

UNCLASSIFIED
SECURITY CLASSIFICATION OF THIS PAGE

(2)

REPORT DOCUMENTATION PAGE

1a. REPORT SECURITY CLASSIFICATION Unclassified		1b. RESTRICTIVE MARKINGS DDC FILE COPY	
2a. 2b. 4. AD-A203 874		3. DISTRIBUTION/AVAILABILITY OF REPORT Distribution Unlimited Approved for Public Release	
6a. NAME OF PERFORMING ORGANIZATION Tufts University		5. MONITORING ORGANIZATION REPORT NUMBER(S) AFOSR-TR- 89-0044-APP	
6b. OFFICE SYMBOL (If applicable)		7a. NAME OF MONITORING ORGANIZATION AFOSR/NP	
6c. ADDRESS (City, State, and ZIP Code) Dept. of Physics & Astronomy Medford, MA 02155		7b. ADDRESS (City, State, and ZIP Code) DKI 410 Bolling Air Force Base Washington, DC 20332	
3a. NAME OF FUNDING/SPONSORING ORGANIZATION AFOSR/NP		8b. OFFICE SYMBOL (If applicable) NP	
9. PROCUREMENT INSTRUMENT IDENTIFICATION NUMBER Grant AFOSR-83-0019		10. SOURCE OF FUNDING NUMBERS	
8c. ADDRESS (City, State, and ZIP Code) BICI 410 Bolling Air Force Base Washington, DC 20332		PROGRAM ELEMENT NO. 61102F	PROJECT NO. 2311
11. TITLE (Include Security Classification) VERY LARGE ARRAY OBSERVATIONS OF THE SUN WITH RELATED OBSERVATIONS USING THE SMM SATELLITE		TASK NO. A1	WORK UNIT ACCESSION NO.
12. PERSONAL AUTHOR(S) Kenneth R. Lang			
13a. TYPE OF REPORT Final Technical		13b. TIME COVERED FROM 830101 TO 880831	14. DATE OF REPORT (Year, Month, Day) 88 10 12
15. PAGE COUNT 30 327		16. SUPPLEMENTARY NOTATION	
17. COSATI CODES FIELD GROUP SUB-GROUP		18. SUBJECT TERMS (Continue on reverse if necessary and identify by block number)	
19. ABSTRACT (Continue on reverse if necessary and identify by block number) X. APPENDIX - REPRINTS OF PAPERS PUBLISHED 1983-1988			
<div style="border: 1px solid black; padding: 5px; width: fit-content;">DISTRIBUTION STATEMENT A Approved for public release; Distribution Unlimited</div>			
20. DISTRIBUTION/AVAILABILITY OF ABSTRACT <input checked="" type="checkbox"/> UNCLASSIFIED/UNLIMITED <input type="checkbox"/> SAME AS RPT. <input type="checkbox"/> DTIC USERS		21. ABSTRACT SECURITY CLASSIFICATION UNCLASSIFIED	
22a. NAME OF RESPONSIBLE INDIVIDUAL DR Henry R. Radaski		22b. TELEPHONE (Include Area Code) 202/767-4906	
22c. OFFICE SYMBOL NP		SECURITY CLASSIFICATION OF THIS PAGE	

DD FORM 1473, 84 MAR

85 APR edition may be used until exhausted.
All other editions are obsolete.

SECURITY CLASSIFICATION OF THIS PAGE

UNCLASSIFIED

DTIC
S E C T E D
FEB 09 1989
9H

VERY LARGE ARRAY OBSERVATIONS OF THE SUN WITH RELATED OBSERVATIONS USING THE
SMM SATELLITE

GRANT AFOSR-83-0019

Final Scientific Report
for 01 Jan. 1983 to 31 Aug. 1988

X. APPENDIX - REPRINTS OF PAPERS PUBLISHED 1983 - 1988

PAGE

1. "Multiple Wavelength Observations of Flaring Active Regions", Kenneth R. Lang and Robert F. Willson, Advances in Space Research, Proceedings of the 24th Plenary Meeting of COSPAR (Committee on Space Research), Volume 2, No. 11, pp. 91-100, Pergamon Press, London 1983.6
2. "Very Large Array Observations of Solar Active Regions III. Multiple Wavelength Observations", Kenneth R. Lang, Robert F. Willson and Victor Gaizauskas, Astrophysical Journal 267, 455-464 (1983).16
3. "High-Resolution Observations of Solar Radio Bursts at 2, 6 and 20 cm Wavelength", Robert F. Willson, Solar Physics 83, 285-303 (1983).....26
4. "The Circularly Polarized Sun at 12.6 cm Wavelength", Kenneth R. Lang and Robert F. Willson, Astronomy and Astrophysics 127, 135-139 (1983).....45
5. "Bright, Rapid, Highly Polarized Radio Spikes from the M Dwarf AD. Leonis", Astrophysical Journal (Letters) 272, L15-L18 (1983).....50
6. "Possible Detection of Thermal Cyclotron Lines from Small Sources within Solar Active Regions", Robert F. Willson, Solar Physics 89, 103-113 (1983).54

7. "Observations of Preburst Heating and Magnetic Field Changes in a 20 cm Loop"; Robert F. Willson, Solar Physics 92 189-198 (1984).....65
8. "Very Large Array Observations of Solar Active Regions IV. Structure and Evolution of Radio Bursts from 20 cm Loops", Robert F. Willson and Kenneth R. Lang, Astrophysical Journal 279, 427-437 (1984).....75
9. "The Structure of a Solar Active Region from RATAN-600 and Very Large Array Observations", Kenneth R. Lang, et. al., Astrophysical Journal 301, 460-464 (1985)86
10. "The Solar-Stellar Connection", Kenneth R. Lang, Proceedings of the INDO-US Workshop on Solar-Terrestrial Physics, (National Physical laboratory: New Delhi, India, 1986) pp. 21-42.....91
11. "Short Term Prediction of Solar Bursts - Radio Wavelength Precursors", Kenneth R. Lang, Proceedings of the Solar Terrestrial Prediction Workshop (Observatoire de Paris, Meudon, 1984) pp. 613.....114
12. "VLA Observations of Flare Build Up in Coronal Loops on the Sun and Solar Type Stars", Kenneth R. Lang and Robert F. Willson, Advances in Space Research, Proceedings of the 25th Plenary Meeting of COSPAR (Committee) on Space Research, Pergamon Press. London, 1984.....117
13. "The Sun and Nearby Stars: Microwave Observations at High Resolution", Mukul R. Kundu and Kenneth R. Lang, Science 228, 9-15 (1985).....123
14. "Microwave Observations of Late-Type Stars with the Very Large Array" Roberto Pallavicini, Robert F. Willson and Kenneth R. Lang, Astronomy and Astrophysics 149, 95-101 (1985).....130 s



A-1

 or
Special

15. "VLA Observations of Narrow-Band Decimetric Burst Emission", Robert F. Willson, Solar Physics 96, 199-207 (1985).....137
16. "VLA Observations of Solar Active Regions at Closely Spaced Frequencies: Evidence for Thermal Cyclotron Line Emission", Robert F. Willson, Astrophysical Journal 298, 911-917 (1985).....146
17. "High-Resolution Microwave Observations of the Sun and Nearby Stars", Kenneth R. Lang, Solar Maximum Analysis (ed. V.E. Stepanov and V.N. Obridko, VNU Science Press, 1986) pp. 69-89.....153
18. "Solar Burst Precursors and Energy Build Up at Microwave Wavelengths", Kenneth R. Lang and Robert Willson, Advances in Space Research 6 no. 6 97-100 (1986).....174
19. "Radio Wavelength Observations of Magnetic Fields On Active Dwarf M, RS CVN And Magnetic Stars", by Kenneth R. Lang, Advances in Space Research 6, no. 6, 109-112 (1986).....178
20. "VLA Observations of Compact, Variable Sources on the Sun", Robert F. Willson and Kenneth R. Lang, The Astrophysical Journal 308, 443-447 (1986).....182
21. "Flare Stars and Solar Bursts: High Resolution In Time and Frequency" Kenneth R. Lang, Solar Physics 104, 227-233 (1986).....187
22. "Coronal Plasmas On The Sun And Nearby Stars", Kenneth R. Lang, Coronal and Prominence Plasmas, (NASA Conference Pub. 2442, 1986) pp. 309-317.....194

23. "Compact, Variable Moving Sources Observed On the Sun At 2 Centimeters Wavelength", Kenneth R. Lang and Robert F. Willson, Coronal and Prominence Plasmas, (NASA Conference Pub. 2442 - 1986) pp. 353-357.....204
24. "Coronal Diagnostics", Kenneth R. Lang, Coronal and Prominence Plasmas NASA Conference Pub. 2442, - U.S. Govt. Printing, 1986) pp. 279-289.....210
25. "Narrow-Band, Slowly Varying Decimetric Radiation From The Dwarf M Flare Star YZ Canis Minoris", Kenneth R. Lang and Robert F. Willson, The Astrophysical Journal (Letters) 302, L17-L22 (1986).....222
26. "Millisecond Radio Spikes From the Dwarf M Flare Star AD Leonis", Kenneth R. Lang and Robert F. Willson, The Astrophysical Journal, 305, 363-368 (1986).....227
27. "Compact, Variable Sources on the Sun at 2 Centimeter Wavelength", Robert F. Willson and Kenneth R. Lang, Solar Physics 114, 93-104 (1987)....233
28. "Multiple Wavelength Microwave Observations of the RS Canum Venaticorum Stars UX Arietis, HR 1099, HR 5110 and II Pegasi", Robert F. Willson and Kenneth R. Lang, Astrophysical Journal 312, 278-283 (1987).....245
29. "VLA Observations of a Solar Noise Storm", Kenneth R. Lang and Robert F. Willson, The Astrophysical Journal 319, 514-519 (1987).....251
30. "Simultaneous SMM Flat Crystal Spectrometer And Very Large Array Observations Of Solar Active Regions", Kenneth R. Lang, Robert F. Willson, Kermit L. Smith, and Keith T. Strong, The Astrophysical Journal 322, 1035-1043 (1987).....257

31. "Solar Active Region Physical Parameters Inferred From A Thermal Cyclotron Line and Soft X-ray Spectral Lines", Kenneth R. Lang, Robert F. Willson, Kermit L. Smith, and Keith T. Strong, The Astrophysical Journal 322, 1044-1051 (1987).....266
32. "Ultraviolet And Radio Flares From UX Arietis And HR 1099", Kenneth R. Lang and Robert Willson, Astrophysical Journal 328, 610-616 (1988).....274
33. "VLA Observations Of Dwarf M Flare Stars And Magnetic Stars", Robert F. Willson, Kenneth R. Lang and Prudence Foster, Astronomy and Astrophysics 199, 255-261 (1988).....281
34. "High Resolution VLA Maps of The Quiescent Corona At 90 cm Wavelength" Kenneth R. Lang, Robert F. Willson and Gerard Trottet, Astronomy and Astrophysics 199, 325-328 (1988).....288
35. "Narrow-Band, Slowly Varying Decimetric Radiation From the Dwarf M Flare Star YZ Canis Minoris II", Kenneth R. Lang and Robert F. Willson, Astrophysical Journal 326, 300-304 (1988).....292
36. "Microwave Observations of Solar and Stellar Coronae", Robert F. Willson in Solar and Stellar Coronal Structure and Dynamics (ed. Richard C. Altrock, National Solar Observatory, 1988) pp. 54-65.....297
37. "Simultaneous VLA-Satellite Observations of the Sun", Kenneth R. Lang. Advances in Space Research, Proceedings of the XXVII Committee on Space Research (COSPAR) Meeting (Pergamon Press, 1988).....310
38. "High-Resolution VLA-Nancay Observations of the Sun", Alain Kerdraon, Gerard Trottet, Kenneth R. Lang and Robert F. Willson, Advances in Space Research; Proceedings of the XXVII Committee on Space Research (COSPAR) Meeting (Pergamon Press, 1988).....319

1. MULTIPLE WAVELENGTH OBSERVATIONS OF FLARING ACTIVE REGIONS

Kenneth R. Lang and Robert F. Willson

Department of Physics, Tufts University, Medford, MA, U.S.A.

ABSTRACT

We present observations of flaring active regions with the Very Large Array (V.L.A. at 6 cm and 20 cm wavelengths) and the Westerbork Synthesis Radio Telescope (W.S.R.T. at 6 cm wavelength). These are compared with photospheric magnetograms (Meudon) and with H α and offband H α photographs (Big Bear and Ottawa River Solar Observatories). The 6 cm radiation of these active regions marks the legs of dipolar loops which have their footpoints in lower-lying sunspots. The intense, million degree radiation at 6 cm lies above sunspot umbrae in coronal regions where the longitudinal magnetic field strength $H_z = 600$ Gauss and the height above the sunspot umbrae $h = 3.5 \pm 0.5 \times 10^9$ cm. Circularly polarized horseshoe structures at 6 cm ring the sunspot umbrae. The high degree of circular polarization ($p_c = 95\%$) of the horseshoes is attributed to gyroresonant emission above sunspot penumbrae. The 20 cm radiation of these active regions exhibits looplike coronal structures which extend across regions of opposite magnetic polarity in the underlying photosphere. The 20 cm loops are the radio wavelength counterparts of the X-ray coronal loops. We infer semilengths $L = 5 \times 10^9$ cm, maximum electron temperatures $T_e(\text{max}) = 3 \times 10^6$ K, emission measures $\int N_e^2 dV = 10^{28}$ cm $^{-5}$, and electron densities $N_e = 10^9$ cm $^{-3}$ (or pressures $p = 1$ dyn cm $^{-2}$) for the 20 cm bremsstrahlung. A total of eight solar bursts were observed at 6 cm or 20 cm wavelength with second-of-arc angular resolution. The regions of burst energy were all resolved with angular sizes between 5" and 30", brightness temperatures between 2×10^7 K and 2×10^8 K, and degrees of circular polarization between 10% and 90%. The impulsive phase of the radio bursts are located near the magnetic neutral lines of the active regions, and between the flaring H α kernels which mark the footpoints of magnetic loops. In one case there was preburst heating in the coronal loop in which a burst occurred. Snapshot maps at 10 s intervals reveal interesting burst evolution including rapid changes of circular polarization and an impulsive burst which was physically separated from both the preburst radio emission and the gradual decay phase of the burst.

INTRODUCTION

Quiescent solar radio emission and solar radio bursts can now be studied with second-of-arc resolution by using the Very Large Array (V.L.A.) and the Westerbork Synthesis Radio Telescope (W.S.R.T.). In addition to providing new information on the sizes, locations and brightness temperatures of the radio bursts, the radio synthesis maps can be compared with optical wavelength data at comparable time intervals and angular resolutions. Furthermore, the V.L.A. and W.S.R.T. are capable of measuring the radio intensity and polarization with high angular and time resolution, thereby providing information about the preburst heating and the evolution of the magnetic fields in the bursting regions. All of this information is, of course, vital to our understanding of the origin, development and prediction of solar bursts.

THE QUIESCENT ACTIVE REGION

Previous related work. High resolution synthesis maps at 6 cm wavelength reveal features which have been associated with a bewildering complexity of optical wavelength counterparts including sunspot umbrae [1,2,3], sunspot penumbrae [4,5] and magnetic neutral lines [6]. In some cases the 6 cm emission delineates structures which join sunspots of opposite magnetic polarity [7,8]. We felt that a more fruitful approach from the physical point of view would be to simultaneously observe the same active region at a variety of radio wavelengths with the same field of view and angular resolution. The highlights of these simultaneous, multiple wavelength observations of quiescent active regions are given in the following three subsections. They are discussed in greater detail elsewhere [4,9,10].

Legs of magnetic dipole loops at 6 cm wavelength. Exploratory multiple wavelength observations were carried out on June 12, 1980 and on September 3-4, 1980, when the Very Large

Array was used to respectively observe AR 2505 and AR 2646 at 2 cm, 6 cm and 20 cm wavelength. The position of AR 2505 on the solar surface was 14°S and 40°W at 13^{h} U.T. on June 12. The position of AR 2646 on the Sun's surface was 11°N and 9.5°W at 13^{h} U.T. on Sept. 3 and 11°N and 22°W at 13^{h} U.T. on Sept. 4. The synthesis maps of the total intensity, I , of the radiation from AR 2505 are shown in Figure 1. Here the contours mark levels of equal brightness temperature corresponding to 0.2, 0.4, 0.6 and 0.8 times the maximum brightness temperatures of 5.1×10^6 K and 1.5×10^6 K at $\lambda = 2$ cm and 6 cm respectively. The enhanced 6 cm emission is associated with a group of three sunspots whose total angular extent is the same as that of the 2 cm emission. We attribute the broader extent of the 6 cm emission to the diverging magnetic fields of a dipolar loop which has one footpoint in the group of sunspots, and a higher lying leg marked by the 6 cm emission. The centroid of the 6 cm emission is displaced with respect to the centroid of the 2 cm emission by $40'' \pm 5''$ to the southwest. This is interpreted as a radial, limbward displacement caused by the greater height of the 6 cm emission. Both the westward component of the displacement ($35'' \pm 5''$) and the southward component ($12'' \pm 5''$) indicate a height $h = 3.5 \pm 0.5 \times 10^9$ cm for the 6 cm emission above the chromosphere. Because this is comparable to the height of the plage-associated component of 6 cm emission in another active region [7] our observations provide no evidence for a difference in the height between the photosphere and the million-degree 6 cm emission above sunspots and plage. When allowance is made for the projection effect caused by a greater height, both the 2 cm and 6 cm emission lie above the group of sunspots. The high brightness temperatures $T_B \approx 10^6$ K and the high degree of circular polarization $p_c \approx 60\%$ of the 6 cm emission are most easily explained as optically thin gyroresonance emission in the low solar corona. The strong radial magnetic fields of the sunspot umbrae allow the detection of the third harmonic of the gyrofrequency at higher, hotter levels in the solar atmosphere. Our 6 cm observations indicate longitudinal magnetic field strengths of $H_L \approx 600$ Gauss (third harmonic at $\lambda = 6$ cm) in regions above sunspot umbrae which have temperatures of 10^6 K.

In Figure 2, the 6 cm emission of AR 2646 on Sept. 3 is superimposed on an offband H α photograph (H α +1.4) taken on the same day. Here the contours mark levels of equal brightness temperature corresponding to 0.2, 0.4, 0.6, 0.8 and 1.0 times the maximum brightness temperature of 2.2×10^6 K. The two main groups of sunspots have opposite magnetic polarity, and the circular polarization of the 6 cm emission corresponds to the extraordinary mode of wave propagation in magnetic fields with the same polarity as the underlying sunspots. The two most intense components of the 6 cm emission are displaced inwards and away from the sunspots as would be expected if they mark the higher lying legs of the magnetic dipole which joins the two sunspot groups. The two peaks found in the largest component of the 6 cm emission probably mark the higher lying parts of the outwardly diverging magnetic flux tubes which join the two umbrae that are separated by a light bridge. There were several H α flares emitted from the light bridge on Sept. 3, even though the two sunspots on either side of it have the same magnetic polarity. To a first approximation we may assume that these groups of sunspots mark the feet of a circular dipole whose radius $r \approx 70'' \approx 5.0 \times 10^9$ cm. We may then infer the heights of the 6 cm components from their inward displacements of $x \approx 25'' \pm 5'' \approx 1.6 \pm 0.4 \times 10^9$ cm. We obtain $h = r \sin[\cos^{-1}\{(x-r)/r\}] = 3.8 \pm 0.4 \times 10^9$ cm above the solar photosphere. The high brightness temperatures $T_B \approx 10^6$ K and high degrees of circular polarization $p_c \approx 67\%$ of the 6 cm emission are most easily explained as optically thin gyroresonance emission in the low solar corona. This provides additional evidence that magnetic fields of $H_L \approx 600$ Gauss exist at heights of $h \approx 3.5 \times 10^9$ cm above sunspots where the temperatures $T \approx 10^6$ K. The 20 cm emission, on the other hand, delineated a coronal loop which joins the two regions of opposite magnetic polarity. The peak brightness temperature at 20 cm was located at the

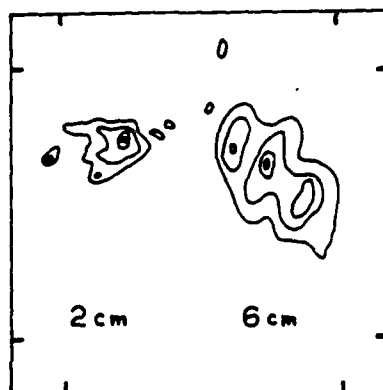


Fig. 1. Synthesis maps of the total intensity, I , of the radiation from active region AR 2505 taken simultaneously with the Very Large Array (V.L.A.) at 2 cm (left) and 6 cm (right) wavelengths on June 12, 1980. Here, north is up, west is to the right, and both maps have the same phase center and the same angular scale denoted by $60''$ spacing between fiducial marks.



Fig. 2. A V.L.A. synthesis map of the total intensity of the 6 cm radiation from active region AR 2646 on Sept. 3, 1980, is superimposed upon an offband H α photograph of the same active region taken at the Ottawa River Solar Observatory (courtesy Victor Gaizauskas) on the same day. The largest component of 6 cm emission has an angular extent of about 60".

central apex or top of the loop, and it had a value of 9.4×10^5 K - suggesting optically thin bremsstrahlung of the hot coronal plasma trapped within the loop.

Polarized horseshoes around sunspots. Multiple wavelength observations were continued during the post-S.M.M. observing interval from June 12 to June 17, 1981, when AR 3159 was observed with the Very Large Array (V.L.A. at 20 cm wavelength), the Westerbork Synthesis Radio Telescope (W.S.R.T. at 6 cm wavelength), the Meudon magnetogram (by Jean Rayrole), and the Big Bear Solar Observatory (B.B.S.O. at H α and offband H α). Here we present the combined W.S.R.T.-B.B.S.O. results, while the combined V.L.A.-Meudon results are discussed in the next subsection. In Figure 3, the W.S.R.T. synthesis maps of AR 3159 for June 14, 1981, are compared with an offband H α photograph taken on the same day. The position of AR 3159 on the solar surface was 26°S and 31°E at 14^h U.T. on June 14. The contours of the V maps (left) mark levels of equal brightness temperature corresponding to 0.3, 0.4, ..., 0.9 times the maximum brightness temperatures of $+3.0 \times 10^5$ K and -2.8×10^5 K. The solid contours of the V map refer to regions of positive, left-hand circular polarization and negative (south or black) magnetic polarity. The dashed contours of the V map correspond to negative right-handed circular polarization and positive (north or white) magnetic polarity. The contours of the I map (right) mark levels of equal brightness temperature corresponding to 0.1, 0.2, ..., 0.9 times the maximum brightness temperature of 2.2×10^6 K.

Of special interest is the horseshoe shaped structure found in the circular polarization map. The horseshoe rings a sunspot umbra and lies above the penumbra where the magnetic fields are

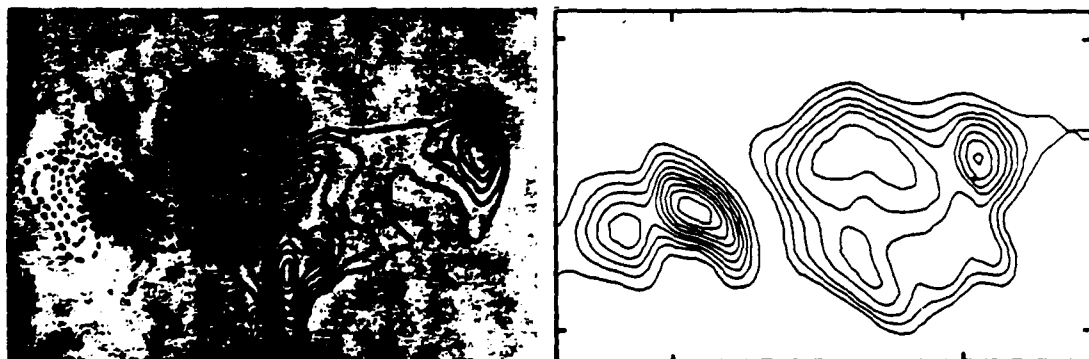


Fig. 3. The 6 cm synthesis map of circular polarization V is superimposed upon an offband H α photograph of the same region AR 3159 taken on the same day (left) and compared with the 6 cm map of total intensity, I (right). The angular scale is denoted by the 60" spacing between the fiducial marks on the axes. The offband H α photograph was taken at the Big Bear Solar Observatory (courtesy of Frances Tang).

strongly curved. Similar horseshoes do not surround nearby sunspots which have more intense magnetic fields. Alissandrakis and Kundu [5] have recently reported their discovery of polarized horseshoes which ring sunspot umbrae, but their result differs from ours in finding a depression of total intensity (or temperature) above the sunspot umbra. We find a peak in the total intensity of the 6 cm emission above sunspot umbrae, where the temperatures $T \approx 10^6$ K and the longitudinal magnetic field strength $H_L \approx 600$ Gauss. The intense magnetic fields of sunspot umbrae probably project radially upwards into the low solar corona with little loss of strength. This enables the third harmonic of the gyrofrequency to occur at higher, hotter levels of the solar atmosphere where the temperature gradient is small. The situation is different for the curved magnetic fields of the sunspot penumbrae. In this case the resonance levels corresponding to the third harmonic occur in the lower-lying cooler regions of the solar atmosphere where the temperature gradients are large. The high degrees of circular polarization ($\rho_c = 95\%$) of the peaks of our newly-discovered horseshoe structures require gyroresonant emission. If this high polarization were due to propagation effects instead of gyroresonance, a higher longitudinal magnetic field strength of $H_L \approx 1800$ Gauss would be required. Furthermore, the gyroresonant interpretation is fully confirmed by the theoretical work [11] which predicted the existence of the circularly polarized horseshoes which we have observed.

Coronal loops at 20 cm wavelength. We have recently detected two looplike structures at 20 cm wavelength which join regions of opposite magnetic polarity in the underlying photosphere [9]. The two loops had maximum brightness temperatures of 2.1×10^6 K and 4.1×10^6 K. They are almost certainly the radio wavelength counterparts of the ubiquitous "coronal loops" detected at soft X-ray wavelengths. The absence of detectable circular polarization suggests that the 20 cm loops are optically thick, and that the brightness temperatures are equal to the electron temperatures of the hot, dense plasma trapped within the loop. In fact, the field of view of the individual V.L.A. antennae at 20 cm wavelength covers the entire Sun. We therefore examined our data for 20 cm coronal loops associated with other active regions. We found a total of 15 coronal loops associated with 3 active regions on 5 days. The 20 cm coronal loops are therefore truly ubiquitous features of the solar atmosphere (see Figure 4 for another example). The maximum electron temperatures, $T_e(\text{max})$, are characteristic of those found in the X-ray coronal loops with $T_e(\text{max}) = 2$ to 4×10^6 K. The total extents of the 20 cm loops range between 2×10^9 cm and 1×10^{10} cm, and these are also comparable to the X-ray coronal loops which have semilengths L of 10^9 cm to 10^{10} cm (L is half the total extent of the loop as measured along the magnetic field). We can use the scaling relationship of Rosner, Tucker and Vaiana [12]: $T_e(\text{max}) = 1.4 \times 10^3 (pL)^{1/3}$ to obtain the loop pressure p . Choosing $T_e(\text{max}) = 3 \times 10^6$ K and $L = 5 \times 10^9$ cm we obtain a pressure of $p = 1.96$ dyn cm^{-2} , which is again characteristic of the X-ray coronal loops. We can also check the consistency of our argument that the 20 cm loops are the optically thick bremsstrahlung of

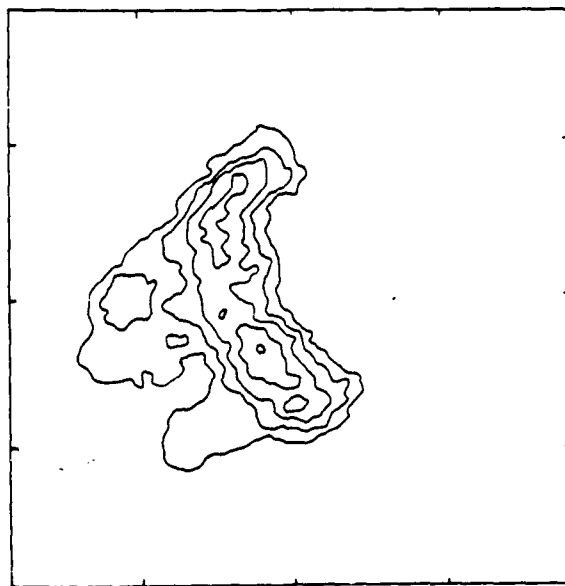


Fig. 4. The 20 cm coronal loop associated with the eastern active region AR 3159 on June 13, 1981. The active region was located about 20° across the solar surface from the east limb, and the 20 cm loop is therefore seen projected eastward (to the left). Here the contours mark levels of equal brightness temperature corresponding to 0.2, 0.4... 1.0 times the maximum brightness temperature of $T_B \approx 2 \times 10^6$ K.

thermal electrons by determining the electron density $N_e = p/(2kT_e) = 2.5 \times 10^9 \text{ cm}^{-3}$. This value of electron density can be used together with an average electron temperature of $T_e \approx 10^6 \text{ K}$ to obtain the optical depth, τ_B , of thermal bremsstrahlung ($\tau_B = 2.5$). Our assumptions are therefore satisfied for brightness temperature $T_B = [1 - \exp(-\tau_B)]T_e = 0.92 T_e$.

SOLAR BURSTS

Previous related work. Previous V.L.A. observations of solar bursts indicate that 6 cm bursts often occur above magnetic neutral lines located between sunspots [13,14], and that both the 2 cm and 6 cm emission are frequently located in the central regions of magnetic arches located between flaring H α kernels [15,16]. These results imply that the energy release at radio wavelengths occurs near the apex of the magnetic loops. In fact, Velusamy and Kundu [17] have reported the observation of postflare loop systems at 20 cm wavelength. Nevertheless, Kattenberg [18] has reported that burst emission at radio wavelengths occurs at the footpoints of magnetic dipoles. V.L.A. observations at 6 cm wavelength [19] indicate that the locations of different peaks of multiple bursts are the same to within $\pm 2''$, although the polarization is not always the same for different peaks. Lang, Willson and Felli [14] have shown that the size, position and circular polarization remain constant during the emission of successive 20 cm bursts. This suggests that one source is emitting the sequence of events, and that the energetic electrons are being accelerated in the same magnetic region of the loop. Lang [20,21] has additionally called attention to dramatic changes in circular polarization which occur before and during flares. These are probably related to changes in the structure of the coronal magnetic field. The highlights of our unpublished observations of solar bursts are given in the next three sections which discuss the location of energy release, preburst heating, and magnetic changes. Much of this data was taken during the post-S.M.M. observing interval in June, 1981. They will be discussed in greater detail elsewhere [22].

Site of energy release and preburst heating. Although it is generally believed that solar radio bursts occur through the conversion of magnetic to particle energy within a complex network of coronal loops, the exact location of the sites of energy release within the loop structures has only recently been determined. We have observed a total of eight bursts at 2 cm, 6 cm or 20 cm wavelength with second-of-arc resolution. The regions of burst energy were all resolved with angular sizes ranging between $5''$ and $30''$, brightness temperatures between $2 \times 10^7 \text{ K}$ and $2 \times 10^8 \text{ K}$, and degrees of circular polarization between 10 and 90 percent. For those cases in which we could compare the positions of the radio bursts and optical features, we found that the radio emission originates near the center of magnetic loops, rather than at the footpoints. In Figure 5 we compare a 10 s snapshot map of the impulsive phase of a burst observed at 6 cm wavelength (B) with both a map of the preburst radio emission (A - three minutes before the burst) and an H α photograph (B - at the time of the burst). The figure indicates that the radio burst (B) was elongated in a direction joining

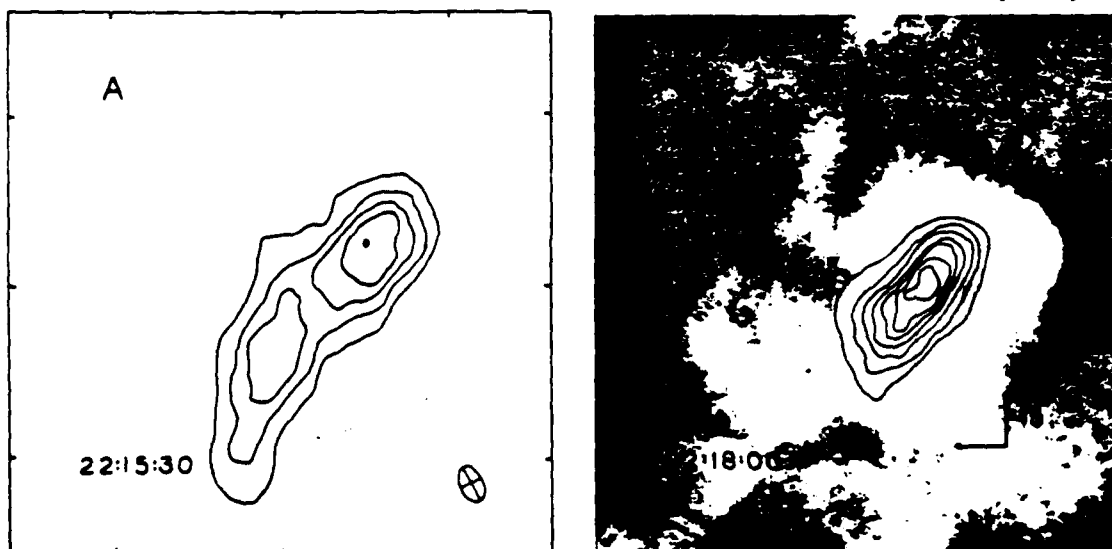


Fig. 5. V.L.A. synthesis maps of the preflare (A) and impulsive phase (B) of a burst detected at 6 cm wavelength on Sept. 4, 1980. Each map of total intensity, I , was made from 10 s of data at the time indicated. The contours of both maps mark levels of equal brightness temperature. For A, the contours are drawn at 1×10^6 , 2×10^6 , ..., $5 \times 10^6 \text{ K}$, while for B, the contours are drawn at 5.5×10^6 , 1.1×10^7 , ..., $3.8 \times 10^7 \text{ K}$. For B, the radio map has been superimposed on an H α photograph of the optical flare taken at the same time. The H α photograph was taken at the Big Bear Solar Observatory (courtesy Frances Tang).

the two bright H α kernels, and that it was most intense at a point located midway between them. The preburst radio emission (A) was contained within a loop-like structure which also joins the sites of subsequent H α emission. Here the peak brightness temperature is 5.5×10^6 K as compared with the peak burst brightness temperature of 4.2×10^7 K. Because the brightness temperature of quiescent coronal emission at 6 cm is typically $\sim 2 \times 10^6$ K [3,7] the somewhat higher temperature observed in the preburst loop could represent thermal (pre-burst heating) or nonthermal emission which precedes the impulsive phase of the solar burst. In order to check that the brightness temperature was in fact higher than normal at this time, we also made several maps of 10 minutes duration centered around one hour before the burst. We found that the radio source has a similar size and shape, but that the peak brightness temperatures were more than a factor of two lower with values of about 1.7×10^6 K. We therefore believe that we have detected preburst heating which occurs minutes before burst emission. Kundu and his colleagues have also found evidence for heating of the plasma in coronal loops before the impulsive phase of a 6 cm burst. There are theoretical explanations for the release of radio energy at the top of magnetic loops [23], and for the expectation of temperature enhancements during pre-flare activity [24]. In Figure 6 we present the time profile of another 6 cm burst whose 10 s snapshot maps are given in Figure 7. The sequence of maps, which were made before, during and after the impulsive phase of the burst, indicate that the impulsive component is smaller and spatially separated from both the preburst radio emission and the gradual decay component of the burst. The gradual decay component is about $10''$ in size and 30% left circularly polarized, while the impulsive component is about $8''$ in size and less than 15% circularly polarized. The absence of circular polarization in the impulsive component suggests that this source is located near the apex of the loop where the longitudinal component of the magnetic field is small, whereas the polarization detected in the gradual decay component suggests an origin in a predominantly longitudinal magnetic field of one polarity, most likely in one leg of the loop.

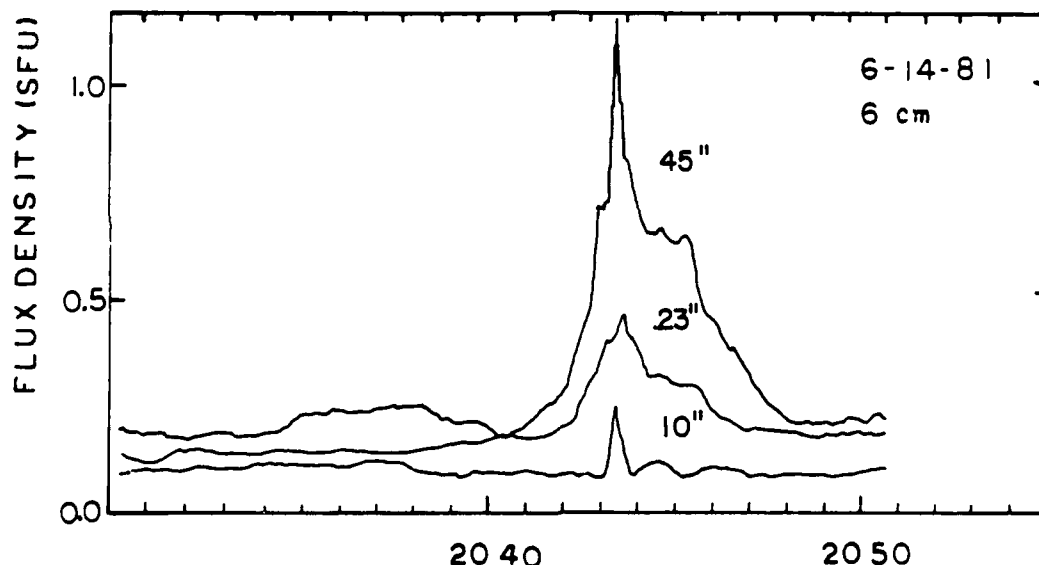


Fig. 6. The fringe amplitude of the total intensity, I , versus time for a burst detected at 6 cm wavelength with the V.L.A. on June 14, 1981. The angular resolution of each interferometer pair is given next to the time profile.

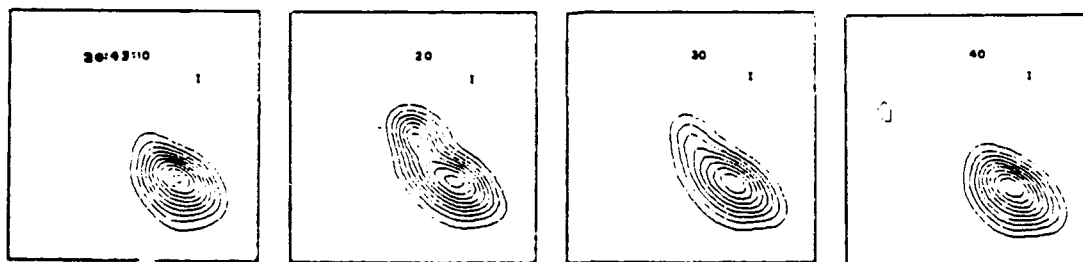


Fig. 7. A series of 10 s V.L.A. snapshot maps of the total intensity, I , for a burst detected at 6 cm wavelength on June 14, 1981. The contours of the I maps mark levels of equal brightness temperature and correspond to 2.8×10^6 , 5.5×10^6 ... 2.5×10^7 K. Note especially the spatial separation of the impulsive component of the burst at 20:43:20 U.T..

Magnetic changes. High resolution interferometric observations have led to the discovery of a high degree of circular polarization for both the slowly varying component and the burst component of active regions. The high polarization is attributed to either propagation effects or to gyroemission of energetic electrons. Both mechanisms require strong magnetic fields of several hundred Gauss in strength. The high brightness temperatures of the radio emission ($> 10^6$ K) indicates that the relevant magnetic fields are in the low solar corona. Previous studies of the evolution of the magnetic fields in the underlying photosphere suggest that some change in the magnetic field topology triggers the emission of solar bursts, but it is probably the coronal magnetic field which supplies the energy for solar bursts. Lang [20,21] has, for example, shown that the degree of circular polarization of the coronal radio emission can increase to 100% about 10 minutes to one hour before the eruption of solar bursts. Kundu and his colleagues have similarly detected dramatic changes in circular polarization before and during a complex flare observed at 6 cm with the V.L.A.. About 10 minutes before the onset of the impulsive phase, the magnetic structure changed from a simple bipolar region to a more complicated quadrupolar configuration; suggesting the appearance of a new system of coronal loops accompanied by the generation of additional magnetic flux.

The time profiles of the total intensity, I , and circular polarization, $p_c = V/I$, of a 20 cm burst are given in Figure 8. It consists of three impulsive spikes, each of 10 to 20 s duration, superimposed on a more gradual burst lasting about 12 minutes. The lower part of the figure shows that the first impulsive spike is highly right circularly polarized while the other two impulsive spikes are highly left circularly polarized. In Figure 9 we display a series of snapshot maps of both I and V made at 10 s intervals. Near the beginning of the burst at 12:40:00 U.T. the slowly varying source has a size of $\sim 30''$ and is $\sim 25\%$ left circularly polarized in the eastern half of the source. The polarized structure changes dramatically during the first impulsive spike, becoming about 90% right circularly polarized in the western half of the region, then reverting back to its unpolarized pre-impulsive state 10 s later. The polarization structure changes again at 12:40:50 and 13:42:50 U.T. when the source becomes more elongated and develops two left circularly polarized spikes ($p_c \sim 50-60\%$) which bracket the previously right circularly polarized spike located near the center of the region. The maximum brightness temperature of the three impulsive spikes ranged from 7×10^7 to 10×10^7 K, whereas the brightness temperature of the more slowly varying source was $\sim 3.5 \times 10^7$ K. These rapid polarization changes are difficult to explain in terms of a simple bipolar loop model of the flaring region. The burst may have occurred in a magnetically complex region containing a number of coronal loops which are undergoing rapid variations.

ACKNOWLEDGEMENTS

We thank Victor Gaizauskas of the Ottawa River Solar Observatory, and Frances Tang of the Big Bear Solar Observatory for providing offband H α data. Jean Rayrole of the Meudon Observatory

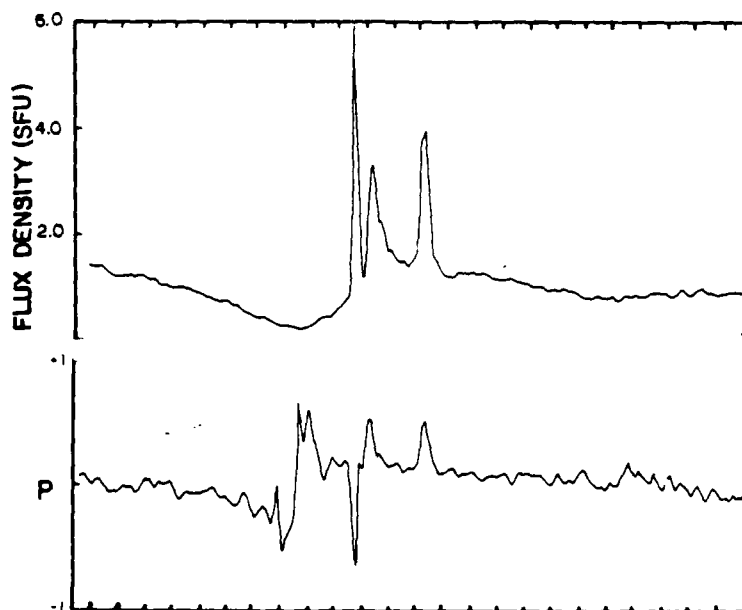


Fig. 8. The time profiles of a multiple spike burst detected at 20 cm wavelength with the V.L.A. on June 12, 1980. Here, both the total intensity, I (top), and the circular polarization, p (bottom), are plotted for an interferometer pair whose angular resolution was $45''$.

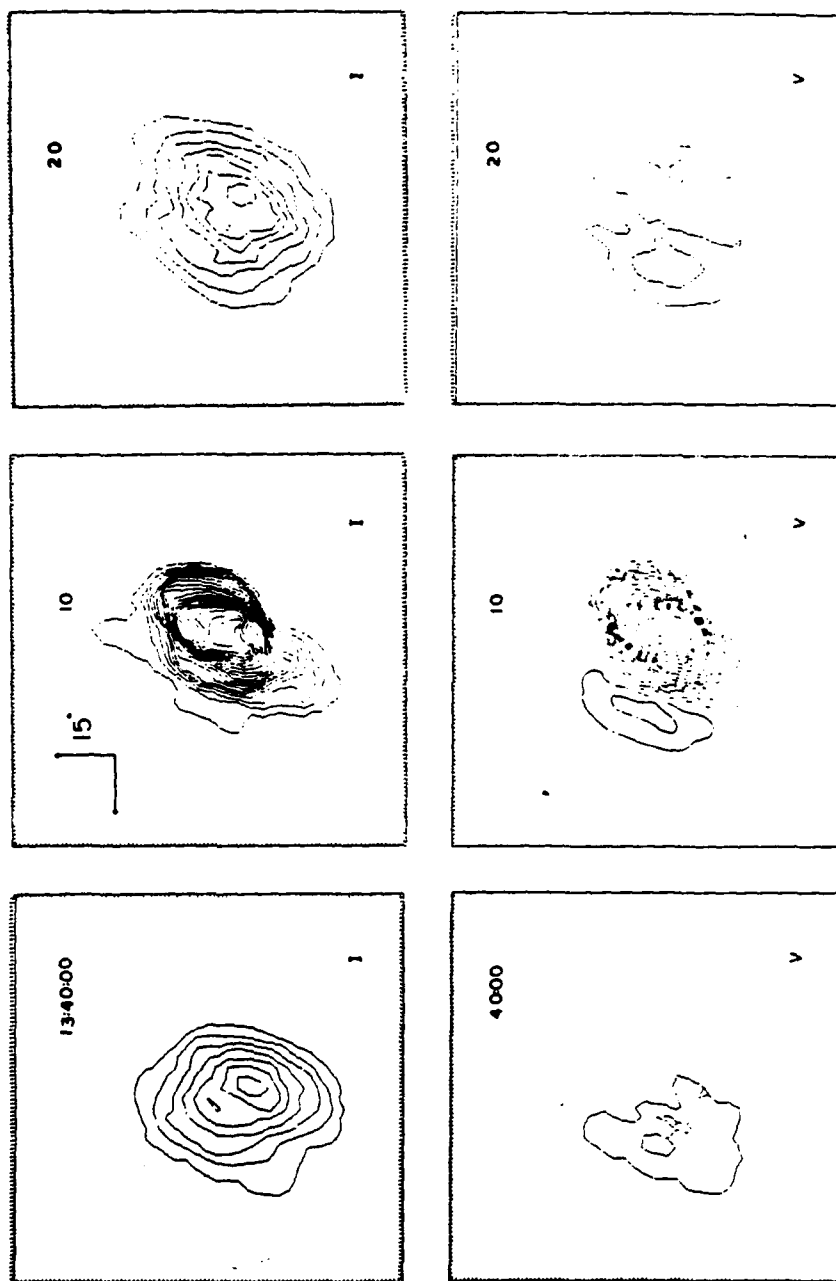
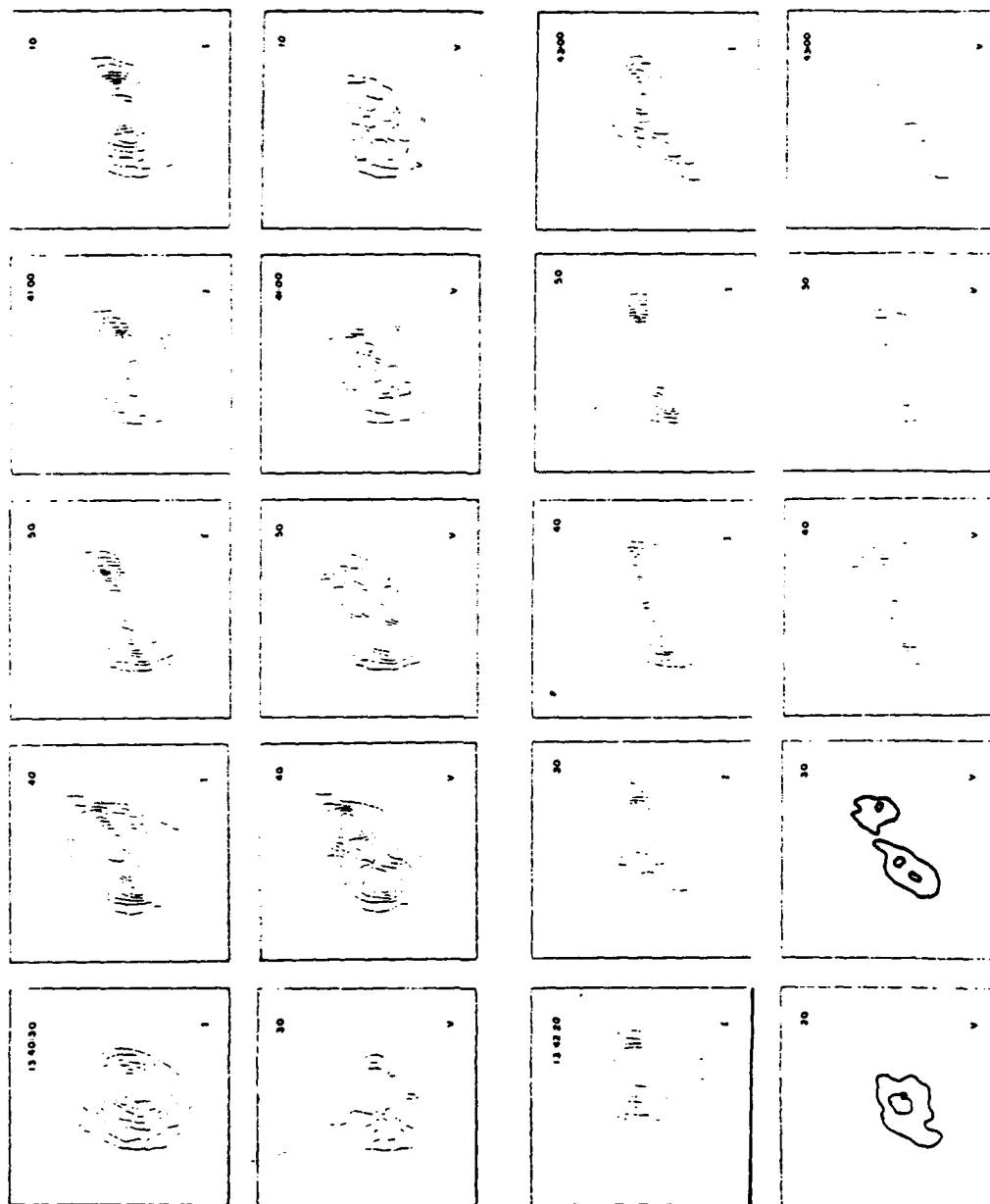


Fig. 9. A series of 10 s snapshot maps of both total intensity, I (top) and circular polarization, V (bottom), for a burst observed at 20 cm wavelength with the V.L.A. on June 12, 1980. For both sets of maps the outermost contour and the contour interval are equal to 6.2×10^6 K.



kindly provided the magnetogram data. We are especially grateful to Dr. Paul Simon for coordinating the post-S.M.M. observing interval.

REFERENCES

1. K.R. Lang and R.F. Willson, Nature 278, 24 (1979).
2. K.R. Lang and R.F. Willson, in Radio Physics of the Sun, I.A.U. Symposium No. 86, Reidel, Dordrecht, 1980.
3. M.R. Kundu, C.E. Alissandrakis, J.D. Bregman and A.C. Hin, Astrophysical Journal 213, 278 (1977).
4. K.R. Lang and R.F. Willson, Astrophysical Journal (Letters) 255, L111 (1982).
5. C.E. Alissandrakis and M.R. Kundu, Astrophysical Journal (Letters) 253, L49 (1981).
6. M.R. Kundu, E.J. Schmahl and A.P. Rao, Astronomy and Astrophysics 94, 72 (1981).
7. M. Felli, K.R. Lang and R.F. Willson, Astrophysical Journal 247, 325 (1981).
8. M.R. Kundu and T. Velusamy, Astrophysical Journal (Letters) 240, L63 (1980).
9. K.R. Lang, R.F. Willson and J. Rayrole, "Very Large Array Observations of Coronal Loops at 20 cm Wavelength", Astrophysical Journal, to be published (July 1982).
10. K.R. Lang, R.F. Willson and V. Gaizauskas, "Very Large Array Observations of Solar Active Regions III. Multiple Wavelength Observations", Astrophysical Journal, submitted, (1982).
11. G.B. Gel'freikh and B.I. Lubyshv, Soviet Astronomy A.J. 23, 216 (1979).
12. R. Rosner, W.H. Tucker and G.S. Vaiana, Astrophysical Journal 220, 643 (1978).
13. C.E. Alissandrakis and M.R. Kundu, Astrophysical Journal 222, 342 (1978).
14. K.R. Lang, R.F. Willson and M. Felli, Astrophysical Journal 247, 338 (1981).
15. K.A. Marsh, H. Zirin and G.J. Hurford, Astrophysical Journal 228, 610 (1979).
16. K.A. Marsh and G.J. Hurford, Astrophysical Journal (Letters) 240, L111 (1980).
17. T. Velusamy and M.R. Kundu, Astrophysical Journal (Letters) 243, L103 (1981).
18. A. Kattenberg, Ph.D. Thesis, Sterrekundig Instituut, Utrecht (1981).
19. M.R. Kundu, M. Bobrowsky and T. Velusamy, Astrophysical Journal 251, 342 (1981).
20. K.R. Lang, Solar Physics 36, 351 (1974).
21. K.R. Lang, in: Solar Terrestrial Predictions, Proceedings III Solar Activity Predictions, N.C.A.A., Boulder, 1980.
22. R.F. Willson, "High Resolution Observations of Solar Radio Bursts at 2 cm, 6 cm and 20 cm Wavelength", Solar Physics, submitted (1982).
23. L. Vlahos and K. Papadopoulos, Astrophysical Journal 233, 717 (1979).
24. S.I. Syrovatskii and V.D. Kuznetsov, in: Radio Physics of the Sun, I.A.U. Symposium No. 86, Reidel, Dordrecht, 1980.

2. VERY LARGE ARRAY OBSERVATIONS OF SOLAR ACTIVE REGIONS. III. MULTIPLE WAVELENGTH OBSERVATIONS

KENNETH R. LANG AND ROBERT F. WILLSON
 Department of Physics, Tufts University

AND

VICTOR GAIZAUSKAS
 Herzberg Institute of Astrophysics

Received 1982 May 20; accepted 1982 September 15

ABSTRACT

Very Large Array (VLA) synthesis maps of the active regions AR 2505 and AR 2646 at wavelengths of 2 cm, 6 cm, and 20 cm are presented and compared with the magnetic structure of the underlying photosphere. At 20 cm wavelength a looplike structure connects two regions of opposite magnetic polarity in AR 2646. The maximum of the 20 cm emission occurs near the central apex or top of the loop, as would be expected from a hydrostatic coronal loop. We interpret the 20 cm radiation in terms of the bremsstrahlung of thermal electrons trapped in magnetic loops. Under the assumption that the electron temperature has a coronal value of $T_e = 2 \times 10^6$ K, our observations indicate that the 20 cm loop has an emission measure $\int N_e^2 dl = 10^{28} \text{ cm}^{-5}$, an electron density of $N_e = 10^9 \text{ cm}^{-3}$, and a pressure $p = 0.8 \text{ dyn cm}^{-2}$. These parameters are similar to those inferred from X-ray observations of coronal loops. The semilength $L = 5 \times 10^9 \text{ cm}$ of the 20 cm loop is also comparable to that of the X-ray coronal loops, and we therefore conclude that we have detected the radio wavelength counterpart of the X-ray loops. The 6 cm radiation of both active regions marks the legs of bipolar loops which have their footprints in lower lying sunspots. The 6 cm brightness temperatures are enhanced above the sunspot umbrae with values of $T_b \approx 10^6$ K. The high brightness temperatures and the high degrees of circular polarization ($\rho_c = 55\% - 70\%$) of the 6 cm radiation are attributed to gyroresonant emission at the third harmonic of the gyrofrequency in a longitudinal magnetic field of strength $H_l = 600$ gauss. We infer a height of the 6 cm emission of $h = (3.5 \pm 0.5) \times 10^9 \text{ cm}$ above the solar photosphere. Our observations show no evidence for cool regions in the solar atmosphere overlying sunspot umbrae, and this is attributed to the unstable, transient nature of cool loops. The 2 cm radiation of AR 2505 has relatively low brightness temperatures $T_b \leq 5 \times 10^4$ K and no detectable circular polarization ($\rho_c < 15\%$), suggesting bremsstrahlung in the transition region. The relatively poor angular resolution did not, however, preclude the existence of highly polarized hot spots of the type detected in AR 2646 at 2 cm wavelength. These small ($\phi \leq 5''$), bright ($T_b \approx 10^5$ K), and highly polarized ($\rho_c \approx 87\%$) hot spots are most plausibly explained in terms of gyroresonant emission in the low solar corona. Although gyroresonant emission in the transition region cannot be completely ruled out, the fact that the hot spots do not exhibit any special relationship with the sunspots argues against this possibility. The 2 cm hot spots may also be transitory phenomena related to H α brightenings or flares, or they may mark the legs of warm ($\approx 10^5$ K) loops.

Subject headings: interferometry — Sun: radio radiation

1. INTRODUCTION

Fan beam observations of solar active regions by Kundu (1959) at 3.2 cm wavelength led to a core-halo model in which bright (10^6 K), polarized cores with angular sizes $\phi \leq 1.8$ are associated with sunspots, and a weaker, extended halo is associated with bright plage. Kakinuma and Swarup (1962) and Zheleznyakov (1962) explained the intensity and polarization spectra of the sunspot-associated cores in terms of the gyroresonant emission of thermal electrons spiraling in the intense magnetic fields of sunspots. This interpretation was given added support when Lang (1974a) used interferometric observations at 3.7 cm wavelength to resolve the core sources which have angular sizes $\phi \approx 20''$ and degrees

of circular polarization up to $\rho_c = 100\%$. The exceptionally high degrees of circular polarization are difficult to explain unless gyroresonant emission is invoked. This is because polarization by propagation effects would require intense magnetic fields which would make the region everywhere optically thick to gyroresonant absorption.

More recently, Alissandrakis, Kundu, and Lantos (1980) and Pallavicini, Sakurai, and Vaiana (1981) have noticed that X-ray observations indicate a low electron density in the coronal atmosphere above sunspots. This low density requires additional radio wavelength opacity due to gyroresonant absorption if radio emission with high brightness temperatures of $T_b \geq 10^6$ K are to be

explained. Furthermore, plane-parallel models of the temperature and density structure of the chromosphere-corona transition region have been used to predict the gyroresonance emission expected in the magnetic fields above sunspots (Lantos 1968; Zlotnik 1968a, b). These theoretical models predict that the total intensity of the emission at 6 cm wavelength will be enhanced above sunspot umbrae where the strong, radial magnetic fields allow the detection of the third harmonic of the gyrofrequency at the higher, hotter levels of the solar atmosphere where the temperature gradient is small. These enhancements have been confirmed by high resolution synthesis maps at 6 cm wavelength which indicate that longitudinal magnetic field strengths of $H_l \approx 600$ gauss are present in the solar atmosphere above sunspots where the temperatures are 10^6 K (Kundu *et al.* 1977; Lang and Willson 1979, 1980; Alissandrakis, Kundu, and Lantos 1980). Final compelling evidence for gyroresonant emission at 6 cm wavelength above sunspots has come from recent observations of circularly polarized horseshoe structures which overlay sunspot penumbrae (Alissandrakis and Kundu 1982; Lang and Willson 1982). These horseshoe structures were predicted from the theory of gyroresonant absorption in the magnetic fields of individual sunspots (Gelfreikh and Lubyshev 1979).

The observations therefore seemed to provide convincing evidence that the 6 cm emission from solar active regions is enhanced above sunspot umbrae where brightness temperatures $T_b \approx 10^6$ K are explained by gyroresonant emission in magnetic fields with strength $H_l \approx 600$ gauss. Curiously enough, however, there has been more recent evidence that there are temperature depressions above some sunspot umbrae at 6 cm wavelength. Felli, Lang, and Willson (1981) showed, for example, that the sunspot-associated emission from one active region occurs at the outer edges of a sunspot where the magnetic field lines are strongly curved, and that the most intense 6 cm emission is correlated with bright chromospheric plage rather than with sunspots. Kundu, Schmahl, and Rao (1981) similarly found that the most intense 6 cm sources in other active regions are associated with filamentary structures and magnetic neutral lines, and that they are not located directly over sunspots. This was attributed to the existence of cool material above the sunspot umbrae. In fact, Foukal (1975, 1976, 1978) has argued several times that the cool "plumes" observed at EUV wavelengths indicate that the coolness of sunspots persists up into the corona. Furthermore, Alissandrakis and Kundu (1982) have reported the detection of a temperature depression at 6 cm wavelength above one sunspot umbra.

High resolution synthesis maps at 6 cm wavelength have therefore revealed a rich diversity of coronal structures which have a variety of optical wavelength counterparts. The 6 cm coronal emission indicates that both temperature enhancements and temperature depressions might occur above sunspot umbrae. Because these single wavelength observations refer to a bewildering complexity of optical wavelength counterparts,

morphological types, and magnetic field configurations, no clear-cut generalizations are possible. We felt that a more fruitful approach from the physical point of view would result from multiple wavelength observations which refer to different levels within the solar atmosphere above active regions. In § II we present VLA synthesis maps at 2 cm, 6 cm, and 20 cm wavelength and compare them with off-band H α photographs. In § III the 20 cm emission is interpreted in terms of the bremsstrahlung of coronal electrons trapped within magnetic loops; the 6 cm emission is interpreted in terms of the gyroresonant emission of thermal electrons spiraling in the legs of magnetic loops, and the 2 cm emission is interpreted in terms of either gyroresonant emission in the low solar corona or bremsstrahlung in the transition region.

II. OBSERVATIONAL RESULTS

We have used the Very Large Array¹ (VLA) to observe the solar active region AR 2505 on 1980 June 12 and the active region AR 2646 on 1980 September 3 and 4. The position of AR 2505 on the solar surface was 14°S and 40°W at 1300 UT on June 12. The position of AR 2646 on the Sun's surface was 11°N and 9.5°W at 1300 UT on September 3 and 11°N and 22°W at 1300 UT on September 4. The incoming signal was sampled at two different wavelengths for alternate 15 minute periods throughout the 11 hours of observation each day. The wavelengths, λ , were $\lambda = 2.0$ cm and 6.2 cm (or 15.016.0 MHz and 4866.3 MHz) on June 12 and September 3, and $\lambda = 6.2$ cm and 20.75 cm (or 1446.1 MHz and 4866.3 MHz) on September 4. In every case the bandwidth was 12.5 MHz. The individual antennae have a diameter of 25 m which provided beamwidths of 3:0, 9:3, and 31:1 at $\lambda = 2$ cm, 6 cm, and 20 cm. On June 12 eleven antennae were used with distances from the array center ranging from 0.04 to 10.5 km and minimum and maximum spacings between interferometer pairs of 0.05 and 11.5 km. On September 3 and 4, 22 antennae were used with distances from the array center ranging from 0.05 to 2.0 km and minimum and maximum spacings between interferometer pairs of 0.11 and 3.4 km. The average correlated flux of 55 and 242 interferometer pairs was respectively sampled on June 12 and September 3 and 4. Both the left-hand circularly polarized (LCP) signal and the right-hand circularly polarized (RCP) signal were sampled every 10 s. These data were then calibrated, edited, and time averaged over 60 s to make synthesis maps of the total intensity $I = (LCP + RCP)/2$ and Stokes parameter $V = (LCP - RCP)/2$.

On June 12 the data were calibrated by observing NRAO 150 for 5 minutes every 30 minutes, and by assuming that the flux density of this calibration was 10.5 and 10.2 Jy at $\lambda = 2$ and 6 cm, respectively. On September 3 and 4 the data were calibrated by observing PKS 0923+392 for 5 minutes every 30 minutes, and by assuming that the flux density of this calibrator was 7.65, 7.36, and 8.53 Jy at $\lambda = 2$ cm, 6 cm, and 20 cm

¹ The Very Large Array is operated by Associated Universities Inc., under contract with the National Science Foundation.

respectively. The amplitude and phase of the correlated flux were calibrated according to the procedure described by Lang and Willson (1979) together with a correction for the differences in the signal from high temperature noise sources detected in each polarization channel. At each wavelength the calibrated amplitude and phase for each polarization and every antenna pair were then taken to be the amplitude and phase of the source visibility function. The source intensity distribution was then obtained by Fourier transforming the calibrated data and using the "CLEAN" procedure developed by Clark (1980). On June 12, roughly 32,000 $u-v$ components were used to obtain maps whose synthesized beams have half-power widths of $2''.4 \times 3''.4$ (tilted at a position angle of 31°) at $\lambda = 2$ cm and $1''.5 \times 2''.2$ (tilted at 26°) at $\lambda = 6$ cm. On September 3 and 4 roughly 54,000 $u-v$ components were used to obtain maps whose synthesized beams were not elongated, and which had half-power widths of $2''.3$, $4''.1$, and $11''.4$ at $\lambda = 2$ cm, 6 cm, and 20 cm, respectively.

The synthesis maps of the total intensity, I , of the radiation from AR 2505 are shown in Figure 1. Here the contours mark levels of equal brightness temperature corresponding to 0.2, 0.4, 0.6, and 0.8 times the maximum brightness temperatures of 5.1×10^4 K and 1.5×10^6 K at $\lambda = 2$ cm and 6 cm, respectively. The enhanced 6 cm emission is associated with a group of three sunspots whose total angular extent is the same as that of the 2 cm

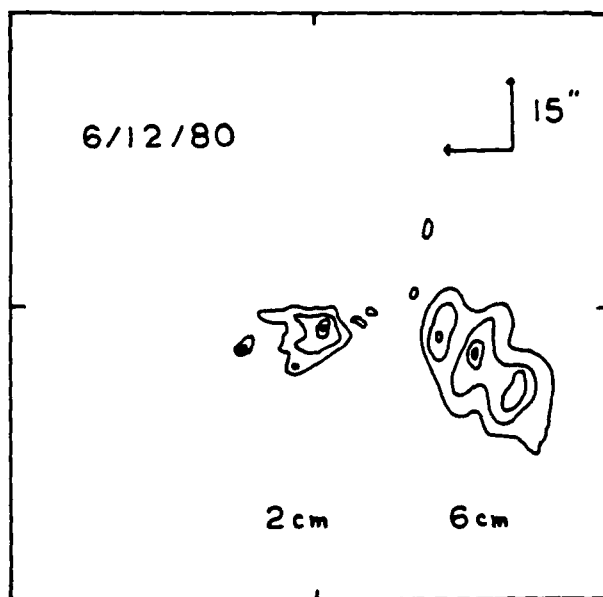


FIG. 1.—Synthesis maps of the total intensity I of the radiation from active region AR 2505 taken simultaneously with the Very Large Array (VLA) at 2 cm (left) and 6 cm (right) wavelengths on 1980 June 12. The position of AR 2505 was near the west limb at about 14° S and 40° W. Here north is up, west is to the right, and both maps have the same phase center and the same angular scale denoted by the $15''$ arrows. Notice that the centroid of the 6 cm emission is displaced with respect to the centroid of the 2 cm emission by $40'' \pm 5''$ to the southwest. This is interpreted as a projection effect caused by the greater height of the 6 cm emission which lies at a height of $(3.5 \pm 0.5) \times 10^9$ cm above the 2 cm emission.

emission. We attribute the broader extent of the 6 cm emission to the diverging magnetic fields of a dipolar loop which has one footprint in the group of sunspots, and a higher lying leg marked by the 6 cm emission. The centroid of the 6 cm emission is displaced with respect to the centroid of the 2 cm emission by $40'' \pm 5''$ to the southwest. This is interpreted as a radial, limbward displacement caused by the greater height of the 6 cm emission. Both the westward component of the displacement ($35'' \pm 5''$) and the southward component ($12'' \pm 5''$) indicate a height $h = (3.5 \pm 0.5) \times 10^9$ cm for the 6 cm emission above the chromosphere. Because this is comparable to the height of the plage-associated component of 6 cm emission in another active region (Felli, Lang, and Willson 1981), our observations provide no evidence for a difference in the thickness of the transition zone above sunspots and plage.

When allowance is made for the projection effect caused by a greater height, both the 2 cm and 6 cm emission lie above the group of sunspots. The low brightness temperatures $T_b \approx 10^4$ K and the low degree of circular polarization $p_c < 15\%$ of the 2 cm emission may be explained in terms of thermal bremsstrahlung in the transition region or low solar corona. The high brightness temperatures $T_b \approx 10^6$ K and the high degree of circular polarization $p_c \approx 60\%$ of the 6 cm emission are most easily explained as optically thin gyroresonance emission in the low solar corona. The strong radial magnetic fields of the sunspot umbrae allow the detection of the third harmonic of the gyrofrequency at higher, hotter levels in the solar atmosphere. Our 6 cm observations indicate longitudinal magnetic field strengths of $H_l \approx 600$ gauss (third harmonic at $\lambda = 6$ cm) at heights $h \approx 3.5 \times 10^9$ cm. This suggests that the radial magnetic field has decreased by a factor of 3 or 4 over an altitude which is comparable to the horizontal scale in the sunspots. Because the observations indicate relatively strong magnetic fields at relatively high altitudes where the temperatures reach 10^6 K, they cannot be explained by a relatively thin transition zone in which high temperatures occur close to sunspots where the magnetic fields are stronger (cf. Bromboz et al. 1981).

Synthesis maps of the total intensity, I , of the 6 cm and 20 cm radiation of AR 2646 are shown in Figure 2. Here the contours mark levels of equal brightness temperature corresponding to 0.2, 0.4, 0.6, 0.8, and 1.0 times the maximum brightness temperatures of 2.9×10^6 K and 9.4×10^5 K at $\lambda = 6$ cm and 20 cm, respectively. The two 6 cm sources lie above two sunspot groups of opposite magnetic polarity (see Fig. 3). The regions of enhanced 6 cm emission have high brightness temperatures of $T_b = (1-3) \times 10^6$ K and high degrees of circular polarization $p_c = 55\%-70\%$ which are most easily explained by gyroresonance emission in the low solar corona. The 6 cm emission marks the legs of a magnetic dipole where the longitudinal magnetic field strength $H_l \approx 600$ gauss and the temperatures reach millions of degrees. The two 6 cm sources mark the higher lying part of the dipole which joins the two sunspot groups. The unpolarized 20 cm emission ($p_c < 12\%$) is

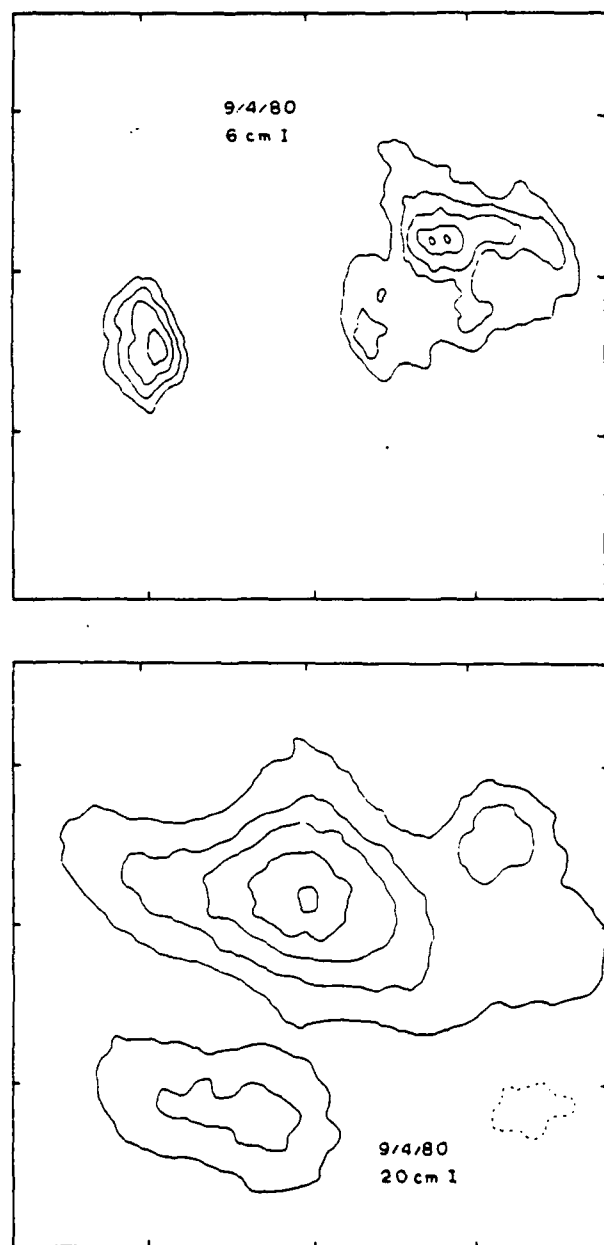


FIG. 2.—Synthesis maps of the total intensity I of the radiation from active region AR 2646 taken simultaneously with the Very Large Array (VLA) at 6 cm (top) and 20 cm (bottom) wavelengths on 1980 September 4. Here, north is up, west is to the right, and both maps have identical fields of view and the same angular scale denoted by the 60° spacing between the fiducial marks on the axes. The two 6 cm sources have brightness temperatures of $T_b \approx 10^6$ K and lie above two sunspot groups of opposite magnetic polarity (see Fig. 3). The larger 20 cm source is interpreted in terms of the optically thin bremsstrahlung of a coronal loop which joins the two sunspot groups. Notice that the peak brightness temperature at 20 cm is located near the central apex or top of the loop and that it has a value of 9.4×10^5 K.

attributed to optically thin bremsstrahlung near the apex of the coronal loop where the magnetic fields are mainly transverse to the line of sight. As discussed in greater detail later, we believe that the 20 cm emission is the radio wavelength counterpart of the ubiquitous coronal loops detected at X-ray wavelengths.

In Figure 3 the 6 cm emission of AR 2646 on September 4 is superposed on an off-band $H\alpha$ photograph ($H\alpha + 1.4 \text{ \AA}$) taken on the same day.² The uncertainty in this superposition is no greater than $10''$. The two main groups of sunspots have opposite magnetic polarity, and the circular polarization of the 6 cm emission corresponds to the extraordinary mode of wave propagation in magnetic fields with the same polarity as the underlying sunspots. The two components of the 6 cm emission are displaced inward and away from the sunspots as would be expected if they mark the higher lying legs of the magnetic dipole which joins the two sunspot groups. To a first approximation, we may assume that these groups of sunspots mark the feet of a loop of circular form whose radius $r \approx 70'' \approx 5.0 \times 10^9$ cm, where $1'' \approx 725$ km on the solar surface. We may then infer the heights of the 6 cm components from their inward displacements of $x \approx 25'' \pm 5'' \approx 1.8 \pm 0.4 \times 10^9$ cm. We obtain $h = r \sin \{ \cos^{-1} [(x - r)/r] \} = 3.8 \pm 0.4 \times 10^9$ cm above the solar photosphere. This provides additional evidence that magnetic fields of $H_i \approx 600$ gauss exist at heights of $h \approx 3.5 \times 10^9$ cm above sunspots where the temperatures $T \approx 10^6$ K.

The inward displacement of the two main components of 6 cm emission with respect to the underlying sunspots is also shown in Figure 4 which compares the 6 cm map of AR 2646 on September 3 with an off-band $H\alpha$ photograph ($H\alpha - 1.0 \text{ \AA}$) taken on the same day. The positional uncertainty in this comparison is no greater than $10''$. Here the contours mark levels of equal brightness temperature corresponding to 0.2, 0.4, ..., 1.0 times the maximum brightness temperature of 2.2×10^6 K. The two peaks found in the largest component of the 6 cm emission probably mark the higher lying parts of the outwardly diverging magnetic flux tubes which join the two umbrae that are separated by a light bridge. A comparison with Figure 3 indicates that changes in the sunspot configuration produced low level changes in the 6 cm emission; but that the more intense dipolar features remain relatively stable during the 2 days.

The synthesis maps of the total intensity, I , and the Stokes parameter, V , of the dominant component of AR 2646 are shown in Figure 5. The contours of the I maps at 6 cm (map A) and 2 cm (map B) mark levels of equal brightness temperature corresponding to 0.2, 0.4, ..., 1.0 times the maximum brightness temperatures of 2.2×10^6 K and 1.6×10^5 K, respectively. The contours of the V maps at 6 cm (map C) and 2 cm (map D) mark levels of equal brightness temperature corresponding to 0.4, 0.6, ..., 1.0 times the maximum brightness temperatures of 1.4×10^6 K and 1.3×10^5 K.

² Offband $H\alpha$ taken at Ottawa River Solar Observatory which is operated by the National Research Council, Canada.



FIG. 3.—A VLA synthesis map of the total intensity of the 6 cm radiation from active region AR 2646 on 1980 September 4 (see Fig. 2) is superposed upon an off-band H α photograph of the same active region taken at the Ottawa River Solar Observatory at 1837 UT on the same day. The largest component of 6 cm emission has an angular extent of about $60''$; but refer to Fig. 2 for exact angular scale. The position of AR 2646 was near the Sun center at about 11°N and 20°W . Notice that the two components of 6 cm emission are displaced inward and away from the sunspots as would be expected if they originate at higher levels in the magnetic loops which join the two sunspot groups. The 6 cm emission appears to be associated with both the sunspot umbrae and penumbrae.

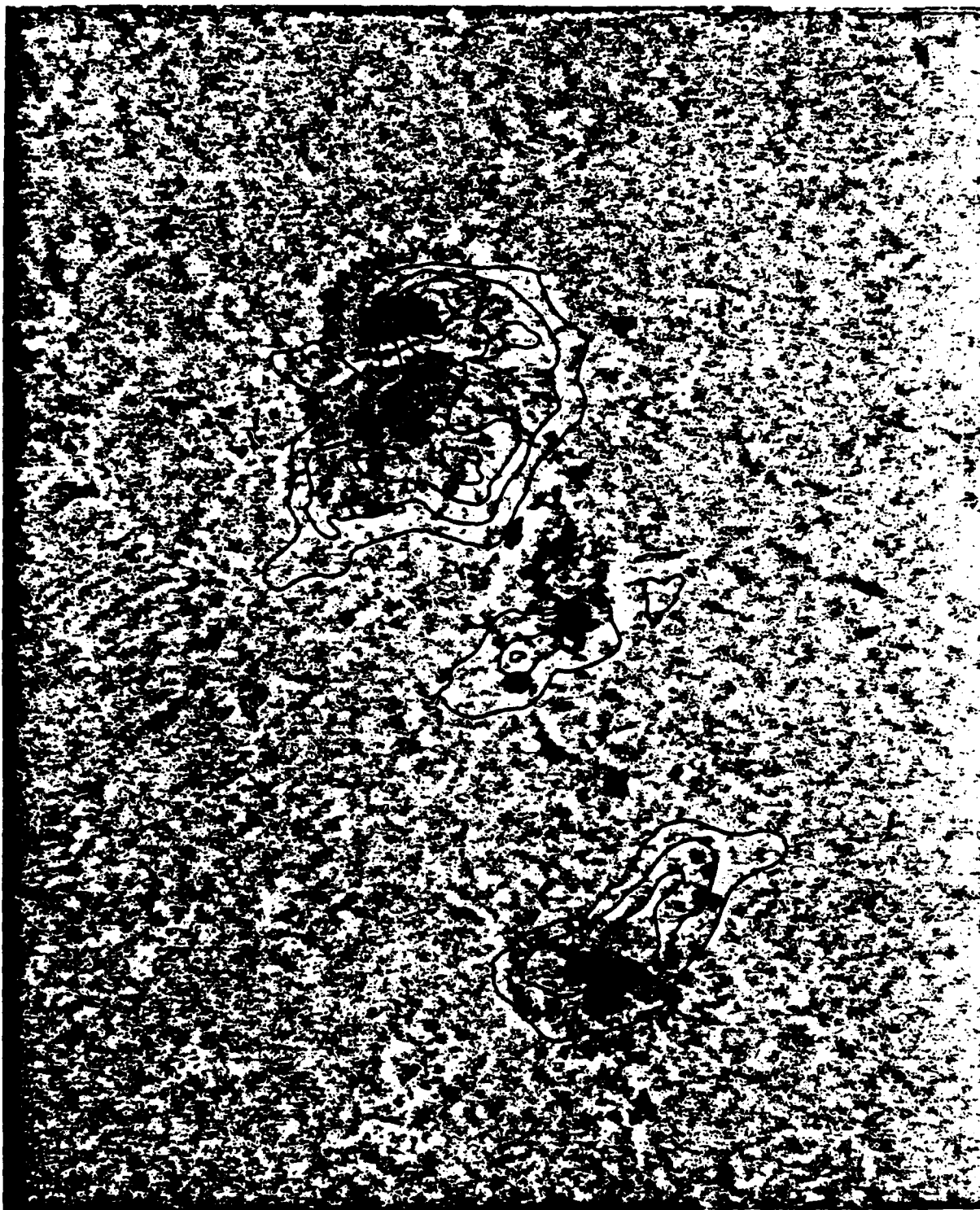


FIG. 4.—A VLA synthesis map of the total intensity of the 6 cm radiation from active region AR 2646 on 1980 September 3 is superposed upon an off-band H α photograph of the same active region taken at the Ottawa River Solar Observatory at 1538 UT on the same day. The field of view and angular scale are the same as those in Fig. 3. The position of AR 2646 on this day was also near the Sun center at about 11°N and 10°W. A comparison with Fig. 3 indicates that changes in the 6 cm emission are associated with changes in the sunspot configuration but that the outermost components of 6 cm emission remain displaced inward and away from the two main sunspot groups.

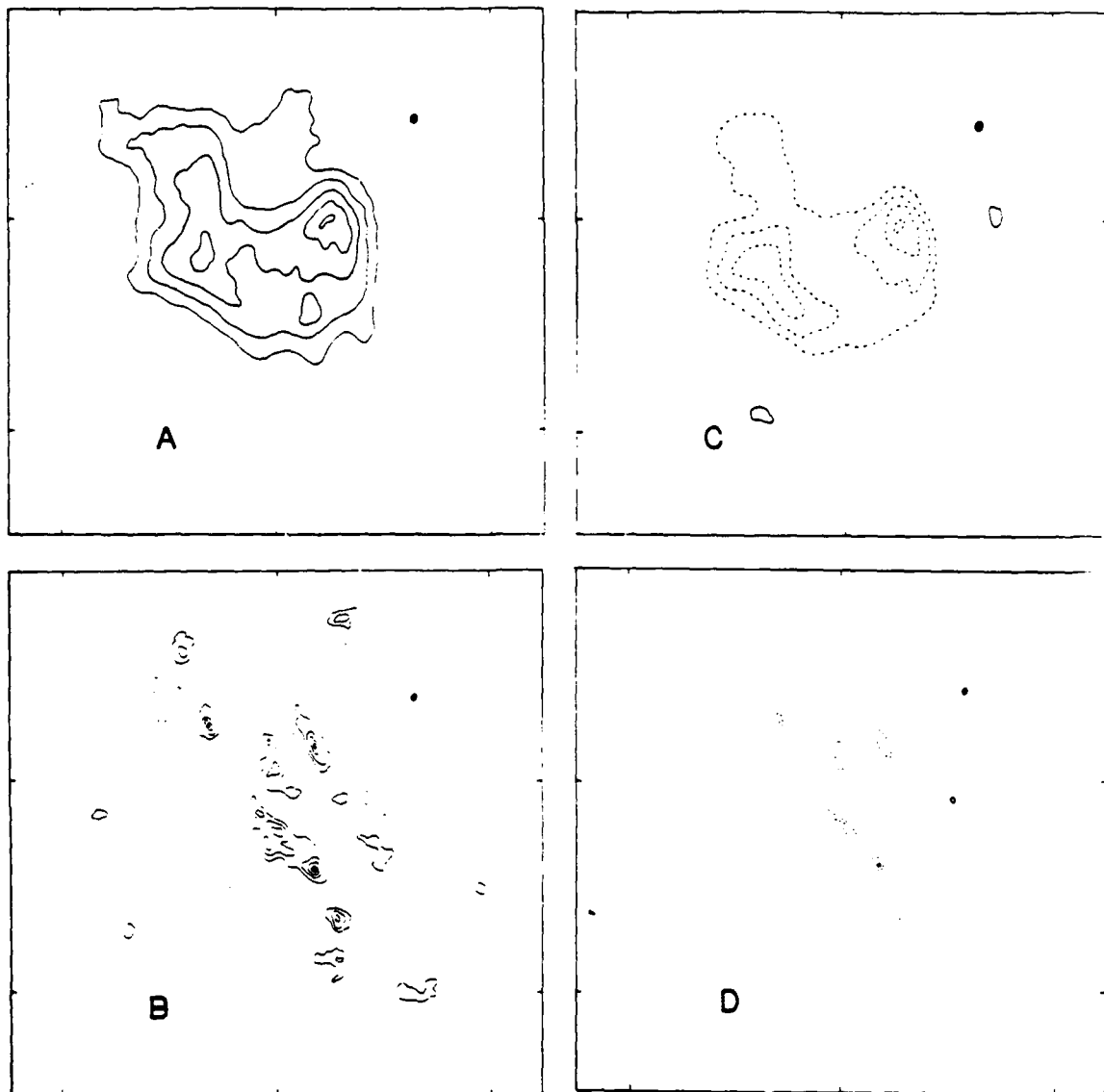


FIG. 5.—VLA synthesis maps of total intensity I at 6 cm (map A) and 2 cm (map B), and the Stokes parameter V at 6 cm (map C) and 2 cm (map D). All of the data refer to the dominant western component of the 6 cm emission from AR 2646, and they were all taken during the same 11 hr period on 1980 September 3. Here, north is up, west is to the right, the black dot denotes the size of the synthesis beam, and all of the maps have the same field of view with angular scales denoted by the $60''$ spacing between the fiducial marks on the axes. Notice that both the 2 cm and 6 cm emission are highly circularly polarized (67% – 86%); but that the emission at 2 cm wavelength is broken up into tiny hot spots with brightness temperatures $T_b \approx 10^3$ K, angular sizes $\phi \approx 5''$, and no special relationship with the sunspot umbrae.

respectively. The dashed contours of the V map refer to regions of negative, right-hand circular polarization and positive (north or white) magnetic polarity. The sense of the circular polarization at both 2 cm and 6 cm wavelengths corresponds to the extraordinary mode of wave propagation in a magnetic field which has the same polarity as the magnetic field in the underlying photosphere. The degrees of circular polarization at 2 cm and 6 cm are similar, with $\rho_c \approx 87\%$ and $\rho_c \approx 67\%$, respectively. The spatial configurations of the 2 cm and 6 cm emissions are, however, different. The peaks of the

6 cm emission have angular sizes of $\phi \approx 20''$ and appear to be the coronal counterparts of the two sunspot umbrae, while the two most intense 2 cm sources have angular sizes of $\phi \approx 5''$, and the 2 cm hot spots do not seem to have any special relation with the sunspots. One of these 2 cm hot spots did, however, coincide, within the uncertainty of the alignment ($10''$), with the light bridge which separates the two westernmost sunspots. Curiously enough, H α flares were emitted from the light bridge on September 3, even though the magnetic field has the same polarity on each side of the bridge.

III. DISCUSSION

a) Coronal Loops at 20 cm Wavelength

We have observed a looplike structure at 20 cm wavelength which extends across two groups of sunspots of opposite magnetic polarity, and which is most intense in the central regions between them. The 20 cm radiation is interpreted in terms of the bremsstrahlung of thermal electrons which are trapped within a single wide loop or an arcade of loops which join the two regions of opposite magnetic polarity. The fact that the 20 cm emission connects two regions whose brightness temperatures exceed 10^6 K at 6 cm wavelength suggests that the electron temperature of the higher lying 20 cm loop has coronal values of $T_e = 2 \times 10^6$ K. We can use this value together with the average brightness temperature $T_B \approx 4.7 \times 10^5$ K of the 20 cm loop to infer an optical depth $\tau = -\ln[1 - (T_B/T_e)] = 0.3$. With these values of optical depth and electron temperature, the bremsstrahlung formulae give an emission measure of (Lang 1974b, 1980)

$$\int N_e^2 dl = 102.2 \frac{v^2 \tau T_e^{3/2}}{\ln[4.7 \times 10^{10} T_e/v]} \approx 10^{28} \text{ cm}^{-5}, \quad (1)$$

where our observing frequency $\nu = 1.446 \times 10^9$ Hz for the wavelength $\lambda = 20.75$ cm. This emission measure is comparable to those inferred from X-ray measurements of coronal loops (Vaiana and Rosner 1978). The semi-length of the 20 cm emission has the value of $L \approx 5 \times 10^9$ cm, which is also comparable to the X-ray coronal loops (L is half the total extent of the loop measured along the magnetic field). The electron density is $N_e \approx [\int N_e^2 dl/L]^{1/2} \approx 1.5 \times 10^9 \text{ cm}^{-3}$, and the loop pressure $p = 2kT_e N_e = 0.83 \text{ dyn cm}^{-2}$ (where Boltzmann's constant $k = 1.38 \times 10^{-16} \text{ ergs K}^{-1}$). The values for the N_e and p of the 20 cm loop are also comparable to those of the X-ray coronal loops (Rosner, Tucker, and Vaiana 1978), and the 20 cm loop parameters satisfy the scaling relationship $T_e(\text{max}) \approx 1.4 \times 10^3 (pL)^{1/3}$ for X-ray loops. The 20 cm emission may therefore be interpreted as the optically thin bremsstrahlung of a hot, dense plasma trapped within an arcade of coronal loops whose physical parameters are similar to those detected at X-ray wavelengths. The fact that the 20 cm emission exhibits no detectable circular polarization may be attributed to the fact that the bremsstrahlung comes mainly from the central regions of the coronal loop where the magnetic fields are mainly transverse to the line of sight. There has incidentally been one previous report of the detection of a low lying coronal loop at 6 cm wavelength (Velusamy and Kundu 1980; Kundu and Velusamy 1980); but these observations were confused by the gyroresonance emission of the sunspots which becomes negligible at the longer 20 cm wavelength.

When the observations given in this paper are combined with our more recent Very Large Array (VLA) observations of hot ($\approx 10^6$ K) coronal loops at 20 cm wavelengths (Lang, Willson, and Rayrole 1982), we may conclude that we have discovered the radio wavelength counterpart of the coronal loops detected at X-ray wave-

lengths. It is the ubiquitous coronal loops which appear to be the dominant structural element in the low solar corona and which seem to outline the three-dimensional configuration of the coronal magnetic field. Future VLA observations at 20 cm wavelength may specify the temperature and density structure of coronal loops with an angular resolution of a few seconds of arc. The evolution of coronal loops can be investigated by taking VLA synthesis maps at intervals of 1 hour or less, and this may lead to the detection of temperature enhancements which are expected during preflare activity (Syrovatskii and Kuznetsov 1980). Our discovery therefore opens up the possibility of using 20 cm synthesis maps to investigate the detailed structure, evolution, and preflare activity of coronal loops. Synthesis maps of several hours' duration may be used to study the relatively stable loops detected at X-ray wavelengths, while maps of shorter duration may be used to study the short-lived, cooler loops.

b) Legs of Dipolar Loops at 6 cm Wavelength

We have detected intense 6 cm emission which marks the legs of a dipolar loop whose two footprints are delineated by lower lying sunspots of opposite magnetic polarity. In contrast to the reports of Alissandrakis and Kundu (1981) and Kundu, Schmahl, and Rao (1981), we do not observe a temperature depression in the 6 cm emission above sunspot umbrae. The brightness temperatures above the umbrae are instead enhanced with values of $T_B \approx 10^6$ K. This is in agreement with the observations of Lang and Willson (1979, 1980) and Alissandrakis, Kundu, and Lantos (1980). The high brightness temperatures, and the high degrees of circular polarization of $\rho_c = 55\% - 70\%$ indicate that the 6 cm radiation is due to gyroresonant emission in the solar atmosphere overlying sunspots (cf. § 1 and references therein). The quasi-longitudinal expression for the optical depth due to gyroresonant absorption is given by (Zlotnik 1968a; Zheleznyakov 1970; Lang 1974a)

$$\tau_2 = 2.985 \times 10^{-22} \lambda N_e T_e L_H \sin^2 \theta (1 \pm \cos \theta)^2$$

for $n = 2$

$$\tau_3 = 3.829 \times 10^{-31} \lambda N_e T_e^2 L_H \sin^4 \theta (1 \pm \cos \theta)^2$$

for $n = 3$

and

$$\tau_4 = 7.224 \times 10^{-40} \lambda N_e T_e^3 L_H \sin^6 \theta (1 \pm \cos \theta)^2$$

for $n = 4$, (2)

where the frequency of the radiation is given by $\nu = 2.8 \times 10^6 n H_i$ for the n th harmonic in a longitudinal magnetic field of strength H_i , the wavelength is λ , the electron density and electron temperature are N_e and T_e , respectively, the scale height for the variation of the magnetic field is L_H , the angle between the line of sight and the magnetic field is θ , and the + and - signs refer, respectively, to the extraordinary and ordinary modes of wave propagation. The 20 cm observation discussed

in § IIIa indicates that the coronal loop which connects the 6 cm sources has $N_e \approx 10^9 \text{ cm}^{-3}$, $T_e \approx 10^6 \text{ K}$, and $L_H \approx 10^9 \text{ cm}$. Using these parameters in equations (2) together with $\lambda = 6 \text{ cm}$, we see that the second harmonic ($n = 2$) is optically thick everywhere, and that the fourth harmonic ($n = 4$) is an ineffective opacity agent. The 10^6 K brightness temperatures require enough opacity to rule out the fourth harmonic, while the circular polarization, which requires an optically thin condition, is most easily accounted for by the third harmonic emission which becomes optically thin at levels where $T_e \approx 10^6 \text{ K}$. Furthermore, the second harmonic must not provide equally bright ordinary mode radiation, either because the field strength is inadequate, or the second harmonic level is below the corona where $T_e \ll 10^6 \text{ K}$. We therefore conclude that the 6 cm radiation is due to gyroresonant emission at the third harmonic ($n = 3$) which corresponds to a longitudinal magnetic field strength of $H_l = 600 \text{ gauss}$.

Our observations also show no evidence for a cool region in the coronal atmosphere above sunspot umbrae. At first sight this would seem to contradict Foukal's (1975, 1976, 1978) argument that the cool "plumes" detected at EUV wavelengths project upward into the solar corona to form cool loops. Static cool loops are unstable, however, and the spiky cool structure observed above sunspot umbrae has short lifetimes of tens of minutes (Sheeley 1980). Furthermore the cool "plumes" fill only a fraction of the umbrae area and change considerably with time (Pallavicini, Sakurai, and Vaiana 1981). The cool loops actually coexist with hot loops which have lifetimes as long as days. Because our 6 cm synthesis maps refer to observations averaged over a 12 hr period, we would only expect to detect the more stable, long-lived hot loops. In fact, we are somewhat skeptical of reports of the detection of cool material above sunspot umbrae in 6 cm synthesis maps (Alissandrakis and Kundu 1982; Kundu, Schmahl, and Rao 1981) for they imply unexpectedly long lifetimes for the cool material. The cool loops might be more effectively detected in "snapshot" maps using 6 cm observations lasting an hour or less.

c) Hot Spots at 2 cm Wavelength

The 2 cm emission from AR 2505 has low brightness temperatures characteristic of the transition region (10^4 – 10^5 K), while the 6 cm emission has high brightness temperatures characteristic of the corona [$(1$ – $3) \times 10^6 \text{ K}$]. Furthermore, the 2 cm emission from AR 2505 is, within the uncertainties of measurement, spatially coincident with the underlying sunspots, and it has no detectable circular polarization. The 6 cm emission, on the other hand, was displaced from the sunspots and

had a high degree of circular polarization ($\rho_c \approx 60\%$). These differences suggest that we are dealing with two different emission mechanisms in this case. The 2 cm radiation may be attributed to bremsstrahlung of thermal electrons in the transition region, while the 6 cm radiation is attributed to gyroresonant emission in the corona. Nevertheless, the overall bright 2 cm region in Figure 1 was observed with relatively poor $u-v$ coverage, and it could be composed of several highly polarized bright spots of the type which were detected in AR 2646 (Fig. 5) when the array configuration permitted the sampling of many more $u-v$ components.

The unexpectedly high degrees of circular polarization ($\rho_c \approx 87\%$) of the 2 cm hot spots observed in AR 2646 suggest gyroresonant emission. The observed polarization could be explained by gyroresonant emission in the low solar corona with longitudinal magnetic field strengths $H_l \approx 1800 \text{ gauss}$ ($n = 3$) provided that the electron density is high ($N_e \approx 10^{10} \text{ cm}^{-3}$). As pointed out by George Dulk (1982, private communication), the appropriate scale length, L_H , for gyroresonance emission in the transition region is a factor of 10^2 or 10^3 smaller than it is in the corona, and for this reason transition region emission is much less plausible. Nevertheless, comparable polarization may occur under imaginable conditions in both the low solar corona ($T_e \approx 5 \times 10^5 \text{ K}$, $N_e \approx 10^{10} \text{ cm}^{-3}$, $L_H \approx 10^9 \text{ cm}$, $H_l = 1800 \text{ gauss}$, $n = 3$) and the transition region ($T_e \approx 10^5 \text{ K}$, $N_e \approx 10^{11} \text{ cm}^{-3}$, $L_H \approx 10^6 \text{ cm}$, $H_l \approx 2700 \text{ gauss}$, $n = 2$). The fact that the 2 cm hot spots are not found everywhere over the sunspots additionally argues against transition region emission, however, for one would expect strong magnetic fields everywhere over the umbrae. An alternative possibility is that the hot spots are transient brightenings similar to those which are often seen at H α wavelengths. In fact, one of the hot spots did coincide with a light bridge in which H α flares were emitted during the observation period. It is also possible that the 2 cm hot spots mark the legs of warm ($\approx 10^5 \text{ K}$) loops.

We are especially indebted to Dave Rust who so effectively coordinated these observations as part of the program of international observations during the Solar Maximum Year (SMY). In carrying out this work, the authors have derived considerable benefit from their participation in the SMY workshops held at the Crimean Astrophysical Observatory in 1981 March and at Annecy, France in 1981 October. We have also benefited from the useful suggestions of our referee, Professor George A. Dulk.

Radio interferometric studies at Tufts University are supported under grant AFOSR-83-0019 with the Air Force Office of Scientific Research.

REFERENCES

- Alissandrakis, C. E., and Kundu, M. R. 1982, *Ap. J. (Letters)*, **253**, L49.
 Alissandrakis, C. E., Kundu, M. R., and Lantos, P. 1980, *Astr. Ap.*, **82**, 30.
 Brzobozek, G., et al. 1981, Report to Crimean Solar Maximum Year Workshop (A. Krüger, private communication).
 Clark, B. G. 1980, *Astr. Ap.*, **89**, 377.
 Felli, M., Lang, K. R., and Willson, R. F. 1981, *Ap. J.*, **247**, 325.
 Foukal, P. V. 1975, *Solar Phys.*, **43**, 327.
 ———. 1976, *Ap. J.*, **210**, 575.
 ———. 1978, *Ap. J.*, **223**, 1046.

- Gel'freikh, G. B., and Lubyshev, B. I. 1979, *Soviet Astr.-AJ*, **23**, 316.
 Kakinuma, T., and Swarup, G. 1962, *Ap. J.*, **136**, 975.
 Kundu, M. R. 1959, *Ann. d'Ap.*, **22**, 1.
 Kundu, M. R., Alissandrakis, C. E., Bregman, J. D., and Hin, A. C. 1977, *Ap. J.*, **213**, 278.
 Kundu, M. R., Schmahl, E. J., and Rao, A. P. 1981, *Astr. Ap.*, **94**, 72.
 Kundu, M. R., and Velusamy, T. 1980, *Ap. J. (Letters)*, **240**, L63.
 Lang, K. R. 1974a, *Solar Phys.*, **36**, 351.
 ———. 1974b, *Astrophysical Formulae* (New York: Springer-Verlag).
 ———. 1980, *Astrophysical Formulae* (2d ed.; New York: Springer-Verlag).
 Lang, K. R., and Willson, R. F. 1979, *Nature*, **278**, 24.
 ———. 1980, in *IAU Symposium 86, Radio Physics of the Sun*, ed. M. R. Kundu and T. E. Gergely (Dordrecht: Reidel), p. 109.
 ———. 1982, *Ap. J. (Letters)*, **255**, L111.
 Lang, K. R., Willson, R. F., and Rayrole, J. 1982, *Ap. J.*, **258**, 384.
 Lantos, P. 1968, *Ann. d'Ap.*, **31**, 105.
 Pallavicini, R., Sakurai, T., and Vaiana, G. S. 1981, *Astr. Ap.*, **98**, 316.
 Sheeley, N. R. 1980, *Solar Phys.*, **60**, 79.
 Rosner, R., Tucker, W. H., and Vaiana, G. S. 1978, *Ap. J.*, **220**, 643.
 Syrovatskij, S. I., and Kuznetsov, V. D. 1980, in *IAU Symposium 86, Radio Physics of the Sun*, ed. M. R. Kundu and T. Gergely (Dordrecht: Reidel), p. 445.
 Vaiana, G. S., and Rosner, R. 1978, *Ann. Rev. Astr. Ap.*, **16**, 393.
 Velusamy, T., and Kundu, M. R. 1980, in *IAU Symposium 86, Radio Physics of the Sun*, ed. M. R. Kundu and T. Gergely (Dordrecht: Reidel), p. 105.
 Zheleznyakov, V. V. 1962, *Soviet Astr.-AJ*, **6**, 3.
 ———. 1970, *Radio Emission of the Sun and Planets* (New York: Pergamon).
 Zlotnik, E. Ya. 1968a, *Soviet Astr.-AJ*, **12**, 245.
 ———. 1968b, *Soviet Astr.-AJ*, **12**, 464.

VICTOR GAIZAUSKAS: Herzberg Institute of Astrophysics, National Research Council of Canada, Ottawa, ON, K1A 0R6, Canada

KENNETH R. LANG and ROBERT F. WILLSON: Department of Physics, Tufts University, Medford, MA 02155

3. HIGH-RESOLUTION OBSERVATIONS OF SOLAR RADIO BURSTS AT 2, 6, AND 20 cm WAVELENGTH

ROBERT F. WILLSON

Department of Physics, Tufts University, Medford, MA 02155, U.S.A.

(Received 25 May; in revised form 7 September, 1982)

Abstract. The Very Large Array and the Westerbork Synthesis Radio Telescope have been used to observe eight solar bursts at 2, 6, or 20 cm wavelength with second-of-arc angular resolution. The regions of burst energy were all resolved with angular sizes between $5''$ and $30''$, brightness temperatures between 2×10^7 K and 2×10^8 K, and degrees of circular polarization between 10 and 90%. A series of 10 s snapshot maps are presented for the more intense bursts, and superimposed on photospheric magnetograms or H α photographs. The impulsive phase of the radio bursts is located near the magnetic neutral line of the active regions, and between the flaring H α kernels which mark the footpoints of magnetic loops. The impulsive phase of one 6 cm burst was smaller and spatially separated from both the preburst radio emission and the gradual decay phase of the burst. Another 6 cm burst exhibited preburst heating of the coronal loop in which the burst occurred. The plasma was probably heated at a lower level in the loop, while the burst energy was released several minutes later at a higher level. A multiple-spike 20 cm burst exhibited polarity inversions with degrees of circular polarization of 90%. The rapid changes in circular polarization are attributed to either a magnetically complex region or the emergence of new magnetic flux at coronal heights where magnetic field strengths $H \approx 300$ to 400 G.

1. Introduction

Solar radio bursts can now be studied with second-of-arc resolution by using the Very Large Array (VLA) and the Westerbork Synthesis Radio Telescope (WSRT). In addition to providing new information on the sizes, locations and brightness temperatures of the radio bursts, the radio synthesis maps can be compared with optical wavelength data at comparable time intervals and angular resolutions. Furthermore, the VLA and the WSRT are capable of measuring the radio polarization with high angular and time resolution, thereby providing information about the evolution of the magnetic fields in the bursting regions. All of this information is, of course, vital to our understanding of the origin, development and prediction of solar bursts.

Previous VLA observations of solar bursts indicate that 6 cm bursts often occur above magnetic neutral lines located between sunspots (Alissandrakis and Kundu, 1978; Lang *et al.*, 1978; Lang *et al.*, 1981); and that both the 2 cm and 6 cm emission are frequently located in the central regions of magnetic arches located between flaring H α kernels (Marsh *et al.*, 1979; Marsh and Hurford, 1980). These results imply that the energy release at radio wavelengths occurs near the apex of the magnetic loops. More recent VLA observations indicate that in some cases the 6 cm emission is most intense at the footpoints of magnetic loops (Kundu *et al.*, 1982). This is consistent with the WSRT observations of complex 6 cm bursts occurring in the widely separated footpoints of coronal loops (Kattenberg, 1981). The observations presented in this paper indicate that the solar radio bursts at 6 cm and 20 cm wavelength are usually located at the apex of magnetic loops rather than at their footpoints.

Solar Physics 83 (1983) 285–303. 0038–0938/83/0832–0285\$02.85.

Copyright © 1983 by D. Reidel Publishing Co., Dordrecht, Holland, and Boston, U.S.A.

Radio interferometric observations can also provide valuable information about the changing magnetic topology before and during the radio bursts. Of special interest are the burst precursors observed in the form of increased intensity and polarization before burst emission. Lang (1974, 1979) has, for example, called attention to dramatic changes in circular polarization which occur on time scales of about one hour before the emission of solar bursts. More recent VLA polarization maps at 6 cm wavelength (Kundu *et al.*, 1982) indicate that the structure of the polarized emission and hence the magnetic field topology, undergoes changes prior to and during radio bursts. These observations are related to models which involve changing magnetic field configurations to explain the release and source of flare energy (Gold and Hoyle, 1960; Heyvaerts *et al.*, 1977; Rust, 1972, 1976). Recent VLA observations at 6 cm wavelength (Kundu *et al.*, 1982) indicate that the locations of different peaks of multiple bursts are the same to within $\pm 2''$, although the polarization is not always the same for different peaks. Lang *et al.* (1981) have shown that the size, position, and circular polarization remain constant during the emission of successive 20 cm bursts. This suggests that one source is emitting the sequence of events, and that the energetic electrons are being accelerated in the same magnetic region of the loop. In this paper we also provide new information on the locations and changing magnetic fields of single and multiple wavelength bursts.

The sizes, brightness temperatures, locations, polarizations, and time evolution of eight solar bursts have been specified using VLA and WSRT observations. In Section 2 we describe our observational procedures and present our basic results on angular sizes and brightness temperatures. In Section 3 we present a series of 10 s snapshot maps made during the more intense bursts and compare them with simultaneous H α photographs. We thereby establish the site of energy release while also providing evidence for preburst heating. In Section 4 we discuss a burst which exhibited dramatic changes in its polarization structure and discuss the possible physical conditions which gave rise to these changes. A summary of our results is given in Section 5.

2. Basic Observational Results

We have used the Very Large Array (VLA) and the Westerbork Synthesis Radio Telescope (WSRT) to observe eight bursts on five days between March 1980 and June 1981. The wavelengths of observation, antenna configurations and synthesized beam-shapes are given in Table I. At the VLA, the individual antennae have diameters of 25 m, which at $\lambda = 2, 6$, and 20 cm, respectively, provide half-power beamwidths of 3.0', 9.3', and 31.1'. The WSRT antennae have individual diameters of 26 m which provide a 9.5' field of view at 6 cm wavelength. At the VLA the average correlated signal of $N(N-1)/2$ interferometer pairs, where N is the number of antennae used on each day, was sampled every 10 s for both the left-hand circularly polarized (LCP) and the right-hand circularly polarized (RCP) signals, thereby providing the data needed to compute maps of total intensity $I = (LCP + RCP)/2$ and the Stokes parameter $V = (LCP - RCP)/2$. The bandwidth used in every case was 12.5 MHz. At the WSRT the average correlated flux

TABLE I
Summary of observations

Date	Instrument	Wavelength	Number of antennae	Baseline range (km)	Synthesized beamshape ("r")
March 20, 1980	VLA	2 cm	10	0.10–1.95	2.2×3.1
June 12, 1980	VLA	20 cm	11	0.08–13.60	6.8×12.6
Sept. 4, 1980	VLA	6 cm	22	0.04–1.95	5.8×7.4
June 13, 1981	VLA	6 cm	26	0.13–6.40	4.2×5.5
June 14, 1981	VLA	20 cm	26	0.13–6.40	7.8×9.2
June 13, 1981	WSRT	6 cm	14	0.05–2.71	4.6×600

of 40 interferometer pairs was sampled every 0.1 s for both the total intensity, I , and circular polarization, V .

The VLA data were calibrated by observing either NRAO 150 or PKS 0923 + 392 for 5 min every 30 min. The flux density of NRAO 150 was assumed to be 10.5, 10.2, and 5.5 Jy at 2, 6, and 20 cm, respectively, while the respective flux densities of PKS 0923 + 392 were taken to be 7.65, 7.36, and 8.53 Jy. The amplitude and phase of the correlated signal were calibrated according to the procedure described by Lang and Willson (1979) together with a correction for the differences in the signal from high temperature noise sources detected in each polarization channel. Details of the observing and calibration procedure at the WSRT are given by Bregman (1980). Here the interferometric phases were calibrated by observing Cassiopeia A whose flux density at 6 cm wavelength was assumed to be 745 Jy. The uncertainty in the calibration at both the VLA and the WSRT is estimated to be $\leq 5^\circ$ in phase and $\leq 10\%$ in amplitude.

A summary of the observed bursts is given in Table II, where we provide the date, time and observing wavelength, the active region number, the full angular width to half intensity, peak brightness temperature and maximum degree of circular polarization,

TABLE II
Observed parameters of radio wavelength flares

Date	Time (UT)	Wave-length	Active region	Angular size ("x")	Maximum brightness temperature (K)	Maximum circular polarization (%)
March 20, 1980	20:40–21:00	2 cm	AR 2339	5×5	2.1×10^7	80
June 12, 1980	13:39–14:44	20 cm	AR 2509	16×35	1.5×10^8	~ 100
June 12, 1980	14:54–14:55	20 cm	AR 2511	15×15	2.0×10^8	75
Sept. 4, 1980	22:15–	6 cm	AR 2645	15×30	4.2×10^7	60
June 13, 1981	11:42–11:55	6 cm	AR 3159	~ 8	–	< 10
June 13, 1981	21:56–21:58	6 cm	AR 3159	5×10	2.7×10^7	≤ 15
June 14, 1981	20:41–20:49	6 cm	AR 3159	5×17	2.6×10^7	25
June 14, 1981	15:10–15:12	20 cm	AR 3159	10×25	5.5×10^7	< 15

$\rho_c = V/I$. The burst was in every case resolved with angular sizes between 5" and 30", peak brightness temperatures between 2×10^7 and 2×10^8 K, and degrees of circular polarization which ranged between 10 and 90%. In the next section we discuss the details of each burst and present snapshot maps which determine the sites of energy release and specify the changing magnetic topology within the bursting regions.

3. Site of Energy Release and Preburst Heating

Although it is generally believed that solar radio bursts occur through the conversion of magnetic to particle energy within a complex network of coronal loops, the exact location of the sites of energy release within the loop structures has only recently been determined. As discussed in the introduction, radio bursts at 2 cm and 6 cm wavelength are usually located at the central regions of magnetic loops, but there are some examples in which the 6 cm burst emission is strongest near the footpoints of the loops. For those cases in which we could compare the positions of the radio bursts and optical features, we found that the radio emission originates near the center of magnetic loops, rather than at the footpoints. In Figure 1 we compare a 10 s snapshot map of the impulsive phase of a burst observed at 6 cm wavelength with both a map of the preburst radio emission (A) three minutes before the peak of the burst and an H α photograph (B) taken at the same time. The figure indicates that the radio burst was elongated in a direction joining the two bright H α kernels, and that it was most intense at a point located midway between them. The preburst radio emission (A) was contained within a looplike structure which also joins the sites of subsequent H α emission. Here the peak brightness temperature is $\sim 5.5 \times 10^6$ K as compared with the peak burst brightness temperature of 4.2×10^7 K. Because the brightness temperature of quiescent coronal emission at 6 cm is typically $\sim 2 \times 10^6$ K (Kundu *et al.*, 1978; Felli *et al.*, 1981) the somewhat higher temperature observed in the preburst loop could represent pre-burst heating of the coronal plasma. In order to check that the brightness temperature was in fact higher than normal at this time, we also made several maps of 10 min duration centered around one hour before the burst. We found that the radio source had a similar size and shape but that the peak brightness temperatures were more than a factor of two lower with values of about 1.7×10^6 K. We therefore believe that we have detected preburst heating which occurs minutes before burst emission. Unfortunately the Solar Maximum Mission satellite was not observing this active region at the time of the burst and so we cannot check to see if there was also an enhancement of soft X-ray emission at the footpoints of the loop. We also note that Kundu *et al.* (1982) have also found evidence for heating of the plasma in coronal loops before the impulsive phase of a 6 cm burst.

The fact that the preburst radio emission lies closer to the H α emission than the peak of the impulsive burst suggests that the plasma is heated at a lower level than the site of the burst emission. The location of the impulsive phase is in agreement with the theoretical models in which the primary release of energy occurs at the top of a magnetic loop (Vlahos and Papadopoulos, 1979; Emslie and Vlahos, 1982; and Holman *et al.*, 1982).

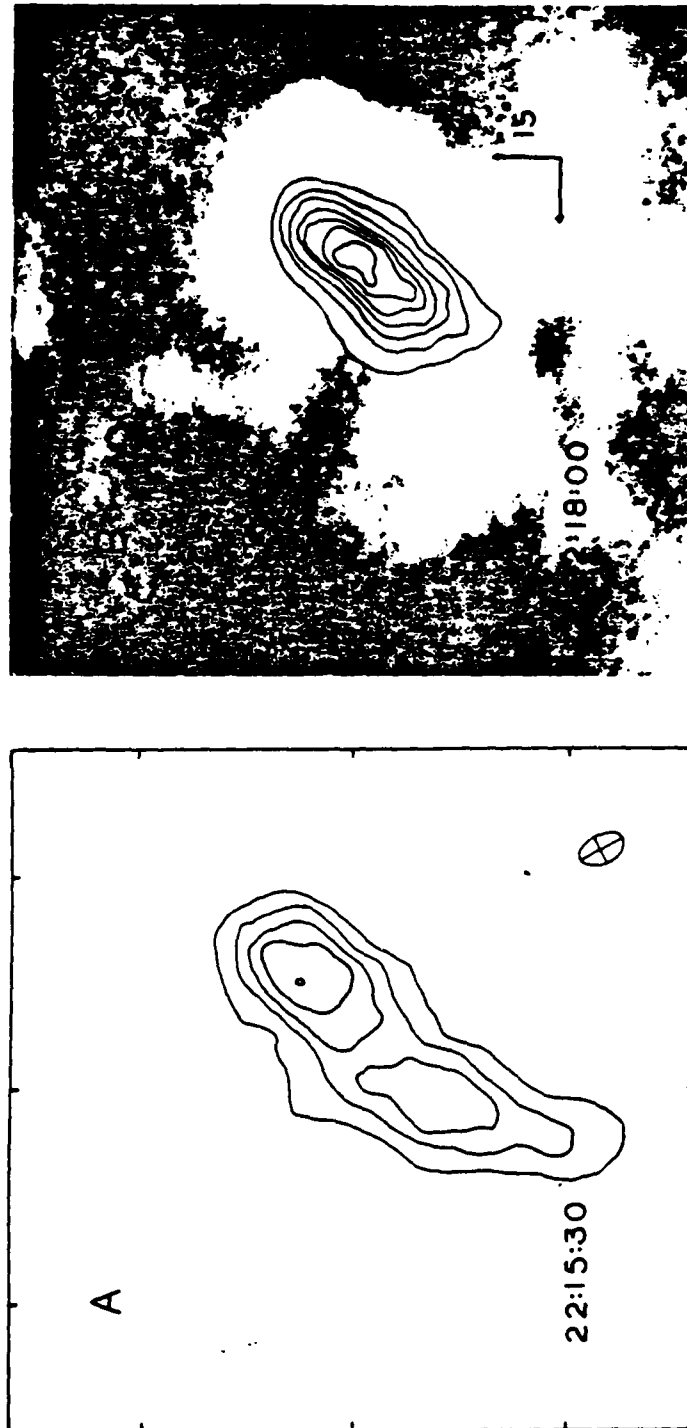


Fig. 1. VLA synthesis maps of the preflare (A) and impulsive phase (B) of a burst detected at 6 cm wavelength on September 4, 1980. Each map of total intensity, I , was made from 10 s of data at the time indicated. The contours of both maps mark levels of equal brightness temperature. For (A), the contours are drawn at 1×10^6 , 2×10^6 , 5×10^6 , and 10^7 K, while for (B), the contours are drawn at 10^6 , 1.1×10^7 , 3.8×10^7 , and 10^8 K. For (A), the radio map has been superimposed on an $H\alpha$ photograph of the optical flare taken at the same time. For both images, north is up, east is to the left and the angular scale is denoted on the figure. Note that the burst emission spans the region between the two $H\alpha$ kernels and is most intense between them and the two peaks of the preburst radio emission. The $H\alpha$ photograph was taken at the Big Bear Solar Observatory. (Courtesy of Frances Tang.)

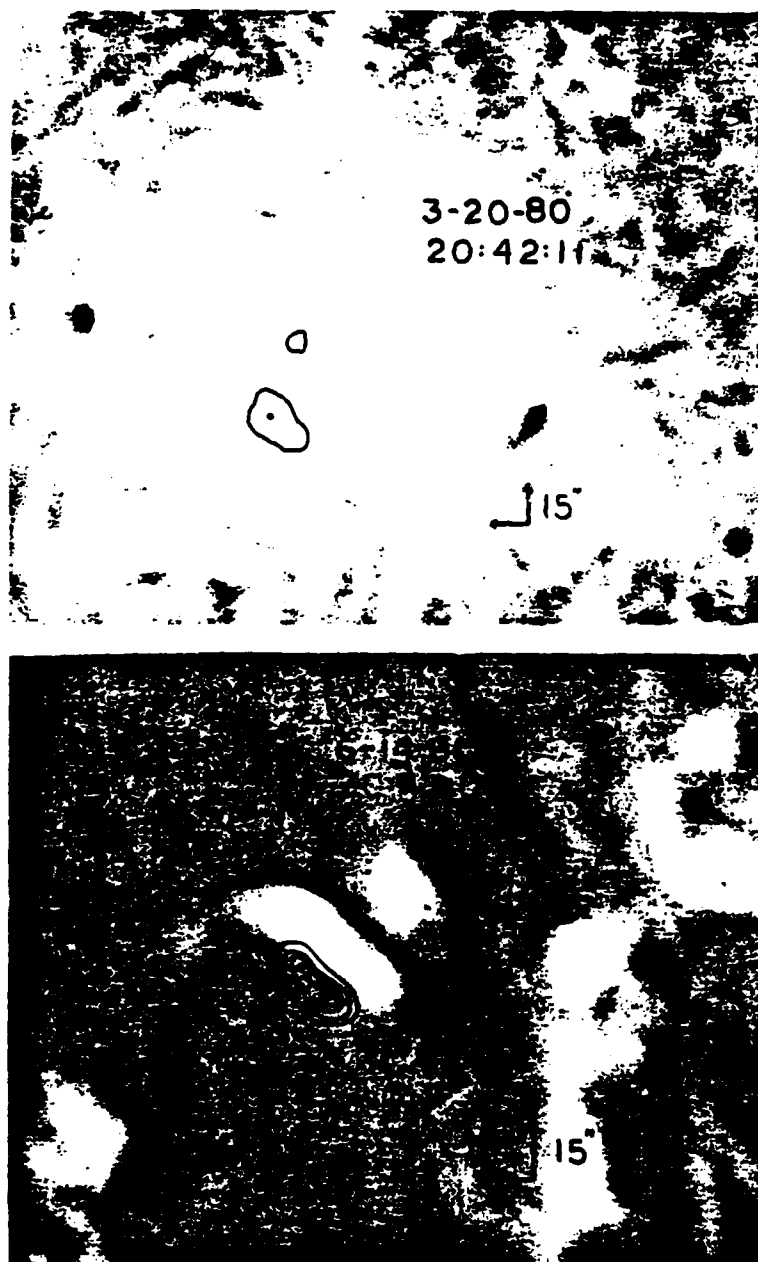


Fig. 2. VLA synthesis of the total intensity, I , of the impulsive phases of two bursts observed at $\lambda = 2$ cm on March 20, 1980 (top) and at $\lambda = 6$ cm on June 14, 1981 (bottom). Here, north is up, east is to the left and the angular scales are given on the figures. The contours of both maps denote levels of equal brightness temperature. For March 20, 1980, the contours are drawn at 3.0×10^6 K and 2.1×10^7 K. For June 14, 1981, the contours are drawn at 2.8×10^6 , 8.3×10^6 ... 2.5×10^7 K. Both maps have been superimposed on H α photographs taken at the same time. The 2 cm burst source is located between two groups of sunspots suggesting that the burst was located near the apex of a magnetic coronal loop which joins the spots. For June 14, 1981, the 10'' south-eastward displacement of the 6 cm radio source relative to the H α flare emission is attributed as a radial, limbward displacement caused by the greater height of the radio source.

In Figure 2 we compare the impulsive phases of two other radio bursts with H α photographs taken at the same time. The 2 cm (A) burst has a size of $\sim 5''$ and is located near the center of the H α emission, which is itself located between two groups of sunspots. Another 6 cm burst (B) consists of two components, both displaced by about $10''$ to the southeast of the H α emission. We attribute the angular displacement between the radio and optical sources as a radial, limbward displacement caused by the greater height of the 6 cm burst emission. Both the eastward component of the displacement ($\sim 10''$) and the southward component ($\sim 10''$) indicate a height of $\sim (1.5 \pm 0.2) \times 10^9$ cm for the 6 cm emission above the photosphere (the active region coordinates were 26° S 32° E).

In Figure 3 we present the time profile of another 6 cm burst where 10 s snapshot maps are given in Figure 4. The sequence of maps, which were made before, during and after the impulsive phase of the burst, indicate that the impulsive component is smaller and spatially separated from both the preburst radio emission and the gradual decay component of the burst. The gradual decay component is about $10''$ in size and 30% left circularly polarized, while the impulsive component is about $\leq 8''$ in size and less than 15% circularly polarized. An examination of a series of H α pictures taken at the Big Bear Solar Observatory showed that the optical emission originated closer to the large sunspot shown in Figure 2 and developed in the north-eastward direction, roughly coinciding with the elongation of the radio image. The absence of circular polarization in the impulsive component suggests that this source is located near the apex of the loop where the longitudinal component of the magnetic field is small, whereas the polariza-

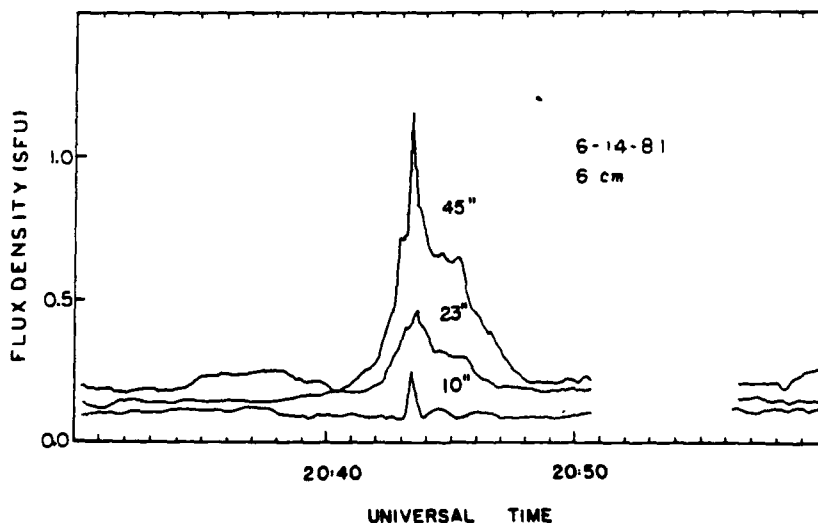


Fig. 3. The fringe amplitude of the total intensity, I , versus time for a burst detected at 6 cm wavelength with the VLA on June 14, 1981. The angular resolution of each interferometer pair is given next to the time profile. The visibility data from 325 interferometer pairs were used to construct the two-dimensional synthesis maps of the burst, shown in Figure 4.

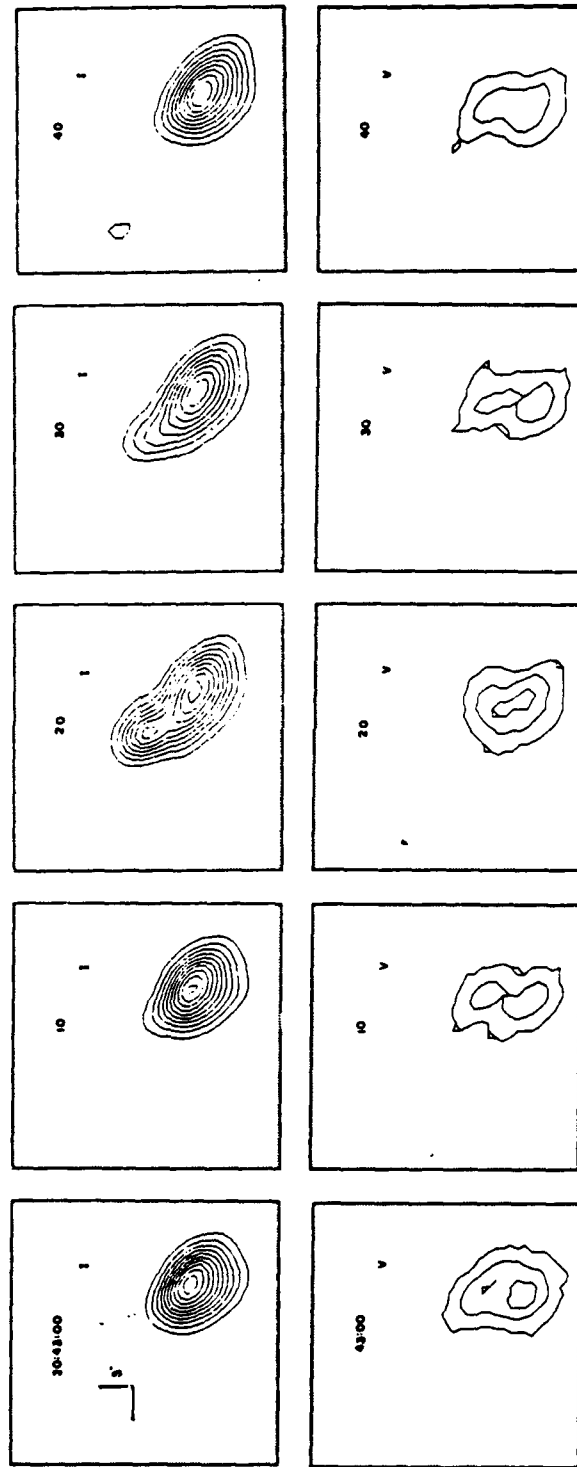


Fig. 4. A series of 10 s VLA snapshot maps of the total intensity, I , (top) and circular polarization, V , (bottom) for a burst detected at 6 cm wavelength on June 14, 1981. The contours of the I maps mark levels of equal brightness temperature and correspond to 2.8×10^6 , 5.5×10^6 , 8.3×10^6 K. The contours of the V maps also mark levels of equal brightness temperature and are drawn at 2.8×10^6 , 5.5×10^6 , 8.3×10^6 K. Note especially the spatial separation of the impulsive and gradual component of the burst at 10:43:20 UT.

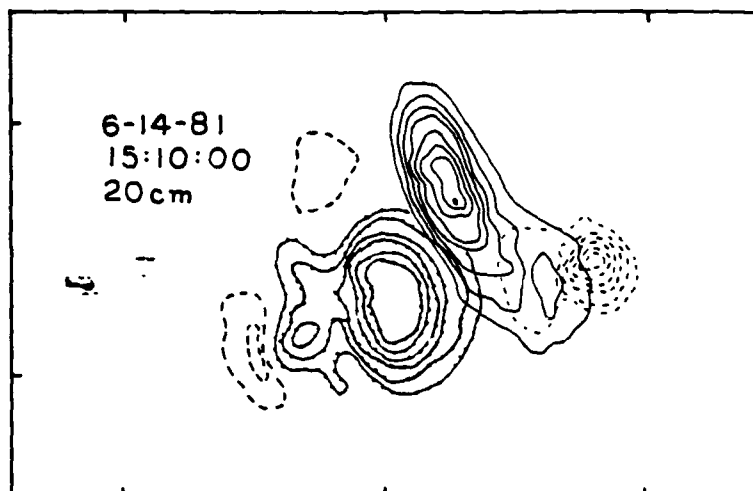


Fig. 5. A VLA snapshot map of the total intensity, I , of a burst detected at 20 cm wavelength on June 14, 1981, superimposed on a magnetogram showing the longitudinal component of the magnetic field in the underlying photosphere. Here, north is up, east is to the left and the angular scale is denoted by the $60''$ spacing between the fiducial marks on the axes. The contours of the radio map mark levels of equal brightness temperature and are drawn at 1.2×10^7 , 1.8×10^7 , ..., 5.5×10^7 K. The dashed contours of the magnetogram denote levels of negative longitudinal field and are drawn at -200 , -400 , -600 , -800 , -1000 , and -1500 G. The dotted contours of the magnetogram denote levels of positive field and are drawn at 100 , 200 , 400 , 600 , 800 , 1000 , and 1500 G.

tion detected in the gradual decay component suggests an origin in a predominantly longitudinal magnetic field of one polarity, most likely in one leg of the loop.

In Figure 5 we have superimposed a 10 s snapshot map of a 20 cm burst on a magnetogram (provided by Jean Rayole of Meudon Observatory) showing the longitudinal component of the magnetic field in the underlying photosphere. The radio burst is located between the regions of opposite magnetic polarity and extends along the magnetic neutral line. A 20 cm synthesis map of the active region made from four hours of observation on the same day shows a hot ($\sim 10^6$ K), looplike structure which connects the regions of opposite polarity. The apex of this 20 cm coronal loop coincides with the location of the burst. We found no detectable preflare heating of the coronal loop before this burst. The maximum brightness temperature of the preflare active region was $\sim 2.5 \times 10^6$ K and did not vary by more than $\sim 25\%$ on timescales of a few minutes to several hours before the burst occurred.

In Figure 6 we show the time profile of a multiple-component 6 cm burst whose individual components had durations of 20 to 60 s. In order to separate the burst structure from that of the quiescent active region we first subtracted the preburst visibility function from the burst data. Maps were then constructed from a 1.0 s average of the corrected visibility function obtained from the 40 available baselines. Because the WSRT is a linear array, these maps gave the one-dimensional brightness distribution of the source integrated perpendicular to a line with a position angle of $\sim 5^\circ$ east of north

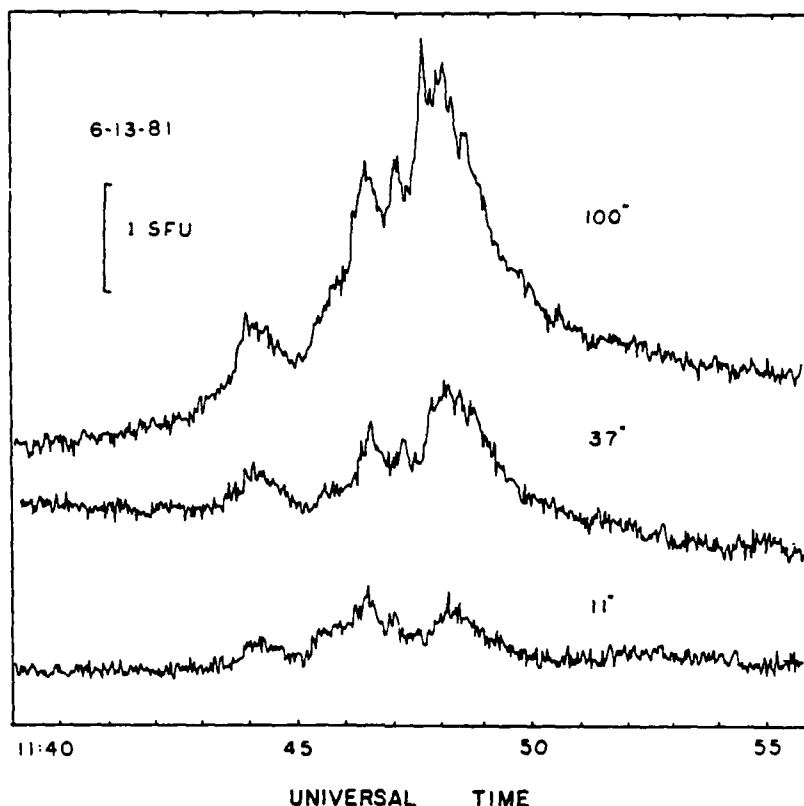


Fig. 6. The time profiles of a complex burst observed at 6 cm wavelength with the WSRT on June 13, 1981. Each profile was detected with one interferometer pair whose angular resolution is given next to the profile. The combined fringe visibilities of 40 interferometer pairs were used to construct one-dimensional snapshot maps throughout the burst.

on the sky. In Figure 7 we display these maps at various times throughout the burst. The data indicate that all the burst components originate from a single source of about $10''$ in size whose position remains constant to within a few arc seconds. This is similar to Lang *et al.* (1981) observations which indicated that the size, position and circular polarization remained constant during the emission of successive 20 cm events in the same burst. A comparison of the 6 cm burst position with a Kitt Peak magnetogram indicated that the radio burst was located within $\pm 5''$ of the neutral line of the active region. This is consistent with the absence of circular polarization throughout the 6 cm burst, which suggests that the source was located in a region of weak longitudinal magnetic field.

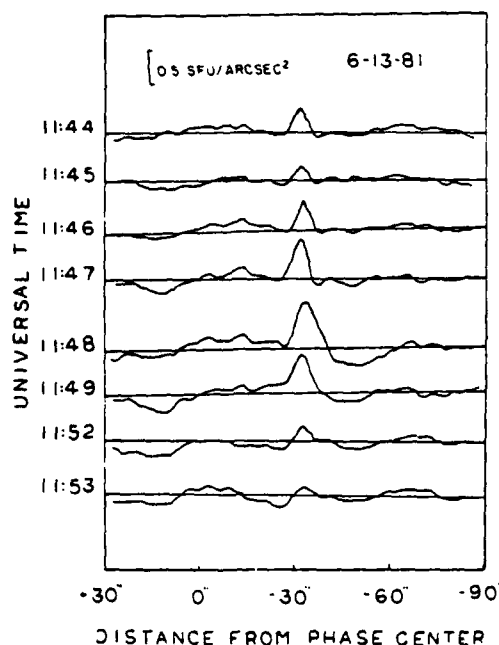


Fig. 7. A sequence of one-dimensional fan beam scans of the total intensity, I , for a burst detected at 6 cm wavelength with the WSRT on June 13, 1981. Each map was constructed from a 1 s average of the visibility data from 40 interferometer pairs. The maps indicate that the burst originates from a source of about $10''$ in size, whose position remains constant to within a few arc seconds.

4. Polarization Changes

High-resolution radio interferometric observations have led to the discovery of a high degree of circular polarization for both the slowly varying component and the burst component of active regions. The high polarization is attributed to either propagation effects or to gyroemission of energetic electrons. Both mechanisms require strong magnetic fields of several hundred gauss. The high brightness temperatures of the radio emission ($\geq 10^6$ K) indicates that the relevant magnetic fields are in the low solar corona. Previous studies of the evolution of the magnetic fields in the underlying photosphere suggest that some change in the magnetic field topology triggers the emission of solar bursts; but it is probably the coronal magnetic field which supplies the energy for solar bursts. Lang (1974, 1979) has, for example, shown that the degree of circular polarization of the coronal radio-emission can increase to 100% about 10 min to one hour before the eruption of solar bursts. Kundu *et al.* (1982) have similarly detected dramatic changes in circular polarization before and during a complex flare observed at 6 cm with the VLA. About 10 min before the onset of the impulsive phase, the magnetic structure changed from a simple bipolar region to a more complicated quadrupolar configuration; suggesting the appearance of a new system of coronal loops accompanied by the generation of additional magnetic flux.

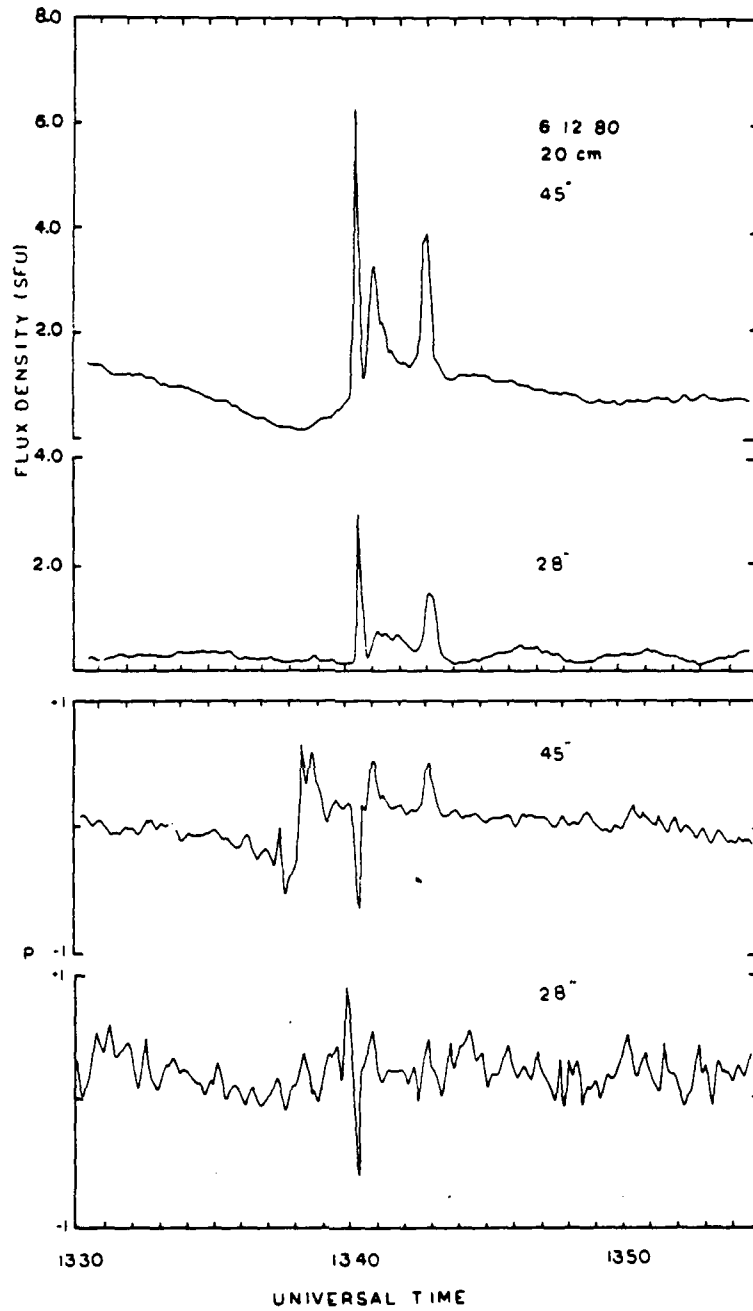
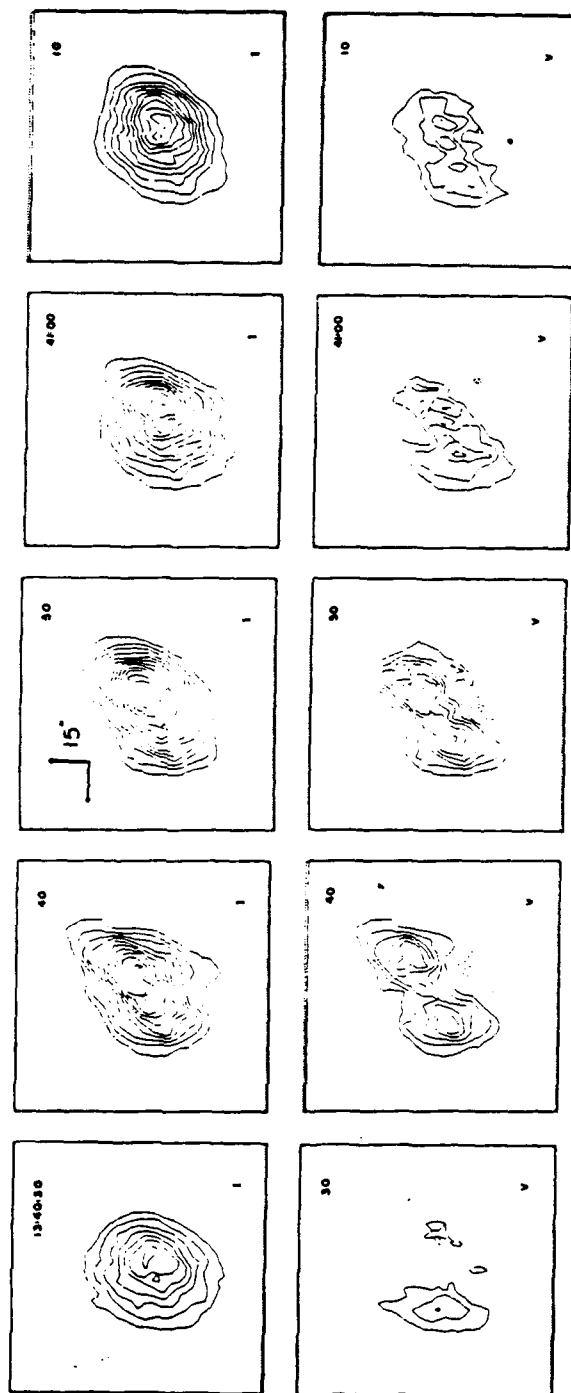


Fig. 8. The time profiles of a multiple spike burst detected at 20 cm wavelength with the VLA on June 12, 1980. Here, both the total intensity I (top), and the circular polarization p (bottom), are plotted for two interferometer pairs whose angular resolutions are given above each profile. Note especially the rapid changes in the circular polarization during the impulsive bursts. The combined fringe visibilities of 55 interferometer pairs were used to make the 10 s snapshot maps of both I and V shown in Figures 9 and 10.

The time profiles of the total intensity, I , and circular polarization, $\rho_c = V/I$, of a 20 cm burst are given in Figure 8. It consists of three impulsive spikes, each of 10 to 20 s duration, superimposed on a more gradual burst lasting about 12 min. The lower part of the figure shows that the first impulsive spike is highly right circularly polarized while the other two impulsive spikes are highly left circularly polarized. In Figures 9 and 10 we display a series of snapshot maps of both I and V made at 10 s intervals. Near the beginning of the burst at 13:40:00 UT the slowly varying source has a size of $\sim 30''$ and is $\sim 25\%$ left circularly polarized in the eastern half of the source. The polarized structure changes dramatically during the first impulsive spike, becoming about 90% right circularly polarized in the western half of the region, then reverting back to its unpolarized pre-impulsive state 10 s later. The polarization structure changes again at 13:40:50 and 13:42:50 UT when the source becomes more elongated and develops two left circularly polarized spikes ($\rho_c \sim 50\text{--}60\%$) which bracket the previously right circularly polarized spike located near the center of the region. The maximum brightness temperature of the three impulsive spikes ranged from 7×10^7 to 10×10^7 K, whereas the brightness temperature of the more slowly varying source was $\sim 3.5 \times 10^7$ K.

These rapid polarization changes are difficult to explain in terms of a simple bipolar loop model of the flaring region. Although we do not have any magnetograms with which to compare these changes, it is unlikely that the magnetic structure of the underlying photosphere can change so rapidly. The high degree of circular polarization implies that the burst emission is optically thin. If the emission is due to thermal bremsstrahlung in a region of $30''$ in size, then the optical depth $\tau_B \leq 0.14$ at 20 cm wavelength for an electron density $N_e \leq 2.5 \times 10^{10} \text{ cm}^{-3}$. For larger electron densities, the plasma frequency would exceed 1.4 GHz, and the 20 cm radiation would not propagate through the solar atmosphere. For an optically thin condition the observed brightness temperatures of $T_B \approx 10^8$ K imply electron temperatures of $T_e \geq 10^8$ K. The optical depth due to gyroresonant absorption with $T_e \approx 10^8$ K, a magnetic scale length of $L_H \approx 10^9$ cm, and electron densities of $N_e \approx 10^9$ to 10^{10} cm^{-3} exceeds unity for all harmonics unless the angle, θ , between the magnetic field and the line of sight is less than $\sim 10^\circ$ (cf. Lang, 1980, for relevant formulae). We therefore conclude that unless θ is unusually small, the gyroemission will be optically thick, and that the high polarization is probably due to propagation effects of the thermal bremsstrahlung. The observed degrees of circular polarization of 50 to 90% indicate magnetic field strengths of $H = 300$ to 400 G. These values are consistent with those obtained by Felli *et al.* (1981) who inferred $H \sim 250$ G for the 2×10^6 K plage-associated component of 6 cm radio emission above active regions.

We next attempt to explain the rapid changes in circular polarization which were observed during the impulsive spikes. One explanation involves frequency-dependent propagation effects which change the magnetoionic mode as the radiation passes through a plasma. Another more straightforward explanation involves the release of energy at different locations within the magnetic loop complex, or the generation of new magnetic flux at coronal levels where the radio emission originates. Cohen (1960) has described the situation in which radiation of predominantly one magnetoionic com-



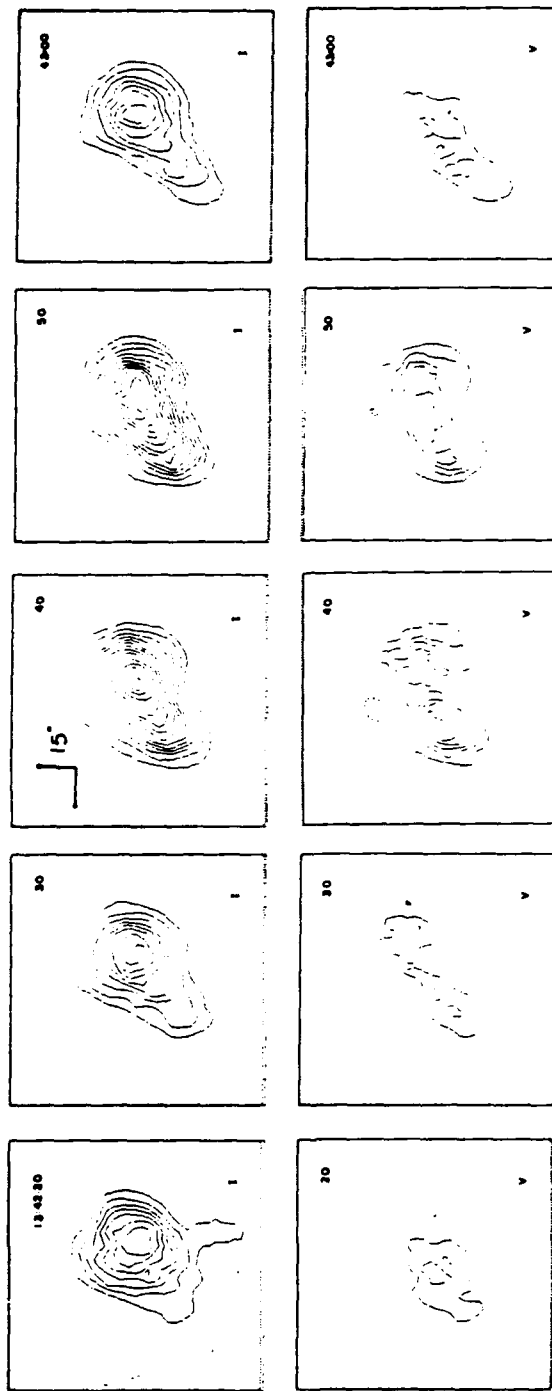


Fig. 9. A series of 10 s snapshot maps of both total intensity I (top), and circular polarization V (bottom), for a burst observed at 20 cm wavelength with the VLA on June 12, 1980. The contours of the maps mark levels of equal brightness temperature, where the solid and dashed contours of the V maps denote positive and negative values of V , respectively. For both sets of maps the outermost contour and the contour interval are equal to 6.2×10^6 K. Here, and in Figure 10, note the dramatic changes in the polarized structure which occurs throughout the burst.

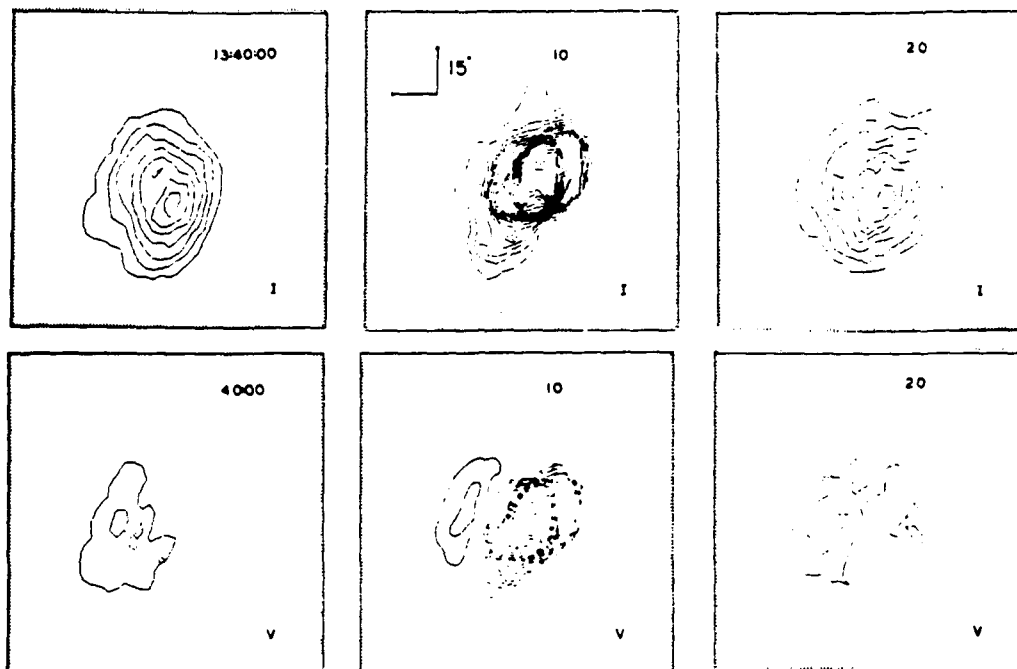


Fig. 10. Same as Figure 9 for the beginning of the burst.

ponent passes through a quasi-transverse region where the longitudinal component of the magnetic field changes sign. At frequencies above some transitional frequency, ν_T , the wave is unaffected by the reversal of the longitudinal field, whereas below ν_T , the two magnetoionic modes will be interchanged, resulting in a reversal in the sense of the circular polarization. The transitional frequency is given by (Cohen, 1960) $\nu_T^4 = 10^{17} N_e L_H H^3$, where N_e is the electron density, L_H is the scale length of the magnetic field, and H is the magnetic field strength. Assuming $N_e = 10^{10} \text{ cm}^{-3}$, $L_H = 10^9 \text{ cm}$, and $\nu_T \geq 1.42 \times 10^9 \text{ Hz}$, we find $H \geq 2 \text{ G}$. The required magnetic field strength is relatively insensitive to changes in the electron density and the scale length. If the coronal plasma is to be confined within looplike structures by the ambient magnetic field, however, then the local magnetic pressure must exceed the gas pressure, i.e., $H^2/8\pi \geq 2N_e kT$. This requires $H \geq 20$ to 120 G for $T_e = 5$ to $10 \times 10^7 \text{ K}$ and $N_e = 10^9$ to 10^{10} cm^{-3} . This indicates that the transitional frequency actually exceeds 1.4 GHz , and that this effect cannot explain the observed polarization changes.

The sense of circular polarization can also change if the source becomes self-absorbed so that only one of the magnetoionic modes becomes optically thick. The frequency of maximum emission, ν_{sa} , resulting from self-absorption of a nonthermal source is given by (Sligh, 1963; Ramaty and Petrosian, 1972) $\nu_{sa} \approx 10^{12.5} I_m^{2/5} H^{1/5}$, where I_m is the maximum brightness, expressed in $\text{erg cm}^{-2} \text{ s}^{-1} \text{ Hz}^{-1} \text{ ster}^{-1}$, and H is the magnetic

field strength perpendicular to the line of sight. For $\nu < \nu_{sa}$, the extraordinary mode is optically thick and the radiation is polarized in the ordinary mode, while for $\nu > \nu_{sa}$, the source is optically thin and polarized in the extraordinary mode. Such effects could explain our observations if, e.g., the number of electrons accelerated during the impulsive phase was different at the sites of the three impulsive bursts, causing one of the burst sources to be self-absorbed. With $I_m = 0.7 \times 10^{-10} \text{ erg cm}^{-2} \text{ s}^{-1} \text{ Hz}^{-1} \text{ ster}^{-1}$, corresponding to $T_b \approx 1 \times 10^8 \text{ K}$ and with $\nu_{sa} \geq 1.4 \times 10^9 \text{ Hz}$, we find $H \geq 3700 \text{ G}$. Because this lower limit is many times higher than expected for coronal magnetic fields we also conclude that self-absorption cannot explain the observed changes in circular polarization.

One interpretation of the complicated polarization structure is that the burst occurred within a magnetically complicated region containing a number of coronal loops, and that the unipolar nature of the bursts is due to emission from different legs of the loops which have different magnetic polarity. As suggested by Kundu *et al.* (1981), the polarization changes could also be explained if the coronal magnetic field undergoes variations on timescales of about one minute. Because both gyroresonant absorption and thermal bremsstrahlung depend on the local value of the magnetic field strength, such variations would also modulate the polarization. Alternatively, the rapid variations could be caused by the generation of new magnetic flux at coronal levels. Several models of burst emission have in fact been proposed in which loops of magnetic flux emerge from below the photosphere to interact with the overlying magnetic field to ultimately produce bursts (Heyvaerts *et al.*, 1977).

5. Summary

We have used the VLA and the WSRT to construct synthesis maps of eight solar bursts at 2, 6, or 20 cm wavelength. The observations have shown that the flares are resolved with angular sizes between $5''$ and $30''$, brightness temperatures between 2×10^7 and $1 \times 10^8 \text{ K}$, and circular polarizations of up to 90%. Superpositions of the radio images on available $H\alpha$ photographs or magnetograms show that the impulsive phases of the bursts are usually located between the $H\alpha$ kernels or close to the magnetic neutral line. These results suggest that the impulsive sources are located near the tops of coronal loops which connect underlying regions of opposite magnetic polarity. A sequence of 10 s snapshot maps for one 6 cm burst revealed that the impulsive source was spatially separated from the component associated with the rise and decay phase of the flare.

We also found evidence for pre-flare heating of a coronal loop minutes before the onset of one burst observed at 6 cm. The brightness temperatures of the pre-burst emission peaks were $\sim 5 \times 10^6 \text{ K}$, about a factor of two larger than the temperature found one hour earlier. These peaks of enhanced emission were located closer to the underlying $H\alpha$ footpoints than was the actual burst suggesting that the heating occurred in a region below the site of primary energy release.

The structure of a multiple spike burst detected at 20 cm wavelength exhibited remarkable changes in circular polarization of up to 90% on timescales of 10 to 20 s.

The polarized emission can be explained as either gyroresonant radiation for which the magnetic field $H \leq 100$ G and for which the angle between the field and the line of sight is $\leq 10^\circ$, or as the bremsstrahlung of a hot, optically thin plasma with a temperature $T_e \geq 10^8$ K and an electron density $\leq 2 \times 10^9 \text{ cm}^{-3}$. The bremsstrahlung requires polarization due to propagation effects at frequencies near the gyrofrequency in magnetic fields of strength $H \approx 300\text{--}400$ G. The most likely explanations for these reversals in polarization are either that the impulsive sources originates at different locations within a magnetically complicated region or that the coronal magnetic topology itself underwent drastic changes during the burst.

Acknowledgements

Solar radio astronomy at Tufts University is supported by the Air Force Office of Scientific Research under grant AFOSR-83-0019. We are indebted to Dave Rust and Paul Simon who very effectively coordinated these observations as part of the international observations during the Solar Maximum Year (SMY) and the post SMY observing session in June, 1981. The data at the WSRT were taken by Kenneth Lang and Mark Allart. We also thank Jaap van Nieuwkoop and Kees Slottje for their help with these observations. We are grateful to Viola Miller of the NOAA and Frances Tang and Margaret Liggett of the Big Bear Solar Observatory for providing the H α photographs. We also warmly thank Ken Lang for useful discussions and a critical review of this manuscript. The Very Large Array is operated by Associated Universities, Inc. under contract with the National Science Foundation. The Westerbork Synthesis Radio Telescope is operated by the Netherlands Foundation for Radio Astronomy with financial support from the Netherlands Organization for the Advancement of Pure Research (ZWO).

References

- Alissandrakis, C. E. and Kundu, M. R.: 1978, *Astrophys. J.* **222**, 342.
- Bregman, J. D.: 1980, Netherlands Foundation for Radio Astronomy Report No. 330.
- Cohen, M. H.: 1960, *Astrophys. J.* **133**, 978.
- Emslie, A. G. and Vlahos, L.: 1980, *Astrophys. J.* **242**, 359.
- Felli, M., Lang, K. R., and Willson, R. F.: 1981, *Astrophys. J.* **247**, 325.
- Gold, T. and Hoyle, F.: 1960, *Monthly Notices Roy. Astron. Soc.* **85**, 553.
- Heyvaerts, J., Priest, E. R., and Rust, D. M.: 1977, *Astrophys. J.* **216**, 123.
- Holman, G. D., Kundu, M. R., and Papadopoulos, K.: 1982, *Astrophys. J.* **257**, 354.
- Kattenberg, A.: 1981, Ph.D. Thesis.
- Kundu, M. R., Alissandrakis, C. E., Bregman, J. D., and Hin, A. C.: 1978, *Astrophys. J.* **213**, 278.
- Kundu, M. R., Bobrowsky, M., and Velusamy, T.: 1981, *Astrophys. J.* **251**, 342.
- Kundu, M. R., Schmahl, E., Velusamy, T., and Vlahos, L.: 1982, *Astron. Astrophys.* **108**, 188.
- Kundu, M. R., Schmahl, E., and Velusamy, T.: 1982, *Astrophys. J.* **253**, 963.
- Lang, K. R.: 1974, *Solar Phys.* **36**, 351.
- Lang, K. R.: 1979, in R. F. Donnelly (ed.), *Solar Terrestrial Prediction Proceedings III. Solar Activity Predictions*, 1980.
- Lang, K. R.: 1980, *Astrophysical Formulae*, 2nd ed., New York: Springer Verlag.
- Lang, K. R. and Willson, R. F.: 1979, *Nature* **278**, 24.

- Lang, K. R., Willson, R. F., and Felli, M.: 1981, *Astrophys. J.* **247**, 338.
Marsh, K. A. and Hurford, G. J.: 1980, *Astrophys. J.* **240**, L111.
Marsh, K. A., Zirin, H., and Hurford, G. J.: 1979, *Astrophys. J.* **228**, 610.
Petrosian, V.: 1982, *Astrophys. J.* **255**, L85.
Ramaty, R. and Petrosian, V.: 1972, *Astrophys. J.* **178**, 241.
Rust, D. M.: 1972, *Solar Phys.* **25**, 141.
Rust, D. M.: 1976, *Solar Phys.* **47**, 21.
Slush, V. I.: 1963, *Nature* **199**, 682.
Vlahos, L. and Papadopoulos, K.: 1979, *Astrophys. J.* **233**, 717.

4. The circularly polarized Sun at 12.6 cm wavelength

K.R. Lang and R.F. Willson

Department of Physics, Tufts University, Medford, Massachusetts 02155, USA

Received March 3, accepted April 15, 1983

Summary. Circular polarization maps of the Sun with 45" angular resolution at 12 cm wavelength are presented for six continuous days. The polarization corresponds to the extraordinary mode of wave propagation. The maps have degrees of circular polarization up to $q_c = 20\%$, and they show an excellent correlation with photospheric magnetograms. A similar correlation exists at 6 cm and 20 cm, and at all three wavelengths the brightness temperatures, T_b , of the circularly polarized emission is $T_b \sim 10^6$ K. This suggests that the emission at all three wavelengths is due to the same hot plasma radiating in the presence of magnetic fields that project radially upwards from the photosphere into the low solar corona. At 6 cm wavelength highly circularly polarized ($q_c \geq 50\%$), core sources with angular sizes $\phi \sim 10''$ to $30''$ occur near sunspots. These core sources are due to gyroresonant emission at the third harmonic of the gyrofrequency, implying longitudinal magnetic field strengths of $H_l \sim 580$ Gauss at altitudes $h \sim 3 \cdot 10^9$ cm above the sunspots. In regions near sunspots, the circularly polarized emission at 6 cm, 12 cm and 20 cm could all be due to the gyroemission of hot electrons spiralling in magnetic fields within the low solar corona. If this is the case, longitudinal magnetic fields of strength $H_l \sim 280$ Gauss and $H_l \sim 170$ Gauss are inferred from the 12 cm and 20 cm data, respectively. An alternative explanation is polarization by bremsstrahlung propagating in magnetic fields of strength $H_l \sim 100$ Gauss and 50 Gauss, respectively. This mechanism probably applies to extended regions of circularly polarized emission that are not near sunspots.

Key words: Sun: radio radiation – Sun: magnetic fields – Sun: active regions

1. Introduction

High resolution observations of solar active regions at 6 cm wavelength indicate that bright (brightness temperatures $T_b \sim 10^6$ K), highly polarized (degrees of circular polarization $q_c \geq 50\%$) core sources (angular sizes $\phi \sim 10''$ to $30''$) overlie sunspots (Lang and Willson, 1979; Alissandrakis et al., 1980). There is an excellent correlation between the 6 cm maps of circular polarization and Zeeman effect magnetograms of the underlying photosphere (Lang

and Willson, 1980). The bright, highly polarized 6 cm cores mark the legs of magnetic dipoles that are connected to lower lying sunspots, and angular displacements indicate that the 6 cm emission lies at a height $h \sim 3 \cdot 10^9$ cm above the photosphere (Lang et al., 1983). The 6 cm maps of circular polarization act as "magnetograms" of the low solar corona, the sense of circular polarization corresponding to the extraordinary mode of wave propagation. The bright, highly polarized core sources at 6 cm have been conclusively shown to radiate by gyroresonant emission in sunspot magnetic fields that project radially upwards into the low solar corona (Lang and Willson, 1982). Longitudinal magnetic field strengths of $H_l \sim 580$ Gauss are inferred from the fact that the detected gyroemission comes mainly from the third harmonic of the gyrofrequency.

Observations at longer radio wavelengths generally refer to higher levels in the solar atmosphere. For instance, Very Large Array (V.L.A.) observations of solar active regions at 20 cm wavelength delineate loop-like structures that connect lower lying sunspots of opposite magnetic polarity. The most intense 20 cm emission occurs near the apex of the loops, and it has been attributed to optically thick bremsstrahlung of a hot plasma trapped within coronal loops (Lang et al., 1982). The 20 cm emission is almost certainly the radio wavelength counterpart of the ubiquitous coronal loops detected at soft X-ray wavelengths. Dulk and Gary (1983) have recently provided supporting evidence for this view by using the V.L.A. to map the entire Sun at 20 cm. They found that intense 20 cm emission comes from bipolar active regions, and that the brightest emission occurs near the line of polarization reversal. They similarly attribute the 20 cm emission to bremsstrahlung from the corona and the upper transition region.

There is no detectable circular polarization at the apex of the 20 cm loops, and this may be attributed to optically thick emission and/or magnetic fields that are transverse to the line of sight (Lang and Willson, 1982). Dulk and Gary (1983) have nevertheless reported the detection of circularly polarized 20 cm emission from the legs of dipolar loops. Under the assumption that the circular polarization ($q_c \sim 20\%$) is due to effects of bremsstrahlung propagating in a magnetic field, they infer longitudinal magnetic field strengths of $H_l \sim 20$ to 70 Gauss at altitudes $h \sim 10^9$ to $5 \cdot 10^9$ cm.

In the next section, we present circular polarization maps of the entire Sun at 12 cm wavelength. They are extraordinarily similar to the 20 cm polarization map given by Dulk and Gary. In both cases the sense of circular polarization refers to the extraordinary mode of wave propagation, and there is an excellent correspondence

Send offprint requests to: K.R. Lang

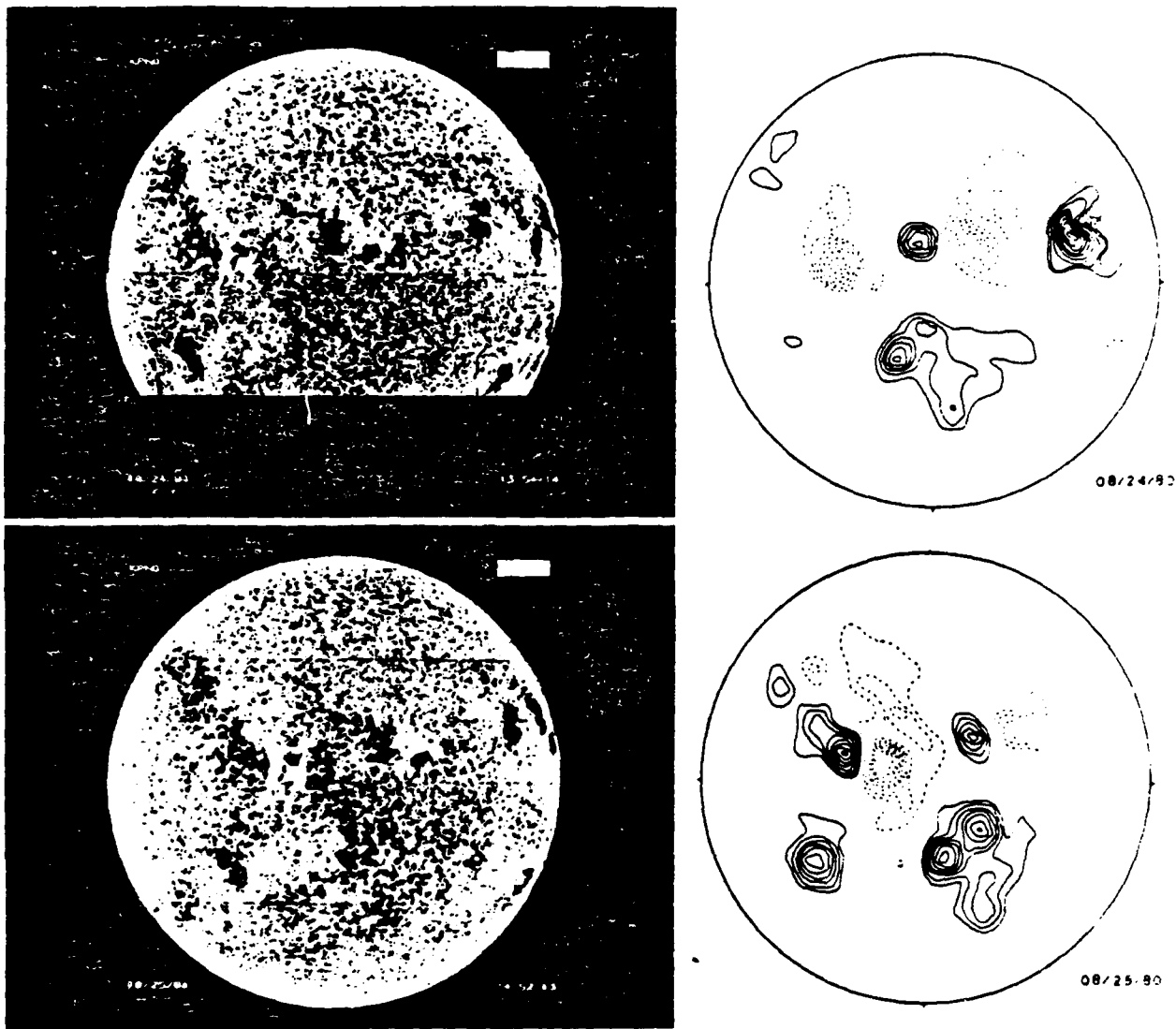


Fig. 1. Photospheric magnetograms (left) and circular polarization maps at 12.6 cm (right). There is a good correlation between the dipolar structures in the photosphere and low solar corona (at 12.6 cm where $T_B \sim 10^6$ K)

between the polarization maps and photospheric magnetograms. In this respect, the data are also similar to those obtained for the 6 cm core sources. The polarized emission at 12 cm and 20 cm is apparently larger in angular extent and lower in circular polarization than the 6 cm core sources, but this may be in part due to an instrumental effect. For instance, the 1.5 beamwidth of the 12 cm observations would not resolve the core sources and the polarization would be diluted. In any event, we conclude our paper by stating that gyroemission may account for the circular polarization observed near sunspots at both 12 cm and 20 cm wavelength. The magnetic field strengths required by the gyroemission explanation have already been inferred from observations at 6 cm for comparable heights $h \sim 3 \cdot 10^9$ cm and temperatures $T_B \sim 10^6$ K, but for smaller areas. Extended regions of circularly polarized emission at 12 cm and 20 cm that are not near sunspots probably owe their polarization to the propagation effects of bremsstrahlung in a magnetic field.

2. Observations

We have observed the Sun at 12.6 cm wavelength (or 2,380 MHz) on 24 August through 29 August 1980 at the Arecibo Observatory where the beamwidth is 1.5. Signals from both the right circularly polarized (RCP) and left circularly polarized (LCP) receivers were simultaneously recorded with a 40 MHz bandwidth and 2 s integration time. An area of 1° in right ascension (α) by $40'$ in declination (δ) was observed by scanning in α at twice the sidereal rate (or at 1° in 2 m) at intervals of $45''$ in declination. A complete map of the Sun was made in slightly less than two hours, which is the approximate time that the Sun can be viewed at favourable zenith angles with the Arecibo telescope. Maps of total intensity $I = (LCP + RCP)/2$ and circular polarization $q_c = (LCP - RCP)/(LCP + RCP)$ were constructed with an angular resolution of $45''$, or half the half-power beamwidth.

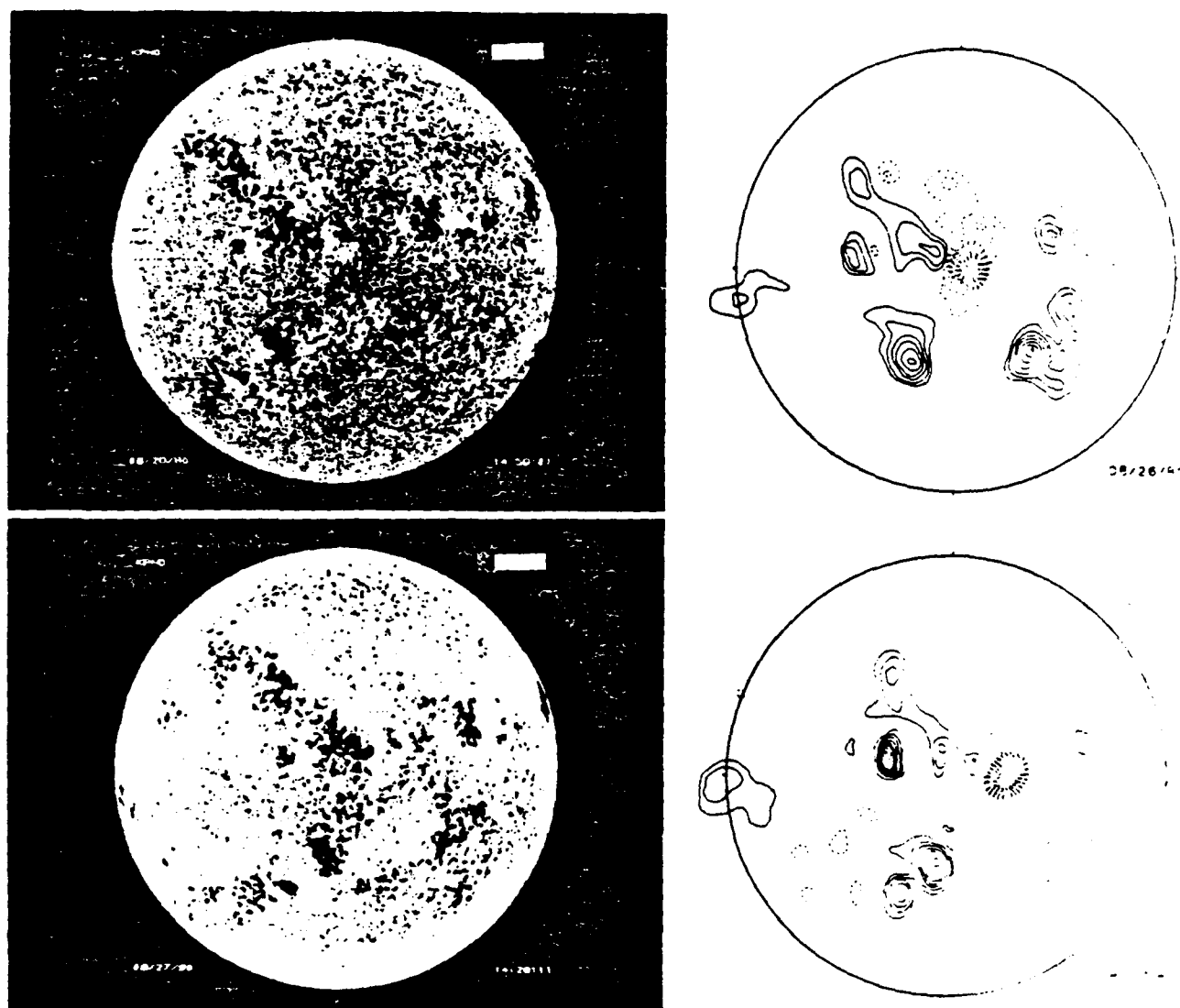


Fig. 1 (continued)

The 12.6 cm circular polarization maps are compared with photospheric magnetograms in the accompanying three figures. The contours are drawn at intervals of $q_c = 0.02, 0.04, 0.06 \dots 0.20$ with solid contours corresponding to positive q_c and dashed contours corresponding to negative q_c . The full disk magnetograms are taken daily at the Kitt Peak National Observatory (KPNO) using the Zeeman effect of the 8680 Å line of neutral iron. Both the circular polarization maps and the KPNO magnetograms delineate the structure of the longitudinal component of the magnetic field. There is an excellent correspondence between the photospheric features seen in the magnetograms and the regions of circular polarization seen at 12.6 cm where the brightness temperatures $T_b \sim 10^6$ K. Dark magnetogram regions refer to negative magnetic polarity and correspond to left hand circular polarization; whereas light magnetogram regions refer to regions of positive magnetic polarity and correspond to right hand circular polarization. The sense of circular polarization at 12.6 cm

therefore corresponds to the extraordinary mode of wave propagation.

In nearly every case, a dipolar feature in the magnetograms corresponds to a dipolar feature in the 12.6 cm maps of circular polarization. (The westernmost region on August 25, 26, and 27 was so intense that it saturated the 12.6 cm receiver, and it is therefore absent from the maps.) The close correspondence between the longitudinal magnetic field structure seen in the photosphere and the low solar corona (12.6 cm when $T_b \sim 10^6$ K) indicates that the magnetic fields project radially outwards from the photosphere into the low solar corona. Our maps of total intensity, which we do not present here, indicate that the maximum brightness occurs between the 12.6 cm dipolar features where there is no detectable circular polarization. This suggests that the intense 12.6 cm emission may be bremsstrahlung from coronal loops. As we shall next see, the circularly polarized emission may have an alternative explanation.

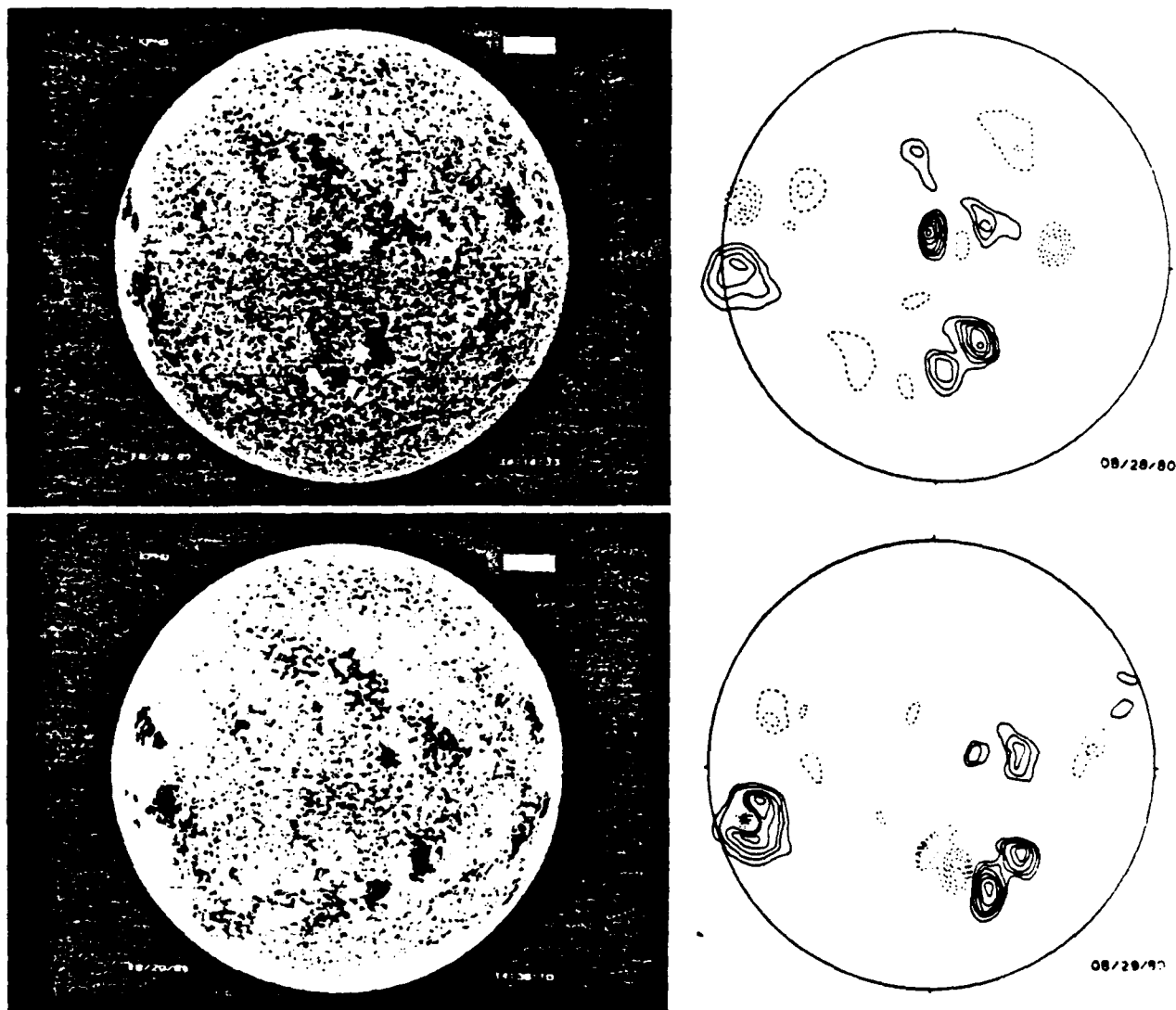


Fig. 1. (continued)

3. Discussion

Maps of circular polarization observed at 6 cm, 12 cm and 20 cm all show bright ($T_b \sim 10^6$ K) features that are strongly correlated with the longitudinal magnetic field structure delineated by photospheric magnetograms. This suggests that the circularly polarized emission at all three wavelengths is due to the same hot plasma radiating in the presence of magnetic fields that project radially upwards from the photosphere into the low solar corona. In fact, the bright ($T_b \sim 10^6$ K), highly polarized emission ($q_c \geq 50\%$), core sources (angular sizes $\varphi \sim 10''$ to $30''$) that lie near sunspots at 6 cm wavelength must be due to gyroemission at the third harmonic of the gyrofrequency, and this means that the longitudinal magnetic field strength $H_l \sim 580$ Gauss at heights $h \sim 3 \cdot 10^9$ cm above sunspots (Lang and Willson, 1982; Lang et al., 1983). Although the circularly polarized emission at both 12 cm and 20 cm is apparently larger in angular extent and lower in circular polarization than the

6 cm core sources, this could be due to the larger beamwidths at the longer wavelengths that do not resolve the core sources and therefore detect a lower polarization. As shown by Lang (1974), angular resolutions of $\sim 10''$ are required to resolve the highly polarized core sources.

The circularly polarized emission at 12 cm and 20 cm wavelength that lies near sunspots may also be due to gyroemission. Observations at X-ray wavelengths have shown that the free-free optical depth is relatively low near sunspots, and that bremsstrahlung only becomes detectable near the apex of coronal loops. That is, the bremsstrahlung from regions overlying sunspots is at least two orders of magnitude weaker than the bremsstrahlung from the coronal loops that join sunspots of opposite magnetic polarity (Pallavicini et al., 1981). We therefore believe that gyroemission is at least a plausible explanation for the circularly polarized emission of active regions at 12 cm and 20 cm wavelength near sunspots. Of course, the gyroresonance emission at 20 cm could be absorbed by

free-free processes, thereby becoming trapped before it can be detected; but this is less likely to be the case at 12 cm for the free-free optical depth scales as ν^{-2} , or as the inverse square of the observing frequency ν and the optical depth for gyroresonant absorption scales as ν^{-1} . In any event, longitudinal magnetic field strengths of $H_l \sim 280$ and 170 Gauss are required if gyroemission explains the 20% circular polarization observed at 12 cm and 20 cm, respectively whereas $H_l \sim 100$ and 50 Gauss if the polarization is caused by bremsstrahlung propagating in a magnetic field. The higher magnetic fields for regions near sunspots have already been inferred from the 6 cm measurements at comparable altitudes and temperatures.

In the cases where broader circularly polarized emission with angular sizes $\phi \gtrsim 45''$ exist in regions that are not near sunspots, the circularly polarized emission at 12 cm and 20 cm is probably due to propagation effects. The magnetic field strengths are probably weaker in these regions, and the optical depth due to bremsstrahlung larger.

Acknowledgements. We gratefully acknowledge Dr. William Livingston of the Kitt Peak National Observatory for providing us with photospheric magnetograms. Radio wavelength observations of solar active regions at Tufts University are supported under grant AFOSR-83-0019 with the Air Force Office of Scientific

Research. The Arecibo Observatory is part of the National Astronomy and Ionosphere Center which is operated by Cornell University under contract with the N.S.F. We also thank our referee, Professor George A. Dulk for useful and constructive suggestions.

References

- Alissandrakis, C.E., Kundu, M.R., Lantos, P.: 1980, *Astron. Astrophys.* **82**, 30
- Dulk, G.A., Gary, D.E.: 1983, *Astron. Astrophys.* submitted
- Lang, K.R.: 1974, *Solar Phys.* **36**, 351
- Lang, K.R., Willson, R.F.: 1979, *Nature* **278**, 24
- Lang, K.R., Willson, R.F.: 1980, in *Radio Physics of the Sun*, IAU Symposium No. 86, ed. M.R. Kundu and T.E. Gergely, Dordrecht: Reidel, p. 109
- Lang, K.R., Willson, R.F.: 1982, *Astrophys. J. Letters* **255**, L111
- Lang, K.R., Willson, R.F., Gaizauskas, V.: 1983, *Astrophys. J.* **267**, 455
- Lang, K.R., Willson, R.F., Rayrole, J.: 1982, *Astrophys. J.* **258**, 384
- Pallavicini, R., Sakurai, T., Vaiana, G.S.: 1981, *Astron. Astrophys.* **98**, 316

5. BRIGHT, RAPID, HIGHLY POLARIZED RADIO SPIKES FROM THE M DWARF AD LEONIS

KENNETH R. LANG

Department of Physics, Tufts University

JAY BOOKBINDER AND LEON GOLUB

Harvard-Smithsonian Center for Astrophysics

AND

MICHAEL M. DAVIS

National Astronomy and Ionosphere Center

Received 1983 March 2; accepted 1983 May 10

ABSTRACT

We have observed a radio burst from the main-sequence (dM4.5e) star AD Leo at 1400 MHz from 0536 to 0556 UT on 1983 February 1 at the Arecibo Observatory. A rapid sequence of highly polarized spikes was observed during the gradual rise of a longer lasting event. The maximum flux density of the spikes was $S_{\max} = 130$ mJy, and they had rise times $\tau \leq 200$ ms. The spikes were all 100% left-hand circularly polarized with an instrumental uncertainty of 5%. The rise times provide an upper limit to the linear size $L \leq 6 \times 10^9$ cm for the emitter. Provided that the source is symmetric, it has an area that is less than 0.03 of the star's surface area. In this case, the lower limit to the brightness temperature of the spikes is $T_B \geq 10^{13}$ K. The high brightness temperatures and high degrees of circular polarization are explained in terms of electron-cyclotron maser emission at the second harmonic of the gyrofrequency in longitudinal magnetic fields of strength $H_l \sim 250$ gauss. The gradual component did not exhibit any rapid fluctuations, and it was entirely analogous to the thermal emission of solar bursts. The Arecibo Observatory has the potential of providing stringent limits on the linear size of "star spots" or "star loops" on active main-sequence stars, and it also provides accurate circular polarization measurements.

Subject headings: radio sources: variable — stars: coronae — stars: flare — stars: late-type — stars: radio radiation — Sun: radio radiation

1. INTRODUCTION

Very Large Array (VLA) observations of the quiescent emission from solar active regions at 1400 MHz (21 cm wavelength) delineate looplike structures connecting regions of opposite magnetic polarity in the underlying photosphere. The quiescent emission at 1400 MHz is, in fact, the radio wavelength counterpart of the ubiquitous coronal loops detected at X-ray wavelengths (Lang, Willson, and Rayrole 1982). VLA observations of solar bursts at 1400 MHz (Lang, Willson, and Felli 1981; Willson 1983) reveal highly polarized (circular polarization $p_c \sim 80\% \pm 15\%$) bursts composed of a sequence of spikes with rise times $\tau < 10$ s (the integration time at the VLA). The high circular polarization implies magnetic field strengths of $H_l \sim 250$ gauss if the 1400 MHz radiation is at the second harmonic of the gyrofrequency. Spike-like events with rise times $\tau \leq 10$ ms have been observed during solar bursts at 1400 MHz (Dröge 1977) and 2600 MHz (Slotje 1978, 1980), indicating high brightness temperatures, $T_B \geq 10^{12}$ K, that require coherent maser-like emission. The very high brightness temperatures and the high circular polarization of these spikes ($p_c \sim 100\%$) have been explained in terms of

electron-cyclotron masers in which amplification occurs at the second harmonic of the gyrofrequency (Melrose and Dulk 1982*a, b*).

Nearby main-sequence stars of late spectral type exhibit quiescent X-ray emission whose absolute luminosity may be as much as 100 times that of the Sun (Vaiana *et al.* 1981; Johnson 1981). This suggests that these stars have large-scale coronal loops and intense magnetic fields. In fact, surface magnetic fields of strength $H_l \sim 1000$ gauss covering as much as 60% of the stellar surface have been observed for several nearby main-sequence stars of late spectral type (Marcy 1983; Giampapa, Golub, and Worden 1983). The nearby dwarf M stars of the UV Ceti type also exhibit X-ray flares in which the X-ray emission can increase by as much as a factor of 30 in a few minutes. This suggests that these stars may exhibit quiescent emission at 1400 MHz which is related to their coronal loops, and that they might exhibit spike-like bursts at 1400 MHz which are analogous to those observed from the Sun. As a matter of fact, VLA observations of the dwarf M stars UV Ceti (L726-8A, B) and YZ Cmi at 1400 MHz (Fisher and Gibson 1982) and L726-8A at 4900 MHz (Gary,

L15

Linsky, and Dulk 1982) indicate that these stars do emit highly polarized radio bursts. Although these VLA observations were limited by large integration times of 10 s and large instrumental uncertainties in circular polarization of up to 15%, lower limits to the burst brightness temperature $T_B \geq 10^{10}$ to 10^{12} K could be obtained by assuming that the bursts cover an area smaller than the stellar disk.

In § II of this *Letter*, we present observations of a burst at 1400 MHz from the dwarf M flare star AD Leo. Highly polarized ($p_c \sim 100\%$), spike-like bursts with rapid rise times ($\tau \leq 200$ ms) occurred during the gradual rise of a longer lasting event. In § III we interpret the high brightness temperatures ($T_B \geq 10^{13}$ K) and high polarization of the spike-like bursts in terms of electron-cyclotron maser emission at the second harmonic of the gyrofrequency with a longitudinal magnetic field strength of $H_l \sim 250$ gauss.

II. OBSERVATIONS

On 1983 February 1, we observed the dM4.5e star AD Leo [$\alpha(1950.0) = 10^h16^m54^s$, $\delta(1950.0) =$

$20^\circ17'18''$] at a frequency of 1400.0 MHz (21.4 cm wavelength) from 0520 to 0619 UT at the Arecibo Observatory. At this frequency the antenna beamwidth is 3.3, and the system sensitivity is 8 K per Jy at zenith ($1 \text{ Jy} = 10^{-23} \text{ ergs s}^{-1} \text{ cm}^{-2} \text{ Hz}^{-1}$). Both the left-hand circularly polarized (LCP) and right-hand circularly polarized (RCP) signals were recorded using separate receivers. The ellipticity was 0.95, and the uncertainty in circular polarization due to cross-talk between the two receivers was 5%. A bandwidth of 20 MHz and an integration time of 0.2 s were employed with digital sampling at the Nyquist rate of 0.1 s. The flux density scale was established using a 2 K noise source which was calibrated by observations of 3C 245 (3.06 Jy at 1400 MHz) immediately after the observations of AD Leo.

As illustrated in Figures 1 and 2, a highly polarized (LCP) impulsive burst lasting almost 3 minutes occurred during the gradual rise of an event that lasted 20 minutes. When the impulsive burst is examined with higher time resolution (Fig. 2), a sequence of 100% left-hand circularly polarized spikes is detected. This is entirely analogous to the microwave bursts from solar active regions where the gradual event is interpreted as the

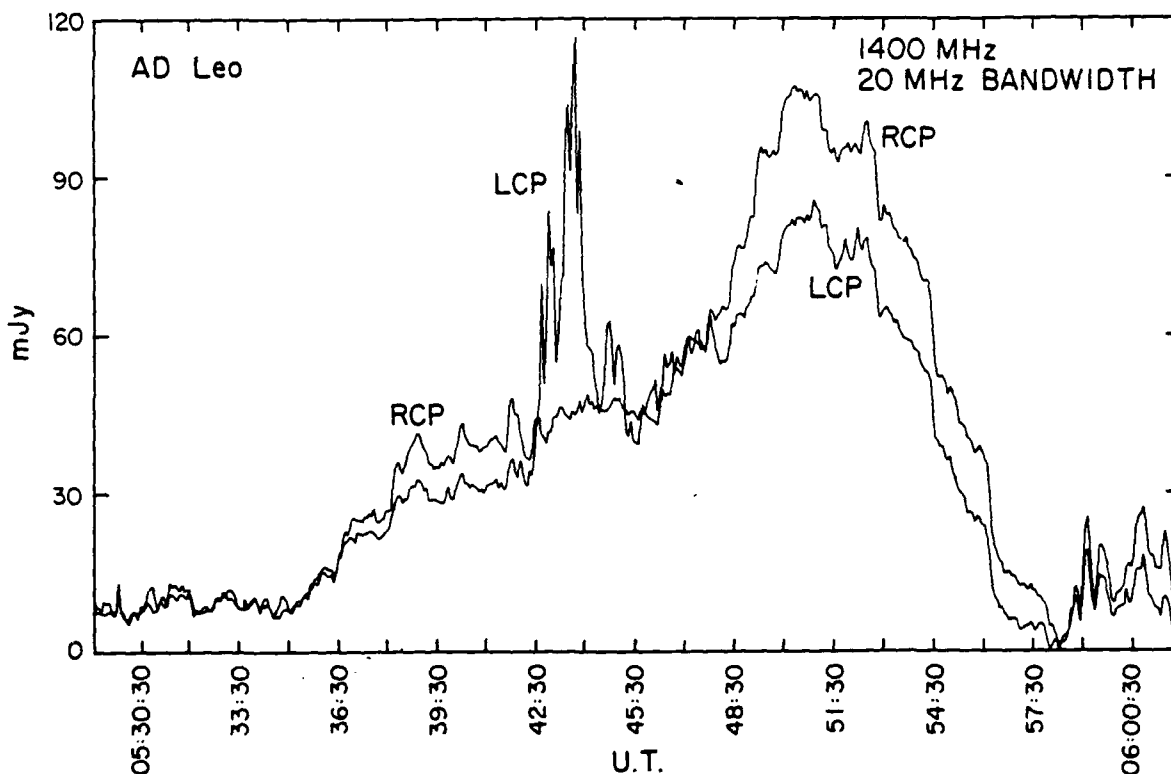


FIG. 1.—The total power detected at a signal frequency of 1400 MHz while tracking the dwarf M star AD Leo. Both the right-hand circularly polarized (RCP) and left-hand circularly polarized (LCP) signals are given. A highly polarized (LCP) impulsive burst lasting almost 3 minutes occurs during the gradual rise of an unpolarized burst lasting about 20 minutes. Because of the long integration time, the rapid-spikes that make up the impulsive burst have been smoothed out and their flux densities underestimated (see Fig. 2 for the correct details).

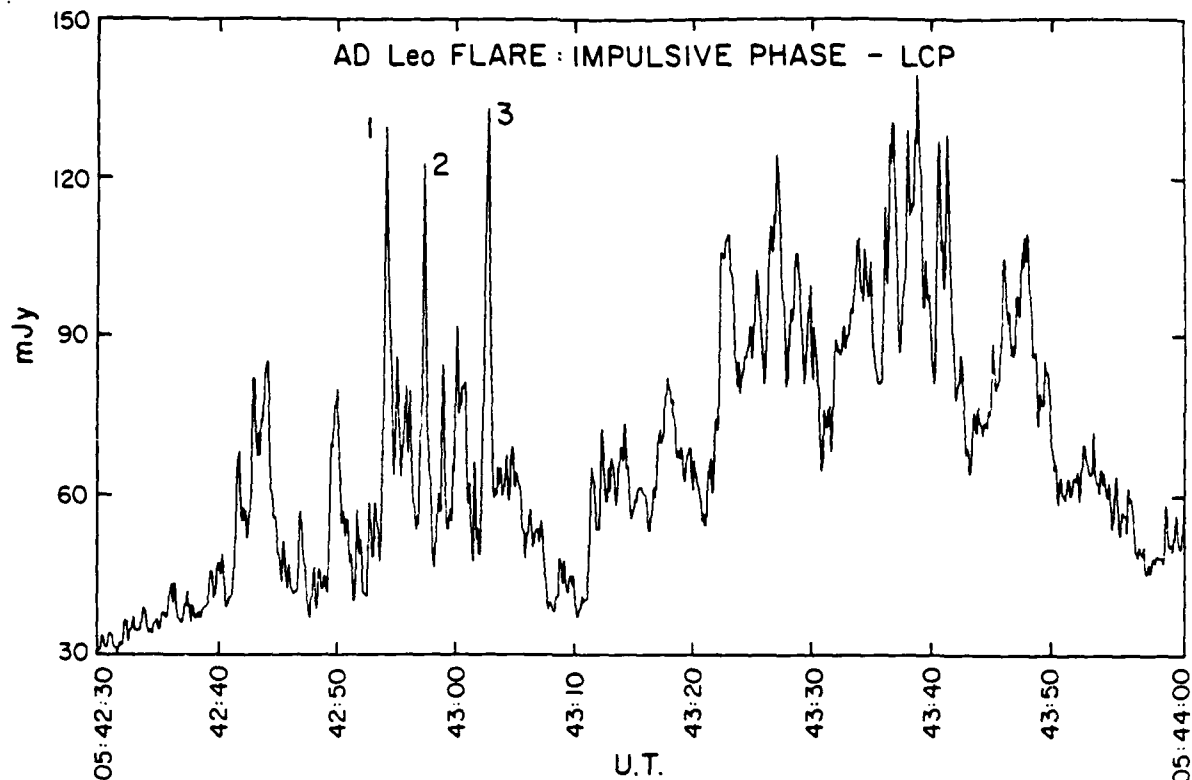


FIG. 2.—Rapid, highly polarized spikes observed during a 1400 MHz radio burst from the dwarf M star AD Leo. Notice that the burst emission occurs in a sequence of spikes which are all 100% left-hand circularly polarized. The time profiles of the spikes denoted by the numbers 1, 2, and 3 are given in Fig. 3.

bremsstrahlung of a high-temperature, thermal plasma, and the spiked emission is attributed to nonthermal radiation that typically occurs during the rise phase of the thermal flare (Lang, Willson, and Felli 1981; Slottje 1978, 1980).

The polarization did not change during the emission of successive spikes, suggesting that the magnetic field structure does not change during spike emission. The maximum flux density of the individual spikes was 130 mJy. Here we notice that current VLA observations with 3 s integration time would still smooth out the individual spikes and lead to an underestimate of their flux density. The data shown in Figure 2 contain "quasi-periodic" fluctuations at time scales of about 2 s, 10 s, and 25 s. Quasi-periodic oscillations with a period of about 56 s have been reported for a microwave flare from the M dwarf L726-8A (Gary, Linsky, and Dulk 1982); but power spectrum analysis of our AD Leo data indicates that no single periodicity dominates the spectrum.

Of special interest is the rise time of the individual spikes. As illustrated in Figure 3, the three most distinct spikes all had a measured rise time of about 300 ms. Because the integration time was 200 ms, the actual rise time $\tau \leq 200$ ms (from the convolution relation). An

upper limit to the linear size, L , of the emitting region, estimated by the distance that light travels in 200 ms, is $L \leq 6 \times 10^9$ cm. A dM4.5e star is expected to have a radius $R = 0.5 R_{\odot} = 3.5 \times 10^{10}$ cm, and the emitting region therefore had a linear size which is at least 6 times smaller than the star's radius. Provided that the burst emitter is symmetric, it has an area which is less than 0.03 of the stellar surface area. We can use the maximum flux density, $S_{\max} = 130$ mJy, to infer a lower limit to the brightness temperature, $T_b \geq 10^{13}$ K, using the Rayleigh-Jeans expression (Lang 1980) and assuming a symmetric source of linear size $L \leq 6 \times 10^9$ cm.

III. DISCUSSION

The high brightness temperature, $T_b \geq 10^{13}$ K, of radio bursts from AD Leo and the Sun can be explained by maser emission. The high degrees of circular polarization ($\rho_c \sim 100\%$) are intimately related to the intense magnetic fields of these stars. For instance, Twiss (1958) and Twiss and Roberts (1958) pointed out that both the high brightness temperatures and the high degrees of circular polarization of solar radio bursts might be explained by the masing action of electrons that are trapped within magnetic loops and radiate at the first

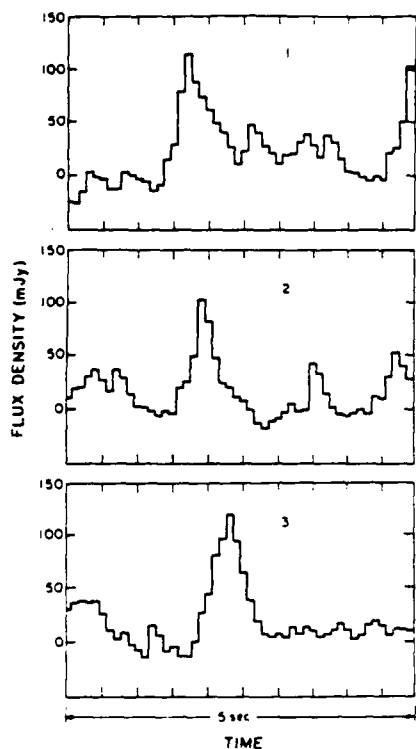


FIG. 3.—Time profiles of the spikes marked 1, 2, and 3 in Fig. 2. The digital sampling rate was 100 ms, the integration time 200 ms, and the distance between fiducial marks on the time axis is 500 ms. Each of these spikes has a rise time $\tau \leq 200$ ms.

few harmonics of the gyrofrequency $\nu_H = 2.8 \times 10^6 H_l$ Hz, where H_l is the longitudinal magnetic field strength. Melrose and Dulk (1982a, b) have applied this radiation mechanism to solar and stellar bursts having rapid variations with high brightness temperatures and high degrees of circular polarization. Because radiation at the first harmonic of the gyrofrequency cannot escape from

such hot, dense plasmas, they attributed the bursts to masers operating at the second harmonic ($n = 2$) of the gyrofrequency, ν_H . At our observing frequency $\nu = 1.4 \times 10^9$ Hz, we obtain a longitudinal magnetic field strength of $H_l = 250$ gauss from $\nu = n\nu_H = 5.6 \times 10^6 H_l$, where $n = 2$ and the gyrofrequency $\nu_H = 2.8 \times 10^6 H_l$. Further evidence for a strong magnetic field is provided by the intense X-ray emission from AD Leo. Its absolute X-ray luminosity is $L_X = 10^{29.0}$ ergs s^{-1} , which is at least 10 times the Sun's X-ray luminosity. The flare star AD Leo must therefore have a magnetic field strength at least as strong as that of the Sun (cf. Golub 1983), and the electron-cyclotron maser interpretation is consistent with this.

We would also like to point out the potential of using the Arecibo Observatory for studies of active main-sequence stars. Accurate circular polarization measurements are one advantage. The rapid time sampling capability of better than 1 ms will allow one to resolve the individual spike-like components of the radio bursts. Measurements of the rise-time of the spikes will establish upper limits to the size of the emitting source, and determine a limit to the fraction of the stellar surface area that is involved in the emission.

We would like to thank Dr. Dan Stinebring for specifying the polarization characteristics of the 20 cm line feed. We would also like to thank Dr. Robert Rosner for useful discussions, and the Department of Astronomy at Harvard University for the travel grant provided for Jay Bookbinder. Radio astronomical studies of the Sun and other active stars at Tufts University are supported under grant AFOSR-83-0019 with the Air Force Office of Scientific Research. Studies of coronal plasma processes at the Harvard-Smithsonian Center for Astrophysics are supported by NASA grant NAGW 112. The Arecibo Observatory is part of the National Astronomy and Ionosphere Center which is operated by Cornell University under contract with the NSF.

REFERENCES

- Dröge, F. 1977, *Astr. Ap.*, **57**, 285.
 Fisher, P. L., and Gibson, D. M. 1982, in *Second Cambridge Workshop on Cool Stars, Stellar Systems and the Sun*, ed. M. S. Giampapa and L. Golub (Smithsonian Observatory Special Report No. 392), pp. 109–114.
 Garv, D. E., Linsky, J. L., and Dulk, G. A. 1982, *Ap. J. (Letters)*, **263**, L79.
 Giampapa, M. S., Golub, L., and Worden, S. P. 1983, *Ap. J. (Letters)*, **268**, L121.
 Golub, L. 1983, in *IAU Colloquium 71, Activity in Red-Dwarf Stars*, ed. P. B. Byrne and M. Rondo (Dordrecht: Reidel), in press.
 Johnson, H. M. 1981, *Ap. J.*, **243**, 234.
 Lang, K. R. 1980, *Astrophysical Formulae* (2d ed.; New York: Springer Verlag), p. 23.
 Lang, K. R., Willson, R. F., and Felli, M. 1981, *Ap. J.*, **247**, 338.
 Lang, K. R., Willson, R. F., and Rayrole, J. 1982, *Ap. J.*, **258**, 384.
 Marcy, G. W. 1983, in *IAU Symposium 102, Solar and Stellar Magnetic Fields: Origins and Coronal Effects*, ed. J. O. Stenflo (Dordrecht: Reidel), in press.
 Melrose, D. B., and Dulk, G. A. 1982a, *Ap. J. (Letters)*, **259**, L41.
 ——— 1982b, *Ap. J.*, **259**, 844.
 Slottje, C. 1978, *Nature*, **275**, 520.
 ——— 1980, in *IAU Symposium 86, Radio Physics of the Sun*, ed. M. R. Kundu and T. E. Gergely (Dordrecht: Reidel), pp. 195–203.
 Twiss, R. Q. 1958, *Australian J. Phys.*, **11**, 564.
 Twiss, R. Q., and Roberts, J. A. 1958, *Australian J. Phys.*, **11**, 424.
 Vaiana, G. S., et al. 1981, *Ap. J.*, **244**, 163.
 Willson, R. F. 1983, *Solar Phys.*, **83**, 285.

JAY BOOKBINDER and LEON GOLUB: Harvard-Smithsonian Center for Astrophysics, 60 Garden Street, Cambridge, MA 02138

MICHAEL M. DAVIS: Arecibo Observatory, P. O. Box 995, Arecibo, Puerto Rico 00613

KENNETH R. LANG: Department of Physics, Tufts University, Medford, MA 02155

6. POSSIBLE DETECTION OF THERMAL CYCLOTRON LINES FROM SMALL SOURCES WITHIN SOLAR ACTIVE REGIONS

ROBERT F. WILLSON

Department of Physics, Tufts University, Medford, MA 02155, U.S.A.

(Received 31 May; in revised form 21 July, 1983)

Abstract. Theoretical spectra of thermal cyclotron line emission from solar active regions are presented for two frequency bands available at the Very Large Array (VLA). VLA synthesis maps of three active regions at 1380, 1540, and 1705 MHz are then presented. The maps of two of these regions show significant changes in the brightness temperature within these narrow frequency ranges. We show that these changes may be attributed to thermal cyclotron line emission in small regions ($\theta = 10''$ to $30''$) where the magnetic field is relatively constant with $H = 125$ – 180 G. An alternative interpretation, involving height-dependent variations in the physical conditions may also explain the changes in one of these regions. The potential to study coronal magnetic fields using VLA observations of cyclotron lines is also discussed.

1. Introduction

It was realized more than two decades ago that the cyclotron radiation (or gyro-emission) of thermal electrons accelerated in solar magnetic fields may compete with the bremsstrahlung of thermal electrons accelerated in the electric fields of coronal ions (Stepanov, 1959; Ginzburg and Zheleznyakov, 1959). At the time, peculiarities in the frequency spectrum and polarization of solar active regions at radio wavelengths were interpreted in terms of the combined effects of cyclotron radiation and bremsstrahlung (Zheleznyakov, 1962; Kakinuma and Swarup, 1962). The observations used in support of this interpretation were, however, made with relatively small antennas whose large beamwidths could not resolve the individual sources within active regions. Interferometric observations at centimeter wavelengths indicated that beam dilution effects had, in fact, previously prevented the detection of small, intense sources which were very highly circularly polarized (Kundu, 1959; Enome *et al.*, 1969; Lang, 1974). This high polarization could only be attributed to cyclotron radiation. Early observations of solar active regions with the Very Large Array (VLA) at 6 cm wavelength then revealed unusually hot ($\approx 10^6$ K) and highly circulated polarized (up to 95%) radiation above sunspots (Lang and Willson, 1979; Kundu *et al.*, 1981). This radiation was attributed to the cyclotron radiation of coronal electrons trapped within the legs of magnetic dipoles whose feet are found in lower lying sunspots (Alissandrakis *et al.*, 1980; Lang *et al.*, 1983). In the meantime, observations at X-ray wavelengths had indicated that magnetic loops are the dominant structural features of the corona, but that the X-ray emission is most intense in the regions which lie between sunspots. The relatively weak X-ray radiation above sunspots implied low electron densities in these regions and this meant that bremsstrahlung could not account for the 6 cm emission above sunspots

Solar Physics 89 (1983) 103–113. 0038-0938/83/0891-0103\$01.65.

© 1983 by D. Reidel Publishing Company

(Pallavicini *et al.*, 1981). Additional opacity due to gyroresonant absorption was required to explain the high brightness temperatures at radio wavelengths. The presence of cyclotron radiation in the coronal atmosphere above sunspots was then confirmed by accurate polarization measurements at 6 cm wavelength using the Westerbork Synthesis Radio Telescope (WSRT) (Lang and Willson, 1982). The observations indicated that highly polarized (up to 100%) horseshoe structures overlie sunspot penumbrae. These structures can only be explained by cyclotron radiation, and they had, in fact actually been predicted by the theory of gyroresonant absorption above individual sunspots (Gel'freikh and Lubyshev, 1979).

The theory of cyclotron absorption indicates that observations at a given frequency, ν , refer to a narrow layer in the solar atmosphere at which $\nu = s\nu_H$, where $s = 2, 3, 4 \dots$ is the harmonic, the gyrofrequency $\nu_H = 2.8 \times 10^6 H$ Hz, and H is the magnetic field strength in gauss. Because the magnetic field strength of dipolar loops decreases systematically with height above the solar photosphere, it was thought that the individual cyclotron lines would be superimposed to give a continuum spectrum, but that observations at longer wavelengths would refer to higher altitudes above the photosphere. Nevertheless, theoretical work predicted that individual cyclotron lines might be detected if the radiation was confined to a fixed altitude where the magnetic field is relatively constant. This might, for example, occur when neutral current sheets develop and subsequently rupture, thereby giving rise to solar bursts (Syrovatskii and Kuznetsov, 1980; Kuznetsov and Syrovatskii, 1981). The cyclotron radiation is able to escape only from a thin edge of the current sheet where the magnetic field is practically homogeneous. It was therefore imagined that thermal cyclotron lines might be detected during the temperature enhancements that occur before and during solar flares or bursts (Zheleznyakov and Zlotnik, 1980a; Zheleznyakov and Tikhomorov, 1980). Zheleznyakov and Zlotnik (1980b) have pointed out that cyclotron lines might also be detected from quiescent active regions if the loop geometry allowed observations of relatively constant magnetic field. Kaverin *et al.* (1980) have, in fact, detected narrow band structures at centimeter wavelengths from several active regions. They suggested that these structures may be attributed to cyclotron line emission from small sources within these regions where the magnetic field is nearly uniform.

The optical depths, τ_s and $\tau_{s,0}$ for the extraordinary and ordinary modes for an individual cyclotron line at harmonic s are given by (Zheleznyakov and Zlotnik, 1980; Zheleznyakov, 1970):

$$\tau_{s,0} = 3.93 \frac{\nu}{c} \left(\frac{\nu_p}{\nu} \right)^2 \frac{s^{2s}}{2^s s!} \beta_T^{2s-3} L_H F(x) \exp(-z^2), \quad (1)$$

where

$$F(x) = (1 \pm \cos x)^2 \frac{\sin x^{2s-2}}{|\cos x|}$$

and

$$z = \frac{v - s v_H}{\sqrt{2 v \beta_T \cos \alpha}}$$

Here, the frequency $v = s v_H$, the gyrofrequency is $v_H = 2.8 \times 10^6 H$, the velocity of light is c , the plasma frequency $v_p = 8.9 \times 10^3 N_e^{1/2}$ for an electron density of N_e , the factor $\beta_T = V_{th}/c = 3.89 \times 10^5 T_e^{1/2}/c$ for an electron thermal velocity V_{th} and an electron temperature of T_e , and L_H is the scale length of the magnetic field. The function $F(x)$ depends on the angle α , between the magnetic field and the line of sight and the + and - signs denote the extraordinary and ordinary modes of wave propagation. The gaussian function $\exp(-z^2)$ describes a Doppler broadened line with a peak value of unity at $v = s v_H$ and a full width to half maximum of $\Delta v_D = 2.335 \beta_T v$.

In addition to cyclotron emission, thermal bremsstrahlung can also contribute to the opacity above active regions. The optical depths τ_{B_e} and τ_{B_o} of the extraordinary and ordinary modes due to thermal bremsstrahlung are given by

$$\tau_{B_e} = \frac{\tau_B}{\left[1 - \frac{v_H \cos \alpha}{v}\right]^2}, \quad (2)$$

$$\tau_{B_o} = \frac{\tau_B}{\left[1 + \frac{v_H \cos \alpha}{v}\right]^2},$$

where

$$\tau_B = \frac{9.78 \times 10^{-3} N_e^2 L}{v^2 T_e^{3/2}} \ln[4.7 \times 10^{10} T_e/v]$$

is the classical expression for the bremsstrahlung optical depth in the absence of a magnetic field. The brightness temperatures $T_{B_{e,o}} = [1 - \exp(-\tau_{e,o})] T_e$, where $\tau_{e,o} = \tau_{s,e,o} + \tau_{B_{e,o}}$. We have calculated the brightness temperature $T_B = (T_{B_e} + T_{B_o})/2$ and the degree of circular polarization $\rho_c = [T_{B_e} + T_{B_o}]/[T_{B_e} - T_{B_o}]$ as a function of frequency for the harmonics 2, 3, 4, and 5 and a number of different values of the magnetic field strength, temperature, density, scale length, and angle. The results of our calculations for two frequency bands between 1000 and 2000 MHz and 4000–5000 MHz are shown in Figures 1 and 2. These frequency ranges were chosen because they are centered on two of the frequency bands available at the VLA. As illustrated in these figures, we obtain thermal cyclotron lines of half-width $\Delta v_D = 50$ –150 MHz, superimposed upon optically thin bremsstrahlung. Because τ depends strongly on the harmonic s , the cyclotron lines become optically thick at $s = 2, 3$, and 4 with flat tops and broad widths which refer to the lower, truncated parts of the gaussian function $\exp(-z^2)$. Because $\Delta v_D/v$ is a constant, the lines between 4 and

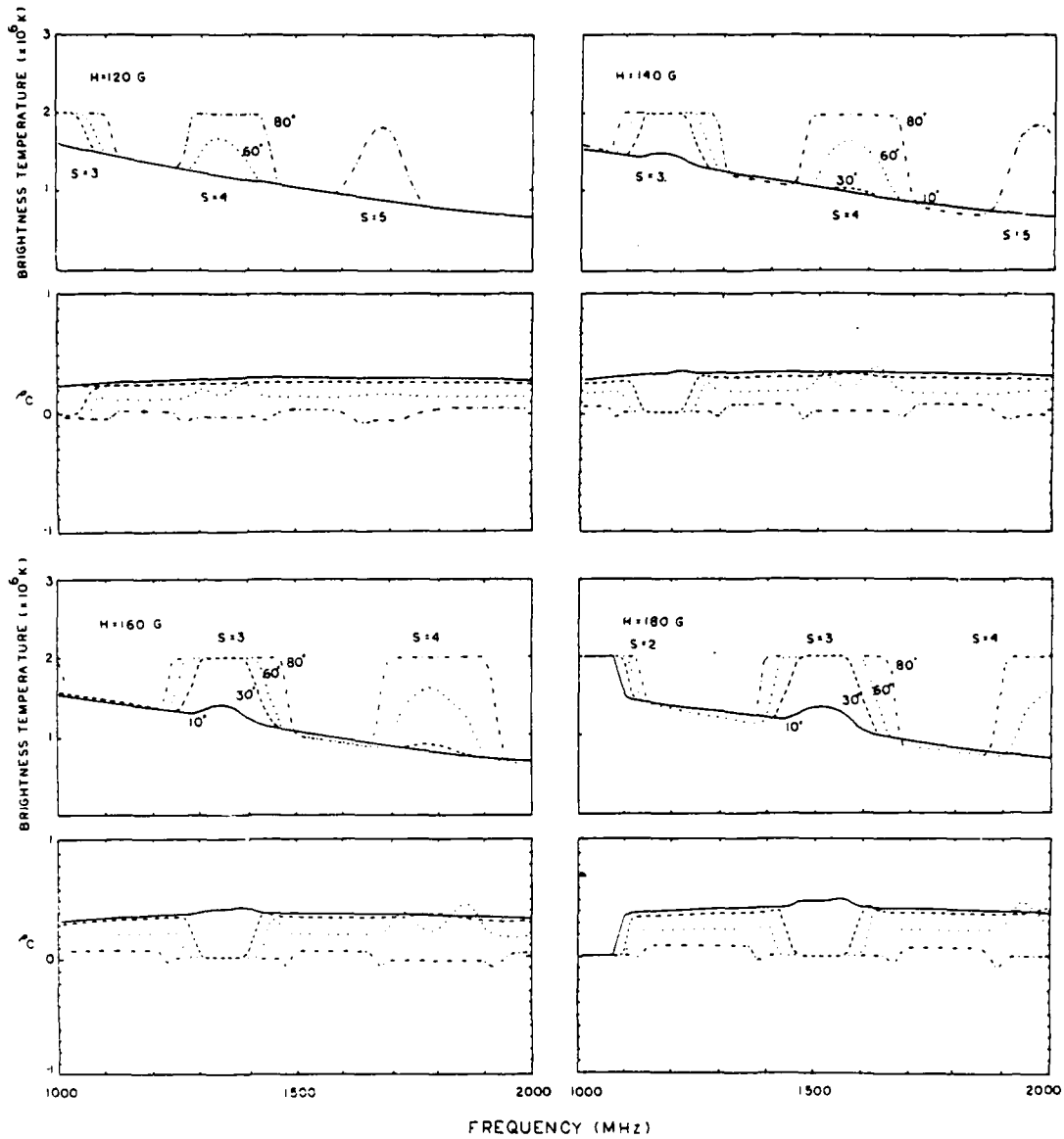


Fig. 1. Theoretical plots of the brightness temperature, T_B , and degree of circular polarization, ρ_c , of thermal cyclotron lines at different harmonics $S = 2, 3, 4$, and 5 for magnetic field strengths $H = 120, 140, 160$, and 180 G, and angles, α , of $10^\circ, 30^\circ, 60^\circ$, and 80° . These curves were generated using an electron temperature $T_e = 2 \times 10^6$ K, an electron density $N_e = 5 \times 10^9 \text{ cm}^{-3}$ and a path length $L = L_H = 1 \times 10^9 \text{ cm}$.

5 GHz are about a factor of 3 wider than those between 1 and 2 GHz. Thus, under favorable conditions, observations of active regions at closely spaced frequencies may show jumps or more complicated variations in both the total intensity and circular

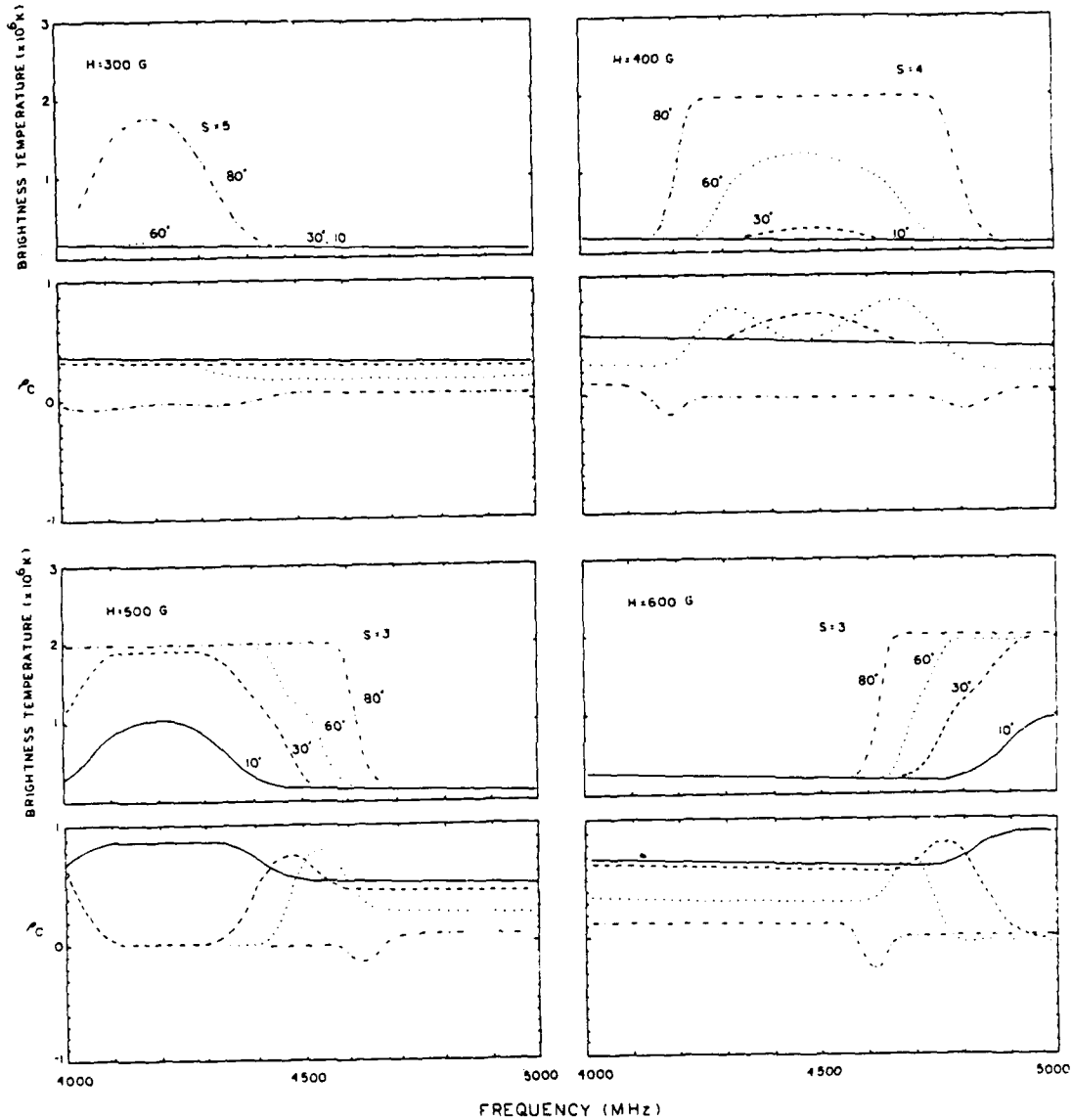


Fig. 2. Theoretical plots of the brightness temperature, T_b , and degree of circular polarization, ρ_c , of thermal cyclotron lines at different harmonics $S = 3, 4$, and 5 for magnetic field strengths $H = 300, 400, 500$, and 600 G, and angles, α , of $10^\circ, 30^\circ, 60^\circ$, and 80° . These curves were generated using an electron temperature $T_e = 2 \times 10^6$ K, an electron density $N_e = 5 \times 10^9 \text{ cm}^{-3}$ and a path length $L = L_H = 1 \times 10^9$ cm.

polarization. In the next section, we describe observations of two active regions which, in fact, show such changes, and which may be attributed to thermal cyclotron line emission.

2. Possible Detection of Thermal Cyclotron Lines

It has been shown that VLA observations of quiescent active regions at centimeter wavelengths delineate the ubiquitous coronal loops that were previously detected at X-ray wavelengths (Kundu and Velusamy, 1980; Lang *et al.*, 1982). The brightness temperatures of $T_B \approx 2 \times 10^6$ K suggested that the radio emission was due to the optically thick bremsstrahlung of a hot plasma trapped within the magnetic loops. Under this interpretation an electron density of $N_e \approx 5 \times 10^9 \text{ cm}^{-3}$ and a line-of-sight thickness of $L \approx 10^9 \text{ cm}$ are inferred. The classical expression for the bremsstrahlung optical depth, τ_B , (Equation (2)) indicates that it is very close to unity at an observing frequency of $\nu \approx 1400 \text{ MHz}$ under these conditions. We therefore planned observations at three frequencies near 1400 MHz with the hope of detecting optically thin bremsstrahlung ($\tau_B < 1$). Because the observations at these frequencies refer to the upper parts of coronal loops, the magnetic field strength may be relatively constant. There was therefore the additional hope that thermal cyclotron lines might be detected as emission that is enhanced above the optically thin bremsstrahlung.

The active regions AR 3804 and AR 3828 were observed on 19 and 28 July, 1982, respectively, with the entire VLA (B configuration) at 1380 MHz, 1540 MHz, and 1705 MHz. The position of AR 3804 was N09 W64 at 13:00 UT on 19 July and the position of AR 3828 was N06 E27 at 13:00 UT on 28 July. The active regions were successively observed for 10 min periods at the three frequencies, and this was followed by successive 2 min observations of the calibrator source O1318. The entire 36 min sequence was repeated for an eight hour period centered on local noon. At these frequencies, the half-power beamwidth of the individual antennas is $\approx 31'$ and the synthesized beamwidth is $\approx 3'' \times 4''$. In all cases the bandwidth was 12.5 MHz. The average correlated flux of 356 interferometer pairs was sampled every 10 s for both the left hand circularly polarized (LCP) and right hand circularly polarized (RCP) signals. The data were then calibrated according to the procedure described by Lang and Willson (1979) together with a correction for the difference in the signal from high temperature noise sources detected in each polarization channel. The assumed fluxes of the calibrator source O1318 at 1380, 1540, and 1705 MHz were 1.73 Jy, 1.65 Jy, respectively. At these frequencies the temperatures of the calibration noise sources are the same to within $\pm 15\%$. The calibrated data were then edited and used together with the standard CLEAN procedure to make the synthesis maps shown in Figures 3 and 4.

These maps show dramatic changes in the structure of the active regions at the three closely spaced frequencies. In Table I we give the brightness temperatures at several locations within the active regions where these temperature differences are particularly striking. The intensity within both the northern and southern components of AR 3804 (Figure 3) varies by as much as a factor of 5 at some locations at the three frequencies. AR 3828 exhibits an enhancement in only one component of the active region (A, Figure 4) where the brightness temperature at 1540 MHz is about a factor of 2.5 greater than at 1380 MHz and 1705 MHz. The V maps shown in Figure 4 indicate that the

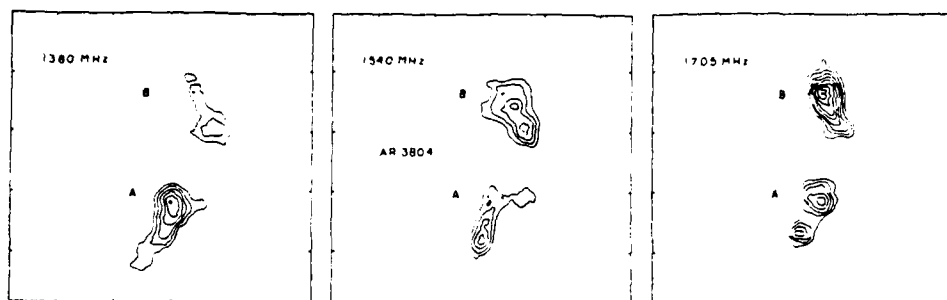


Fig. 3. VLA synthesis maps of the total intensity, I , of AR 3804 at three closely spaced frequencies using data obtained during an eight hour period on 19 July, 1982. The synthesized beamwidth is $\theta \approx 3'' \times 4''$. The contours of the map mark levels of equal brightness temperature. The outermost contour and the contour level are equal to 3.2×10^5 and 1.6×10^5 K, respectively. The positions of components A and B, referred to in the text and Table I, are marked with a cross. The angular scale can be determined from the $60''$ spacing between the fiducial marks on the axes.

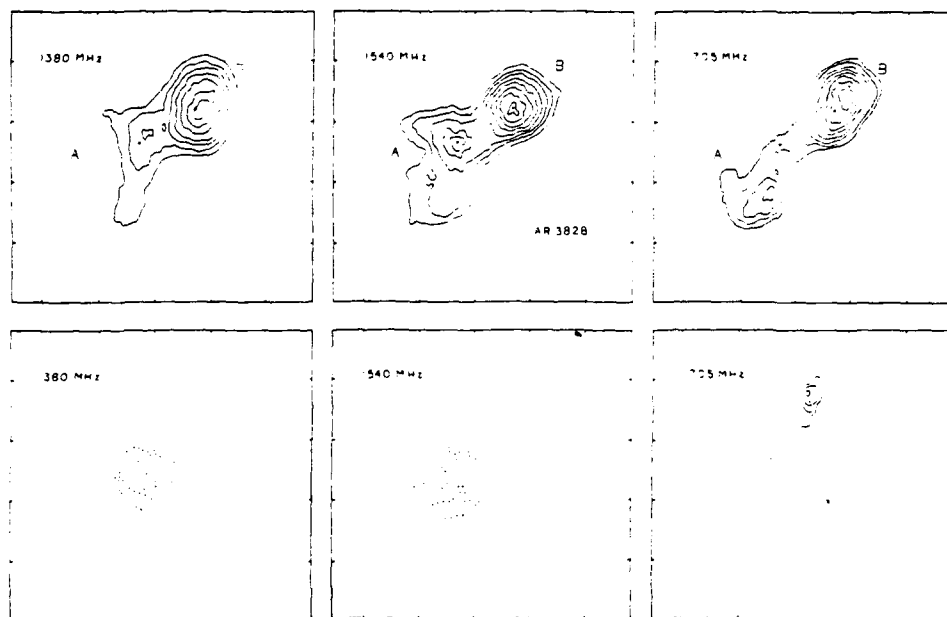


Fig. 4. VLA synthesis maps of the total intensity, I (top), and circular polarization, V (bottom) of AR 3828 at three closely spaced frequencies using data obtained during an eight hour period on 28 July, 1982. The synthesized beamwidth is $\theta \approx 3'' \times 4''$. The contours of the maps mark levels of equal brightness temperature, and the solid and dashed contours of the V maps denote positive and negative values of V , respectively. The outermost contour and the contour level of the I maps are equal to 4.3×10^5 and 2.2×10^5 K, respectively. The contours of the V maps are drawn at -3.6×10^5 , -3.2×10^5 , -2.8×10^5 ... 2.1×10^5 K. The positions of components A and B, referred to in the text and Table I, are marked with a cross. The maximum degree of circular polarization, ρ_c , is $\approx 35\%$ at each of the three frequencies in component A. The angular scale can be determined from the $30''$ spacing between the fiducial marks on the axes.

TABLE I
Maximum brightness temperatures, T_b (max), of components within AR 3804,
AR 3828, and AR 3828 NW at different frequencies

Component T_b		1380 MHz (K)	1540 MHz (K)	1705 MHz (K)
AR 3804	A	1.3×10^6	4.6×10^5	5.3×10^5
	B	3.1×10^5	4.7×10^5	1.5×10^6
AR 3828	A	6.2×10^5	1.5×10^6	6.5×10^5
	B	1.9×10^6	1.9×10^6	2.1×10^6
AR 3828 NW	A	1.2×10^6	1.4×10^6	1.4×10^6

circularly polarized emission is also enhanced in the same part of the active region where the total intensity is the highest. We were unable to detect any polarized emission from AR 3804 to a limit of $< 10\%$.

These striking changes in source structure cannot be due to an artifact of the cleaning process, as they were also visible in the uncleaned, or 'dirty' maps. If these changes were due to a systematic error in calibration or to the confusion from neighboring sources located on the Sun, then we would expect similar variations in all of the sources located within the antenna beam. For comparison, in Figure 5 we show synthesis maps of an active region located $\approx 3.2'$ W and $\approx 2.5'$ N of AR 3828 (AR 3828 NW) on 28 July. These maps of total intensity indicate that the source structure and peak brightness temperature at the three frequencies are the same to within $\approx 15\%$.

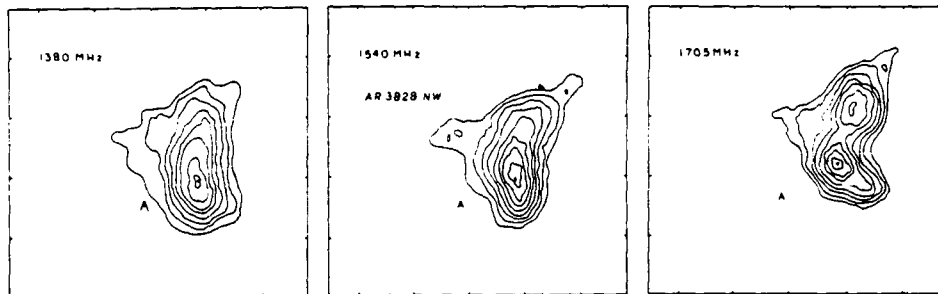


Fig. 5. VLA synthesis maps of the total intensity, I , of an active region, AR 3828 NW, located $\approx 5'$ NW of AR 3828 on 28 July, 1982. The contours of the maps mark levels of equal brightness temperature, where the outermost contour and the contour interval are equal to 2.9×10^5 and 1.4×10^5 K, respectively. The position of maximum intensity is marked with a cross. The angular scale can be determined from the $30''$ spacing between the fiducial marks on the axes.

3. Discussion

The changes in source structure are difficult to explain by the conventional radiation mechanisms of gyroemission or thermal bremsstrahlung which predict gradual changes

in brightness temperature and polarization over the observed frequency range. In the optically thick regime, the brightness temperature of a uniform source due to the bremsstrahlung and gyro-emission vary as ν^{-2} and ν^{-1} , respectively, where ν is the observing frequency. Our observations however indicate much more rapid brightness temperature variations, with $T_b \sim \nu^{\pm 5}$ for some components (see Table I). These abrupt changes in brightness temperature can, however, be explained by cyclotron line emission.

The maximum brightness temperatures as a function of frequency of components *A* and *B* of AR 3804 and component *A* of AR 3828 NW have been plotted in Figure 6 with

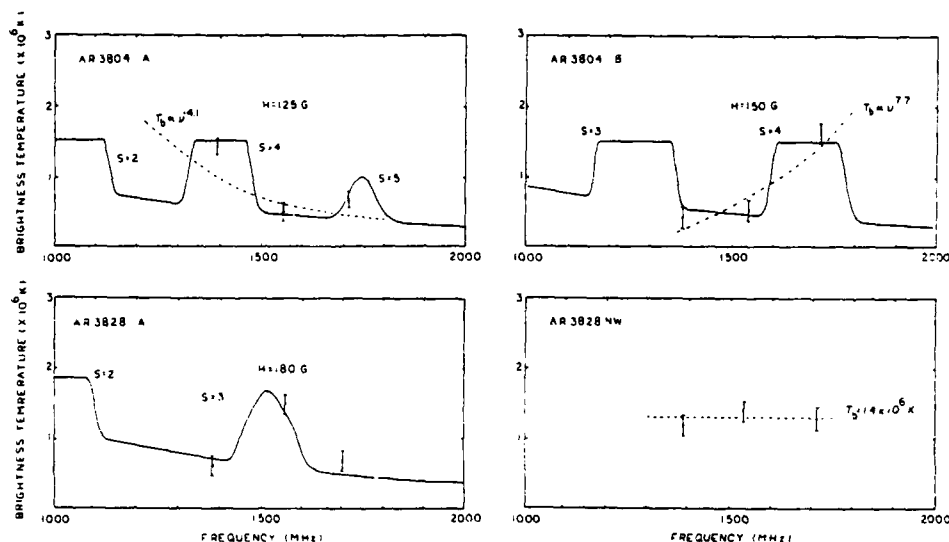


Fig. 6. Theoretical plots of the brightness temperature of thermal cyclotron lines at different harmonics $S = 2, 3, 4$, and 5 for magnetic field strengths of $H = 125, 150$, and 180 G. The maximum brightness temperatures observed for components *A* and *B* of AR 3804 and components *A* of AR 3828 and AR 3828 NW are also plotted with error bars corresponding to the peak-to-peak fluctuations in the background temperature of the synthesis maps. The theoretical curves for AR 3804 were calculated assuming an electron temperature of $T_e = 1.5 \times 10^6$ K, an electron density $N_e = 3 \times 10^9$ cm $^{-3}$, a path length $L = L_H = 1 \times 10^9$ cm, and an angle $\alpha = 80^\circ$. The curves for AR 3828 were calculated with the same values of electron density and path length but with $T_e = 1.8 \times 10^6$ K, and $\alpha = 20^\circ$. The dashed lines refer to power-law fits to the observed brightness temperatures. The data for AR 3828 NW are fit by optically thick thermal bremsstrahlung with $T_b = T_e = 1.4 \times 10^6$ K.

conservative error bars corresponding to the peak-to-peak fluctuations in the background noise temperature of the synthesis maps. We also show the brightness temperature of theoretical curves of cyclotron line emission for the harmonics $s = 3, 4$, and 5 and a number of different values of the magnetic field strength, temperature, density, scale length and angle. We find that thermal cyclotron lines can explain the observed total intensity and polarization of AR 3804 and AR 3828 with plausible physical parameters $H = 125$ – 180 G, an electron density $N_e = 3 \times 10^9$ cm $^{-3}$, an electron temperature $T_e = 1.5 \times 10^6$ K, and a scale length $L = L_H = 1 \times 10^9$ cm. The

observations of AR3828NW, can, however, be explained as either optically thick bremsstrahlung or gyro-emission with $T_b = T_e = 1.4 \times 10^6$ K. The polarization data constrain the angle α to be $\geq 80^\circ$ for AR3804 and $\approx 20^\circ$ for AR3828. Under the assumption that the magnetic field projects radially outward from the surface of the Sun into the corona, these angles are also plausible, as AR3804 and AR3828 were, respectively, near the solar limb and near central meridian, at the time of observation. These model curves are not unique, however, as the parameters can be adjusted to give acceptable agreement with the data.

There may also be alternative explanations of our data. One possibility is that the emission at each frequency originates at a different height above the active region where the physical conditions are also different. Observations at successively lower frequencies refer to successively higher levels in the solar atmosphere where the electron temperature and density and magnetic field systematically increase and decrease, respectively. The brightness temperature of optically thick emission ($T_b = T_e$) can therefore only decrease with increasing frequency, whereas the brightness temperature of optically thin emission ($T_b \approx T_e \tau$) may increase with increasing frequency. In Figure 6 we show power law fits to the brightness temperatures of components A and B of AR3804. For component A, $T_b \sim \nu^{-4.1}$ so that the decrease in brightness temperatures might be attributed to an optically thick source in which the temperature systematically decreases with decreasing height. For component B, $T_b \sim \nu^{+7.7}$, suggesting an optically thin source in which the temperature or the density or both change with height. This alternative explanation however, cannot explain the observations of AR3828 which show neither a systematic increase or decrease of the brightness temperature with frequency. Because thermal cyclotron lines can explain the observed data with plausible physical parameters while conventional radiation mechanisms cannot, we believe that we have a possible detection of cyclotron lines. This has important implications for the combined measurements of bremsstrahlung and cyclotron lines provide a sensitive probe of the physical properties of coronal loops. For instance, it is known that the electron temperature of quiescent coronal loops have a narrow range of temperature between 1 and 3×10^6 K. A measurement of the electron temperature, say using the Solar Maximum Mission X-ray instruments (when it is repaired in 1984) combined with VLA observations of the radio brightness temperature and bremsstrahlung optical depth will give a reliable measurement of the emission measure. As illustrated in Figures 1, 2, and 6, the central frequencies of the cyclotron lines provide a sensitive measurement of the magnetic field strength, for a change of only 20 G produces a 170 MHz shift in the central frequency of the line. Carefully calibrated, high resolution maps of the total intensity and circular polarization of active regions at uniformly spaced frequencies over a frequency range of ≈ 1 GHz may provide a detailed description of the magnetic field, temperature and density of the active region. Measurements of these effects can probably best be made with the VLA which provides sufficient angular resolution to resolve the different sources of cyclotron lines. The poorer angular resolution of single antennas would combine the signals from different sources, and the cyclotron lines might be lost in the superposition of the different sources which radiate at different frequencies.

Acknowledgements

The author wishes to thank Kenneth R. Lang for helpful discussions. Radio interferometric studies at Tufts University are supported under grant AFOSR-83-0019 with the Air Force Office of Scientific Research. The VLA is operated by Associated Universities, Inc., under contract with the National Science Foundation.

References

- Alissandrakis, C. E., Kundu, M. R., and Lantos, P.: 1980, *Astron. Astrophys.* **82**, 30.
 Enome, S., Kakinuma, T., and Tanaka, H.: 1969, *Solar Phys.* **6**, 428.
 Gel'freikh, G. B. and Lubyshev, B. I.: 1979, *Soviet Astron. A.J.* **23**, 316.
 Ginzburg, V. L. and Zheleznyakov, V. V.: 1959, *Soviet Astron. A.J.* **3**, 235.
 Kakinuma, T. and Swarup, G.: 1962, *Astrophys. J.* **136**, 975.
 Kaverin, N. S., Kobrin, M. M., Kovshunov, A. I., and Sushunov, V. V.: 1980, *Soviet Astron. A.J.* **24**, 442.
 Kundu, M. R.: 1959, *Ann. Astrophys.* **22**, 1.
 Kundu, M. R. and Velusamy, T.: 1980, *Astrophys. J. Letters* **240**, L63.
 Kundu, M. R., Schmahl, E. J., and Rao, A. P.: 1981, *Astron. Astrophys.* **94**, 72.
 Kuznetsov, V. D. and Syrovatskii, S. I.: 1981, *Solar Phys.* **69**, 361.
 Lang, K. R.: 1974, *Solar Phys.* **36**, 351.
 Lang, K. R. and Willson, R. F.: 1979, *Nature* **278**, 24.
 Lang, K. R. and Willson, R. F.: 1982, *Astrophys. J. Letters* **255**, L111.
 Lang, K. R., Willson, R. F., and Rayrole, J.: 1982, *Astrophys. J.* **258**, 384.
 Lang, K. R., Willson, R. F., and Gaizauskas, V.: 1983, *Astrophys. J.* **267**, 455.
 Pallavicini, R., Sakurai, T., and Vaiana, G. S.: 1981, *Astron. Astrophys.* **98**, 316.
 Stepanov, K. N.: 1959, *Soviet Phys. JETP* **8**, 195.
 Syrovatskii, S. I. and Kuznetsov, V. D.: 1980, in M. R. Kundu and T. E. Gergely (eds.), 'Radio Physics of the Sun', *IAU Symp.* **86**, 109.
 Zheleznyakov, V. V.: 1962, *Soviet Astron. A.J.* **6**, 3.
 Zheleznyakov, V. V.: 1970, in *Radio Physics of the Sun and Planets*, New York, Pergamon Press.
 Zheleznyakov, V. V. and Tikhomorov, Yu. V.: 1982, *Solar Phys.* **81**, 121.
 Zheleznyakov, V. V. and Zlotnik, E. Ya.: 1980a, *Solar Phys.* **68**, 317.
 Zheleznyakov, V. V. and Zlotnik, E. Ya.: 1980b, *Soviet Astron. A.J.* **24**, 448.

7. OBSERVATIONS OF PREBURST HEATING AND MAGNETIC FIELD CHANGES IN A CORONAL LOOP AT 20 cm WAVELENGTH

ROBERT F. WILLSON

Department of Physics, Tufts University, Medford, MA 02155, U.S.A.

(Received 12 December, 1983; in revised form 27 February, 1984)

Abstract. The Very Large Array (VLA) has been used at 20 cm wavelength to study the evolution of a burst loop with 4" resolution on timescales as short as 10 s. The VLA observations show that the coronal loop began to heat up and change its structure about 15 min before the eruption of two impulsive bursts. The first of these bursts occurred near the top of the loop that underwent preburst heating, while the second burst probably occurred along the legs of an adjacent loop. These observations evoke flare models in which coronal loops twist, develop magnetic instabilities and then erupt. We also combine the VLA observations with GOES X-ray data to derive a peak electron temperature of $T_e = 2.5 \times 10^7$ K and an average electron density of $N_e \approx 1 \times 10^{10} \text{ cm}^{-3}$ in the coronal loop during the preburst heating phase.

1. Introduction

High resolution VLA observations of centimeter radio bursts have recently provided a wealth of new information about the flare emission process. Of special interest are the changes in both intensity and circular polarization which are sometimes observed on timescales of minutes to tens of minutes before the onset of the impulsive phase. These changes are thought to be related to preburst heating and the reorientation or emergence of magnetic flux in coronal loops. Willson (1983), for example, recently observed a coronal loop that began to heat up about 2 min before the eruption of one 6 cm burst. By comparing the preburst VLA snapshot maps with the locations of the $H\alpha$ flare kernels, he argued that the loop was heated in the legs, rather than at the top where the impulsive energy release took place. Kundu *et al.* (1982) have also observed an active region in which a quadruple magnetic loop structure may have emerged a few tens of seconds before a 6 cm burst, and which they believe may be related to the impulsive energy release. More recent 21 cm VLA observations by Willson and Lang (1984) showed evidence for preburst heating and magnetic field changes in burst sources that were spatially separated from the sites of the impulsive sources. These radio wavelength results are similar to those that have been detected at X-ray wavelengths in which adjacent loops brighten and perhaps trigger the eruption of other bursts (Vorpahl *et al.*, 1975; Kahler *et al.*, 1975; Kahler *et al.*, 1976). It is unclear however, that preburst heating is a general property of all solar bursts, for Kahler (1979) and Wolfson (1982) have found that soft X-ray bursts of weak to moderate strength ($\leq 1.5 \times 10^{25} \text{ erg s}^{-1}$, a C5 level in the Solrad and GOES classification schemes) are typically not preceded by an enhancement in the X-ray flux. Nevertheless, many theoretical models of solar flares include a preflare phase in which the coronal loop is heated, becomes unstable

and then erupts, giving rise to the impulsive phase (Heyvaerts *et al.*, 1977; Spicer, 1981; Somov and Syrovatskii, 1982). High resolution observations of the preburst evolution of coronal loops may therefore place useful constraints on these models as well as allow comparisons with other preflare phenomena, such as filament eruption, preflare vortical structure, H α and X-ray brightening and coronal transients, for which direct association with flares has been implied (cf. Martin, 1980).

In this paper we present 20 cm VLA observations of an active region that underwent significant structural changes before the eruption phase of two spikelike bursts. The radio observations are compared with simultaneous X-ray and H α observations which also show evidence for preburst activity. We also discuss these results in light of theoretical models that have been proposed for the preburst heating of coronal loops and the triggering of bursts. Finally, we combine the radio and X-ray data to estimate the kinetic temperature and electron density in the coronal loop that underwent these preburst changes.

2. Observations

The Very Large Array (B configuration) was used to observe the active region AR 3806 on July 13, 1982. The location of AR 3806 at 13:00 UT on this day was S23, E06. The entire VLA, consisting of 27 antennas was used to observe for successive 15 min periods at wavelengths of 21.7 and 17.6 cm (1377 MHz and 1698 MHz). At these wavelengths, the half power beamwidth of the individual 25 m antennas is $\sim 31'$ and the synthesized beamwidth is $\sim 3'' \times 4''$. Each 15 min solar observation was followed by a 2 min observation of the calibrator source OI318 whose flux was assumed to be 1.7 Jy. The data were calibrated according to the procedure given by Lang and Willson (1979). These data were then used to produce synthesis maps of the total intensity $I = (RCP + LCP)/2$ and circular polarization, $V = (RCP - LCP)/2$, (where RCP and LCP denote the right and left handed circularly polarized signals) of the preburst, impulsive and postburst phases at intervals as short as 10 s. Finally, these maps were cleaned to produce microwave images with a dynamic range of about 10:1.

Figure 1 shows the time profile of the radio burst together with the profiles of X-ray emission in the 1.6–12.5 keV and 3.1–25 keV energy bands as observed by the GOES X-ray satellite. This burst was classified as a type M1.1 event by *Solar Geophysical Data*. The X-ray profiles are similar for the two bands; both show a rapid increase beginning $\sim 21:40$ UT with a peak near 21:50 UT followed by a more gradual decrease lasting nearly half an hour. This X-ray burst was also accompanied by H α brightenings which also began $\sim 21:40$ UT (see below).

The radio burst profile has a different structure with two impulsive spikes of less than 10 s in duration at 21:58:10 UT and 22:00:50 UT. These spikes, which do not have X-ray counterparts, are also superimposed on a more gradual intensity increase that may also have begun as early as 21:40 UT.

In Figure 2 we show a series of VLA snapshot maps of both I and V which depict the evolution of the active region about 30 min before the first impulsive radio burst.

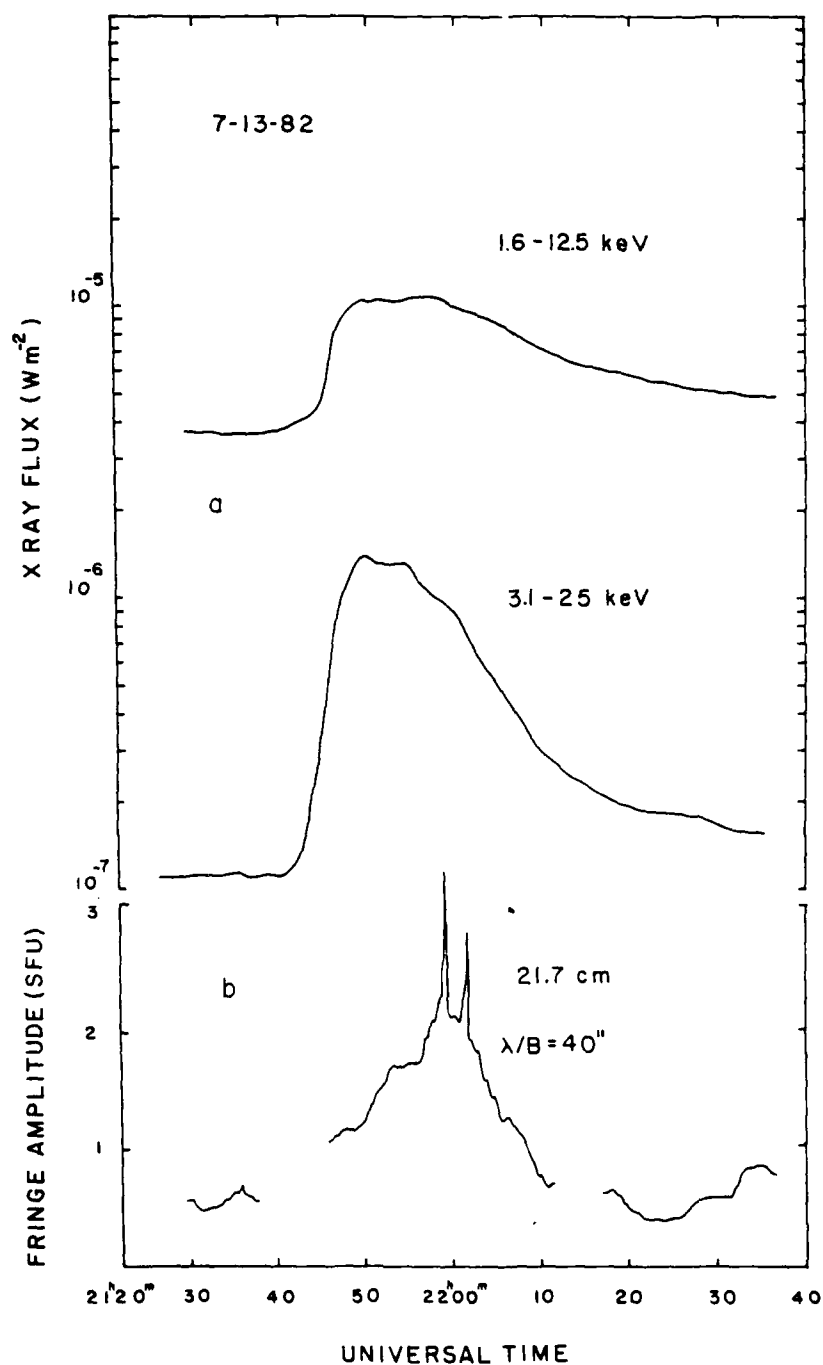


Fig. 1. (a) Time profiles in the 1.6–12.5 keV and 3.1–25 keV energy bands of X-rays as observed by the GOES satellite during the burst on July 13, 1982. (b) The fringe amplitude, versus time, of the total intensity I , for the burst detected at 20 cm wavelength at the VLA on a baseline of 40'' fringe spacing.

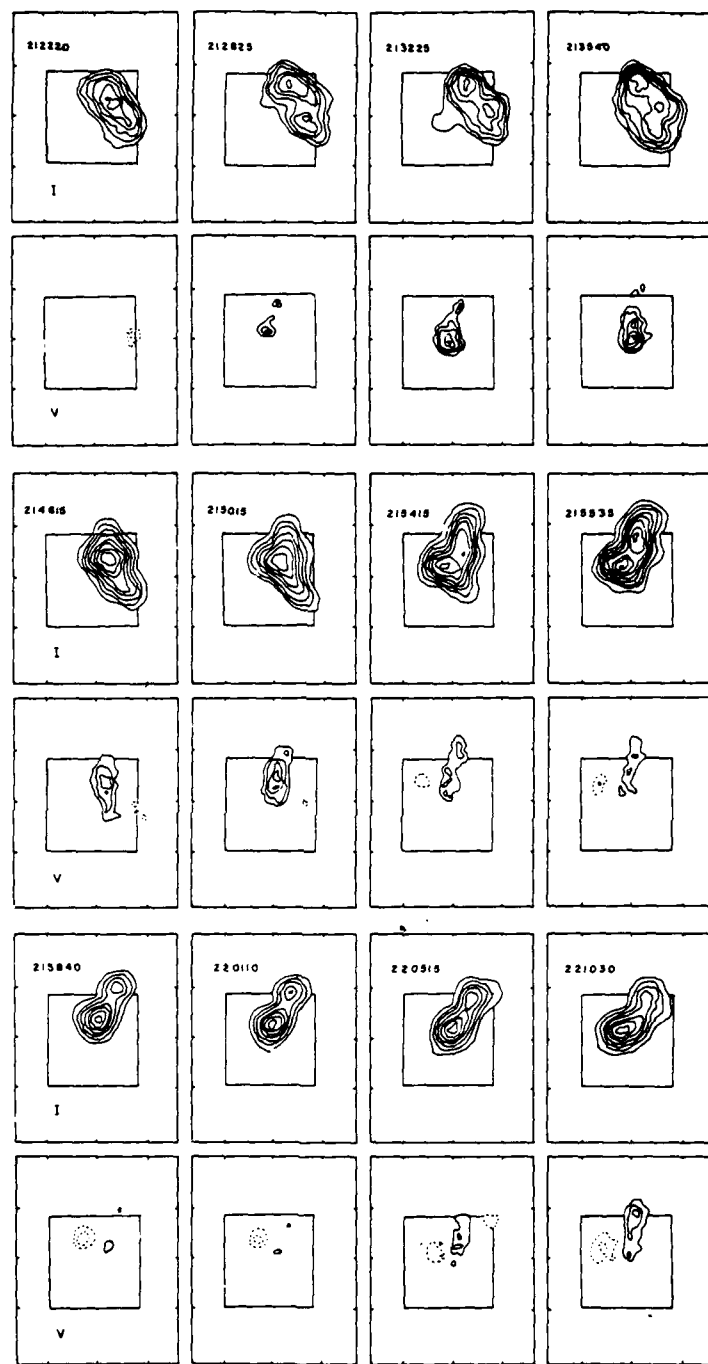


Fig. 2. A series of VLA maps of total intensity I , and circular polarization V , for the burst shown in Figure 1. Each map was made from 2 min of data beginning at the time indicated. Here north is up and east is to the left. The contours of both sets of maps mark levels of equal brightness temperature and the solid and dashed line, of the V maps denote positive and negative values of V , respectively. The outermost contour and the contour interval of the I maps are both equal to 4×10^5 K. The outermost contour and contour interval of the V maps are equal to 4×10^5 K and 2×10^5 K, respectively. The angular scale is determined from the $60''$ spacing between the fiducial marks on the axes. The area within the boxes corresponds to the field of view of the 10 s snapshot maps of the two impulsive sources which are shown in Figure 4.

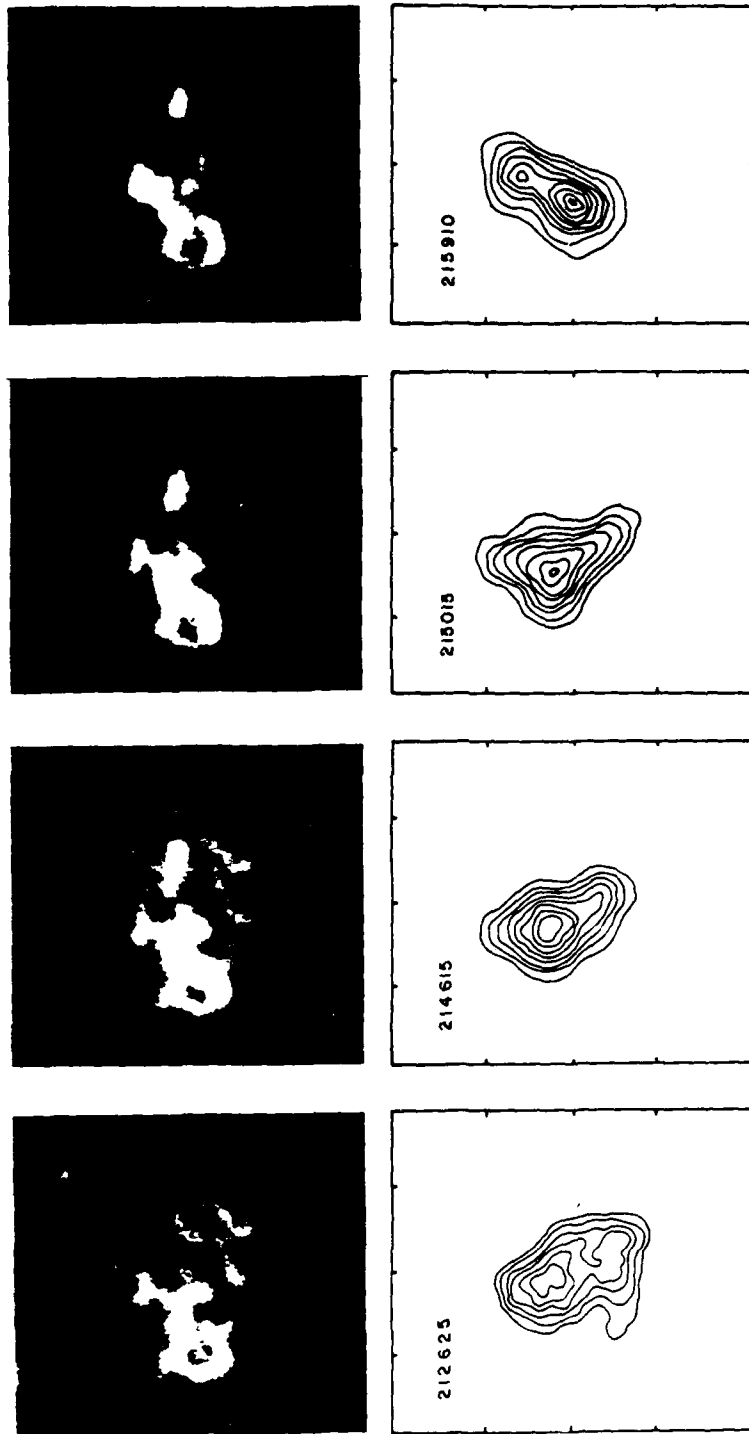


Fig. 3. Simultaneous $H\alpha$ photographs (top) and VLA synthesis maps (bottom) of total intensity during the gradual phase of the burst shown in Figure 1. The contour of the radio maps are the same as those given in Figure 2. The $H\alpha$ photographs were taken at the Big Bear Solar Observatory (courtesy of Frances Tang). The angular scales of both sets of pictures can be determined from the 60'' spacing between the fiducial marks on the radio maps. Note that both the optical and radio data indicate significant changes during the gradual phase of the burst.

Each map was made from 2 min of data beginning at the time indicated. Between 21:22 and 21:50 UT the radio emission is contained within a looplike structure of about $1.5'$ in length with a NE-SW orientation. During this time interval, the peak brightness temperature gradually increased from $\sim 2 \times 10^6$ K to 3.5×10^6 K, while the circular polarization increased from $\leq 20\%$ to $\sim 60\%$. A comparison with a Kitt Peak magnetogram taken at 13:50:26 UT indicated that the source bridges regions of opposite magnetic polarity, suggesting a magnetically confined coronal loop. At $\sim 21:50$ UT, and well after the start of the X-ray burst, the loop began to twist in a clockwise direction, developed a second intensity peak, and finally became oriented in a NW-SE direction. Maps of the post-impulsive phase also show a looplike structure, oriented

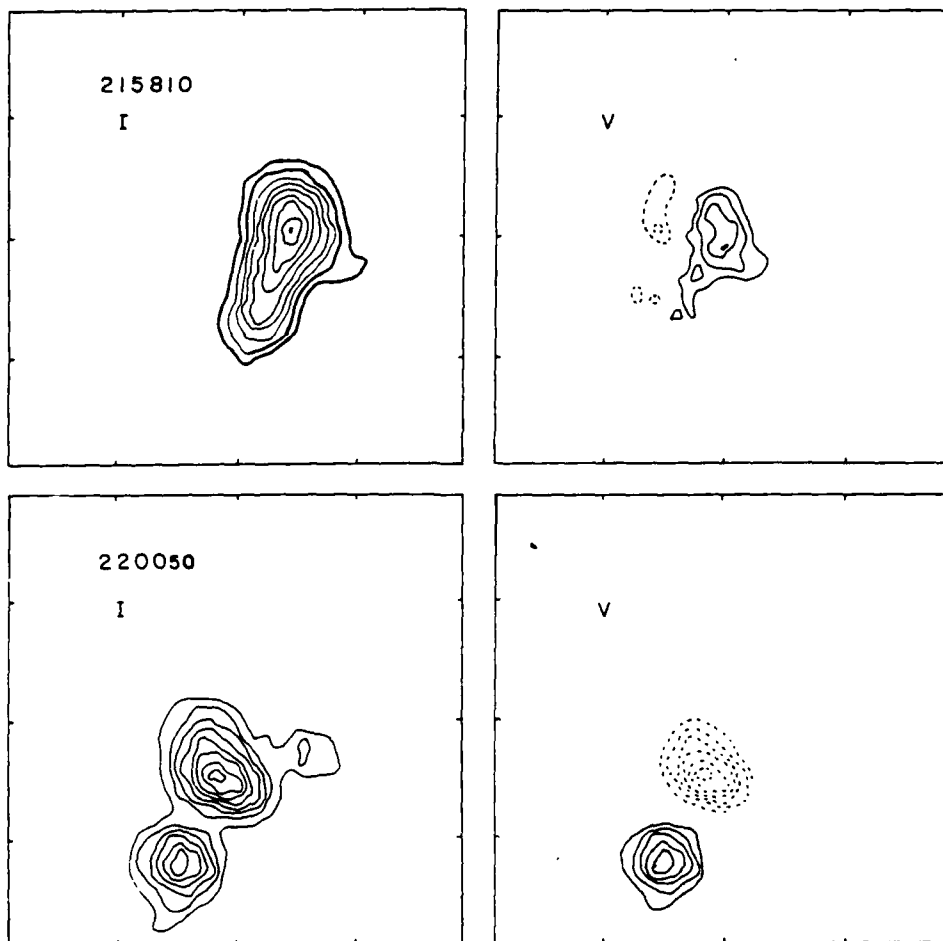


Fig. 4. VLA 10s snapshot maps of the total intensity I , and circular polarization V , for the two impulsive bursts shown in Figure 1. The outermost contour and contour interval of the I maps are both equal to 3.5×10^6 K and 1.7×10^6 K, respectively. The angular scale is determined by the $30''$ spacing between the fiducial marks on the axes.

NW-SE, whose peak brightness temperature decreased steadily from $\sim 2.5 \times 10^6$ K at 22:05 UT to $\sim 1.5 \times 10^6$ K at 22:20 UT.

The GOES X-ray data are spatially unresolved and thus it is impossible to compare the morphologies of the radio and X-ray sources. We have, however, made a comparison between the radio maps and simultaneous Big Bear Solar Observatory H α data (courtesy of Frances Tang) which also show evidence for preflare changes. This comparison is shown in Figure 3 where the uncertainty in alignment between the radio and optical images is $\sim \pm 5''$. The first panel, at 21:20 UT, shows the preflare H α emission in which the plage is concentrated mainly in the eastern half of the region. The next three panels show that the H α brightenings occurred primarily in the plage, with a fainter brightening near the large spot in the west. In contrast, the radio emission was most intense $\sim 10''$ - $20''$ to the west of the strongest H α brightenings. This shift in position of the radio emission with respect to the underlying H α emission suggests that the radio wavelength heating occurred in the upper regions of a coronal loop that connects the large spot and the bright plage.

In Figure 4 we show maps of the two impulsive bursts. These 10 s snapshot maps cover the smaller field of view contained within the boxes shown in Figure 2. The first impulsive spike at 21:58:10 UT has a peak brightness temperature of 3.1×10^7 K and a looplike structure of $\sim 30''$ in size which is nearly spatially coincident with the most intense peak of the preburst loop. The second, less intense, burst at 22:00:50 UT is shifted $\sim 30''$ to the south of the first and consists of two compact ($\theta \sim 10''$ - $15''$) oppositely polarized sources (pc $\sim 100\%$) with peak brightness temperatures of $\sim 2.5 \times 10^7$ K. The bipolar structure of these sources as well as their separation from the preburst emission suggests that they are located near the footpoints of an adjacent loop that may have become activated by the eruption of the larger loop to the north. A similar pattern of multiple burst emission has been observed at 20 cm by Willson and Lang (1984) in which sequential triggering of burst loops may have occurred in a magnetically complicated region.

3. Discussion

Our observations show that the active region underwent significant changes before the eruption of the two impulsive bursts. In this case a large ($L \sim 6 \times 10^9$ cm) 20 cm loop began to twist and heat up about 15 min before these bursts occurred. These dramatic structural changes were also accompanied by changes in circular polarization suggesting the reorientation or emergence of magnetic fields in the loop. An interesting feature of these changes is their large physical scale. Other high resolution radio studies of the preburst state of active regions have, for example, revealed changes in both intensity and circular polarization (Kundu *et al.*, 1982; Willson and Lang, 1984) but these changes appear to have occurred on angular scales of a few to tens of arc seconds ($L \sim 10^8$ - 10^9 cm) and therefore involved changes in much smaller loops.

The changes seen in this loop are reminiscent of flare models in which coronal loops twist and develop kinks in response to motions in the photospheric footprints (Priest,

1983). In these models, the loop slowly heats up and remains stable until the twist exceeds a critical value (Raadu, 1972; Giachetti *et al.*, 1977; Hood and Priest, 1979) after which the loop is heated explosively (Spicer, 1977). The fact that the first of the impulsive bursts occurred within the loop that appeared to twist and heat up lends support to these models. Unfortunately, there are no simultaneous optical wavelength magnetograms that would allow us to check for the presence of such motions in the photosphere.

On the other hand, the fact that the second impulsive burst appears to have occurred in an adjacent loop lends support to the interacting loop model developed by Emslie (1982) in which an energy release in one loop triggers, through a magnetohydrodynamic disturbance, an energy release in a neighboring loop. In this case, the second loop did not show a gradual heating phase, and in fact was invisible on the 20 cm maps before and after it erupted.

The bipolar structure of this burst also provides evidence that microwave sources do not always lie at the top of loops as has been observed, for example, at 1.3 and 2.0 cm by Marsh and Hurford (1980) and 6 and 20 cm by Willson (1983) but they may also occur along the legs or near the footpoints as has been observed at 6 cm by Kundu *et al.* (1982). Petrosian (1982) has shown, for example, that if the magnetic field strength increases very rapidly from the top of the loop to the footpoints, or if the accelerated particles injected in the loop have an anisotropic distribution of pitch angles, then the microwave brightness can be greatest near the footpoints, as in the case for this burst.

Our observations of preburst heating were also accompanied by an enhancement of the soft X-ray flux. This is not surprising since theoretical investigations by Mätzler (1978) and Dulk *et al.* (1979) indicate that X-ray and radio bursts may arise from the same population of thermal or non-thermal electrons. In this case, it is possible to estimate the temperature and density of the loop by combining the radio and X-ray data. Marsh *et al.* (1981) and Hoyng *et al.* (1983) have analyzed several bursts and concluded that the microwave and *hard* X-rays are probably *not* produced by a common population of either thermal or non-thermal electrons. However, Hoyng *et al.* (1981) and Duijve-man and Hoyng (1983) have found that the soft (3.5–5.5 keV) and hard (16–30 keV) X-rays originate in different parts of the flare loop, with the former originating at the top of the loop and the latter near the footpoints. In the following analysis, we therefore assume that the soft X-ray enhancement, which represents the thermal phase of the burst, occurred in the 20 cm loop and that the X-ray and microwave sources therefore share a common temperature and density. This assumption is probably not valid for the two impulsive bursts which do not have soft X-ray counterparts and which therefore likely arise from a different population of electrons.

A recently shown by Schmahl (1984 and personal communication) the kinetic temperature of the X-ray emitting plasma can be estimated directly from the ratio of the flares in the two GOES energy channels. His technique uses the spectra of Raymond and Smith (1977) and Mewe and Gronenschild (1981). Near the peak of the X-ray enhancement at 21:50 UT the ratio $I(1-8 \text{ \AA})/I(0.5-4 \text{ \AA}) \sim 6.1$ corresponds to a temperature of $\sim 1 \times 10^7 \text{ K}$. By 22:10 UT, this ratio had decreased to ~ 20 , corresponding to a

lower temperature of $\sim 5 \times 10^7$ K. Because these temperatures are higher than the 20 cm brightness temperatures of between 1.5×10^6 and 3.5×10^6 K, we infer that the radio emission is optically thin. Comparing the X-ray and radio brightness temperatures throughout the gradual burst, we find that the 20 cm optical depth increased from 0.32 at 21:50 UT to 0.65 at 22:10 UT. These results are consistent with the relatively high degree of circular polarization which also requires that the 20 cm loop be optically thin. Finally, assuming that the loop geometry is a cylinder of length $L \approx 6.5 \times 10^9$ cm and radius $R \sim 1 \times 10^9$ cm, we derive an average electron density of $N_e \sim 9.0 \times 10^9 \text{ cm}^{-3}$, consistent with the densities typically found in pre-impulsive X-ray burst loops (Dere *et al.*, 1977; McKenzie *et al.*, 1980; Moore *et al.*, 1980).

Acknowledgements

Solar radio astronomy at Tufts University is supported under grant AFOSR-83-0019 with the Air Force Office of Scientific Research. The author is grateful to Frances Tang of the Big Bear Solar Observatory for providing the H α photographs. He also thanks Kenneth Lang for useful discussions. The Very Large Array is operated by Associated Universities, Inc., under contract with the National Science Foundation.

References

- Dere, K. P., Horan, M., and Kreplin, R. W.: 1977, *Astrophys. J.* **217**, 976.
 Duijveman, A. and Hoyng, P.: 1983, *Solar Phys.* **86**, 279.
 Dulk, G. A., Melrose, D. B., and White, S. M.: 1979, *Astrophys. J.* **234**, 1137.
 Giachetti, R., Van Hoven, G., and Chivderi, C.: 1977, *Solar Phys.* **55**, 371.
 Heyvaerts, J., Priest, E. R., and Rust, D. M.: 1977, *Astrophys. J.* **216**, 123.
 Hood, A. W. and Priest, E. R.: 1979, *Solar Phys.* **64**, 303.
 Hoyng, P. *et al.*: 1981, *Astrophys. J. Letters* **244**, L153.
 Hoyng, P., Marsh, K. A., Zirin, H., and Dennis, B. R.: 1983, *Astrophys. J.* **268**, 865.
 Kahler, S. W.: 1979, *Solar Phys.* **62**, 347.
 Kahler, S. W., Krieger, A. S., and Vaina, G. S.: 1975, *Astrophys. J. Letters* **199**, L57.
 Kahler, S. W., Petrasso, R. D., and Kane, S. R.: 1976, *Solar Phys.* **50**, 179.
 Kundu, M. R., Schmahl, E. J., Velusamy, T., and Vlahos, L.: 1982, *Astron. Astrophys.* **108**, 188.
 Landini, M. and Monsignori-Fossi, B. C.: 1979, *Astron. Astrophys.* **72**, 171.
 Marsh, K. A., Hurford, G. J., Zirin, H., Dulk, G. A., Dennis, B. R., Frost, K. J., and Orwig, L. E.: 1981, *Astrophys. J.* **251**, 797.
 Martin, S.: 1980, *Solar Phys.* **68**, 217.
 Mätzler, C.: 1978, *Astron. Astrophys.* **70**, 181.
 McKenzie, D. L., Broussard, R. M., Landecker, P. B., Rugge, H. R., and Young, R. M.: 1980, *Astrophys. J. Letters* **238**, L43.
 Mewe, R. and Gronenschild, E. H. B. M.: 1981, *Astron. Astrophys. Suppl. Ser.* **45**, 11.
 Moore, R., McKenzie, D. L., Švestka, Z., Widing, K. G., and 12 co-authors: 1980, in P. A. Sturrock (ed.), *Solar Flares*, Colorado Associated University Press, p. 341.
 Priest, E. R.: 1983, *Solar Phys.* **86**, 33.
 Raadu, M. A.: 1972, *Solar Phys.* **22**, 425.
 Raymond, J. C. and Smith, B. W.: 1977, *Astrophys. J. Suppl. Ser.* **35**, 419.
 Schmahl, E. J.: 1984, *Bull. Am. Astron. Soc.* (Jan. 1984 meeting).
 Somov, B. V. and Syrovatskii, S. I.: 1982, *Solar Phys.* **75**, 237.

- Spicer, D. S.: 1977, *Solar Phys.* 53, 305.
Spicer, D. S.: 1981, *Solar Phys.* 70, 149.
Willson, R. F.: 1983, *Solar Phys.* 83, 285.
Willson, R. F. and Lang, K. R.: 1984, *Astrophys. J.* (to be published).
Wolfson, C. J.: 1982, *Solar Phys.* 76, 377.

8. VERY LARGE ARRAY OBSERVATIONS OF SOLAR ACTIVE REGIONS. IV. STRUCTURE AND EVOLUTION OF RADIO BURSTS FROM 20 CENTIMETER LOOPS

ROBERT F. WILLSON AND KENNETH R. LANG

Department of Physics, Tufts University

Received 1983 April 18; accepted 1983 September 19

ABSTRACT

The Very Large Array (VLA) has been used to study the structure and evolution of six solar bursts near 20 cm wavelength. In most cases the burst emission has been resolved into looplike structures with total lengths, $L \sim 3 \times 10^9$ cm, brightness temperatures $T_B \sim 10^7$ – 10^8 K, and degrees of circular polarization $p_c \lesssim 90\%$. Changes in the total intensity and circular polarization of the bursts occur on time scales as short as 10 s. The individual peaks of one multiple-component burst originated in different locations within a magnetically complicated region. Preburst heating occurred minutes before the onset of the impulsive phase of one burst, and circular polarization changes occurred minutes before the onset of the impulsive phase of another burst. In one case, a loop system emerged in the vicinity of the impulsive source, and two adjacent loop systems may have emerged and triggered the burst.

Subject headings: interferometry — polarization — Sun: radio radiation

1. INTRODUCTION

Centimeter wavelength ($\lambda = 2$ cm or 6 cm) observations with the Very Large Array (VLA) at high angular resolution ($\theta \geq 1''$) and moderate time resolution ($\tau \approx 10$ s) have provided new insights into the physics of solar radio bursts. The radio bursts are usually located above magnetic neutral lines rather than sunspots, while the H α flares often occur near the sunspots (Alissandrakis and Kundu 1978; Marsh, Zirin, and Hurford 1979; Marsh and Hurford 1980; Lang, Willson, and Felli 1981; Willson 1983). The total intensity and circular polarization of the radio emission often change before the bursts, suggesting that they are triggered by preburst heating or by magnetic changes. Variations in the distribution of circular polarization also reflect changes in the magnetic field configuration during solar bursts (Kundu, Bobrowsky, and Velusamy 1982; Velusamy and Kundu 1982; Willson 1983). The observations at $\lambda = 2$ cm and 6 cm therefore suggest that radio bursts are emitted near the apices of magnetic loops, rather than at their feet and that either preburst heating within loops or emerging loops trigger burst emission.

There have been comparatively few VLA observations of solar bursts at the longer 20 cm wavelength. Observations of the quiescent emission from solar active regions at $\lambda = 20$ cm delineate looplike structures which are the radio wavelength counterpart of the ubiquitous coronal loops detected at soft X-ray wavelengths (Lang, Willson, and Rayrole 1982). Velusamy and Kundu (1981) have reported the detection of a postflare loop at $\lambda = 20$ cm, and Lang, Willson, and Felli (1981) have shown that some 20 cm bursts have small angular sizes $\theta \sim 3''$ – $5''$ and brightness temperatures $T_B \sim 2 \times 10^7$ K that are similar to those of hard X-ray kernels and soft X-ray bursts. The 20 cm data are nevertheless meager, and in this paper we therefore present a VLA analysis of six bursts from 20 cm loops. In § II we present time profiles and 10 s snapshot maps that describe the evolution of the 20 cm bursts, preburst heating, and changes in magnetic structure before and

during the bursts. The angular sizes $\theta \sim 20''$ – $60''$, total linear extents $L \sim (0.7$ – $5) \times 10^9$ cm and brightness temperatures $T_B \sim (2$ – $20) \times 10^7$ K of the 20 cm bursts are similar to those observed at soft X-ray wavelengths. In § III we discuss the implications of our observations and place them within the framework of other observational and theoretical work.

II. OBSERVATIONS OF RADIO BURSTS FROM 20 CENTIMETER LOOPS

The Very Large Array (B configuration) was used to observe the active region AR 3804 on 1982 July 12–20 at 1380 MHz, 1540 MHz, or 1705 MHz (or wavelengths $\lambda = 21.7$, 19.4, and 17.6 cm). On July 12 the active region was observed for successive 10 minute periods at 1380 MHz and 1705 MHz, while on July 19 and 20 the region was observed at all three frequencies for successive 10 minute intervals. At these

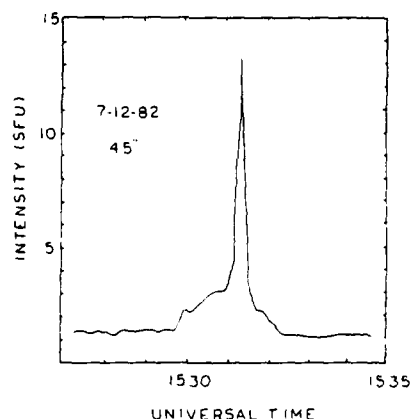


FIG. 1. — The fringe amplitude and total intensity, I , vs. time for a spikelike burst detected at 20 cm wavelength with an interferometer pair with angular resolution $\theta = 45''$ on 1982 July 12.



FIG. 2.—A series of 10 s snapshot maps of the total intensity, I , and circular polarization, V , for the burst shown in Fig. 1. The contours of the map mark levels of equal brightness temperature, and the solid and dashed contours of the V maps denote positive and negative values of V , respectively. The development of the gradual burst emission is shown on the left-hand side. Maps of the impulsive phase are shown on the right-hand side. The outermost contour level and the contour interval of the gradual component maps are 2.4×10^6 K and 1.2×10^6 K, respectively. The outermost contour and contour interval of the impulsive phase maps are both equal to 7.2×10^6 K. The angular scale can be determined from the $30''$ spacing between the fiducial marks on the axes.

TABLE 1
OBSERVED PARAMETERS OF SOLAR BURSTS NEAR 20 CENTIMETER WAVELENGTH

Date	Time (UT)	Wavelength (cm)	Maximum Brightness Temperature (K)	Maximum Circular Polarization (percent)	Angular Size (arcsec)
1982 Jul 12	15:31-15:32	21.7	1.5×10^8	~90	~45
1982 Jul 12	19:05-19:09	17.6	1.4×10^8	~70	~30
1982 Jul 12	20:03-20:07	21.7	2.0×10^7	~20	~40
1982 Jul 19	18:41-18:43	19.4	1.2×10^7	~40	~60
1982 Jul 20	21:49-21:51	19.4	1.3×10^7	~60	~60
1982 Jul 20	23:10-23:12	17.6	4.9×10^7	~25	~45

frequencies the half-power beamwidth of the individual antenna is $\sim 31'$ and the synthesized beamwidth was $3'' \times 4''$. Each 10 minute observation was followed by a 2 minute observation of the calibrator source OI 318. In all cases the bandwidth was 12.5 MHz, and the assumed calibrator flux was 1.7 Jy. The average correlated flux of 356 interferometer pairs was sampled every 10 s for both the left-hand circularly polarized (LCP) and right-hand circularly polarized (RCP) signals. The amplitude and phase of the correlated signal were then calibrated according to the procedure described by Lang and Willson (1979) together with a correction for the difference in the signal from high temperature noise sources detected in each polarization channel. These data were then edited and used to produce synthesis maps of both the total intensity, $I = (RCP + LCP)/2$ and circular polarization $V = (RCP - LCP)/2$ of the burst emission at intervals of 10 s. The CLEAN procedure developed by Clark (1980) was then used to produce synthesis maps with a dynamic range of about 10:1.

The date, time, observing wavelength, maximum brightness temperature and maximum degree of circular polarization, and angular size for six bursts are given in Table 1. In Figure 1 we show the time profile of the spikelike burst on July 12. The rapid impulsive spike lasting ~ 60 s is superposed on a more gradual component lasting about 2 minutes. In Figure 2 we present 10 s snapshot maps of both the total intensity, I , and circular polarization, V , for both of these components. The impulsive spike consists of two components of unequal

intensity and size that are separated by about $45''$ and which are nearly 100% oppositely circularly polarized. These two components are also connected by a bridge of weaker, unpolarized emission. The gradual component, which began about 1 minute before the impulsive spike, is contained within an adjacent source having a peak brightness temperature of $T_B \sim 6 \times 10^6$ K and a polarization of about 100%, suggesting that preburst heating in an adjacent part of the active region triggered the impulsive spike. An alternative explanation is that this component represents heating in an adjacent loop which was unrelated to the triggering of the burst. The impulsive emission occurred mainly along the legs of a magnetic loop. Kundu and Vlahos (1979) have shown that if the magnetic field strengths at the feet of a loop are different or if unequal numbers of particles are injected downward along each leg, then both the intensity and degree of circular polarization of the two microwave sources will be different, as is the case here. The bipolar structure of this burst is nevertheless uncommon, for the impulsive component of most microwave bursts occurs at the apices of coronal loops, rather than along their legs.

Figure 3 shows the time profile of a multiple-spike burst on July 12. The fourth and fifth spikes were associated with an H α flare. Snapshot maps coinciding with the peaks of the spikes (Fig. 4) show that the most intense peaks (1, 4, and 5 in Fig. 3) arise from spatially separated structures having peak brightness temperatures between 2×10^7 K and 1.5×10^8 K and angular extents between $20''$ and $50''$ [linear extents

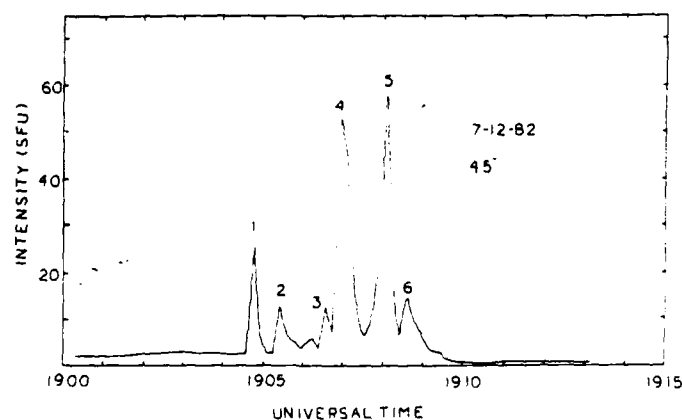


FIG. 3.—The time profile of a multiple-spike burst detected at 20 cm wavelength with an interferometer pair with angular resolution $\theta = 45''$ on 1982 July 12

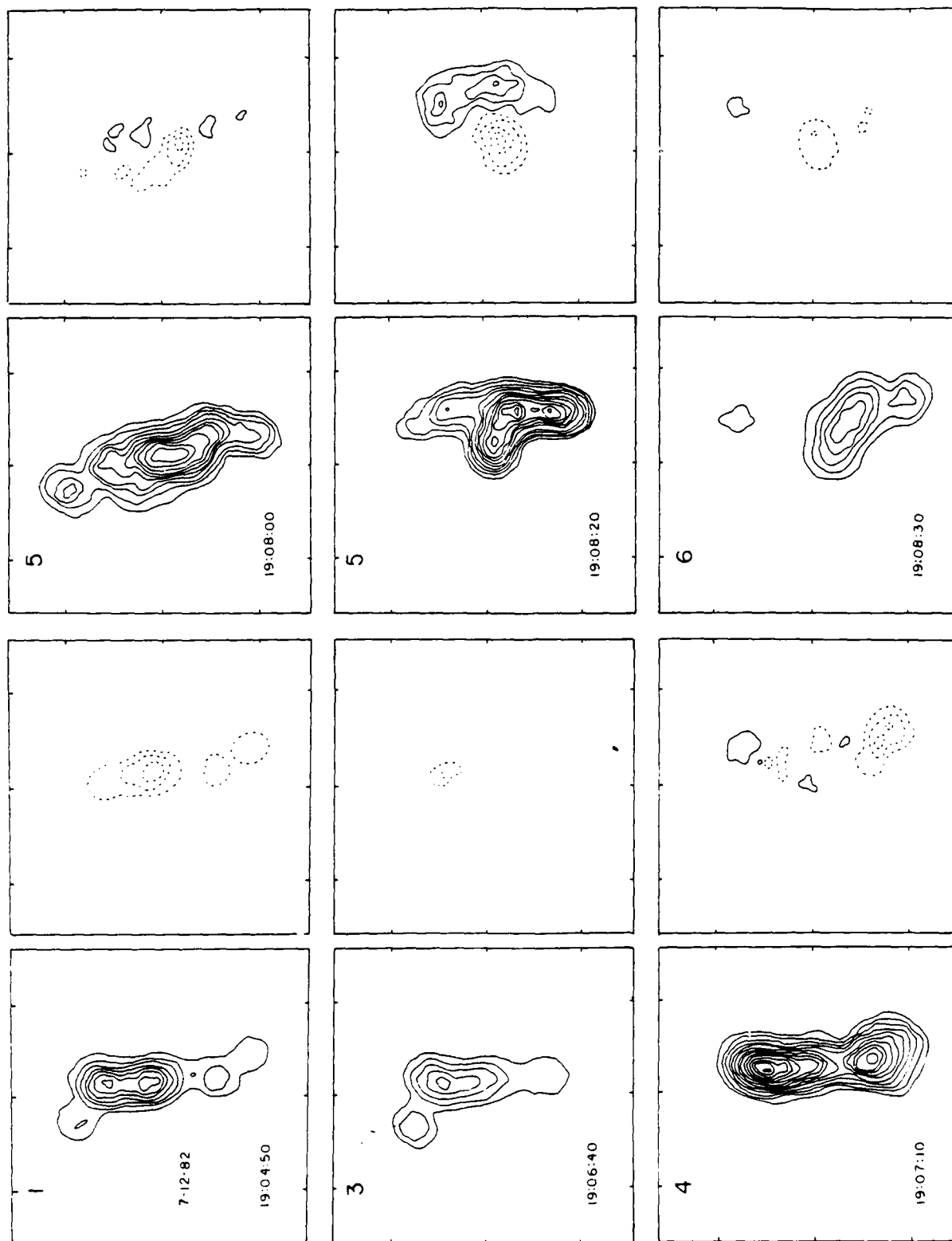


FIG. 4. A series of 10 s snapshot maps made at the most intense peaks (1, 4, and 5) of the impulsive spikes of the complex burst whose time profile is shown in Fig. 3. The contours of the maps mark levels of equal brightness temperature and the solid and dashed contours of the 1' maps denote positive and negative values of 1', respectively. For both sets of maps the outermost contour and the contour interval are both equal to 1.0×10^7 K. The angular scale can be determined from the 30" spacing between the fiducial marks on the axes

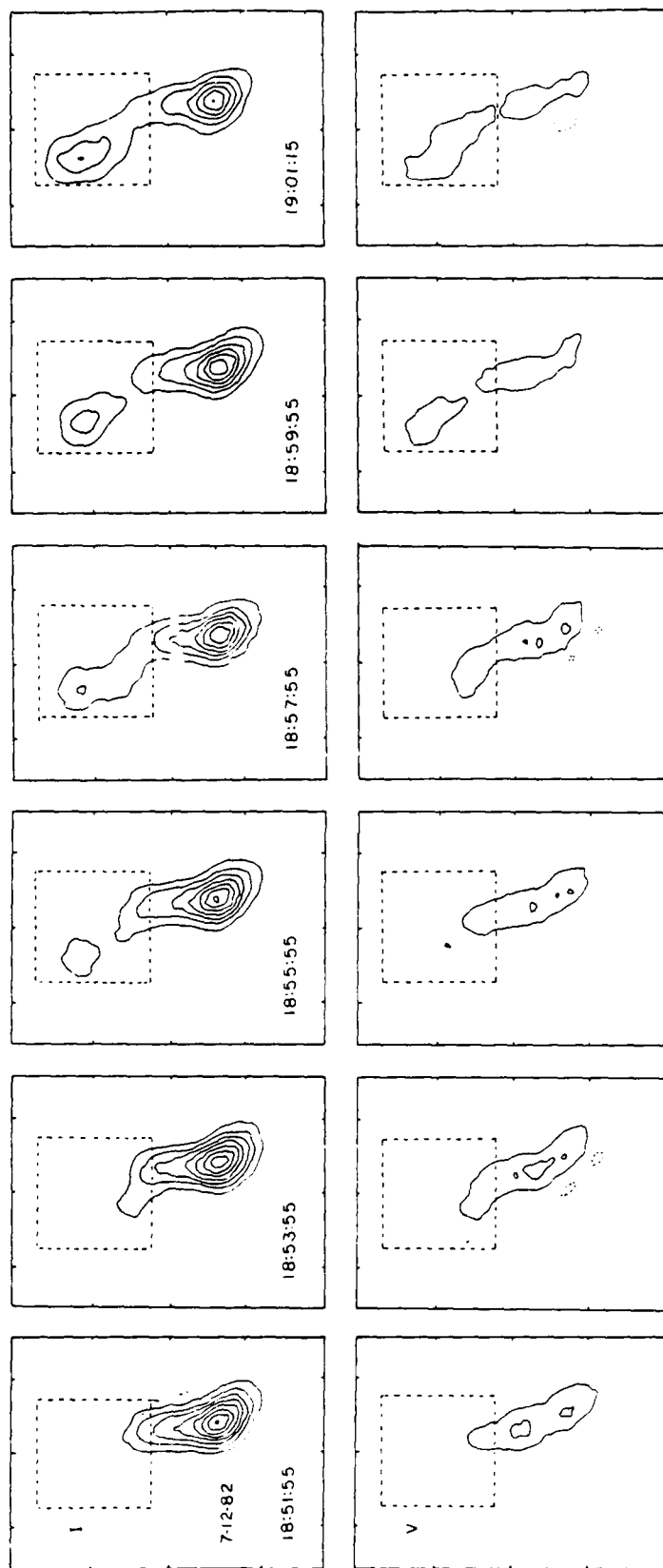


FIG. 5. A series of VLA maps showing the development of the active region AR 3804 before the complex burst shown in Fig. 3. Each map of total intensity, I (top), and circular polarization, V (bottom), was made from 2 minutes of data beginning at the time indicated. The contours of both sets of maps mark levels of equal brightness temperature, and the solid and dashed lines of the V maps denote positive and negative values of V , respectively. For both sets of maps the outermost contour level and the contour interval are equal to 1.7×10^6 K. The angular scale can be determined from the $60''$ spacing between the fiducial marks on the axes. The area within the dashed boxes corresponds to the field of view of the 10 s snapshot maps which are shown in Figure 4.

$L = (1.4-3.5) \times 10^9$ cm]. The weaker spikes (2, 3, and 6 in Fig. 3) that followed a more intense spike were, however, located in the same source as the intense one. Thus, successive weak spikes seem to be emitted in the same loop, while successive intense spikes are emitted from different loops. This last conjecture is supported by the circular polarization changes that reflect different magnetic structures at the times of successive intense spikes.

In Figure 5 we show VLA synthesis maps of the preburst emission made during a 15 minute interval before the start of the first impulsive spike shown in Figure 3. Each map was made from 2 minutes of data beginning at the time indicated. Here the dashed boxes refer to the field of view of the 10 s snapshot maps of the impulsive spikes shown in Figure 4. Both the total intensity and circular polarization increased and changed in an adjacent source during the 15 minutes preceding the first spike. At 18:51:55 UT the peak brightness temperature of this adjacent source was $T_B \sim 7 \times 10^6$ K, about a factor of 3 to 4 above the brightness temperature typically observed in coronal radio loop structures (Kundu *et al.* 1977; Felli, Lang, and Willson 1981; Lang, Willson, and Rayrole 1982). The adjacent source began to heat up about 30 minutes before the onset of the impulsive spikes and remained at $T_B \sim 7 \times 10^6$ K until 5 minutes before the first impulsive spike. At this time the region of spiked emission began to heat up, while the adjacent source cooled to $T_B \sim 4 \times 10^6$ K. This newly heated region of spiked emission was about 60% right circularly polarized, suggesting that it occurred in one leg of a coronal loop.

In Figure 6 we show the time profile of the July 19 burst whose evolution is shown in Figures 7a and 7b. This event consists of two components, whose combined duration was 70 s. The burst structure at first consists of two sources separated by a bridge of weaker emission. The polarization maps (Fig. 7b) indicate that these two sources were oppositely circularly polarized ($p_c \approx 20\%-30\%$) and that they therefore probably mark the legs of magnetic loops. One interpretation of the burst structure in total intensity (Fig. 7a) is that mass motions are occurring within the coronal loop. Craig and McClymont (1970) and Antiochos and Sturrock (1982) have pointed out that mass motions may play a role in the cooling of flare loops.

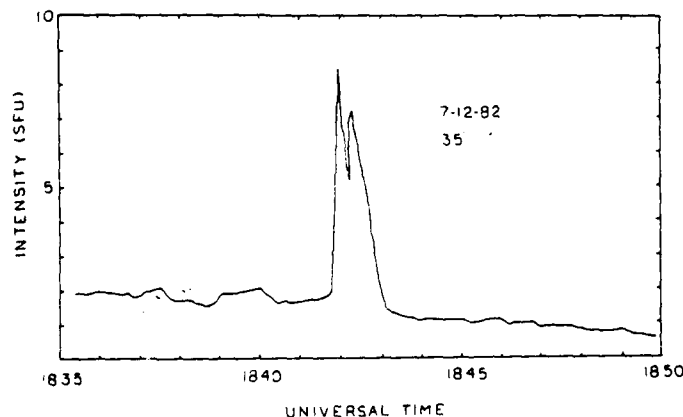


FIG. 6.—The fringe amplitude of the total intensity, I , vs. time for a burst detected at 20 cm wavelength with an interferometer pair with an angular resolution $\theta = 35''$ on 1982 July 19.

In Figure 8 we show the time profile of the July 20 burst, whose evolution is shown in Figure 9. A looplike structure having a peak brightness temperature of $\sim 5 \times 10^6$ K corresponds to the peak precursor, shown in Figure 8. Rapid polarization changes occurred before the main burst (see Fig. 9). The dipolar loop A-B either brightened or emerged at 23:09:50 UT, while the dipolar loop C-D brightened or emerged at 23:10:00 UT. There was also a brightening of A-B at 23:10:10 UT and a dimming of B and C at 23:10:20 UT. All of these changes occurred before the main burst that was emitted at 23:10:40 UT. This impulsive peak is contained within a looplike structure, but it is oriented perpendicular to the present loop. The impulsive peak is also located nearly between the oppositely polarized sources A and B and may have been triggered by the brightening or emergence of this loop. The impulsive source apparently moved by $\sim 10''$ to the west during this time interval. This limbward displacement could be explained as an outward motion of the burst source or as the brightening of progressively higher lying loops. If the burst is moving radially outward from the surface of the Sun, then the inferred velocity is ~ 370 km s $^{-1}$. For comparison, the velocities of moving type IV bursts typically range between 250 and 1200 km s $^{-1}$ (Pick and Trotter 1978; Robinson 1978; Kai 1978) while outward motions of 250–400 km s $^{-1}$ have been detected in coronal X-ray burst loops (Poland *et al.* 1982; Antonucci *et al.* 1982).

In Figure 10 we compare the impulsive phase of this burst as well as that of another burst which began on the same day with simultaneous H α photographs showing the underlying optical flares. Here the uncertainty in the alignment between the radio and optical pictures is $\pm 5''$. The figure shows that the centroids of both radio images are displaced limbward by $\sim 30''-40''$ with respect to the H α kernels. This displacement can be attributed as a radial, limbward displacement caused by the greater height of the 20 cm emission, indicating a height $h = (2-3 \pm 0.4) \times 10^9$ cm above the solar photosphere. These values are consistent with the height $h \sim (3-4) \times 10^9$ cm for quiescent loops (Lang, Willson, and Gaizauskas 1983).

III. DISCUSSION

The observations presented here provide new insight into the evolution of solar microwave bursts and the physical

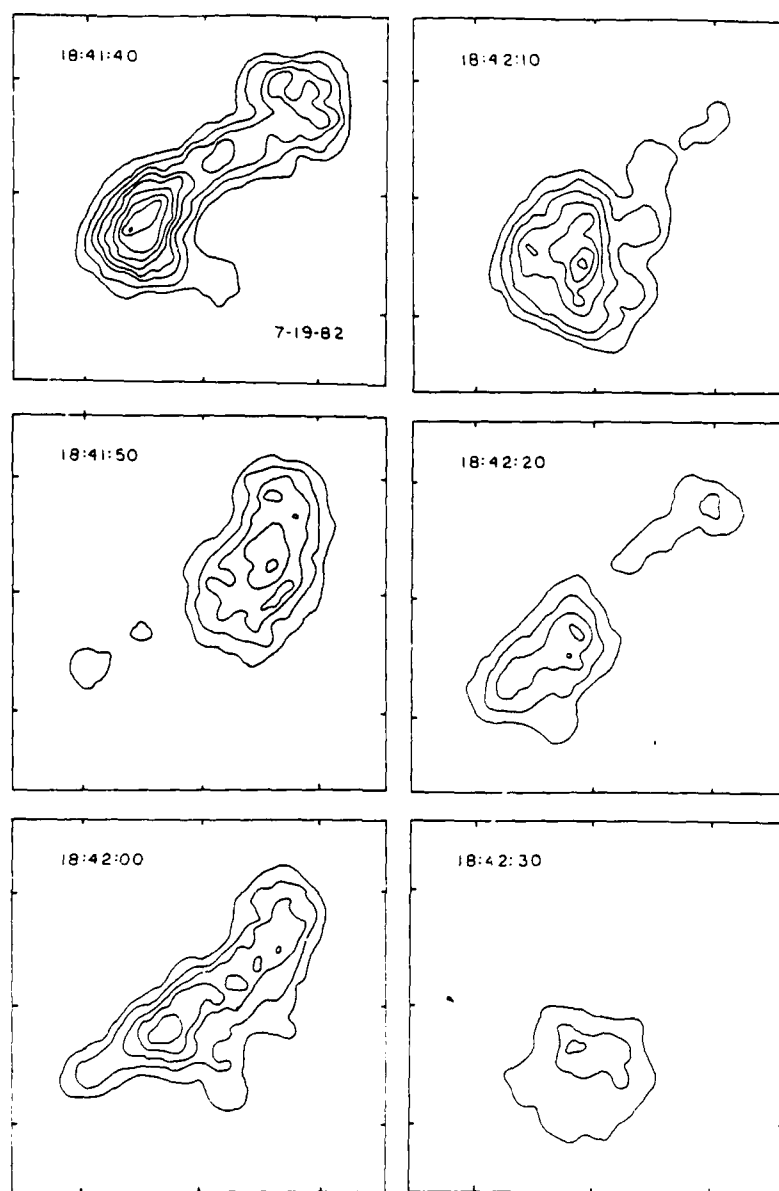


FIG. 7a

FIG. 7.—A series of 10 s snapshot maps of the total intensity, I (Fig. 7a), and circular polarization, V (Fig. 7b), for the burst shown in Fig. 6. The outermost contour and the contour interval of the I maps are both equal to 1.3×10^6 K. The outermost contour and the contour interval of the V maps are equal to 1.3×10^6 K and 6.5×10^5 K, respectively. The angular scale is determined by the $30''$ spacing between the fiducial marks on the axes.

processes which may trigger them. In one case, the intense components of multiple bursts originated in different sources, suggesting that a number of loops may have become successively activated like some complex X-ray bursts (Vorpahl *et al.* 1975; Kahler, Krieger, and Vaiana 1975). There is evidence for different magnetic field strengths at different times in the evolution of these X-ray bursts (Karpen, Crannell, and Frost 1979). Because only a small percentage of the magnetic energy is expected to be converted to particle energy during the impulsive phase (Baum and Bratenahl 1976), both the radio and X-ray results suggest that the components of intense

multiple bursts originate in separate locations within an active region. On the other hand, this does not always occur, for Kundu, Bobrowsky, and Velusamy (1982) and Lang, Willson, and Felli (1981) found that the positions of the individual peaks of multiple component microwave bursts were at the same location to within a few seconds of arc, and we also found that weaker successive components originate in the same source.

We also found evidence for both preburst heating and magnetic changes that may have triggered the impulsive energy release in the loops. (Also see Lang 1974; Syrovetskii and

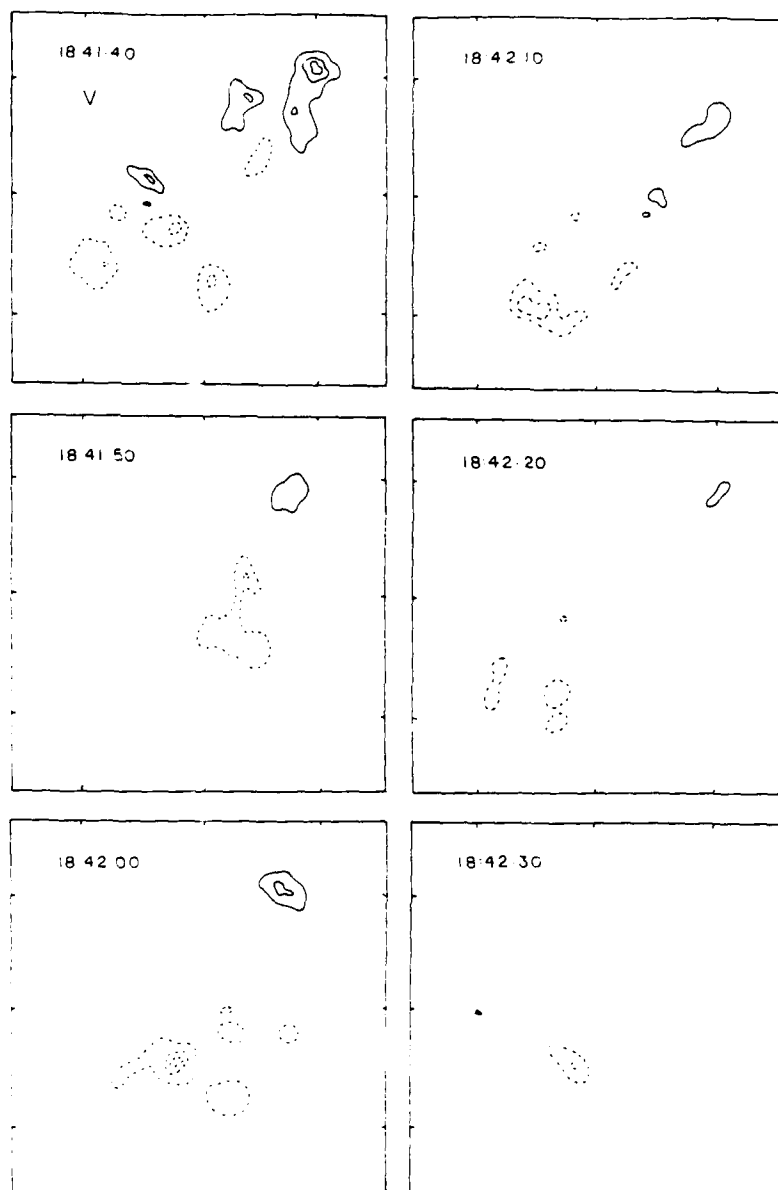


FIG. 7b

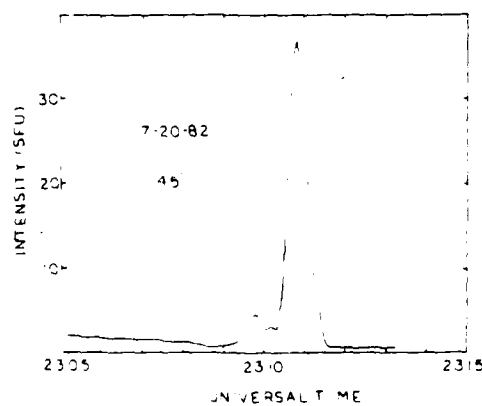


FIG. 8 - The fringe amplitude, I , vs. time for a burst detected at 20 cm wavelength with an interferometer pair whose angular resolution $\theta = 45''$ on 1982 July 20.

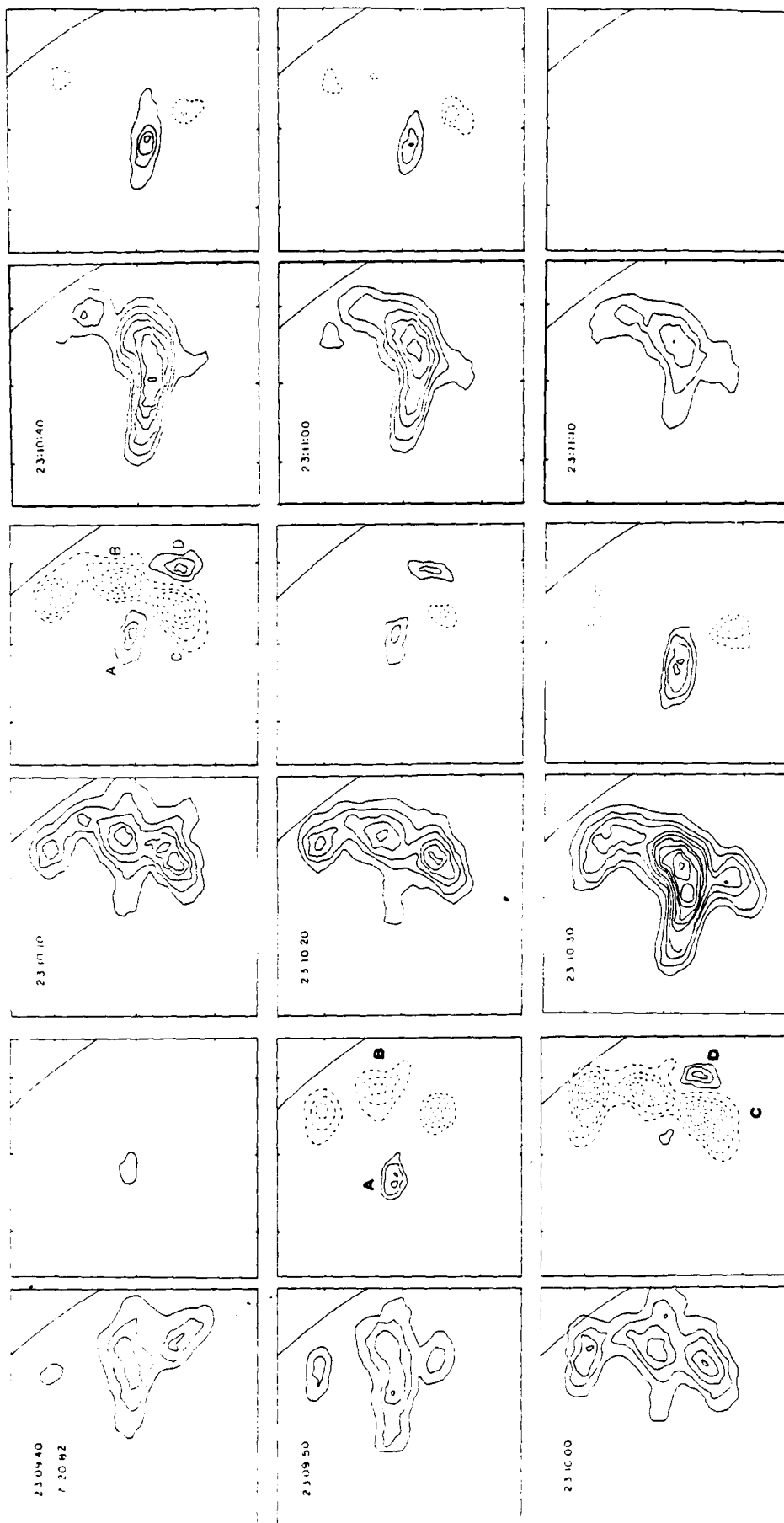


FIG. 9. A series of 40 s VLA snapshot maps of the total intensity, I , and circular polarization, V , for the burst shown in Fig. 8. The development of the preburst emission is shown between 23:09:40 and 23:10:50 UT. Maps of the impulsive phase are shown between 23:11:00 and 23:11:20 UT. The outermost contours of the preburst maps are equal to 1.7×10^5 K. The contour interval of the I and V maps are equal to 1.7×10^5 K and 8.5×10^5 K, respectively. The outermost contours of the impulsive phase maps are equal to 8.2×10^5 K. The contour interval of the I and V maps are equal to 8.2×10^5 K and 4.1×10^6 K, respectively. The curved line in the upper right-hand side of each box denotes the solar west limb. The angular scale can be inferred from the 30'' spacing between fiducial marks on the axes.

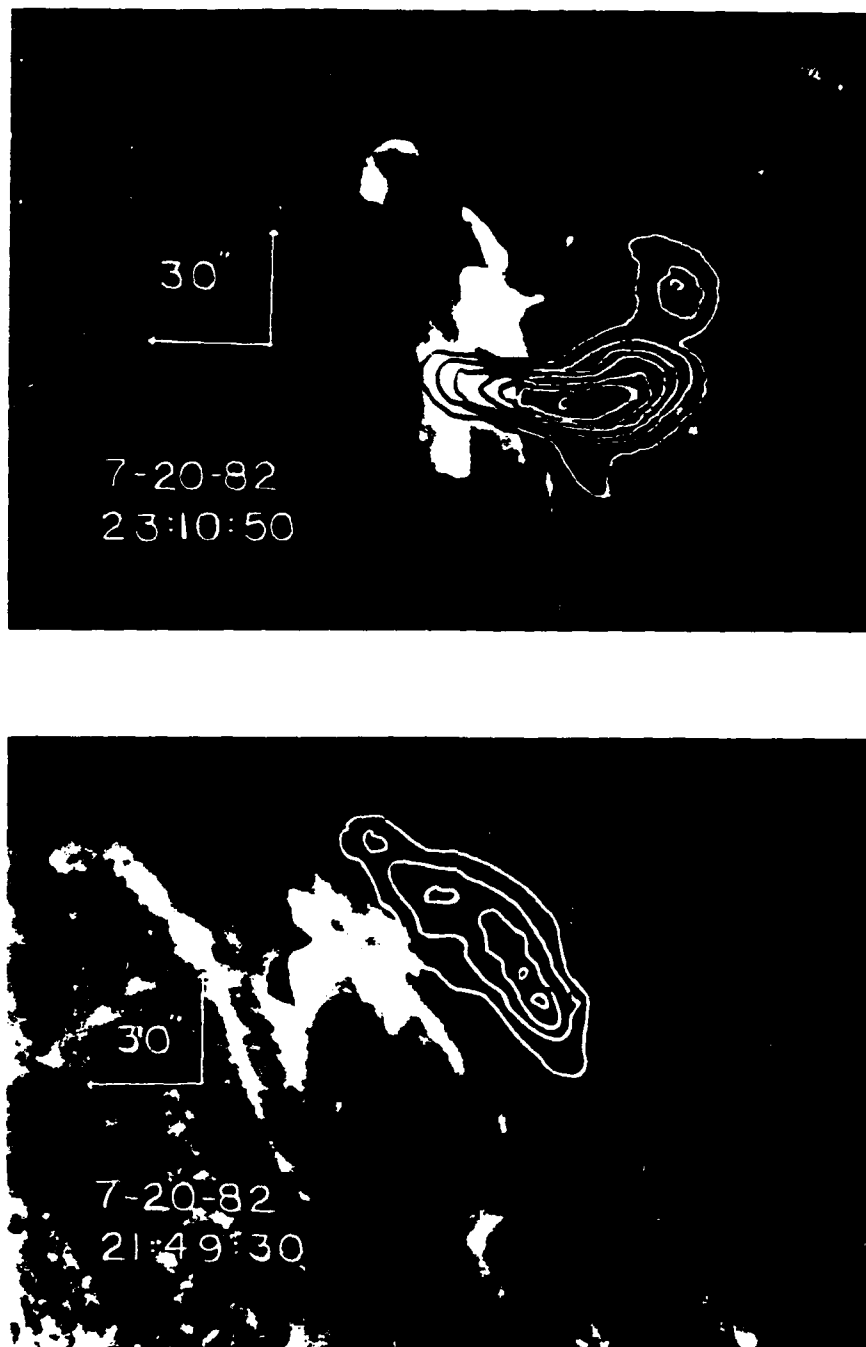


FIG. 10.—A 10 s VLA synthesis map of the impulsive phase of two bursts detected at 20 cm wavelength on 1982 July 20. The radio maps have been superposed on an H α photograph of the optical flares taken at the same time. For both images, north is up, west is to the right. The H α photograph was taken at the Big Bear Solar Observatory (courtesy of Margaret Liggett).

Kuznetsov 1980; Syrovotskii and Somov 1980; Webb and Kundu 1978; Webb 1980). The cause of the sudden temperature enhancements is uncertain. It is possible that we are viewing portions of magnetic loops where the opacity due to either gyroemission or thermal bremsstrahlung increased, thereby causing a temperature increase. Kundu *et al.* (1982) have speculated that if the dominant radiation mechanisms in preflare coronal loops is gyroemission, then the onset of

currents in the loop could increase the magnetic field strength to make the source optically thick at the third harmonic of the gyrofrequency (170 gauss at 20 cm). It is interesting to note, however, that for the burst which began at 19:04 UT on July 12, the impulsive sources were both left and right circularly polarized, whereas the newly heated preburst source was only right circularly polarized, suggesting that the impulsive and preburst sources were located in a different set of loops. In

another case we found that a loop system emerged about 20 s before the impulsive phase of the burst. Recently Kundu *et al.* (1982) observed a similar polarization change only a few tens of seconds before a 6 cm burst, which they believe to be related to the impulsive energy release. The quadrupole field configuration observed in these cases evokes flare models in which neighboring loops merge together and form current sheets between the interface of the loops, thereby triggering the impulsive phase of the burst (Gold and Hoyle 1960; Heyvaerts, Priest, and Rust 1977; Emslie 1982).

There were also cases where preburst changes were undetectable on time scales of minutes to several hours before the onset of the impulsive phase. Out of eight bursts observed at 2, 6, and 20 cm by Willson (1983), only one exhibited detectable preburst heating of the coronal loop in which the

burst took place. These results suggest that preburst changes in the centimeter wavelength emission of coronal loops are not a general feature of the burst process, at least for relatively small bursts of a few solar flux units in size. A similar conclusion was reached by Kahler (1979) and Mosher and Acton (1980) who found no compelling evidence for X-ray enhancements during the few tens of minutes before weak X-ray events.

Solar radio astronomy at Tufts University is supported under grant AFOSR-83-0019 with the Air Force Office of Scientific Research. We are grateful to Margaret Liggett of the Big Bear Solar Observatory for providing the Hz photographs. The Very Large Array is operated by Associated Universities Inc., under contract with the National Science Foundation.

REFERENCES

- Alissandrakis, C. E., and Kundu, M. R. 1978, *Ap. J.*, **222**, 342.
 Antiochos, S. K., and Sturrock, P. A. 1982, *Solar Phys.*, **254**, 343.
 Antonucci, E., *et al.* 1982, *Solar Phys.*, **78**, 107.
 Baum, P. J., and Bratenahl, A. 1976, *Solar Phys.*, **47**, 331.
 Clark, B. G. 1980, *Astr. Ap.*, **89**, 377.
 Craig, I. J. D., and McClymont, A. N. 1976, *Solar Phys.*, **50**, 133.
 Emslie, A. G. 1982, *Ap. Letters*, **22**, 41.
 Felli, M., Lang, K. R., and Willson, R. F. 1981, *Ap. J.*, **247**, 325.
 Gold, T., and Hoyle, F. 1960, *M.N.R.A.S.*, **85**, 553.
 Heyvaerts, J., Priest, E. R., and Rust, D. M. 1977, *Ap. J.*, **216**, 123.
 Kahler, S. W. 1979, *Solar Phys.*, **63**, 347.
 Kahler, W. S., Krieger, A. S., and Vaiana, G. S. 1975, *Ap. J. (Letters)*, **199**, L57.
 Kai, K. 1978, *Solar Phys.*, **61**, 187.
 Karpen, J. T., Crannell, C. J., and Frost, K. J. 1979, *Ap. J.*, **234**, 370.
 Kundu, M. R., Alissandrakis, C. E., Bregman, J. D., and Hin, A. C. 1977, *Ap. J.*, **213**, 278.
 Kundu, M., and Vlahos, L. 1979, *Ap. J.*, **232**, 595.
 Kundu, M. R., Bobrowsky, M., and Velusamy, T. 1982, *Ap. J.*, **251**, 342.
 Kundu, M. R., Schmahl, E. J., Velusamy, T., and Vlahos, T. 1982, *Astr. Ap.*, **108**, 188.
 Lang, K. R. 1974, *Solar Phys.*, **36**, 351.
 Lang, K. R., and Willson, R. F. 1979, *Nature*, **278**, 24.
 Lang, K. R., Willson, R. F., and Felli, M. 1981, *Ap. J.*, **247**, 338.
 Lang, K. R., Willson, R. F., and Gaizauskas, V. 1983, *Ap. J.*, **267**, 455.
 Lang, K. R., Willson, R. F., and Rayrole, J. 1982, *Ap. J.*, **258**, 284.
 Marsh, K. A., and Hurford, G. J. 1980, *Ap. J. (Letters)*, **240**, L111.
 Marsh, K. A., Zirin, H., and Hurford, G. J. 1979, *Ap. J.*, **228**, 610.
 Mosher, J., and Acton, L. 1980, *Solar Phys.*, **66**, 105.
 Pick, M., and Trotter, G. 1978, *Solar Phys.*, **60**, 353.
 Poland, A. I., *et al.* 1982, *Solar Phys.*, **78**, 201.
 Robinson, R. D. 1978, *Solar Phys.*, **60**, 383.
 Syrovatskii, S. I., and Kuznetsov, V. D. 1980, in *IAU Symposium 86, Radio Physics of the Sun*, ed. M. R. Kundu and T. E. Gergeley (Dordrecht: Reidel), p. 445.
 Syrovatskii, S. I., and Somov, B. V. 1980, in *IAU Symposium 91, Solar and Interplanetary Dynamics*, ed. M. Dryer and E. Tandberg-Hanssen (Dordrecht: Reidel), p. 425.
 Velusamy, T., and Kundu, M. R. 1981, *Ap. J. (Letters)*, **243**, L103.
 ———, 1982, *Ap. J.*, **258**, 388.
 Vorpahl, J. A., Gibson, E. G., Landecker, P. B., McKenzie, D. L., and Underwood, J. H. 1975, *Solar Phys.*, **45**, 199.
 Webb, D. F. 1980, in *IAU Symposium 91, Solar and Interplanetary Dynamics*, ed. M. Dryer and E. Tandberg-Hanssen (Dordrecht: Reidel), p. 189.
 Webb, D. F., and Kundu, M. R. 1978, *Solar Phys.*, **57**, 155.
 Willson, R. F. 1983, *Solar Phys.*, **83**, 285.

KENNETH R. LANG and ROBERT F. WILLSON: Department of Physics, Tufts University, Medford, MA 02155

9. STRUCTURE OF A SOLAR ACTIVE REGION FROM RATAN 600 AND VERY LARGE ARRAY¹ OBSERVATIONS

SH. B. AKHMEDOV, V. N. BOROVIK, AND G. B. GELFREIKH
 Main Astronomical Observatory, Academy of Science of the USSR, Leningrad

V. M. BOGOD, A. N. KORZHAVIN, AND Z. E. PETROV
 Special Astrophysical Observatory of the USSR, Academy of Science, Leningrad Branch

V. N. DIKIJ
 Leningrad Polytechnical Institute

AND

KENNETH R. LANG AND ROBERT F. WILLSON
 Department of Physics and Astronomy, Tufts University

Received 1985 February 19; accepted 1985 June 12

ABSTRACT

Solar active region AR 3804 was observed on the same days with the RATAN 600 and the VLA in 1982 July. The emission at wavelengths between 2 and 4 cm consisted of narrow ($\phi < 40''$), bright ($T_b \approx 0.2$ to 6×10^6 K) core sources surrounded by a weaker ($T_b \approx 10^4$ – 10^5 K), extended ($\phi \approx 200''$) halo. The brightest core sources are associated with sunspots and are interpreted in terms of the gyroradiation of thermal electrons at the second and third harmonics of the gyrofrequency. Two of the core sources were associated with a filament that lies above the magnetic neutral line in the photosphere. One of these filament-associated sources has a flat spectrum and is attributed to thermal bremsstrahlung. Relatively high magnetic field strengths of $H \approx 536$ G are inferred if the circular polarization of this source is due to propagation of the bremsstrahlung in the presence of a magnetic field, and even higher magnetic field strengths are required if the radiation is thermal gyroemission. Lower magnetic fields can be obtained if the radiation propagates through a region of transverse magnetic fields higher in the corona where polarization inversion occurs. The other filament-associated source had a high brightness temperature and steep radiation spectrum that cannot be attributed to either thermal bremsstrahlung or thermal gyroradiation. The weak magnetic field strengths at photospheric levels require implausibly high electron temperatures if the high brightness temperatures are to be explained. This source might be attributed to currents that enhance coronal magnetic fields. In this event gyroemission might account for the radiation. Alternatively, it may be due to nonthermal radiation such as the gyrosynchrotron radiation of subrelativistic electrons. VLA synthesis maps at 20 cm reveal hot ($T_b \approx 10^6$ K) coronal loops that connect underlying sunspots of opposite magnetic polarity, but RATAN 600 observations reveal the presence of a much more extended source that accounts for the vast majority of the flux detected at this wavelength. This extended source may also be attributed to the gyrosynchrotron radiation of subrelativistic electrons.

Subject headings: radiation mechanisms — Sun: radio radiation — Sun: sunspots

1. INTRODUCTION

Very Large Array (VLA) observations with high angular resolution ($\theta \gtrsim 1''$) at different microwave wavelengths ($\lambda = 2, 6, \text{ and } 20 \text{ cm}$) have been used to specify the temperature and magnetic structure at different heights in solar active regions. These multiple-wavelength observations specify the three-dimensional structure of active regions in the transition region and the low solar corona (Lang and Willson 1983, 1984; Lang, Willson, and Gaizauskas 1983; Shevgaonkar and Kundu 1984; Kundu and Lang 1985). However, active regions often have a complex structure with local sources that have different emission mechanisms (Gelfreikh *et al.* 1970; Kundu 1982).

Measurements of the spectrum and polarization of the local sources can help specify their emission mechanisms, while also supplementing the interpretation of the VLA observations. We have therefore begun collaborative observations in which the

same active region is observed by the VLA and the Soviet RATAN 600 (Radio Astronomy Telescope of the Academy of Sciences [Nauk]). The RATAN 600 observations provide high angular resolution in the east-west direction at five wavelengths between 2 and 4 cm, thereby determining the radiation spectra of the local sources. Accurate polarization measurements (to 0.5%) are also made at these wavelengths, while more extended structures are detected at decimetric wavelengths (see Table 1).

The VLA and RATAN 600 observations complement each other. The VLA provides high angular resolution in two dimensions at three wavelengths, but the wavelengths are not close enough to determine the spectra of the local sources, and the polarization accuracy is only $\sim 10\%$. The RATAN 600 provides information on extended sources that are not detected with the VLA because of incomplete UV coverage. On the other hand, confusion arising because of the poor angular resolution (in one dimension) of the RATAN 600 can be overcome by VLA observations.

In this paper we will emphasize the unique capabilities of the

¹ The Very Large Array (VLA) is a facility of the National Radio Astronomy Observatory, which is operated by Associated Universities, Inc., under contract with the National Science Foundation.

TABLE 1
BEAM WIDTHS* OF RATAN 600 AT
WAVELENGTHS USED IN SOLAR OBSERVATIONS

WAVELENGTH (cm)	BEAM WIDTH	
	East-West	North-South
2.0	18"	12.5
2.3	21	14.4
2.7	25	16.9
3.2	29	20.0
4.0	36	25.0
13.0	120	81.0
21.0	190	131.0
30.0	270	187.0

* Full width to half-maximum.

RATAN 600. It consists of a ring-shaped primary reflector that is 576 m in diameter and provides a total collecting area of 13,000 m². The radiation reflected off a sector of this ring is collected by a secondary reflector that transforms the cylindrical waves from the primary ring sector into spherical waves that are detected by a set of radiometers operating at different wavelengths (see Table 1 and Parijskij *et al.* 1976). At each wavelength the total intensity I and circular polarization V are measured.

In the work reported here, a flat, tiltable reflector was used to direct solar radiation toward the southern sector of the primary ring. This periscope reflector is ~8 m high and 400 m long in the east-west direction. It permitted observations at five different azimuths (19°, 11°, 0°, 348°, and 340°), two on each side of meridian (Shivris 1980). Although the RATAN 600 provides fan beam scans with high angular resolution in only one direction (close to east-west), the observations at different azimuths provide fan beam scans in slightly different directions. They can be combined to specify the positions of the local sources.

The VLA is a system of 27 antennae with individual diameters of 25 m (or 30' beam width at 20 cm) spread out in a Y-configuration with separations as large as 34 km. The antennae are interconnected electronically to provide a total of 351 interferometer pairs and a combined angular resolution of a few seconds of arc. Synthesis maps of total intensity I and circular polarization V are made for time intervals as short as 10 s for solar bursts and over longer time intervals of several hours for quiescent microwave emission when complete UV coverage is desired.

II. OBSERVATIONS OF SOLAR ACTIVE REGION AR 3084

Solar active region AR 3084 was observed with the RATAN 600 at daily intervals between 1982 July 7 and August 2. As illustrated in Figure 1, the local radio sources could be most easily identified with their optical counterparts on July 15 when the active region was in the center of the disk and was very extended.

Several narrow (angular size $\phi \leq 40''$), bright (brightness temperature $T_B \approx 0.2\text{--}6 \times 10^6$ K) core sources were superposed upon a weaker ($T_B \approx 10^4\text{--}10^5$ K), extended ($\phi \approx 200''$) halo. The halo is the residual radiation left over when Gaussian-shaped core sources are subtracted from the one-dimensional fan beam scans. Here we will concentrate on the core sources designated by the letters "A," "B," and "C," and "D" in Figure 1. The location of these sources was accurately

specified by combining one-dimensional fan beam scans taken in different directions. The core sources A and C are associated with sunspots whose longitudinal magnetic field strengths (at the photosphere) are between 2100 and 2500 gauss. In contrast, core sources B and D are associated with the filament designated by the solid line in the sunspot picture. This filament lies above the magnetic neutral line in the photosphere.

The observed one-dimensional intensities I , the angular sizes, ϕ , in the east-west direction, the degree of circular polarization, ρ_c , and the estimated brightness temperatures, T_B , of the four core sources are given in Table 2 at various wavelengths. Here the data have been corrected for the convolution effects of the antenna beam, and the brightness temperature has been inferred under the assumption of circular symmetry. The two filament-associated sources have angular sizes, ϕ , that do not change with wavelength, but the sunspot-associated sources have angular sizes that increase with wavelength.

The flux density $S = I \times \phi$ has been plotted as a function of wavelength in Figure 2. Three of the core sources have a flux density that increases with wavelength between 2.0 and 4.0 cm. The filament-associated source B has the flat spectrum that is associated with optically thin thermal bremsstrahlung.

A 20 cm VLA synthesis map of AR 3084 on July 12 is superposed on the relevant sunspot picture in Figure 3. The 20

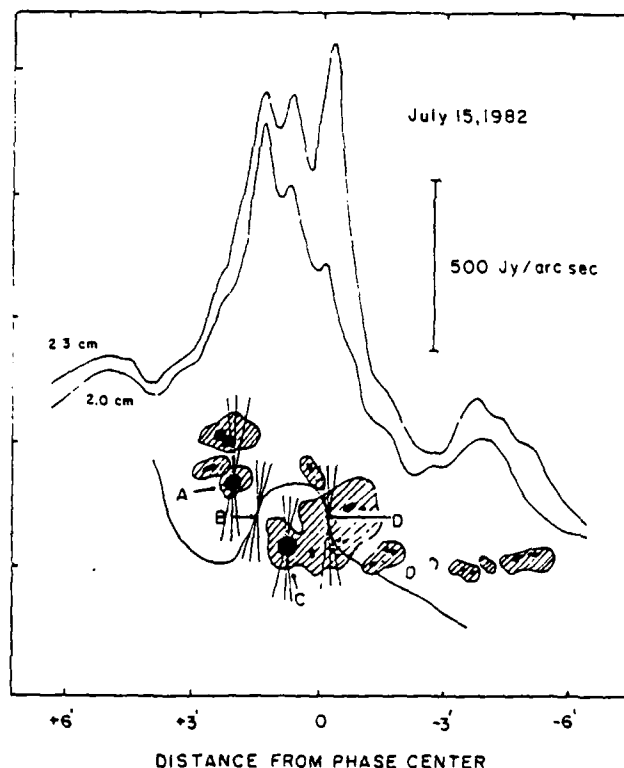


FIG. 1.—One-dimensional fan beam scans of AR 3084 taken at wavelengths of 2.0 and 2.3 cm with the RATAN 600 on 1982 July 15. They are compared with a sunspot picture (umbrae black and penumbrae crosshatched) provided by M. N. Gnevyshev using the photoheliogram at the Kislovodsk station of the Pulkovo Observatory. RATAN 600 scans in slightly different directions, or azimuths, have been combined to determine the positions of the four core radio sources designated by "A," "B," "C," and "D." Their positions are inferred from the four sets of three intersecting lines, each set corresponding to three different azimuths.

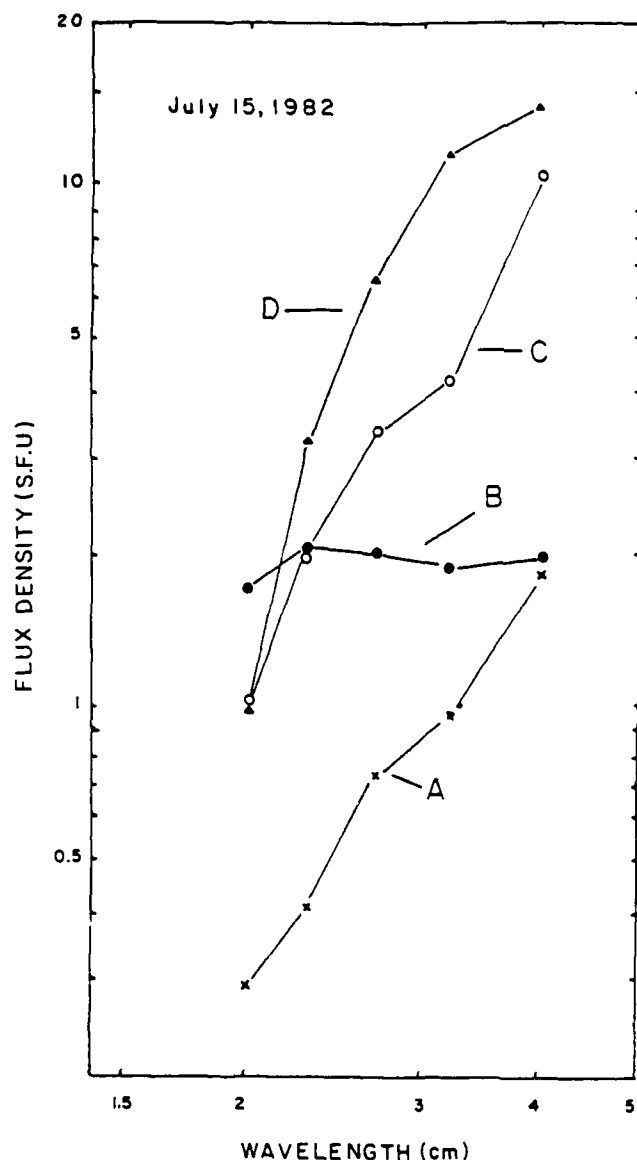


FIG. 2.—Radiation spectrum of four core sources. Here the flux density in solar flux units (sfu) has been plotted as a function of wavelength. For comparison purposes, $1 \text{ sfu} = 10^4 \text{ Jy} = 10^{-19} \text{ ergs cm}^{-2} \text{ s}^{-1} \text{ Hz}^{-1}$.

cm emission consists of two components: one elongated component that connects underlying sunspots of opposite magnetic polarity, and a more compact source that also lies between oppositely polarized sunspots. The radiation at 20 cm wavelength is therefore attributed to the hot ($T_B \approx 10^6 \text{ K}$), dense plasma that is trapped within magnetic loops that connect underlying sunspots of opposite magnetic polarity. The linear extent of the 20 cm coronal loops is 10^9 – 10^{10} cm . These results confirm previous work indicating that 20 cm VLA observations delineate the structure of the ubiquitous coronal loops that had previously only been detected at X-ray wavelengths (Lang, Willson, and Rayrole 1982; Dulk and Gary 1983; McConnell and Kundu 1983).

The RATAN 600 observations at 13 and 21 cm indicate an extended source whose angular size $\phi \approx 4'$ is comparable to that of the entire active region. Such extended sources are often

TABLE 2
PARAMETERS FOR FOUR CORE RADIO SOURCES

Core	Wavelength (cm)	I (Jy per arcsec)	ϕ	ρ_c (%)	T_B (10^6 K)
A	2.0	≥ 315	$\leq 8''$...	≥ 0.23
	2.3	360	10	53	0.28
	2.7	535	13	100	0.43
	3.2	560	17	100	0.49
	4.0	765	23	...	0.77
B	2.0	941	17	...	0.32
	2.3	1374	14	8	0.75
	2.7	1162	16	30	0.77
	3.2	972	18	40	0.80
	4.0	1024	18	...	1.32
C	2.0	807	12	...	0.39
	2.3	1356	14	7	0.74
	2.7	2080	15	19	1.46
	3.2	1944	20	11	1.44
	4.0	4012	24	...	3.88
D	2.0	315	30	...	0.06
	2.3	1308	23	28	0.44
	2.7	2648	23	45	1.22
	3.2	4212	25	33	2.50
	4.0	6675	24	...	6.45

undetectable on VLA synthesis maps. The total flux density of the 21 cm extended source detected with the RATAN 600 is $1.5 \times 10^5 \text{ Jy}$, whereas the total flux density of the 20 cm loops detected with the VLA is $3.0 \times 10^3 \text{ Jy}$. This indicates that the flux of the 20 cm coronal loops detected with the VLA is only $\sim 2\%$ of the total flux of the entire active region at 21 cm. Thus, the coronal loops may be superposed upon much more extended sources that account for most of the active region flux at these wavelengths.

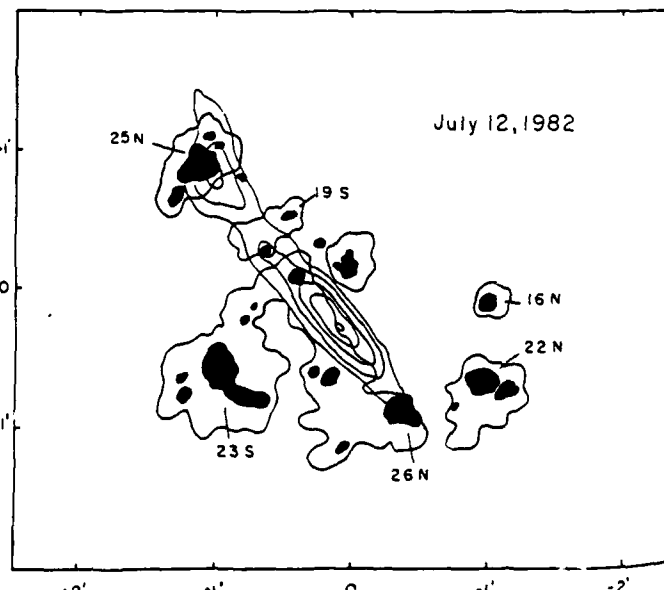


FIG. 3.—VLA synthesis map of the 20 cm emission from AR 3084 on 1982 July 12 is superposed upon the sunspot picture provided by M. N. Gnevyshev. The sunspots (black) have numbers corresponding to the longitudinal magnetic field strength in hundreds of gauss and letters denoting the magnetic polarity ("N" or "S"). The 20 cm contours are of equal brightness temperature corresponding to 0.2, 0.4, 0.6, 0.8, and 1.0 times the peak brightness temperature of $1.8 \times 10^6 \text{ K}$.

III. DISCUSSION

The sunspot-associated core sources A and C may be attributed to gyroradiation of thermal electrons at the second and third harmonic of the gyrofrequency. Strong evidence for gyroresonance absorption at coronal levels in solar active regions was provided by Kundu, Schmahl, and Gerassimenko (1980) through a comparison of microwave, EUV, and X-ray observations. The near equality of the microwave brightness and electron temperatures indicated that the microwave emission was thermal. The measured electron densities and temperatures indicated that free-free absorption is inadequate and that gyroresonance absorption at the second or third harmonic of the gyrofrequency provides sufficient optical depth at microwave wavelengths. Thermal gyroradiation at coronal levels above sunspots was additionally confirmed by the detection of circularly polarized ring-shaped or horseshoe structures (Alissandrakis and Kundu 1982; Lang and Willson 1982) that were predicted using the theory of gyroresonant emission from individual sunspots (Gelfreikh and Lubyshev 1979). It is also consistent with the 100% circular polarization observed for the core source A.

The magnetic field intensity, H_c , at the bottom of the corona may be inferred from the short wavelength limit, λ_c , of the polarized gyroresonant emission through the relation (Akhmedov *et al.* 1982)

$$H_c = \frac{3570}{\lambda_c} \text{ gauss}, \quad (1)$$

for the third harmonic. For core source A, a value of $H_c = 1690$ gauss is obtained. This may be compared with the magnetic field strength $H = 2100$ – 2600 gauss for the sunspots in the underlying photosphere.

The filament-associated core source B has the flat spectrum of optically thin thermal bremsstrahlung. A lower estimate to the emission measure, $\int N_e^2 dl$, can be obtained by assuming that the electron temperature, T_e , is equal to the brightness temperature, T_b , at longer wavelength $\lambda = 4.0$ cm. The relevant formulae (Lang 1974) then give $\int N_e^2 dl = 5.6 \times 10^{29} \text{ cm}^{-5}$ and an electron density $N_e \approx 2.1 \times 10^{10} \text{ cm}^{-3}$ for core source B.

The observed circular polarization of the filament-associated source B might be explained in terms of a propagation effect in which the optical depths of the ordinary and extraordinary waves differ. In the quasi-longitudinal (Q-L) approximation for wave propagation in the direction of an external magnetic field, the degree of circular polarization $\rho_c \approx 2\nu_H \cos \theta / \nu$, where the gyrofrequency $\nu_H = 2.8 \times 10^6 H$ Hz in a longitudinal magnetic field strength of H , the angle between the line of sight and the direction of the magnetic field is θ , and ν is the frequency of the radiation. At our observing wavelength of $\lambda \approx 3$ cm where the circular polarization $\rho_c \approx 30\%$ we obtain $H = 536$ gauss for Q-L propagation. Although this longitudinal magnetic field strength may be large for a filament associated source, it cannot be avoided by an appeal to the alternative gyroresonant emission process.

The optical thickness due to gyroresonant absorption increases with increasing angle, θ , between the line of sight and the direction of the magnetic field, and we might expect a large θ near the magnetic neutral line. However, even with $\theta = 85^\circ$, plausible values for the electron temperature, $T_e \approx 2 \times 10^6$ K, electron density $N_e \approx 10^{10} \text{ cm}^{-3}$, and extent $L \approx 10^9$ cm indicate that the highest harmonic, s , of the gyrofrequency that is consistent with the observed brightness temperature of $T_b =$

1.0×10^6 K is $s = 5$ (see McConnell and Kundu 1983, for the relevant formulae). This harmonic corresponds to a longitudinal magnetic field strength of $H \approx 714$ gauss if the gyrofrequency is at $\lambda = 3$ cm. Higher harmonics that correspond to weaker magnetic fields require implausibly high electron temperatures to produce the observed brightness temperature.

One method of accounting for circular polarization with lower magnetic field strengths involves a polarization inversion in a region of quasi-transverse (Q-T) magnetic field (Cohen 1960). The coupling of the ordinary and extraordinary modes as the radiation passes through the Q-T region will cause an inversion in the sense of circular polarization if the frequency ν is less than the critical frequency, ν_T , given by $\nu_T^2 = 10^{17} N_e L_H H^2$. Assuming $N_e = 10^{10} \text{ cm}^{-3}$, a magnetic scale length of $L_H = 10^9$ cm and $\nu_T \geq 10^{10}$ Hz, we find $H \geq 46$ gauss. This inversion occurs high in the corona above the region where the radiation is formed. However, because source B is located above a magnetic neutral line, we have no evidence for whether or not a polarization inversion has taken place.

Kundu *et al.* (1977) and Kundu and Alissandrakis (1984) have provided evidence for polarization inversion in the regions of bright 6 cm sources ($T_b \approx 2 \times 10^6$ K) associated with magnetic neutral lines. Their observations led to an estimate of $H \sim 20$ gauss for the Q-T region. Similar values of magnetic field strength in the Q-T region have been inferred from centimeter-wavelength polarization inversions by Peterova and Akhmedov (1973).

Of special interest is the filament-associated core source D. This source has a large brightness temperature of $T_b \approx 7 \times 10^6$ K at $\lambda = 4$ cm and an exceptionally rapid increase of flux density with wavelength. Because the optical depth must be less than unity in order to account for the observed circular polarization, the electron temperature must be greater than 7×10^6 K. This unusually high electron temperature argues against thermal emission processes. Moreover, the steep radiation spectrum rules out thermal bremsstrahlung.

Although one can obtain a steep spectrum from thermal gyroemission as the result of an exponential term in the optical depth (see McConnell and Kundu 1983), the region must have an implausibly high magnetic field strength. If the radiation were due to gyroemission at the second harmonic of the gyrofrequency, then a magnetic field strength of $H = 1800$ gauss is implied. This is inconsistent with the fact that the source lies above a magnetic neutral line in the solar photosphere where much weaker magnetic fields prevail. When more plausible magnetic field strengths of $H \sim 140$ gauss are assumed for the regions where $T_e \approx 10^6$ K, then the observed radiation must occur at high harmonics of the gyrofrequency ($s = 26$ for $\lambda = 3$ cm). The optical depth due to gyroresonance absorption is then negligibly small, and implausibly high electron temperatures of $T_e \gg 10^7$ K are inferred. However, there is the possibility that strong currents produce higher magnetic fields in the low corona than those expected from current-free extrapolations from photospheric values. In this event thermal gyroemission might account for the radiation.

An alternative explanation for the radiation from the core source D may be some sort of nonthermal emission mechanism (Gelfreikh *et al.* 1970). Such a mechanism was suggested by observations of 6 cm sources of high brightness temperature in regions where the magnetic fields are weak (Webb *et al.* 1983). These sources have been attributed to the nonthermal synchrotron emission of mildly relativistic electrons (Chiuderi Drago and Melozzi 1984).

One possibility is that source D is the gyrosynchrotron radiation of subrelativistic electrons. The theoretical formulae describing gyrosynchrotron radiation have been given (Ramaty 1969; Takakura and Scalise 1970; Ramaty and Petrosian 1972; Petrosian 1981). Theoretical results of the gyrosynchrotron radiation from mildly relativistic electrons have been summarized by Dulk and Marsh (1982), who provide simplified expressions for nonthermal (power-law) and thermal (Maxwellian) distributions. Using their formulae, we find that a nonthermal electron energy distribution with a power-law index $\delta = -4.0$ and a magnetic field strength of $H = 40$ gauss describes the flux density spectrum of source D between 2.0 and 4.0 cm. The observed flux density can be accounted for with a magnetic field of strength $H = 40$ gauss and an electron density $N = 2 \times 10^9 \text{ cm}^{-3}$ for electrons with energies $E > 10 \text{ keV}$. These values of H and N may plausibly account for the observed emission from source D.

The extended component of decimetric emission at 13 and 21 cm wavelength may be similarly accounted for by gyrosynchrotron radiation. Plausible magnetic field strengths of $H \approx 80$ gauss can be inferred from the observed circular polarization (15%–50%) and Takakura and Scalise's (1970) formulae for the volume emissivity of the ordinary and extra-

ordinary waves. Because of the much larger volume of the extended emission, the required electron density $N_e \approx 10^2 \text{ cm}^{-3}$ may be relatively low.

One possible difficulty with this explanation is that some as yet unspecified mechanism must be continually accelerating the electrons. For example, the energy loss by synchrotron radiation (Lang 1974) with a power-law electron energy distribution has a half-time for the total emitted radiation (Chiuderi and Chiuderi-Drago 1967) of several hours for a magnetic field strength of $H = 40$ gauss.

We are especially grateful to Yu. N. Parijskij, the late D. V. Korolkov and V. K. Abalakin for their support of collaborative observations between the RATAN 600 and the VLA. We thank D. Rust, P. Simon, and V. E. Stepanov for the stimulus to international collaboration provided by support activities for the *Solar Maximum Mission* satellite. We also thank the staff of the RATAN 600 and VLA telescopes for their support and help. Travel support for use of a foreign telescope (the RATAN 600) was provided by the NSF. Radio astronomical studies of the Sun and other active stars at Tufts University are supported under grant AFOSR-83-0019 with the Air Force Office of Scientific Research.

REFERENCES

- Akhmedov, Sh. B., Gelfreikh, G. B., Bogod, V. M., and Korshavin, A. N. 1982, *Solar Phys.*, 79, 41.
 Alissandrakis, C. E., and Kundu, M. R. 1982, *Ap. J. (Letters)*, 253, L49.
 Chiuderi, C., and Chiuderi-Drago, F. 1967, *Nuovo Cimento*, 48, 186.
 Chiuderi-Drago, F., and Melozzi, M. 1984, *Astr. Ap.*, 131, 103.
 Cohen, M. H. 1960, *Ap. J.*, 131, 664.
 Dulk, G. A., and Gary, D. E. 1983, *Astr. Ap.*, 124, 103.
 Dulk, G. A., and Marsh, K. A. 1982, *Ap. J.*, 259, 350.
 Felli, M., Lang, K. R., and Willson, R. F. 1981, *Ap. J.*, 247, 325.
 Gelfreikh, G. B., and Lubyshev, B. I. 1979, *Soviet Astr.*, 23, 316.
 Gelfreikh, G. B., Akhmedov, Sh. B., Borovic, V. N., Golnev, V. Ja., Korshavin, A. N., Nagnibeda, V. G., and Peterova, N. G. 1970, *Izvestia GAO*, N185, 167.
 Kundu, M. R. 1982, *Rept. Progr. Phys.*, 45, 1435.
 Kundu, M. R., and Alissandrakis, C. E. 1984, *Solar Phys.*, 94, 249.
 Kundu, M. R., Alissandrakis, C. E., Bregman, J. D., and Hin, A. C. 1977, *Ap. J.*, 213, 278.
 Kundu, M. R., and Lang, K. R. 1985, *Science*, 228, 9.
 Kundu, M. R., Schmahl, E. J., and Gerassimenko, M. 1980, *Astr. Ap.*, 82, 265.
 Lang, K. R. 1974, *Astrophysical Formulae* (New York: Springer-Verlag).
 Lang, K. R., and Willson, R. F. 1982, *Ap. J. (Letters)*, 255, L111.
 ———, 1983, *Adv. Space Res.*, 2, No. 11, 91.
 ———, 1984, *Adv. Space Res.*, 4, No. 7, 105.
 Lang, K. R., Willson, R. F., and Gaizauskas, V. 1983, *Ap. J.*, 267, 455.
 Lang, K. R., Willson, R. F., and Rayrole, J. 1982, *Ap. J.*, 258, 384.
 McConnell, D., and Kundu, M. R. 1983, *Ap. J.*, 269, 698.
 Parijskij, Yu. N., et al. 1976, *Soviet Astr.*, 53, 1017.
 Peterova, N. G., and Akhmedov, Sh. B. 1973, *Soviet Astr.*, 17, 768.
 Petrosian, V. 1981, *Ap. J.*, 251, 727.
 Ramaty, R. 1969, *Ap. J.*, 158, 753.
 Ramaty, R., and Petrosian, V. 1972, *Ap. J.*, 178, 241.
 Shevgaonkar, R. K., and Kundu, M. R. 1984, *Ap. J.*, 283, 413.
 Shrivis, O. N. 1980, *Ap. Issledovanie (Izvestia SAO)*, 12, 134.
 Takakura, T., and Scalise, C. 1970, *Solar Phys.*, 11, 434.
 Webb, D. F., Davis, J. M., Kundu, M. R., and Velusamy, T. 1983, *Solar Phys.*, 85, 267.

SH. B. AKHMEDOV, V. N. BOROVIC, and G. B. GELFREIKH: Main Astronomical Observatory, Academy of Science of the USSR, 196140 Leningrad M-140, USSR

V. M. BOGOD, A. N. KORSHAVIN, and Z. E. PETROV: Special Astrophysical Observatory of the USSR, Academy of Science, Leningrad Branch, 196140 Leningrad M-140, USSR

V. N. DIKIJ: Leningrad Polytechnical Institute, 196140 Leningrad M-140, USSR

KENNETH R. LANG and ROBERT F. WILLSON: Department of Physics and Astronomy, Tufts University, Medford, MA 02155

10. **SOLAR TERRESTRIAL PHYSICS**

**PROCEEDINGS OF
SECOND INDO-US WORKSHOP ON
SOLAR-TERRESTRIAL PHYSICS**

Edited by

**M.R. KUNDU, B. BISWAS
B.M. REDDY, S. RAMADURAI**



**National Physical Laboratory (CSIR)
Hillside Road, New Delhi-110012 (India)**

1986

THE SOLAR-STELLAR CONNECTION

Kenneth R. Lang

Department of Physics and Astronomy
Tufts University, Medford, MA 02155

ABSTRACT

In this paper we review high resolution V.L.A. observations of the microwave emission from solar active regions, and then use the solar analogy to interpret the microwave emission of nearby dwarf M flare stars.

INTRODUCTION

Nearby main sequence stars of late spectral type exhibit a variety of phenomena that are closely related to our understanding of solar active regions including dark spots, strong magnetic fields, activity cycles, and flare emission at optical, ultraviolet, radio and X-ray wavelengths. A consideration of solar active regions may therefore provide a useful background for future studies of solar-type stars. The solar analogy is, in fact, particularly relevant for the dwarf M flare stars that exhibit slowly varying quiescent, or non-flaring, microwave emission and microwave bursts that are very similar to those of solar active regions.

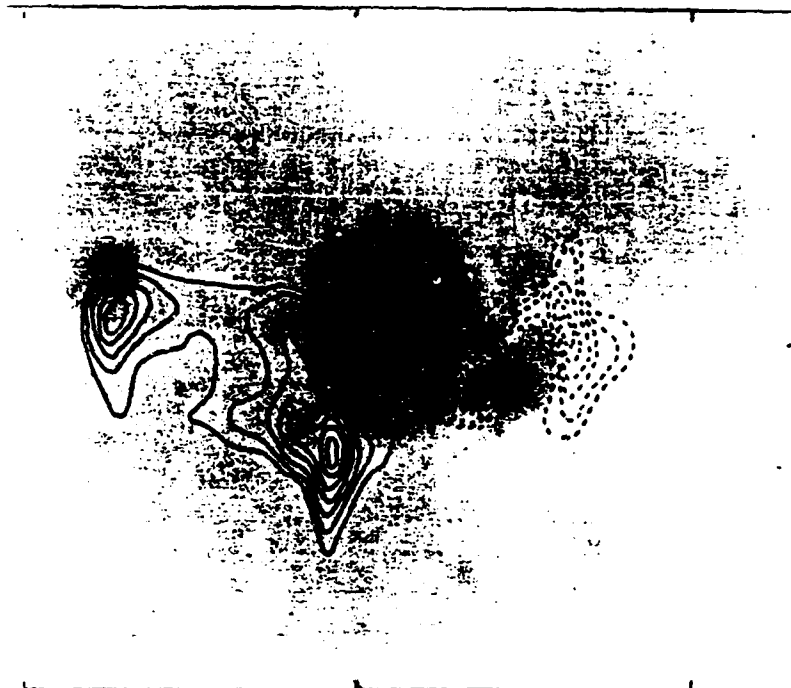


Fig. 1. A V.L.A. synthesis map of circular polarization, V , of the 6 cm radiation superimposed upon an off-band $H\alpha$ photograph of the same active region taken at the Big Bear Solar Observatory on the same day. The angular scale is denoted by the $60''$ spacing between the fiducial marks on the axes. There is no detectable circular polarization above the sunspot umbrae where the magnetic fields are strong and nearly vertical. The polarized emission is concentrated above the penumbrae, where the magnetic field lines are curved with a sharp gradient. The contours of the V map mark levels of equal brightness temperature corresponding to 0.3, 0.4, ... 0.9 times the maximum brightness temperatures of $+3.0 \times 10^5$ K and -2.8×10^5 K.

THE SLOWLY VARYING COMPONENT OF SOLAR MICROWAVE RADIATION

The radio emission from quiescent, or non-flaring, active regions has an intensity that is correlated with sunspot number and area. It arises at all levels within the solar atmosphere above active regions, from the chromosphere to the corona. Because this quiescent emission is only slowly varying over time scales of several hours, its detailed structure can be investigated using aperture synthesis techniques. These techniques have been employed at the Very Large Array, or V.L.A., to map different levels within the solar atmosphere with second-of-arc angular resolutions that are either better or comparable to those obtained from ground-based optical telescopes.

Synthesis maps at longer microwave wavelengths, λ , refer to higher levels within the solar atmosphere above active regions. For example, typical brightness temperatures T_B , range from $T_B \sim 10^4$ K at $\lambda = 2$ mm in the low chromosphere through $T_B \sim 10^5$ K at $\lambda = 2$ cm in the transition region to $T_B \sim 10^6$ K at $\lambda = 20$ cm in the low solar corona. At each wavelength, the synthesis maps of total intensity, I , describe the two-dimensional distribution of brightness temperature, while the synthesis maps of circular polarization, or Stokes parameter V , describe the two-dimensional structure of the magnetic field. The heights of the microwave structures can be inferred from their angular displacements from underlying photospheric features, and the two-dimensional maps at different microwave wavelengths can be combined to specify the three-dimensional structure of solar active regions.

The slowly varying component of solar microwave emission is thermal in nature, with brightness

temperatures that do not normally exceed the local electron temperatures. The radiation at millimeter wavelengths is the thermal bremsstrahlung of hot, dense plasma in the chromosphere. At centimeter wavelengths the gyroresonant radiation of thermal electrons accelerated by magnetic fields can compete with the bremsstrahlung of thermal electrons accelerated in the electric fields of ions. The dominant emission mechanism depends upon the wavelength and the physical conditions within the active regions.

The most intense emission from solar active regions at 6 cm wavelength originates in the legs of magnetic dipoles that have their footpoints in underlying sunspots. Coronal temperatures are inferred from the high brightness temperatures of $T_B \sim 10^6$ K, whereas heights $h \sim 40,000$ km are inferred from angular displacements from the underlying sunspots (Lang, Willson and Gaizauskas, 1983). The low electron density above sunspots requires gyroresonance absorption if the bright 6 cm emission is to be explained (Alissandrakis, Kundu and Lantos, 1980; Pallavicini, Sakurai and Vaiana, 1980).

Gyroresonant emission in the legs of magnetic dipoles at 6 cm wavelength has been confirmed by the detection of circularly polarized horseshoe or ring shaped structures that lie above the curved magnetic fields of sunspot penumbrae (see Figure 1; Lang and Willson, 1982; and Alissandrakis and Kundu, 1982). The high degrees of circular polarization $p_c \sim 95\%$ of these horseshoes requires gyroresonant emission, and the structures were, in fact, predicted from the theory of gyroresonant emission of individual sunspots (Gel'freikh and Lubyshev, 1979). There is no detectable circular polarization above the central sunspot umbrae whose magnetic fields project radially upwards into the hot coronal regions. In

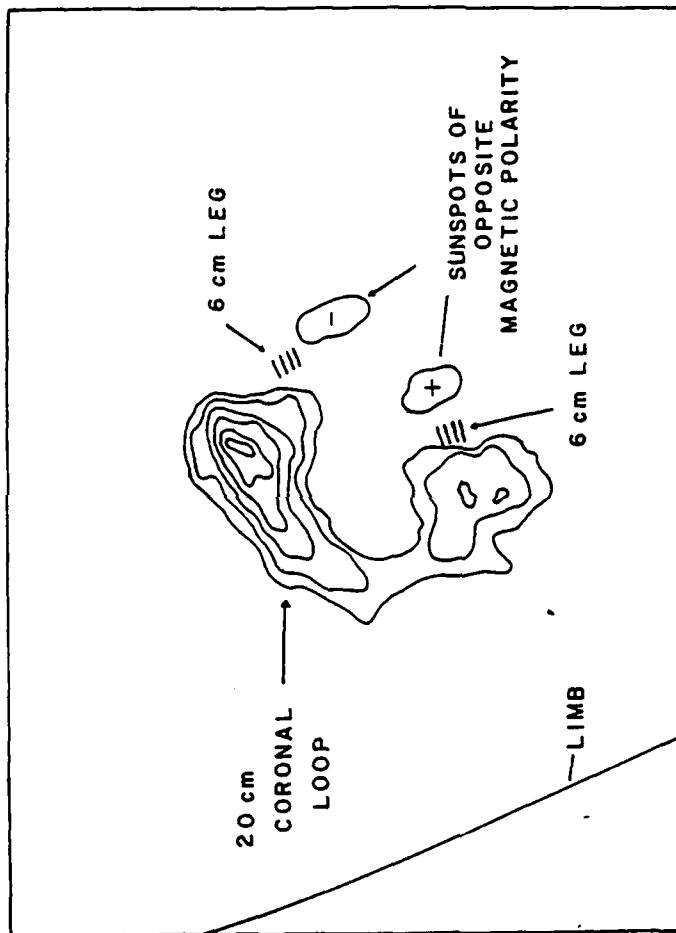


Fig. 2. A V.L.A. synthesis map of the total intensity, I , of the 20 cm emission from a coronal loop. The contours mark levels of equal brightness temperature corresponding to 0.2, 0.4, ..., 1.0 times the maximum brightness temperature of $T_B = 2 \times 10^6$ °K. A schematic portrayal of the 6 cm emission, which comes from the legs of the magnetic loops, has been added together with the underlying sunspots that are detected at optical wavelengths.

contrast, the total intensity of the 6 cm radiation is often enhanced above the sunspot umbrae, with brightness temperatures $T_B \sim 10^6$ K.

A connection with intense magnetic fields is indicated by the high degrees of circular polarization of the microwave emission. These magnetic fields permeate every level of the solar atmosphere above active regions. In fact, magnetic loops that confine the hot coronal plasma are the dominant structural element in the solar corona. The microwave observations of circular polarization uniquely provide direct measurements of the strength and structure of these magnetic fields. Longitudinal magnetic field strengths of $H_z \sim 600-900$ Gauss are, for example, inferred from the 6 cm gyroemission that comes mainly from the second or third harmonic of the gyrofrequency. In fact, circular polarization maps at 6 cm wavelength act as coronal magnetograms, with the sense of circular polarization corresponding to the extraordinary mode of wave propagation (Kundu and Alissandrakis, 1975; Kundu *et. al.*, 1977; Lang and Willson 1979, 1980). Observations of circular polarization at longer wavelengths of $\lambda = 12.6$ cm and $\lambda = 20$ cm also act as coronal magnetograms that specify the strength and structure of the longitudinal component of the magnetic field in the low solar corona (Dulk and Gary, 1983; Lang and Willson, 1983a).

V.L.A. observations at 20 cm wavelength describe the magnetic, temperature and density structure of coronal loops. The ubiquitous coronal loops have previously only been detected during rare and expensive satellite observations at soft X-ray wavelengths (Vaiana and Rosner, 1978). Now, the loops can be routinely investigated using 20 cm V.L.A. observations (Lang, Willson and Rayrole, 1982;



Fig. 3. The ten second V.L.A. synthesis maps of the impulsive phase of two solar bursts at 20 cm wavelength superimposed on H α photographs of the optical flares taken at the same time at the Big Bear Solar Observatory. The 20 cm bursts originate near the tops of coronal loops that are about 40,000 km above the flaring region seen at optical wavelengths. The western solar limb is visible in both photographs.

Lang and Willson, 1983b; McConnell and Kundu, 1983; Shevgaonkar and Kundu, 1984). The unique aspect of the 20 cm observations is that they can be used to specify the structure and strength of the magnetic field. This is not possible with any other technique, either at optical or X-ray wavelengths.

Much, if not all, of the 20 cm emission is due to the thermal bremsstrahlung of the same hot plasma that gives rise to the soft X-ray emission. Because the magnetic energy density dominates the thermal energy density in the low solar corona, this plasma usually remains trapped within the magnetic loops. Electron temperatures of $T_e = 2$ to 4×10^7 K, electron densities of $N_e = 10^9$ to 10^{10} cm^{-3} and loop extents $L = 10^9$ to 10^{10} cm are inferred from the 20 cm bremsstrahlung, while longitudinal magnetic field strengths of $H_{\parallel} \sim 50$ Gauss are inferred from the circular polarization if it is due to propagation effects. Thermal gyroresonance emission may also play a role in the 20 cm coronal loops, and in this case stronger magnetic fields of $H_{\parallel} \sim 200$ Gauss are inferred from the polarization data.

MICROWAVE BURSTS FROM THE SUN - PRECURSORS AND LOCATION

Microwave bursts from the Sun are characterized by a compact (5" to 30"), circularly polarized ($\rho_c = 10\%$ to 90%) impulsive component with a brightness temperature of $T_B = 10^7$ to 10^{10} K lasting between 1 and 5 minutes. This is often followed by a larger, longer post-burst component with relatively low polarization and brightness temperature. The impulsive part of the microwave energy is usually released in the upper parts of coronal loops and

between the flaring H α kernels that mark the foot-points of magnetic loops (see Figure 3; Marsh and Hurford, 1980; Lang, Willson and Felli, 1981; Kundu and Vlahos, 1982). A nonthermal tail of electrons with energies greater than 100 KeV is created near the top of the coronal loop. Some of these electrons are trapped in the upper parts of the loop, producing the impulsive microwave bursts by synchrotron radiation. Other electrons stream down to the loop foot-points, producing hard X-ray bursts and the H α kernels.

Changing magnetic fields within solar active regions must provide the energy source for solar bursts, or flares, and trigger their eruption (Gold and Hoyle, 1960). The location of these changes could not, however, be accurately specified from observations at optical wavelengths alone. This is because it is changes in the invisible coronal magnetic fields and temperature enhancements within coronal loops that seem to play the dominant role in the excitation of solar bursts. Theoretical considerations indicate, for example, that magnetic shear within coronal loops and interacting coronal loops can trigger solar bursts and supply their energy (Emslie, 1982; Heyvaerts, Priest and Rust, 1977; Priest, 1983; Somov and Syrovetskii, 1982; and Spicer, 1977, 1981).

Preburst activity is associated with increases in the intensity and the degree of circular polarization of the centimeter wavelength emission of solar active regions (Lang, 1974). These increases precede solar bursts on time scales of tens of minutes to an hour. The high angular resolution provided by the V.L.A. on time intervals as short as 3.3 seconds has now shown that these increases are associated with changes in the coronal magnetic

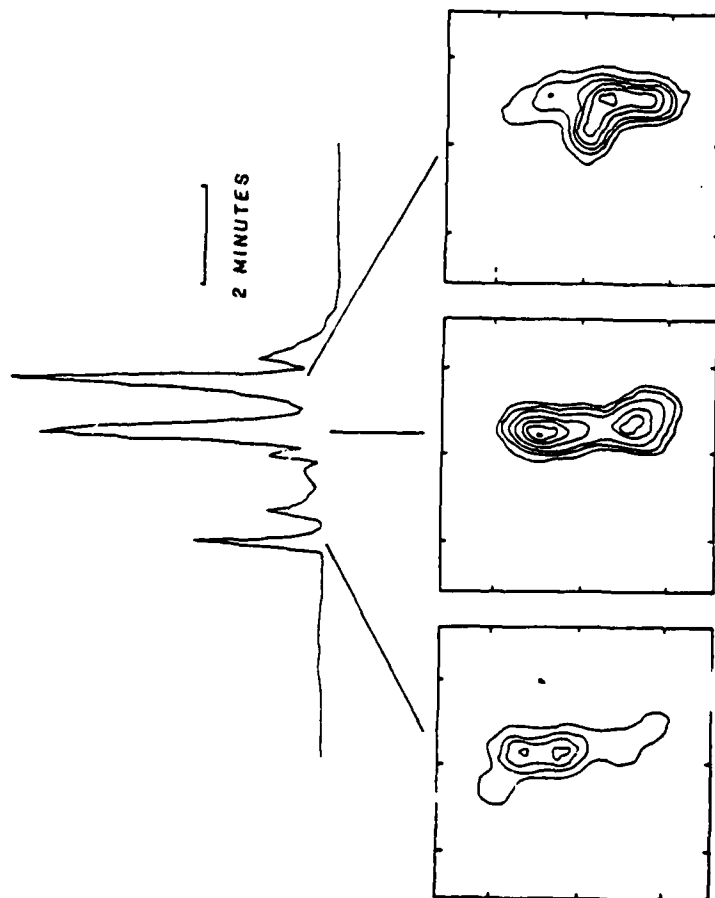


Fig. 4. The time profile of successive impulsive bursts at 20 cm wavelength is compared with ten second V.L.A. synthesis maps at the same wavelength. Here the countour intervals are in steps of 1.0×10^7 K and the angular scale can be inferred from the 30" spacing between fiducial marks on the axes.

field and with preburst heating in coronal loops. (Kundu 1982, 1983; Willson, 1983, 1984; Willson and Lang, 1984).

Single coronal loops or arcades of loops often begin to heat up and change structure about fifteen minutes before the eruption of impulsive bursts. A comparison of the X-ray and radio data (Willson, 1984) indicate a peak electron temperature of $T_e = 2.5 \times 10^7$ K and an average electron density of $N_e = 10^{10} \text{ cm}^{-3}$ during the preburst heating for one case. Preburst heating can also occur in coronal loops that are adjacent to, but spatially separated from, the sites of impulsive bursts. (Willson and Lang, 1984).

New bipolar loops can emerge and interact with preexisting ones, thereby triggering solar bursts. When the polarity of the new emerging flux differs from that of the preexisting flux, current sheets are produced that trigger the emission of bursts. A similar process can occur when preexisting adjacent loops undergo magnetic changes and trigger eruptions in nearby coronal loops.

Microwave bursts can be sequentially triggered within magnetically complex regions. As illustrated in Figure 4, successive intense bursts can be emitted from spatially separated coronal loops. Here the total intensity of the 20 cm burst emission is mapped. The polarization data indicate that the spatially separated structures are dipolar loops. In contrast to the intense bursts, the successive weaker bursts shown in the time profile were emitted from the same loop as the immediately preceding intense burst.

THE SLOWLY VARYING COMPONENT OF MICROWAVE EMISSION FROM DWARF M FLARE STARS

Nearby main-sequence stars of late spectral type exhibit quiescent, or non-flaring, X-ray emission whose absolute luminosity may be as much as 100 times that of the Sun (Vaiana et al., 1981). The X-ray radiation has generally been interpreted as the thermal bremsstrahlung of hot stellar coronae with electron temperatures $T_e \sim 10^7$ K, or an order of magnitude hotter than the Sun's corona. Because the absolute X-ray luminosity increases with stellar rotation speed (Pallavicini et al., 1981), the brighter X-ray stars rotate faster than the Sun and could thereby generate stronger magnetic fields. In fact, surface magnetic fields of strength $H_s \sim 1,000$ Gauss covering as much as 60% of the stellar surface have been observed for several nearby main-sequence stars of late spectral type (Marcy, 1983). This suggests that these nearby stars may exhibit star spots and stellar loops that are detectable at radio wavelengths.

The solar analogy suggests that the magnetic fields and coronal plasma of other stars will be detected as slowly varying microwave emission. Nearby dwarf M stars of the UV Ceti type do, in fact, exhibit quiescent, or non-flaring, microwave emission that is slowly variable with time scales of tens of minutes to hours (Gary and Linsky, 1981; Linsky and Gary, 1983; Topka and Marsh, 1982). The variation is not related to stellar rotation whose periods are on the order of 100 hours.

At the distance of the nearby dwarf M stars, the stellar disks have angular extents of about 10^{-3} seconds of arc. They therefore remain un-

resolved even with the V.L.A.; but the two components of the binary system EQ Pegasi have been detected (Topka and Marsh, 1982). A summary of microwave detections is given in Table 1.

As illustrated in Table 1, brightness temperatures, $T_B \sim 10^7$ to 10^8 K are inferred if the microwave emitting source covers the entire visible surface of the star. Brightness temperatures comparable to that expected from the Sun ($T_B \sim 10^6$ K) or inferred from the absolute X-ray luminosity ($T_B \sim 10^7$ K), are obtained if the stellar emitting region is three times as large as the visible star. If this is the case, the slowly variable microwave radiation, which is often circularly polarized with $p_c \sim 30\%$, can be explained as the gyroresonant emission of thermal electrons spiralling in magnetic fields of strength $H_i \sim 300$ Gauss. Alternatively, the gyrosynchrotron emission of a relatively small number of electrons from much smaller sources could explain the microwave emission (Linsky and Gary, 1983). Thermal bremsstrahlung is incidentally ruled out as a dominant microwave emitting mechanism, for the required electron temperatures are an order of magnitude higher than those inferred from the X-ray emission.

MICROWAVE BURSTS FROM DWARF M FLARE STARS

The nearby dwarf M stars of the UV Ceti type also emit X-ray flares in which the X-ray emission can increase by as much as a factor of thirty in a few minutes. This suggests that stellar active regions can undergo magnetic changes that trigger stellar microwave bursts. Microwave bursts have, in fact, been detected from nearby dwarf M stars by several observers (Spangler, *et. al.*, 1974; Fisher

Table 1: Microwave emission from dwarf M flare stars at 6 cm wavelength

STAR	SPECTRAL TYPE	DISTANCE (parsecs)	RADIUS (R_{\odot}^{-1})	FLUX (mJy)	T_B^* (°K)	$\log L_X^{**}$ (erg s^{-1})
X^1 Ori	GO + M4V	10.0	1.18	0.6	3×10^7	29.6
UV Cet	M5.6eV + M5.Gev	2.7	0.5	2.2	1×10^7	27.5
YY Gem	dM1e + dM1e	14.7	1.25	1.8	2×10^8	29.6
Wolf 630	dM4e + dM4e	6.4	0.68	1.5	1×10^8	29.3
EQ Peg	dM3.5e + dM4.5e	6.5	0.4	0.7	1×10^8	28.9
AD Leo	dM4.5e	4.9	0.5	1.5	1×10^8	29.0
YZ Cmi	dM4.5e	6.0	0.5	4.0	4×10^8	28.5

* Brightness temperature T_B assuming that the microwave emitter is equal in size to the visible stellar surface. For comparison, $T_B = 10^6$ K for the Sun's corona.

** The absolute X-ray luminosity is L_X . For comparison, the mean value for the Sun is $L_X = 10^{27.5} \text{ erg s}^{-1}$.

and Gibson, 1982; Gary Linsky and Dulk, 1982, and Lang et. al., 1983). The stellar microwave bursts are very similar to those emitted by the Sun, with high degrees of circular polarization $\rho_c \sim 100\%$ and relatively brief durations of a few minutes.

Recent observations of a 20 cm burst from the dwarf M star AD Leonis are of particular interest, for they indicate that the impulsive burst is emitted by a coherent radiation mechanism (Lang et. al., 1983). The highly polarized impulsive burst of a few minutes duration occurred during the gradual rise of an unpolarized burst that lasted about twenty minutes. When the impulsive burst is examined with higher time resolution (Figure 5), a sequence of 100% left-hand circularly polarized spikes is detected. This situation is entirely analogous to the microwave bursts from solar active regions where the gradual event is interpreted as the bremsstrahlung of a high-temperature, thermal plasma and the circularly polarized impulsive emission is attributed to non-thermal radiation that typically occurs during the rise phase of a thermal burst.

The polarization did not change during the emission of successive spikes, suggesting that the magnetic field structure does not change during spike emission. A close examination of individual spikes indicates that their rise times were less than the integration time of 200 milliseconds. An upper limit to the linear size, L , of the emitting region, estimated by the distance that light travels in 200 milliseconds, is $L \sim 6 \times 10^9$ cm. If the microwave burst emission grows at the Alfvén speed, then $L \sim 6 \times 10^7$ cm. A dM4.5e star like AD Leonis is expected to have a radius $R = 0.5R_\odot = 3.5 \times 10^{10}$ cm. The emitting region is therefore between 6 and 600 times smaller than the star's radius. Provided that

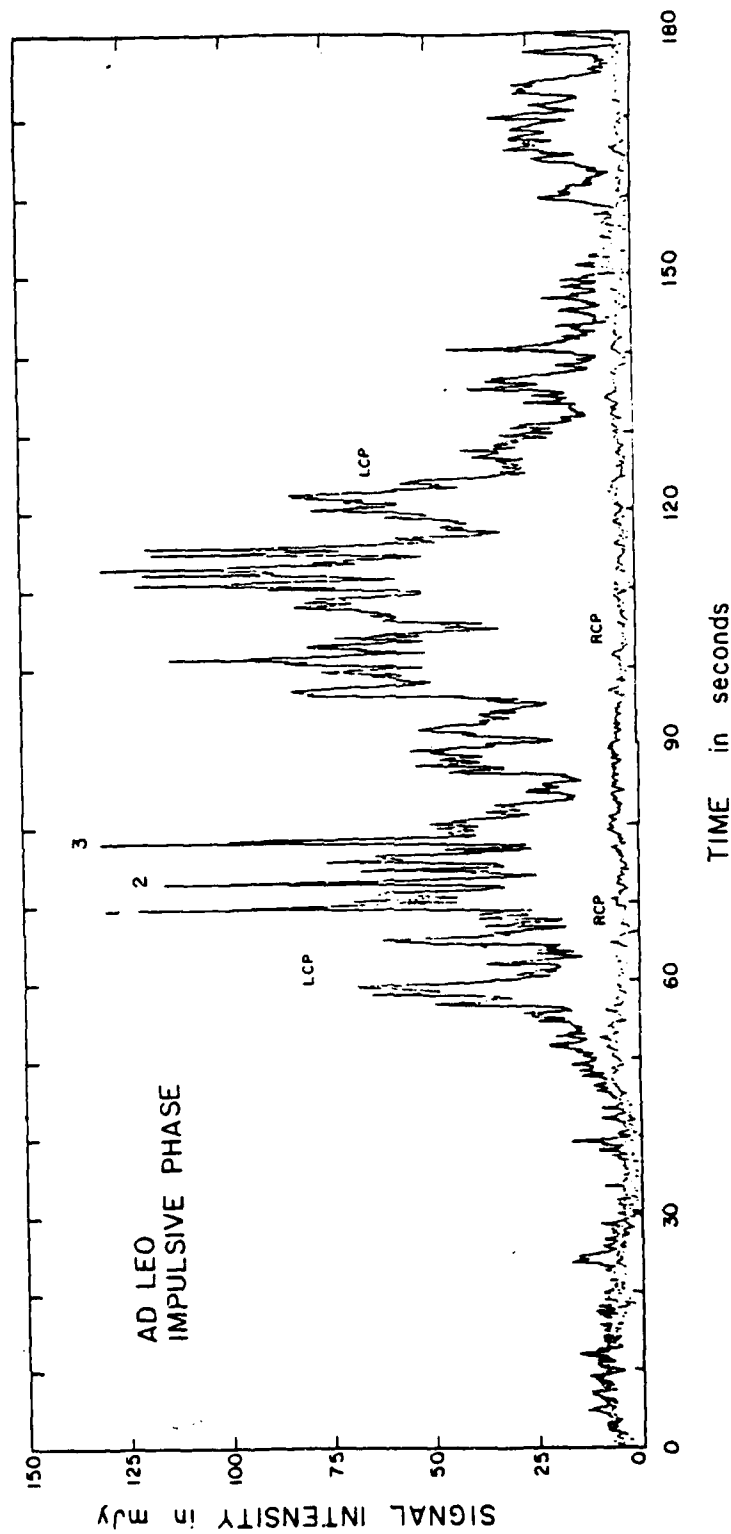


Fig. 5. An impulsive burst from the dwarf M flare star AD Leo observed with right and left hand circular polarization (RCP and LCP) at 20 cm wavelength. It is composed of a sequence of rapid spikes which are all 100% left-hand circularly polarized.

the burst emitter is symmetric, it has an area that is between 3×10^{-6} and 3×10^{-2} of the stellar surface area, and a brightness temperature $T_B \sim 10^{13}$ to 10^{17} K.

The high brightness temperatures of the microwave spikes from AD Leonis require a coherent radiation mechanism similar to a maser. The high degrees of circular polarization $\rho_c = 100\%$ indicate that an intense magnetic field is involved in the emission process. Melrose and Dulk (1982) have attributed the high brightness temperatures and the high degrees of circular polarization of solar and stellar bursts to the masing action of electrons trapped within magnetic loops. Because radiation at the first harmonic of the gyrofrequency cannot escape from such hot, dense plasmas, they attribute the bursts to masers operating at the second harmonic of the gyrofrequency cannot escape from such hot, dense plasmas, they attribute the bursts to masers operating at the second harmonic of the gyrofrequency. At our 20 cm observing wavelength, the second harmonic corresponds to a longitudinal magnetic field strength of $H_z = 250$ Gauss.

We conclude this review of the solar-stellar connection by noticing that observational limitations may lead to incorrect interpretations of the microwave emission from the Sun and stars. For example, it was once thought that the quiescent microwave emission from solar active regions had a low degree of circular polarization with $\rho_c \sim 30\%$. This was due to beam dilution effects rather than an intrinsic property of the emitter. When the core microwave sources were eventually resolved using interferometers (Lang, 1974), it was realized that $\rho_c = 100\%$ was possible. A similar resolution problem

may be occurring in the time domain, for most synthesis arrays and satellite equipment have integration times that are no shorter than a few seconds (for the V.L.A. it is 3.3 seconds). Such integration times preclude the detection of rapid, spiked emission of the AD Leonis type. They may also lead to serious underestimates of the burst flux density by averaging brief events over long time intervals.

ACKNOWLEDGEMENTS

The research leading up to this review was done in collaboration with Robert F. Willson at Tufts University. Radio astronomical studies of the Sun and other active stars at Tufts University are supported under grant AFOSR-83-0019-B with the Air Force Office of Scientific Research. Investigations of flare stars at Tufts University are also supported by NASA grant NAG 5-477.

REFERENCES

- Alissandrakis, C.E. and Kundu, M.R.: 1982, Ap. J. (Letters), 253, L49.
- Alissandrakis, C.E., Kundu, M.R. and Lantos, P.: 1980 Astr. Ap., 82, 30.
- Dulk, G.A. and Gary, D.E.: 1983, Astr. Ap., 124, 103.
- Emslie, A.G.: 1982, Ap. Lett. 22, 41.
- Fisher, P.L. and Gibson, D.M.: 1982; in Second Cambridge Workshop on Cool Stars, Stellar Systems and the Sun, ed. M.S. Giampapa and L. Golub (Smithsonian Observagory Special Report No.392), pp.109-114.
- Gary, D.E. and Linsky, J.L.: 1981, Ap. J., 250, 284.

- Gary, D.E., Linsky, J.L. and Dulk, G.A.: 1982, Ap. J. (Letters), 263, L79.
- Gel'freikh, G.B. and Lubyshev, B.I.: 1979, Soviet Astr. - A.J., 23, 316.
- Gold T. and Hoyle, F.: 1960, M.N.R.A.S., 120, 89.
- Heyvaerts, J., Priest, E.R. and Rust, D.M.: 1977, Ap. J., 216, 123.
- Kundu, M.R.: 1982, Rep. Prog. Phys., 45, 1435.
- Kundu, M.R.: 1983, Solar Phys. 86, 205.
- Kundu, M.R. and Alissandrakis, C.E.: 1975, Nature, 257, 465.
- Kundu, M.R., et al.: 1977, Ap. J., 213, 278.
- Kundu, M.R. and Vlahos, L.: 1982, Space Sci. Rev., 32, 405.
- Lang, K.R.: 1974, Solar Phys., 36, 351.
- Lang, K.R. and Willson, R.F.: 1979, Nature, 278, 24.
- Lang, K.R. and Willson, R.F.: 1980, in I.A.U. Symposium 86, Radio Physics of the Sun, ed. M.R. Kundu and T.E. Gergely (Dordrecht: Reidel), p.109.
- Lang, K.R. and Willson, R.F.: 1982, Ap. J. (Letters), 255, L111.
- Lang, K.R. and Willson, R.F.: 1983a, Astr. Ap., 127, 135.
- Lang, K.R. and Willson, R.F.: 1983b, in Adv. Space Res. Proc. XXIV COSPAR (Pergamon: London), p. 91-100.
- Lang, K.R., Willson, R.F. and Gaizauskas, V.: 1983, Ap. J., 267, 455.
- Lang, K.R., Willson, R.F. and Felli, M.: 1981, Ap. J., 247, 338.
- Lang, K.R., Willson, R.F. and Rayrole, J.: 1982, Ap. J., 258, 384.

- Lang, K.R., Bookbinder, J., Golub, L. and Davis, M.M.:
1983, Ap. J. (Letters), 272, L15.
- Linsky, J.L. and Gary, D.E.: 1983, Ap. J., 274, 776.
- Marcy, G.W.: 1983, in I.A.U. Symposium 102, Solar and
Stellar Magnetic Fields: Origins and Coronal
Effects, ed. J.O. Stenflo (Dordrecht: Reidel).
- Marsh, K. and Hurford, G.J.: 1980, Ap. J. (Letters),
240, L111.
- McConnell, D. and Kundu, M.R.: 1983, Ap. J. 269, 698.
- Melrose, D.B. and Dulk, G.A.: 1982, Ap. J., 259, 844.
- Pallavicini, R., Sakurai, T. and Vaiana, G.S.: 1981,
Astr. Ap., 98, 316.
- Pallavicini, R. et al.: 1981, Ap. J., 248, 279.
- Priest, E.R.: 1983, Solar Phys., 86, 33.
- Shevgaonkar, R.K. and Kundu, M.R.: 1984, Ap. J.
283, 413.
- Spangler, S.R., Rankin, J.M. and Shawhan, S.D.: 1974,
Ap. J. (Letters), 194, L43.
- Somov, B.V. and Syrovetskii, S.I.: 1982, Solar Phys.,
75, 237.
- Spicer, D.S.: 1977, Solar Phys., 53, 305.
- Spicer, D.S.: 1981, Solar Phys., 70, 149.
- Topka, K. and Marsh, K.A.: 1982, Ap. J., 254, 641.
- Vaiana, G.S. and Rosner, R.: 1978, Ann. Rev. Astr.
Ap., 16, 393.
- Vaiana, G.S., et al.: 1981, Ap. J., 244, 163.
- Willson, R.F.: 1983, Solar Phys., 83, 285.
- Willson, R.F.: 1984, Solar Phys., to be published.
- Willson, R.F. and Lang, K.R.: 1984, Ap. J., 279, 427.

DISCUSSION

KUNDU: 1. For AD Leo when you talk about masering, did you estimate its brightness temperature?

2. How did you estimate that the burst emitting region of AD Leo is less than 3 per cent of the total star area?

LANG: 1. An upper limit to the size of the emitter is inferred from the relativity theory argument that nothing can move faster than the velocity of light $c = 3 \times 10^{10}$ cm/sec. The observed rise times = 200 msec then give the size limit. $L \leq C \times \tau = 6 \times 10^9$ cm. Then, assuming a symmetric emitter, the observed radio flux density of 130 mJy can be used to infer a lower limit to the brightness temperature $T_B \geq 10^{13}$ K.

2. AD Leo is a dM 4.5e star with a radius $R = 0.5 R_{\odot} = 3.5 \times 10^{10}$ cm. The above (Q1) limit to linear size, L , is six times smaller than the radius. Assuming a symmetric emitter, the source area is then $A \leq 0.03$ or 3 per cent of the stellar surface area (see Lang et al. *Astrophysical Journal (Letters)* 272, L15-18 (1983) for details).

KUNDU: In one of your slides showing the two components of UV ceti, it appeared that the two components were of equal intensity, I know from my own observations as well as of others that the two components are of dissimilar strengths. Could you please explain your slide?

LANG: The UV ceti system contains two stars L 726-8A; a radio flare star, and UV cet or L 726-8B, that exhibits most of the quiescent emission at 6 cm wavelength. When L 726-8A is flaring the two components can be of equal intensity. When it is not, the continuum emission of UV cet may be dominant. We must also remember that even this quiescent emission is time variable and can fade to undetectable levels.

SINGH: Do the absence of right-handed polarization (RHP) and hundred per cent presence of left-handed polarization (LHP) or arbitrary polarization provide additional clues about the radio emission processes, region of emission and interaction with the plasma?

LANG: Yes, the high circular polarization observed in the 6 cm emission of active region does provide clues about the radiation mechanism. In the first place, the ring like or horse shoe structure of the circular polarization above sunspots shows rather conclusively that the radiation mechanism is gyroresonance emission of thermal electrons ($T_e \sim 10^6$ K) at the low harmonics of the gyrofrequency (second harmonic with longitudinal magnetic field strength $H_{\parallel} = 600$ gauss).

11. SOLAR-TERRESTRIAL PREDICTIONS:

Proceedings of a Workshop at Meudon, France, June 18 -22, 1984

MEUDON, 1984

Science Sponsors

COSPAR
IAG
IAU
SCOSTEP
URSI

Committee on Space Research
International Association of Geomagnetism and Aeronomy
International Astronomical Union
Scientific Committee on Solar-Terrestrial Physics
Union Radio Scientifique Internationale

Science and Financial Sponsors

CNES
ESA
IUWDS
OP
TAAF

Centre National d'Etude Spatiale
European Space Agency
International Ursigram and World Days Service
Observatoire de Paris
Terres Australes et Antarctiques Francaises

edited by

P. A. Simon

Paris-Meudon Observatory, Meudon, France

G. Heckman

NOAA, Boulder, Colorado, U.S.A.

M. A. Shea

AFGL, Bedford, Massachusetts, U.S.A.

Prepared and published through the cooperative efforts of the

National Oceanic and Atmospheric Administration.

325 Broadway, Boulder, Colorado 80303, U.S.A.

and

Air Force Geophysics Laboratory

Hanscom AFB, Bedford, Massachusetts 01731, U.S.A.

1986

APPENDIX A

ABSTRACTS OF INVITED REVIEW PAPERS

FORECASTING SUNSPOT MAXIMUM: A REVIEW

G. M. BROWN
Department of Physics
University College of Wales
Aberystwyth, UK

ABSTRACT. A general review is given of the various techniques which have been used to predict the magnitude of a forthcoming sunspot maximum. For convenience, these are discussed under two main headings: methods which use statistical/numerical analyses of the time series of past solar activity data, including secular cycles, and methods which use a wide range of solar or geophysical precursors measured prior to the sunspot peak. Full bibliographical references are given so that readers can follow up detailed study of individual methods. No attempt is made here to describe specific approaches, or to rank the methods in any league table.

ACTIVE SOLAR LONGITUDES

V. Gaizauskas
Herzberg Institute of Astrophysics
Ottawa, Canada

ABSTRACT. The tendency for recurrent activity to cluster in longitude is discussed in terms of observational tracers of magnetic fields. Locations of recurrent activity are by definition predictable but not their strengths owing to the lack of a clear understanding of the process behind this behaviour.

HIGH RESOLUTION MICROWAVE OBSERVATIONS OF THE SUN AND NEARBY STARS

K. R. LANG
Department of Physics and Astronomy
Robinson Hall
Tufts University
Medford, MA 02155 U.S.A.

ABSTRACT. High resolution microwave observations are providing new insights to the nature of active regions and eruptions on the Sun and nearby solar-like stars. The strength, evolution, and structure of magnetic fields in coronal loops are specified by multiple wavelength V.L.A. observations. Unique tests of flare models can be made using V.L.A. snapshot maps with angular resolutions of better than one second of arc for time intervals as short as 3.3 seconds. Magnetic changes that precede solar eruptions on time scales of tens of minutes include magnetic shear within isolated coronal loops, emerging coronal loops, and the interaction of two orthogonal loops. Nearby main sequence stars of late spectral type emit slowly varying microwave radiation and stellar microwave bursts that show striking parallels with those of the Sun.

EFFECTS OF THE SOLAR-TERRESTRIAL ENVIRONMENT ON SATELLITE OPERATIONS

D. N. BAKER
University of California
Los Alamos National Laboratory
Los Alamos, NM 87545 U.S.A.

ABSTRACT. Hot plasma and energetic particle populations in space are known to produce spacecraft operational anomalies. In the inner part of the earth's magnetosphere, these effects are primarily due to durably trapped radiation belt particles, and the integrated doses can be calculated quite accurately for any given orbit. In the outer magnetosphere many spacecraft operational problems appear to be due to intense, transient phenomena. It is shown that three types of naturally-occurring, and highly variable, hostile particle radiation environments are encountered at, or near, the geostationary orbit: (1) High-energy protons due to solar flares; (2) Very high energy electrons (2-10 MeV) of unknown origin; and (3) Energetic ions and electrons produced by magnetospheric substorms. Present particle sensor systems provide energetic particle detection and assessment capabilities during these kinds of high-energy radiation events. Numerous operational anomalies and subsystem problems have occurred during each type of event period, and the association of such upsets is demonstrated in this paper. Methods of prediction of magnetospheric disturbances are discussed, and overall recommendations are made for dealing with this continuing problem.

GEOMAGNETIC ACTIVITY AND THE SOLAR CYCLE

P. A. SIMON
LA 326, DASOP
Paris Meudon Observatory
J. P. LEGRAND
INAG Mesure
Saint Maur

ABSTRACT. We analyze the relationships with the sunspot cycle, and we discuss the origin of the four categories of solar phenomena which contribute to geomagnetic activity. The shock event activity has a loose link, if any, with the sunspot number but a quite definite cycle behavior. The temporary expansion of polar wind streams generates the so-called recurrent geomagnetic activity occurring just before a sunspot minimum. The remaining activity is related to the distribution around the sun and to the time evolution of both the coronal streamers and the heliosheet, which are the sources, in the ecliptic plane, of the slow undisturbed wind of the quiet days and of the low density areas in between which are at the origin, in the ecliptic plane, of the fluctuating wind activity.

12. V.L.A. OBSERVATIONS OF FLARE BUILD-UP IN CORONAL LOOPS

Kenneth R. Lang and Robert F. Willson

Department of Physics, Tufts University, Medford, MA 02155, U.S.A.

ABSTRACT

Very Large Array (V.L.A.) measurements at 20 cm wavelength map emission from coronal loops with second-of-arc angular resolution at time intervals as short as 3.3 seconds. The total intensity of the 20 cm emission describes the evolution and structure of the hot plasma that is detected by satellite X-ray observations of coronal loops. The circular polarization of the 20 cm emission describes the evolution, strength and structure of the coronal magnetic field. Preburst heating and magnetic changes that precede burst emission on time scales of between 1 and 30 minutes are discussed. Simultaneous 20 cm and soft X-ray observations indicate an electron temperature $T_e \sim 2.5 \times 10^7$ K and electron density $N_e \sim 10^{10} \text{ cm}^{-3}$ during preburst heating in a coronal loop that was also associated with twisting of the entire loop in space. We also discuss the successive triggering of bursts from adjacent coronal loops; highly polarized emission from the legs of loops with large intensity changes over a 32 MHz change in observing frequency; and apparent motions of hot plasma within coronal loops at velocities $V > 2,000$ kilometers per second.

OBSERVING CORONAL LOOPS WITH THE V.L.A.

Because 356 interferometer pairs are sampled at the Very Large Array (V.L.A.), it is possible to create synthesis maps of solar active regions with second-of-arc angular resolution at time intervals as short as 3.3 seconds. Both the left-hand circularly polarized (LCP) and right-hand circularly polarized (RCP) signals are sampled, making it possible to create synthesis maps of the total intensity $I = (RCP + LCP)/2$ and circular polarization $V = (RCP - LCP)/2$. The total intensity maps describe the structure and evolution of the brightness temperature, whereas the circular polarization maps delineate the structure, evolution and strength of the magnetic field. Synthesis maps at longer microwave wavelengths, λ , refer to higher levels within the solar atmosphere where the brightness temperatures, T_B , are comparable to the electron temperature. Observations at $\lambda = 2$ cm refer to the footpoints of coronal loops where $T_B \sim 10^5$ K, while 6 cm observations often delineate the legs of magnetic dipoles where $T_B \sim 10^6$ K. The coronal loops are more reliably detected using the V.L.A. at 20 cm wavelength where emission from the entire loop is routinely detected [1,2,3,4,5,6]. These ubiquitous loops are the dominant structural element in the solar corona, but they have previously only been detected during rare and expensive satellite observations at soft X-ray wavelengths. Much, if not all, of the 20 cm emission is due to the thermal bremsstrahlung of the same hot plasma that gives rise to the soft X-ray emission.

The magnetic, temperature and density structure of the coronal loops can be specified from the 20 cm observations. Because the magnetic energy density dominates the thermal energy density at coronal heights, the hot plasma remains trapped within the magnetic loops. Electron temperatures $T_e = 2$ to 4×10^6 K, electron densities $N_e \sim 10^9$ to 10^{10} cm^{-3} and loop extents $L \sim 10^9$ to 10^{10} cm are inferred from the 20 cm bremsstrahlung, while longitudinal magnetic field strengths of $H_z \sim 50$ Gauss are inferred from the circular polarization, if it is due to propagation effects. Thermal gyroresonance emission may also sometimes play a role in the 20 cm coronal loops, and in this case stronger magnetic fields of $H_z \sim 200$ Gauss are inferred from the polarization data.

The microwave bursts are themselves characterized by a strongly polarized, compact (5" to 30") impulsive component with a brightness temperature of $T_B = 10^7$ to 10^{10} K lasting between 1 and 5 minutes. The impulsive phase of the microwave burst is usually located near the neutral line between two H α kernels in magnetic fields of opposite magnetic polarity. That is, the site of microwave energy release is usually at the apex of coronal loops, whereas the H α emission occurs at the footpoints of the magnetic loops in the chromosphere [3,7,8,9,10,11]. The impulsive bursts are due to the gyrosynchrotron radiation of mildly

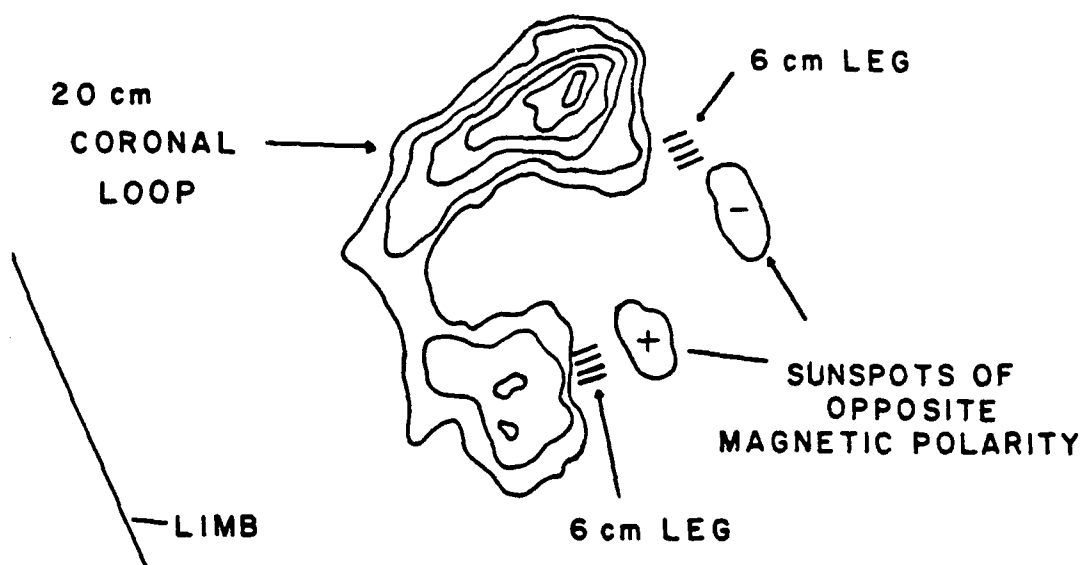


Fig. 1. A V.L.A. synthesis map of the total intensity, I , of the 20 cm emission from a coronal loop. The contours mark levels of equal brightness temperature corresponding to 0.2, 0.4, ..., 1.0 times the maximum brightness temperature of $T_b = 2 \times 10^6$ K. A schematic portrayal of the 6 cm emission, which comes from the legs of the magnetic loops, has been added together with the underlying sunspots that are detected at optical wavelengths.

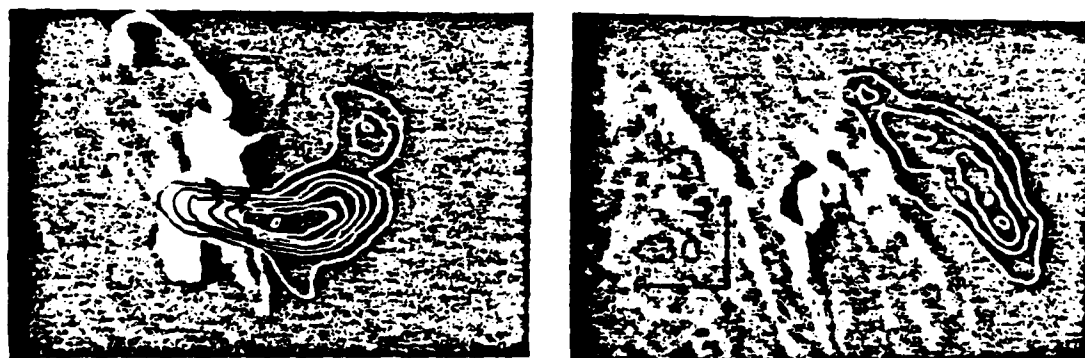


Fig. 2. The ten second V.L.A. synthesis maps of the impulsive phase of two solar bursts at 20 cm wavelength superimposed on $H\alpha$ photographs of the optical flares taken at the same time at the Big Bear Solar Observatory. The 20 cm bursts originate near the tops of coronal loops that are about 40,000 km above the flaring region seen at optical wavelengths. The western solar limb is visible in both photographs.

relativistic electrons with energies of 100 to 500 keV. Some of these electrons are trapped in the upper parts of the loop, producing the microwave bursts. Other electrons stream down to the loop footpoints, producing hard X-ray bursts and the $H\alpha$ kernels. This is often followed by a larger, longer post-burst component of microwave radiation with relatively low polarization and brightness temperature.

TRIGGERING SOLAR BURSTS IN CORONAL LOOPS

Preburst activity is associated with increases in the intensity and the degree of circular polarization of the centimeter wavelength emission of solar active regions [12,13]. These increases precede solar bursts on time scales of tens of minutes to an hour. The high angular resolution provided by the V.L.A. has now shown that the intensity increases are associated with preburst heating in coronal loops [10,11,14], and that the changes in circular polarization are associated with changes in the coronal magnetic field [10,11,15]. Both the preburst heating and the magnetic field changes may trigger solar eruptions.

Single coronal loops or arcades of loops often begin to heat up and change structure about 30 minutes before the eruption of impulsive bursts. Many theoretical models of solar flares include such a preflare phase in which the coronal loop is heated, becomes unstable and then erupts /16,17,18,19/. As illustrated in Figure 3, a magnetic loop can heat up and twist in space. The magnetic shear produces a current sheet that triggers impulsive burst emission. The magnetic shear produces a current sheet that triggers impulsive burst emission. The preburst heating shown in Figure 3 was also detected at soft X-ray wavelengths with the GOES satellite. A comparison of the X-ray and radio data /14/ indicate a peak electron temperature of $T_e = 2.5 \times 10^7$ K and an average electron density of $n_e = 10^{10} \text{ cm}^{-3}$ during the preburst heating. Preburst heating can also occur in coronal loops that are adjacent to, but spatially separated from, the sites of impulsive bursts /11/.

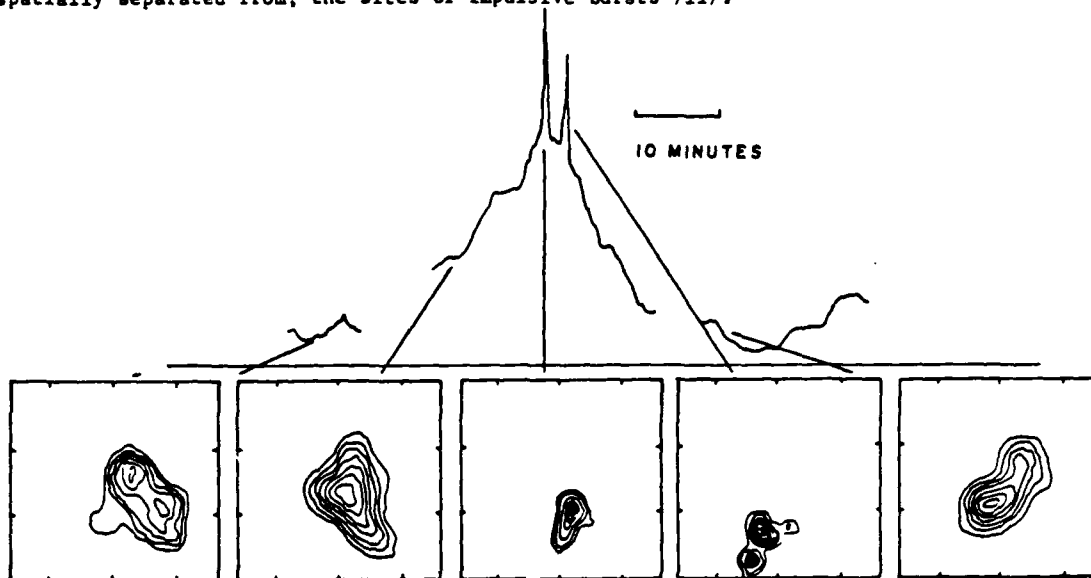


Fig. 3. The time profile of a solar burst at 20 cm wavelength illustrates heating within a coronal loop prior to the emission of two impulsive bursts. The 20 cm V.L.A. synthesis maps for ten second intervals are given below. The angular scale can be inferred from the 60" spacing between fiducial marks on the axes. The maps show that the coronal loop twisted in space, producing magnetic shear that led to impulsive burst emission from the same loop. This emission triggered a second burst from an adjacent source.

New bipolar loops can emerge and interact with preexisting ones, thereby triggering solar bursts. When the polarity of the new emerging flux differs from that of the preexisting flux, current sheets are produced that trigger the emission of bursts. A similar process can occur when preexisting adjacent loops undergo magnetic changes and trigger eruptions in nearby coronal loops.

Because of intense competition from celestial observers, it is not possible to routinely use the V.L.A. to obtain statistical data about the preburst heating and magnetic changes that trigger solar bursts. Other users of the V.L.A. have, however, reported the detection of magnetic changes that trigger bursts, including the interaction of orthogonal dipoles /15/. Preheating up to 30 minutes before flare onset has been detected for 70 percent of the flares observed at soft X-ray wavelengths using the Skylab satellite /20/, and minor energy release at 1.7 cm wavelength has preceded 25 percent of the main bursts observed at this wavelength at time intervals of between 10 to 35 minutes /21/.

Microwave bursts can be sequentially triggered within magnetically complex regions. As illustrated in Figure 4, successive intense bursts can be emitted from spatially separated coronal loops. Here the total intensity of the 20 cm burst emission is mapped. The polarization data indicate that the spatially separated structures are dipolar loops. In contrast to the intense bursts, the successive weaker bursts in the time profile were emitted from the same loop as the immediately preceding intense burst. The sequential triggering of intense impulsive bursts may be related to theoretical models of interacting loops in which an energy release in one loop triggers, through a magnetohydrodynamic disturbance, an energy release in a neighboring loop /22/.

Successive impulsive bursts can also be triggered within one leg of a coronal loop when a more gradual, oppositely polarized component is emitted from the other leg of the loop (see Figures 5 and 6). The most interesting aspect of this observation is that the last impulsive burst of the sequence (number 7) has an intensity difference of almost a factor of two over a very narrow frequency range of only 32 MHz. This might be explained by narrow-band maser emission.

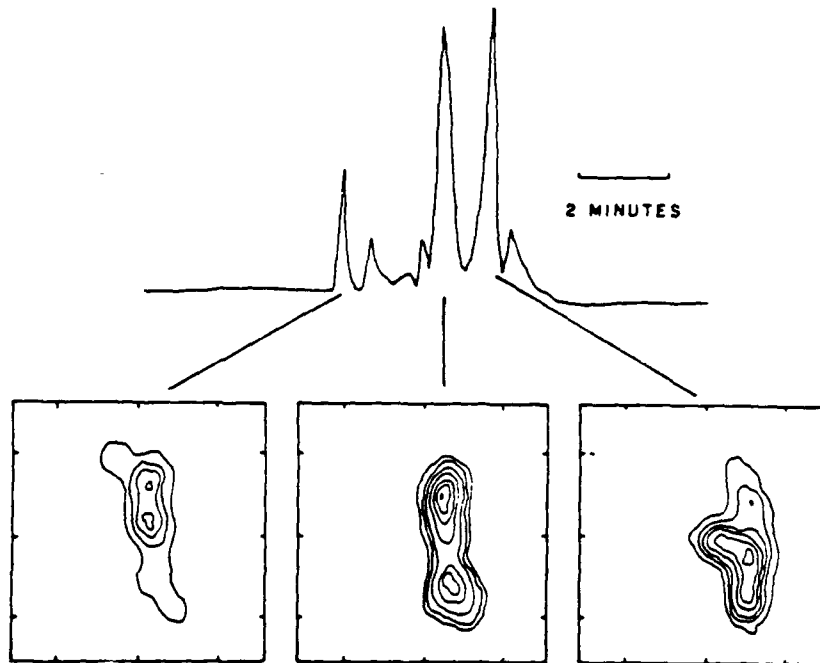


Fig. 4. The time profile of successive impulsive bursts at 20 cm wavelength is compared with ten second V.L.A. synthesis maps at the same wavelength. Here the contour intervals are in steps of 1.0×10^7 K and the angular scale can be inferred from the $30''$ spacing between fiducial marks on the axes.

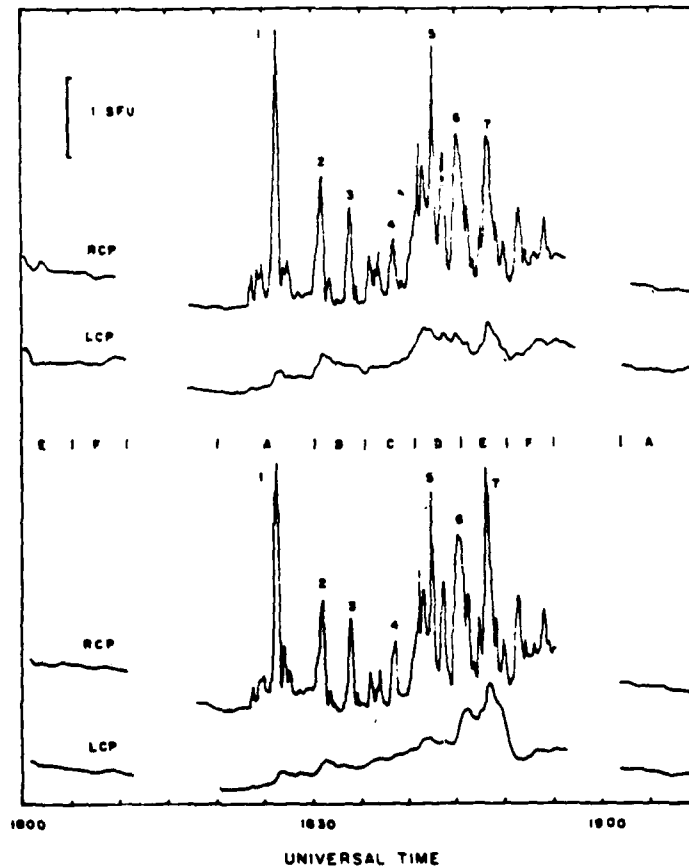


Fig. 5. A sequence of right circularly polarized (RCP) impulsive bursts observed at wavelengths near 20 cm on January 29, 1984 from AK 4398. The top and bottom profiles are at closely spaced frequencies designated by A: 1410 and 1375 MHz, B: 1480 and 1440 MHz, C: 1550 and 1515 MHz, D: 1620 and 1585 MHz, E: 1690 and 1658 MHz, and F: 1720 and 1705 MHz. Each pair of frequencies was observed for about 5 minutes. The 10 second snapshot maps at the peak of each burst are shown in Figure 6.

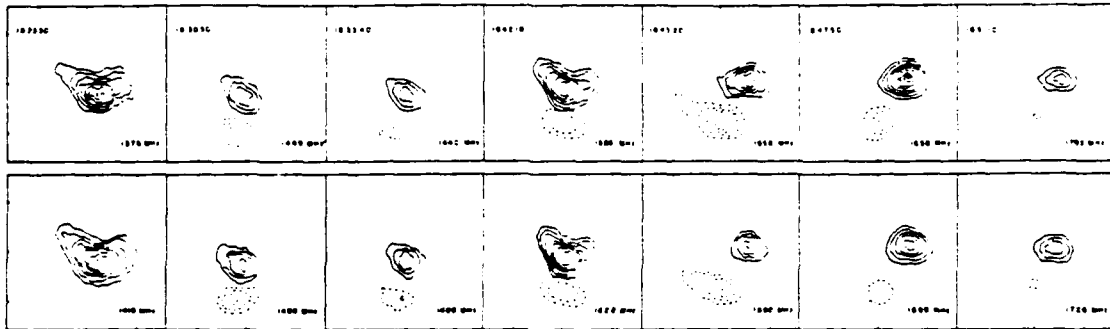


Fig. 6. Ten second snapshot maps made at the peak of the impulsive bursts shown in Figure 5. The right circularly polarized (RCP) bursts originated from a source (solid lines) that was spatially separated from the left circularly polarized (LCP) emission (dashed lines). The outermost contour and contour interval is 2.3×10^7 K for RCP and 9.0×10^6 K for LCP. Peak 7 occurring at $18^h 47^m 50^s$ (right) has a large difference in brightness temperature with $T_B(1658) = 1.1 \times 10^8$ K and $T_B(1690) = 6.0 \times 10^7$ K. The angular scale can be determined from the $30''$ spacing between the hatchmarks.

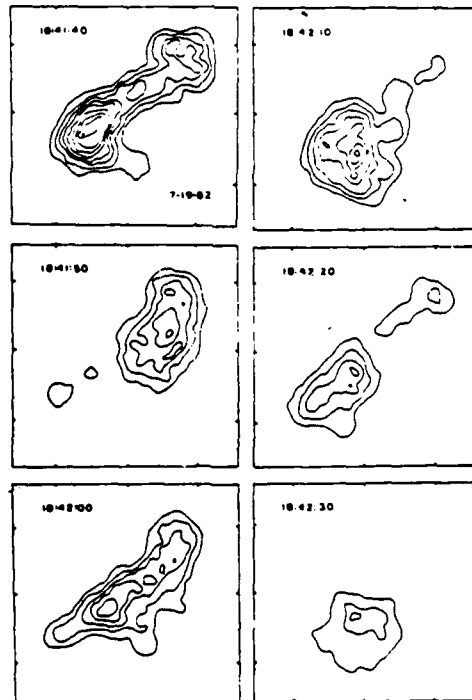


Fig. 7. A series of ten second snapshot maps of the total intensity, I , of an impulsive burst at 20 cm wavelength. The outermost contour and the contour interval are both equal to 1.3×10^6 K. The angular scale is determined by the $30''$ spacing between the fiducial marks on the axes.

As illustrated in Figure 7, the V.L.A. 20 cm snapshot maps also reveal the apparent motion of hot plasma within coronal loops at rates of more than 30" in 10 seconds, or a velocity $V > 2,000$ kilometers per second. Thermal conduction fronts might reach these velocities, exciting the plasma as they move through it. Although this speed is an order of magnitude higher than those detected spectroscopically during other bursts, there is abundant evidence for high speed excitations during solar bursts. Shocks with velocities of 1,000 kilometers per second are found in large flares /23/, and distant activation by electron beams travelling along large coronal loops at velocities $V > 6,000$ kilometers per second have been reported /24/. Electron beams moving with velocities of 100,000 kilometers per second may even have been the exciting agent for two large flares /25/.

ACKNOWLEDGEMENTS

Radio astronomical studies of the Sun and other active stars are supported under Grant AFOSR-83-0019-B with the Air Force Office of Scientific Research.

REFERENCES

1. K.R. Lang, R.F. Willson, and J. Kayrole, Astrophysical Journal **258**, 284 (1982).
2. K.R. Lang, R.F. Willson and V. Gaizauskas, Astrophysical Journal **267**, 455 (1983).
3. K.R. Lang and R.F. Willson, Adv. Space Res. **2**, No. 11, 91 (1983).
4. D. McConnell and M.R. Kundu, Astrophysical Journal **269**, 698 (1983).
5. G.A. Dulk and D.E. Gary, Astronomy and Astrophysics **124**, 103 (1983).
6. R.K. Shevgaonkar and M.R. Kundu, Astrophysical Journal, in press (1984).
7. K. Marsh and G.J. Hurford, Astrophysical Journal (Letters) **240**, L111 (1980).
8. K.R. Lang, R.F. Willson and M. Felli, Astrophysical Journal **247**, 338 (1981).
9. M.R. Kundu and L. Vlahos, Space Science Reviews **32**, 405 (1982).
10. R.F. Willson, Solar Physics **83**, 285 (1983).
11. K.R. Lang and R.F. Willson, Astrophysical Journal **279**, 427 (1984).
12. K.R. Lang, Solar Physics **36**, 351 (1974).
13. M.R. Kundu, T. Velusamy and R.H. Becker, Solar Physics **34**, 217 (1974).
14. R.F. Willson, Solar Physics, in press (1984).
15. M.R. Kundu, Solar Physics **86**, 205 (1983).
16. J. Heyvaerts, E.R. Priest and D.M. Rust, Astrophysical Journal **216**, 123 (1977).
17. S.I. Syrovatskii and V.D. Kuznetsov, in I.A.U. Symposium No. 86, Radio Physics of the Sun, ed. M.R. Kundu and T. Gergeley (Dordrecht: Reidel, 1980) p. 445.
18. D.S. Spicer, Solar Physics **70**, 149 (1981).
19. B.V. Somov and S.I. Syrovatskii, Solar Physics **75**, 237 (1982).
20. D.F. Webb, in I.A.U. Symposium No. 91, Solar and Interplanetary Dynamics, ed. M. Dwyer and E. Tandberg-Hanssen (Dordrecht: Reidel, 1980), p.189.
21. K. Kai, H. Nakajima and T. Kosugi, Publications of the Astronomical Society of Japan **35**, 285 (1983).
22. A.G. Emslie, Astrophysical Letters **22**, 41 (1982).
23. D.M. Rust and D.F. Webb, Solar Physics **54**, 403 (1977).
24. M.R. Kundu, D.M. Rust and M. Bobrowsky, Astrophysical Journal **265**, 1084 (1983).
25. P. Tang and R.L. Moore, Solar Physics **77**, 263 (1982).

13. The Sun and Nearby Stars: Microwave Observations at High Resolution

Mukul R. Kundu and Kenneth R. Lang

Microwave observations in the 1960's and 1970's added new dimensions to studies of solar active regions. The quiescent, or nonflaring, microwave emission at different wavelengths originates in levels of the solar atmosphere where the brightness temperatures (T_B) are comparable to the local electron tem-

perature. The dominant emission mechanism depends upon the wavelength and the physical conditions within the active region (1).

The solar active regions have intense magnetic fields that result in high degrees of circular polarization of the microwave emission. Magnetic fields permeate every level of the solar atmo-

Summary. High-resolution microwave observations are providing new insights into the nature of active regions and eruptions on the sun and nearby stars. The strength, evolution, and structure of magnetic fields in coronal loops can be determined by multiple-wavelength observations with the Very Large Array. Flare models can be tested with Very Large Array snapshot maps, which have angular resolutions of better than 1 second of arc in time periods as short as 10 seconds. Magnetic changes that precede solar eruptions on time scales of tens of minutes involve primarily emerging coronal loops and the interactions of two or more loops. Magnetic reconnection at the interface of two closed loops may accelerate electrons and trigger the release of microwave energy in the coronal parts of the magnetic loops. Nearby main-sequence stars of late spectral type emit slowly varying microwave radiation and stellar microwave bursts that show striking similarities to those of the sun.

peratures. Values of T_B increase with increasing wavelength, λ , from $\sim 6.5 \times 10^3$ K at $\lambda = 2$ mm in the low chromosphere through $\sim 10^5$ K at $\lambda = 2$ cm in the chromosphere-corona transition region to $\sim 10^6$ K at $\lambda = 20$ cm in the low corona.

The microwave radiation of solar active regions is, with the exception of bursts, thermal in nature. The radiation at millimeter wavelengths is thermal bremsstrahlung. At centimeter wavelengths the gyroresonant radiation of thermal electrons accelerated by magnetic fields can compete with the bremsstrahlung of thermal electrons accelerated in the electric fields of ions. The

sphere above active regions. The microwave observations uniquely provide direct measurements of the strength and structure of the magnetic fields in the low corona and the transition region (between the photosphere and the corona). The observed radiation is circularly polarized in the extraordinary mode of wave propagation, with right-handed circular polarization corresponding to a positive magnetic field directed toward the observer. When thermal bremsstrahlung is the dominant radiation mechanism, the circular polarization is due to a propagation effect in the presence of a magnetic field. An electromagnetic wave passing through a magnetoionic medium

is split into ordinary and extraordinary components, and the degree of circular polarization of the emergent radiation depends upon the optical depth for these two components. The longitudinal magnetic field strength (H_l) can be inferred from the polarization and the optical depths. When gyroresonance dominates, the circularly polarized radiation is emitted at the second or third harmonic of the gyrofrequency. One is thus able to infer the magnetic field strength from the observed frequency (2).

The development of aperture synthesis instruments at radio wavelengths in the 1970's made possible the spatial resolution of the solar microwave sources and opened the way for comparisons with observations of similar angular resolution at optical and x-ray wavelengths. The high-resolution microwave observations were initially carried out at wavelength $\lambda = 6$ cm with the Westerbork Synthesis Radio Telescope in the Netherlands and the Very Large Array (VLA) spread out on a desert near Socorro, New Mexico. These observations indicated that gyromagnetic effects predominate in the regions above sunspots and that maps of circular polarization at 6 cm specify the structure of the coronal magnetic field (3). The high-resolution observations also indicated that the impulsive component of microwave bursts is usually located near the top of magnetic loops and that brightness and polarization changes precede solar bursts on time scales of tens of minutes (4, 5).

Three reviews, written when the solar application of microwave aperture synthesis was at an early stage, dealt almost solely with observations at 6 cm (6). This research area has matured in recent years, with multiple-wavelength VLA observations and snapshot synthesis maps produced in time periods as short as 10 seconds. We provide here a review of these recent developments. We begin with a discussion of the results of the multiple-wavelength studies that specify the three-dimensional structure of quies-

Mukul R. Kundu is professor and director of the Astronomy Program at the University of Maryland, College Park 20742. Kenneth R. Lang is an associate professor of astronomy at Tufts University, Medford, Massachusetts 02155.

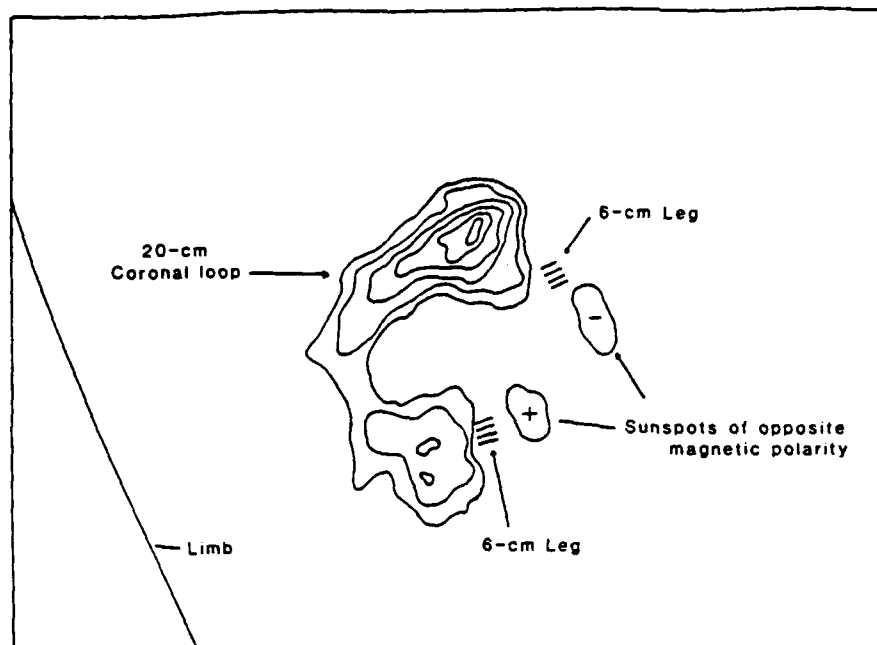


Fig. 1. Very Large Array synthesis map of a coronal loop at wavelength $\lambda = 20$ cm. The contours mark levels of equal T_B corresponding to 0.2, 0.4 . . . 1.0 times the maximum T_B of 2.0×10^6 K. A schematic portrayal of the 6-cm microwave emission, which comes from the legs of magnetic dipoles, is also shown, together with the underlying sunspots that are detected at optical wavelengths.

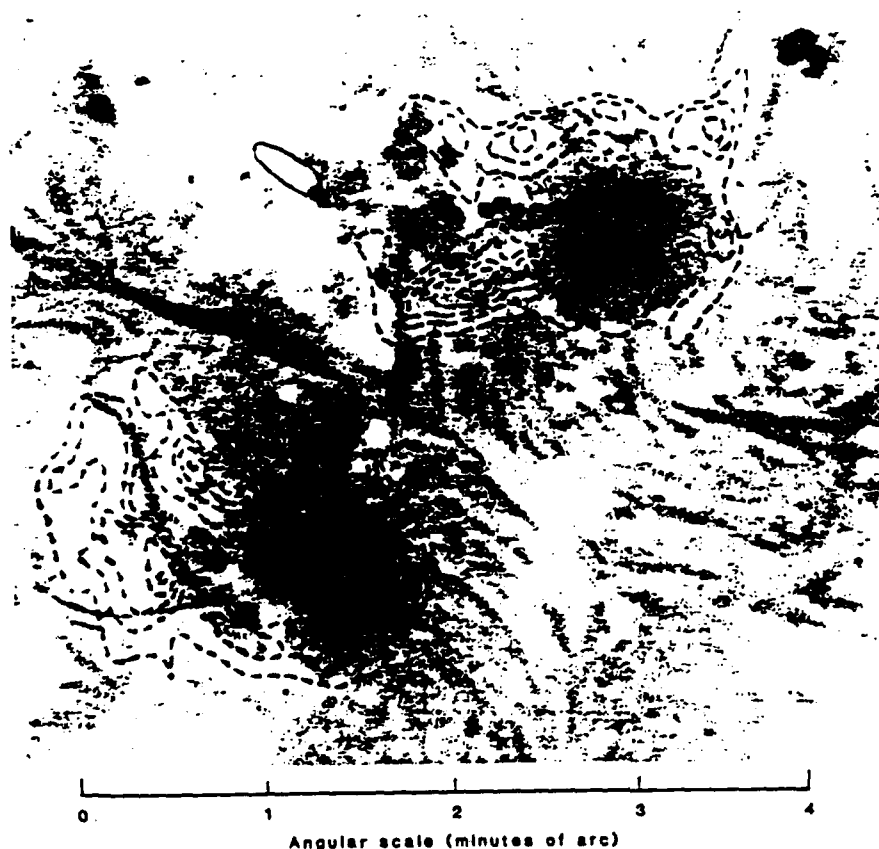


Fig. 2. A Westerbork Synthesis Radio Telescope synthesis map of circular polarization at $\lambda = 6$ cm overlaid on an H α photograph obtained from the observatory at Athens. The contours are in steps of 1.5×10^5 K. The circularly polarized horseshoe structure that rings the sunspot umbra is due to gyroresonant emission in the curved magnetic fields of the sunspot penumbra. [Courtesy of *Astrophysical Journal (Letters)*]

cent, or nonflaring, active regions. Perhaps the most important new development has been the discovery of the microwave counterpart of the ubiquitous coronal loops, which heretofore have been observable only with satellite-borne x-ray telescopes.

Quiescent (Nonflaring) Microwave Emission from Solar Active Regions

Because the microwave emission from nonflaring active regions varies slowly over time scales of several hours, one may investigate its detailed structure by using the earth-rotation aperture synthesis technique (7). The instruments that one uses for this technique are generally composed of one or several linear arrays and utilize the rotation of the earth to change the relative orientation of the array and the radio source; Fourier inversion methods are used to determine the angular power distribution of a radio source from the array response (visibility functions). Synthesis maps of total intensity, I , describe the two-dimensional distribution of source brightness, whereas synthesis maps of circular polarization, or Stokes parameter V , describe the two-dimensional structure of the longitudinal magnetic field. Observations at different wavelengths sample different levels within the solar atmosphere, with longer wavelengths referring to higher levels. The heights of the microwave structures can be inferred from their angular displacements from underlying photospheric features, and the two-dimensional maps at different wavelengths in the microwave domain can be combined to specify the three-dimensional structure of solar active regions.

Multiple-wavelength synthesis observations of solar active regions have been carried out mainly at the VLA with $\lambda = 2, 6$, and 20 cm (8). The emission at these wavelengths often originates at different heights within the coronal loops that join sunspots of opposite magnetic polarity (Fig. 1). The 2-cm emission has been attributed to thermal bremsstrahlung of the 10^5 K plasma that overlies sunspots at heights $h \sim 5,000$ km where H_i is $\sim 10^3$ G. Bright, highly polarized 6-cm cores mark the legs of dipolar loops with $T_B \sim 2 \times 10^6$ to 5×10^6 K and $h \sim 30,000$ km above the underlying sunspots (Fig. 1). Values of H_i of ~ 600 to 900 G are inferred from the fact that these cores emit gyroresonance at the second or third harmonic of the gyrofrequency. The 20-cm emission comes from the hot, dense plasma trapped within the

magnetic loops that connect underlying sunspots. These coronal loops have $T_B = 2 \times 10^6$ to 4×10^6 K and extents of about 100,000 km. The 20-cm emission may be attributed to thermal bremsstrahlung or gyroresonant radiation, or both.

One of the most satisfying observational results has been the detection of circularly polarized ring-shaped or horseshoe structures predicted by the theory of gyroresonant emission from individual sunspots (9). Circular polarization maps at $\lambda = 6$ cm reveal highly polarized (up to 100 percent) structures that lie above the curved magnetic fields of sunspot penumbrae (see Fig. 2). There is no detectable circular polarization above the central sunspot umbrae where the magnetic fields project radially upward into the hot coronal regions. The total intensity of the 6-cm radiation is often enhanced above the sunspot umbrae, with $T_B \sim 10^6$ K; but it is also often enhanced above sunspot penumbrae and depressed over the umbrae. A 6-cm brightness depression above sunspot umbrae may be attributed to cool material above sunspot umbrae or to geometrical effects. For instance, there is negligible gyroresonant absorption when the angle between the magnetic field and the line of sight is small. Both cool material and variable absorption may be present, but the two effects cannot be easily disentangled.

Although gyroresonance in the legs of magnetic loops usually dominates the 6-cm emission, weaker bremsstrahlung can sometimes be detected at 6 cm near the loop apex. The coronal loops are more reliably mapped out if one uses the VLA at $\lambda = 20$ cm, where emission from the entire loop is routinely detected (10). The magnetic and temperature structure of coronal loops can be specified from the 20-cm observations. This emission is due to thermal gyroresonant absorption and/or bremsstrahlung of the same hot plasma that gives rise to x-ray emission by thermal bremsstrahlung. Because the magnetic energy density dominates the thermal energy density at coronal heights, this plasma remains trapped within the magnetic loops. Electron temperatures T_e of 2×10^6 to 4×10^6 K, electron densities N_e of 10^9 to 10^{10} cm $^{-3}$, loop extents of 10^9 to 10^{10} cm, and H_t values of 200 G can be inferred from the 20-cm intensity and polarization maps. Thermal bremsstrahlung may also sometimes play a role in the 20-cm coronal loops, and in this case stronger magnetic fields of $H_t \sim 500$ G are inferred from the circular polarization if it is due to propagation effects.

Microwave Bursts from Solar Active Regions

The VLA has also recently been used to detect changes in the configuration of coronal magnetic fields and temperature enhancements within coronal loops that are important in the excitation of solar

bursts. The origin and prediction of these powerful bursts is one of the most important and interesting problems of solar physics. It has long been known that solar eruptions are intimately connected with the magnetic fields in active regions, for the ultimate source of energy for these bursts must be magnetic ener-

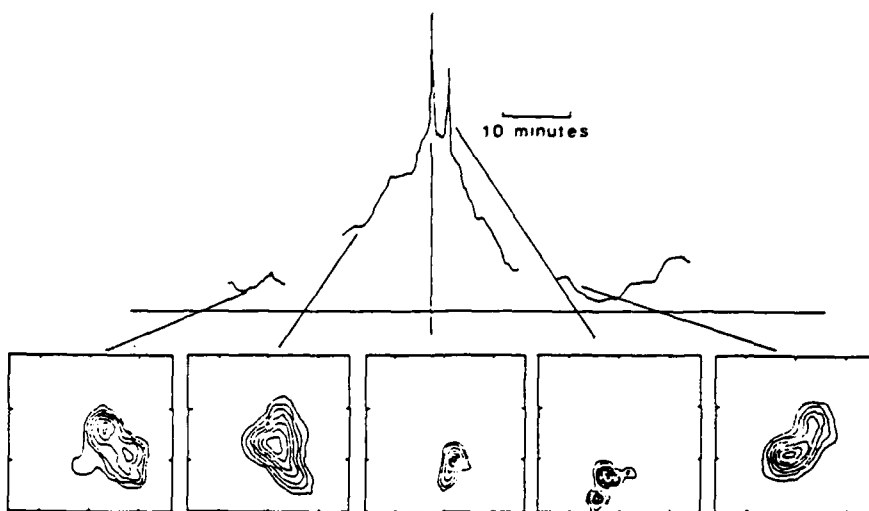


Fig. 3. The time profile of a solar burst at $\lambda = 20$ cm (top of figure) suggests heating within a coronal loop prior to the emission of two impulsive microwave bursts. The 20-cm VLA synthesis maps for 10-second intervals (bottom of figure) suggest that a coronal loop twisted in space. Energetic particles associated with hard x-ray emission at relatively low levels that occurred during the calibration gap shown in the figure may have either initiated the heating in the coronal loop or supplied it with microwave-emitting particles.

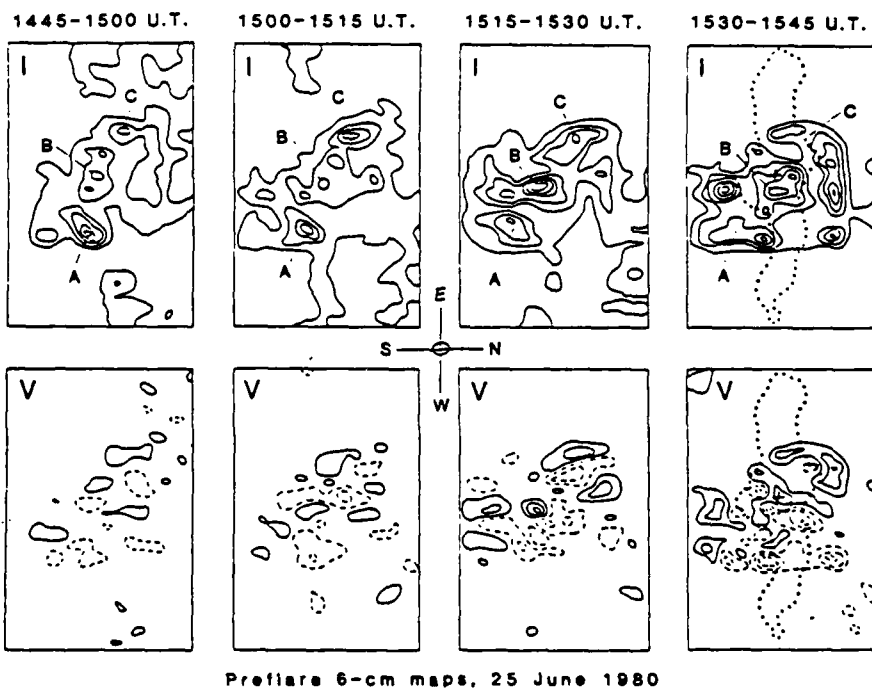


Fig. 4. Central $1'.1 \times 1'.6$ regions of preflare (15 minutes) maps of total intensity (I) and circular polarization (V) from $14^h 45^m$ to $15^h 45^m$ U.T. on 25 June 1980. The beam size is $4'' \times 6''$. The first contour is 1×10^6 K, and the contour interval is 2×10^6 K. Note the reversal of polarity in component B in the last map, close to the subsequent burst peak (marked by +). The dotted outline shows the extent of the burst source in the impulsive phase, $15^h 51^m$ to $16^h 00^m$ U.T. [Courtesy of Astronomy and Astrophysics]

gy. It has only recently been realized, however, that evolving magnetic fields in the solar corona may play a dominant role in triggering solar eruptions (11). Theoretical considerations indicate that loops emerging into the corona, magnetic shear within these loops, and interacting coronal loops can trigger solar bursts and supply their energy (12). One can now observe these effects for the first time by using the VLA to specify the magnetic field topology in active regions with angular resolutions of better than 1 second of arc in time periods as short as 10 seconds.

It has been known for several years that preflare changes in active regions are detected as increases in the intensity

and polarization of the microwave emission at centimeter wavelengths. These increases precede solar eruptions on time scales of 10 minutes to an hour (13). They suggest that new magnetic loops are emerging or that existing magnetic fields are becoming more ordered. The high angular resolution provided by the VLA has now shown that these increases are related to preburst heating in coronal loops and to changes in the coronal magnetic field topology. The VLA snapshot maps have also made possible tests of flare models that could not be carried out at optical wavelengths.

The VLA results indicate that no single flare model is versatile enough to explain the diverse ways in which mag-

netic energy is dissipated in solar bursts. This is not terribly surprising in view of the magnetic complexity of solar active regions. Preburst changes can nevertheless be ordered into three major categories: (i) changes within a single coronal loop, (ii) the emergence of coronal loops, and (iii) interaction between coronal loops (14).

Single coronal loops or arcades of loops often begin to heat up and change structure about 15 minutes before the eruption of impulsive bursts. As illustrated in Fig. 3, heating within a magnetic loop was followed by impulsive microwave emission. Energetic particles associated with hard x-ray emission (high-energy x-ray photons) may have initiated or contributed to this heating. Radio and soft x-ray data have been combined to derive a peak T_e of 2.5×10^7 K and an average N_e of 10^{10} cm^{-3} during the heating phase of the example shown in Fig. 3. Future comparisons with observations at optical wavelengths may indicate whether the changing orientation of the microwave flaring region (Fig. 3) is related to the shear of photospheric magnetic fields, which is sometimes observed before a flare. Preburst heating and magnetic field changes can also occur in loops that are adjacent to, but spatially separated from, the sites of the impulsive bursts.

Preburst activity is also detected in coronal loops that are adjacent to those that emit bursts. New bipolar loops can emerge and interact with preexisting ones. When the polarity of the new emerging flux differs from that of the preexisting flux, current sheets are produced that trigger the emission of bursts.

An example of a reversal of polarization in a bipolar feature prior to the onset of a flare is shown in Fig. 4. It suggests either the emergence of new magnetic flux or a change in the topology of the magnetic field. Joint studies based on the use of $H\alpha$ data and the ultraviolet spectrometer polarimeter aboard the Solar Maximum Mission Satellite led to the conclusion that rising and twisting of magnetic loops around the site of the flare triggered its onset (15).

Recent VLA solar observations may provide direct evidence of magnetic reconnection in microwave bursts (16). This is exemplified by a 6-cm burst, shown in Fig. 5, in which a gradual burst first appears with an east-west magnetic neutral line; superposed on it an intense emission extending along a new north-south neutral line appeared just before the impulsive burst occurred. This north-south line is indicative of the appearance of a new system of loops, possibly due to

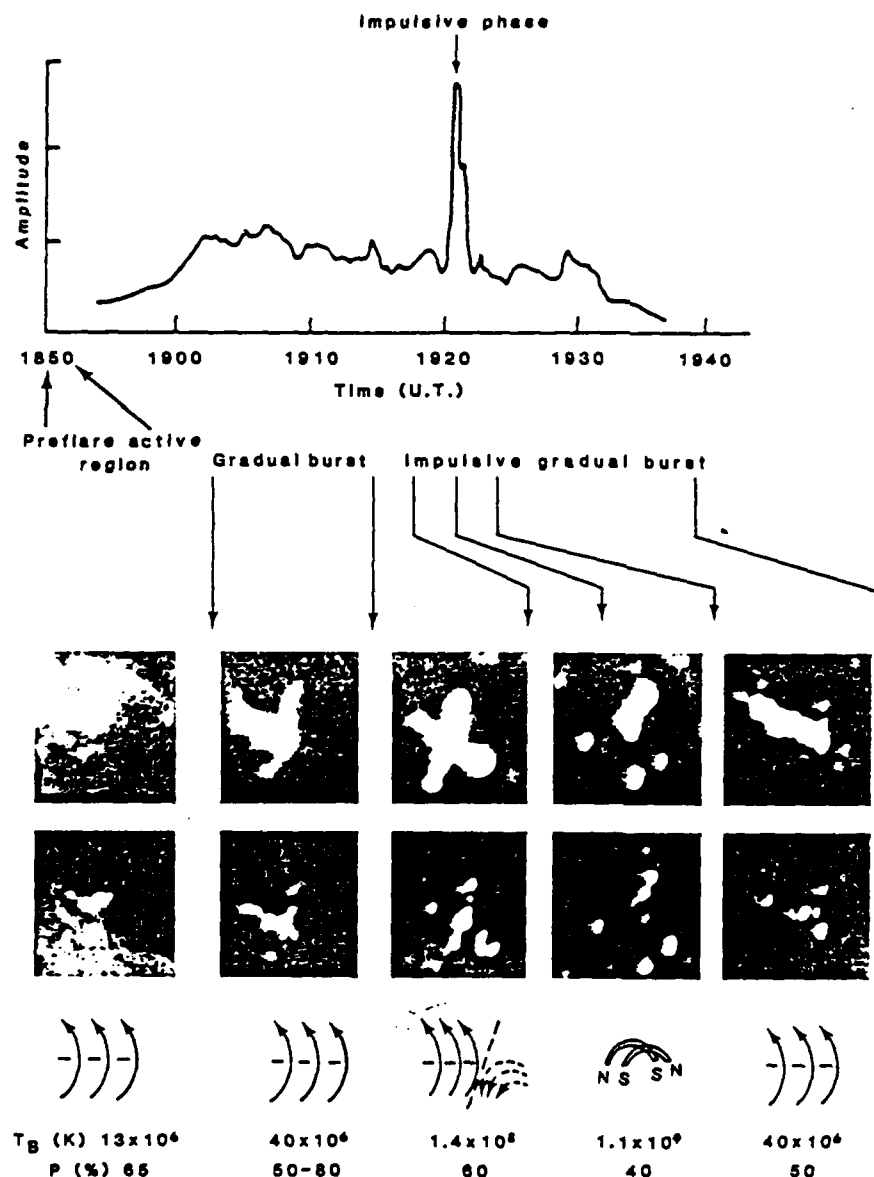


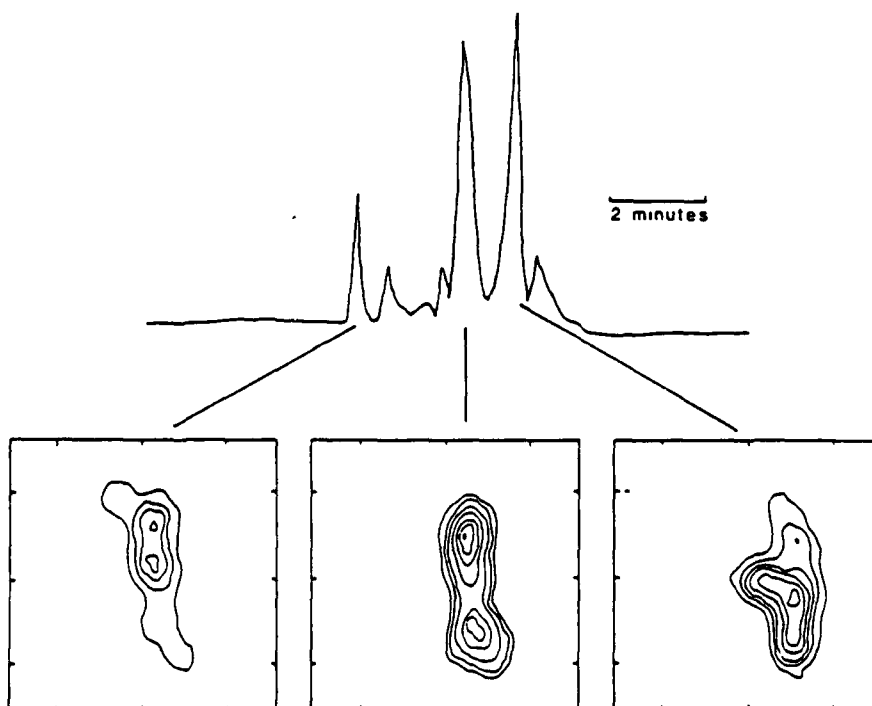
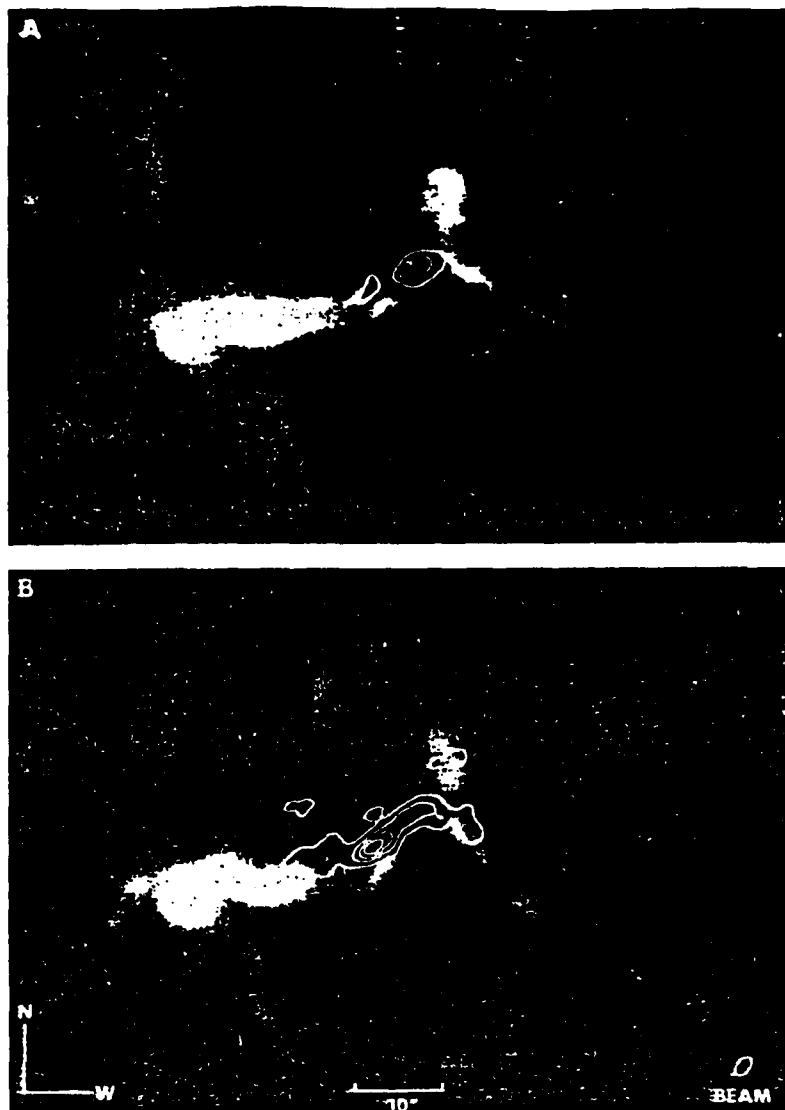
Fig. 5. The time profile and 10-second VLA synthesis maps of a solar burst at $\lambda = 6$ cm. The loop structure, peak brightness temperatures, T_B , and degrees of circular polarization (P) are given below the synthesis maps. Two dipolar loops emerged to form a quadrupolar structure. The interacting loops created a change in the orientation of the neutral plane and triggered the emission of an impulsive burst. [Courtesy of *Advances in Space Research*, Academic Press, New York]

reconnections. At the impulsive peak, the burst source structure changes and ultimately develops into two oppositely polarized bipolar regions or a quadrupole structure. A current sheet may have developed at the interface of two closed loops, thereby triggering the burst onset. The impulsive energy was probably due to magnetic reconnections of the field lines connecting the two oppositely polarized bipolar regions. It remains to be seen if the reconnection process can accelerate electrons to energies of the order of 100 keV or higher, which are responsible for microwave burst emission.

The microwave bursts are characterized by a strongly polarized, compact ($5''$ to $30''$) impulsive component with a T_B of 10^7 to 10^9 K lasting between 1 and 5 minutes. This is followed by a larger, longer postburst component with relatively low polarization and T_B . The impulsive bursts are due to the gyrosynchrotron radiation of mildly relativistic electrons with energies of 100 to 500 keV.

The primary release of microwave energy takes place in the coronal part of magnetic loops. The impulsive part of the microwave energy is usually released in the upper parts of coronal loops and between the flaring H α kernels (small regions) that mark the footpoints of magnetic loops (Fig. 6). The impulsive emitting region at $\lambda = 6$ cm occupies a large fraction of the flaring loops near their tops, whereas the 2-cm emission is more concentrated toward the loop apex. The microwave emission of the gradual phase that follows the impulsive burst at 2 cm is larger and is elongated along the magnetic field lines joining the H α kernels.

Fig. 6 (top). Very Large Array synthesis maps of the impulsive phase (A) and gradual phase (B) of a solar burst at $\lambda = 2$ cm (15.05 GHz) superimposed upon an H α photograph of the flare taken at the same time at the Big Bear Solar Observatory, Big Bear, California. The microwave emission of the impulsive phase (peak $T_B = 2.5 \times 10^8$ K) was released at the top part of a dipolar loop, while the H α kernels were emitted at the loop footpoints. The microwave emission of the gradual phase, which followed the impulsive phase and lasted for several minutes, is larger and is elongated along the magnetic field lines joining the H α kernels (22). [Courtesy of *Astrophysical Journal (Letters)*] Fig. 7 (bottom). The time profile of successive impulsive bursts at $\lambda = 20$ cm (top) is compared with 10-second VLA synthesis maps at the same wavelength (bottom). Although the successive weak bursts were emitted from the same coronal loop, the successive intense bursts arose from spatially separated coronal loops having peak T_B values between 2×10^7 and 2×10^8 K. The contour intervals are in steps of 1.0×10^7 K.



The loop or arcade model of flares postulates the release of energy in the coronal part of a magnetic loop. This energy release [possibly through magnetic reconnection brought on by a tearing-mode instability (12)] impulsively heats the plasma in the upper part of the loop. A nonthermal tail of high-energy electrons (energies up to a few hundred kiloelectron volts) may also be produced at this time. The hot plasma is confined between a pair of conduction fronts which propagate down the legs of the loop with a velocity near the ion sound speed (17). Electrons with velocities greater than approximately three times the electron thermal speed in this region, however, are not confined by the conduction fronts and escape to the lower part of the loop. When the electron gyrofrequency exceeds the plasma frequency, the escaping electrons are unstable to the generation of electrostatic plasma waves which scatter the particles in pitch angle to a nearly isotropic distribution (17). This scattering can enhance the microwave emission from the upper part of the loop because more electrons are trapped in that part of the loop, and the scattered electrons have a higher mean pitch angle. Using an isotropic particle distribution and a uniform magnetic field, one can show (12) that microwave emission originates predominantly from the upper part of the loop and that a loop would appear larger in the optically thick regime than in the optically thin regime.

During the course of impulsive bursts, the microwave source sometimes drifts

toward the limb. This apparent limbward motion can be attributed to a radial movement of expanding magnetic loops at velocities of a few hundred kilometers per second. Alternatively, bursts could be sequentially triggered at higher levels in the solar atmosphere.

There is also evidence for the sequential triggering of microwave bursts in different loops within magnetically complicated regions. As illustrated in Fig. 7, successive intense bursts can originate in adjacent coronal loops, whereas successive weaker bursts are located in the same coronal loop.

Microwave Emission from Nearby Stars of Late Spectral Type

Nearby main-sequence stars of late spectral type exhibit quiescent x-ray emission whose absolute luminosity may be as much as one hundred times that of the sun. These stars thus may have large-scale coronal loops and intense magnetic fields. The solar analogy indicates that the hot coronal plasma ought to be detected at $\lambda = 20$ cm and that polarized 6-cm emission should reveal the presence of large-scale magnetic structures.

In fact, the dwarf M flare stars exhibit slowly varying, circularly polarized microwave emission at $\lambda = 6$ cm that is analogous to the quiescent, or nonflaring, microwave emission from solar active regions (18). Brightness temperatures of 10^7 to 10^8 K are inferred if the microwave-emitting source covers the

entire visible surface of the star. Brightness temperatures comparable to that of the sun's quiescent microwave emission ($T_B \sim 10^6$ K) are obtained if the stellar emitting region is three times as large as the visible star. The detected emission might then be explained as the gyroresonant emission from thermal electrons spiraling in magnetic fields with $H_t \sim 300$ G. Alternatively, the gyrosynchrotron emission of a small number of energetic electrons in starspots may account for the stellar microwave emission.

The dwarf M flare stars also exhibit microwave bursts that are similar to those emitted by the sun (19). For example, impulsive microwave bursts from the sun sometimes exhibit rapid millisecond fine structure that is 100 percent circularly polarized (20). Brightness temperatures as high as $\sim 10^{15}$ K have been inferred for the solar fine structure.

One impulsive burst from the dwarf M star AD Leo is composed of a rapid sequence of highly polarized (100 percent) spikes with rise times of less than 200 msec (Fig. 8). An upper limit to the linear size of the emitting region is 6×10^9 cm, the distance that light travels in 200 msec. If the emitting starspot is symmetric, it has an area that is less than 3 percent of the star's surface area, and its T_B exceeds 10^{13} K. The high T_B and high degrees of circular polarization of these star bursts can be explained in terms of electron-cyclotron maser emission at the second harmonic of the gyrofrequency in longitudinal magnetic fields of $H_t \sim 250$ G (21).

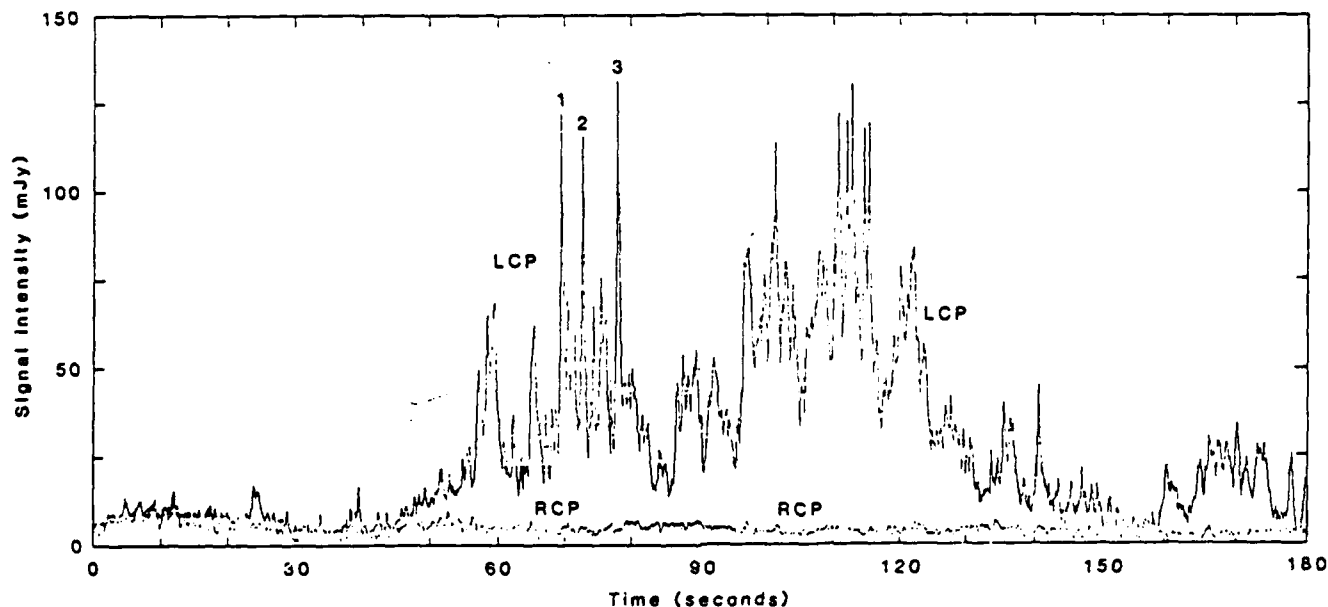


Fig. 8. Rapid, highly polarized spikes make up this 20-cm burst from the dwarf M star AD Leo. The spikes marked 1, 2, and 3 had rise times of less than 200 msec, indicating that the emitting source was less than 6×10^9 cm in diameter. Brightness temperatures in excess of 10^{13} K are inferred for these spikes; LCP and RCP designate, respectively, left-handed and right-handed circularly polarized emission. [Courtesy of *Astrophysical Journal (Letters)*]

References and Notes

1. V. V. Zheleznyakov, *Sov. Astron. AJ* 6, 3 (1962); T. Kakinuma and G. Swarup, *Astrophys. J.* 136, 975 (1962); M. R. Kundu, *Solar Radio Astronomy* (Interscience, New York, 1965); P. Lantos, *Ann. Astrophys.* 31, 101 (1968); E. Ya. Zlotnik, *Sov. Astron. AJ* 12, 245 (1968); *ibid.*, p. 464; V. V. Zheleznyakov, *Radio Emission from the Sun and Planets* (Pergamon, New York, 1970); A. Kruger, *Introduction to Solar Radio Astronomy and Radio Physics* (Reidel, Boston, 1979).
2. J. A. Ratcliffe, *The Magneto-Ionic Theory* (Cambridge Univ. Press, Cambridge, 1962); K. R. Lang, *Astrophysical Formulae* (Springer, New York, 1974, 1980).
3. M. R. Kundu and C. E. Alissandrakis, *Nature (London)* 257, 465 (1975); J. D. Bregman, A. C. Hin, *Astrophys. J.* 213, 278 (1977); K. R. Lang and R. F. Willson, *Nature (London)* 278, 24 (1979); in *Radio Physics of the Sun* (International Astronomical Union Symposium 86), M. R. Kundu and T. E. Gergely, Eds. (Reidel, Dordrecht, 1980), p. 109; M. R. Kundu, E. J. Schmahl, M. Gerassimenko, *Astron. Astrophys.* 82, 265 (1980); M. Felli, K. R. Lang, R. F. Willson, *Astrophys. J.* 247, 325 (1981); R. Pallavicini, T. Sakurai, G. S. Vaiana, *Astron. Astrophys.* 98, 316 (1981).
4. M. R. Kundu, T. Velusamy, R. H. Becker, *Sol. Phys.* 34, 217 (1974); K. R. Lang, *ibid.* 36, 351 (1974); C. E. Alissandrakis and M. R. Kundu, *Astrophys. J.* 222, 342 (1978); M. R. Kundu, in *Radio Physics of the Sun* (International Astronomical Union Symposium 86), M. R. Kundu and T. E. Gergely, Eds. (Reidel, Dordrecht, 1980), p. 157; K. Marsh, G. J. Hurford, H. Zirin, *ibid.*, p. 191; K. R. Lang, R. F. Willson, M. Felli, *Astrophys. J.* 247, 338 (1981).
5. K. A. Marsh and G. J. Hurford, *Astrophys. J.* 240, L111 (1980).
6. —, *Annu. Rev. Astron. Astrophys.* 20, 497 (1982); M. R. Kundu, *Rep. Prog. Phys.* 45, 1435 (1982); — and L. Vlahos, *Space Sci. Rev.* 32, 405 (1982).
7. E. B. Fomalont, *Proc. Inst. Elec. Eng.* 61, 1211 (1973).
8. K. R. Lang and R. F. Willson, in *Advances in Space Research—Proceedings of the 24th Meeting of COSPAR* (Pergamon, London, 1983), vol. 1, p. 91; —, V. Gaizauskas, *Astrophys. J.* 267, 455 (1983); R. K. Shevgaonkar and M. R. Kundu, *ibid.* 283, 413 (1984).
9. G. B. Gel'freikh and B. I. Lyubyshev, *Sov. Astron. AJ* 23, 316 (1979); C. E. Alissandrakis, M. R. Kundu, P. Lantos, *Astron. Astrophys.* 82, 30 (1980); C. E. Alissandrakis and M. R. Kundu, *Astrophys. J.* 253, L49 (1982); K. R. Lang and R. F. Willson, *ibid.* 255, L111 (1982).
10. M. R. Kundu and T. Velusamy, *Astrophys. J.* 240, L63 (1980); T. Velusamy and M. R. Kundu, *ibid.* 243, L103 (1981); K. R. Lang, R. F. Willson, J. Kavrole, *ibid.* 258, 384 (1982); G. A. Dulk and D. E. Gary, *Astron. Astrophys.* 124, 103 (1983); K. R. Lang and R. F. Willson, *ibid.* 127, 135 (1983); D. McConnell and M. R. Kundu, *Astrophys. J.* 269, 698 (1983).
11. D. Rust, *Sol. Phys.* 47, 21 (1976); M. R. Kundu et al., *Astron. Astrophys.* 108, 188 (1982); R. F. Willson, *Sol. Phys.* 83, 285 (1983); K. R. Lang and R. F. Willson, in *Advances in Space Research—Proceedings of the 24th Meeting of COSPAR* (Pergamon, London, 1983), vol. 2, p. 91; M. R. Kundu, *Proc. Int. Astron. Union Symp.* 107 (1984), p. 185.
12. T. Gold and F. Hoyle, *Mon. Not. R. Astron. Soc.* 120, 89 (1960); J. Heyvaerts, E. R. Priest, D. M. Rust, *Astrophys. J.* 216, 123 (1977); D. S. Spicer, *Sol. Phys.* 53, 305 (1977); S. I. Syrovatskii and V. D. Kuznetsov, in *Radio Physics of the Sun* (International Astronomical Union Symposium 86), M. R. Kundu and T. E. Gergely, Eds. (Reidel, Dordrecht, 1980), p. 445; V. D. Kuznetsov and S. I. Syrovatskii, *Sol. Phys.* 69, 361 (1981); D. S. Spicer, *ibid.* 70, 149 (1981); V. Petrosian, *Astrophys. J.* 255, L85 (1982); B. V. Somov and S. I. Syrovatskii, *Sol. Phys.* 75, 237 (1982); E. R. Priest, *ibid.* 86, 33 (1983).
13. K. R. Lang, *Sol. Phys.* 52, 63 (1977); M. R. Kundu, in *Radio Physics of the Sun* (International Astronomical Union Symposium 86), M. R. Kundu and T. E. Gergely, Eds. (Reidel, Dordrecht, 1980), p. 157; G. Hurford and H. Zirin, *Air Force Geophys. Lab. Rep. AFGL-TR-62-0017* (1982); R. K. Shevgaonkar and M. R. Kundu, *Astrophys. J.*, in press; K. R. Lang and R. F. Willson, *Advances in Space Research—Proceedings of the 25th Meeting of COSPAR* (Pergamon, London, in press).
14. M. R. Kundu, E. J. Schmahl, T. Velusamy, *Astrophys. J.* 253, 963 (1982); —, L. Vlahos, *Astron. Astrophys.* 108, 188 (1982); T. Velusamy and M. R. Kundu, *Astrophys. J.* 258, 388 (1982); M. R. Kundu, *Sol. Phys.* 86, 205 (1983); M. R. Kundu, in *Advances in Space Research—Proceedings of the 24th Meeting of COSPAR* (Pergamon, London, 1983), vol. 1, p. 159; M. R. Kundu, D. M. Rust, M. Bobrowsky, *Astrophys. J.* 265, 1084 (1983); R. F. Willson and K. R. Lang, *Astrophys. J.* 279, 427 (1984); R. F. Willson, *Sol. Phys.* 92, 189 (1984).
15. M. R. Kundu, V. Gaizauskas, B. Woodgate, E. J. Schmahl, R. Shine, H. Jones, *Astrophys. J. Suppl. Ser.*, in press.
16. M. R. Kundu, *Proc. Int. Astron. Union Symp.* 107 (1984), p. 185.
17. J. C. Brown, D. B. Melrose, D. S. Spicer, *Astrophys. J.* 228, 592 (1979); D. F. Smith and C. G. Lillquist, *ibid.* 232, 582 (1979); L. Vlahos and K. Papadopoulos, *ibid.* 233, 717 (1979); G. D. Holman, M. R. Kundu, K. Papadopoulos, *ibid.* 257, 354 (1984).
18. D. E. Gary and J. L. Linsky, *ibid.* 250, 284 (1981); K. Topka and K. A. Marsh, *ibid.* 254, 641 (1982); J. L. Linsky and D. E. Gary, *ibid.* 274, 776 (1983).
19. D. E. Gary, J. L. Linsky, G. A. Dulk, *ibid.* 263, L79 (1982); D. B. Melrose and G. A. Dulk, *ibid.* 259, 844 (1982); K. R. Lang, J. Bookbinder, L. Golub, M. M. Davis, *ibid.* 272, L15 (1983).
20. C. Slotje, *Nature (London)* 275, 520 (1978); in *Radio Physics of the Sun* (International Astronomical Union Symposium 86), M. R. Kundu and T. E. Gergely, Eds. (Reidel, Dordrecht, 1980), p. 195; R. Zhao and S. Jin, *Sci. Sin. A* 25, 422 (1982).
21. G. D. Holman, D. S. Eichler, M. R. Kundu, in *Radio Physics of the Sun* (International Astronomical Union Symposium 86), M. R. Kundu and T. E. Gergely, Eds. (Reidel, Dordrecht, 1980), p. 457; G. D. Holman, *Adv. Space Res.* 2, 181 (1982); R. R. Sharma, L. Vlahos, K. Papadopoulos, *Astron. Astrophys.* 112, 337 (1982); L. Vlahos, R. R. Sharma, K. Papadopoulos, *Astrophys. J.* 275, 374 (1983).
22. Adapted from (5), plate 2.
23. This review would have been impossible without the fine contributions to solar radio astronomy made by R. F. Willson at Tufts University and C. E. Alissandrakis, E. J. Schmahl, T. Velusamy, and L. Vlahos while working for the University of Maryland. Radio astronomical studies of the sun and other active stars at Tufts University are supported under Air Force Office of Scientific Research grant AFOSR-83-0019-B. Investigations of flare stars at Tufts University are also supported by NASA grant NAG 5-477; whereas comparisons of VLA and Solar Maximum Mission satellite data are supported by NASA Guest Investigator grant NAG 5-501. Solar research in the Astronomy Program at the University of Maryland is supported under NSF grant ATM 84-15388, NASA grant NGR 21-002-199, and NASA contract NSG 5320. The Very Large Array is operated by Associated Universities Inc., under contract with the National Science Foundation.

14. Microwave observations of late-type stars with the Very Large Array

R. Pallavicini¹, R. F. Willson², and K. R. Lang²

¹ Osservatorio Astrofisico di Arcetri, Largo Fermi 5, I-50125 Firenze, Italy

² Department of Physics and Astronomy, Tufts University, Medford, MA 02125, USA

Received November 27, 1984; accepted February 21, 1985

Summary. The Very Large Array was used to search for microwave emission from 32 stars of late spectral type including RS CVn type stars, dwarf M flare stars, and stars with active chromospheres, coronae or intense magnetic fields. We have detected four RS CVn stars at 6 cm wavelength and have established upper limits for another six. Radio emission was detected from three dwarf M flare stars, UV Cet, EQ Peg and YZ CMi. Both impulsive (≤ 20 s) and more gradual (\geq ten minutes) bursts were observed from the flare star YZ CMi. We do not confirm radio emission at 6 cm from the solar type star χ^1 Ori, with an upper limit that is three times lower than the detections reported by other observers. We failed to detect microwave emission from any other solar type star of spectral class F to K. The quiescent radio emission from dwarf M flare stars is interpreted as non-thermal gyrosynchrotron emission by mildly relativistic electrons accelerated more or less continuously in the magnetic fields of starspots.

Key words: late-type stars

1. Introduction

Observations of stellar coronae at X-ray and ultraviolet wavelengths from the EINSTEIN and IUE satellites have revealed that magnetic fields play a dominant role in the outer atmospheres of cool stars (Vaiana, 1981, 1983; Linsky, 1983). This is in agreement with what we know from observations of the sun. Spatially resolved observations of the solar corona from Skylab, OSO-8 and the Solar Maximum Mission have shown that magnetic fields are responsible for the structure and variability of the corona as well as for directly heating the coronal plasma (Vaiana and Rosner, 1978). Recently, observational evidence has been found for the presence of magnetic fields in late-type stars (Marcy, 1984).

If dynamo-generated magnetic fields are prominent in all late-type stars, as they appear to be for the sun, then one might expect their effects to be detectable at radio wavelengths, provided instrumentation of sufficiently high sensitivity is available. With the completion of the Very Large Array (VLA) such high sensitivity measurements have indeed become possible.

Magnetic fields affect microwave emission in a number of ways. For example, they increase the opacity of the coronal plasma by the thermal gyroresonance process, as observed in the sun above sunspots (Alissandrakis et al., 1980; Pallavicini et al., 1981; Lang and Willson, 1982). Alternatively, electric fields associated with restructuring and dissipation of magnetic fields in solar and

stellar active regions may accelerate particles to high energies and produce gyrosynchrotron emission as seen in solar microwave bursts (Takakura, 1967; Ramaty, 1973). In such cases, the microwave emission produced by magnetic processes is more intense than thermal free-free emission.

In the past few years a number of investigators have used the VLA to search for microwave emission from stars of late spectral type (Bowers and Kundu, 1981; Gary and Linsky, 1981; Topka and Marsh, 1982; Fisher and Gibson, 1982; Linsky and Gary, 1983; Mutel et al., 1984). Flaring, as well as quiescent microwave emission has been detected from dwarf M flare stars as well as from RS CVn binary systems. Even more interesting, quiescent emission has been reported from one solar-type star of spectral type G0 V (χ^1 Ori, Gary and Linsky, 1981). This particular observation, if confirmed, would open up unexpected possibilities of using radio observations as a diagnostic tool of coronal magnetic fields and plasma properties in other stars similar to, although more active than, the sun.

In this paper, we report on a new search for microwave emission from stars of late spectral type using the VLA. Our main objective was to determine if detectable radio emission from cool stars is common, as well as to elucidate the nature of the emission mechanism. In particular, we wanted to assess the relative importance of thermal gyroresonance vs. non-thermal gyrosynchrotron emission in producing quiescent microwave emission from stars of late spectral type.

2. Observations

The observations were made in August and October 1983, and in January and March 1984 using the VLA. Our initial survey was made at a wavelength of 6.1 cm (4885 MHz and 4935 MHz) with subsequent observations at 2.0 cm (14.984 MHz and 15.035 MHz) and 20.7 cm (1446 MHz and 1496 MHz) wavelengths. The entire VLA, consisting of 27 antennas, was used to observe each star for 30 min followed by a 3 min observation on a nearby calibrator source. For a few particular interesting objects (χ^1 Ori, 59 Vir, 53 Aqr, π^1 UMa, λ And, EQ Peg) we used somewhat longer integration times of up to 3 h in order to lower our detection threshold. In all cases the bandwidth was 50 MHz. The absolute flux density of all sources were determined from observations of 3C 286 whose flux densities at 2.0, 6.1, and 20.7 cm were assumed to be 3.9, 7.4, and 14.51 Jy, respectively. The data were edited and calibrated and used to produce synthesis maps of the total intensity, I , and circular polarization, V , within an area of $2' \times 2'$ centered on the position of the stars. For those fields which

Send offprint requests to: R. Pallavicini

Table 1. Detected stars

Star	Sp	d (pc)	Flux (mJy)	Cir. pol. (%)	$\log L_R$ ($\text{erg s}^{-1} \text{Hz}^{-1}$)	Type
UX Ari	G5V + K0IV	50	20.7 ± 0.24	10	16.8	RSCVn
HR 1099	G5IV + K1IV	33	7.7 ± 0.15	20	16.0	RSCVn
WW Dra	G5V + K0IV	180	3.6 ± 0.17	< 5	17.1	RSCVn
λ And	G8III-IV	24	0.84 ± 0.12	< 23	14.8	RSCVn
UV Cet	dM5.5e	2.7	0.95 ± 0.24	< 21	12.9	Flare star
EQ Peg A	dM3.5e	6.4	0.81 ± 0.12	< 20	13.6	Flare star
YZ CMi	dM4.5e	6.1	2.5 - 8.5	50-90	14.0-14.5	Flare star

Table 2. Upper limits

Star	Sp	d (pc)	Flux (mJy)	$\log L_R$	Type
α Aur	G0III + G5III	14	< 0.39	< 14.0	1
ζ And	K1II-III	31	< 0.45	< 14.7	1
σ Gem	K1III	59	< 0.45	< 15.3	1
54 Cam	G0V + G2V	38	< 0.42	< 14.9	1
ε UMi	G5III	71	< 0.42	< 15.4	1
MM Her	G2V + K2IV	190	< 0.41	< 16.3	1
YY Gem	dM1e + dM1e	14.5	< 0.45	< 14.1	2
EQ Vir	K5Ve	16.4	< 0.42	< 14.1	2
κ Ceti	G5V	9.5	< 0.45	< 13.7	3
ε Eri	K2V	3.3	< 0.42	< 12.7	3
111 Tau	F8V	15.6	< 0.39	< 14.1	3
β Lep	G5III	71.4	< 0.42	< 15.4	3
γ^1 Ori	G0V	9.8	< 0.23	< 13.4	3
π^1 UMa	G0V	15.4	< 0.36; < 0.24	< 13.8	3
24 UMa	G2IV	26.0	< 0.45	< 14.6	3
59 Vir	F8V	13.3	< 0.21	< 13.6	3
.					
ξ Boo A	G8V	4.7	< 0.36	< 13.0	3
HR 8314	G0V	15.0	< 0.45	< 14.1	3
53 Aqr A + B	G1V + G2V	18.5	< 0.17	< 13.8	3
ξ UMa B	G0V	7.3	< 0.45	< 13.5	3
61 UMa	G8V	8.4	< 0.45	< 13.6	3
σ Dra	K0V	5.6	< 0.36	< 13.1	3
40 Eri A	K1V	4.8	< 0.39	< 13.0	3
HD 131511	K2V	11.5	< 0.45	< 13.9	3
HD 131977	K4V	5.8	< 0.39	< 13.2	3

1) RSCVn's, 2) Flare stars, 3) Stars with active chromospheres and/or detected magnetic fields

contained a source, the maps were cleaned using the CLEAN algorithm developed by Clark (1980).

Our target stars were chosen on the basis of various criteria, all implying the likelihood of strong magnetic fields and high magnetic activity on the star surface. Our list of objects includes:

1. Stars known to have active chromospheres and coronae (Linsky et al., 1979; Vaiana et al., 1981), or known to be rapidly rotating for their spectral type (Pallavicini et al., 1981).

2. Stars for which magnetic fields may have been detected by direct spectroscopic methods (Marcy, 1984).

3. Binary systems of the RSCVn type (Hall, 1981).

4. Flare stars of the UV Cet type (Petterson, 1983).

In all, 32 stars were observed and 7 were detected. For the remaining 25 objects we have determined 3σ upper limits. In all cases, the data from the two closely-spaced frequency channels were averaged together. Table 1 gives the observed 6 cm fluxes S (in mJy), degree of circular polarization and computed radio luminosities L_R in $\text{erg s}^{-1} \text{Hz}^{-1}$ for the seven detected objects. Table 2 gives the 3σ upper limits of the observed fluxes and of the derived radio luminosities for the 25 non-detected stars. In Table 3 we give the fluxes and circular polarization of the RSCVn stars HR 1099 and UX Ari that were measured simultaneously at 2.6

Table 3. Multiple wavelength observations of UX Ari and HR 1099 at different epochs

Star	Date	Wave-length (cm)	Total intensity, I (mJy)	Circular polarization, (mJy)
UX Ari	1-12-84	2.0	9.5 ± 1.0	≤ 0.7
	1-12-84	6.1	13.7 ± 0.5	-8.4 ± 0.3
	1-12-84	20.7	17.1 ± 0.6	≤ 0.25
UX Ari	1-29-84	2.0	8.1 ± 0.8	≤ 1.0
	1-29-84	6.1	10.1 ± 0.6	-1.6 ± 0.3
	1-29-84	20.7	13.2 ± 0.5	≤ 0.4
UX Ari	3-23-84	2.0	32.3 ± 0.8	-3.2 ± 0.5
	3-23-84	6.1	50.5 ± 0.5	≤ 0.8
	3-23-84	20.7	40.4 ± 0.5	2.1 ± 0.4
HR 1099	1-12-84	2.0	16.4 ± 1.2	5.5 ± 0.7
	1-12-84	6.1	21.9 ± 0.8	3.5 ± 0.3
	1-12-84	20.7	27.1 ± 0.6	-3.0 ± 0.3
HR 1099	1-29-84	6.1	17.6 ± 0.5	3.2 ± 0.4
	1-29-84	20.7	21.7 ± 0.8	≤ 0.5
HR 1099	3-23-84	2.0	13.0 ± 0.7	-2.8 ± 0.6
	3-23-84	6.1	10.4 ± 0.5	2.4 ± 0.5

and 20 cm wavelength at three different epochs. The radiation from these stars has a spectrum with an average spectral index of $\alpha = -0.25 \pm 0.05$ (where the flux density is proportional to ν^α where ν is the frequency) and circular polarizations of up to 60%.

3. Comparison with other observations

In this section we discuss the observed sources class by class. Comparison with other previous work is given in Tables 4 and 5.

3.1. RS CVn stars

We have observed 10 RS CVn binaries (including both long and short period systems of Hall, 1981), and we have detected four. Of these, one (WW Dra) is a new detection. The derived luminosity for this star ($\log L_R = 17.1 \text{ erg s}^{-1} \text{ Hz}^{-1}$) falls in the range ($10^{15} - 10^{18} \text{ erg s}^{-1} \text{ Hz}^{-1}$) typical of radio luminosities observed in RS CVn stars (Hjellming and Gibson, 1980). For HR 1099 and UX Ari the derived luminosities are one to two orders of magnitude lower than the maximum radio luminosities previously reported (Hjellming and Gibson, 1980). This suggests that the flux levels we have detected are at, or close to, the quiescent level of radio emission from these objects. Our results for other epochs (Table 3) clearly show that the source intensity and polarization change with time and that the source of polarization is wavelength dependent.

The observed degree of circular polarization and the relatively low fluxes of these two sources suggest that the emission detected by us refers to the extended "halo" component observed by Mutel and Lestrade (1984) using VLBI techniques. The latter component is comparable in size to the overall binary system. On the contrary, the unpolarized emission has been shown to originate from volumes smaller than the component stars, possibly associated with flaring activity on the later spectral type component (Mutel and Lestrade, 1984).

Table 4. RS CVn stars

Star	$\log L_R$ (this work)	Other VLA Obs.	$\log L_R$ max (prev. obs.)
UX Ari	16.8	17.5 ^a	17.9 (at 8 GHz) ^a 18.0 (at 10 GHz) ^b
HR 1099	16.0	16.4 ^a	18.2 (at 10 GHz) ^{a, b}
WW Dra	17.1		New detection
λ And	14.8	14.8 ^c 14.7 - 15.3 ^c	16.1 (at 8 GHz) ^a
α Aur	< 14.0	< 14.0 ^b < 14.6 ^c < 13.6 ^c	Never detected
ζ And	< 14.7	< 14.7 ^c < 14.5 ^c	Never detected
σ Gem	< 15.3	< 15.9 ^c 15.4 - 16.1 ^c	16.9 ^a
54 Cam	< 14.9	< 14.9 ^b	16.3 ^a
ϵ Umi	< 15.4	< 15.0 ^a	Never detected
MM Her	< 16.3		Never detected

^a Hjellming and Gibson (1980) ^d Mutel et al. (1984)

^b Mutel and Lestrade (1984) ^e Drake et al. (1985)

^c Bowers and Kundu (1981)

Table 5

Star	Flux (mJy) This work	Flux (mJy) Previous obs.
------	----------------------	--------------------------

a) Stars with active chromospheres and Coronae

κ Cet	< 0.45	< 0.2 ^a
ϵ Eri	< 0.42	< 0.3 ^a
111 Tau	< 0.39	< 0.2 ^a
χ^1 Ori	< 0.23	0.6 ^b 0.3 - 1.4 ^a
π^1 UMa	< 0.24	< 0.6 ^a
24 UMa	< 0.45	< 0.8 ^a
ξ Boo A	< 0.36	< 0.2 ^a

b) UV Cet-type flare stars

UV Cet	0.95	1.5 ^{a, b} 1.3 ^d
EQ Peg	0.81 (comp. A)	0.69 + 0.4 ^c
YY Gem	< 0.45	0.41 - 1.8 ^c

^a Linsky and Gary (1983)

^b Gary and Linsky (1981)

^c Topka and Marsh (1982)

^d Kundu and Shevgaonkar (1985)

3.2. Dwarf M flare stars

We have observed five dwarf M stars and have detected three. All of these stars belong to the class of BY Draconis variables (Bopp and Fekel, 1977) characterized by optical photometric variability attributed to emission from a rotating spotted star. The BY Dra variables constitute a subclass of UV Ceti-type flare stars.

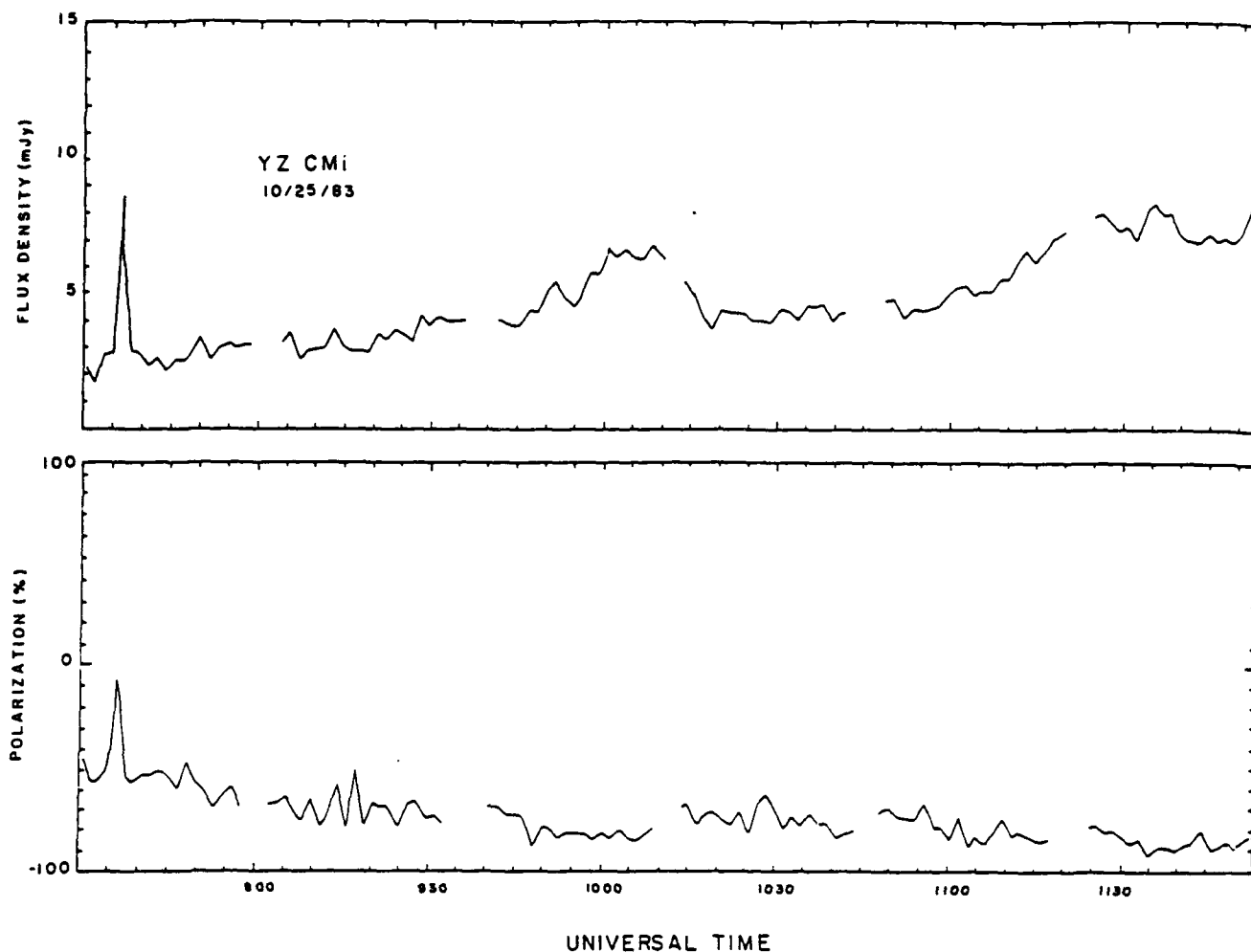


Fig. 1. A plot of the total intensity I (top) and circular polarization q , (bottom) observed at 6.1 cm wavelength from the star YZ CMi on October 25, 1983

The flux we observed from UV Cet is 20% to 100% lower than reported at 6 cm by other observers (see Table 5). Taking into account observational uncertainties we conclude that the observations are consistent with each other and indicate a rather stable (within a factor of 2) quiescent level from this star over a period of almost three years. This contrasts with the case of other dwarf M stars which have been shown to exhibit a larger degree of variability (Linsky and Gary, 1983).

In Fig. 1, for example, we show a plot of the 6.1 cm total intensity and circular polarization that was observed from YZ CMi during a 3.5 h interval on October 25, 1983. This plot was constructed by first making a 3.5 h synthesis map of a $5' \times 5'$ field surrounding YZ CMi. Inspection of this map revealed a ~ 4.5 mJy source within $0.4''$ of the phase center. There were also no strong confusing sources within this field of view. The visibility data were then phase shifted to bring the source exactly to the center of the map. These data were then averaged, baseline by baseline, over a 30 s interval and then vector averaged. The theoretical 1σ noise level obtained by averaging both the 4885 MHz and 4935 MHz data is ~ 0.45 mJy. The minimum flux level shown in Fig. 1 of ~ 2.5 mJy is therefore, in our opinion, significant. During this time interval YZ CMi exhibited variations on three different timescales: 1. an impulsive burst which occurred at ~ 0837 UT and which

lasted less than 30 s; 2. two gradual bursts at ~ 1000 UT and 1115 UT which had a duration of between 20 and 30 min, and 3. a more slowly varying component which became more negatively (left circular) polarized with increasing intensity.

Impulsive bursts, together with gradual and slowly varying emission are commonly observed on the sun. Centimeter wavelength bursts, for example, are thought to be triggered by the rapid reorientation of coronal magnetic fields, while more gradual bursts may be related to preburst heating caused by slower changes in these fields. Finally, the slowly varying component of the sun's centimeter wavelength emission may be related to evolutionary changes in the active regions themselves. Alternatively, this component may be due to slow burst emission analogous to the centimeter wavelength component of solar Type IV bursts. The fact that similar variations are observed on YZ CMi suggests that the same processes are operating on this star.

3.3. Stars with active chromospheres and coronae

We have observed 17 stars of spectral type F, G, and K, and known to possess active chromospheres and coronae and/or detected magnetic fields. We have detected none. The upper limits of radio luminosities determined for dwarf stars (which comprise most of

the objects in this class) are in the range $\sim 10^{13}$ – 10^{14} erg s $^{-1}$ Hz $^{-1}$. These are comparable with quiescent radio emission typically observed in dwarf M stars (Linsky and Gary, 1983, and Tables 1 and 2).

Although our observations do not constitute a complete sample in any sense, the absence of detectable emission from all G and K stars at the same luminosity level of detected M stars, argues in favor of an emission mechanism in dwarf M stars that is substantially different from that of G and K stars. If the sun may be taken as a representative of the physical processes in single or widely separated G dwarfs, we must conclude that the emission process operating at radio wavelengths in dwarf M stars, even at the quiescent level, are on a much larger scale than those on the Sun. More importantly, the radio emission processes (perhaps due to a more efficient acceleration process) in these stars must also be more efficient than in those G and K stars which have a degree of magnetic activity far in excess of that of the sun. Typically, the X-ray luminosity of most of our program stars is one hundred times larger than for the sun, and the chromospheric emission is typically an order of magnitude larger (Linsky et al., 1979; Vaiana et al., 1981). In spite of this, no radio emission has been detected from these active late-type stars.

3.4. The G0 V star χ^1 Ori

Gary and Linsky (1981) reported detection of χ^1 Ori at a level of 0.60 ± 0.27 mJy in a 3 h observation on 2 October 1980. In a subsequent observation 10 months later they failed to detect the source, but the star may have been detected again on 16 October 1981 at a 3σ level of 0.3 ± 0.2 mJy (Linsky and Gary, 1983). So far this is the only dwarf star of spectral type G detected at microwave frequencies. This observation has a special interest as it gives us an opportunity to investigate radio emission processes in a true solar-type star which is younger (age = $5 \cdot 10^4$ yr) and more rapidly rotating ($V_{\text{eq}} \approx 10$ km s $^{-1}$) than the sun. The degree of magnetic activity of χ^1 Ori is believed to be much higher than for the sun, as indicated by its high level of chromospheric and coronal activity (Linsky et al., 1979; Mewe et al., 1981).

If radio emission from χ^1 Ori has been reliably detected, and there is some question about this, then it is difficult to explain. If the emission mechanism is thermal gyroresonance (cyclotron emission) as suggested by Gary and Linsky (1981), the source size must be larger than ≈ 2 – 3 times the stellar radius [see Eq. (1) in the next section]. Magnetic fields of several hundred gauss must fill this extended volume, which implies that either the star is completely covered by starspots, or that the magnetic fields at photospheric levels are much stronger ($B \sim 10^4$ G) than those measured on the sun and in other G and K stars (Marcy, 1984). Both alternatives are difficult to accept, if the solar analogy is of any value. Moreover, Boesgaard and Simon (1984) have estimated from IUE observations that active regions cover at most 20% of the stellar surface in χ^1 Ori. Alternatively, the detected emission might be non-thermal and due to a transient flare-like brightening on the star. If this is the case, flares in active solar-type stars may be about one order of magnitude larger than the strongest bursts ever observed on the sun (the derived radio luminosity for χ^1 Ori is $\log L_R = 13.9$ erg cm $^{-2}$ s $^{-1}$ Hz $^{-1}$). We would expect to observe similar flares in other stars with the same age, rotation, chromosphere/coronal activity and distance as χ^1 Ori.

For these reasons we included χ^1 Ori in our program, and we also included a number of nearby active solar-type stars (111 Tau, π^1 UMa, 59 Vir, HR 8314, ξ UMa, 53 Agr) which appear indistinguishable from χ^1 Ori with regard to atmospheric parameters such

as spectral type, rotation, chromosphere, and coronal emission, magnetic activity, etc. All are young stars of spectral type F8 V to G2 V, with rotation rates of the order of ~ 10 km s $^{-1}$ and coronal X-ray fluxes which are two orders of magnitude higher than for the sun. We have failed to detect χ^1 Ori, as well as all other G and K dwarf stars in our program. Our upper limit for χ^1 Ori ($S < 0.23$ mJy) is a factor of three lower than the detection level reported by Gary and Linsky (1981). Similarly low upper limits were determined for the other stars (see Table 2). Indeed, if flares much stronger than solar bursts occur in active G stars, they must be rather infrequent.

A possible solution to the χ^1 Ori dilemma may be the recent discovery by infrared speckle interferometry (McCarthy, 1983) of a previously unknown dwarf M companion of χ^1 Ori, separated by only 0.65" (notice that the detection of χ^1 by Gary and Linsky, 1981, was done in the C configuration which has insufficient spatial resolution to separate the two component stars). The detected emission might have been due to a flare on the dM companion. If this is the case, we can take it as evidence that: a) radio emission from single dwarf stars at the present sensitivity levels is limited to dwarf M stars; b) the dwarf M companion of χ^1 Ori is not a steady 6 cm source at a level larger than $\log L_R \sim 13.4$ erg s $^{-1}$ Hz $^{-1}$.

4. Discussion

Our results can be summarized as follows:

We have detected four RS CVn binaries and established upper limits for another six. Of the detected stars, one (WW Dra) is a new detection, while the radio luminosities of the other three were one to two orders of magnitude lower than the maximum luminosities reported by other observers.

Detectable circular polarization was observed for UX Ari and HR 1099. Multiple wavelength monitoring of these stars indicates that both the shape of the spectrum and the degree of circular polarization change with time.

We have confirmed radio emission from three flare stars (UV Cet, EQ Peg, and YZ CMi) at about the same level as previous detections and have established upper limits for two others (YY Gem and EQ Vir). We have also observed both impulsive (~ 10 s) and more gradual (10–20 min) burst emission from the flare star YZ CMi. These bursts appear to be superimposed on a more slowly varying component which becomes more polarized with increasing intensity.

We have failed to detect microwave emission from any other solar-type star of spectral type F to K. For those stars observed previously, our upper limits are consistent with, and sometimes lower than, those reported by other authors.

We do not confirm radio emission at 6 cm from the G star χ^1 Ori, and we establish an upper limit that is three times lower than the detection level reported by Gary and Linsky (1981).

In what follows, we discuss the implications of these observations for the mechanism of stellar radio emission at 6 cm.

Most of the stars in our program have been observed at X-ray wavelengths by the EINSTEIN and EXOSAT satellites. From the temperatures and emission measures derived from X-ray observations (Vaiana, 1983; Landini et al., 1985) we estimate that the coronae of all these stars are optically thin at 6 cm by thermal free-free emission. The expected flux due to thermal bremsstrahlung for these sources is typically $\sim 10^{-2}$ mJy, well below the present VLA sensitivity level.

The expected flux may be somewhat higher if the stellar corona becomes optically thick at centimeter wavelengths by the thermal gyroresonant process (Kakinuma and Swarup, 1962; Zheleznyakov, 1970). This is suggested by the analogy with the sun where the slowly-varying emission associated with active centers is made up of two components, one diffuse and of low brightness temperature overlying plages, and the other component of small size and high brightness temperature, usually but not exclusively associated with spots (Kundu et al., 1977; Pallavicini et al., 1979; Felli et al., 1981). While the first component can be easily explained by optically thin free-free emission, sunspot associated components require an additional opacity mechanism, usually attributed to thermal gyroresonance absorption at the first few harmonics of the gyrofrequency, ν_{gr} , in which $\nu_{gr} = 2.8 \cdot 10^6 H$, where H is the magnetic field in Gauss. Fields of the order of 600–900 Gauss are required for $\lambda = 6$ cm if the gyroresonance absorption occurs at the second or third harmonic. Models based on the gyroresonance interpretation have been able to satisfactorily explain coordinated high-resolution observations of solar active regions at radio and EUV wavelengths (Alissandrakis et al., 1980; Pallavicini et al., 1981; Schmahl et al., 1982).

If extraordinarily large spots are present in active stars of late spectral type, then it is possible that thermal gyroresonance emission could substantially contribute to the emission at centimeter wavelengths. One might even hope to infer from the observed radio emission the strength and area covered by magnetic fields in these stars. Unfortunately, simple order of magnitude estimates show that these expectations are not easily fulfilled. Assuming that the stellar coronae become optically thick by the gyroresonance process over a source of radius R_s , the expected flux at $\lambda = 6$ cm from a star at distance d (pc) radius R_* and coronal temperature T_{cor} is

$$S_{6cm}(\text{mJy}) = 1.2 \cdot 10^{-6} \left(\frac{R_s}{R_*} \right)^2 \left(\frac{R_*}{R_\odot} \right)^2 T_{cor}(d_{pc})^{-2}, \quad (1)$$

where R_\odot is the sun's radius.

For a coronal temperature $T_{cor} = 3\text{--}5 \cdot 10^6$ K as constrained by X-ray observations (Vaiana, 1983; Golub, 1983; Swank, 1984; Landini et al., 1984) and a typical distance of 10 pc, a star with $R_* = R_\odot$ would be detected at a level of 0.5 mJy only if the size of the optically thick source is $R_s = 3R_*$. For a dM star with $R_* = 0.5R_\odot$, the source size must be $R_s = 6R_*$. In order to have magnetic fields of several hundred Gauss at distances $R = 3\text{--}6R_*$, the photospheric magnetic field must decrease with height much more slowly than a potential configuration. Alternatively, if a potential magnetic field configuration is assumed to be valid, as it is for the sun, at least in a first approximation (Poletto et al., 1975), the inferred magnetic fields at photospheric levels must be much larger than in sunspots, and of the order of 10^4 Gauss. Such high magnetic fields have never been observed in G and K stars (Robinson et al., 1980; Marcey, 1984), although they have been shown to be inconsistent with nearly simultaneous observations of some stars at 6 cm and 20 cm (Kundu and Shevarture ($T_e = 10^4$ K) electrons producing microwave emission has been shown to be inconsistent with nearly simultaneous observations of some stars at 6 cm and 20 cm (Kundu and Shevgaonkar, 1985).

The above difficulties make the thermal interpretation of quiescent emission from stars of late spectral type rather unattractive. An alternative mechanism suggested to explain the high brightness temperatures of compact sources on the sun (Pallavicini et al., 1979; Melozzi, 1984) is non-thermal gyroresonance

emission similar to that used to explain some solar microwave bursts (Ramaty, 1973; Dulk and Marsh, 1982). Mildly relativistic electrons with energy of a few hundred keV and a density of $\sim 10^{-4}$ of the ambient thermal electron density are required. The main problem here is the short lifetime (typically 1 h) of the non-thermal electrons against radiative and collisional energy losses, which requires a continuous acceleration to explain the quasi-steady emission observed. This may well occur in dwarf M stars which have a level of activity and a frequency of flaring much larger than the sun. If this interpretation is correct, the "quiescent" emission observed in dMe flare stars results from the integrated flaring emission of non-thermal electrons accelerated quasi-continuously in stellar spots. If the emission is non-thermal gyrosynchrotron, we may expect high circular polarization which occasionally has been observed (Gary and Linsky, 1983). We further expect that this type of emission should be highly variable because of the stochastic nature of the process, and to be important only in stars with large spots and continuous flaring activity. This is consistent with the observed variability on timescales of tens of minutes (see Fig. 1) to hours (Linsky and Gary, 1983) and with the observed higher level of microwave emission in dwarf M stars with respect to G and K dwarf stars.

Finally, we comment on RSCVn stars. Radio emission from RSCVn stars has usually been interpreted as non-thermal gyrosynchrotron emission by mildly relativistic electrons in fields of 30–100 Gauss (Hjellming and Gibson, 1980). This interpretation has been proposed in the past to explain the strong flaring behavior of RSCVn stars (Feldman et al., 1978). A non-thermal emission mechanism is probably correct as our multiple wavelength observations (see Table 3) yield high circular polarizations of up to 60% and spectral indices of $\alpha \approx -0.25$ for both UX Ari and HR 1099, where the flux density is proportional to ν^α and ν is the frequency, which cannot be explained by thermal bremsstrahlung. Our observations also show the existence of emission levels much lower than during strong flares. This indicates that the VLA may indeed have the capability of observing "quiescent" emission from RSCVn stars. Long-term monitoring of RSCVn stars with the VLA should be pursued with the aim of distinguishing between the "quiescent" emission and the low-level flaring activity.

Acknowledgements. Solar and stellar radio astronomy at Tufts University is supported under grant AFOSR-83-0019 with the Air Force of Scientific Research. Investigations of dwarf M flare stars at Tufts University are also supported by NASA grant NAG 5-477. The Very Large Array is operated by Associated Universities, Inc. under contract with the National Science Foundation. Solar and stellar research at the Arcetri Astrophysical Observatory is partially supported by the Consiglio Nazionale delle Ricerche.

References

- Allissandrakis, C.E., Kundu, M.R., Lantos, P.: 1980, *Astron. Astrophys.* **82**, 30
- Boesgard, A.M., Simon, T.: 1984, *Astrophys. J.* **273**, 241
- Bopp, B.W., Fekel, F.: 1977, *Astron. J.* **82**, 490
- Bowers, P.F., Kundu, M.R.: 1981, *Astron. J.* **86**, 569
- Clark, B.G.: 1980, *Astron. Astrophys.* **89**, 377
- Drake, S., Simon, T., Linsky, J.: 1985, in *Stellar Continuum Radio Astronomy* (R. M. Hjellming and D. M. Gibson, eds) (in press)
- Dulk, G.A., Marsh, K.A.: 1982, *Astrophys. J.* **259**, 350
- Feldman, P.A., Taylor, A.R., Gregory, P.C., Seaquist, E.R., Balonek, T.J., Cohen, N.L.: 1978, *Astron. J.* **83**, 1471

R. Pallavicini et al.: Microwave observations of late-type stars

- Felli, M., Lang, K.R., Willson, R.F.: 1981, *Astrophys. J.* **247**, 325
- Fisher, P.L., Gibson, D.M.: 1982, in *Cool Stars, Stellar Systems and the Sun*, eds. M. S. Giampapa, L. Golub, SAO Special Rep. No. 392, Vol. II, p. 109
- Gary, D.E., Linsky, J.L.: 1981, *Astrophys. J.* **250**, 284
- Golub, L.: 1983, in *Activity in Red Dwarf Stars*, eds. P. B. Byrne, M. Rodonò, p. 83
- Hjellming, R.M., Gibson, D.M.: 1980, in *Radio Physics of the Sun*, eds. M. R. Kundu, T. E. Gergeley, p. 209
- Hall, D.S.: 1981, in *Solar Phenomena in Stars and Stellar Systems*, eds. R. M. Bonnet, A. K. Dupree, p. 431
- Kakinuma, T., Swarup, G.: 1962, *Astrophys. J.* **136**, 975
- Kundu, M.R., Alissandrakis, C.E., Bregman, J.D., Hin, A.C.: 1977, *Astron. Astrophys.* **213**, 278
- Kundu, M.R., Shevgaonkar, R.K.: 1984, in *Stellar Continuum Radio Astronomy* (R. M. Hjellming and D. M. Gibson, eds.) (in press)
- Lang, K.R., Willson, R.F.: 1982, *Astrophys. J. Letters* **255**, L 111
- Landini, M., Monsignori-Fossi, B.C., Pallavicini, R.: 1985, in *X-ray Astronomy '84* (in press)
- Linsky, J.L., Worden, S.P., McClintock, W., Robertson, R.M.: 1979, *Astrophys. J. Suppl.* **41**, 47
- Linsky, J.L., Gary, D.E.: 1983, *Astrophys. J.* **274**, 776
- Linsky, J.L.: 1983, in *Solar and Stellar Magnetic Fields: Origins and Coronal Effects*, ed. J. O. Stenflo, p. 313
- Marcy, G.W.: 1984, *Astrophys. J.* **276**, 286
- McCarthy, D.W., Jr.: 1983, in *Nearby Stars and the Stellar Luminosity Function*, eds. A. G. D. Philip, A. R. Uggren, p. 107
- Melozzi, M.: 1984, Ph. D. Thesis, Arcetri Observatory. Also see *Astron. Astrophys.* **131**, 103 (1984)
- Mewe, R., Schrijvers, C.J., Zwaan, C.: 1981, *Space Sci. Rev.* **30**, 191
- Mullan, D.J.: 1984, *Astrophys. J.* **279**, 746
- Mutel, R.L., Lestrade, J.F.: 1984, *Astrophys. J.* (submitted)
- Mutel, R.L., Lestrade, J.F., Preston, R.A., Phillips, R.B.: 1984, *Astrophys. J.* (submitted)
- Pallavicini, R., Vaiana, G.S., Tofani, Felli, M.: 1989, *Astrophys. J.* **229**, 375
- Pallavicini, R., Golub, L., Rosner, R., Vaiana, G.S., Ayres, T., Linsky, J.L.: 1981, *Astrophys. J.* **248**, 279
- Pallavicini, R., Sakurai, T., Vaiana, G.S.: 1981, *Astron. Astrophys.* **98**, 316
- Pettersen, B.R.: 1983, in *Activity in Red Dwarf Stars*, eds. P. B. Byrne, M. Rodonò, p. 17
- Poletto, G., Vaiana, G.S., Zombeck, M.V., Krieger, A.S., Timothy, A.F.: 1975, *Solar Phys.* **44**, 93
- Ramaty, R.: 1973, in *High Energy Phenomena on the Sun*, eds. R. Ramaty, R. G. Stone, NASA SP-342, p. 188
- Robinson, R.D., Wordern, S.P., Harvey, J.W.: 1980, *Astrophys. J. Letters* **236**, L 155
- Schmahl, E.J., Kundu, M.R., Strong, K.T., Bentley, R.D., Smith, J.B., Krall, K.R.: 1982, *Solar Phys.* **80**, 253
- Swank, J.H.: 1984, in *Proceedings of Conference on Early-Type Stars*, ed. A. Underhill (in press)
- Takakura, T.: 1967, *Solar Phys.* **1**, 304
- Topka, K., Marsh, K.A.: 1982, *Astrophys. J.* **254**, 641
- Vaiana, G.S., Rosner, R.: 1978, *Ann. Rev. Astron. Astrophys.* **16**, 393
- Vaiana, G.S. et al.: 1981, *Astrophys. J.* **244**, 163
- Vaiana, G.S.: 1981, *Space Sci. Rev.* **30**, 151
- Vaiana, G.S.: 1983, in *Solar and Stellar Magnetic Fields: Origins and Coronal Effects*, ed. J. O. Stenflo
- Zheleznyakov, V.V.: 1970, *Radio Emission of the Sun and Planets*, Pergamon Press, Oxford

15. VLA OBSERVATIONS OF NARROW-BAND DECIMETRIC BURST EMISSION

ROBERT F. WILLSON

Department of Physics, Tufts University, Medford, MA 02155, U.S.A.

(Received 24 October, 1984; in revised form 10 January, 1985)

Abstract. The Very Large Array was used to observe a multiply-impulsive solar radio burst at several wavelengths near 20 cm. The observations indicate that the impulsive emission was nearly 100% circularly polarized and originated in small regions of $\sim 10''$ – $20''$ in size. For one of the impulsive spikes, we find evidence of narrow-band emission that could be attributed to an electron-cyclotron maser. The radio data are also compared with soft X-ray data and interpreted in light of a model in which the coronal plasma is heated by maser burst emission.

1. Introduction

VLA observations of solar radio bursts near 20 cm wavelength indicate that the regions of impulsive emission are often compact ($\theta \leq 10''$), highly circularly polarized ($p_c \geq 50\%$) sources with brightness temperatures in excess of 2×10^7 K (Willson, 1982; Willson and Lang, 1984). In most cases, the regions of energy release appear to be localized near the tops of bipolar loops, while in rarer instances they appear to originate in two spatially separated regions of opposite magnetic polarity, possibly from the legs or feet of loops. Although the radiation mechanisms of thermal bremsstrahlung and gyroresonance absorption contribute to the quiescent emission of 20 cm loops (Lang *et al.*, 1983a; McConnell and Kundu, 1983; Dulk and Gary, 1983; Lang *et al.*, 1982), they cannot explain the high brightness temperatures and high degrees of circular polarization of impulsive bursts. Instead, it has been generally believed that the burst mechanism is gyrosynchrotron emission from mildly relativistic electrons trapped in a magnetic loop (e.g. Kundu and Vlahos, 1982).

Recently, however, it has been suggested that electron-cyclotron maser emission may play an important role in some decimetric bursts (Holman *et al.*, 1980; Melrose and Dulk, 1982a, b). A coherent emission mechanism has been invoked in order to explain, for example, intense ($T_b \geq 10^{12}$ K), narrow-band, millisecond spikes that have been detected from the Sun at decimeter wavelengths (Droge, 1977; Slottje, 1978) as well as rapid, highly circularly polarized bursts that have been observed from nearby flare stars (Brown and Crane, 1978; Gibson and Fisher 1981; Slee *et al.*, 1981; Lang *et al.*, 1983b). Melrose and Dulk (1982a, b) have interpreted these observations in terms of electron-cyclotron masers which operate at the first or second harmonic of the gyrofrequency. Under conditions that are expected to prevail in the coronae of the Sun and active stars, maser emission can produce burst sources with brightness temperatures in excess of 10^{12} K and 100% circular polarization over a narrow frequency range of $\Delta\nu/\nu \leq 10^{-2}$. More recently, Melrose and Dulk, (1984) have shown that decimetric wavelength

masers may generate sufficient energy to heat the surrounding thermal plasma to a temperature of $1-3 \times 10^7$ K. The heated plasma will be detected as an enhancement at soft X-ray wavelengths, which is expected to lag behind the impulsive maser emission. Their model thereby provides an explanation for observations that often indicate time differences between impulsive radio spikes and the later more gradual soft X-ray emission.

Although there have been several multi-frequency observations of solar radio bursts (Marsh and Hurford, 1980; *et al.*, 1981) they have been made at such widely spaced frequencies as to be insensitive to narrow-band features of the kind expected from maser emission. In this paper we present VLA observations of a multiply impulsive burst that was observed simultaneously at two closely spaced frequencies near 1446 MHz (20.7 cm). For one of these spikes we find evidence for narrow-band 100% circularly polarized emission that could be attributed to an electron-cyclotron maser. We also compare the VLA results with soft X-ray data and interpret them in light of the radiofrequency heating model of Melrose and Dulk (1984).

2. Observations

The VLA (B configuration) was used to observe the active region AR 4398 on January 29, 1984. The position of AR 4398 on the solar surface at 13:00 UT was 14° N 24° W. The primary goal of our observations was to search for cyclotron line emission from the quiescent active region itself by making synthesis maps at 12 different frequencies between 1375 MHz and 1720 MHz. The results of these observations are given elsewhere (Willson, 1984). At the frequencies of observation, the half-power beamwidth of the individual antennas is $\sim 31'$ and the synthesized beamwidth is $\sim 3'' \times 4''$. The four independent intermediate frequency channels available at the VLA made it possible to record the left and right circularly polarized signals at two different frequencies at once from all 351 antenna pairs at a rate of once every 10 s. The active region was observed at successive pairs of frequencies for a period of 5 min each so that all twelve frequencies could be observed in 30 min. In all cases the bandwidth was 12.5 MHz. By choosing the frequency separation to be sufficiently narrow (typically 50 MHz), it was possible to compare observations at two nearby frequencies and thereby search for narrow-band features characteristic of maser emission.

The sequence of solar observations was followed by successive 2 min observations of the calibrator source 3C 48. The 10 s visibility data were calibrated using 3C 48 together with a correction for the difference in signals from high temperature noise sources located on four of the antennas. The calibrated data were then edited and used to produce snapshot maps of both the left (LCP) and right circularly polarized (RCP) emission at 10 s intervals. The maps were then cleaned to produce microwave images with a dynamic range of 10:1.

In Figure 1 we show the fringe amplitudes of a multiply-impulsive burst that occurred during our observations. Here, the data were measured on a baseline having a fringe spacing of $25''$. We also show the time profiles of the 1.6–12.5 keV (1–8 Å) and the

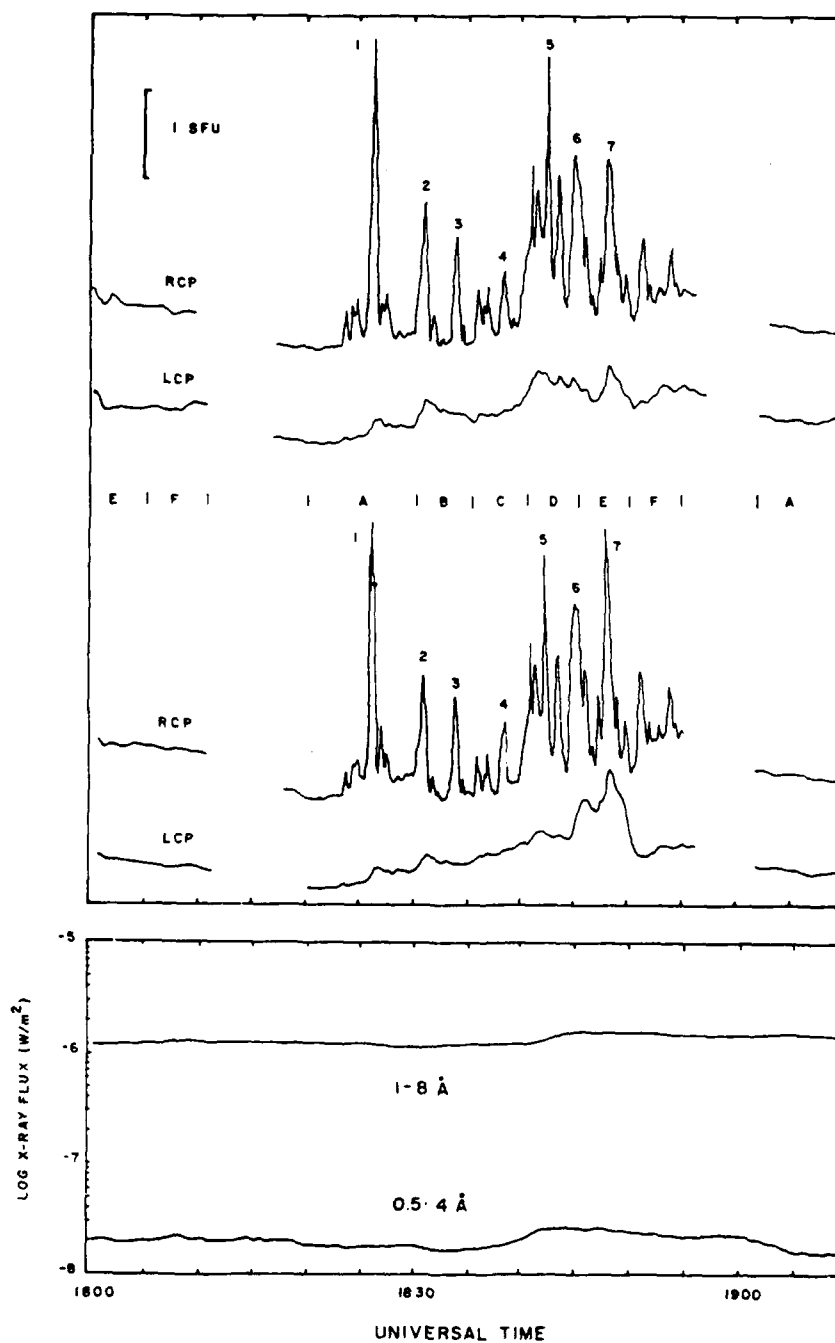


Fig. 1. A sequence of right circularly polarized (RCP) impulsive bursts observed at wavelengths near 20 cm on January 29, 1984. The top and bottom profiles are at closely spaced frequencies designated by A: 1375 and 1410 MHz, B: 1440 and 1480 MHz, C: 1515 and 1550 MHz, D: 1585 and 1620 MHz, E: 1658 and 1690 MHz, and F: 1705 and 1720 MHz. Each pair of frequencies was observed for about 5 min. The 10 s snapshot maps at the peak of each burst are shown in Figure 2.

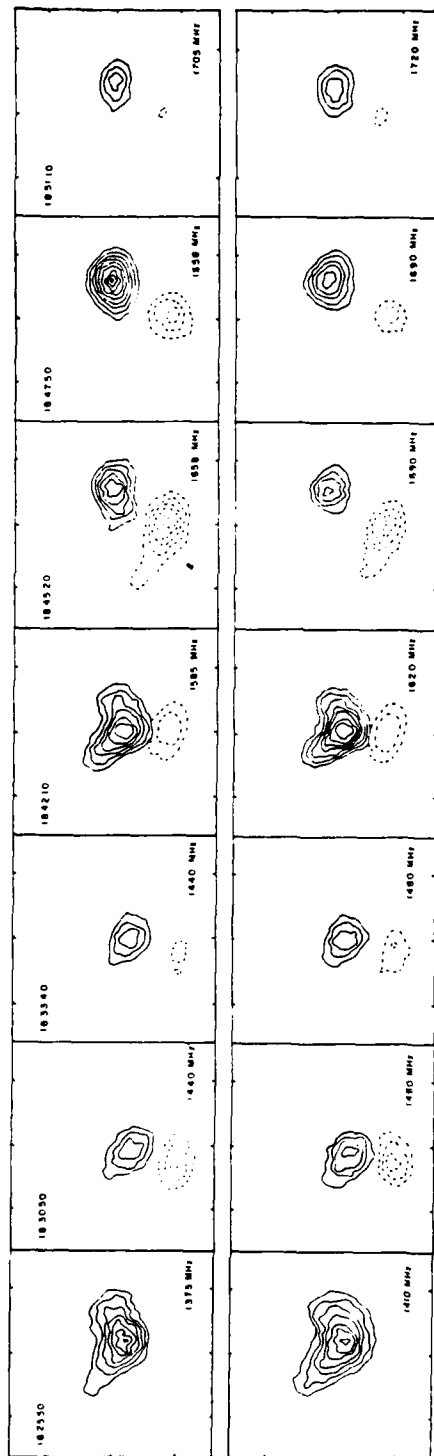


Fig. 2. Ten-second snapshot maps made at the peak of the impulsive bursts shown in Figure 1. The right circularly polarized (RCP) bursts originated from a source (solid lines) that was spatially separated from the left circularly polarized (LCP) emission (dashed lines). The outermost contour and contour interval is 2.3×10^7 K for RCP and 9.0×10^6 K for LCP. Peak 7 occurring at 18:47:50 has a large difference in brightness temperature with T_R (1658) = 1.5×10^8 K and T_H (1690) = 8.5×10^7 K. The angular scale can be determined from the $30''$ spacing between the fiducial marks.

3.1–25.0 keV (0.5–4.0 Å) X-ray flux as observed by the GOES satellite. The radio burst is particularly interesting because of the striking difference in the time behavior of the polarized emission. The left circularly polarized flux shows a gradual increase that began ~ 18:25 UT with a peak near 18:47 UT. In contrast, the right circularly polarized burst component shows a number of impulsive spikes each lasting between 10 and 30 seconds. We particularly draw attention to spike number 7, (18:47:50 UT) which is about 1.6 times more intense at 1658 MHz than at 1690 MHz.

In Figure 2 we show a series of 10 s snapshot maps which depict the structure of the burst source at the peaks of the impulsive spikes. In order to more clearly illustrate the weaker left circularly polarized emission the LCP contours have been enhanced by a factor of 2.5. The maps clearly indicate the burst emission comes from two spatially separated 100% circularly polarized regions whose angular sizes are well resolved and range from 10" to 30". The structure of the impulsive right circularly polarized source changes from peak to peak. The location of this source also shifts eastward by 10" to 15" between the peaks at 18:42:10 and 18:45:20, as the left circularly polarized source remains stationary. The maximum brightness temperatures (Table I) of the RCP sources range between 5.0×10^7 K and 1.5×10^8 K, while the LCP sources have lower brightness temperatures of between 6.4×10^6 K and 2.8×10^7 K.

TABLE I
Peak brightness temperatures

Time (UT)	Frequency (MHz)	T_b (RCP) (K)	T_b (LCP) (K)
18:25:50	1375	1.1×10^8	$\leq 5.0 \times 10^6$
	1410	1.2×10^8	$\leq 5.0 \times 10^6$
18:30:50	1440	5.4×10^7	1.9×10^7
	1480	6.3×10^7	1.9×10^7
18:33:40	1440	4.8×10^7	1.1×10^7
	1480	4.9×10^7	1.3×10^7
18:42:10	1585	1.3×10^8	1.3×10^7
	1620	1.3×10^8	1.3×10^7
18:45:20	1658	1.1×10^8	4.1×10^7
	1690	8.9×10^7	2.6×10^7
18:47:50	1658	1.5×10^8	2.8×10^7
	1690	8.5×10^7	1.7×10^7
18:51:10	1705	4.8×10^7	6.5×10^6
	1720	5.0×10^7	6.4×10^6

In Figure 3 we compare the location of the burst peak at 18:45:20 UT with a Kitt Peak magnetogram taken at 16:41:05 UT on the same day. This figure shows that the active region consists of two main spots located almost east-west on the Sun and that the burst occurred near the leading spot of positive magnetic polarity. The right circularly

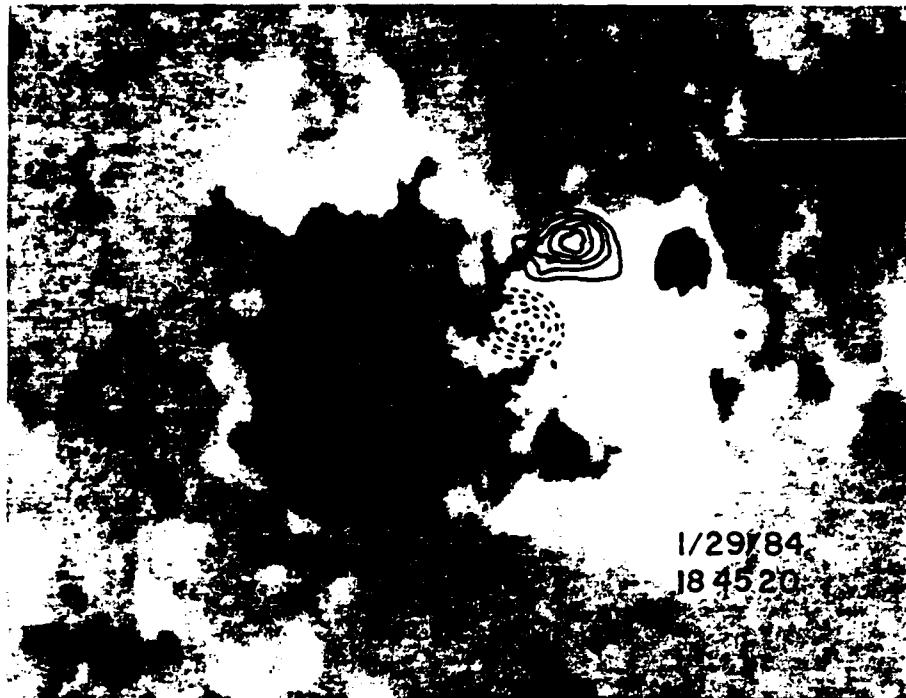


Fig. 3. A ten-second snapshot map of the LCP (dashed) and RCP (solid) burst sources at 18:45:20 UT, superimposed on a Kitt Peak magnetogram.

polarized source is displaced eastward by $\approx 10''$ – $15''$ from the center of the spot. This displacement, together with the bipolar nature of the burst sources, suggests that the burst emission occurred along the legs of a magnetic loop that joins the regions of opposite polarity, but that the loop is not centered between the two spots.

3. Discussion

The most interesting aspect of these observations is the difference in intensity of spike number 7 at 1658 and 1690 MHz for which T_B (1658) = 1.5×10^8 K and T_B (1690) = 8.5×10^7 K. The observed reduction in brightness temperature by a factor of 1.6 over a frequency range of only 32 MHz implies a spectral index ($T_b \sim \nu^\alpha$) of $\alpha \approx -2.5$. The steep slope of the burst spectrum excludes any thermal or nonthermal mechanism such as bremsstrahlung or gyrosynchrotron emission, which is intrinsically broadband. In principle, there are several mechanisms, such as Razin suppression or free-free absorption that could reduce the intensity of a broadband source at lower frequencies (Benz and Tarnstrom, 1976), but they cannot account for the high frequency decrease observed in this burst peak.

The high degree of circular polarization and narrow bandwidth of this spike are reminiscent of bursts observed between 1.0 and 1.4 GHz by Dröge (1977) and at 2.6 GHz by Slottje (1978). Narrow-band impulsive bursts or 'blips' have also been observed between 0.6 and 1.0 GHz by Benz *et al.* (1981) and by Fürst *et al.* (1982). These bursts are often associated with hard X-ray emission and show some of the properties of type III bursts, such as decay time, polarization, and drift rate. Benz *et al.* (1983) suggest that the narrow bandwidth of blips may be caused by beams of electrons which either decay rapidly or else increase their radio luminosity locally because of special conditions in the coronal loop plasma. Blips differ qualitatively from other higher frequency bursts, however, in that the former exhibit relatively low degrees of circular polarization. The narrow band width of the burst discussed in this paper may therefore require a different physical explanation.

Both high circular polarization and narrow bandwidths are, for example, signatures of electron-cyclotron-maser emission, for Melrose and Dulk (1982a, b) calculate $\rho_c \approx 100\%$ and $\Delta\nu/\nu_0 \approx 10^{-2}$ for a typical maser spike. The observed peak brightness temperature of 1.5×10^8 K observed in spike number 7 is, however, far below that expected ($T_b \geq 10^{10}$ K) from masers, but the lower observed brightness temperature could be due to the relatively long VLA integration time of 10 s which almost certainly averages over many maser spikes. Melrose and Dulk (1984) have suggested that the maser operates in a number of small regions, each of which produces an 'elementary burst' lasting a few milliseconds. The size of each burst may be only 30–300 km, corresponding to an angular size of 0.04" to 0.4". These bursts would therefore be spatially and temporally unresolved by the VLA. The fact that the impulsive source is resolved with an angular size of $\sim 10''$ may indicate that many maser bursts occurred within the region during the 10 s time interval. Maser emission that escapes and is observed is expected to occur at the second harmonic of the gyrofrequency, so that small variations in the magnetic field strength across the bursting region would cause the maser spikes to shift in frequency and thereby produce a broadening of the maser spectrum when many spikes are averaged together. This could explain why the intensity of the other burst peaks are the same over a frequency separation of ~ 50 MHz.

Finally, we comment on the flare heating model of Melrose and Dulk (1984) in which the soft X-ray emitting plasma is heated by decimetric maser emission.

In Figure 1 we compare the radio burst with soft X-ray data in the 0.5–4.0 Å and 1–8 Å wavelength ranges as observed by the GOES satellite. This figure shows that the X-ray emission began to increase at $\sim 18:40$ UT and reached a peak at $\sim 18:45$ UT, about 20 min after the first impulsive spike. Unfortunately, there was no hard X-ray observations of this burst by the HXRBS instrument aboard the Solar Maximum Mission satellite.

Schmahl (1984) has shown that the kinetic temperature of the X-ray emitting plasma may be estimated directly from the ratio of the fluxes in the two GOES energy channels. At the peak of the X-ray burst, the ratio of fluxes $F(0.5-4 \text{ Å})/F(1-8 \text{ Å}) \approx 0.65$, corresponding to a temperature of 1.5×10^7 K.

The time delay between the radio spikes and the soft X-ray emission is consistent with

the heating model recently proposed by Melrose and Dulk (1984). In their model, maser emission generated at the first harmonic of the gyrofrequency, ν_B , is reabsorbed at the second harmonic, $2\nu_B$. The radiofrequency energy thus provided can then be used to heat the surrounding thermal plasma to a temperature of $1-3 \times 10^7$ K.

A potential difficulty with the heating model may arise because as the second harmonic maser emission propagates outward through the solar corona, it may be absorbed within these higher layers at different harmonics of the local gyrofrequency. For example, if the third harmonic layer has a temperature of $T_e = 2.5 \times 10^6$, a density of $n_e = 5 \times 10^8 \text{ cm}^{-3}$, and a thickness of $1.0 \times 10^9 \text{ cm}$ then the optical depth due to gyroresonance absorption (the angle $\theta = 80^\circ$ between the magnetic field and the line of sight) is $\tau_{gr} \approx 40$. In this case, radiation emitted at the second harmonic will not escape from the burst site. We note, however, that a significantly smaller value of θ is not excluded, for if the burst emission occurs along the legs of a dipolar loop (Figure 3) then given the location of the active region at the time of the burst ($14^\circ \text{ N } 29^\circ \text{ W}$) and the eastward displacement of the impulsive source from the underlying spot, then the angle θ , could be as small as 10° . For the same values of temperature, density and thickness the third harmonic will be nearly optically thin with $\tau_{gr} (\theta < 10^\circ) \leq 0.1$.

In conclusion, our VLA observations show evidence for impulsive narrow-band decimetric burst emission which could be explained by an electron-cyclotron maser. The soft X-ray enhancement that followed the impulsive radio burst is consistent with the radio frequency heating model proposed by Melrose and Dulk (1984) only under certain restrictive conditions. However, we cannot rule out that the X-ray emitting plasma was heated by maser emission. Future multiple frequency VLA observations with higher time and spatial resolution together with spatially resolved X-ray data may provide a more definitive test of this model as well as yield important information about solar maser burst emission.

Acknowledgements

Solar Radio Astronomy at Tufts University is supported under grant AFOSR-83-0019 with the Air Force Office of Scientific Research. The author thanks Kenneth Lang for useful discussions and Jack Harvey for providing the Kitt Peak magnetogram. The author is also grateful to the referee, George Dulk, for a critical review of the paper. The Very Large Array is operated by Associated Universities, Inc., under contract with the National Science Foundation.

References

- Benz, A. O. and Tarnstrom, G. L.: 1976, *Astrophys. J.* **204**, 597.
- Benz, A. O., Furst, E., Hirt, W., and Perrenoud, M. R.: 1981, *Nature* **291**, 239.
- Benz, A. O., Bernold, T. E. X., and Dennis, B. R.: 1983, *Astrophys. J.* **271**, 355.
- Brown, R. L. and Crane, P. C.: 1978, *Astron. J.* **83**, 1504.
- Droge, F.: 1977, *Astron. Astrophys.* **57**, 285.
- Dulk, G. A. and Gary, D. E.: 1983, *Astron. Astrophys.* **124**, 103.

- Fürst, E., Benz, A. O., and Hirth, W.: 1982, *Astron. Astrophys.* **107**, 178.
- Holman, G. D., Eichler, D., and Kundu, M.: 1980, in M. Kundu and T. Gergely (eds.), 'Radio Physics of the Sun', *IAU Symp.* **86**, 205.
- Kundu, M. R. and Vlahos, L.: 1982, *Space Sci. Rev.* **32**, 405.
- Lang, K. R., Willson, R. F., and Rayrole, J.: 1982, *Astrophys. J.* **258**, 384.
- Lang, K. R., Willson, R. F., and Gaizauskas, V.: 1983a, *Astrophys. J.* **267**, 455.
- Lang, K. R., Bookbinder, J., Golub, L., and Davis, M. M.: 1983b, *Astrophys. J. Letters* **272**, L15.
- Marsh, K. A. and Hurford, G. J.: 1980, *Astrophys. J. Letters* **240**, L111.
- Marsh, K. A., Hurford, G. J., Zirin, H., Dulk, G. A., Dennis, B. R., Frost, K. J., and Orwig, L. E.: 1981, *Astrophys. J.* **251**, 797.
- Melrose, D. B. and Dulk, G. A.: 1982a, *Astrophys. J.* **259**, 844.
- Melrose, D. B. and Dulk, G. A.: 1982b, *Astrophys. J. Letters* **259**, L141.
- Melrose, D. B. and Dulk, G. A.: 1984, *Astrophys. J.* **282**, 308.
- McConnell, D. and Kundu, M. R.: 1983, *Astrophys. J.* **269**, 698.
- Schmahl, E.: 1984, *Bull. Am. Astron. Soc.* (Jan. 1984 meeting).
- Slee, O. B., Tuohy, I. R., Nelson, G. J., and Rennie, C. J.: 1981, *Nature* **292**, 220.
- Slotje, C.: 1978, *Nature* **275**, 520.
- Willson, R. F.: 1982, *Solar Phys.* **83**, 285.
- Willson, R. F.: 1984 (submitted to *Astrophys. J.*).
- Willson, R. F. and Lang, K. R.: 1984, *Astrophys. J.* **279**, 427.

16. VLA OBSERVATIONS OF SOLAR ACTIVE REGIONS AT CLOSELY SPACED FREQUENCIES: EVIDENCE FOR THERMAL CYCLOTRON LINE EMISSION

ROBERT F. WILLSON

Department of Physics, Tufts University

Received 1984 August 10; accepted 1985 May 20

ABSTRACT

VLA observations of a solar active region at 10 closely spaced frequencies between 1440 and 1720 MHz are presented. The synthesis maps show, on two successive days, significant changes in the brightness temperature within this narrow frequency range. We show that these changes cannot be due to either thermal bremsstrahlung or gyroresonance emission from a coronal loop in which the temperature, density, or magnetic field varies monotonically with height. Instead, we attribute the brightness spectrum to cyclotron line emission from a narrow layer where the temperature is elevated above the surrounding part of the loop.

Subject headings: interferometry — radiation mechanisms — Sun: radio radiation

1. INTRODUCTION

Very Large Array (VLA)¹ observations of solar active regions near 20 cm wavelength delineate looplike structures that appear to connect lower lying areas of opposite magnetic polarity (Lang, Willson, and Rayrole 1982; Dulk and Gary 1983; Lang, Willson, and Gaizauskas 1983; McConnell and Kundu 1983). These sources have peak brightness temperatures of between 1.5×10^6 and 4.0×10^6 K, suggesting that they are the radio wavelength counterparts of coronal loops seen at soft X-ray wavelengths.

The radiation mechanism responsible for this emission is, however, the subject of some controversy. Lang, Willson, and Rayrole (1983) and Dulk and Gary (1983) have, for example, attributed 20 cm emission to optically thick thermal bremsstrahlung of a hot plasma trapped within magnetic arches connecting underlying sunspots. There is no detectable polarization near the magnetic neutral lines, and this has been attributed to optically thick emission or to magnetic fields that are transverse to the line of sight. A few 20 cm loops exhibit small circular polarization ($\rho_c \leq 20\%$) near their legs, and this has been attributed to the effects of bremsstrahlung propagating in longitudinal magnetic fields of strength $H_l \approx 20$ –70 G (Dulk and Gary 1983).

Other VLA observations suggest that low-harmonic gyroresonance absorption may provide the bulk of the opacity in 20 cm loops. McConnell and Kundu (1983) have, for example, found that the brightness of one loop could be best explained by gyroemission near the loop top and thermal bremsstrahlung near the feet. Velusamy and Kundu (1981) also compared radio and X-ray observations of systems of postflare loops, and found that gyroresonance emission was the most likely mechanism in these sources.

Both competing processes of bremsstrahlung and gyroresonance emission predict a smoothly varying continuum spectrum that decreases slowly with increasing frequency. The theory of cyclotron absorption, for example, indicates that observations at a given frequency, ν , refer to a narrow layer in the solar atmosphere at which $\nu = s\nu_H$, where $s = 2, 3, 4$ is the harmonic number and ν_H is the gyrofrequency. If the magnetic field in a

coronal loop decreases uniformly with height, then it was thought that the individual cyclotron lines would merge to form a smooth continuum. Theoretical work has shown however, that individual cyclotron lines might also be detected as narrow-band enhancements in the radio-frequency spectra of solar active regions if the radiation were emitted from relatively thin layers in the corona where the magnetic field is relatively constant (Syrovatskii and Kuznetsov 1980; Kuznetsov and Syrovatskii 1981). The presence of neutral current sheets, in which the temperature and density are higher than in the surrounding parts of the loop, might also lead to abrupt changes in the brightness temperature over a small frequency range (Syrovatskii 1977; Syrovatskii and Kuznetsov 1980). Recently, Willson (1983) mapped several active regions at three closely spaced frequencies near 1446 MHz and found that two of the sources showed striking changes in brightness within these narrow frequency ranges. These changes could not be explained by either thermal bremsstrahlung or gyroresonance emission from a loop in which the temperature, density, or magnetic field varied uniformly with height. They could, however, be explained by individual cyclotron lines emitted in small regions (10"–30") where the magnetic field was relatively constant with $H \approx 125$ –180 G.

Observations of cyclotron line emission are potentially important because they provide a means of specifying the physical conditions within coronal loops and current sheets. We have now tried to confirm the presence of cyclotron lines on the Sun by using the VLA to map an active region on two successive days at 10 different frequencies between 1440 and 1720 MHz. In this paper we present these observations and compare them with theoretical spectra of cyclotron line emission from coronal loops.

II. OBSERVATIONS

The VLA (B-configuration) was used to observe the active region AR 4398 on 1984 January 28 and 29. The position of AR 4398 at 1300 UT on January 28 and 29 was $14^\circ\text{N } 11^\circ\text{W}$ and $14^\circ\text{N } 24^\circ\text{W}$, respectively. The active region was observed at 10 different frequencies between 1440 MHz (21.8 cm) and 1720 MHz (17.4 cm) with bandwidths of 12.5 MHz during a 10 hr period between 1300 UT and 2300 UT on each day. At these frequencies the half-power beamwidth of the individual antennas ranges between 26.0 and 31.2 and the synthesized

¹ The VLA is a facility of the National Radio Astronomy Observatory, which is operated by Associated Universities, Inc., under contract with the National Science Foundation.

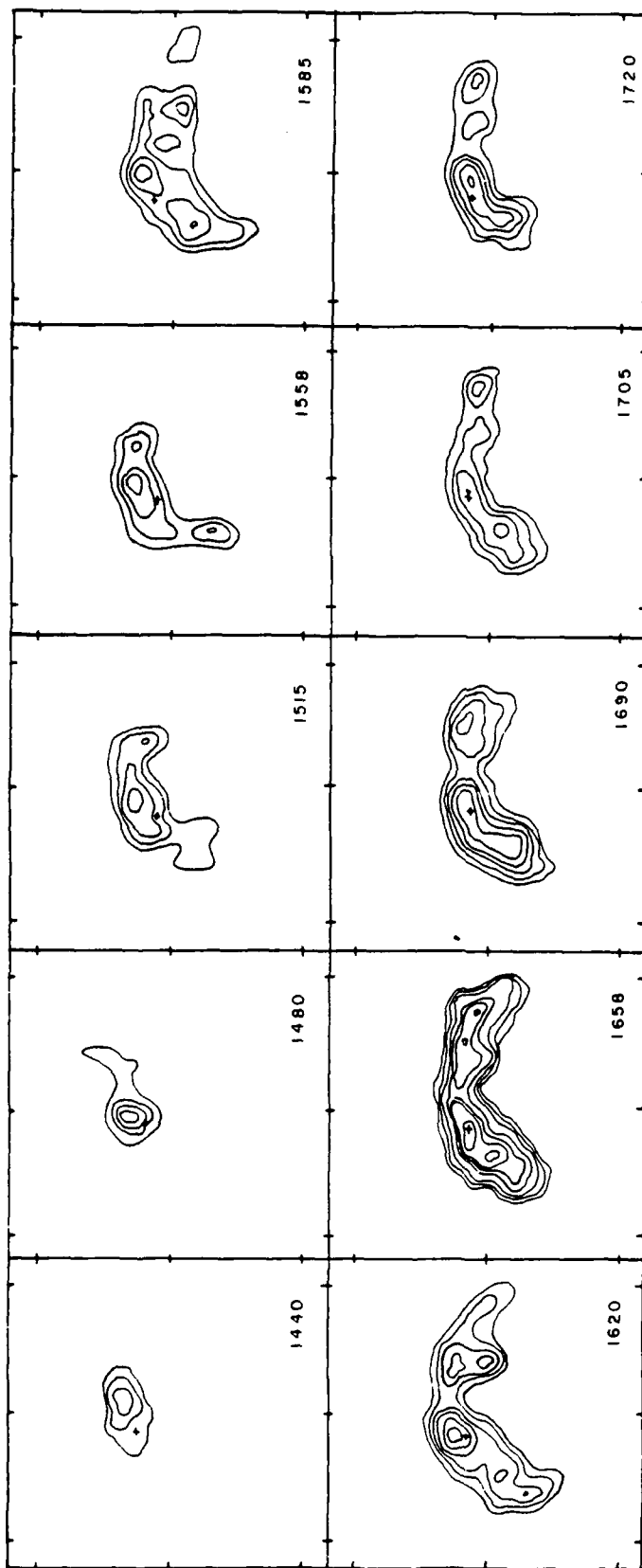


FIG. 1.—VLA synthesis maps of total intensity, I , of AR 4398 at 10 closely spaced frequencies during a 10 hr period on 1984 January 28. Synthesized beamwidth is $\theta \approx 3'' \times 4''$. Contours of the maps mark levels of equal brightness temperature. Outermost contour and contour interval are equal to 1.1×10^6 and 4.0×10^5 K, respectively. Angular scale can be determined from the $60''$ spacing between fiducial marks on the area.

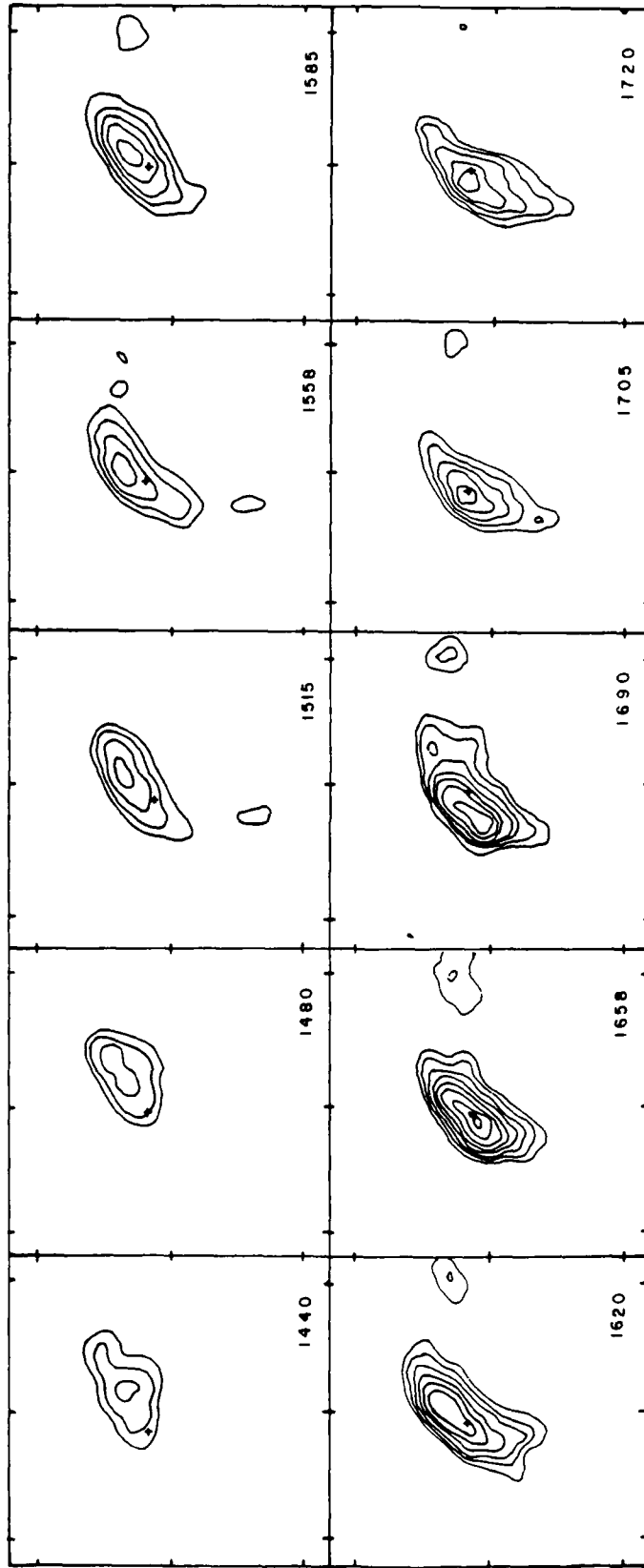


FIG. 2.—VLA synthesis maps of total intensity, I , of AR 4398 at 10 closely spaced frequencies using data obtained during a 10 hr interval on 1984 January 29. Contour levels and angular scale are same as in Fig. 1.

beamwidth varies between $3''.0 \times 3''.5$ and $3''.6 \times 4''.2$. The four independent intermediate frequency channels now available at the VLA made it possible to record the left and right circularly polarized signals of two different frequencies at once. The active region was observed at successive pairs of frequencies for a period of 5 minutes, so that all 10 frequencies could be observed in 25 minutes. This sequence of observations was followed by successive 2 minute observations of the calibrator source 3C 48. The data were calibrated using 3C 48 together with a correction for the difference in the signals from high-temperature noise sources located on four of the antennas. The temperatures of these sources were measured at each frequency and polarization prior to the solar observations and are believed to be accurate to $\leq 5\%$. The flux of 3C 48 at each frequency was determined from its flux of 15.37 Jy at 1465 MHz and its spectral index of $\alpha = -0.81$. Since some of the observations were made outside of the nominal protected radio band near 1421 MHz , the total power signal from two of the antennas was monitored for the presence of interference. No interference was detected during these observations, however. We also examined the data for the presence of solar bursts which could have corrupted the maps at one or more frequencies. Only one burst was detected, between 1820 and 1950 UT on January 29, and these data were edited before maps were made. The calibrated data were edited and used together with the standard CLEAN procedure to make synthesis maps of both total intensity, I , and circular polarization, V .

The maps of total intensity are shown in Figures 1 and 2. There was no detectable circular polarization ($V/I \leq 15\%$) on either day, suggesting that the regions were optically thick to both the ordinary and extraordinary modes of wave propagation. On both days the region shows a looplike structure of 1.0 to 1.5 in length, whose peak brightness temperature first increases systematically from $\sim 1.5 \times 10^6 \text{ K}$ at 1440 MHz to $\sim 4.0 \times 10^6 \text{ K}$ at 1658 MHz , and then begins to decrease at the highest frequencies. In Table 1 we give the brightness temperatures at a point denoted by a cross on the peak intensity at 1658 MHz , and in Figure 3 we plot these temperatures as a function of frequency. The error bars in Figure 3 represent 3σ uncertainties determined from the residual noise left on the CLEANed maps.

As a check on the integrity of the solar calibration procedure, we have also plotted the brightness temperatures observed in a loop within the active region AR 4399, located ~ 6.5 to the east of AR 4398. This was the only other major active region on the Sun during these 2 days. In contrast to AR 4398, the brightness spectrum of AR 4399 is nearly constant on both days, with an average brightness temperature of $T_b \approx 1.5 \times 10^6 \text{ K}$. This result seems to indicate that the changes in brightness temperature observed from AR 4398 are not common to all sources, and therefore not due to an artifact of the calibration or CLEANing procedure.

In Figure 4 we compare the radio maps at the peak frequency of 1658 MHz with Kitt Peak magnetograms taken on

the same day. The radio emission appears to connect regions of opposite magnetic polarity, suggesting that the sources are dipolar loops which join the underlying sunspots. Observations made at Mount Wilson Observatory (R. Howard, private communication) indicate that the two dominant spots have magnetic field strengths of $|H| \approx 2000 \text{ G}$, and that the morphology and surface fields of these spots did not change appreciably from one day to the next. As we will argue in the next section, this may explain why the spectrum and morphology of the radio loops were also similar on the two days.

III. DISCUSSION

In this section we will show that the observed changes in brightness temperature of about a factor of 2.5 over a frequency range of $\sim 300 \text{ MHz}$ are difficult to explain by either thermal bremsstrahlung or gyroresonance emission from a loop in which the temperature, density, and magnetic field vary uniformly with height. These radio results, then, appear to conflict with the results of numerical models of quasi-static coronal loops which predict smooth gradients in both temperature and density along the loop (e.g., Rosner, Tucker, and Vaiana 1978; Vesecky, Antiochos, and Underwood 1979). On the other hand, these sharp changes in brightness temperature are consistent with the existence of neutral current sheets or thin inhomogeneous layers in the coronal loop where the temperature or density are thought to be higher than in their surroundings (Syrovatskii 1977).

As a starting point in our analysis, we assume that the magnetic field strength $B(Z)$ in the loop can be represented by a dipole function, $B(Z) = B_0 R_D^3 / (Z + R_D)^3$, where Z is the height above the photosphere, B_0 ($\sim 2000 \text{ G}$) is the magnetic field at the solar surface, and R_D is the depth of the dipole below the loop base. If R_D is taken to be equal to one-half the distance, D , between the two footpoints, then Mount Wilson sunspot observations indicate $D \approx 8.0 \times 10^9 \text{ cm}$ and $R_D \approx 4 \times 10^9 \text{ cm}$. We next divide the loop into thin layers of thickness $1.0 \times 10^8 \text{ cm}$ and compute the optical depth due to thermal bremsstrahlung and gyroresonance emission with assumed values of temperature and density at each height, Z , in the loop. In the simplest models, we assume that the loop has a constant temperature and density between $Z = 2 \times 10^9 \text{ cm}$ and $5 \times 10^9 \text{ cm}$, the approximate height of 20 burst centimeter loop emission (Willson and Lang 1984). The equation of transfer for the emergent brightness temperature and circular polarization as a function of frequency was then solved for temperatures between 1.5×10^5 and $4.0 \times 10^6 \text{ K}$, and densities between 1.0×10^9 and $5.0 \times 10^9 \text{ cm}^{-3}$, using the equations for the thermal bremsstrahlung and gyroresonance optical depth given by Willson (1983). Models were also computed for different values of the parameter θ ($20^\circ < \theta < 90^\circ$), the angle between the magnetic field and the line of sight.

The results of these calculations indicate that for this range of temperatures and densities, and for $\theta > 60^\circ$, gyroresonance absorption would render the loop optically thick with a nearly

TABLE 1
MAXIMUM BRIGHTNESS TEMPERATURES, $T_b(\text{max})$, WITHIN AR 4398 AT DIFFERENT FREQUENCIES

Date	1440*	1480	1515	1558	1585	1620	1658	1690	1705	1724
1984 Jan 28	1.4×10^6	1.4×10^6	1.6×10^6	1.8×10^6	2.2×10^6	3.0×10^6	3.7×10^6	3.2×10^6	2.5×10^6	2.6×10^6
1984 Jan 29	1.3×10^6	1.7×10^6	1.8×10^6	2.0×10^6	2.2×10^6	3.2×10^6	4.0×10^6	2.8×10^6	2.7×10^6	2.3×10^6

* All frequencies are in megahertz, all temperatures are in kelvins.

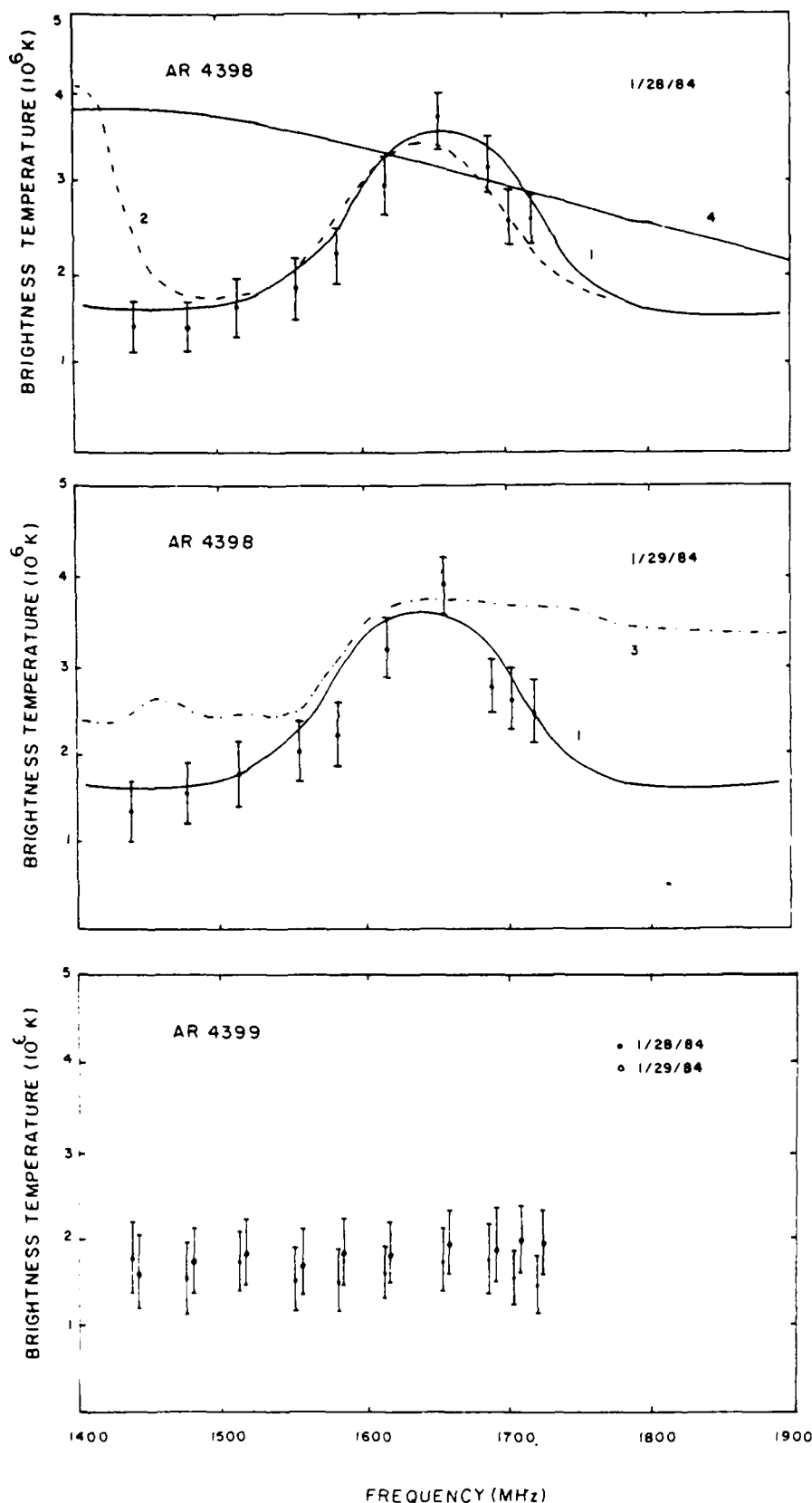


FIG. 3.—Theoretical plots of brightness temperature for different values of temperature density, and magnetic field strength in a coronal loop (top, middle). Maximum brightness temperatures of the loops in AR 4398 (top, middle) and AR 4399 (bottom) are also plotted with error bars corresponding to peak-to-peak fluctuations in background temperature of the synthesis maps. Curves 1 and 2 correspond to a coronal loop model that contains a thin ($\Delta L = 1.0 \times 10^8$ cm) layer where the magnetic field is $H = 145$ and 119 G, respectively, and where the temperature and density at $T_e = 3.8 \times 10^6$ K and $N_e = 1.0 \times 10^9$ cm $^{-3}$. The temperature and density in the rest of the loop are taken to be equal to $T_e = 1.5 \times 10^6$ K and $N_e = 1.0 \times 10^9$ cm $^{-3}$. Curve 3 corresponds to the same parameters as model 1, except that $N_e = 2.0 \times 10^{10}$ cm $^{-3}$. Curve 4 corresponds to a loop in which electron temperature increases monotonically from $T_e = 1.5 \times 10^6$ at $z = 5 \times 10^9$ cm to $T_e = 3.8 \times 10^6$ K at $z = 6 \times 10^9$ cm. In all cases, the angle θ between magnetic field and line of sight was taken to be equal to $\theta = 70^\circ$.

Brightness temperature of active region AR 4399, located ~ 6.5 east of AR 4398, together with typical error bars, is plotted on bottom panel of figure.

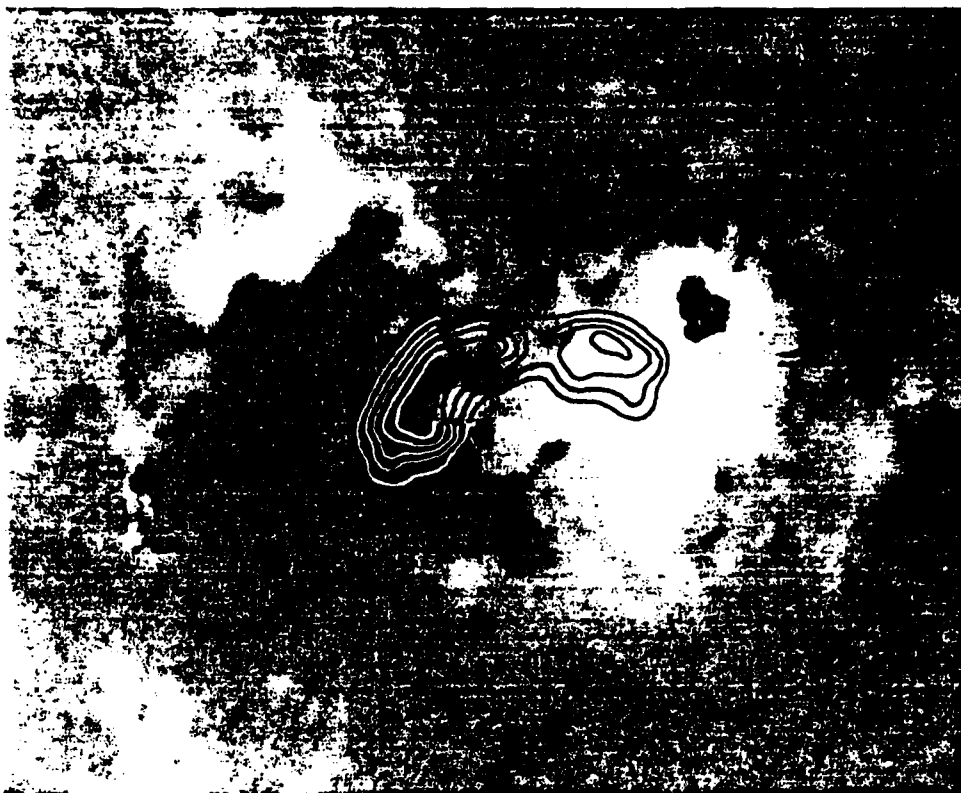


FIG. 4.—VLA synthesis maps of total intensity at 1658 MHz on 1984 January 28 (*top*) and 29 January (*bottom*), superposed on Kitt Peak magnetograms taken on the same day. Note that radio emission appears to connect areas of opposite magnetic polarity, and that peak brightness temperature occurs nearly along magnetic neutral line.

constant brightness temperature between 1.5×10^6 and 4×10^6 K, and a low degree of circular polarization ($p_c < 20\%$) throughout the range of frequencies observed. This is because the individual cyclotron lines at different harmonics that are emitted from a layer with constant temperature would merge to form a continuum. These results are in agreement with those of McConnell and Kundu (1983) who found that 20 cm coronal loops would be optically thick to gyroresonance emission at the third harmonic of the gyrofrequency for magnetic fields $H \approx 130$ –170 G, temperatures $T \approx 1.5 \times 10^6$ K, and densities of $N_e \approx 5 \times 10^8 \text{ cm}^{-3}$. We also found that these results are unchanged if the temperature and density are allowed to vary monotonically with height. In Figure 3 we show one such model in which the temperature varied from $T_e = 1.5 \times 10^6$ K at $Z = 5 \times 10^9$ cm to $T_e = 3.8 \times 10^6$ K at $Z = 6 \times 10^9$ cm.

Instead, we find that the peak in brightness temperature can be produced if the temperature, say T_e , in one of the layers with constant magnetic field is assumed to be higher than in the other layers. In this case, the individual cyclotron line with peak brightness temperature T_e will appear above the continuum spectrum produced by the other layers in the loop. The results of these model calculations are shown in Figure 3 for different values of the magnetic field strength, temperature, and density for which the peak at ~ 1658 MHz is a harmonic of the gyrofrequency. We find that the spectrum can be satisfactorily fit if the loop contains a thin layer in which $T_e = 3.5$ – 4.0×10^6 K, where the magnetic field is $H \approx 145$ G ($n = 4$), or possibly $H = 119$ G ($n = 5$). For $n = 3$ ($H = 197$ G), the line profile is too wide and flat-topped, while for $n > 6$ ($H > 100$ G) the lines are optically thin. That is, one explanation of these brightness temperature variations is the existence of a thin layer in which the temperature is ~ 3 times higher than in the rest of the loop where $T_e \approx 1.5 \times 10^6$ K. For an electron density of $N_e = 10^9 \text{ cm}^{-3}$, we obtain good fits for $1 \times 10^7 \text{ cm} < \Delta L < 1 \times 10^8 \text{ cm}$. For narrower layers, the lines become optically thin and do not give a good fit to the data. The data also constrain the angle θ to $\theta \approx 65^\circ$ – 80° , since smaller values would yield unacceptably high circular polarization ($p_c > 30\%$), and higher values would result in cyclotron line profiles that are too wide and flat-topped. We also find

that these results are relatively insensitive to the assumed density in the heated layer, up to $N_e \approx 2 \times 10^{10} \text{ cm}^{-3}$. For higher densities, thermal bremsstrahlung becomes dominant in the layer, resulting in a sharp step in brightness temperature above ~ 1600 MHz (Fig. 3).

The fact that the brightness spectrum is nearly identical on both days suggests that the physical conditions in the loop were similar on these days. As noted earlier, the magnetic fields of underlying sunspots were relatively constant, so that one might also expect the coronal extension of these photospheric fields to be also relatively unchanged. The frequency of the cyclotron line emission would, under these conditions be relatively unaffected, and this might explain the similarity of the microwave spectrum from one day to the next.

The physical mechanism that gives rise to a thin, apparently stable, hot layer in the corona is uncertain. We note, however, that EUV observations of coronal loops have revealed the presence of temperature inhomogeneities in a number of sources (Foukal 1975, 1976; Raymond and Foukal 1982; Pye *et al.* 1978). These inhomogeneities cannot be explained by quasi-static loop models in which the pressure is assumed to be uniform (e.g., Rosner, Tucker, and Vaiana 1978), but they may be accommodated in more sophisticated models in which the pressure and heat deposition are allowed to vary with height and distance in the loop (Serio *et al.* 1981). Whether these structures represent current sheets or regions where the heating rate is higher than in the surrounding parts of the loop is also an open question at this time. Future observations with the VLA and other multifrequency radio interferometers, together with observations at ultraviolet and X-ray wavelength with the repaired SMM, may provide a more complete description of the magnetic field temperature and density stratification of active region coronal loops.

The author wishes to thank Kenneth R. Lang for useful discussions and an anonymous referee for helpful suggestions. Solar radio interferometric studies at Tufts University are supported under grant AFSOR-83-0019 with the Air Force Office of Scientific Research. Comparisons of VLA and *Solar Maximum Mission* satellite data are supported under NASA Guest Investigator grant NAG 5-501.

REFERENCES

- Dulk, G. A., and Gary, D. E. 1983, *Astr. Ap.*, **124**, 103.
 Foukal, P. 1975, *Solar Phys.*, **43**, 327.
 ———, 1976, *Ap. J.*, **210**, 575.
 Kuznetsov, V. D., and Syrovatskii, S. I. 1981, *Solar Phys.*, **69**, 361.
 Lang, K. R., Willson, R. F., and Gaizauskas, V. 1983, *Ap. J.*, **267**, 455.
 Lang, K. R., Willson, R. F., and Rayrole, J. 1982, *Ap. J.*, **258**, 384.
 McConnell, D., and Kundu, M. R. 1983, *Ap. J.*, **269**, 698.
 Pye, J. P., Evans, K. D., Hutcheon, R. J., Gerassimenko, M., Davis, J. M., Krieger, A. S., and Vesecky, J. F. 1978, *Astr. Ap.*, **65**, 123.
 Raymond, J. C., and Foukal, P. 1982, *Ap. J.*, **253**, 323.
 Rosner, R., Tucker, W. H., and Vaiana, G. S. 1978, *Ap. J.*, **220**, 643.
 Serio, S., Peres, G., Vaiana, G. S., Golub, L., and Rosner, R. 1981, *Ap. J.*, **243**, 288.
 Syrovatskii, S. I., and Kuznetsov, V. D. 1980, in *IAU Symposium 86, Radio Physics of the Sun*, ed. M. R. Kundu and T. E. Gergeley (Dordrecht: Reidel), p. 109.
 Syrovatskii, V. D. 1977, *Astr. Zh. (Letters)*, **3**, 133.
 Velusamy, T., and Kundu, M. R. 1981, *Ap. J. (Letters)*, **243**, L103.
 Vesecky, J. F., Antiochos, S. K., and Underwood, J. H. 1979, *Ap. J.*, **233**, 987.
 Willson, R. F. 1983, *Solar Phys.*, **89**, 103.
 Willson, R. F., and Lang, K. R. 1984, *Ap. J.*, **279**, 427.

ROBERT F. WILLSON: Department of Physics, Tufts University, Medford, MA 02155

17. HIGH-RESOLUTION MICROWAVE OBSERVATIONS OF THE SUN AND NEARBY STARS

Kenneth R. Lang
Department of Physics and Astronomy
Robinson Hall
Tufts University
Medford, MA 02155
U.S.A.

ABSTRACT

Multiple-wavelength VLA observations uniquely specify the three-dimensional structure of the magnetic field and the plasma in the coronal atmosphere above solar active regions. Synthesis maps at 20 cm wavelength specify the density, temperature, and magnetic fields of the ubiquitous coronal loops that are the dominant structural element of the low solar corona; the 6 cm maps delineate the magnetic structure of the legs of coronal loops that radiate at the second or third harmonic of the gyrofrequency. Individual cyclotron lines have been detected at 20 cm wavelength at the apex of a coronal loop where the magnetic field strength is relatively constant and neutral current sheets may lead to enhanced emission from a relatively thin coronal layer. Although thermal bremsstrahlung and/or thermal gyroresonance emission dominate the quiescent microwave emission from solar active regions, some plage-associated microwave sources require nonthermal emission mechanisms in the presence of weak magnetic fields. Intense filament-associated sources might be attributed to the nonthermal gyrosynchrotron emission of subrelativistic electrons.

Snapshot synthesis maps for time intervals as short as ten seconds have led to a new understanding of the excitation and eruption of solar bursts. The impulsive phase of 20 cm bursts is released near the apex of coronal loops located at a height of about 40,000 km above the solar photosphere. Solar bursts are triggered by preburst heating and/or magnetic changes that precede the bursts on time scales of 10 minutes to an hour. The preburst changes can occur within single coronal loops or arcades of coronal loops. Magnetic triggering can also be caused by current sheets that develop during the emergence of coronal loops or the interaction of preexisting coronal loops. Successive bursts can be excited in adjacent coronal loops. Observations of microwave bursts at closely spaced wavelengths provide evidence for narrow-band, highly circularly polarized bursts that may be attributed to gyrosynchrotron masers or electron-cyclotron masers.

Observations of nearby stars with high time resolution provide stringent limits to the size of the stellar bursting sources; highly circularly polarized emitters with very high brightness temperatures suggest coherent emission mechanisms. The slowly varying emission from one nearby flare star also exhibits narrow-band microwave emission characteristic of a coherent mechanism.

I. QUIESCENT (NONFLARING) MICROWAVE EMISSION FROM SOLAR ACTIVE REGIONS

Because the microwave emission from quiescent (non-flaring) active regions varies slowly over time scales of several hours, one may investigate its detailed structure by using the Earth-rotation aperture synthesis technique. When the Very Large Array is used in this way, the rotation of the Earth changes the relative orientation of the array and the radio source; Fourier inversion methods are then used to determine the angular power distribution of the radio source from the array response (visibility functions). Angular resolutions of better than one second of arc are achieved for fields of view that can be as large as the entire solar disk. These angular resolutions exceed those of optical telescopes or existing spacecraft telescopes at X-ray or ultraviolet wavelengths.

Synthesis maps of total intensity, I , describe the two-dimensional distribution of source brightness, whereas synthesis maps of circular polarization, or Stokes parameter V , describe the two-dimensional structure of the magnetic field. The observed radiation from quiescent active regions is circularly polarized in the extraordinary mode of wave propagation, with right-handed circular polarization corresponding to a positive magnetic field directed toward the observer.

The microwave synthesis maps of circular polarization uniquely provide direct measurements of the strength and structure of the magnetic fields in the low corona and the transition region (between the photosphere and the corona). This is not possible with any other technique. When thermal bremsstrahlung is the dominant radiation mechanism, the circular polarization is due to propagation effects in the presence of a magnetic field; the longitudinal magnetic field strength is then inferred from the polarization and the optical depth. When gyroresonant radiation of thermal electrons dominates, the circularly polarized radiation is emitted at the second or third harmonic of the gyrofrequency. One is then able to infer the longitudinal magnetic field strength from the observed frequency.

Single wavelength V.L.A. synthesis maps of quiescent active regions at 20 cm wavelength have been used as coronal magnetograms that specify the strength and structure of the magnetic field in the low solar corona, while also specifying the temperature distribution

along the coronal loops that are the dominant structural element in the low corona. [Lang et al. (1982); McConnell and Kundu (1984); Lang et al. (1983); Lang and Willson (1983); Shevgoankar and Kundu (1984, 1985); Kundu and Lang (1985)]

Our recent Very Large Array observations have revealed three powerful new approaches to the study of these ubiquitous coronal loops. They include multiple wavelength observations that establish the three-dimensional structure of active regions and specify the physical parameters and radiation mechanisms at different levels in the solar atmosphere (following Section I A), observations of cyclotron line emission from individual loops (following Section B), and observations of nonthermal emission in regions of relatively weak magnetic fields (following Section I C).

I A. Quiescent Microwave Emission at Widely Spaced Wavelengths

The quiescent, or nonflaring, radio emission at longer wavelengths originates at higher levels in the atmosphere. This is because the local electron density, N_e , decreases with height, and emission at a given frequency, ν , can arise only from regions where the electron plasma frequency, $\nu_p = 8.9 \times 10^3 N_e^{1/2} \text{ Hz}$ is equal to or lower than ν .

Radiation at longer microwave wavelengths, λ , also originates at higher hotter levels in the solar atmosphere. The brightness temperatures, T_B , are comparable to the local electron temperature, T_e . They range from $T_B \sim 6.5 \times 10^3 \text{ K}$ at $\lambda = 2 \text{ mm}$ in the low chromosphere through 10^5 K at $\lambda = 2 \text{ cm}$ in the chromosphere-corona transition region to 10^6 K at $\lambda = 20 \text{ cm}$ in the low corona.

The heights, h , of the microwave structures can be inferred from their angular displacements from underlying photospheric features. Very Large Array observations indicate that 2 cm emission overlies sunspots at heights $h \sim 5,000 \text{ km}$, and that the 6 cm emission marks the legs of magnetic dipoles at $h \sim 30,000 \text{ km}$ above the photosphere. As illustrated in Figure 1, the 20 cm emission comes from the hot, dense plasma trapped within coronal loops with total extents of about 100,000 km. [Lang and Willson (1983); Lang et al. (1983); Shevgoankar and Kundu (1984); Kundu and Lang (1985)]

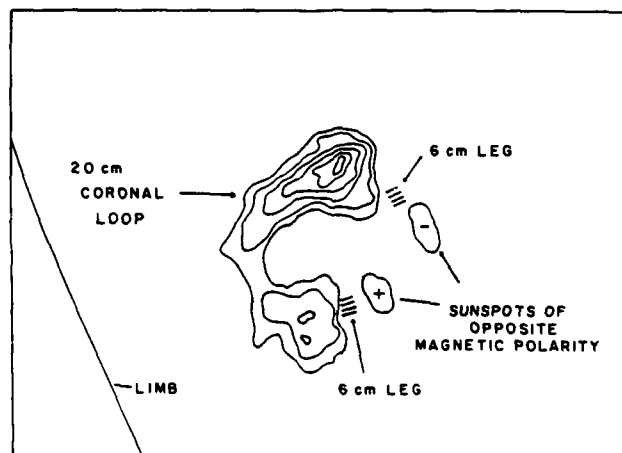


Figure 1. A Very Large Array synthesis map of a coronal loop at 20 centimeters wavelength. The contours mark levels of equal brightness temperature corresponding to 0.2, 0.4,...1.0 times the maximum value of 2.0×10^6 K. A schematic portrayal of the 6 cm microwave emission, which comes from the legs of magnetic dipoles, is also shown, together with the underlying sunspots that are detected at optical wavelengths.

One of the most satisfying observational results at 6 cm wavelength has been the detection of circularly polarized horseshoe structures predicted by the theory of gyroresonant emission from individual sunspots (see figure 2 and Kundu and Lang (1985)). The circular polarization maps at 6 cm reveal highly polarized (up to 100 percent) structures that lie above the curved magnetic fields of sunspot penumbrae. There is no detectable circular polarization above the central sunspot umbrae where the magnetic fields project radially upward into the hot coronal regions. Values of a longitudinal magnetic field strength of $H = 600$ to 900 Gauss are inferred from the fact that the 6 cm radiation is emitted at the second or third harmonic of the gyrofrequency. These magnetic field strengths apply to the legs of coronal loops.

We have also carried out simultaneous observations of solar active regions with Very Large Array (VLA) and the Solar Maximum Mission (SMM) satellite. The VLA observations at 20 cm wavelength can be compared with the soft X-ray polychromator (XRP) data from SMM (see figure 3). Physical parameters such as electron temperature,

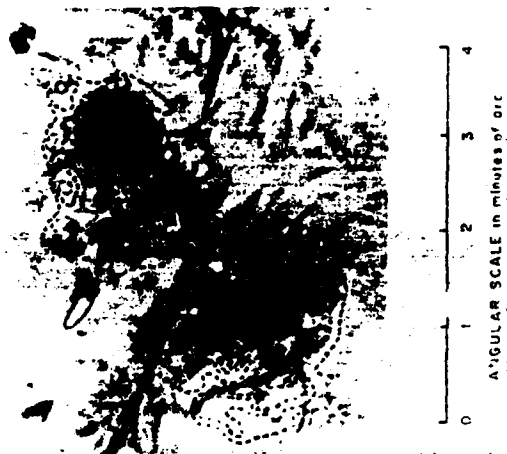


Figure 2. A Westbork Synthesis Radio Telescope synthesis map of circular polarization at 6 cm wavelength superposed on a $H\alpha$ photograph from the observatory at Athens. The contours are in steps of 1.5×10^5 K. The circularly-polarized horseshoe structure that rings the sunspot umbra is due to gyroresonant emission in the curved magnetic fields of the sunspot penumbra.

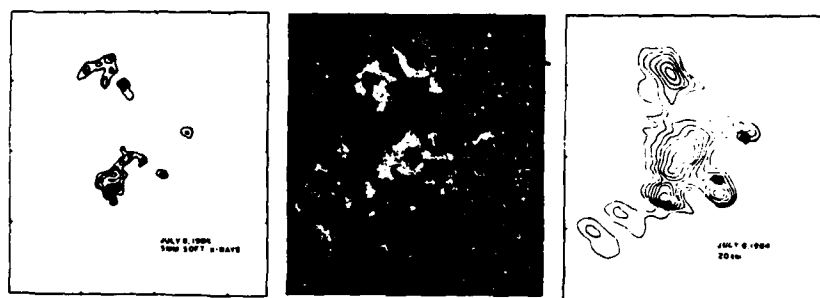


Figure 3. Plots the soft X-ray, $H\alpha$ and 20 cm (right) emission of a solar active region taken on the same day. The most intense radio emission is spatially correlated with the most intense $H\alpha$ and soft X-ray radiation, but there is intense 20 cm emission associated with the sunspots where there is no detectable $H\alpha$ or soft X-ray emission. There is a 60" spacing between fiducial marks on the axes.

T_e , and electron density, N_e , can be independently inferred and compared at two wavelengths. For instance, the intense 20 cm emission from the apex of coronal loops can be interpreted in terms of thermal bremsstrahlung with an electron temperature and emission measure that are consistent with those inferred from bright X-ray sources at the same regions. However, there is intense 20 cm emission above and near sunspots where there is no detectable X-ray emission (see figure 3). The 20 cm emission from these regions requires an extra source of opacity that may be attributed to gyroresonance absorption. Although this effect has been previously noticed at 6 cm, Schmahl et al. (1980), this is the first time that it has been observed at the longer 20 cm wavelength. We also notice the excellent correlation between bright H α plage, intense X-ray emission and intense 20 cm emission over a range of 10^8 in wavelength.

I B. Quiescent Microwave Emission at Closely Spaced Wavelengths

As previously mentioned, the gyroresonant radiation of thermal electrons accelerated by magnetic fields can compete with the bremsstrahlung of thermal electrons accelerated in the electric field of ions. The discovery of circularly polarized ring-shaped or horse-shoe structures above individual sunspots at 6 cm wavelength (see Figure 2) showed that gyroemission dominates the radiation from the legs of magnetic dipoles; these results have played an important role in theoretical models of the quiescent radio emission from solar active regions.

The thermal electrons gyrate around the magnetic fields, emitting cyclotron lines at harmonics of the gyrofrequency. The frequency, ν , of the cyclotron lines therefore provides a sensitive measurement of the longitudinal magnetic field strength, H , through the relation $\nu = 2.8 \times 10^6 n \text{ MHz}$, where the harmonic number $n = 2, 3, 4, \dots$. However, because the magnetic field strength in a coronal loop decreases uniformly with height, it was thought that the individual cyclotron lines would merge to form a smooth continuum.

Theoretical speculations have nevertheless led to two hypothetical situations in which individual cyclotron lines might be observed. The presence of neutral current sheets might lead to enhanced emission from relatively thin coronal layers where the magnetic field

is constant, Syrovatskii and Kuznetsov (1980); Kuznetsov and Syrovatskii (1981); Somov and Syrovatskii (1982). The individual cyclotron lines might then be detected if the region of current sheet emission was resolved and appropriate spectral data were obtained. Alternatively, the thermal cyclotron emission from a dipolar loop might be detected through spatial and polarization structures that are sensitive to both observation frequency and the angle of observation, Holman and Kundu (1985).

Preliminary Very Large Array observations at three closely spaced wavelengths near 21 cm showed significant brightness changes that suggested cyclotron line emission from the apex of a coronal loop where the magnetic field strength is relatively constant. These results were substantiated in greater detail, Willson (1985), when observations at ten closely spaced frequencies revealed the spectral shape of a cyclotron line that could not be attributed to alternative emission mechanisms (see Figure 4). The brightness spectrum was attributed to cyclotron emission from a narrow layer where current sheets resulted in enhanced temperatures in regions of relatively constant magnetic field.

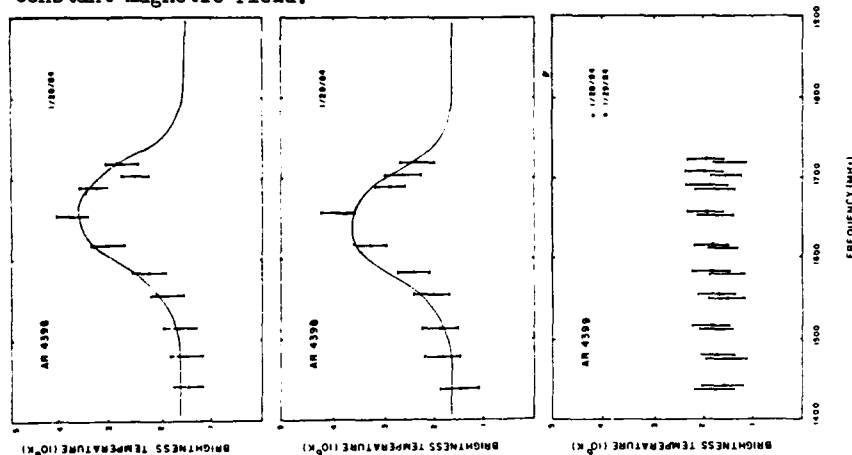


Figure 4. The maximum brightness temperature observed from a coronal loop at ten closely-spaced frequencies near 1446 MHz (20cm) showing a thermal cyclotron line from active region AR 4389 on two successive days, together with optically thick thermal bremsstrahlung spectra from active region AR 4399 on the same days.

The discovery of individual cyclotron lines provides a sensitive new diagnostic tool for specifying the magnetic and plasma properties of coronal loops. For example, a change in the magnetic field strength of only 20 Gauss produces a 170 MHz shift in the central frequency of a cyclotron line near 1420 MHz (or 21 cm wavelength). Measurements of the central frequency therefore specify the magnetic field strength with unprecedented precision.

I C. Thermal and Nonthermal Emission Mechanisms for Quiescent Microwave Emission

The quiescent microwave emission from solar active regions has generally been attributed to thermal radiation from hot electrons, Kundu and Lang (1985). Thermal bremsstrahlung and/or thermal gyroresonance effects dominate both the 6 cm and the 20 cm emission from the legs of coronal loops.

Nonthermal microwave emission has been recently suggested by the detection of high brightness temperatures in regions where the magnetic fields are weak, Webb et al. (1983); Akhmedov et al. (1985) - see figures 5 and 6. Thermal bremsstrahlung cannot account for the radiation because the temperatures are too high and the electron

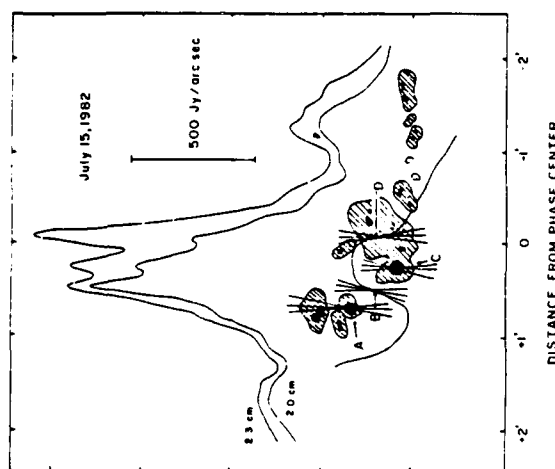


Figure 5. One-dimensional fan beam scans of AR 3084 taken with the RATAN 600 at wavelengths of 2.0 and 2.3 centimeters. Sources A and C are associated with sunspots; sources B and D are associated with filaments.

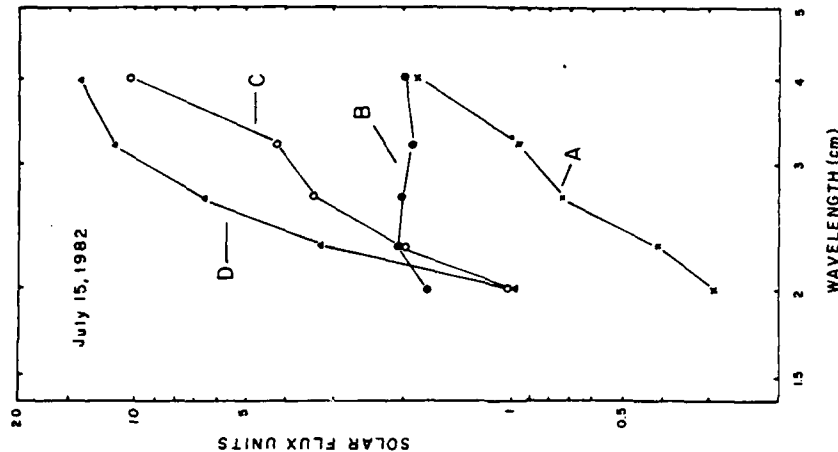


Figure 6. The radiation spectra of the four sources shown in Figure 5. The steep spectrum of the filament-associated source D is attributed to the gyrosynchrotron radiation of mildly relativistic electrons, whereas the flat spectrum of source B is attributed to thermal bremsstrahlung. The sunspot-associated sources A and C are attributed to gyroresonant emission.

densities are too low. Thermal gyroemission is similarly ruled out because the weak magnetic fields require a high harmonic of the gyro-frequency where the optical depth is far too small to account for the high brightness temperatures. The nonthermal radiation might be explained by the gyrosynchrotron emission of subrelativistic electrons, Akhmedov et al. (1985); Chiuderi-Drago and Melozzi (1984); but the acceleration mechanism is difficult to explain because of the short lifetime of the electrons.

II. MICROWAVE BURSTS FROM SOLAR ACTIVE REGIONS

The 27 antennae of the Very Large Array are interconnected electronically to provide a total of 356 interferometer pairs. Signals recorded every three seconds of time therefore provide sufficient data to construct snapshot synthesis maps with angular resolutions of a few seconds of arc without relying on the Earth's rotation to provide variable interferometric baselines. Snapshot maps of total intensity, I , and circular polarization, or Stokes parameter V , can be made at time intervals as short as three seconds. These maps can be used to detect changes in the configuration of coronal magnetic fields and temperature enhancements within coronal loops that are important triggering

agents for solar bursts.

The origin and prediction of these powerful bursts is one of the most important and interesting problems of solar physics. It has long been known that solar eruptions are intimately connected with the magnetic fields in active regions, for the ultimate source of energy for these bursts must be magnetic energy. It has only recently been realized, however, that evolving magnetic fields in the solar corona may play a dominant role in triggering solar eruptions.

Snapshot maps of the impulsive phase of 20 cm bursts indicate, for example, that the microwave energy is released near the apex of coronal loops, while the underlying optical flares occur near the footpoints of these loops. The examples shown in Figure 7 indicate that the 20 cm bursts are displayed by about 40,000 km above the solar photosphere. The loop plasma is impulsively heated at the loop tops where most of the electrons remain trapped, but some high-speed electrons escape to the lower parts of the loop detected at H α wavelengths.

Theoretical considerations indicate that loops emerging into the



Figure 7. Ten second V.L.A. synthesis maps (white contours) of the impulsive phase of two solar bursts at 20 cm wavelength superposed on H α photographs of the optical flares taken at the same time at the Big Bear Solar Observatory. The 20 cm bursts originate near the tops of coronal loops that are about 40,000 kilometers above the flaring region seen at optical wavelengths. The contours mark levels of equal brightness corresponding to 0.2, 0.4, ... 1.0 times the maximum value of 10^8 K. The angular scale can be inferred from the 30" arrows, and the western solar limb is visible on both photographs.

corona, magnetic shear within these loops, and interacting coronal loops can trigger solar bursts and supply their energy, Heyvaerts et al. (1977); Spicer (1977); Hood and Priest (1979); Syrovatski and Kuznetsov (1980); Kuznetsov and Syrovatski (1981); Spicer (1981); Emslie (1982); Somov and Syrovatskii (1982); Priest (1983). Very Large Array solar observations have played a crucial role in demonstrating that many of these theoretical effects actually take place on the Sun, Kundu and Lang (1985). These observations indicate that no single theoretical model is versatile enough to explain the diverse ways in which magnetic energy is dissipated in solar bursts. They nevertheless indicate that preburst changes can be ordered into three major categories - changes within a single coronal loop, the emergence of coronal loops, and interaction between coronal loops, Lang and Willson (1983, 1984); Willson and Lang (1983); Kundu (1984); Kundu and Lang (1985).

Our recent Very Large Array observations have revealed two new approaches to an understanding of the excitation and eruption of solar bursts. They include the observation of preburst heating and magnetic triggering in coronal loops (following Section II A), and the observation of coherent burst mechanisms at closely spaced frequencies (following Section II B).

II A. Prebust Heating and Magnetic Triggering

Interferometric observations at microwave wavelengths first indicated that preburst activity is associated with brightness and polarization changes that precede solar bursts on time scales of tens of minutes; but these observations had inadequate resolution to determine the sources of this activity. The high two-dimensional angular resolution provided by the Very Large Array has recently shown that the intensity or brightness increases are associated with preburst heating in coronal loops, Lang and Willson (1984); Willson (1984) and that the changes in circular polarization are associated with changes in the coronal magnetic field, Lang and Willson (1984); Willson and Lang (1984); Kundu (1984); Kundu and Lang (1985). Both the preburst heating in coronal loops and the changes in coronal magnetic fields may trigger solar eruptions.

There is evidence for sequential triggering of microwave bursts in

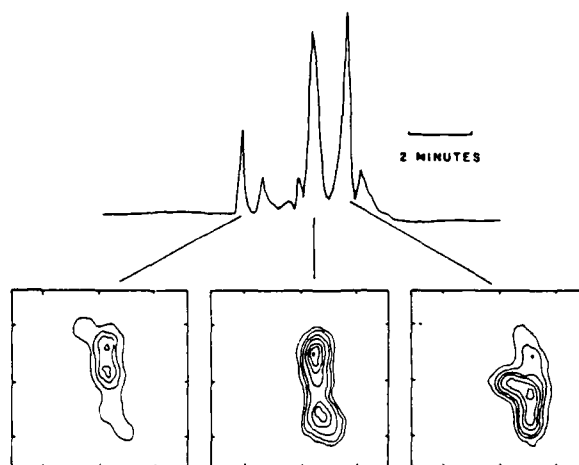


Figure 8. The time profile of successive impulsive bursts at 20 cm wavelength (top) is compared with ten second V.L.A. synthesis maps at the same wavelength (bottom). Here the contour intervals are in steps of 1.0×10^7 K and there is a $30''$ spacing between the fiducial marks on the axis. Although the successive weak bursts were emitted from the same coronal loop or arcade of loops, the successive intense bursts arose from spatially separated loops or arcades of loops.

different loops within magnetically complicated regions. VLA 20 cm maps of total intensity (Figure 8) show that successive intense bursts can originate in adjacent coronal loops, whereas successive weaker bursts are located in the same coronal loop. The 20 cm maps of circular polarization indicate that the feet or legs of the loop-like feature shown in Figure 8 originate in regions of opposite magnetic polarity.

As illustrated in Figure 9, single coronal loops or arcades of loops often begin to heat up and change structure about 15 minutes before the eruption of impulsive bursts. Radio and soft X-ray data have been combined for this example to derive a peak electron temperature of $T_e = 2.5 \times 10^7$ K and an average electron density of $N_e = 10^{10} \text{ cm}^{-3}$ during the heating phase. This heating may be related to the development of current sheets at the apex or tops of coronal loops.

New bipolar loops can also emerge and interact with preexisting ones. When the polarity of the new emerging flux differs from that of the preexisting flux, current sheets are produced that trigger the emission

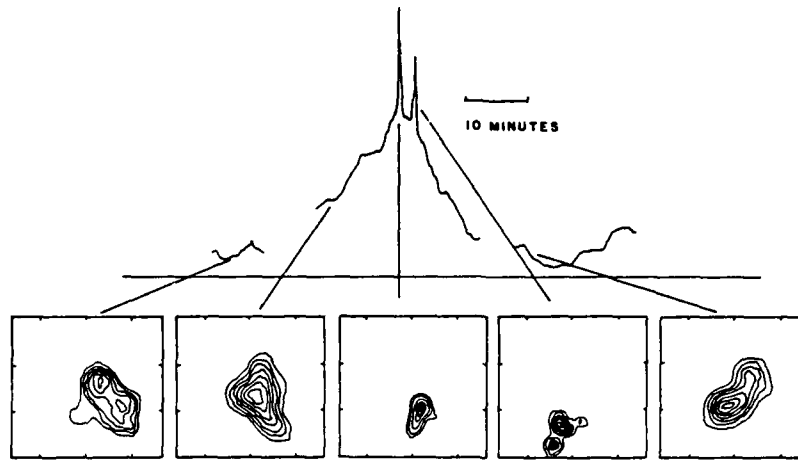


Figure 9. The time profile of a solar burst at 20 centimeters wavelength (top) suggests preburst heating within a coronal loop prior to the emission of two impulsive microwave bursts. The ten second V.L.A. synthesis maps (bottom) suggest that adjacent coronal loops were successively excited or that a coronal loop twisted in space. The outermost contour and contour interval are both equal to 4×10^5 K, and there is a 60" spacing between the fiducial marks on the axes.

of bursts. Two oppositely polarized bipolar loops may also interact and reconnect, Kundu (1984); Kundu and Lang (1985). A current sheet can develop at the interface of the two closed loops, thereby triggering the burst onset.

II B. Burst Emission at Closely Spaced Wavelengths and Coherent Mechanisms

Microwave bursts from the Sun are characterized by compact (angular sizes $\theta \leq 10''$), highly circularly polarized (degrees of circular polarization $P_c \geq 50\%$) sources with high brightness temperatures, T_B , in excess of 10^7 K, Lang and Willson (1984); Willson and Lang (1984). The high brightness temperatures and high degrees of circular polarization have generally been attributed to the gyrosynchrotron radiation of mildly relativistic electrons with energies of 100 to 500 keV (see Kundu and Lang (1985) for a review).

Recently, however, it has been suggested that electron-cyclotron maser emission may play a role in solar microwave bursts, Holman et al. (1980); Melrose and Dulk (1982). Such a coherent emission mechanism

ism has been invoked to explain intense ($T_B \leq 10^{12}$ K), narrow-band, millisecond spikes that have been detected from the Sun at decimeter wavelengths, Droege (1977); Slottje (1978).

The long integration times ($\gamma \geq 10$ seconds), broad bandwidths ($\Delta\nu \geq 50$ MHz), and large beamwidths ($\theta \geq 30''$) of most radio telescopes nevertheless preclude the detection of coherent burst emission. Rapidly varying emission is smoothed by the long time constants, leading to large upper limits to burst duration. This provides unrealistically large upper limits to the source size from the argument that nothing can move faster than the velocity of light. Large upper limits to source size are also constrained by the large antenna beamwidths. As a result, the brightness temperatures of the burst emission may be seriously underestimated. Narrow-band coherent emission is also smoothed in frequency by the large bandwidths.

Although the high angular resolution of the Very Large Array provides the possibility of isolating and perhaps even resolving individual coherent emitters, previous multi-frequency observations have been made over such widely spaced frequencies that the narrow-band features characteristic of coherent emission processes could not be detected. We have recently used the Very Large Array with narrow bandwidths ($\Delta\nu=12.5$ MHz) and closely spaced frequencies (30 MHz) near 1440 MHz (or 20.7 cm) to isolate a coronal loop that exhibited narrow-band burst emission, Lang and Willson (1984); Willson (1985) - see figure 10). The impulsive burst emission was nearly 100% circularly polarized and originated in a loop-like structure 10" or less in angular size. One burst exhibited a factor of two difference in brightness temperature (1.5×10^8 K and 0.8×10^8 K) at two wavelengths separated by only 32 MHz (burst 7 of Figure 10 at 1658 MHz and 1690 MHz). The high circular polarization and narrow bandwidth ($\Delta\nu/\nu \leq 10^{-2}$) of this burst are comparable to those expected from gyrosynchrotron masers, Holman et al. (1980) or electron-cyclotron masers, Melrose and Dulk (1982). Although the burst source was apparently resolved, the 10 second integration time of the VLA may have smoothed or integrated several briefly, spatially-separated coherent spikes.

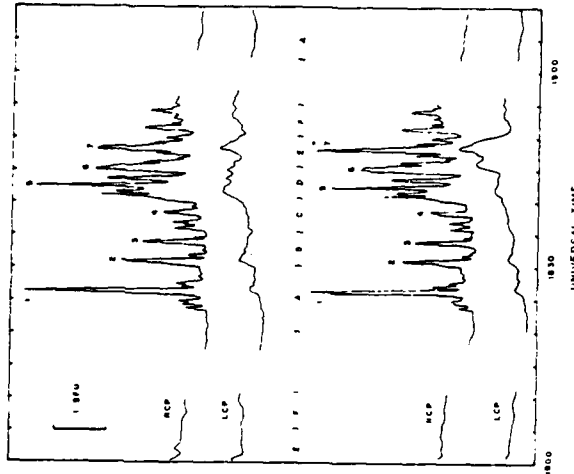


Figure 10. A sequence of right circularly polarized (RCP) impulsive bursts from a solar active region observed at wavelengths near 20 cm. The top and bottom profiles are separated by only 30 MHz; burst 7 has a factor of two difference in brightness temperature over this narrow frequency interval; suggesting coherent burst emission.

III. MICROWAVE EMISSION FROM NEARBY STARS OF LATE SPECTRAL TYPE

Nearby main-sequence stars of late spectral type exhibit a variety of phenomena that are closely related to our understanding of solar active regions including dark spots, activity cycles and bursts at ultraviolet, optical, radio and X-ray wavelengths. These stars also emit quiescent X-ray emission whose absolute luminosity is as much as one hundred times that of the Sun. They may therefore have large-scale coronal loops and intense magnetic fields. The solar analogy suggests that the magnetic fields and coronal plasma of these nearby stars will be detected as slowly varying microwave emission, and that their stellar bursts may exhibit coherent microwave emission similar to that suspected for the Sun.

Nearby dwarf M flare stars do, in fact, exhibit quiescent, or non-flaring microwave emission that is slowly variable with time scales of tens of minutes to hours [Linsky and Gary (1983); Pallavicini, Willson and Lang (1985)]. Brightness temperatures of 10^7 to 10^8 K are inferred if the microwave-emitting source covers the entire visible surface of the star. The detected emission might then be explained as the gyroresonant emission of thermal electrons gyrating in gigantic

coronal loops that exceed the stars in size. Alternatively, the slowly-varying stellar microwave emission might be attributed to the gyrosynchrotron emission of energetic electrons in magnetic fields associated with smaller coronal loops of star spots.

The dwarf M flare stars also exhibit intense, highly circularly polarized microwave bursts that are similar to those emitted by the Sun. Both the high circular polarization and the high brightness temperatures might be explained by electron-cyclotron maser emission, Melrose and Dulk (1982). As discussed in the preceding Section IIB, a similar coherent burst mechanism may have to be invoked to explain microwave bursts from the Sun.

Another class of microwave-emitting stars is the RS CVn binary stars. Their microwave emission is intense, highly variable and often circularly polarized [Mutel and Lestrade (1985); Pallavicini, Willson and Lang (1985).] There is a slowly varying component that varies on time scales of hours and days. Bursts of short duration that are close to 100% circularly polarized have occasionally been observed; speculation about the origin of these bursts have involved electron-cyclotron masers and expanding coronal loops. Very Long Baseline Interferometry (VLBI) has been used to resolve a few of the RS CVn microwave sources, indicating that they are comparable with the binary separation and/or an individual stellar diameter (or smaller) in size, Mutel et al. (1984, 1985).

Observations of the dwarf M star AD Leonis with high time resolution have provided dramatic evidence for coherent burst emission, Lang et al. (1983). A microwave stellar eruption from AD Leonis was composed of highly circularly polarized (100%) spikes with rise times of less than 200 milliseconds. An upper limit to the linear size of the emitting region is 6×10^9 cm, the distance that light travels in 200 milliseconds. If the emitting region is symmetrical, it has an area that is less than 3 percent of the star's surface area, and its brightness temperature exceeds 10^{13} K. The high brightness temperature requires a coherent burst mechanism. Both the high degree of circular polarization and the high brightness temperature may be explained by electron-cyclotron maser emission.

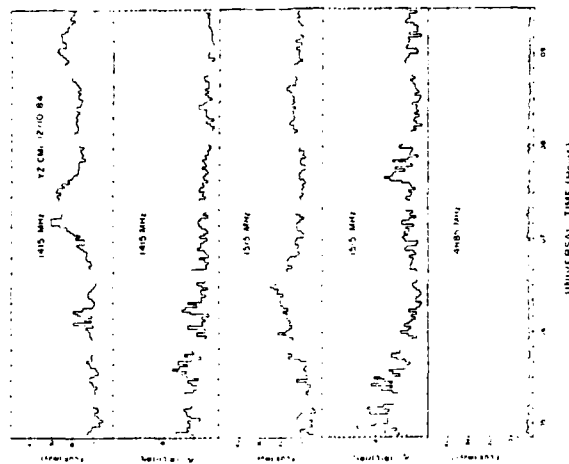


Figure 11. Slowly-varying emission from the dwarf M flare star YZ Canis Minoris at two closely spaced frequencies of 1415 and 1515 MHz and at 4885 MHz. The emission at the two nearby frequencies peaks at different times, suggesting a coherent emission mechanism with a bandwidth of less than 100 MHz. There are no detectable variations at 4885 MHz.

VLA observations of the slowly varying emission from the dwarf M flare star YZ Canis Minoris indicate that its microwave emission peaks at different times at two frequencies near 1420 MHz (21 cm) that are separated by only 100 MHz (Figures 11 and 12). This emission exhibits narrow-band characteristics that are suggestive of coherent emission mechanisms, Lang and Willson (1985). Moreover, the mechanism appears to be confined to the stellar corona, and the intensity is far in excess of that expected from gyroresonance radiation.

IV. CONCLUSIONS

Multiple-wavelength VLA observations of the quiescent microwave emission from solar active regions at widely spaced wavelengths specify the three-dimensional structure of the magnetic field and plasma in the low corona. Gyroresonance effects dominate the 6 cm emission from the legs of magnetic dipoles; whereas thermal radiation from the ubiquitous coronal loops is detected at 20 cm wavelength. Individual cyclotron lines have been detected at the apex of coronal loops, providing sensitive probes of the magnetic field strength. Nonthermal radiation mechanisms are required to explain intense microwave emission with a steep radiation spectrum in regions of relatively weak magnetic

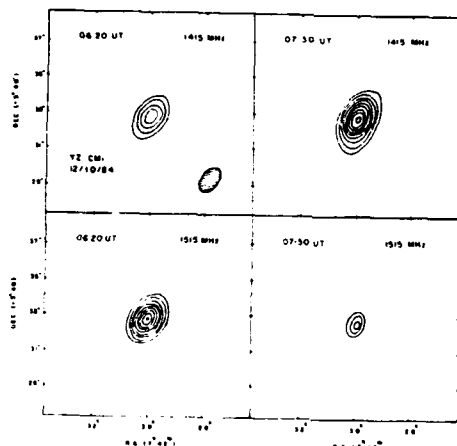


Figure 12. VLA snapshot maps of the emission from the dwarf M flare star YZ Canis Minoris. The unresolved emission peaks at different times at two frequencies separated by only 100 MHz, suggesting a coherent burst mechanism. The contours are at intervals of 4, 8, 12, ... Jy/beam area, with maximum values of 14 and 22 at 0620 UT and 1415 and 1515 MHz, respectively, and 25 and 10 at 0730 for the same respective frequencies.

fields.

Snapshot synthesis maps provide evidence for the excitation of solar bursts by preburst heating within coronal loops or by magnetic triggering due to emerging coronal loops or interacting coronal loops. Narrow band, highly circularly polarized solar bursts require coherent emission mechanisms like gyrosynchrotron masers or electron-cyclotron masers. Coherent mechanisms are also required to explain both stellar bursts and the slowly varying microwave emission from some dwarf M flare stars.

Radio astronomical studies of the Sun and other active stars at Tufts University are supported under Air Force Office of Scientific Research grant AFOSR-83-0019 and by Solar Maximum Mission NASA grant NAG 5-501. Investigations of flare stars at Tufts University are supported by NASA grant NAG 5-477.

REFERENCES

- Akhmedov, Sh.B., Borovik, V.N., Gelfreikh, G.B., Bogod, V.M., Korzhavin, A.N., Petrovo, A.E., Dikij, V.N., Lang, K.R. and Willson, R.F. (1985). The Structure of a Solar Active Region from RATAN 600 and Very Large Array Observations. *Ap. J.* in press.
- Chiuderi-Drago, F. and Melozzi, M. (1984). Non-Thermal Radio Sources in Solar Active Regions. *Astr. Ap.* 131, 103-110.
- Droge, F. (1977). Millisecond Fine Structures of Solar Burst Radiation in the Range 0.2-1.4 GHz. *Astr. Ap.* 57, 285-290.
- Emslie, A.G. (1982). An Interacting Loop Model for Solar Flare Bursts. *Ap. Lett.* 22, 41-47.
- Hayvaerts, J., Priest, E.R. and Rust, D.M. (1977). An Emergin Flux Model for Solar Flare Phenomenon. *Ap. J.* 216, 123-130.
- Holman, G.D., Eichler, D. and Kundu, M.R. (1980). An Interpretation of Solar Flare Microwave Spikes as Gyrosynchrotron Maser. In: *IAU Symp. No. 86: Radiophysics of the Sun*, M.R. Kundu and T. Gergeley (eds.). Reidel, Dordrecht, pp. 457-459.
- Holman, G.D. and Kundu, M.R. (1985). The Microwave Structure of Hot Coronal Loops. *Ap. J.* in press.
- Hood, A.W. and Priest, E.R. (1979). Kink Instability of Solar Coronal Loops as the Cause of Solar Flares. *Solar Ph-s.* 64, 287-301.
- Kundu M.R. (1984). Observational Evidence for Magnetic Reconnection in Microwave Solar Bursts. In: *Proc. IAU Symp. No. 107*. M.R. Kundu and G.D. Holman (eds.). Reidel, Boston, pp. 185-190.
- Kundu, M.R. and Lang, K.R. (1985). The Sun and Nearby Stars: Microwave Observations at High Resolution. *Science* 228, 9-15.
- Kuznetsov, V.D. and Syrovatskii, S.I. (1981). On the Possibility of Observations of Current Sheets in Radio Band. *Solar Phys.* 69, 361-372.
- Lang, K.R., Bookbinder, J., Golub, L. and Davis, M. (1983). Bright, Rapid, Highly Polarized Radio Spikes from the M Dwarf AD Leonis. *Ap. J. (Letters)* 272, L15-L18.
- Lang, K.R. and Willson, R.F. (1983). Multiple Wavelength Observations of Flaring Active Regions. *Adv. Space Res.* 2, No. 11, 91-100.
- Lang, K.R. and Willson, R.F. (1984). Observations of Flare Build Up in Coronal Loops on the Sun and Solar-Type Stars, *Adv. Space Res.* 4, 105.
- Lang, K.R. and Willson, R.F. (1985). Narrow-Band, Slowly Varying Decimetric Radiation from the Dwarf M Star YZ Canis Minoris. *Ap. J. (Letters)* in press.

- Lang, K.R., Willson, R.F. and Gaizauskas, V. (1983). Very Large Array Observations of Solar Active Regions III. Multiple Wavelength Observations. *Ap. J.* 267, 455-464.
- Lang, K.R., Willson, R.F. and Rayrole, J. (1982). Very Large Array Observations of Coronal Loops at 20 cm Wavelength. *Ap. J.* 258, 384-387.
- Linsky, J.L. and Gary, D.E. (1983). Microwave Emission from the Coronae of Late-Type Dwarf Stars. *Ap. J.* 274, 776-783.
- Marsh, K.A. and Hurford, G.J. (1980). Two-Dimensional VLA Maps of Solar Bursts at 15 and 23 GHz with Arcsec Resolution. *Ap. J. (Letters)* 240, L111-L114.
- McConnell, D. and Kundu, M.R. (1983). VLA Observations of a Solar Active Region and Coronal Loops. *Ap. J.* 269, 698-705.
- Melrose, D.B. and Duld, G. (1982). Electron-Cyclotron Masers as the Source of Certain Solar and Stellar Radio Bursts. *Ap. J.* 259, 844-858.
- Melrose, D.B. and Dulk, G.A. (1984). Radio Frequency Heating of the Coronal Plasma During Flares. *Ap. J.* 282, 308-315.
- Mutel, R.L., Doiron, D.J., Lestrade, J.F. and Phillips, R.B. (1984). VLBI Observations of the RS Canium Venaticorum Binary Systems UX Arietis and HR 1099 at 1.69 GHz. *Ap. J.* 278, 220-223.
- Mutel, R.L., Lestrade, J.F., Preston, R.A., and Phillips, R.B. (1985). Dual Polarization VLBI Observations of Stellar Binary Systems at 5 GHz. *Ap. J.* 289, 262-268.
- Pallavicini, R., Willson, R. and Lang, K.R. (1985). Microwave Observations of Late-Type Stars with the Very Large Array. *Astr. Ap.* 149, 95-101.
- Priest, E.R. (1983). Magnetic Theories of Solar Flares. *Solar Phys.* 86, 33-45.
- Schmahl, E.J., Kundu, M.R., Strong, K.T., Bentley, R.D., Smith, J.B. and Krall, K.R. (1982). Active Region Magnetic Fields Inferred from Simultaneous VLA Microwave Maps, X-ray Spectroheliograms and Magnetograms. *Solar Phys.* 80, 233-249.
- Shevgaonkar, R.K. and Kundu, M.R. (1984). Three-Dimensional Structures of Two Solar Active Regions from VLA Observations at 2, 6 and 20 Centimeter Wavelengths. *Ap. J.* 283, 413-420.
- Slottje, C. (1978). Millisecond Microwave Spikes in a Solar Flare. *Nature* 275, 520-521.
- Somov, B.V. and Syrovatskii, S.I. (1982). Thermal Trigger for Solar Flares and Coronal Loops Formation. *Solar Phys.* 75, 237-244.

- Spicer, D.S. (1977). An Unstable Arch Model of a Solar Flare. *Solar Phys.* 53, 305-345.
- Spicer, D.S. (1981). Loop Models of Solar Flares: Revisions and Comparisons. *Solar Phys.* 70, 149-172.
- Syrovatskii, B.V. and Kuznetsov, V.D. (1980). On the Possibility of Radio Observations of Current Sheets on the Sun. In: *Radio Physics of the Sun*. IAU Symp. No. 86. M.R. Kundu and T. Gergely (eds.). Reidel, Dordrecht, 445-455.
- Webb, D.F., Davis, J.M., Kundu, M.R. and Velusamy T. (1983). X-Ray and Microwave Observations of Active Regions. *Solar Phys.* 85, 267-283.
- Willson, R.F. (1985). VLA Observations of Solar Active Regions at Closely Spaced Frequencies: Evidence for Thermal Cyclotron Line Emission. *Ap. J.* in press.
- Willson, R.F. (1985). VLA Observation of Narrow Band Decimetric Burst Emission, *Solar Phys.* in press.
- Willson, R.F. and Lang, K.R. (1983). Very Large Array Observations of Solar Active Regions IV. Structure and Evolution of Radio Bursts from 20 cm Loops. *Ap. J.* 279, 427-437.
- Zheleznyakov, V.V. and Tikhomirov, Yu. V. (1984). Microwave Radiation from Magnetic Stars. *Ap. Space Sci.* 102, 189-209.

18. SOLAR BURST PRECURSORS AND ENERGY BUILD-UP AT MICROWAVE WAVELENGTHS

Kenneth R. Lang and Robert F. Willson

*Department of Physics, Tufts University, Medford, MA 02155,
U.S.A.*

ABSTRACT

We summarize high-resolution microwave observations (VLA) of heating and magnetic triggering in coronal loops. Magnetic changes that precede solar eruptions on time scales of tens of minutes involve primarily emerging coronal loops and the interaction of two or more loops. Thermal cyclotron lines have been detected in coronal loops, suggesting the presence of hot current sheets that enhance emission from relatively thin layers of enhanced temperature and constant magnetic field. These current sheets may play a role in the excitation of solar bursts. A filament-associated source with a high brightness temperature and steep radiation spectrum occurs above a region of apparently weak photospheric field. This source might be attributed to currents that enhance coronal magnetic fields. Compact ($\phi = 5''$) transient sources with lifetimes of 30 to 60 minutes have also been detected in regions of apparently weak photospheric field. We conclude by comparing VLA observations of coronal loops with simultaneous SMM-XRP observations.

MAGNETIC CHANGES AND PREBURST HEATING

The VLA has recently been used to detect changes in the configuration of coronal magnetic fields and temperature enhancements within coronal loops that are important in the excitation of solar bursts. It has long been known that solar eruptions are intimately connected with the magnetic fields in active regions, for the ultimate source of energy for these bursts must be magnetic energy. It has only recently been realized, however, that evolving magnetic fields in the solar corona may play a dominant role in triggering solar eruptions /1/.



Fig. 1. The ten second V.L.A. synthesis maps of the impulsive phase of two solar bursts at 20 cm wavelength superposed on H α photographs of the optical flares taken at the same time at the Big Bear Solar Observatory. The 20 cm bursts originate near the tops of coronal loops that are about 40,000 kilometers above the flaring region seen at optical wavelengths. The western solar limb is visible in both photographs.

Preflare changes in active regions are detected as increases in the intensity and polarization of the microwave emission at centimeter wavelengths. These increases precede solar eruptions on time scales of 10 minutes to an hour. The high angular resolution provided by the Very Large Array (VLA) has shown that these increases are related to preburst heating in coronal loops and to changes in the coronal magnetic field topology /2/. The VLA snapshot maps have also made possible tests of flare models that could not be carried out at optical wavelengths. For instance, the region of microwave energy release occurs at the

apex of coronal loops, while the optical flares occur at the loop footpoints (See Fig. 1). The VLA results indicate that preburst changes can be ordered into three major categories: (I) changes within a single coronal loop, (II) the emergence of coronal loops, and (III) interaction between coronal loops. As illustrated in Figure 2, coronal loops or arcades of loops often begin to heat up and change structure about 15 minutes before the eruption of impulsive bursts. Examples of the other types of magnetic interaction detected by the University of Maryland and Tufts groups are given in the review by Kundu and Lang /2/.

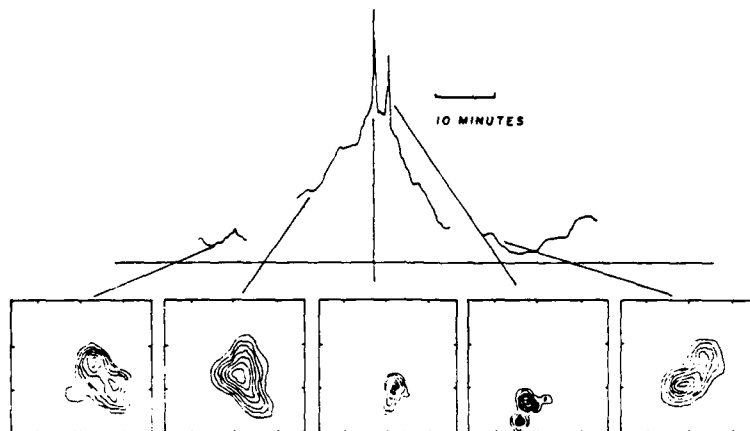


Fig. 2. The time profile of a solar burst at 20 cm wavelength suggests heating within a coronal loop prior to the emission of two impulsive microwave bursts. Radio and X-ray data have been combined to derive a peak electron temperature T_e of 2.5×10^7 K and an average electron density N_e of 10^{10} cm^{-3} during the heating phase. The changing orientation illustrated in the 10 second VLA snapshot maps could be related to the shear of photospheric fields.

THERMAL CYCLOTRON LINES AND EVIDENCE FOR CURRENTS

Theoretical work has shown that individual cyclotron lines might be detected as narrow-band enhancements in the radio-frequency spectra of solar active regions /3/. The spectra of individual cyclotron lines have subsequently been observed at wavelengths near 20 cm when the apex of a coronal loop is resolved /4/ - see Figure 3. This is because the magnetic field strength is relatively constant near the loop apex; the cyclotron lines would merge into a continuum along the loop legs where the magnetic field strength decreases uniformly with height. Neutral current sheets might also play a role, leading to intense radio emission from a thin layer near the loop apex. Both a uniform field and a steep temperature gradient in the uniform region are probably required to detect the cyclotron lines. In any event, observations of individual cyclotron lines indicate magnetic field strengths of $H = 145 \pm 5$ G at the apex of some coronal loops. Observations of individual cyclotron lines provide an unusually accurate method of specifying the coronal magnetic field strength, while also suggesting the presence of currents.

Evidence for current amplification of the coronal magnetic field may be provided by sources of high brightness temperature and steep radiation spectrum above regions of apparently-weak magnetic field /5/. An example is the filament associated source D whose spectrum is shown in Figure 4. If this emission is due to thermal gyroradiation, strong magnetic fields are required to produce gyroradiation at the first few harmonics of the gyrofrequency. Higher harmonics produce insufficient optical depth to account for the high brightness temperatures. The strong magnetic fields could be obtained if currents amplify the magnetic field in the low corona to values greater than those expected from extrapolations from the photosphere. The emission could alternatively be due to nonthermal radiation in weak magnetic fields. Nonthermal synchrotron radiation from mildly relativistic electrons is one possibility, but some as yet unspecified mechanism must be continuously accelerating the electrons.

COMPACT VARIABLE SOURCES

We have recently discovered compact, variable highly-polarized sources in regions of apparently-weak photospheric magnetic field /6/. Our subsequent VLA observations have confirmed the existence of compact, variable 2 cm sources that are not associated with active regions, but these sources had no detectable circular polarization.

The 2 cm maps showed two compact ($\theta = 5''$), highly circularly polarized ($P_c = 80$ to 90%) sources that vary on time scales of 30 to 60 minutes. The left circularly polarized source varied in maximum brightness temperature from $T_B = 2.0 \times 10^5$ K to $T_B < 0.5 \times 10^5$ K.

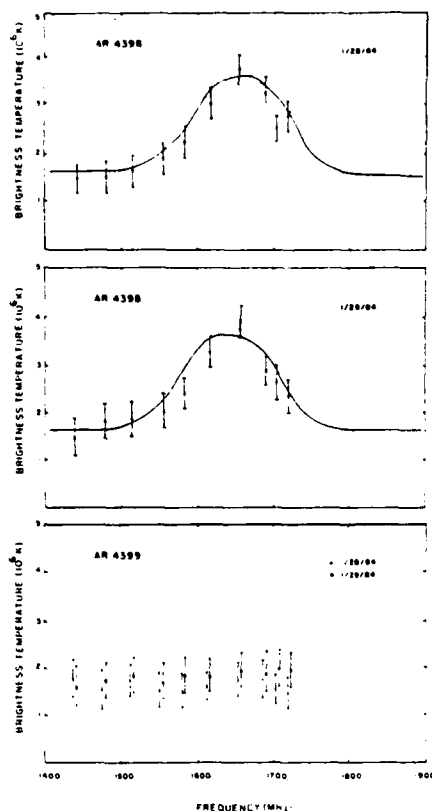


Fig. 3.

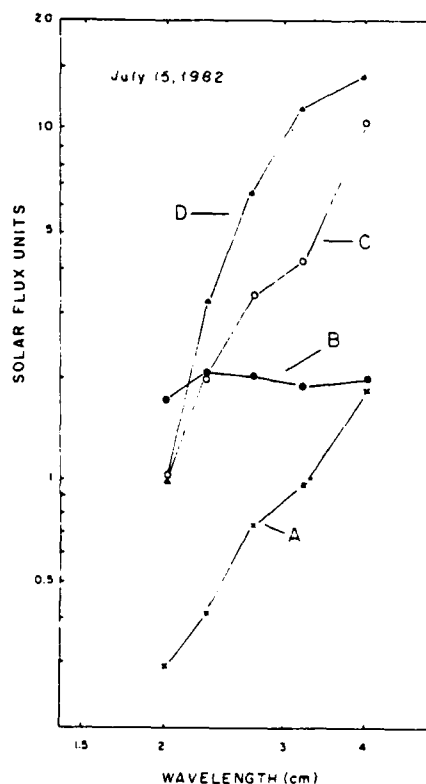


Fig. 4.

Fig. 3. VLA data at ten closely-spaced frequencies near 1440 MHz (20 cm) showing thermal cyclotron line spectra from active region AR 4398 on successive days, together with optically-thick thermal bremsstrahlung spectra from active region AR 4399 on the same days.

Fig. 4. The radiation spectra for the three types of sources usually detected at short centimeter wavelengths. The most common type of source is the sunspot-associated component (A and C) that is attributed to thermal gyroresonance radiation in the legs of coronal loops that are connected to the underlying sunspots. Source D is a filament-associated component located above a magnetic neutral line in regions of apparently-weak magnetic field. It may be due to thermal gyroradiation in current-amplified magnetic fields. The filament-associated source B has the flat spectrum of optically-thin thermal bremsstrahlung.

Comparisons with Mr. Wilson magnetograms indicate that the two compact, variable sources were located in regions of apparently-weak photospheric magnetic field ($H < 80$ G), and that they did not overlie sunspots. The high polarization of these sources is therefore somewhat enigmatic, for the polarization of thermal radiation requires strong magnetic fields of $H = 2,000$ G.

The enigmatic presence of highly polarized sources in regions of apparently-weak photospheric magnetic field may be explained by any one of three hypothesis. First, the photospheric field may have strengths of up to 2,000 G in compact regions that are not readily detected by the photospheric magnetograms. Alternatively, the magnetic field in the transition region or the low corona may be amplified by currents to a strength above that in the underlying photosphere. If either of these hypothesis is true, then the high circular polarization of the 2 cm sources can be attributed to either thermal gyroradiation or the propagation of thermal bremsstrahlung in the presence of a magnetic field of strength $H = 2,000$ G. A third hypothesis is that the compact 2 cm sources are due to non-thermal gyrosynchrotron radiation of mildly relativistic electrons in relatively weak magnetic fields of strength $H = 50$ G.

ONGOING COMPARISONS OF VLA AND SMM-XRP DATA

We are continuing with a comparison of 20 cm coronal loop data (VLA) with soft X-ray data obtained with the SMM satellite. In some instances, there is radiation at 20 centimeters

wavelength near sunspots where no X-ray radiation is detected /7/. In other cases, the 20 centimeter radiation appears at the apex of coronal loops, but with a slightly lower brightness temperature, $T_B = 1.4$ to 1.7×10^6 K, than the electron temperature, $T_e = 3.0 \times 10^6$ K, inferred from the X-ray data. This may be explained by a low temperature plasma with $T_e = 10^5$ K that lowers the effective brightness temperature of the radio bremsstrahlung while not affecting the X-ray data that only detects the 10^6 K plasma /8/.

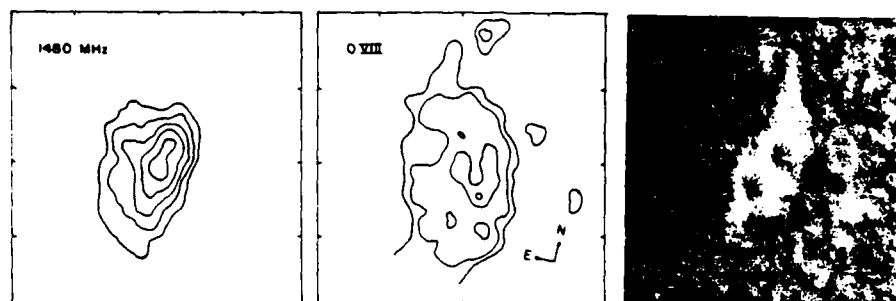


Fig. 5. A comparison of the 20 cm emission (V.L.A.-left), soft X-ray (S.M.M.-middle) and H α (SOON-right) emission of an active region on the same day. The angular spacing between fiducial marks on the axes is 60 arc-seconds.

As illustrated in Figure 5, there are other instances in which the 20-cm radiation and the soft X-ray emission have the same angular extent. In this case, the maximum brightness temperature of the radio emission has the same value as the electron temperature, $T_e = 3 \times 10^6$ K, inferred from the X-ray data. At first sight it would seem that the 20-cm emission is the thermal bremsstrahlung of the X-ray emitting plasma (electron density $N_e = 2 \times 10^{10} \text{ cm}^{-3}$), but in this instance we have also detected a cyclotron line. Preliminary modeling indicates a thin layer of $T_e = 4 \times 10^6$ K with a magnetic field strength of $H = 145$ or 187 G (harmonic $n = 4$ or 3). The thermal electrons that give rise to the X-ray radiation therefore also seem to produce strong gyroresonant radiation at 20 centimeters wavelength.

ACKNOWLEDGEMENTS

Radio astronomical studies of the Sun at Tufts University are supported under grant AFOSR-83-0019 with the Air Force Office of Scientific Research and by contract N00014-86-K-0068 with the Office of Naval Research (ONR). Comparisons of VLA and Solar Maximum Mission satellite data are supported under NASA Guest Investigator grant NAG 5-501.

REFERENCES

1. K.R. Lang and R.F. Willson, V.L.A. observations of flare build-up in coronal loops, Advances in Space Research 4, No. 7, 105 (1984).
2. M.R. Kundu and Kenneth R. Lang, The Sun and nearby stars: microwave observations at high resolution, Science, 228, 9 (1985).
3. V.S. Kuznetsov and S.I. Syrovatskii, On the possibility of observations of current sheets in the radio band, Solar Physics, 69, 361 (1981).
4. R.F. Willson, V.L.A. observations of solar active regions at closely spaced frequencies: evidence for thermal cyclotron line emission, Astrophysical Journal, 298, 911 (1985).
5. S.B. Akmedov, et al., Structure of a solar active region from RATAN 600 and Very Large Array observations, Astrophysical Journal, 301, 460 (1986).
6. R.F. Willson and K.R. Lang, VLA observations of compact, variable sources on the Sun, Astrophysical Journal (1986) - to be published.
7. K.R. Lang, R.F. Willson, K.T. Strong and K.L. Smith, Simultaneous Solar Maximum Mission and Very Large Array observations of solar active regions, Astrophysical Journal (1986) - to be submitted.
8. K.R. Lang, R.F. Willson, K.T. Strong and K.L. Smith, Physical parameters of solar active regions inferred from thermal cyclotron lines and soft X-ray spectral lines, Astrophysical Journal (1986) - to be submitted.

19. RADIO WAVELENGTH OBSERVATIONS OF MAGNETIC FIELDS ON ACTIVE DWARF M, RS CVn AND MAGNETIC STARS

Kenneth R. Lang

Department of Physics, Tufts University, Medford, MA 02155, U.S.A.

ABSTRACT

The dwarf M stars YZ Canis Minoris and AD Leonis exhibit narrow-band, slowly varying (hours) microwave emission that cannot be explained by conventional thermal radiation mechanisms. The dwarf M stars AD Leonis and Wolf 424 emit rapid spikes whose high brightness temperatures similarly require a nonthermal radiation process. We attribute them to coherent mechanisms such as an electron-cyclotron maser or coherent plasma radiation. If the electron-cyclotron maser emits at the second or third harmonic of the gyrofrequency, the coronal magnetic field strength $H = 250$ G or 167 G and constraints on the plasma frequency imply an electron density of $N_e = 6 \times 10^9 \text{ cm}^{-3}$. Coherent plasma radiation requires similar values of electron density but much weaker magnetic fields. Radio spikes from AD Leonis and Wolf 424 have rise times $\tau_r < 5$ ms, indicating a linear size of $L < 1.5 \times 10^8 \text{ cm}$, or less than 0.005 of the stellar radius. Although Ap magnetic stars have strong dipole magnetic fields, they exhibit no detectable gyroresonant radiation, suggesting that these stars do not have hot, dense coronae. The binary RS CVn star UX Arietis exhibits variable emission at 6 cm wavelength on time scales ranging from 30 s to more than one hour. The shortest variation implies a linear size much less than that of the halo observed by VLBI techniques, and most probably sizes smaller than those of the component stars. The observed variations might be due to absorption by a thermal plasma located between the stars.

DWARF M FLARE STARS

The dwarf M flare stars exhibit relatively weak microwave bursts (a few tenths of one Jy) with a rate comparable to that of optically visible flares from the same stars. Quiescent, or nonflaring, microwave emission has also now been detected from several dwarf M stars using the Very Large Array (VLA). These stars exhibit quiescent X-ray emission whose absolute luminosity may be as much as 100 times that of the Sun. Both the microwave and the X-ray emission suggest that dwarf M stars have hot stellar coronae and large-scale coronal loops with strong magnetic fields. In this section we will demonstrate that both the quiescent microwave emission and the microwave bursts from dwarf M stars cannot be attributed to thermal radiation mechanisms. The required non-thermal emission processes can provide stringent constraints on the electron density and magnetic field strength in the stellar coronae.

What accounts for the slowly varying microwave emission from dwarf M stars? The X-ray observations rule out detectable thermal bremsstrahlung at microwave wavelengths; the temperatures and emission measures inferred from the X-ray data indicate that the microwave flux density is at least two orders of magnitude below the detection threshold of the VLA. Thermal electrons gyrating about large-scale magnetic fields might emit detectable gyroresonant, or cyclotron, radiation. The radiation will be emitted in gyroresonant layers that lie outside the visible star at a radius, R , given by the Rayleigh-Jeans law /1/

$$R^2 = 10^{13} \frac{SD^2}{\nu^2} \text{ cm}^2, \quad (1)$$

where S is the source flux density in Jy; D is the distance in cm; T is the temperature in K; and the observing frequency ν , is given by

$$\nu = 2.8 \times 10^6 \text{ nH Hz}$$

(2)

where n is the maximum harmonic for which the stellar corona still remains optically thick.

Gyroresonance radiation of thermal electrons in extensive coronae was once believed to be the most likely explanation for the slowly varying quiescent emission of dwarf M flare stars. Values of R amounting to a few stellar radii were obtained following detection of low flux densities at 6 cm wavelength, and gigantic coronal loops of about three times larger than the visible star were envisaged. However, we have now detected stronger slowly-varying emission at longer wavelengths (20 cm) from YZ Canis Minoris /2/. Substituting the relevant data ($S = 0.02$ Jy, $D = 5.99$ pc = 1.8×10^{19} cm, $\nu = 1.5 \times 10^9$ Hz and $T = 10^6$ K) into equation 1, we obtain $R = 5.4 \times 10^{12}$ cm, which is 200 times larger than the visible star's radius. Strong, large-scale magnetic fields extending out to 200 stellar radii are inconceivable.

Our observations of narrow-band structure from YZ Canis Minoris additionally rule out a thermal radiation mechanism for its slowly-varying microwave emission /2/. Moreover, other observers subsequently found narrow-band structure in hour-long variations from AD Leonis and shorter bursts from UV Ceti /3/. The narrow-band radiation has bandwidth $\Delta\nu < 0.1 \nu$. Continuum emission processes like thermal bremsstrahlung, thermal gyroresonant radiation or gyrosynchrotron radiation will not normally exhibit such spectral features. Coherent radiation processes like electron-cyclotron masers can give rise to the observed narrow-band structure, but before explaining these processes we will provide additional evidence for coherent burst emission from dwarf M stars.

After several hours of observation at the Arecibo Observatory, a stellar eruption was detected from AD Leonis at 20 cm wavelength with a maximum flux density of 30 mJy. The burst was composed of highly left-handed circularly polarized (100%) spikes with rise times of $\tau_R < 200$ ms. An upper limit to the linear size $L < 6 \times 10^9$ cm, and a brightness temperature of $T_B < 10^{13}$ K (symmetric emitter) were inferred from these rise times /4/.

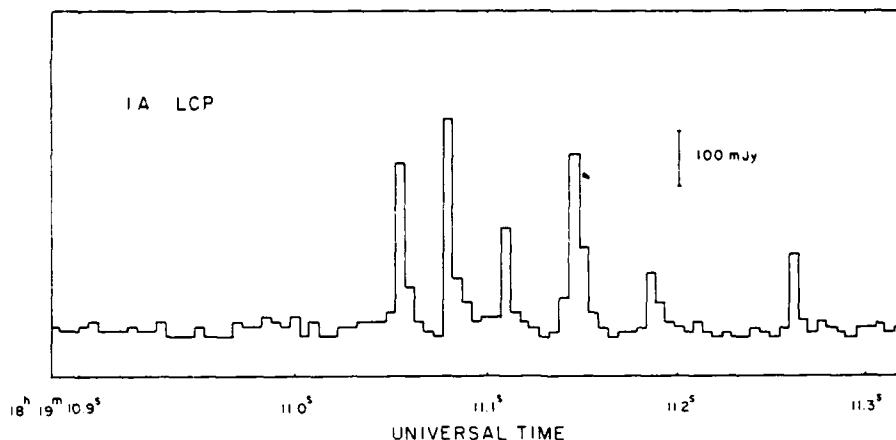


Fig. 1. The total power detected at a frequency of 1415 MHz (21.2 cm) while tracking the dwarf M star AD Leonis. The left-hand circularly polarized (LCP) signal has been displayed with a 5 ms integration time. There are five quasi-periodic spikes with a mean periodicity of $\tau_p = 32 \pm 5$ ms and a total duration of $\tau_t = 150$ ms. Each of these spikes had a rise time of $\tau_R < 5$ ms, leading to an upper limit to the linear size $L < 1.5 \times 10^8$ cm for the spike emitter. A symmetric source of this size would have a brightness temperature of $T_B > 10^{16}$ K, requiring a coherent radiation mechanism.

As illustrated in Figure 1, subsequent Arecibo observations resulted in the detection of quasi-periodic, highly polarized spikes at 20 cm wavelength from AD Leonis /5/. The spikes had rise times of $\tau_R < 5$ ms. An upper limit to the linear size of the spike emitting region is $L < 1.5 \times 10^8$ cm, the distance that light travels in 5 milliseconds. This size is only five hundredths of the estimated radius of AD Leonis. Provided that the emitter is symmetric, it has a brightness temperature greater than 10^{16} K.

We have subsequently detected spikes of shorter rise time $\tau_R = 0.1$ s from AD Leonis that are 100% right- and circularly polarized, as well as spikes from Wolf 424 with rise times $\tau_R < 5$ ms. All of these spikes require high brightness temperatures in excess of 10^{13} K. The high degrees of circular polarization (up to 100%) indicate an intimate connection with the star's magnetic field, and the high brightness temperatures suggest a coherent radiation mechanism such as an electron-cyclotron maser or coherent plasma radiation. The coherent process provides constraints on the electron density, N_e , and the magnetic field strength, H , in the stellar coronae /6/. If the electron-cyclotron maser emits at the second or third harmonic of the gyrofrequency, the longitudinal magnetic field $H = 250$ G or 167 G and constraints on the plasma frequency imply an electron density of $N_e = 6 \times 10^9 \text{ cm}^{-3}$. Although we do not know the harmonic with certainty, the high circular polarization requires a strong magnetic field, and high harmonics provide slow growth and insufficient optical depth. Coherent plasma radiation at the first or second harmonic of the plasma frequency respectively require $N_e = 2 \times 10^{10} \text{ cm}^{-3}$ and $H \ll 500$ G or $N_e = 6 \times 10^9 \text{ cm}^{-3}$ and $H \ll 250$ G.

MAGNETIC STARS

Although we have ruled out thermal gyroresonant radiation from dwarf M stars, such radiation might be detected from the magnetic stars that have large, strong magnetic fields /7/. These stars have magnetic field strengths of a few hundred to a few thousand gauss. The observed field strengths vary in a roughly sinusoidal fashion with periods in the range of 1 to 10 days. Most of these magnetic stars also vary in brightness and have spectral lines that vary in strength; the period of variation is always the same as the magnetic period. The magnetic variations are explained by a dipolar magnetic field that is frozen into the rotating star. As the star rotates, the observer sees different aspects of the magnetic geometry. It is typically dipolar with two magnetic poles of opposite sign and unequal strength.

Detailed calculations indicate that the gyroresonant layers lie fully outside the star and form closed surfaces around it /8/. The degree of circular polarization depends on the angle between the line of sight and the axis of the magnetic dipole. The magnetic field strength can be inferred from the harmonic of the gyrofrequency. As an example, the magnetic stars ϵ Ursae Majoris and α^2 Canum Venaticorum have maximum magnetic field strengths of 960 and 3,500 gauss respectively, and respective distances of 20.0 and 43.5 parsecs. For these parameters and assuming an electron temperature $T_e = 10^7$ K, and electron density $N_e = 10^9 \text{ cm}^{-3}$, the computed flux density for gyroresonant emission at $\nu = 10$ GHz is 0.8 mJy.

We have observed the 11 magnetic stars listed in Table 1 with the VLA for at least one hour each at 6 cm wavelength. No emission was detected from these stars at a 3 sigma level of about 0.2 mJy (see Table). The results indicate that strong surface magnetic fields are not sufficient to produce detectable radio emission. The magnetic Ap stars probably do not have the hot, dense coronae and stellar winds required to produce significant radio luminosity. In contrast, radio emission has been detected from at least two helium-rich, magnetic variable Bp stars with kilogauss photospheric fields (σ Ori E and HR 1890) /8/.

THE RS CVN STAR UX ARIETIS

As illustrated in Figure 2, the binary RS CVn star UX Arietis exhibits variable emission at 6 cm wavelength on time scales ranging from 30 s to more than one hour /8/. In contrast, the flux at 20 cm wavelength had a nearly constant value of about 30 mJy. From the shortest variations of 30 s, we place an upper limit of $L < 9 \times 10^{11} \text{ cm}$ for the size of the emitting region under the assumption that the source cannot move faster than the velocity of light. This size is four times smaller than that of the halo component obtained from 6 cm VLBI observations, but comparable to the upper limit given by VLBI for the core component.

Velocities considerably below the velocity of light are most likely. For example, plausible magnetic field strengths of $H = 10$ -100 gauss and electron densities of $N_e = 10^7$ - 10^8 cm^{-3} , result in an Alfvén velocity of $2 \times 10^8 \text{ cm s}^{-1} < V_A < 7 \times 10^9 \text{ cm s}^{-1}$. This implies a source size of $L = 6 \times 10^9 \text{ cm}$ to $2 \times 10^{11} \text{ cm}$ and a brightness temperature of $T_B > 10^{11} \text{ K}$ to $T_B > 10^{13} \text{ K}$ for the rapid 30 s variations. These sizes are small compared to the separation between the two stars ($L = 1.4 \times 10^{12} \text{ cm}$) and to the sizes of the stars themselves ($L = 1.4 \times 10^{11} \text{ cm}$ and $4.2 \times 10^{11} \text{ cm}$).

A model that might explain the relatively abrupt variations of less than 10-20 minutes is one in which the variable emission is absorbed by a thermal plasma lying between the two stars. High temperature plasma may reside in coronal loops which are comparable in size to the binary system. Absorption of radio emission from one component of UX Arietis by the thermal plasma in coronal loops lying along the line of sight might then explain both the variations at 6 cm and the absence of variations at 20 cm wavelength /9/.

Table 1. Upper limits at the 3 sigma level to the 6 cm flux density, S, of magnetic stars that exhibit no detectable radiation at this wavelength.

STAR	ME	m_V	P (days)	H (gauss)	D (pc)	S (mJy)
α	Andromedae	2.1	0.9636	500	41.6	0.23
γ	Cassiopeiae	4.5	1.7405	1030	47.6	0.35
53	Camelopardi	6.0	8.0278	17000	7.0	0.21
30H	Ursae Majoris	5.0	11.58	1200	25.0	0.20
γ	Virginis	3.0	—	436	9.9	0.15
ϵ	Ursae Majoris	1.8	50.0887	960	20.0	0.25
α^2	Canum Venaticorum	2.9	5.4694	3500	43.5	0.20
γ	Librae	4.5	—	300	43.5	0.20
β	Coronae Borealis	3.7	18.4870	6100	32.3	0.18
χ	Serpentis	5.3	1.5958	1840	33.3	0.20
γ	Equulei	4.7	—	3500	47.6	0.23

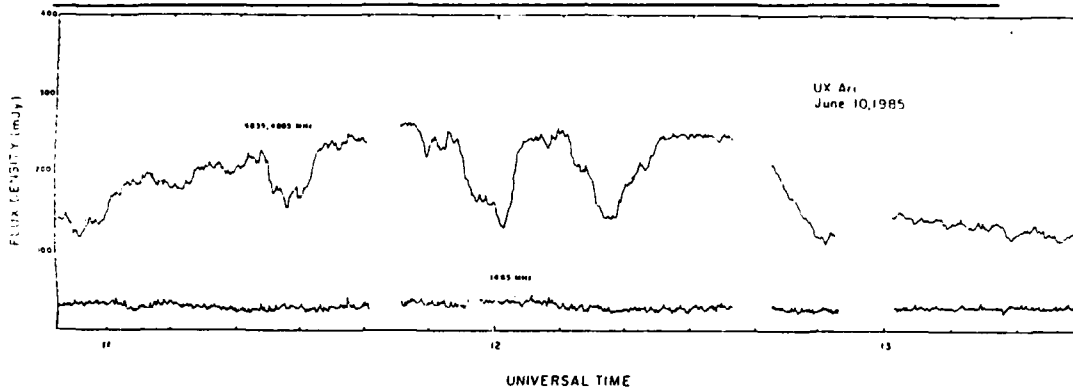


Fig. 2. A plot of the total intensity, I, observed at 1465 MHz, 4835 MHz, and 4885 MHz from the RS CVn star UX Arietis on June 10, 1985. The visibility data were phase shifted to the source center and then vector averaged, baseline by baseline, over a 6.67 s interval to produce these time profiles.

ACKNOWLEDGEMENTS

Radio astronomical studies of the Sun and other active stars at Tufts University are supported under grant AFOSR-83-0019 with the Air Force Office of Scientific Research and by contract N00014-86-K-0068 with the Office of Naval Research (ONR). Investigations of dwarf M flare stars and RS CVn stars at Tufts University are also supported by NASA grant NAG 5-477.

REFERENCES

1. K.R. Lang, *Astrophysical Formulae*, (2d ed., New York, Springer-Verlag, 1986), p. 23.
2. K.R. Lang and R.F. Willson, Narrow-band, slowly-varying decimetric radiation from the dwarf M flare star YZ Canis Minoris, *Astrophysical Journal (Letters)*, 302, L17 (1986).
3. S.M. White, M.R. Kundu and P.D. Jackson, Narrow-band radio flares from red dwarf stars, *Astrophysical Journal*, 305, 363, (1986).
4. K.R. Lang, J. Bookbinder, L. Golub and M. Davis, Bright, rapid, highly polarized radio spikes from the dwarf star AD Leonis, *Astrophysical Journal (Letters)* 272, L15 (1983).
5. K.R. Lang and R.F. Willson, Millisecond radio spikes from the dwarf M flare star AD Leonis, *Astrophysical Journal* (1986) - to be published.
6. G.A. Dulk, Radio emission from the Sun and stars, *Annual Reviews of Astronomy and Astrophysics* 23, 169 (1985).
7. V.V. Zheleznyakov and Yu. V. Tikhomirov, Microwave Radiation from Magnetic Stars, *Astrophysics and Space Science* 102, 189 (1984).
8. S.A. Drake, D.C. Abbott, J.H. Bieging, E. Churchwell, and J.L. Linsky, VLA Observations of A and B Stars with kilogauss magnetic fields, in *Radio Stars*, ed. R.M. Hjellming and D.M. Gibson, D. Reidel, Dordrecht, 1985, p. 247.
9. R.F. Willson and K.R. Lang, Multiple wavelength microwave observations of the RS CVn stars UX Arietis, HR 1099, HR 511C and II Pegasi, *Astrophysical Journal* (1986) - to be published.

20. VLA¹ OBSERVATIONS OF COMPACT, VARIABLE SOURCES ON THE SUN

ROBERT F. WILLSON AND KENNETH R. LANG

Department of Physics and Astronomy, Tufts University

Received 1985 September 24; accepted 1986 February 12

ABSTRACT

Very Large Array (VLA) observations of a solar active region at 2 cm wavelength have revealed a new class of compact, variable sources on the Sun. The compact sources vary on two different time scales of 10–20 s and 30–60 minutes. They are small (angular size $\theta = 5''$), hot (brightness temperatures $T_b = 0.5\text{--}3 \times 10^5$ K), and highly circularly polarized (degrees of circular polarization $\rho_c = 80\%\text{--}90\%$). This emission originates in regions of low magnetic field strength $H \leq 80$ G. The high circular polarization must nevertheless be associated with magnetic fields, and a plausible explanation for the source variability is variations in the magnetic fields on the two time scales. Alternatively, the variability might be attributed to a variable nonthermal electron density, perhaps resulting from a variable acceleration mechanism. The compact sources are attributed to gyrosynchrotron emission from mildly relativistic electrons with a power-law spectrum.

Subject headings: interferometry — polarization — radiation mechanisms — Sun: activity — Sun: radio radiation

1. INTRODUCTION

The radiation mechanisms of quiescent (nonflaring) microwave emission from solar active regions at 6 cm and 20 cm wavelength are now well understood. This emission is attributed to the gyroresonant radiation or the bremsstrahlung of thermal electrons at the legs or apex of coronal loops, or both (Lang, Willson, and Gaizauskas 1983; Lang and Willson 1983; Shevgaonkar and Kundu 1984; Kundu and Lang 1985). In contrast, the quiescent emission of solar active regions at 2 cm wavelength is poorly understood.

There are only two published reports of 2 cm VLA observations of solar active regions (Lang, Willson, and Gaizauskas 1983; Shevgaonkar and Kundu 1984). Both papers report the presence of several (2–6) compact (angular sizes $\theta \leq 15''$), highly polarized (degrees of circular polarization $\rho_c = 80\%\text{--}90\%$) sources at the feet of coronal loops and overlying sunspots. The brightness temperatures ($T_b \approx 10^5$ K) of these compact polarized sources suggests an origin in the transition region, while the high polarization is attributed to intense magnetic fields of strength $H \approx 2000$ G.

The relationship of the compact, highly polarized sources to the magnetic field geometry is controversial. Shevgaonkar and Kundu (1984) report the presence of two compact sources underlying larger 6 cm emission. This suggested that coronal loops diverge as they rise toward their apex, and contradicted loop models that assume a constant cross section (Rosner, Tucker, and Vaiana 1978). In contrast, Lang, Willson, and Gaizauskas (1983) find at least six compact 2 cm sources scattered over an area that is comparable to that of the 6 cm emission. They also notice that the 2 cm sources are not found everywhere over sunspots, suggesting an origin in the low corona rather than the transition region where uniformly strong magnetic fields are expected above umbrae.

Previous VLA observations of compact, highly polarized 2 cm sources were used to make synthesis maps over intervals

of 11–12 hr. These maps revealed long-lasting sources that overlaid sunspots in regions of strong magnetic field. Our recent VLA observations at 2 cm wavelength have been used to make snapshot synthesis maps for time intervals as short as 10 s. These maps indicate the presence of variable compact sources that vary over intervals of ~ 20 s and ~ 30 minutes. The variable sources originate in regions of low magnetic field strength $H \leq 80$ G, but they are highly circularly polarized. These observations are discussed in greater detail in § II. The compact ($\theta \approx 5''$), highly circularly polarized ($\rho_c = 80\%\text{--}90\%$) sources have brightness temperatures $T_b = 0.5\text{--}3 \times 10^5$ K, and they vary in brightness on two different time scales of 10–20 s and 30–60 minutes. In § III we associate the high circular polarization with magnetic fields. Since the sources appear above regions of low magnetic field strength, the high circular polarization and high brightness temperatures cannot be explained by thermal radiation mechanisms. Here we explain the polarization and temperatures in terms of the nonthermal gyrosynchrotron emission from mildly relativistic electrons. The source variability is attributed to varying magnetic fields or a varying nonthermal electron density.

II. OBSERVATIONS

The VLA was used to observe the active region AR 4508 in the C configuration between 1530 and 2330 UT on 1984 June 4. The position of AR 4508 was N06 E57 at 1300 UT on this day. Wavelengths of 2.1 cm and 20.7 cm were used for alternate 15 minute periods, followed by 5 minute observations of the calibration source PKS 0528+134. In all cases, the bandwidth was 12.5 MHz. In the C configuration the synthesized beamwidths are $\sim 1.2''$ and $2''$ at 2.1 and 20.7 cm, respectively. The data were sampled every 10 s and were calibrated using the standard solar calibration procedures at the VLA. These data were then used to make synthesis maps of both the total intensity, I , and circular polarization, V , at each wavelength. These maps were finally CLEANed to produce images having a dynamic range of $\sim 10:1$.

The synthesis maps of total intensity at both wavelengths are shown in Figure 1. The 20.7 cm map was made using the data taken during the entire 8 hr observation period, whereas

¹ The VLA is a facility of the National Radio Astronomy Observatory, which is operated by Associated Universities, Inc., under contract with the National Science Foundation.

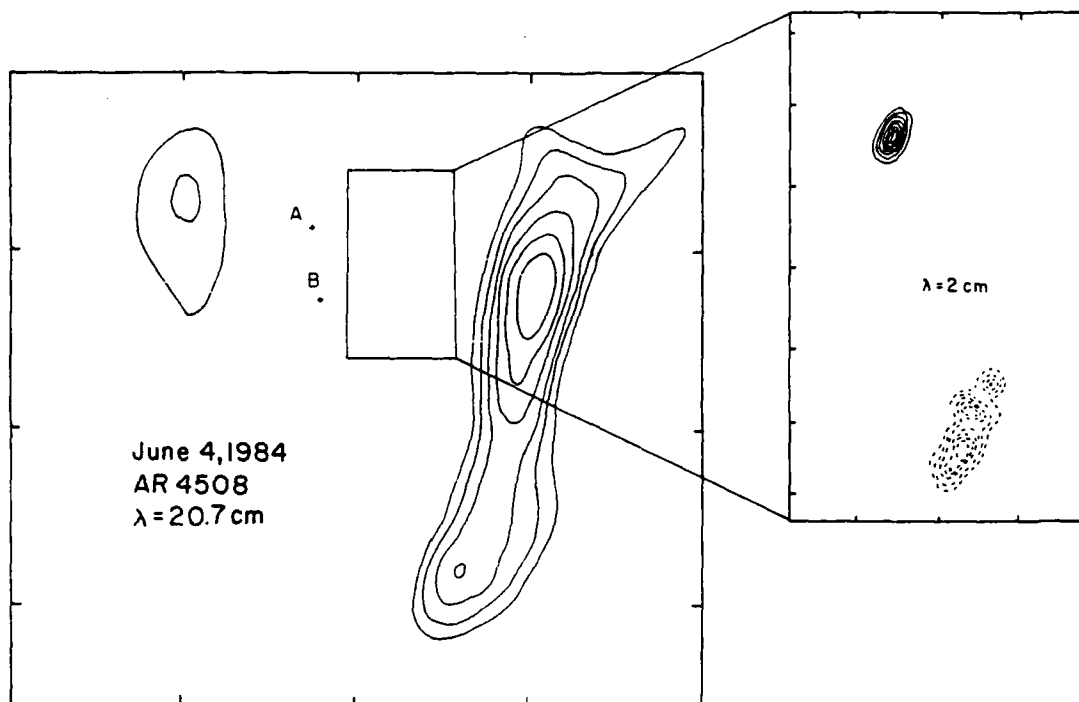


FIG. 1.—VLA synthesis maps of total intensity, I , at 20.7 cm for 8 hr of data and 2.1 cm (box) for 15 minutes of data (also see Fig. 2). The points marked "A" and "B" denote the positions of compact, variable 2 cm sources with lifetimes of 10–20 s (see Fig. 3). All of the compact 2 cm sources lie in regions of weak magnetic fields and do not overlie sunspots. The contours mark levels of equal brightness, and the fiducial marks on the axes are separated by $1''$ at 20 cm and $10''$ at 2 cm. The outermost contour and contour intervals are 4.5×10^5 K and 1.5×10^5 K at 20 cm and 6.1×10^4 K and 3.1×10^4 K at 2 cm.

the 2 cm map refers to a shorter 15 minute interval beginning at 1547 UT. The most intense 20 cm emission is contained within an elongated looplike structure of $\sim 2.5''$ in extent which has a peak brightness temperature of 1.0×10^6 K. There was no detectable 20 cm circular polarization to a limit of 10% or less. A comparison with Kitt Peak and Mount Wilson magnetograms indicates that the extended 20 cm component lies along the magnetic neutral line in the western part of the active region. The weaker component lies $\sim 30''$ to the east of a pair of sunspots.

In contrast, the 2 cm map shows two compact ($\theta \approx 5''$), highly circularly polarized ($p_c = 80\%–90\%$) sources that vary on time scales of 30–60 minutes (Fig. 2). Comparisons with Mount Wilson magnetograms indicate that the two compact, variable sources appeared in regions of weak magnetic field with strengths $H \leq 80$ G, and that they did not overlie sunspots. The left circularly polarized sources (solid contours) varied in brightness temperature from $T_b = 2.0 \times 10^5$ K to $T_b \leq 0.5 \times 10^5$ K, while also moving systematically to the northwest with a total movement of $12''$ in 3 hr, or at a rate of $\sim 0.8 \text{ km s}^{-1}$ ($1'' = 725.3 \text{ km}$ on the Sun). The right circularly polarized source (dashed contours) ranged between 3.0 and 1.0×10^5 K.

Figure 3 shows 30 s snapshot maps of additional 2 cm compact sources with angular sizes $\theta \approx 4''$ and peak brightness temperatures of $T_b = 1.0–3.0 \times 10^5$ K. These sources are denoted by "A" and "B" in Figure 1. They also appeared in regions of weak magnetic field ($H \leq 80$ G) and did not overlie sunspots. An examination of 10 s snapshot maps indicates that sources A and B had respective lifetimes of 10 s and 20 s. The A source appeared at about 165740 UT and was unpolarized,

whereas the B source appeared at 173130 UT and had a dipolar structure. Source B suggests the emergence of a small dipolar loop with a lifetime of 20 s and a temperature characteristic of the transition region.

III. DISCUSSION

The high degree of circular polarization of the compact, transient 2 cm sources is somewhat enigmatic. This polarization cannot be accounted for by propagation effects (thermal bremsstrahlung) or gyroresonant absorption. The compact, transient 2 cm sources are in regions of weak magnetic field ($H \leq 80$ G) and do not overlie sunspots. The circular polarization of these sources cannot be explained by propagation effects of the thermal bremsstrahlung, for magnetic fields of $H \approx 2000$ G are required. Although gyroresonant absorption might account for the circular polarization, the weak magnetic field requires a very high harmonic of the gyrofrequency. The optical depth due to gyroresonant absorption is then negligibly small and the observed brightness temperatures $T_b \approx 10^5$ K cannot be accounted for by a plausible electron temperature. (The electron temperatures would be much too high.)

Conventional thermal radiation mechanisms like bremsstrahlung and gyroresonant, or cyclotron, radiation cannot explain the high circular polarization and high brightness temperature in the presence of weak photospheric magnetic fields. However, nonthermal gyrosynchrotron radiation might explain the observations. This mechanism has been invoked to explain 6 cm sources of high brightness temperature in regions of weak magnetic fields (Webb *et al.* 1983; Chiuderi Drago and Melozzi 1984), as well as a filament-associated source with a

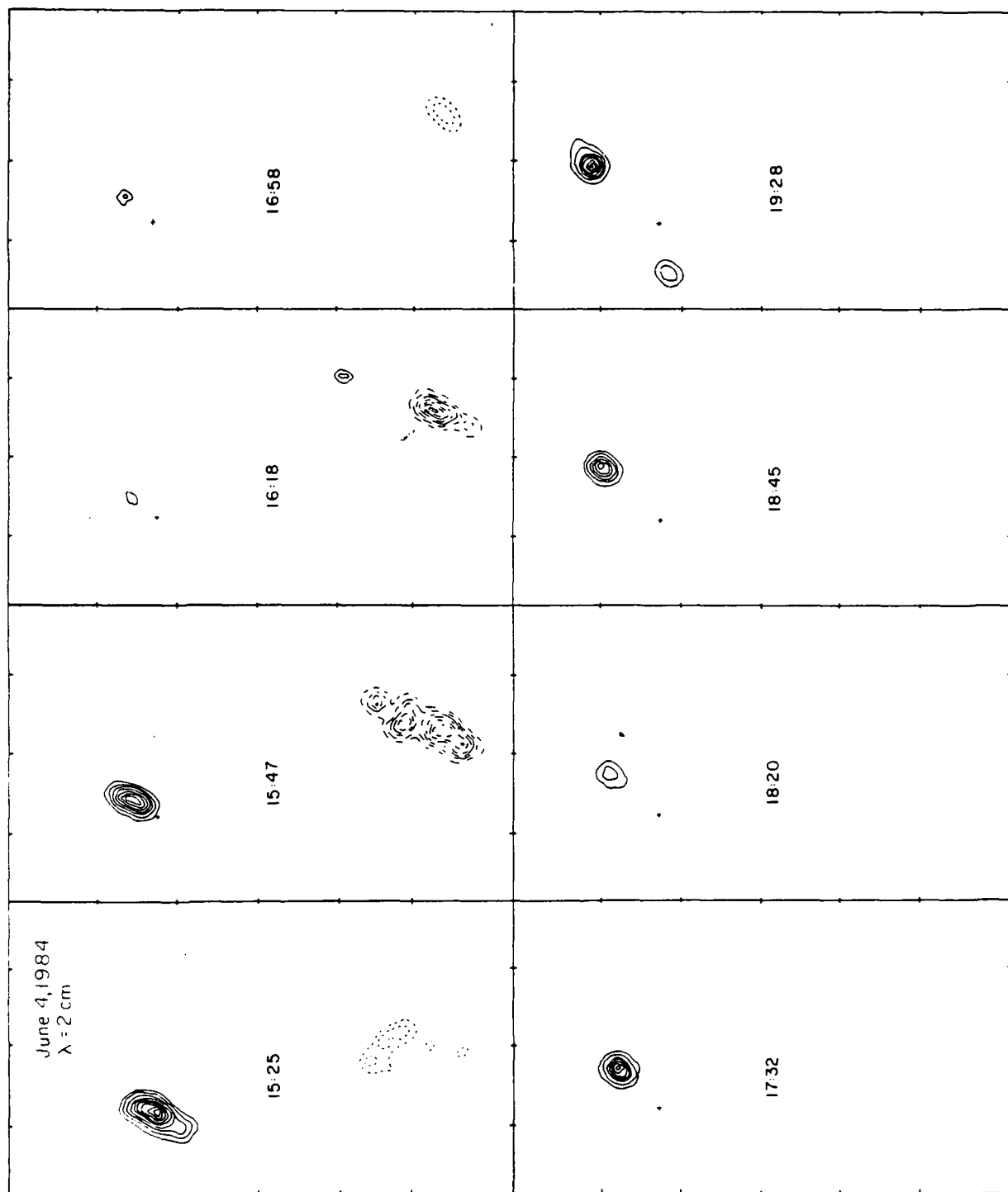


FIG. 2.—VLA synthesis maps of left circularly polarized (solid contours) and right circularly polarized (dashed contours) radiation at 2 cm wavelength. Each map begins at the UT time indicated. The map beginning at 1525 UT is for only 2 minutes of data, those beginning at 1618 and 1732 UT covered a 20 minute interval, and all of the other maps were for 15 minute intervals. The northern (top) source varied over time scales of 30 minutes, the southernmost (bottom) source had a lifetime of ~ 60 minutes, and the complex of sources just above the southernmost source lasted for ~ 30 minutes. Here the contours mark levels of equal brightness with an outermost contour of 6.1×10^4 K and a contour interval of 3.1×10^4 K. The fiducial marks on the axes are separated by $10''$.

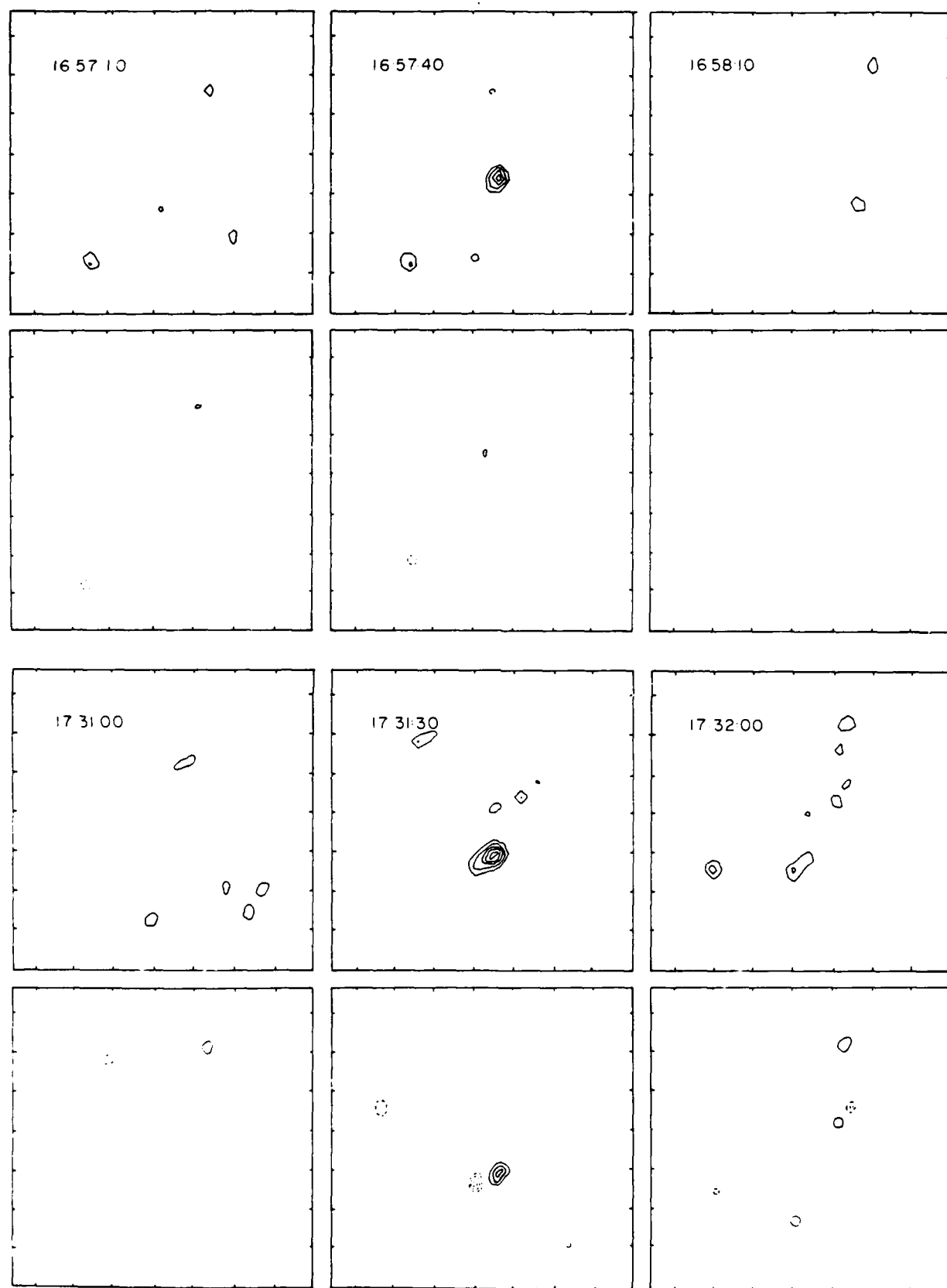


FIG. 3—A series of 30 s snapshot maps of total intensity I (top) and circular polarization V (bottom). The maps reveal the presence of compact sources at 165740 and 173130 UT, respectively denoted by "A" and "B" in Fig. 1. An examination of 10 s snapshot maps indicates that compact sources A and B had respective lifetimes of 10 s and 20 s. Here the contour intervals mark levels of equal brightness temperature, and the fiducial marks on the axes are separated by $10''$. The outermost contour and the contour interval are 6.1×10^4 K and 3.1×10^4 K for the I maps and 1.5×10^4 K for the V maps. The solid and dashed contours of the V maps respectively refer to positive and negative values of V .

high brightness temperature and steep radiation spectrum (Akhmedov *et al.* 1986).

Simplified expressions for the gyrosynchrotron emission from mildly relativistic electrons with both a thermal (Maxwellian) and nonthermal (power-law) energy distribution have been given by Dulk and Marsh (1982). For nonthermal electrons with a power-law energy distribution of index δ , the degree of circular polarization, ρ_c , of the radiation and the effective temperature, T_{eff} , of the radiating electrons are given by

$$\rho_c = 0.20 \times 10^{0.5\delta} 10^{1.93 \cos \theta - 1.16 \cos^2 \theta} (v/v_H)^{-0.21 - 0.37 \sin \theta} \quad (1)$$

and

$$T_{\text{eff}} = 2.2 \times 10^9 10^{-0.31\delta} (\sin \theta)^{-0.36 - 0.06\delta} (v/v_H)^{0.50 + 0.085\delta}, \quad (2)$$

where θ is the angle between the line of sight and the direction of the magnetic field, the observing frequency is v and the gyrofrequency $v_H = 2.8 \times 10^6$ Hz. For an observing frequency of $v = 15.0 \times 10^9$ Hz and a magnetic field strength of $H = 50$ G, we have $v/v_H = 107.1$, and for $\theta = 20^\circ$ – 40° we obtain:

$$\rho_c = 22\% \text{--} 36\%$$

and

$$T_{\text{eff}} = 1.1 \times 10^{10} \text{ K to } 1.5 \times 10^{10} \text{ K}$$

for an energy spectral index of $\delta = 3$.

The high effective temperatures permit brightness temperatures $T_B \approx 10^5$ K under the optically thin conditions (optical depth $\tau \ll 1$) that occur when one is observing at such high harmonics, n , of the gyrofrequency. (For our case, $v = nv_H = 2.8 \times 10^6 n$ Hz so that $n = 107$.) In contrast, the effective temperature of thermal electrons is equal to the kinetic temperature of 10^5 – 10^6 K, and the expected brightness temperatures are very much lower than those observed. For nonthermal electrons of density N_{nt} above some cutoff energy E_0 , we have

$$T_B = \tau T_{\text{eff}} = HLN_{nt} \frac{c^2}{kv^2} \times \left(\frac{\eta_v}{HN_{nt}} \right), \quad (3)$$

where E_0 is assumed to be $E_0 = 10$ keV $= 1.6 \times 10^{-8}$ ergs, and

$$\frac{\eta_v}{HN_{nt}} = 3.3 \times 10^{-24} 10^{-0.52\delta} (\sin \theta)^{-0.43 + 0.65\delta} \times (v/v_H)^{1.22 - 0.90\delta}, \quad (4)$$

If the magnetic field strength $H = 50$ G and the dimension along the line of sight is $L = 10^9$ cm, then a nonthermal electron density of $N_{nt} = 5 \times 10^9 \text{ cm}^{-3}$ give

$$\tau = 8.6 \times 10^{-6} \text{ to } 3.0 \times 10^{-5}$$

and

$$T_B = 1.2 \times 10^5 \text{ K to } 3.3 \times 10^5 \text{ K}.$$

These brightness temperatures are comparable to those observed.

The absence of nonthermal gyrosynchrotron radiation at 20 cm wavelength can be explained by the large optical depth in the overlying corona. With an electron temperature of $T_e = 10^6$ K and an electron density of $N_e = 5 \times 10^9 \text{ cm}^{-3}$, the optical depth due to thermal bremsstrahlung at 20 cm is $\tau = 20$. In this case, the nonthermal gyrosynchrotron radiation would be completely absorbed at 20 cm. Because the optical depth scales as the square of the wavelength, the corona would be optically thin at 2 cm wavelength.

Because the compact 2 cm sources are transient with lifetimes as short as 10 s, continual acceleration of the electrons is not required. The energy loss by synchrotron radiation with a power-law electron energy distribution has a half-life, T , for the total emitted radiation given by

$$T \approx \frac{10^8}{H^2} \text{ s}. \quad (5)$$

A magnetic field of strength $H = 50$ G, gives $T \approx 4 \times 10^4$ s or ~ 11 hr. But how are the electrons initially accelerated? Spicer (1979) and Shoub (1983) showed that large electric fields can be produced in the transition region as a result of the steep temperature gradient there. One possibility is that the electric fields become unstable and generate numerous nonthermal electrons. Spicer's calculations indicate that the number density of nonthermal electrons is $N_{nt} = 5 \times 10^6 \text{ cm}^{-3}$ for a thermal electron density of $N_e = 3 \times 10^9 \text{ cm}^{-3}$. This is consistent with the number of nonthermal electrons required to account for the compact, transient 2 cm sources.

But what causes the variability of the observed emission? According to equation (3), the observed brightness temperature decreases with decreasing magnetic field strength and decreasing nonthermal electron density. We have observed an apparent emergence and disappearance of a dipolar magnetic field in one case. A plausible explanation for the source variability is therefore variations in the magnetic fields. Alternatively, the variability might be attributed to a variable nonthermal electron density, perhaps resulting from a variable acceleration mechanism.

Yet another possibility is that currents amplify the magnetic fields, leading to magnetic field strengths of $H \approx 2000$ G in the transition region that are apparently not observed by photospheric magnetograms.

Radio astronomical studies of the Sun at Tufts University are supported under grant AFOSR-83-0019 with the Air Force Office of Scientific Research (AFOSR) and contract N0014-86-K-0068 with the Office of Naval Research (ONR). Comparisons of VLA and *Solar Maximum Mission* (SMM) data are supported by our NASA-SMM Guest Investigator grant NAG 5-501.

REFERENCES

- Akhmedov, Sh. B., *et al.* 1986, *Ap. J.*, **301**, 760.
 Chiuderi Drago, F., and Mellozzi, M. 1984, *Astr. Ap.*, **131**, 103.
 Dulk, G. A., and Marsh, K. A. 1982, *Ap. J.*, **259**, 350.
 Kundu, M. R., and Lang, K. R. 1985, *Science*, **228**, 9.
 Lang, K. R., and Willson, R. F. 1983, *Adv. Space Res.*, Vol. 2, No. 11, ed. Z. Svestka, D. M. Rust, and M. Dryer (Oxford: Pergamon), p. 91.
 Lang, K. R., Willson, R. F., and Gaizauskas, V. 1983, *Ap. J.*, **267**, 455.
 Rosner, R., Tucker, W. H., and Vaiana, G. S. 1978, *Ap. J.*, **283**, 413.
 Shevgaonkar, R. K., and Kundu, M. R. 1984, *Ap. J.*, **283**, 413.
 Shoub, E. C. 1983, *Ap. J.*, **266**, 339.
 Spicer, D. S. 1979, *Solar Phys.*, **62**, 295.
 Webb, D. F., Davis, J. M., Kundu, M. R., and Velusamy, T. 1983, *Solar Phys.*, **85**, 267.

KENNETH R. LANG and ROBERT F. WILLSON: Department of Physics and Astronomy, Robinson Hall, Tufts University, Medford, MA 02155

21. FLARE STARS AND SOLAR BURSTS: HIGH RESOLUTION IN TIME AND FREQUENCY*

KENNETH R. LANG

Department of Physics and Astronomy, Tufts University, Medford, MA 02155, U.S.A.

Abstract. Coronal loops on the Sun and nearby stars are investigated using observations at 20 cm wavelength with high resolution in time and frequency. Observations of the dwarf M star AD Leonis with high time resolution using the Arecibo Observatory have resulted in the discovery of a quasi-periodic train of circularly polarized spikes with a mean periodicity of 32 ± 5 ms and a total duration of 150 ms. The individual spikes had rise times of ≤ 5 ms, leading to an upper limit to the linear size $L \leq 1.5 \times 10^8$ cm for the spike emitter. This size is only 0.005 of the estimated radius of AD Leonis. Provided that the emitter is symmetric, it has a brightness temperature of $T_B \geq 10^{16}$ K, suggesting a coherent burst mechanism such as an electron-cyclotron maser. Coronal oscillations might modulate the maser output, producing the quasi-periodic spikes. Observations at closely spaced wavelengths, or high frequency resolution, using the Very Large Array have revealed narrow-band structure ($\Delta\nu/\nu \leq 0.01$) in solar bursts and in the slowly-varying radiation of the dwarf M star YZ Canis Minoris. The narrow-band emission cannot be explained by continuum emission processes, but it might be attributed to electron-cyclotron maser radiation. Maser action at the second or first harmonic of the gyrofrequency implies magnetic field strengths of 250 and 500 G, respectively. Thus, observations with high resolution in time and frequency suggest coherent processes in the coronae of the Sun and dwarf M stars. The scientific potential of these discoveries may be best fulfilled by the construction of a solar-stellar synthesis radiotelescope.

1. Introduction

Very Large Array (VLA) observations at widely spaced wavelengths refer to different levels within the ubiquitous coronal loops that are the dominant structural element of solar active regions. The slowly-varying 6 cm emission often originates in the legs of coronal loops, while the slowly-varying 20 cm emission comes from the hot dense plasma trapped within the legs and apex of coronal loops (Lang *et al.*, 1982; Lang and Willson, 1983, 1984; Lang *et al.*, 1983; McConnell and Kundu, 1983; Kundu and Lang, 1985). VLA snapshot maps indicate that the impulsive component of microwave bursts is usually located near the apex of coronal loops (Marsh and Hurford, 1981; Lang and Willson, 1983, 1984; Willson and Lang, 1984; Kundu and Lang, 1985). These bursts may be triggered by temperature enhancements within coronal loops or by changes in the configuration of coronal magnetic fields.

The solar analogy suggests that coronal loops may also play a dominant role in the microwave emission from dwarf M flare stars. These stars exhibit slowly-varying microwave radiation that may be similar to the quiescent, or nonflaring, slowly-varying radiation of solar active regions. These stars also exhibit microwave bursts that are similar to those emitted by the Sun (Linsky and Gary, 1983; Pallavicini *et al.*, 1985).

Recent investigations have revealed two new approaches to the study of coronal loops on the Sun and nearby stars. They involve observations at 20 cm wavelength with high

* Proceedings of the Workshop on Radio Continua during Solar flares, held at Duino (Trieste), Italy, 27-31 May, 1985.

resolution in time and frequency. Observations with high time resolution using the Arecibo Observatory have led to the discovery of quasi-periodic spiked emission from the dwarf M star AD Leonis (Section 2). Observations at closely spaced wavelengths, or high frequency resolution, reveal narrow-band structure during solar bursts and in the slowly-varying radiation of the dwarf M star YZ Canis Minoris (Section 3). This paper highlights these recent results that seem to require coherent radiation mechanisms. It also draws attention to their possible implications for a solar-stellar synthesis radiotelescope.

2. Quasi-Periodic Spikes from AD Leonis

If the solar analogy is applicable, slowly-varying emission and stellar bursts from nearby stars ought to be emitted from coronal loops that are a fraction of a stellar radius in linear extent. Thermal bremsstrahlung from coronal loops on nearby stars would, however, be too weak to be detected, and thermal gyroresonant radiation would require impossibly large coronal loops for this radiation to be detected at 20 cm wavelength.

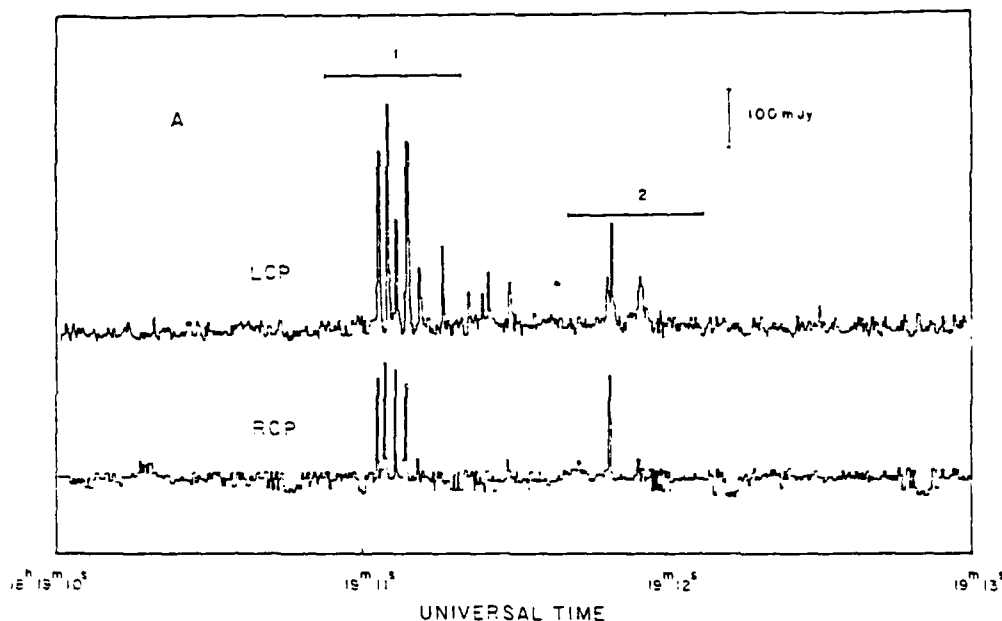


Fig. 1. The total power detected at a frequency of 1415 MHz (21.2 cm) while tracking the dwarf M star AD Leonis. Both the left-hand circularly polarized (LCP-top) and the right-hand circularly polarized (RCP-bottom) signals are shown. Here the integration time is 5 ms. The data exhibit a train of five quasi-periodic spikes with a mean periodicity of $\tau_p = 32 \pm 5$ ms, a total duration of $\tau_D = 150$ ms (horizontal bar 1), and circular polarizations of about 33%. The data also include individual spikes that are 100% left-hand circularly polarized. Each of the spikes had a rise time of $\tau_r \leq 5$ ms, leading to an upper limit to the linear size $L \leq 1.5 \times 10^8$ cm and a brightness temperature of $T_B \geq 10^{16}$ K if the spike emitter is symmetric.

Non-thermal and/or coherent emission processes are required if the slowly-varying or burst emission originates from stellar loops or star spots that are similar in size to their counterparts on the Sun.

As illustrated in Figure 1, observations of AD Leonis at 1415 MHz (21.2 cm) indicate a train of quasi-periodic spikes that suggest a coherent burst emitter that is modulated by coronal oscillations. The quasi-periodic spikes have a mean periodicity of 32 ± 5 ms and a total duration of 150 ms. They have a maximum flux density of 300 mJy and circular polarizations of about 33%. Each of the spikes have rise times of ≤ 5 ms, the integration time employed.

An upper limit to the linear size of the emitting region is $L \leq 1.5 \times 10^8$ cm, the distance that light travels in 5 ms. This is only 0.005 of the estimated radius of AD Leonis ($R = 3.0 \times 10^{10}$ cm). Provided that the spike emitter is symmetric, it has an area that is less than 2.5×10^{-5} of the surface area of the star's visible disk. The maximum flux density and linear size can be combined with the star's distance (4.85 pc) to infer a brightness temperature of $T_b \geq 10^{16}$ K from the Rayleigh-Jeans expression.

The high circular polarization of the spikes indicates an intimate connection with strong stellar magnetic fields, whereas the high brightness temperatures suggest a coherent emission mechanism. Similar highly circularly polarized spikes with high brightness temperatures ($T_b \geq 10^{12}$ K) have been observed during solar bursts (Dröge, 1977; Slottje, 1978). The spikes emitted from both the Sun and AD Leonis may be explained by electron-cyclotron maser emission (Melrose and Dulk, 1982). Magnetic field strengths of $H = 250$ and 500 G are inferred if the radiation is at the second or first harmonic of the gyrofrequency, respectively.

But what accounts for the quasi-periodic spikes? Some process must modulate the coherent burst emitter in a quasi-periodic manner. One possibility is coronal oscillations that provide a currently-popular explanation for longer (50 ms to 5 s) quasi-periodic pulsations during some solar bursts (Roberts *et al.*, 1984). An inhomogeneity of size $a = 2 \times 10^7$ cm might account for the quasi-periodic spikes with an Alfvén velocity corresponding to $H = 250$ G and plausible values of density.

3. Narrow-Band Structure in Solar Bursts and in the Slowly-Varying Radiation from YZ Canis Minoris

Recent VLA observations at closely spaced wavelengths near 20 cm have provided evidence for coherent emission processes during solar bursts (Lang and Willson, 1984). One highly circularly polarized (100%) burst exhibited a factor of two difference in brightness temperature (1.5×10^8 K and 0.8×10^8 K) at two wavelengths separated by only 32 MHz (burst 7 of Figure 2 at 1658 and 1690 MHz). The high circular polarization and narrow bandwidth ($\Delta\nu/\nu \leq 0.01$) of this burst are comparable to those expected from electron-cyclotron masers. Although the burst source was apparently resolved, the 10 s integration time of the VLA may have integrated several briefer, spatially-separated coherent spikes.

Narrow-band, slowly-varying microwave radiation has been detected from the dwarf

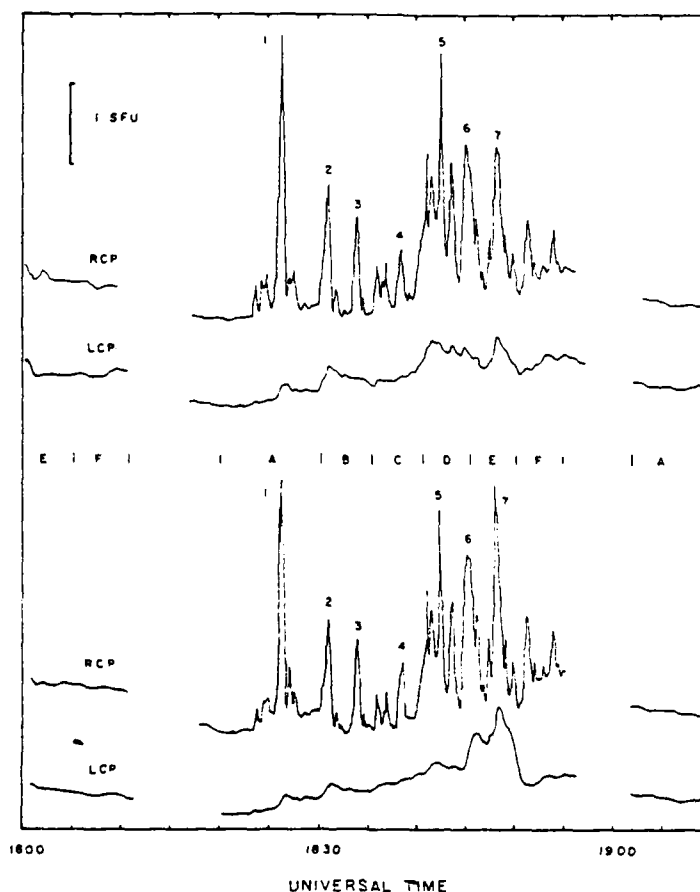


Fig. 2. A sequence of right circularly polarized (RCP) impulsive bursts from a solar active region observed at wavelengths near 20 cm (1400 MHz). The top and bottom profiles are separated by only 30 MHz; burst 7 has a factor of two difference in brightness temperature over this narrow frequency interval, suggesting coherent burst emission. This figure originally appeared in Lang and Willson (1984).

M star YZ Canis Minoris at frequencies near 1465 MHz. Slow variations over time-scales of an hour and as much as 20 mJy in strength peak at different times for frequencies $\nu = 1415$ and 1515 MHz (Figures 3 and 4), indicating narrow-band structure of bandwidth $\Delta\nu \leq 100$ MHz, or $\Delta\nu/\nu \leq 0.1$. Cyclotron line structure from gyroresonant radiation can be ruled out because the high flux density and large observing frequency would require coronal loops that are more than one hundred times larger than the star.

We might speculate that the slowly-varying radiation from YZ Canis Minoris is due to continuous low-level, coherent burst activity. High circular polarization would be expected to be occasionally observed if the coherent mechanism is associated with

FLARE STARS AND SOLAR BURSTS

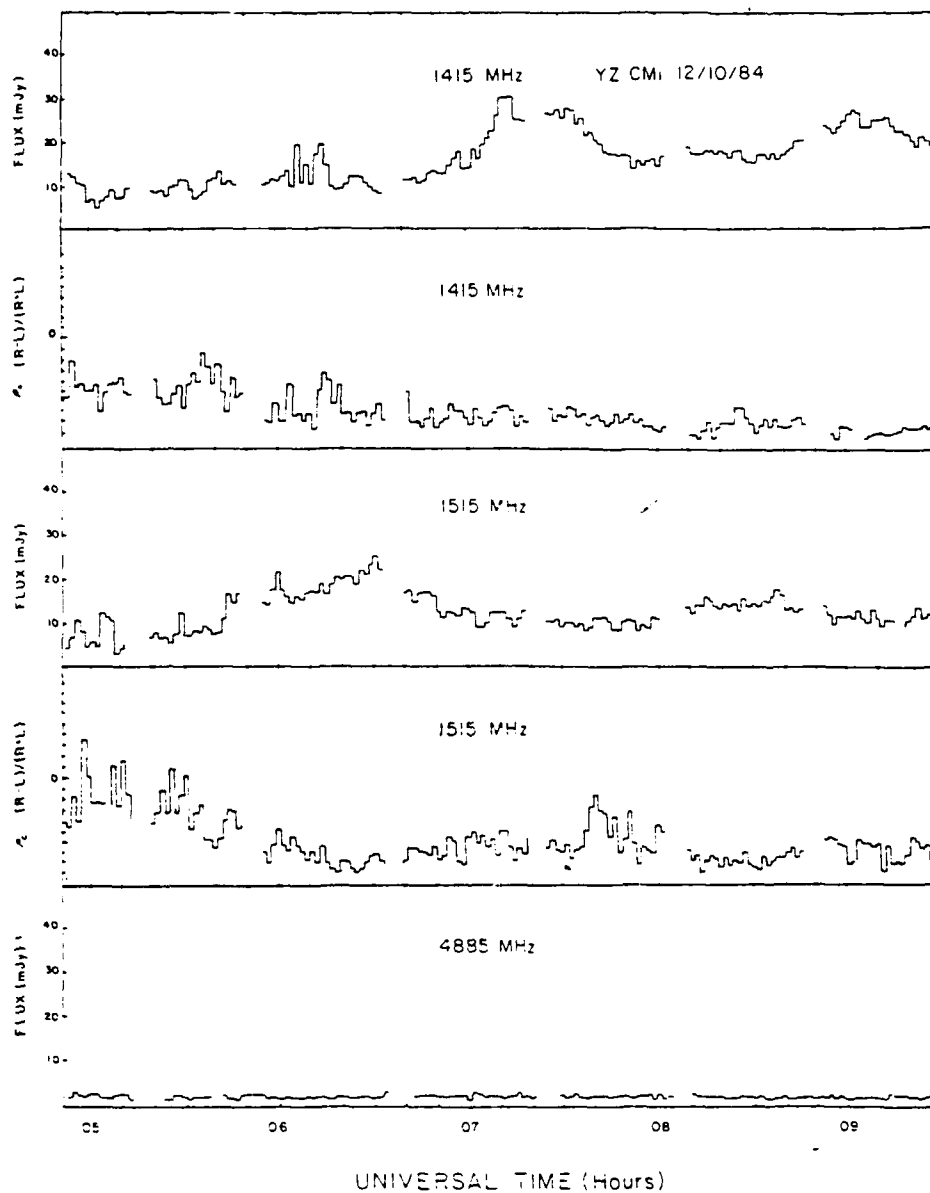


Fig. 3. Slowly-varying emission from the dwarf M flare star YZ Canis Minoris at two closely spaced frequencies of 1415 and 1515 MHz and at 4885 MHz. The emission at the two frequencies peaks at different times, suggesting a coherent emission mechanism with a bandwidth of less than 100 MHz. There are no detectable fluctuations at 4885 MHz.

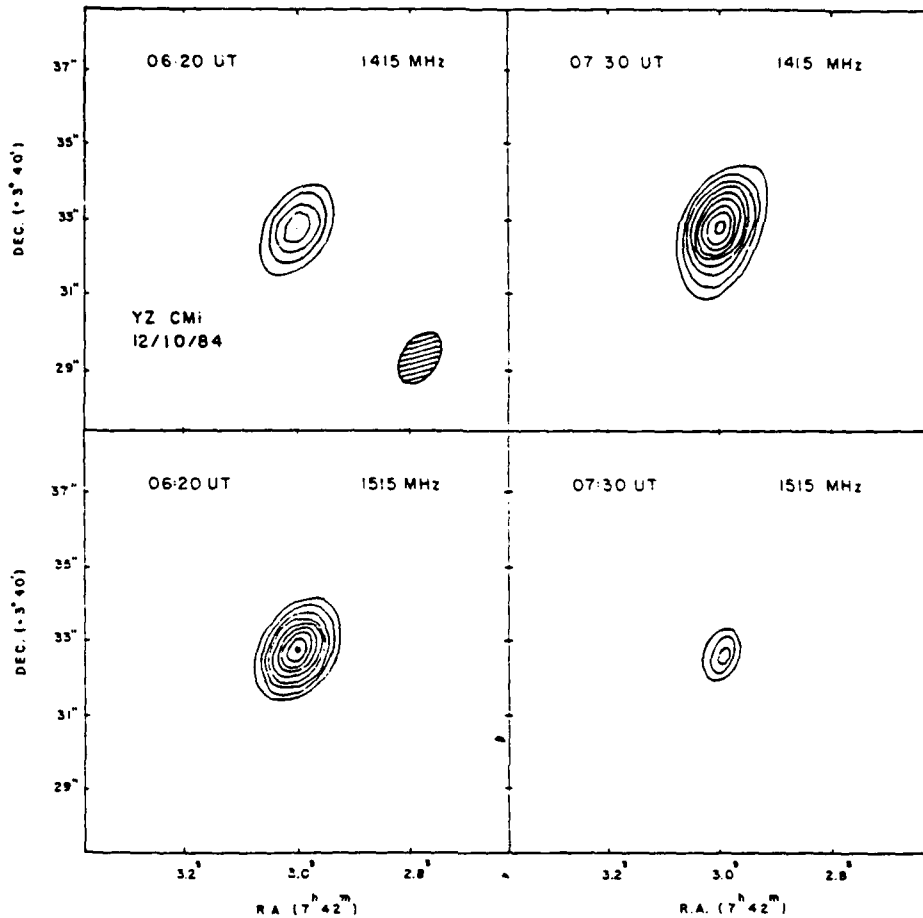


Fig. 4. VLA snapshot maps of the emission from the dwarf M flare star YZ Canis Minoris. The unresolved emission peaks at different times at two frequencies separated by only 100 MHz, suggesting a coherent burst mechanism. The contours are at intervals of 6, 8, 10, 12, ... Jy beam area, with maximum values of 14 and 22 Jy beam area at 06:20 UT and 1415 and 1515 MHz, respectively, and 25 and 10 Jy beam area at 07:30 UT for the same respective frequencies.

intense magnetic fields, and the stochastic nature of continued bursts might explain the variability of the observed microwave radiation.

4. Conclusions

Observations at 20 cm wavelength with high resolution in time and frequency have provided evidence for coherent emission mechanisms on the Sun and nearby stars. However, observations are limited by infrequent use of the Arecibo Observatory and the Very Large Array for solar and stellar observations. The scientific potential suggested

by the data presented here can only be fully realized by the development of a solar-stellar synthesis radiotelescope. Such an instrument would be dedicated to solar and stellar observations with high angular, temporal and frequency resolution.

Acknowledgements

Radio astronomical studies of the Sun at Tufts University are supported under Air Force Office of Scientific Research grant AFOSR-83-0019 and contract N0014-86-K-0068 with the Office of Naval Research. Investigations of flare stars at Tufts University are also supported by NASA grant NAG 5-477, and our simultaneous VLA and Solar Maximum Mission observations of the Sun are supported by NASA grant NAG 5-501.

References

- Dröge, F.: 1977, *Astron. Astrophys.* **57**, 285.
 Kundu, M. R. and Lang, K. R.: 1985, *Science* **228**, 9.
 Lang, K. R. and Willson, R. F.: 1983, *Adv. Space Res.* **2**, 91.
 Lang, K. R. and Willson, R. F.: 1984, *Adv. Space Res.* **4**, 105.
 Lang, K. R., Willson, R. F., and Gaizauskas, V.: 1983, *Astrophys. J.* **267**, 455.
 Lang, K. R., Willson, R. F., and Rayrole, J.: 1982, *Astrophys. J.* **258**, 384.
 Linsky, J. L. and Gary, D. E.: 1982, *Astrophys. J.* **274**, 776.
 Marsh, K. A. and Hurford, G. J.: 1980, *Astrophys. J.* **240**, L111.
 McConnell, D. and Kundu, M. R.: 1983, *Astrophys. J.* **269**, 698.
 Melrose, D. B. and Dulk, G.: 1982, *Astrophys. J.* **259**, 844.
 Pallavicini, R., Willson, R. F., and Lang, K. R.: 1985, *Astron. Astrophys.* **149**, 95.
 Roberts, B., Edwin, P. M., and Benz, A. O.: 1984, *Astrophys. J.* **279**, 857.
 Slottje, C.: 1978, *Nature* **275**, 520.
 Willson, R. F. and Lang, K. R.: 1984, *Astrophys. J.* **279**, 427.

22. CORONAL PLASMAS ON THE SUN AND NEARBY STARS

KENNETH R. LANG

Department of Physics and Astronomy
Tufts University
Medford, MA 02155

INTRODUCTION

The Very Large Array (VLA) has been used to observe solar microwave sources with second-of-arc angular resolution. Both the quiescent, or non-flaring, microwave sources and the flaring ones are usually resolved. They are often associated with the apex and/or legs of the ubiquitous coronal loops, which heretofore have been observable only with X-ray telescopes sent above the atmosphere. Multiple-wavelength VLA observations can specify the strength, evolution and structure of the magnetic fields in coronal loops, while also providing constraints on the electron density and electron temperature of the plasma trapped within the coronal loops.

VLA observations are providing new insights to the preburst heating and magnetic interaction that precede eruptions from solar active regions [Lang and Willson, (1983, 1984)]; but these interesting studies are not discussed here [see Kundu and Lang (1985) for a review]. We instead summarize our current understanding of the quiescent, or non-flaring, microwave emission from solar active regions. The next section briefly reviews the thermal radiation mechanisms that account for most of the quiescent emission, while also pointing out that current-amplified magnetic fields or non-thermal radiation may be required in some instances. This is followed by a discussion of the 20 cm radiation of coronal loops and the thermal cyclotron lines that accurately specify their magnetic field strength. The 20 cm and X-ray emission of the coronal plasma are then compared. We next discuss the coronae of nearby stars, where coherent radiation processes seem to prevail, and then conclude our summary with promising research opportunities for the future.

THERMAL RADIATION, CURRENTS AND NON-THERMAL RADIATION

The quiescent microwave emission of solar active regions has been attributed to the thermal radiation of hot electrons trapped within the strong magnetic fields of coronal loops. The microwave brightness temperature is then on the order of the million-degree electron temperature, and either thermal bremsstrahlung or thermal gyroresonant radiation dominate the emission. Bremsstrahlung, or braking radiation, is emitted when the thermal electrons are accelerated in the electric fields of ions and gyroresonant radiation is emitted when the thermal electrons are accelerated by magnetic fields.

Strong evidence for gyroresonant radiation at coronal levels above sunspots was provided by a comparison of microwave, EUV and X-ray observations [Kundu, Schmahl and Gerassimenko (1980); Pallavicini, Sakurai and Vaiana (1981)]. The near equality of the microwave brightness and electron temperatures indicated that the microwave emission was thermal, but the absence of detectable X-ray radiation above sunspots indicated a relatively low electron density there. This meant that the high microwave brightness temperature above sunspots could not be due to bremsstrahlung, but it could be explained by thermal gyroresonant radiation at the second or third harmonic of the gyrofrequency.

NASA Conference Publication 2442

Coronal and Prominence Plasmas

*Edited by
A. I. Poland
NASA Goddard Space Flight Center
Greenbelt, Maryland*

Proceedings of Workshops
Held at Goddard Space Flight Center
April 9-11, 1985
April 8-10, 1986



National Aeronautics
and Space Administration

Scientific and Technical
Information Branch

1986

Thermal gyroradiation at coronal levels above sunspots was fully confirmed by the detection of circularly polarized ring-shaped or horseshoe structures [Allisandrakis and Kundu (1982); Lang and Willson (1982)] that were predicted using the theory of gyroresonant radiation in the curved magnetic fields above individual sunspots [Gel'freikh and Lubyshev (1979)]. These structures were observed at 6 cm wavelength where circular polarizations as high as 100% were detected. Bright sunspot-associated sources observed at 2 to 6 centimeters wavelength are now widely believed to be due to the gyroradiation of million-degree electrons spiralling about strong magnetic fields above sunspots.

But there is another class of compact, bright microwave sources in this wavelength range that are not associated with sunspots. They occur above regions of apparently-weak photospheric magnetic fields. For instance observations at 6 cm wavelength revealed sources with coronal brightness temperatures $T_B > 10^6$ K in regions away from sunspots [Schmahl et al. (1982); Webb, Davis, Kundu and Velusamy (1983)]. Force-free (potential) magnetic field extrapolations from the known photospheric values indicate that the magnetic field in the low solar corona is too weak to account for the observed emission by gyroradiation.

The situation is even worse at shorter wavelengths where stronger magnetic fields are required to produce gyroradiation at the first few harmonics of the gyrofrequency. (Higher harmonics produce insufficient optical depth to account for the high brightness temperatures.) Lang and Willson (1986a-this proceedings) and Willson and Lang (1986) report the presence of compact, bright 2-cm sources that require magnetic field strengths of $H \approx 2,000$ G in the low solar corona at regions away from sunspots if they are attributed to gyroresonance radiation.

Bright microwave sources in regions of apparently-weak photospheric fields can be explained by two different hypotheses. First, the emission could be thermal gyroradiation at the second or third harmonic of the gyrofrequency in strong magnetic fields. Currents might amplify the magnetic field in the low corona to values greater than those expected from extrapolations from the photosphere. Alternatively the photospheric magnetograms could be misleading, and strong magnetic fields could exist in isolated regions away from sunspots. Secondly, the emission could be nonthermal radiation in weak magnetic fields. Nonthermal synchrotron radiation from mildly relativistic electrons is one possibility, but some as yet unspecified mechanism must be continuously accelerating the electrons [Akhmedov et al. (1986), Chiuderi-Drago and Melozzi (1984); Willson and Lang (1986)].

Figure 1 provides the radiation spectra for the three types of sources usually detected at short centimeter wavelengths [see Akmedov et al. (1986) for greater details]. The most common type of source is the sunspot-associated component (A and C) that is attributed to thermal gyroresonance radiation in the legs of coronal loops that are connected to the underlying sunspots. Source D is a filament-associated component located above a magnetic neutral line in regions of apparently-weak magnetic field. Yet, this source has a steep radiation spectrum and high brightness temperature of $T_B > 7 \times 10^6$ K. It may be attributed to non-thermal radiation or to thermal gyroradiation in current-amplified magnetic fields. Then there is the filament-associated source B that has the flat spectrum of optically-thin thermal bremsstrahlung. Electron densities $n_e \approx 10^9$ to 10^{10} cm⁻³ are consistent with this interpretation, suggesting that in this case we are detecting the same thermal plasma that is observed at X-ray wavelengths from coronal loops. But this plasma is more commonly detected at the longer radio wavelength of 20 centimeters.

Individual cyclotron lines from AR 4398 are shown in Figure 3 together with the flat spectrum of the nearby active region AR 4399. The flat spectrum of AR 4399 is attributed to thermal bremsstrahlung, whereas the spectrum of AR 4398 can be explained by cyclotron line emission from a narrow layer of width $\Delta L \approx 10^8$ cm, electron density $N_e \approx 10^9$ cm $^{-3}$ and a relatively high electron temperature $T_e \approx 4 \times 10^6$ K (solid line). Here the harmonic number $n = 4$ and the magnetic field strength $H = 145$ G. A key aspect of this discovery is the extraordinary precision in measuring the magnetic field strength; a change of only $\Delta H = 20$ G shifts the central frequency of the line by 170 MHz.

COMPARISON OF THE 20 CM AND X-RAY EMISSION

As previously mentioned, comparisons between the X-ray and short microwave (3 to 6 cm) radiation from solar active regions provided evidence for a new source of opacity at microwave wavelengths above sunspots. It has been attributed to gyroresonance effects in the legs of coronal loops connecting with underlying sunspots. Recent comparisons of the 6 cm radiation from the apex of coronal loops indicates that its brightness temperature is less than the electron temperature measured at X-ray wavelengths; this has been explained by a cool ($\approx 10^5$ K) external plasma [Holman (1986 - this proceedings); Weis, Holman, Davis and Kundu (1986)].

However, there have been no published comparisons of X-ray data with the 20 cm emission of the coronal plasma. In some instances, there is radiation at 20 centimeters wavelength near sunspots where no X-ray radiation is detected. The radio emission may be attributed to gyroresonant radiation of a low density plasma in magnetic fields of strength $H = 145$ to 290 G (harmonic $n = 4$ to 2), [see Lang, Willson, Strong and Smith (1986a) for greater details].

In other cases, the 20 centimeter radiation appears at the apex of coronal loops, but with a slightly lower brightness temperature, $T_B \approx 1.4$ to 1.7×10^6 K, than the electron temperature, $T_e \approx 3.0 \times 10^6$ K, inferred from the X-ray data. This may be explained by a low temperature plasma with $T_e \approx 10^5$ K that lowers the effective brightness temperature of the radio bremsstrahlung while not affecting the X-ray data that only detects the 10^6 K plasma [see Holman (1986 - this proceedings); Lang (1986 - this proceedings); and Lang, Willson, Strong and Smith (1986a) for greater details]. Because the line of sight through the low temperature plasma is greatest along the legs of coronal loops, it can reduce the size of the radio source below that of the X-ray emission. That is, the low temperature plasma can, under the right circumstances, confine the detectable radio radiation to the apex of coronal loops.

As illustrated in Figure 4, there are other instances in which the 20-cm radiation and the soft X-ray emission have the same angular extent. In this case, the maximum brightness temperature of the radio emission has the same value as the electron temperature, $T_e \approx 3 \times 10^6$ K, inferred from the X-ray data. At first sight it would seem that the 20-cm emission is the thermal bremsstrahlung of the X-ray emitting plasma (electron density $N_e \approx 2 \times 10^{10}$ cm $^{-3}$), but in this instance we have also detected a cyclotron line. Preliminary modeling indicates a thin layer of $T_e \approx 4 \times 10^6$ K with a magnetic field strength of $H = 145$ or 187 G (harmonic $n = 4$ or 3). The thermal electrons that give rise to the X-ray radiation therefore also seem to produce strong gyroresonant radiation at 20 centimeters wavelength.

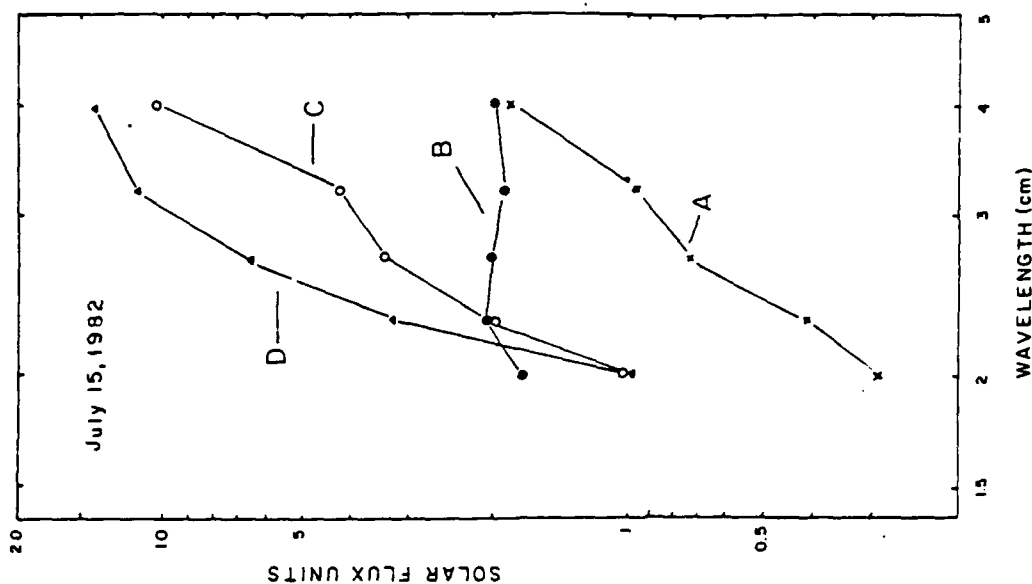


Figure 1. The radiation spectra of four sources associated with an active region. The steep spectrum of the filament-associated source D is attributed to the gyrosynchrotron radiation of mildly relativistic electrons whereas the flat spectrum of the source B is attributed to thermal bremsstrahlung. The sunspot-associated sources A and C are attributed to gyroresonance emission in the legs of coronal loops.

CORONAL LOOPS AT 20 CM WAVELENGTH AND THERMAL CYCLOTRON LINES

Radiation from a post-flare loop at 20 centimeters wavelength was reported by Velusamy and Kundu (1981); but there is a much more extensive literature regarding the quiescent 20-cm radiation of coronal loops [Lang, Willson and Rayrole (1982); Lang, Willson and Gaizauskas (1983); McConnell and Kundu (1983); Shevgaonkar and Kundu (1984); Kundu and Lang (1985); Kundu (1986 - this proceedings); Lang (1986 - this proceedings)]. The radiation at this longer wavelength often comes from the hot, dense plasma trapped within the coronal loop (see Figure 2 for a typical example). The 20-cm coronal loops have peak brightness temperatures of 1×10^6 to 4×10^6 K and extents of about 10^{10} cm. Their radio emission can be attributed to thermal bremsstrahlung or thermal gyroresonant radiation, or both.

Of special interest is the recent detection of thermal cyclotron lines near the apex of coronal loops at wavelengths near 20 centimeters [see Figure 3 and Willson (1985) for greater details]. These cyclotron lines are emitted at harmonics of the gyrofrequency, with a wavelength that depends only on the harmonic number and the magnetic field strength. However, because the magnetic field in the legs of coronal loops decrease uniformly with height, the individual cyclotron lines at short wavelengths will usually merge into a smooth continuum.

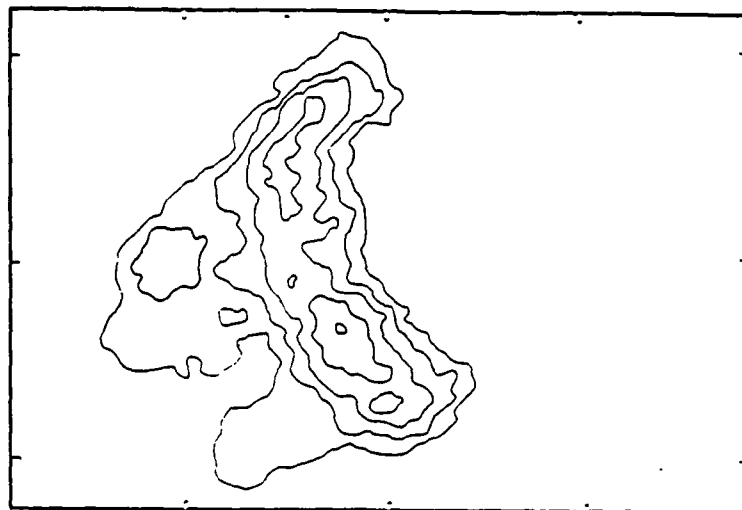


Figure 2. A typical radio wavelength (20 cm) V.L.A. map of the hot, million-degree plasma trapped in a coronal loop. The angular scale between fiducial marks on the axes is 60 arc-seconds.

At 20 centimeters wavelength we can observe the apex of coronal loops where the magnetic field is nearly constant and the spectrum of individual cyclotron lines can be resolved. This will be particularly true if currents or some other process confine the intense emission to a thin, hot layer within the loop apex.

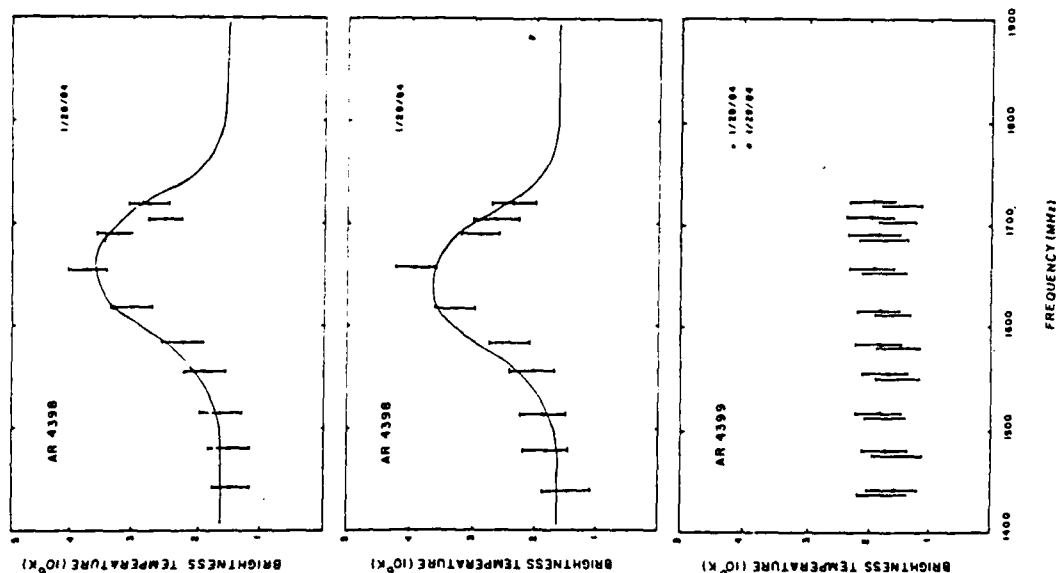


Figure 3. VLA data at ten closely-spaced frequencies near 1446 MHz (20 cm) showing thermal cyclotron line spectra from active region AR 4398 on successive days, together with optically-thick thermal bremsstrahlung spectra from active region AR 4399 on the same days.

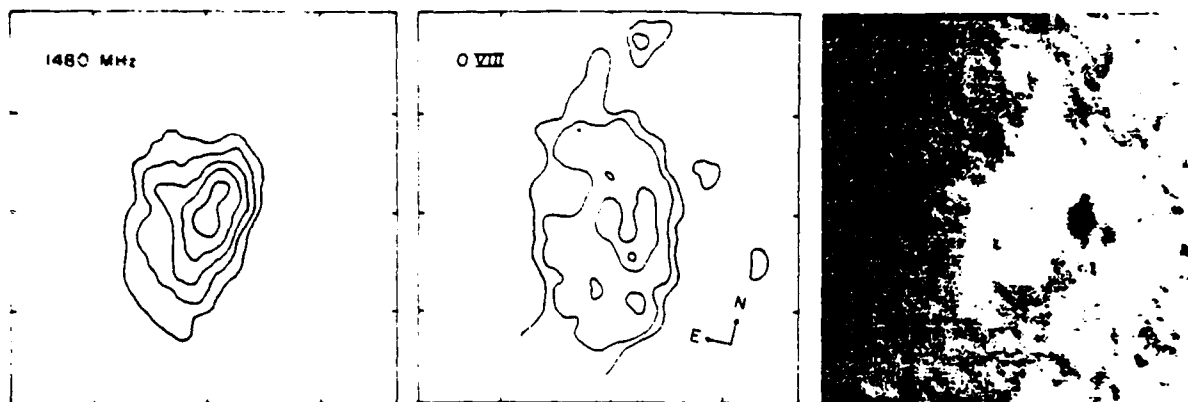


Figure 4. A comparison of the 20 cm emission (V.L.A.-left), soft-X-ray (S.M.M.-middle) and H α (SOON-right) emission of an active region on the same day. The angular spacing between fiducial marks on the axis is 60 arc-seconds.

CORONAE OF NEARBY STARS

Nearby dwarf M stars exhibit slowly-varying, quiescent microwave radiation and microwave bursts that have been detected with the Very Large Array (VLA) and the Arecibo Observatory. Observations with high resolution in frequency and time provide strong evidence for coherent radiation mechanisms in the coronae of these stars [Lang (1986b)]. Such mechanisms provide stringent constraints on the electron density and magnetic field strength in the stellar coronae.

Narrow-band, slowly varying radiation has been detected from the dwarf M star YZ Canis Minoris when using the VLA at wavelengths near 20 centimeters [Lang and Willson (1986b)]. White, Kundu and Jackson (1986) subsequently repeated this experiment, finding narrow-band bursts from the dwarf M stars AD Leonis and UV Ceti. The narrow-band structure cannot be explained by continuum emission processes such as thermal bremsstrahlung, thermal gyroresonant radiation or nonthermal gyrosynchrotron radiation. Although gyroresonant radiation can give rise to narrow-band cyclotron lines, it requires an implausibly large source that is hundreds of times larger than the star. The observations of narrow-band structure can apparently only be explained by coherent mechanisms like electron-cyclotron lines or coherent plasma radiation.

Independent evidence for coherent radiation mechanisms is provided by high-time-resolution observations of the dwarf M star AD Leonis at the Arecibo Observatory [Lang, Bookbinder and Golub (1983), Lang and Willson (1986c)]. As illustrated in Figure 5, quasi-periodic, highly polarized spikes are observed at 20 centimeters wavelength with rise times of less than 5 milliseconds. An upper limit to the linear size of the spike emitting region is $L < 1.5 \times 10^8$ cm, the distance

that light travels in 5 milliseconds. This size is only five hundredths of the estimated radius of AD Leonis. Provided that the emitter is symmetric, it has a brightness temperature greater than 10^{16} K. The high degrees of circular

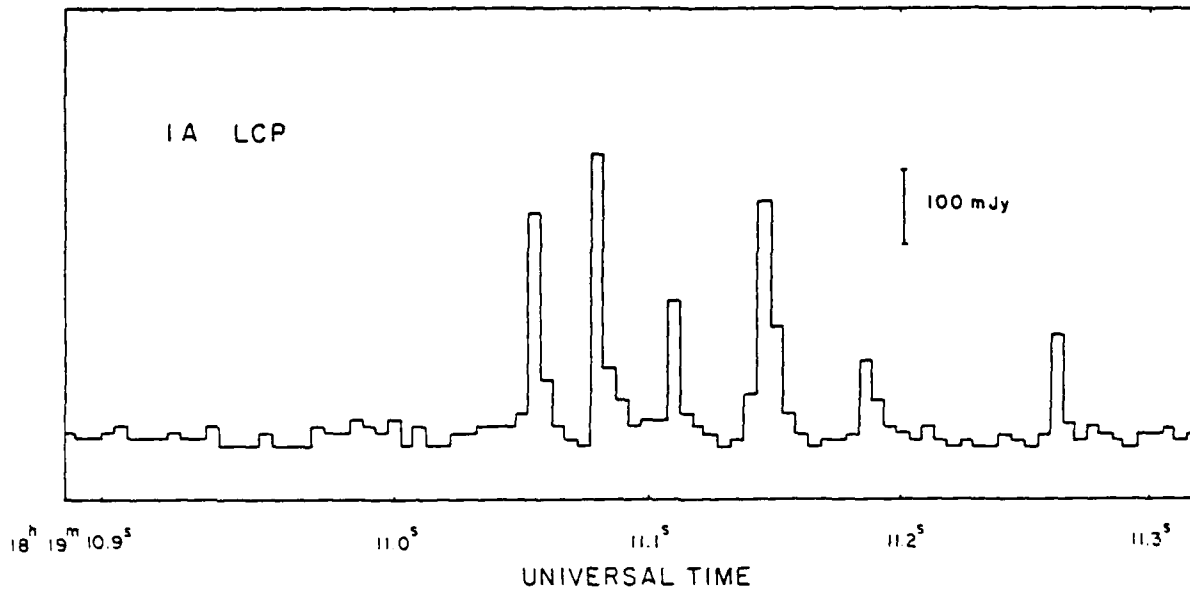


Figure 5. The total power detected at a frequency of 1415 MHz (21.2 cm) while tracking the dwarf M star AD Leonis. The left-hand circularly polarized (LCP) signal has been displayed with a 5 ms integration time. There are five quasi-periodic spikes with a mean periodicity of $T_p = 32 \pm 5$ ms and a total duration of $T_D = 150$ ms. Each of these spikes had a rise time of $\tau_R < 5$ ms, leading to an upper limit to the linear size $L < 1.5 \times 10^8$ cm for the spike emitter. A symmetric source of this size would have a brightness temperature of $T_B > 10^{16}$ K, requiring a coherent radiation mechanism.

polarization (up to 100%) indicate an intimate connection with the star's magnetic field, and the high brightness temperatures suggest a coherent radiation mechanism such as an electron-cyclotron maser or coherent plasma radiation.

The coherent process provides constraints on the electron density, N_e , and the magnetic field strength, H , in the stellar coronae [see Dulk (1985) for the relevant formulae]. If the electron-cyclotron maser emits at the second harmonic of the gyrofrequency, the longitudinal magnetic field strength $H = 250$ G and constraints on the plasma frequency imply an electron density of $N_e = 6 \times 10^9$ cm $^{-3}$. Coherent plasma radiation at the first or second harmonic of the plasma frequency respectively require $N_e = 2 \times 10^{10}$ cm $^{-3}$ and $H \ll 500$ G or $N_e = 6 \times 10^9$ cm $^{-3}$ and $H \ll 250$ G.

PROMISING DIRECTIONS FOR THE FUTURE

Future VLA observations at 20 centimeters wavelength will continue to provide diagnostic tools for the solar corona. Observations of thermal cyclotron lines offer a promising method of accurately determining the coronal magnetic field strength. Comparisons with soft X-ray spectral lines will help delineate the

electron density and temperature, while also specifying the radiation mechanisms. One promising approach that grew out of this conference involves simultaneous observations with the VLA and the Owens Valley Radio Observatory (OVRO). The OVRO will provide spectral information that is not obtainable with the VLA, whereas the high angular resolution of the VLA will remove ambiguities in the OVRO data. Future collaborations between the Tufts University group and the Observatoire de Paris - Nancay Radio Heliograph will provide new perspectives to coherent radiation processes on the Sun. The rapidly growing studies of the microwave radiation from dwarf M and RS CVn stars will continue to provide new insights to physical processes in stellar coronae. The full potential of these studies of the Sun and nearby stars will only be realized by the development of a solar-stellar synthesis radiotelescope. Such an instrument would be dedicated to solar and stellar observations with high angular, temporal and frequency resolution.

ACKNOWLEDGEMENTS

Radio astronomical studies of the Sun at Tufts University are supported under Air Force of Scientific Research grant AFOSR-83-0019 and contract N0014-86-K-0068 with the Office of Naval Research. Simultaneous VLA and Solar Maximum Mission observations of the Sun are supported by NASA grant NAG 5-501.

REFERENCES

- Akhmedov, S.B., et al., 1986, "Structure of a Solar Active Region from RATAN 600 and Very Large Array Observations," *Astrophys. J.*, 301, 460-464.
- Alissandrakis, C.E. and M.R. Kundu, 1982, "Observations of Ring Structure in a Sunspot Associated Source at 6 centimeter Wavelength", *Astrophys. J. (Letters)*, 253, L49-L52.
- Chiuderi-Drago, F. and M. Melozzi, 1984, "Non-Thermal Radio Sources in Solar Active Regions," *Astrophys. J.* 131, 103-110.
- Dulk, G.A., 1985 "Radio Emission from the Sun and Stars," *Ann. Rev. Astron. Ap.*, 23 169-180
- Dulk, G.A. and D.E. Gary, 1983, "The Sun at 1.4 GHz: Intensity and Polarization," *Astron. Astrophys.*, 124, 103-107
- Gel'frikh, G.B. and B.I. Lubyshev, 1979, "Structure of Local Sources of the S Component of Solar Radio Emission " *Sov. Astron. A.J.*, 23, 316.
- Holman, G.D., 1986, "Determining Magnetic and Plasma Structure of Coronal Loops from Microwave and Soft X-ray Observations", : this Proceedings.
- Kundu, M.R., 1986, "Three Dimensional Structure of Solar Active Regions," this Proceedings.
- Kundu, M.R. and K.R. Lang, 1985, "The Sun and Nearby Stars," *Science*, 228, 9-15.
- Kundu, M.R., E.J. Schmahl and M. Gerassimenko, 1980, "Microwave, EUV and X-ray Observations of Active Region Loops: Evidence for Gyroresonance Absorption in the Corona," *Astron. Astrophys.* 82, 265-271.
- Kundu, M.R. and T. Velusamy, 1980, " Observation with the VLA of a Stationary Loop Structure in the Sun at 6 cm Wavelength," *Astrophys. J. (Letters)*, 240, L62-L65.
- Lang, K.R., 1986a, "Coronal Diagnostics "-this Proceedings.
- Lang, K.R., 1986b, "Flare Stars and Solar Bursts: High Resolution in Time and Frequency," *Solar Phys.*, in press.
- Lang, K.R., J. Bookbinder, L. Golub and M. Davis, 1983, "Bright, Rapid, Highly Polarized Radio Spikes from the Dwarf AD Leo," *Astrophys. J. (Letters)*, 272, L15-L18.

- Lang, K.R. and R.F. Willson, 1982, "Polarized Horseshoes Around Sunspots at 6 Centimeter Wavelength," *Astrophys. J. (Letters)*, 255 L111-L117.
- Lang, K.R. and R.F. Willson, 1983, "Multiple Wavelength Observations of Flaring Active Regions," *Adv.Space Res.* 2, No. 11, 91-100.
- Lang, K.R. and R.F. Willson, 1984, "V.L.A. Observations of Flare Build-Up in Coronal Loops," *Adv. Space Res.* 4, no. 7, 105-110.
- Lang, K.R. and R.F. Willson, 1986a, "Compact, Variable, Moving Sources on the Sun at 2 Centimeters Wavelength," this Proceedings.
- Lang, K.R. and R.F. Willson, 1986b, "Narrow-Band, Slowly Varying Decimetric Radiation from the Dwarf M Flare Star YZ Canis Minoris," *Astrophys. J. (Letters)*, 302, L17-L21.
- Lang, K.R. and R.F. Willson, 1986c, "Millisecond Radio Spikes from the Dwarf M Flare Star AD Leonis," *Astrophys. J.*, in press.
- Lang, K.R., R.F. Willson and V. Gaizauskas, 1983, "Very Large Array Observations of Solar Active Regions III. Multiple Wavelengths Observations," *Astrophys. J.* 267, 455-464.
- Lang, K.R., R.F. Willson and J. Rayrole, 1982, "Very Large Array Observations of Coronal Loops at 20 Centimeter Wavelength," *Astrophys. J.*, 258, 384-387.
- Lang, K.R., R.F. Willson, K.T. Strong and K.L. Smith, 1986a, "Simultaneous Solar Maximum Mission and Very Large Array Observations of Solar Active Regions", *Astrophys. J.*, to be submitted.
- Lang, K.R., R.F. Willson, K.T. Strong and K.L. Smith, 1986b, "Physical Parameters of Solar Active Regions Inferred from Thermal Cyclotron Lines and Soft X-ray Spectral Lines, *Astrophys. J.*, to be submitted.
- McConnell, D. and M.R. Kundu, 1983, "VLA Observations of a Solar Active Region and Coronal Loops," *Astrophys. J.*, 269, 698-705.
- Schmahl, E.J., et al., 1982, "Active Region Magnetic Fields Inferred from Simultaneous VLA Microwave Maps, X-ray Spectroheliograms, and Magnetograms", *Solar Phys.* 80, 233-249.
- Shevgaonkar, R.K. and M.R. Kundu, 1984, "Three-Dimensional Structures of Two Solar Active Regions from VLA Observations at 2, 6 and 20 Centimeter Wavelengths," *Astrophys. J.*, 283, 413-420.
- Strong, K.T., C.E. Alissandrakis and M.R. Kundu, 1984, "Interpretation of Microwave Active Region Structures Using SMM Soft X-ray Observations," *Astrophys. J.* 277, 865-873.
- Velusamy, T. and M.R. Kundu, 1981, "VLA Observations of Postflare Loops at 20 Centimeter Wavelength," *Astrophys. J. (Letters)*, 243, L103-L107.
- Webb, D.M. J.M. Davis, M.R. Kundu and T. Velusamy, 1983, "X-ray and Microwave Observations of Active Regions," *Solar Phys.* 85, 267-283.
- Webb, D.F., G.D. Holman, J.M. Davis and M.R. Kundu, 1986, "High-Spatial-Resolution Microwave and Soft X-ray Observations as Diagnostics of Solar Magnetic Loops", *Astrophys. J.*, submitted
- White, S.M., M.R. Kundu and P.D. Jackson, 1986, "Narrowband Radio Flares from Red Dwarf Stars," *Astrophys. J.*, submitted.
- Willson, R.F., 1985, "VLA Observations of Solar Active Regions at Closely Spaced Frequencies: Evidence for Thermal Cyclotron Line Emission," *Astrophys. J.*, 298, 911-917.
- Willson, R.F. and K.R. Lang, 1986, "VLA Observations of Compact, Variable Sources on the Sun," *Astrophys. J.*, in press.

23. COMPACT, VARIABLE, MOVING SOURCES
OBSERVED ON THE SUN AT 2 CENTIMETERS WAVELENGTH

KENNETH R. LANG
ROBERT F. WILLSON

Department of Physics and Astronomy
Tufts University
Medford, MA 02155

INTRODUCTION

The high angular resolution provided by the Very Large Array (VLA) has permitted the spatial resolution of solar microwave sources and opened the way for comparisons with observations of similar angular resolution at optical and X-ray wavelengths. High-resolution VLA observations of solar active regions at relatively long wavelengths of 6 cm and 20 cm have, for example, led to the discovery of the microwave counterpart of the ubiquitous coronal loops that had previously only been observed by X-ray telescopes lofted above the Earth's atmosphere. The microwave emission of the coronal loops is attributed to the gyroresonant radiation and/or the bremsstrahlung of million-degree, thermal electrons trapped within the loops by strong magnetic fields; observations of this emission have provided valuable new insights into the nature of solar active regions and eruptions from the Sun and nearby stars [Kundu and Lang (1985); Lang (1986 a,b - this proceedings)].

In contrast, the short wavelength 2 cm emission of solar active regions is poorly understood. In spite of numerous VLA solar observations at 2 cm, there are only two published results [Lang, Willson and Gaizauskas (1983); Shevgaonkar and Kundu (1984)]. In both instances, compact (angular sizes $\theta \approx 15''$), highly polarized (degrees of circular polarization $p_c = 80\%$ to 90%) sources were found in regions of strong magnetic field (strength $H \approx 2,000$ G) above sunspots. The brightness temperatures of $T_B \approx 10^5$ K were characteristic of the electron temperature in the transition region.

Subsequent examination of the compact 2 cm sources in active regions indicated that they are variable over time scales of an hour or shorter. This probably explains the paucity of VLA results; synthesis maps averaged over 11 or 12 hours would not reveal several relatively-weak, time-variable sources.

To further complicate the matter, we have recently discovered compact, variable, highly-polarized 2 cm sources in regions of apparently-weak, photospheric magnetic field [Willson and Lang (1986)]. Our subsequent VLA observations have confirmed the existence of compact, variable 2 cm sources that are not associated with active regions, but these sources had no detectable circular polarization. In addition, both the unpolarized and polarized 2 cm sources were found to move laterally across the solar surface with velocities $V \approx 1 \text{ km s}^{-1}$. In the next section we present observations of these compact, variable, moving sources. The concluding discussion mentions possible radiation mechanisms and implications for studies of the quiet Sun.

NASA Conference Publication 2442

Coronal and Prominence Plasmas

*Edited by
A. I. Poland
NASA Goddard Space Flight Center
Greenbelt, Maryland*

*Proceedings of Workshops
Held at Goddard Space Flight Center
April 9-11, 1985
April 8-10, 1986*



National Aeronautics
and Space Administration

Scientific and Technical
Information Branch

1986

OBSERVATIONS

The VLA was used to observe the active region AR 4508 in the C configuration between 1530 and 2330 UT on June 4, 1984. The position of this region was NO6 E57 at 1300 UT on this day. Follow-up observations were made between 1500 and 2300 UT on January 17, 1986 in the D configuration. In this case, a region of bright plage and relatively-weak magnetic fields (no sunspots) was observed; its position was S10 W62 at 1300 UT on this day.

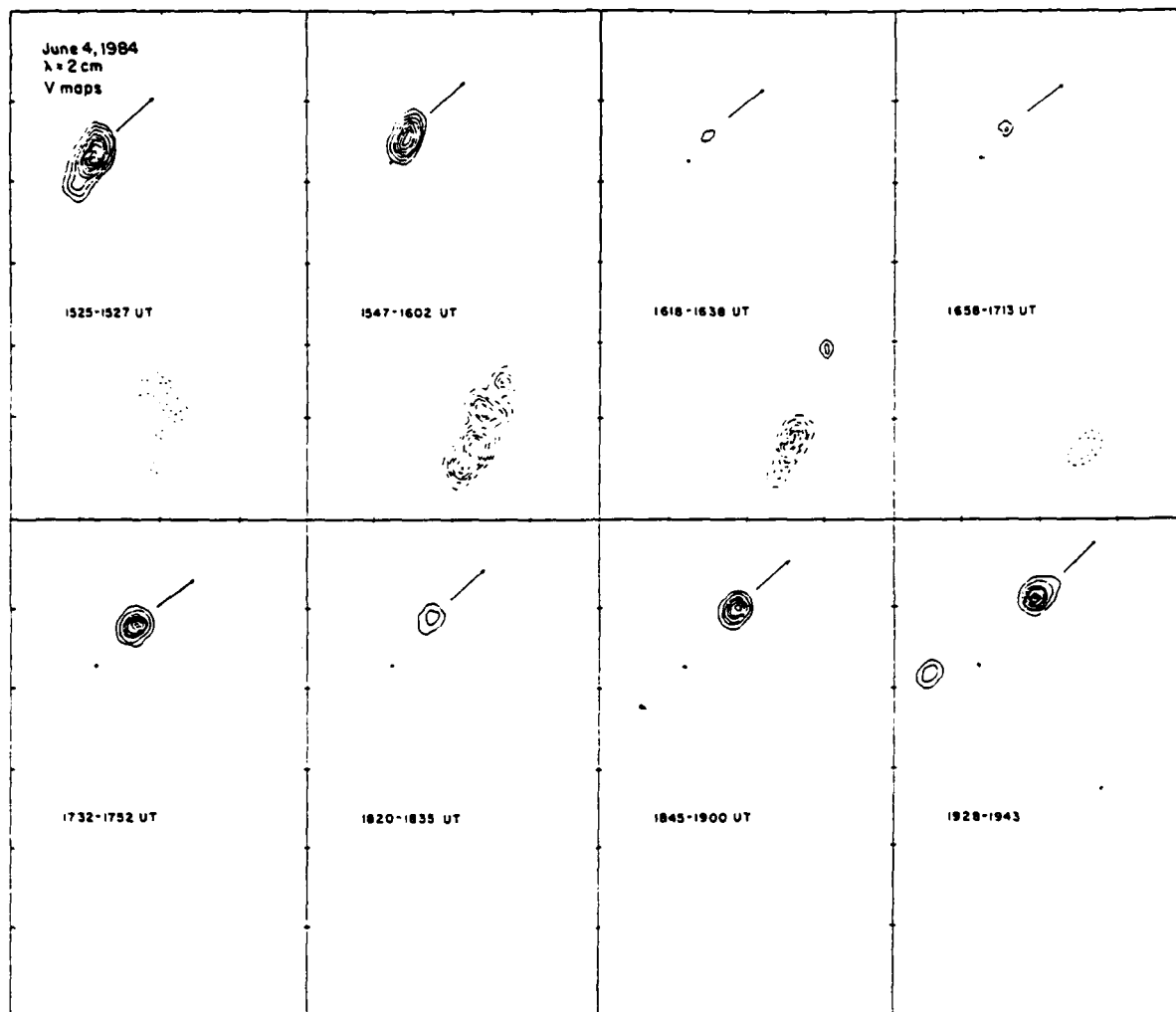


Figure 1. VLA synthesis maps of left circularly polarized (solid contours) and right circularly polarized (dashed contours) radiation at 2 cm wavelength. Here each box refers to the same area on the surface of the Sun, and the fiducial marks on the axes are separated by 10 arc-seconds. The northern source (top) varied over time scales of 30 minutes and moved laterally across the solar surface in the northwest direction a velocity of $\sim 1 \text{ km s}^{-1}$. The southernmost source varied over a time scale of about 60 minutes, and moved laterally towards the southwest at a velocity of $\sim 2 \text{ km s}^{-1}$. Here the contours mark levels of equal brightness with an outermost contour of 6.1×10^4 and a contour interval of $3.1 \times 10^4 \text{ K}$.

As illustrated in Figure 1, the 2 cm maps on June 4 showed two compact ($\theta \approx 5''$), highly circularly polarized ($p_c = 80$ to 90%) sources that vary on time scales of 30 to 60 minutes. The left circularly polarized source (solid contours) varied in maximum brightness temperature from $T_B = 2.0 \times 10^5$ K to $T_B < 0.5 \times 10^5$ K. Here each box refers to the same area of the Sun, and the arrows illustrate systematic motion to the northwest with a total motion of about $15''$ in three hours. The left circularly polarized source was therefore moving laterally across the surface of the Sun with a velocity of $V \approx 1$ km s $^{-1}$. The right circularly polarized source (dashed contours) apparently moved towards the southwest at about twice this speed, but the motion is confused by the presence of more than one source.

Comparisons with Mt. Wilson magnetograms indicate that the two compact, variable, moving sources were located in regions of apparently-weak photospheric magnetic field ($H < 80$ G), and that they did not overliesunspots. The high polarization of these sources is therefore somewhat enigmatic, for the polarization of thermal radiation requires strong magnetic fields of $H \approx 2,000$ G. We will return to this paradox in the discussion.

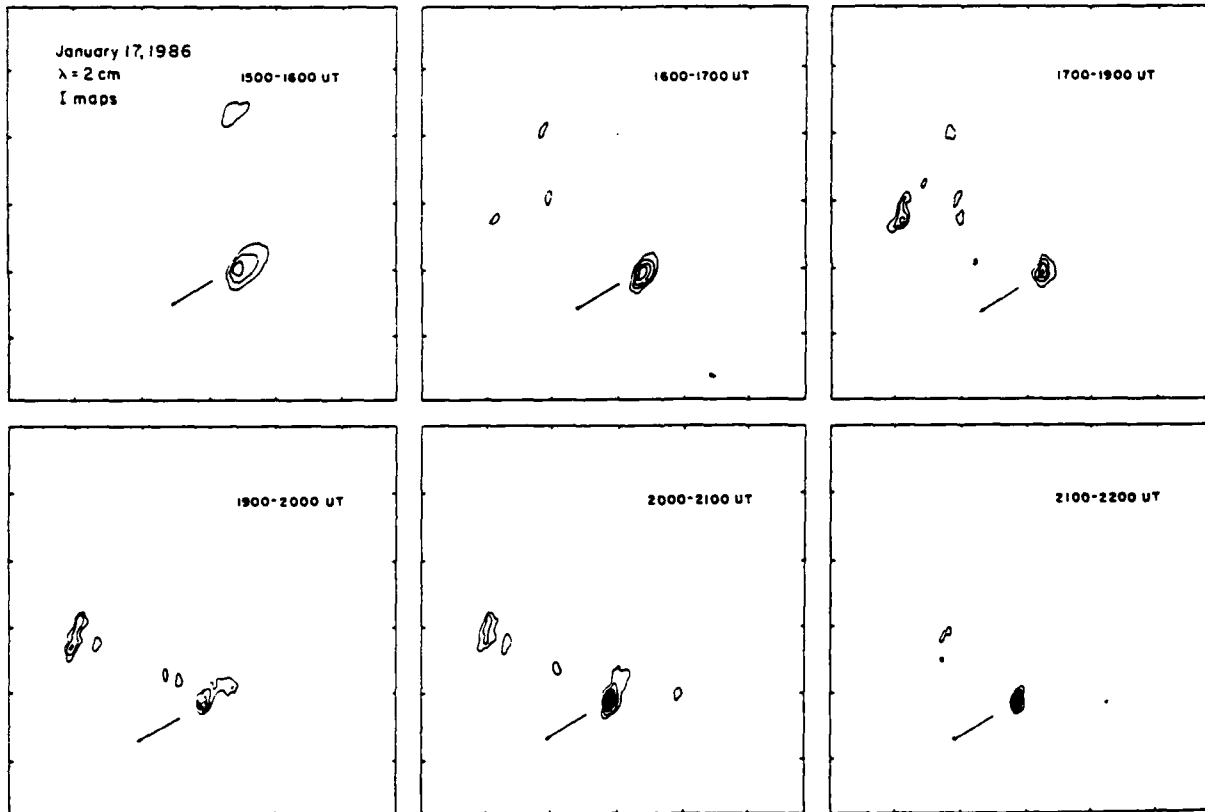


Figure 2. VLA synthesis map of the total intensity of the radiation at 2 cm wavelength. Here each box refers to the same area on the surface of the Sun, and the fiducial marks on the axes are separated by 60 arc-seconds. The southern source (bottom) increased slowly in brightness over a seven hour period while moving laterally across the solar surface in the southeast direction at a velocity of ~ 1 km s $^{-1}$. The northern source (top) varied over a time scale of 180 minutes, but showed no detectable lateral motion. Here the contours mark levels of equal brightness with an outermost contour of 5.2×10^4 K and a contour interval of 1.8×10^4 K.

Our confirming observations on January 17, 1986 revealed compact 2 cm sources with angular sizes $\theta \approx 25''$ and maximum brightness temperatures of $T_B = 2.0 \times 10^5$ K. These sources were observed in plage regions with apparently-weak photospheric magnetic field and no sunspots, but in this case the compact sources had no detectable circular polarization ($\rho_C < 15\%$).

As illustrated in Figure 2, the compact unpolarized sources either varied substantially in intensity over time scales of hours (top sources) or slowly increased in brightness over a seven hour period (bottom source). Here each box refers to the same area on the surface of the Sun, and the arrows indicate a lateral motion at a velocity of $V \approx 1 \text{ km s}^{-1}$. Curiously, the relatively-unvarying source exhibited this motion, but the variable one showed no detectable motion.

DISCUSSION

We have discovered previously-unobserved sources at 2 cm wavelength in regions of apparently-weak photospheric magnetic field. The brightness temperatures of $T_B \sim 10^5$ K are characteristic of the transition region. The angular sizes are $\theta \sim 5''$ to $25''$, and they vary in intensity over time-scales of 30 minutes to more than 180 minutes. We have observed at least two of these compact, variable 2-cm sources within the $3'$ field of view every time we have observed the Sun; extrapolating to the $30'$ - wide Sun, we would expect hundreds of them on the visible surface of the quiet Sun. The compact, variable sources can either be highly circularly polarized ($\rho_C \approx 90\%$) or they can exhibit no detectable circular polarization ($\rho_C < 15\%$).

The enigmatic presence of highly polarized sources in regions of apparently-weak photospheric magnetic field may be explained by any one of three hypothesis. First, the photospheric field may have strengths of up to 2,000 G in compact regions that are not readily detected by the photospheric magnetograms. Alternatively, the magnetic field in the transition region or the low corona may be amplified by currents to a strength above that in the underlying photosphere. If either of these hypothesis is true, then the high circular polarization of the 2 cm sources can be attributed to either thermal gyroradiation or the propagation of thermal bremsstrahlung in the presence of a magnetic field of strength $H \approx 2,000$ G. A third hypothesis, developed by Willson and Lang(1985), is that the compact 2 cm sources are due to nonthermal gyrosynchrotron radiation of mildly relativistic electrons in relatively weak magnetic fields of strength $H \approx 50$ G.

But what accounts for the variability and lateral motion of both the polarized and the unpolarized sources? The source variability might be due to a variable magnetic field that comes and goes within the transition region and low solar corona. Alternatively, the variations could be interpreted in terms of thermal electron density variations related to heating changes or to non-thermal electron density variations resulting from a variable acceleration mechanism. The lateral motion can be attributed to an upward expansion of dipolar loops; the 2-cm observations detect the apparent lateral motion of the loop legs.

Finally, we would like to point out certain resemblances between the compact, variable 2-cm sources and other phenomena reported in this proceeding. These sources are resolved (they are not points) with angular sizes comparable to those of small erupting filaments [Martin (1986 - this proceedings)] and the 20 cm observations of so-called coronal bright points [Habbal (1986 - this proceedings)]. The time scale of the variations and the lateral motions of the 2-cm sources are

comparable to those of the small erupting filaments. The brightness temperatures of the 2-cm sources are the same as those of the 20-cm ones. Comparisons with features seen at the He I, λ 10830 transition are very misleading, for there are so many of these features that the statistical significance of a correlation has to be very low.

ACKNOWLEDGEMENTS

Radio astronomical studies of the Sun at Tufts University are supported under grant AFOSR-83-0019 with the Air Force Office of Scientific Research (AFOSR) and contract N0014-86-K-0068 with the Office of Naval Research (ONR).

REFERENCES

- Habbal, S., 1986, " Spatial and Temporal Observations of Coronal Bright Points" - this Proceedings.
- Kundu, M.R. and K.R. Lang, 1985, "The Sun and Nearby Stars: Microwave Observations at High Resolution, " Science 228, 9-15
- Kundu, M.R., 1986 a, "Coronal Plasmas on the Sun and Nearby Stars" - this Proceedings.
- Lang, K.R., 1986a "Coronal Plasmas on the Sun and Nearby Stars"- this Proceedings.
- Lang, K.R., 1986b, "Coronal Diagnostics - this proceedings.
- Lang, K.R., R.F. Willson and V. Gaizauskas, 1983, " Very Large Array Observations of Solar Active Regions III. Multiple Wavelength Observations," Astrophysical J., 267, 455-464.
- Martin, S., 1986, : Small Eruptive Filamentary Sources" - this Proceedings.
- Shevgaonkar, R.K. and M.R. Kundu, 1984 "Three Dimensional Structures of two Solar Active Regions from VLA Observations at 2,6 and 20 cm. Centimeter Wavelength", Astroph. J., 283, 413-420.
- Willson, R.F. and K.R. Lang, 1986, "VLA Observations of Compact, Variable Sources on the Sun," Astrophysical Journal - to be published.

24. CORONAL DIAGNOSTICS

KENNETH R. LANG

Department of Physics and Astronomy
Tufts University
Medford, MA 02155

INTRODUCTION

The relatively recent development of satellite-borne X-ray telescopes and ground-based aperture synthesis radio telescopes has led to an examination of the solar corona with unprecedented resolution in space, time and frequency. The high spatial and spectral resolution of the X-ray instruments aboard Skylab and the Solar Maximum Mission (SMM) satellite have, for instance, showed that coronal loops dominate the structure of the Sun's lower corona [see Vaiana and Rosner (1978) for a review]. Strong magnetic fields hold a hot, dense plasma within the ubiquitous coronal loops.

Observations of soft X-ray spectral lines indicate that the quiescent, or non-flaring, coronal loops have electron temperatures $T_e \sim 2$ to 4×10^6 K and electron densities $N_e \sim 10^9$ to 10^{11} cm⁻³ with total extents $L \sim 10^9$ to 10^{10} cm. Similar temperatures are inferred from radio-wavelength brightness temperatures that are comparable to the local electron temperatures.

The detailed temperature and magnetic structure of the quiescent, or non-flaring, coronal loops has been inferred from radio wavelength synthesis observations. Synthesis maps describe the two-dimensional distribution of source brightness and the two-dimensional structure of the magnetic field [see Kundu and Lang (1985) for a review]. The unique ability to specify the strength and structure of the coronal magnetic fields is an important aspect of the radio wavelength synthesis maps.

Our current understanding of coronal loops is summarized in this chapter. It includes observations from ground-based radio telescopes and from X-ray telescopes lofted above the atmosphere, as well as theoretical interpretations of these observations.

The remaining sections of this introductory overview highlight both the observational and theoretical results that are discussed in greater detail in the following papers. We begin by discussing the three-dimensional structure of coronal loops. Alternative radiation mechanisms are then described within the context of both the radio and X-ray emission. Various methods of determining the strength and structure of the coronal magnetic field are then described. The final sections of

NASA Conference Publication 2442

Coronal and Prominence Plasmas

*Edited by
A. I. Poland
NASA Goddard Space Flight Center
Greenbelt, Maryland*

**Proceedings of Workshops
Held at Goddard Space Flight Center
April 9-11, 1985
April 8-10, 1986**



**National Aeronautics
and Space Administration**

**Scientific and Technical
Information Branch**

1986

this introduction include the coronae of nearby stars and future prospects for radio diagnostics of coronal loops.

THREE DIMENSIONAL STRUCTURE OF CORONAL LOOPS

Observations at different radio wavelengths generally sample different levels within coronal loops, with longer wavelengths referring to higher levels. The heights of the radio structures can be inferred from their angular displacements from underlying photospheric features, and the two-dimensional maps at different radio wavelengths can be combined to specify the three-dimensional structure of coronal loops. The accuracy of these height determinations depends on the geometry of the magnetic field, and the accuracy is greatest near the limb.

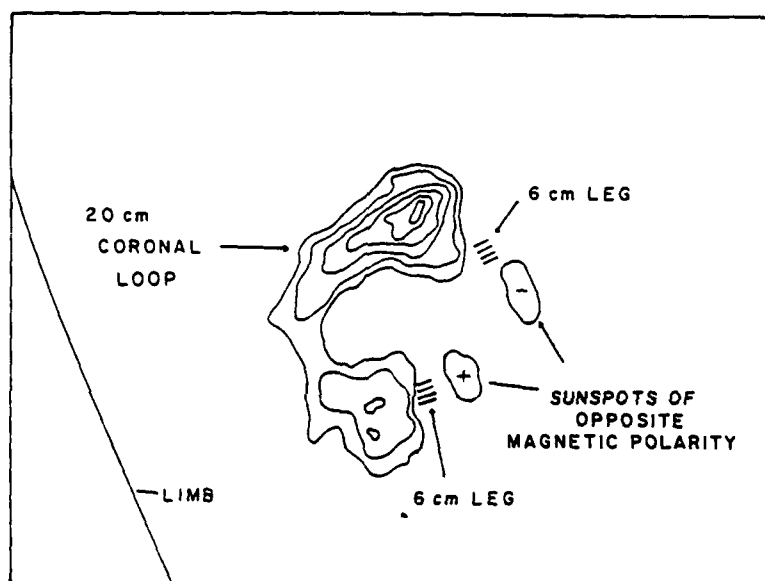


Figure 1. A VLA synthesis map of the total intensity, I , of the 20 cm emission from a coronal loop. The contours mark levels of equal brightness temperature corresponding to 0.2, 0.4, ...1.0 times the maximum brightness temperature of $T_b = 2 \times 10^6$ K. A schematic portrayal of the 6 cm emission, which comes from the legs of the magnetic loops, has been added together with the underlying sunspots that are detected at optical wavelengths.

Multiple-wavelength synthesis observations with the Very Large Array (VLA) have been carried out at wavelengths $\lambda = 20, 6$ and 2 cm (see Figure 1). The radiation at 20 cm can originate at both the apex and legs of coronal loops, and sometimes delineates the hot, dense plasma detected at X-ray wavelengths. The 20-cm coronal loops have brightness temperatures $T_b = 1 \times 10^6$ to 4×10^6 K and extents of $L = 10^9$ to 10^{10} cm. Magnetic field strengths of $H \sim 145$ G have been inferred from cyclotron lines at the apex of the 20-cm loops. Bright, highly polarized 6-cm cores often mark the legs of dipolar loops with $T_b = 2 \times 10^6$ to 5×10^6 K and heights $h \approx 10^9$ cm above the underlying sunspots. Values of H of ~ 600 to 900 G are inferred from the fact that these cores emit gyro radiation at the second or third harmonic of the gyrofrequency. The 2-cm emission has brightness temperatures of $T_b \approx 10^5$ K and often overlies sunspots at heights $h \approx 5 \times 10^8$ cm where H is $\approx 10^3$ G.

The 20-cm coronal loops have been discussed by Velusamy and Kundu (1981), Lang, Willson and Rayrole (1982), Dulk and Gary (1983), and McConnell and Kundu (1984). Multiple-wavelength VLA observations at 2, 6 and 20 cm have been presented by Lang, Willson and Gaizauskas (1983), Shevgaonkar and Kundu (1984), Kundu and Lang (1985) and Kundu (1986 - this proceedings). Most recently, Gary and Hurford (1986) have used microwave spectroscopy during a solar eclipse to delineate the physical conditions at a variety of levels within the legs and apex of a coronal loop (see Figure 2).

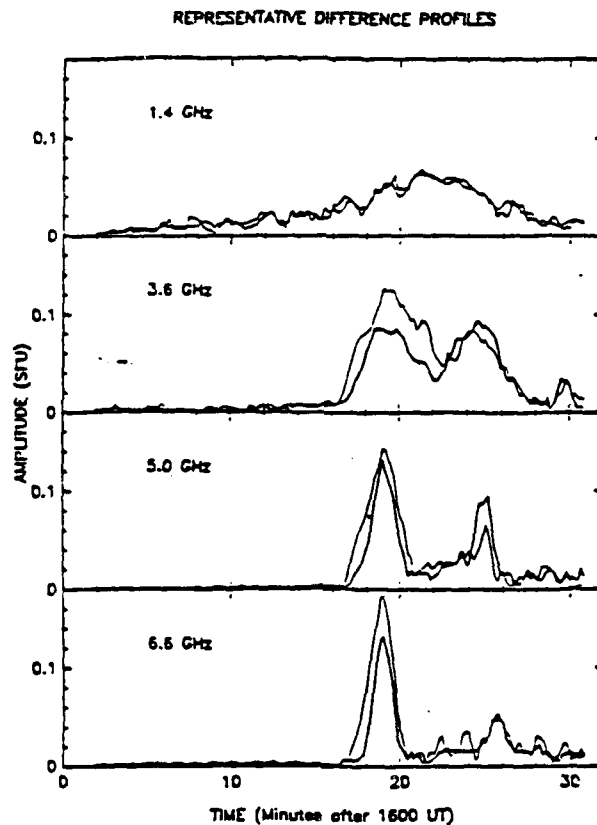


Figure 2. Differenced OVRO time profiles at four representative frequencies. Right hand circular (RH) polarization is shown by the heavy lines, and left hand (LH) polarization by the light lines. Below 3 GHz, the active region appears as a single board source. At higher frequencies, the region bifurcates into two main sources, becoming more localized to the sunspots as the observing frequency increases. The sense of polarization in the two spot sources is consistent with gyroresonance emission.

RADIATION MECHANISMS OF CORONAL LOOPS

The quiescent, or non-flaring, radiation of coronal loops is usually thermal in nature. The soft X-ray radiation is, for example, attributed to the thermal bremsstrahlung of hot million-degree electrons. However, at centimeter wavelengths there are two different thermal mechanisms: the bremsstrahlung of thermal electrons accelerated in the electric field of ions and the gyroresonant radiation of thermal electrons accelerated by magnetic fields can contribute to the emission. While the thermal bremsstrahlung emission is sensitive to the electron temperature and emission measure, gyroresonant emission is sensitive to the local magnetic field and electron temperature. It is this gyroresonant radiation which provides a sensitive measure of coronal magnetic field strength. Thus, it is important to distinguish which of these mechanisms is responsible for the emission from any given source at these wavelengths.

Strong evidence for thermal gyroradiation at coronal levels above sunspots has been provided by comparing the soft X-ray and centimeter-wavelength radiation of active regions [Kundu, Schmahl and Gerassimenko (1980); Pallavicini, Sakurai and Vaiana (1981); Schmahl et al. (1982)]. Although there is intense X-ray emission from the apex of coronal loops, the X-ray radiation often falls to undetectable levels in the legs of coronal loops above sunspots. Yet, intense radio radiation has sometimes been observed from both the apex and the legs of coronal loops. At other times radio emission has been detected from just the apex or just the legs of the loops, depending on the wavelength and observing conditions.

The near equality of the radio brightness and electron temperatures indicates that the radio emission from coronal loops is usually thermal. But the low electron densities inferred from the X-ray data above sunspots indicate that thermal bremsstrahlung is too weak to account for the intense radio radiation. The extra source of opacity has been attributed to gyroresonance absorption at the second or third harmonic of the gyrofrequency.

GYRORESONANT EMISSION



Figure 3. A Westerbork Synthesis Radio Telescope synthesis map of circular polarization at $\lambda = 6$ cm overlaid on an H α photograph obtained from the observatory at Athens. The contours are in steps of 1.5×10^5 K. The circularly polarized horseshoe structure that rings the sunspot umbra is due to gyroresonant emission in the curved magnetic fields of the sunspot penumbra.

Thermal gyroradiation at coronal levels above sunspots has been additionally confirmed by the detection of circularly polarized ring-shaped or horseshoe structures at 6 cm wavelength [Alissandrakis and Kundu (1982); Lang and Willson (1982)]. The highly-polarized (up to 100 percent) structures were predicted by the theory of gyroradiation in the curved magnetic fields above sunspot penumbrae [Gel'freikh and Lubyshev (1979)]. There is no detectable circular polarization above the central sunspot umbrae where the magnetic fields project radially upward into the hot coronal regions (see Figure 3). Depressions in the radio brightness temperature above sunspot umbrae have been attributed to cool material in these regions [Strong, Allisandrakis and Kundu(1984)].

At the longer, 20 cm, wavelength, emission is detected sometimes from both the apex and the legs of coronal loops (Lang, Willson, Strong, and Smith, 1986, and see Figure 4), and sometimes from just the apex (Webb et al., 1986). In the latter case, the electron densities and temperatures inferred from the X-ray spectral lines indicate that the plasma is optically thick at 20 cm, and hence that the observed brightness temperature should be equal to the electron temperature. However, the observed brightness temperature is a factor of 2 - 3 lower than the local electron temperature. Brosius and Holman (1986--this proceedings) and Holman (1986--this proceedings) explain this low brightness temperature in terms of a relatively cool, $<10^5$ K external plasma around the hot 2.5×10^6 K loops. Such material absorbs emissions primarily from the loop footpoints, where the optical depth along the line of sight is greatest. The loops and the external plasma are separated by a thin transition zone. The emission measure distributions for such models have been calculated, and have been found not only to agree well with recent observational emission measure curves for solar active region loops, but also to rise on both the cool and the hot side of the emission measure minimum. This is the first time that a theoretical emission measure curve for a single active region loop has been found to do this (cf. Antiochos and Noci, 1986).

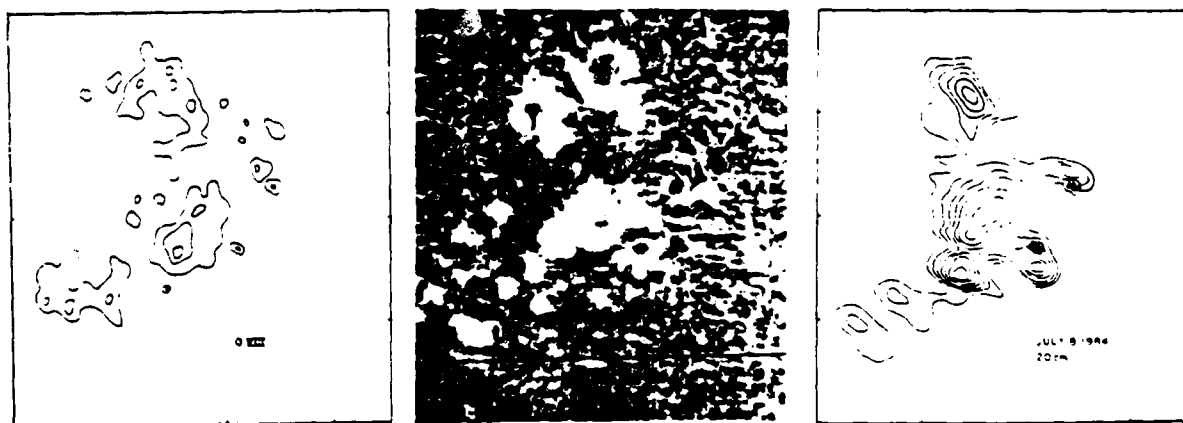


Figure 4. A comparison of the soft X-ray (S.M.M.-left), H (SOON-middle) and 20 cm (V.L.A.-right) emission of an active region on the same day. The most intense soft X-ray emission is well correlated with intense 20 cm and H emission; but the 20 cm emission also extends across the areas near the sunspots where it is also intense. The angular spacing between fiducial marks on the axes is 60 arc-seconds.

Alternative radiation mechanisms may be required for intense radio emission from regions overlying weak photospheric magnetic fields. Observations of these regions have been reported by Akmedov et al. (1986), Lang (1986a-this proceedings), Lang and Willson (1986a-this proceedings), Webb, Davis, Kundu and Velusamy (1983), and Willson and Lang (1986). A possible explanation, first studied in detail by Chiuderi, Drago and Melozzi (1984), is the nonthermal synchrotron emission of mildly relativistic electrons; but some currently-unspecified mechanism must be accelerating the electrons. An equally plausible explanation is that currents amplify the magnetic field in the low solar corona to strengths that are a factor of ten larger than those inferred from magnetograms of the underlying photosphere. The observed radio emission might then be attributed to the gyroradiation of thermal electrons at the second and third harmonic of the gyrofrequency.

SPECIFYING THE CORONAL MAGNETIC FIELD

Measurements of the spectrum, polarization and angular size of active region sources at centimeter wavelengths have been pioneered by Soviet astronomers using the RATAN 600 [Radio Astronomy Telescope of the Academy of Sciences (Nauk)-see Akmedov et al. (1986)], and further developed and extended using the frequency-agile interferometer at the OVRO [Owens Valley Radio Observatory-see Hurford and Gary (1986) this proceedings]. By measuring both the angular size and the flux density at a variety of wavelengths, one can uniquely determine the brightness temperature spectrum of the sources. Circular polarization data can additionally be used to specify the magnetic field strength. Hurford and Gary (1986-this proceedings) have used this technique of microwave spectroscopy to measure the field distribution in the lower corona above sunspots.

In fact, both the strength and structure of the coronal magnetic field can be specified along the legs of coronal loops where gyroradiation dominates. The observations indicate that the magnetic fields systematically diverge and decrease in strength at higher heights (longer wavelengths) above single sunspots [see Hurford and Gary (1986) - this proceedings].

The magnetic field strength can also be inferred from individual cyclotron lines when gyroradiation dominates the emission. The observations at a single wavelength refer to a predetermined height where the radiation frequency is at one of the low harmonics of the gyrofrequency. Multiple-frequency observations provide information at a fixed height, regardless of field strength.

Holman and Kundu (1985) and Holman (1986 - proceedings) have pointed out that the emitting layers might be spatially resolved when a thin loop is observed. The magnetic field strength within each layer can then be inferred from the observing wavelength and the relevant harmonic. However, the cyclotron lines may overlap when the loop is thick or when a thin loop is observed along its legs.

The spectrum of an individual cyclotron line may also be obtained when observing at several wavelengths. For example, the spectra of individual cyclotron lines have been observed at wavelengths near 20 cm when the apex of a coronal loop is resolved [Willson (1985), Lang (1986a-this proceedings), Lang, Willson, Strong and Smith (1986)]. This is because the magnetic field strength is relatively constant near the loop apex; the cyclotron lines would merge into a continuum along the loop legs where the magnetic field strength decreases uniformly with height. Neutral current sheets might also play a role, leading to intense radio emission from a thin layer near the loop apex. Both a uniform field and a steep temperature gradient in the uniform region are probably required to detect the cyclotron lines. In any event observations of individual cyclotron lines indicate magnetic field strengths of $H = 145 \pm 5$ G at the apex of some coronal loops.

Solar bursts might also be used to infer the strength and configuration of coronal magnetic fields. Roberts, Edwin and Benz (1984) and Roberts (1984, 1986 - proceedings) have shown that bursts can impulsively generate magneto-acoustic oscillations in a coronal loop. These oscillations may be observed as quasi-periodic radio variations whose onset, duration and periodicity can be used to infer the height, size and magnetic field strength of the emitting region.

THE CORONAE OF NEARBY STARS

Nearby main-sequence stars of late spectral type exhibit quiescent, or non-flaring, X-ray emission whose absolute luminosity may be as much as 100 times that of the Sun [Vaiana et al. (1981)]. This suggests that these stars have hot stellar coronae with large-scale coronal loops and strong magnetic fields. The solar analogy suggests that these coronae might also be detected at radio wavelengths.

Nearby dwarf M flare stars do, in fact, exhibit slowly varying radio emission at 6 and 20 cm wavelength that is analogous to that of solar active regions. However, the X-ray observations rule out detectable thermal bremsstrahlung at radio wavelengths; the temperatures and emission measures inferred from the X-ray data indicate that the radio bremsstrahlung would be at least two orders of magnitude below detection thresholds. Moreover, thermal gyroradiation is an unlikely source of the intense 20 cm radiation from some of these stars; implausibly large coronal loops would have to be up to 10 times larger than the star with magnetic field strengths larger than 100 G at these remote distances. The most likely source of this slowly varying radiation in M-dwarf stars is gyrosynchrotron radiation from nonthermal electrons (Holman, 1986; Lang and Willson, 1986b).

In other words, the fact that we detect radio emission from these stars means that something unusual is happening on them. As an example, radio bursts from the dwarf M₁ stars have been attributed to coherent emission mechanisms like electron-cyclotron masers or coherent plasma radiation [Melrose and Dulk (1982); Dulk (1985)].

Quasi-periodic and individual spikes have been detected from the dwarf M star AD Leonis at 20 cm wavelength [Lang et al. (1983), Lang and Willson (1986a), Lang (1986a)-this proceedings]. These spikes are up to 100% circularly polarized with rise times less than 5 milliseconds. The rapid rise time indicates that the emitter's size is less than 0.005 of the star's radius, and that a symmetric emitter has a brightness temperature in excess of 10^{16} K. Such a high brightness temperature requires a coherent radiation mechanism. Similar high brightness temperature spikes

have been observed during solar flares. Unlike solar flares, however, the underlying nonspiky emission from the AD Leonis flare is probably also coherent [Holman, Bookbinder and Golub (1985)].

Coherent emission is also suggested by the narrow-band, slowly varying, 20-cm emission from the dwarf M star YZ Canis Minoris [Lang and Willson (1986)], as well as narrow-band 20 cm flares from the red dwarf stars AD Leo and UV Ceti [White, Kundu and Jackson (1986)]. The narrow-band structure cannot be explained by continuum emission processes such as thermal bremsstrahlung, thermal gyroradiation, or nonthermal gyrosynchrotron radiation. Coherent radiation processes seem to be required.

If the radiation is emitted by an electron-cyclotron maser at the second harmonic of the gyrofrequency, then the magnetic field strength is $H = 250$ G, and constraints on the plasma frequency imply an electron density of $N_e \approx 6 \times 10^9 \text{ cm}^{-3}$. Coherent plasma radiation at the first or second harmonic of the plasma frequency respectively require $N_e = 2 \times 10^{10} \text{ cm}^{-3}$ and $H \ll 500$ G or $N_e = 6 \times 10^9 \text{ cm}^{-3}$ and $H \ll 250$ G. Thus, the coherent burst mechanisms suggest that the coronae of dwarf M stars have physical parameters similar to those of solar active regions.

FUTURE PROSPECTS FOR CORONAL DIAGNOSTICS

Probable observations of coherent radiation processes on nearby stars are stimulating further searches for coherent signatures in the Sun's radio radiation. In fact, narrow-band structure has been observed in a solar burst [Lang and Willson (1984); Lang (1986b)], and rapid spikes during some solar bursts have been interpreted in terms of electron-cyclotron masers [Holman, Eichler and Kundu (1980); Holman (1983)]. Future observations with high resolution in time and frequency at the VLA, OVRO and Nancay will help determine the role that coherent radiation processes play in solar active regions.

The next decade will also include detailed comparisons of radio and X-ray observations with model coronal loops that include both thermal bremsstrahlung and thermal gyroradiation. Coronal magnetic fields may be directly inferred from observations and models in which the expected radio emission is computed as a function of wavelength, polarization and viewing angle. A comparison of the observed radiation with theoretical expectations will determine magnetic field strengths, electron densities and electron temperatures.

The evolution of coronal loops has strong future potential. Of special interest are the preheating and magnetic changes that trigger solar bursts [see Kundu and Lang (1985) for a review]. Emerging coronal loops and the magnetic interaction of existing coronal loops will be particularly interesting topics.

Future studies of the evolution of the three-dimensional magnetic and plasma structure of coronal loops will lead to valuable new insights to the nature of solar active regions and eruptions on the Sun and nearby stars. Such insights can only be fully realized by the development of a solar-stellar synthesis radiotelescope. Such an instrument would be dedicated to solar and stellar observations with high angular, temporal and frequency resolution.

ACKNOWLEDGEMENTS

Radio astronomical studies of the Sun at Tufts University are supported under Air Force Office of Scientific Research grant AFOSR-83-0019 and contract N0014-86-K-0068 with the Office of Naval Research. Our simultaneous VLA and Solar Maximum Mission satellite observations of the Sun are supported under NASA grant NAG 5-501.

REFERENCES

- Akhmedov, S.B., et al., 1986, "Structure of a Solar Active Region from RATAN 600 and Very Large Array Observations," *Astrophys. J.*, 301, 460-464.
- Alissandrakis, C.E. and M.R. Kundu, 1982, "Observations of Ring Structure in a Sunspot Associated Source at 6 Centimeter Wavelength," *Astrophys. J. (Letters)*, 253, L49-L52.
- Alissandrakis, C.E. and M.R. Kundu, 1984, "Center-to-Limb Variation of a Sunspot-Associated Microwave Source," *Astron. Astrophys.*, 139, 271-284.
- Antiochos, S.K. and G. Noci, 1986 "The Structure of the Static Corona and Transition Region," *Astrophys. J.*, 301, 440-447
- Brosius, J.W. and G.D. Holman, 1986, "Theoretical Models of Free-Free Microwave Emission from Solar Magnetic Loops," this Proceedings.
- Chiuderi-Drago, F. and M. Melozzi, 1984, "Non-Thermal Radio Sources in Solar Active Regions," *Astron. Astrophys.* 131, 103-110.
- Dulk, G.A., 1985, "Radio Emission from the Sun and Stars," *Ann. Rev. Astron. Ap.*, 23, 169-180.
- Dulk, G.A. and D.E. Gary, 1983, "The Sun at 1.4 GHz: Intensity and Polarization," *Astron. Astrophys.* 124, 103-107.
- Gary, D.E. and G.J. Hurford, 1986, "Multi-Frequency Observations of a Solar Active Region During a Partial Eclipse, BBSO 259, submitted to *Astrophys. J.*
- Gel'friekh, G.B. and B.I. Lubyshev, 1979, "Structure of Local Sources of the S Component of Solar Radio Emission," *Sov. Astron. A.J.*, 23, 316-322.
- Holman, G.D., 1983, "Some Recent Results in the Interpretation of High Brightness Temperature Microwave Spike Emission," *Adv.Space Res.*, 2, No.11, 181-183
- Holman, G.D., 1986, "Coronal Heating and the X-ray and Microwave Emission from M-Dwarf Flare Stars," in Proceedings of the Fourth Cambridge Workshop on Cool Stars, Stellar Systems, and the Sun, eds. M. Zeilik and D.M. Gibson (Springer-Verlag), in press.
- Holman, G.D., 1986, "High-Spatial-Resolution Microwave and Related Observations as Diagnostics of Coronal Loops," - this Proceedings.
- Holman, G.D., J. Bookbinder and L. Golub, 1985, "Implications of the 1400 MHz Flare Emission from AD Leo for the Emission Mechanism and Flare Environment," in *Radio Stars*, ed. R.M. Hjellming and D.M. Gibson, (Dordrecht: Reidel), 35-37.
- Holman, G.D., D. Eichler and M.R. Kundu, 1980, "An Interpretation of Solar Flare Microspikes as Gyrosynchrotron Maser," in *Radio Physics of the Sun - I.A.U. Symposium No. 86*, ed. M.R. Kundu and T.E. Gergely, (Dordrecht: Reidel), 457-459.
- Holman, G.D. and M.R. Kundu, 1985, "The Microwave Structure of Hot Coronal Loops," *Astrophys. J.*, 292, 291-296.
- Hurford, G.J. and D.E. Gary, 1986, "Measurement of Coronal Fields Using Spatially Resolved Microwave Spectroscopy," - this Proceedings.
- Kundu, M.R., 1986, "Three Dimensional Structures of Solar Active Regions," this Proceedings."

- Kundu, M.R. and C.E. Alissandrakis, 1984, "Structure and Polarization of Active Region Microwave Emission," *Solar Phys.*, 94, 249-283.
- Kundu, M.R. and K.R. Lang, 1985, "The Sun and Nearby Stars," *Science*, 228, 9-15.
- Kundu, M.R., E.J. Schmahl and M. Gerassimenko, 1980, "Microwave, EUV and X-ray Observations of Active Region Loops: Evidence for Gyroresonance Absorption in the Corona," *Astron. Astrophys.* 82, 265-271.
- Kundu, M.R. and T. Velusamy, 1980, "Observation with the VLA of a Stationary Loop Structure in the Sun at 6 cm Wavelength," *Astrophys. J. (Letters)*, 240, L63-L65.
- Lang, K.R., 1986a, "Coronal Plasmas on the Sun and Nearby Stars," this Proceedings.
- Lang, K.R., 1986b, "Flare Stars and Solar Bursts: High Resolution in Time and Frequency," *Solar Phys.*, in press.
- Lang, K.R., J. Bookbinder, L. Golub and M. Davis, 1983, "Bright, Rapid, Highly Polarized Radio Spikes from the M Dwarf AD Leo," *Astrophys. J. (Letters)*, 272, L15-L18.
- Lang, K.R. and R.F. Willson, 1982, "Polarized Horseshoes Around Sunspots at 6 Centimeter Wavelength," *Astrophys. J. (Letters)*, 255, L111-L117.
- Lang, K.R. and R.F. Willson, 1983, "Multiple Wavelength Observations of Flaring Active Regions," *Adv. Space Res.* 2, No. 11, 91-100.
- Lang, K.R. and R.F. Willson, 1984, "V.L.A. Observations of Flare Build-Up in Coronal Loops," *Adv. Space Res.* 4, No. 7, 105-110.
- Lang, K.R. and R.F. Willson, 1986a, "Compact, Variable, Moving Sources on the Sun at 2 Centimeters Wavelength," this Proceedings.
- Lang, K.R. and R.F. Willson, 1986b, "Narrow-Band, Slowly Varying Decimetric Radiation from the Dwarf M Flare Star YZ Canis Minoris," *Astrophys. J. (Letters)*, 302, L17-L21.
- Lang, K.R. and R.F. Willson, 1986c, "Millisecond Radio Spikes from the Dwarf M Flare Star AD Leonis," *Astrophys. J.*, in press.
- Lang, K.R., R.F. Willson and V. Gaizauskas, 1983, "Very Large Array Observations of Solar Active Regions III. Multiple Wavelength Observations," *Astrophys. J.*, 267, 455-464.
- Lang, K.R., R.F. Willson and J. Rayrole, 1982, "Very Large Array Observations of Coronal Loops at 20 Centimeter Wavelength," *Astrophys. J.*, 258, 384-387.
- Lang, K.R., R.F. Willson, K.T. Strong and K.L. Smith, 1986a, "Physical Parameters of a Solar Active Region Inferred from Thermal Cyclotron Lines and Soft X-Ray Spectral Lines," *Astrophys. J.*, to be submitted.
- Lang, K.R., R.F. Willson, K.T. Strong and K. L. Smith, 1986b, "Simultaneous Solar Maximum Mission and Very Large Array Observations of Solar Active Regions," *Astrophys. J.*, to be submitted.
- McConnell, D. and M.R. Kundu, 1983, "VLA Observations of a Solar Active Region and Coronal Loops," *Astrophys. J.*, 269, 698-705.
- Melrose, D.B. and G.A. Dulk, 1982, "Electron-Cyclotron Masers as the Source of Certain Solar and Stellar Bursts," *Astrophys. J.*, 259, 844-858.
- Pallavicini, R., T. Sakurai and G.S. Vaiana, 1981, "X-Ray, EUV and Centimetric Observations of Solar Active Regions: an Empirical Model for Bright Radio Sources," *Astron. Astrophys.*, 98, 316-327.
- Roberts, B., 1984, "Waves in Inhomogeneous Media," in *The Hydrodynamics of the Sun*, ESA SP-220, November.
- Roberts, B., 1986, "Guided MHD Waves as a Coronal Diagnostic Tools," this Proceedings.
- Roberts, B., P.M. Edwin and A.O. Benz, 1984, "On Coronal Oscillations," *Astrophys. J.*, 279, 857-865.
- Schmahl, E.J., et al., 1982, "Active Region Magnetic Fields Inferred from Simultaneous VLA Microwave Maps, X-Ray Spectroheliograms, and Magnetograms," *Solar Physics* 80, 233-249.

- Shevgaonkar, R.K. and M.R. Kundu, 1984, "Three-Dimensional Structures of Two Solar Active Regions from VLA Observations at 2, 6 and 20 Centimeter Wavelengths" *Astrophys. J.*, 283, 413-420.
- Strong, K.T., C.E. Alissandrakis and M.R. Kundu, 1984, "Interpretation of Microwave Active Region Structures Using SMM Soft X-Ray Observations," *Astrophys. J.*, 277, 865-873.
- Vaiana, G.S. and R. Rosner, 1978, "Recent Advances in Coronal Physics," *Ann. Rev. Astron. Ap.* 16, 393-405.
- Vaiana, G.S., et al., 1981, "Results From An Extensive Einstein Stellar Survey," *Astrophys. J.*, 245, 163-182.
- Velusamy, T. and M.R. Kundu, 1981, "VLA Observations of Postflare Loops at 20 Centimeter Wavelength," *Astrophys. J. (Letters)*, 243, L103-L107.
- Webb, D.F., J.M. Davis, M.R. Kundu and T. Velusamy, 1983, "X-Ray and Microwave Observations of Active Regions," *Solar Phys.* 85, 267-283.
- Webb, D.F., G.D. Holman, J.M. Davis, M.R. Kundu and R.K. Shevgaonkar, 1986, "The Plasma and Magnetic Field Properties of Coronal Loops Observed At High Spatial Resolution," submitted to *Astrophys. J.*
- White, S.M., M.R. Kundu and P.D. Jackson, 1986, "Narrowband Radio Flares from Red Dwarf Stars," *Astrophys. J.*, submitted.
- Willson, R.F., 1983, "Possible Detection of Thermal Cyclotron Lines from Small Sources Within Solar Active Regions," *Solar Phys.*, 89, 103-113.
- Willson, R.F., 1985, "VLA Observations of Solar Active Regions at Closely Spaced Frequencies: Evidence for Thermal Cyclotron Line Emission," *Astrophys. J.*, 298, 911-917.

25. NARROW-BAND, SLOWLY VARYING DECIMETRIC RADIATION FROM THE DWARF M FLARE STAR YZ CANIS MINORIS

KENNETH R. LANG AND ROBERT F. WILLSON

Department of Physics and Astronomy, Tufts University

Received 1985 September 24; accepted 1985 December 13

ABSTRACT

Narrow-band, slowly varying microwave radiation has been detected from the dwarf M star YZ Canis Minoris at frequencies near 1465 MHz. This quiescent, or nonflaring, emission cannot be attributed to gyroresonant radiation from coronal loops; the loops would have to be more than 200 times the stellar radius in size with magnetic field strengths of $H \geq 100$ G at this distance. The narrow-band structure ($\Delta\nu/\nu \leq 0.1$) of the slowly varying radiation cannot be explained by continuum emission processes such as thermal bremsstrahlung, thermal gyroresonant radiation, or nonthermal gyrosynchrotron radiation. Our observations may be explained by coherent burst mechanisms like electron-cyclotron masers or coherent plasma radiation. Maser action at the second harmonic of the gyrofrequency implies a longitudinal magnetic field strength of 250 G and an electron density of $N_e = 6 \times 10^9 \text{ cm}^{-3}$. Coherent plasma radiation at the second harmonic of the plasma frequency similarly requires $N_e = 6 \times 10^9 \text{ cm}^{-3}$ but a longitudinal magnetic field strength of $H_l \ll 250$ G. The slow variation of the narrow-band emission might be explained by the stochastic nature of continued low-level, coherent burst activity. There are possible analogies with narrow-band decimetric bursts observed on the Sun.

Subject headings: stars: corone — stars: flare — stars: radio radiation

1. INTRODUCTION

Nearby main-sequence stars of late spectral type exhibit quiescent, or nonflaring, X-ray emission whose absolute luminosity may be as much as 100 times that of the Sun (Johnson 1981; Vaiana *et al.* 1981). This suggests that these stars may have hot stellar coronae and large-scale coronal loops with strong magnetic fields. Quiescent microwave radiation might be emitted by electrons trapped within stellar loops or by electrons spiraling about magnetic fields above starspots.

Quiescent microwave emission has, in fact, been detected from six dwarf M stars using the Very Large Array (VLA). They are UV Ceti (Gary and Linksy 1981), both components of the binary star system EQ Pegasi (Topka and Marsh 1982), YY Geminorum and Wolf 630 (Linksy and Gary 1983), the suspected spectroscopic binary AU Microscopii (Cox and Gibson 1985), and YZ Canis Minoris (Pallavicini, Willson, and Lang 1985; Kundu and Shevgaonkar 1985). YZ Canis Minoris is curiously unique in being the only single, or nonbinary, dwarf M star that is known to exhibit quiescent microwave radiation.

The quiescent radiation from dwarf M stars is slowly variable over time scales of hours (Linksy and Gary 1983; Pallavicini, Willson, and Lang 1985). An example is shown in Figure 1 where the 6 cm flux density from YZ Canis Minoris rises to 7 mJy over periods of half an hour. Kundu and Shevgaonkar (1985) have pointed out that the microwave radiation from this star is highly variable with a flux density that varied by a factor of 5 in 2 days and reached a peak value of 3 mJy at 20 cm wavelength, but their 2 hr synthesis maps may have underestimated the peak flux density of the slowly

varying component that varies on time scales shorter than 2 hr. In addition, Rondonò *et al.* (1984) have reported variable microwave radiation from YZ Canis Minoris at 6 cm wavelength with a peak flux density of 5 mJy and a duration of ≥ 30 minutes. If this was the slowly varying radiation illustrated in Figure 1, its association with an ultraviolet flare that occurred 7 minutes earlier may have been purely coincidental.

Most of the dwarf M stars detected at microwave wavelengths exhibit X-ray radiation with absolute X-ray luminosities of $L_x = 10^{27.5}$ ergs s^{-1} (UV Ceti), $10^{28.8}$ ergs s^{-1} (EQ Peg), $10^{29.6}$ ergs s^{-1} (YY Gem), $10^{29.3}$ ergs s^{-1} (Wolf 630), and $10^{28.5}$ ergs s^{-1} (YZ CMi). By way of comparison, the Sun has an average $L_x = 10^{27.0}$ ergs s^{-1} that is attributed to thermal bremsstrahlung of hot electrons trapped in the ubiquitous coronal loops that dominate the structure of the solar corona. This suggests that the slowly varying, quiescent microwave radiation of dwarf M stars may be due to thermal electrons trapped in extensive coronal loops.

The X-ray observations rule out detectable thermal bremsstrahlung at microwave wavelengths; the temperatures and emission measures inferred from the X-ray data indicate that the microwave bremsstrahlung flux density is at least two orders of magnitude below the detection threshold of the VLA. Thermal gyroresonant, or cyclotron, radiation might nevertheless account for the quiescent microwave emission from dwarf M stars. This process explains most, if not all, of the quiescent microwave emission from coronal loops on the Sun (Kundu and Lang 1985). However, gigantic coronal loops with intense magnetic fields (several hundred gauss) and enormous heights of three stellar radii are required to explain the

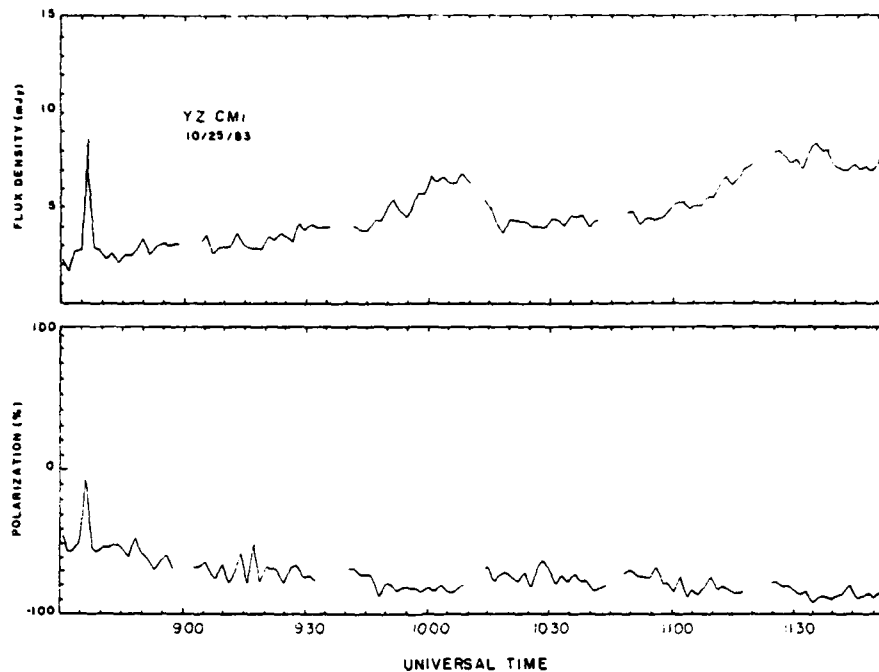


FIG. 1.—A plot of the total intensity I (top) and degree of circular polarization, p_c (bottom) observed at 4885 MHz from the dwarf M star YZ CMi on 1983 October 25. A circularly polarized impulsive (≤ 20 s) burst and circularly polarized, slowly varying (~ 1 hr) radiation are observed. The visibility data were phase shifted to source center and then averaged, baseline by baseline, over a 30 s interval. They were then vector averaged to produce these time profiles. The theoretical 3σ noise level of these data is ~ 1.35 mJy.

6 cm (or 5000 MHz) emission from dwarf M stars. Gyroresonance radiation of thermal electrons in extensive coronae was nevertheless once believed to be the most likely explanation for the slowly varying quiescent emission from these stars (Gary and Linsky 1981; Topka and Marsh 1982).

An alternative microwave emission mechanism is nonthermal gyrosynchrotron emission by mildly relativistic electrons (Linsky and Gary 1983; Pallavicini, Willson, and Lang 1985). An attractive aspect of this mechanism is that the emitting sources can be relatively small with sizes comparable to those of starspots. The unattractive aspect of the nonthermal gyrosynchrotron hypothesis is that the mildly relativistic electrons must be accelerated more or less continuously in the magnetic fields of starspots.

Our recent VLA observations of YZ CMi indicate that neither thermal gyroresonant radiation nor nonthermal gyrosynchrotron radiation can account for the slowly varying, quiescent microwave radiation of this star. In § II we present observations of the slowly varying radiation with a maximum flux density of 20 mJy and narrow-band frequency structure ($\Delta\nu/\nu \leq 0.1$) at frequencies near 1465 MHz. Possible explanations for this radiation are examined in § II. Thermal gyroresonant radiation would require impossibly large coronal loops and magnetic field strengths. The narrow-band structure cannot be explained by continuum emission processes such as thermal bremsstrahlung, thermal gyroresonant radiation, or nonthermal gyrosynchrotron radiation. Coherent burst mechanisms seem to be required.

II. OBSERVATIONS

The dwarf M star YZ Canis Minoris (GL 285, dM4.5e) was observed with two subarrays of the VLA on 1984 December 10 in the A configuration. One subarray of 13 antennas had signal frequencies of 1415 MHz and 1515 MHz, and the other subarray of 14 antennas had signal frequencies of 4835 MHz and 4885 MHz. The bandwidth at all four frequencies was 50 MHz. The total intensity, I , and circular polarization, p_c , or Stokes parameter V , were sampled for every 10 s, and the data were calibrated by observing 3C 286 (14.51 Jy at 1415 MHz and 7.4 Jy at 4885 MHz) and 0735+178 (2.2 Jy at 1415 MHz and 2.1 Jy at 4885 MHz).

The calibrated visibility data were used to construct a 4.5 hr synthesis map of the unresolved source. The calibrated data were then phase shifted to bring the microwave source exactly at the center of the 4.5 hr map. There were no confusing sources in the field of view.

The calibrated, phase-shifted visibility data were then averaged, baseline by baseline, with running means over a 1.5 minute time interval, and then vector averaged. The theoretical 3σ noise level obtained in this way was 2.3 mJy at 4885 MHz and 2.9 mJy at 1415 MHz. The total intensity at 1415 MHz and 1515 MHz exhibited slowly varying fluctuations of as much as 20 mJy, which is well above the noise level (see Fig. 2). However, there were no detectable variations at 4885 MHz for this observation.

An examination of the calibration amplitudes at the times of the gaps in Figure 2 indicates that they are constant and

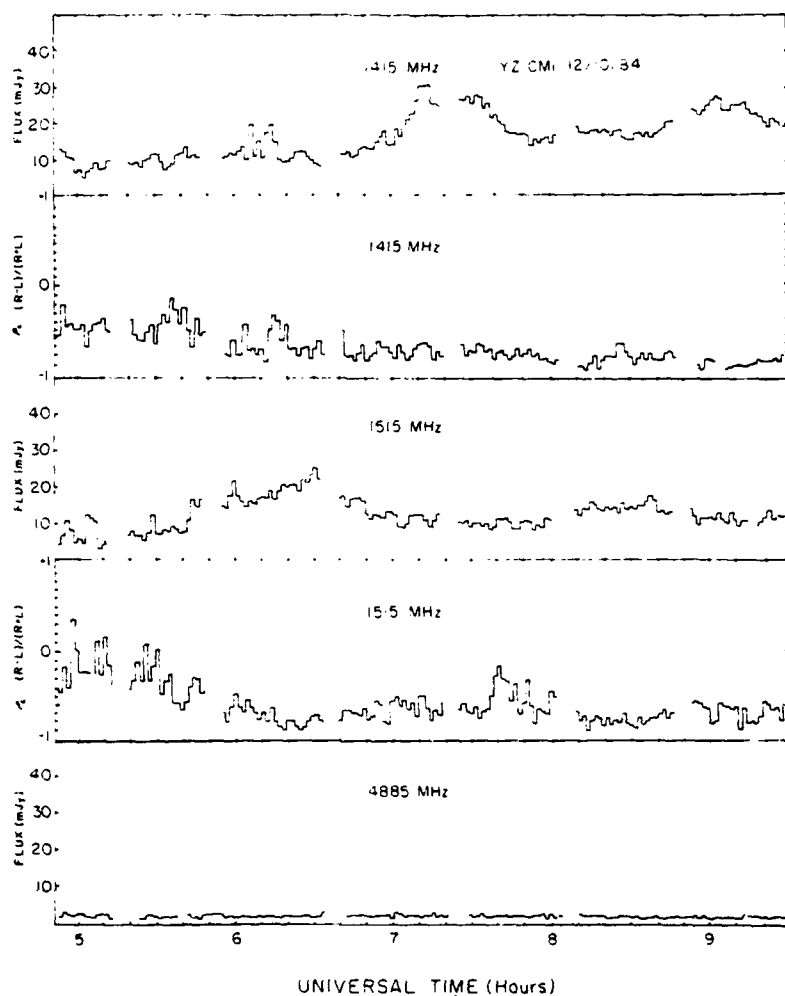


FIG. 2.—Plots of the slowly varying emission from the dwarf M flare star YZ CMi observed at two closely spaced frequencies of 1415 MHz and 1515 MHz and at 4885 MHz on 1984 December 10. Both the total intensity (flux) and degree of circular polarization (p_c) are plotted as a function of time. Notice that the total intensity at two frequencies separated by 100 MHz near 1465 MHz peak at different times, indicating a narrow-band radiation mechanism. Also notice that there are no detectable variations at 4885 MHz on this day. Here the visibility data were phase shifted to source center and then averaged, baseline by baseline, over a 1.5 minute interval. They were then vector averaged to produce time profiles with 3σ noise levels of 2.9 mJy at 1415 MHz and 1515 MHz and 2.3 mJy at 4885 MHz. No quiescent emission was detected at 6 cm where the plot represents the nonzero vector-averaged noise level.

have the same value at 1415 MHz and 1515 MHz within the 5σ noise level of 3.3 mJy for the 3 minute calibration interval. Changing calibrator amplitudes therefore do not produce the flux variations shown in Figure 2. This is confirmed by the unchanging peak-to-peak noise level of about 3 mJy depicted in the figure.

The interesting aspect of Figure 2 is that the slow variations in total intensity peak at different times for frequencies $\nu = 1415$ and 1515 MHz, indicating narrow-band structure of bandwidth $\Delta\nu \ll 100$ MHz, or $\Delta\nu/\nu \ll 0.1$. This narrow-band structure was confirmed by constructing snapshot synthesis maps over time intervals of 1.5 minutes centered at 06:20 UT and 07:30 UT (Fig. 3). The snapshot maps had an effective half-power beamwidth of $1''.0 \times 1''.6$. The maximum flux values at 06:20 were 14 and 22 mJy per beam area at 1415

and 1515 MHz, respectively, while at 07:30 they were 25 and 10 mJy per beam area at 1415 and 1515 MHz, respectively.

Although 1415 MHz and 1515 MHz lie outside the protected band for radio astronomy, there was no indication of interference. This is reflected by the unchanging calibrator amplitudes and the absence of interference patterns in the 1.5 minute maps (Fig. 3) and in a 2 hr map (not shown).

III. DISCUSSION

What accounts for the observed narrow-band structure? Continuum emission processes like thermal bremsstrahlung, thermal gyroresonant radiation, or gyrosynchrotron radiation will not normally exhibit such spectral features. Of course, thermal electrons gyrate around magnetic fields, emitting

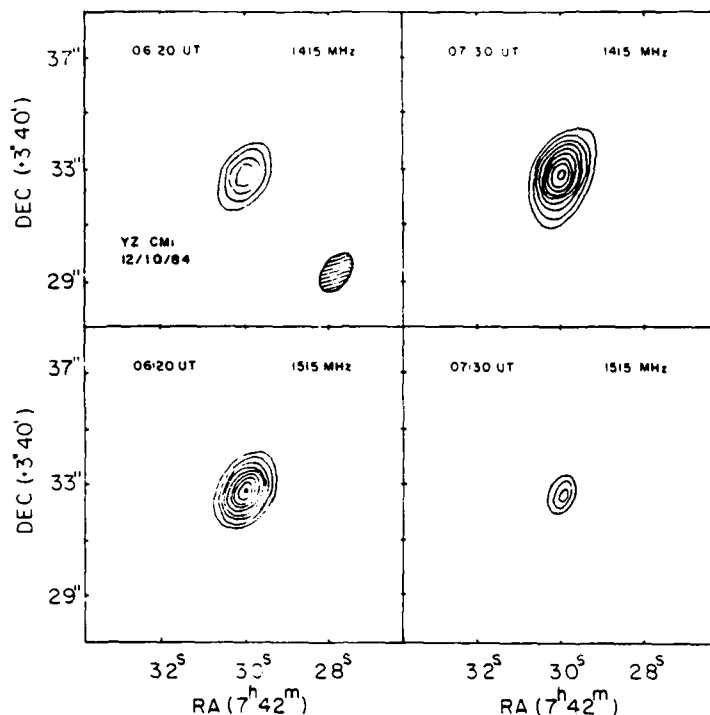


FIG. 3.—VLA snapshot synthesis maps of the total intensity over a 1.5 minute time interval centered at 06:20 UT and 07:30 UT for signal frequencies of 1415 MHz and 1515 MHz. The contour intervals of these maps are 6, 8, 10... mJy per beam area, and the synthesized beam ($1''.0 \times 1''.6$) is illustrated by the cross-hatched ellipsoid at the upper left. Notice that the unresolved emission peaks at different times at two frequencies separated by only 100 MHz near 1465 MHz, indicating a narrow-band radiation mechanism.

cyclotron lines at harmonics of the gyrofrequency. Current sheets could lead to enhanced gyroresonant radiation from relatively thin coronal layers where the magnetic field is constant, and in this case, individual cyclotron lines might be observed. In fact, the VLA has been used to resolve individual coronal loops on the Sun, thereby detecting individual cyclotron lines (Willson 1985a). However, when an entire star is observed, the complex magnetic geometry should lead to varying magnetic field strengths and the cyclotron lines ought to be smoothed into a continuum.

Moreover, we can rule out gyroresonant radiation for the observations presented here. The gyroresonant layers in a stellar corona will lie fully outside the star and form closed surfaces around it. The observed radiation will be generated at the maximum harmonic, n , for which the corona still remains optically thick, for this outermost layer absorbs underlying radiation at lower harmonics. The maximum observed flux density, S , will be given by the Rayleigh-Jeans law (Lang 1980), and the radius of the emitting source will be given by

$$R^2 = 10^{13} \frac{SD^2}{\nu^2 T} \text{ cm}^2, \quad (1)$$

where S is the source flux density in Jy; D is the distance in cm; T is the temperature in K; and the observing frequency, ν , is given by

$$\nu = 2.8 \times 10^6 n H_i \text{ Hz}, \quad (2)$$

for a longitudinal magnetic field of strength H_i . (Slightly larger values of R will be obtained when the magnetic field geometry and the visible area of the gyroresonant surface are taken into account.) For YZ CMi, we substitute $S = 0.02$ Jy, $D = 5.99$ pc $\approx 1.8 \times 10^{19}$ cm, $\nu = 1.5 \times 10^9$ Hz, and $T \approx 10^6$ K to obtain $R = 5.4 \times 10^{12}$ cm.

Thus, the hypothetical gyroresonant radiator must have a radius of $R = 5.4 \times 10^{12}$ cm which is 200 times as large as the star's radius of 2.6×10^{10} cm (Pettersen 1980). (Smaller values of R amounting to a few stellar radii were previously obtained because lower flux densities were observed at higher frequencies.) Because the gyroresonant layers remain optically thick out to no more than $n = 6$ for normal stellar coronae (Zheleznyakov and Tikhomirov 1984), the required magnetic field strength for radiation at 1500 MHz is $H \geq 100$ G. Such strong magnetic fields at 200 stellar radii are simply inconceivable. Even a well-ordered dipolar field has a strength that goes as the cube of the radius, implying a surface magnetic field strength of 0.8×10^9 G.

Thus, the narrow-band, slowly varying radiation from YZ CMi cannot be explained by conventional radiation mechanisms. We might speculate that the star could be continually radiating coherent bursts. Coherent radiation processes like electron-cyclotron masers have been used to explain some microwave bursts on the Sun and nearby stars (Melrose and Dulk 1982; Holman 1983). Some solar bursts exhibit high brightness temperatures, $T_b \geq 10^{15}$ K, that require coherent mechanisms (Slottje 1978), and other solar bursts have ex-

hibited narrow-band ($\Delta\nu/\nu < 10^{-2}$) structure that suggests coherent emission (Lang and Willson 1984; Willson 1985b). In addition, microwave bursts from the dwarf M star AD Leo have millisecond rise times and high brightness temperatures that require coherent emission processes (Lang *et al.* 1983; Lang and Willson 1986). Coherent burst mechanisms might therefore be adopted to explain the observed narrow-band, slowly varying microwave radiation through continuous burst activity.

High circular polarization would be expected to be occasionally observed if the coherent mechanism is associated with intense magnetic fields, and the stochastic nature of continued bursts might explain the variability of the observed microwave radiation.

If the electron-cyclotron maser radiates at the second harmonic, or $n = 2$, of the gyrofrequency as suggested by Melrose and Dulk (1982), then we obtain a longitudinal magnetic field strength of $H_l = 250$ G for a radiation frequency of 1400 MHz. The first harmonic radiation is expected to be attenuated by gyroresonant absorption in overlying atmospheric layers, and second harmonic radiation may dominate the emission when the gyrofrequency is roughly equal to the plasma frequency $\nu_p = 8.9 \times 10^3 N_e^{1/2}$ Hz, where the electron density is in cm^{-3} (see Dulk 1985). This means that the electron density $N_e \approx 6 \times 10^9 \text{ cm}^{-3}$.

The coherent process might alternatively be attributed to plasma radiation. For example, type IV bursts with $\Delta\nu/\nu \leq 0.1$ have been observed at frequencies $\nu = 200\text{--}1500$ MHz. Benz and Tarnstrom (1976) have shown that a coherent synchrotron mechanism for the narrow-band type IV bursts requires either an excessively large number of relativistic electrons or an unstable pitch angle anisotropy. They argue that plasma emission processes might explain these bursts. Plasma processes involving electron beams have also been invoked to explain weaker, narrow-band ($\Delta\nu/\nu \leq 0.1$) bursts or blips observed at decimetric wavelengths during other solar bursts (Furst, Benz, and Hirth 1982; Benz, Bernold, and Dennis 1983). However, analogies with these solar features may be constrained by their rapid temporal variations. The narrow-band type IV bursts have lifetimes of several minutes, and the weaker blips last less than 0.25 s. In contrast, the narrow-band

slowly varying radiation from YZ Canis Minoris lasts for hours.

If YZ Canis Minoris has a solar-like corona, then the first harmonic of the plasma frequency will be absorbed by electron-ion collisions at frequencies $\nu = 1400$ MHz, but the second harmonic will escape. For this case we obtain $N_e = 6 \times 10^9 \text{ cm}^{-3}$, but for plasma radiation to dominate we require $\nu_H \ll \nu_p$ or the longitudinal magnetic field strength $H_l \ll 250$ G.

Radio astronomical studies of the Sun and other active stars at Tufts University are supported under grant AFOSR-83-0019 with the Air Force Office of Scientific Research. Our VLA observations of the Sun are supported by contract N00014-86-K-0068 with the Office of Naval Research (ONR). Investigations of dwarf M flare stars and RS CVn stars at Tufts University are also supported by NASA grant NAG 5-477. The Very Large Array is operated by Associated Universities Inc., under contract with the National Science Foundation.

Note added in manuscript.—Dr. Ronald D. Ekers (private communication) has pointed out that the narrow bandwidths and long fluctuation times of the decimetric radiation from YZ CMi are comparable to the decorrelation frequencies and decorrelation times of the interstellar scintillation of pulsar radiation. Our observations might therefore be explained by interstellar scintillation, but YZ CMi is about 100 times closer than the scintillating pulsars. The fluctuating electron number density would therefore have to be 100 times greater than that detected along the line of sight to these pulsars if the observed decorrelation is attributed to interstellar scintillation. Multiple-wavelength VLA observations can be used to test the scintillation hypothesis; the decorrelation frequency and time, respectively, scale as the fourth and first power of the observing frequency. An emitter located at the distance of YZ CMi must have a linear size smaller than 10^4 km in order to give rise to detectable scintillation in this dense interstellar medium (see Lang 1971 for relevant formulae and pulsar data). If a source of this size accounts for the decimetric flux density from YZ CMi, then its brightness temperature is $T_b \geq 10^{14}$ K, which may again require a coherent radiation mechanism.

REFERENCES

- Benz, A. O., Bernold, T. E. X., and Dennis, B. R. 1983, *Ap. J.*, **271**, 355.
 Benz, A. O., and Tarnstrom, G. L. 1976, *Ap. J.*, **204**, 597.
 Cox, J. J., and Gibson, D. M. 1985, in *Radio Stars*, ed. R. M. Hjellming and D. M. Gibson (Dordrecht: Reidel), p. 233.
 Dulk, G. A. 1985, *Ann. Rev. Astr. Ap.*, **23**, 169.
 Furst, E., Benz, A. O., and Hirth, W. 1982, *Astr. Ap.*, **107**, 178.
 Gary, D. E., and Linsky, J. L. 1981, *Ap. J.*, **250**, 284.
 Holman, G. D. 1983, *Adv. Space Res.*, Vol. 2, No. 11, p. 181.
 Johnson, H. M. 1981, *Ap. J.*, **243**, 234.
 Kundu, M. R., and Lang, K. R. 1985, *Science*, **228**, 9.
 Kundu, M. R., and Shevgaonkar, R. K. 1985, in *Radio Stars*, ed. R. M. Hjellming and D. M. Gibson (Dordrecht: Reidel), p. 229.
 Lang, K. R. 1971, *Ap. J.*, **164**, 249.
 ———. 1980, in *Astrophysical Formulae* (2d ed.; New York: Springer-Verlag), p. 23.
 Lang, K. R., Bookbinder, J., Golub, L., and Davis, M. 1983, *Ap. J. (Letters)*, **272**, L15.
 Lang, K. R., and Willson, R. F. 1984, *Adv. Space Res.*, Vol. 4, No. 7, p. 105.
 ———. 1986, *Ap. J.*, in press.
 Linsky, J. L., and Gary, D. E. 1983, *Ap. J.*, **274**, 776.
 Melrose, D. B., and Dulk, G. A. 1982, *Ap. J.*, **259**, 844.
 Pallavicini, R., Willson, R. F., and Lang, K. R. 1985, *Astr. Ap.*, **149**, 95.
 Pettersen, B. R. 1980, *Astr. Ap.*, **82**, 53.
 Rodono, M., *et al.* 1984, in *Proc. 4th European IUE Conference* (ESA SP-214), p. 247.
 Slottje, C. 1978, *Nature*, **275**, 520.
 Topka, K., and Marsh, K. A. 1982, *Ap. J.*, **254**, 641.
 Vaiana, G. S., *et al.* 1981, *Ap. J.*, **244**, 163.
 Willson, R. F. 1985a, *Ap. J.*, **298**, 911.
 ———. 1985b, *Solar Phys.*, **96**, 199.
 Zheleznyakov, V. V., and Tikhomirov, Yu. V. 1984, *Ap. Space Sci.*, **102**, 189.

KENNETH R. LANG and ROBERT F. WILLSON: Department of Physics and Astronomy, Robinson Hall, Tufts University, Medford, MA 02155

26. MILLISECOND RADIO SPIKES FROM THE DWARF M FLARE STAR AD LEONIS

KENNETH R. LANG AND ROBERT F. WILLSON

Department of Physics and Astronomy, Tufts University

Received 1985 September 24; accepted 1985 November 25

ABSTRACT

The Arecibo Observatory was used to detect two circularly polarized bursts at 1415 MHz from the dwarf M star AD Leonis with total durations of 50 s and 25 s. A sequence of quasi-periodic pulsations with a mean periodicity of $\tau_p = 3.2 \pm 0.3$ s and a total duration of $\tau_D = 25$ s was superposed on the 50 s burst. The strong-pulse was itself composed of a train of quasi-periodic spikes with a mean periodicity of $\tau_s = 32 \pm 5$ ms and a total duration of $\tau_D = 150$ ms. Both the quasi-periodic spikes and individual spikes had rise times of $\tau_R \leq 5$ ms, and they were up to 100% circularly polarized. An upper limit to the linear size of the spike-emitting region is $L \leq 1.5 \times 10^8$ cm, the distance light travels in 5 ms. This size is only 0.005 of the estimated radius of AD Leonis. Provided that the emitter is symmetric, it has an area which is less than 2.5×10^{-3} of the area of the stellar disk and a brightness temperature of $T_b \geq 10^{16}$ K. The high degrees of circular polarization indicate an intimate connection with the star's magnetic field, and the high brightness temperatures suggest a coherent burst mechanism such as an electron-cyclotron maser or coherent plasma radiation. If the electron-cyclotron maser emits at the second harmonic of the gyrofrequency, the longitudinal magnetic field strength $H_l = 250$ G and constraints on the plasma frequency imply an electron density of $N_e \approx 6 \times 10^9$ cm $^{-3}$. Coherent plasma radiation at the first or second harmonic of the plasma frequency, respectively, require $N_e = 2 \times 10^{10}$ cm $^{-3}$ and $H_l \leq 500$ G or $N_e = 6 \times 10^9$ cm $^{-3}$ and $H_l \leq 250$ G. The quasi-periodic pulsations and spikes may be due to some process that modulates the coherent burst emitter. One possibility is radial oscillations in a coronal loop that are excited by energetic trapped particles or by an impulsive source. In this event, an Alfvén velocity of $v_A = 2 \times 10^9$ cm s $^{-1}$, a coronal loop of extent $a_1 = 2 \times 10^9$ cm, and a loop inhomogeneity of size $a_2 = 2 \times 10^7$ cm are inferred for the dwarf M star. Energetic particles that are trapped within closed magnetic structures might alternatively modulate the coherent emission.

Subject headings: polarization — radio sources: variable — stars: flare — stars: individual — stars: radio radiation

1. INTRODUCTION

Rare, powerful (10–20 Jy), long-lasting (several hours) radio bursts from dwarf M flare stars have been occasionally observed at meter wavelengths (frequencies of a few hundred MHz) during many thousands of hours of observations in the 1970s (Lovell 1969; Spangler and Moffet 1976; Davis *et al.* 1978). Brightness temperatures of $T_b \geq 10^{12}$ – 10^{15} K were derived from the measured flux densities under the assumption that the radio emitter was smaller than the stellar disk. Weaker (a few tenths of 1 Jy) radio bursts of shorter duration (tens of seconds) occur more frequently with a rate comparable to that of optically visible flares from the same stars (one every 5.4 hours; Spangler, Shawhan, and Rankin 1974).

The first polarimetric study of these stellar radio bursts was provided by Spangler, Rankin, and Shawhan (1974) who showed that a burst from AD Leonis with a duration of $\tau = 40$ s was as high as 92% circularly polarized. The maximum amplitude of this burst was 520 mJy, which corresponds to $T_b \geq 10^{16}$ K at 430 MHz if the emitter has a radius equal to that of the dwarf M star ($R = 3.0 \times 10^{10}$ cm; Pettersen 1980). This highly circularly polarized burst was also the first radio burst to be observed from AD Leonis.

The improvement in sensitivity made possible by the large collecting area of the Very Large Array (VLA)¹ led to the

detection of relatively weak (10 mJy), highly circularly polarized bursts from dwarf M flare stars at decimetric wavelengths. For example, nearly 100% right-hand circularly polarized bursts have been observed at 1420 MHz at about the same time from both components of the dwarf M binary star system UV Ceti (L726–8B) and L726–8A (Fisher and Gibson 1982); one 100% right-hand circularly polarized 6 cm burst from L726–8A exhibited quasi-periodic flux variations with a period of $\tau_p = 56 \pm 5$ s (Gary, Linsky, and Dulk 1982). The VLA has also been used to detect relatively weak, highly circularly polarized bursts from the single dwarf M star YZ Canis Minoris (Fisher and Gibson 1982; Pallavicini, Lang, and Willson 1985), as well as slowly varying quiescent, or non-flaring, emission of a few mJy from YZ Canis Minoris (Lang and Willson 1985), both components of the binary star system EQ Pegasi (Topka and Marsh 1982), and the binary dwarf M stars YY Geminorum and Wolf 630 (Linsky and Gary 1983). Two 6 cm bursts with nearly 100% left-hand circular polarization have also been observed from the single dwarf M star AD Leonis (Gary 1985); these bursts showed significant structure at the limiting 3.3 s time scale provided by the fastest VLA integration time.

This suggests a serious limitation for the VLA and most other large radio telescopes. The large integration times of ~ 10 s that are used to detect weak signals prohibit the detection of rapid bursts. In fact, individual microwave bursts, or variations within microwave bursts, from dwarf M stars are often unresolved in time when observed with the VLA. We have therefore begun a program of monitoring these stars with

¹ The VLA is a facility of the National Radio Astronomy Observatory, which is operated by Associated Universities, Inc., under contract with the National Science Foundation.

high time resolution (better than 1 ms) at the Arecibo Observatory.

After several hours of observation, a stellar eruption was observed from AD Leonis at 1400 MHz with a maximum flux density of 130 mJy. This burst was composed of highly left-hand circularly polarized (100%) spikes with rise times of $\tau_R \leq 200$ ms (Lang *et al.* 1983). An upper limit to the linear size $L \leq 6 \times 10^9$ cm and a brightness temperature of $T_b \geq 10^{13}$ K were inferred from these rise times. Twenty hours of subsequent observations led to the detection of two other bursts at 1415 MHz that are discussed here.

In § II of this paper we present observations of highly left-hand circularly polarized (up to 100%) spikes from AD Leonis at 1415 MHz with rise times $\tau_R \leq 5$ ms. These rise times provide an upper limit of $L \leq 1.5 \times 10^8$ cm, and a lower limit to $T_b \geq 10^{16}$ K for a symmetric emitter. Some of the spikes were part of a quasi-periodic train of spikes with a mean periodicity of $\tau_p = 32 \pm 5$ ms and a total duration of $\tau_D = 150$ ms. This spike train was itself one pulse in a quasi-periodic sequence of pulsations with a mean periodicity of $\tau_p = 3.2 \pm 0.3$ s and total duration of $\tau_D = 25$ s; the pulsations were superposed upon a longer lasting (50 s) burst. In § III we interpret the high brightness temperatures and high circular polarization of the spikes in terms of coherent maser emission processes. The quasi-periodic trains of pulses and spikes are discussed within the framework of similar effects that have been observed during solar bursts. One possible explanation of the quasi-periodic pulsations and spikes is magnetoacoustic oscillations in a coronal loop that modulate the maser action.

II. OBSERVATIONS

On 1985 July 15, we observed the dwarf M star AD Leonis (Gliese 388, dM3.5e) at a frequency of 1415.0 MHz from 1745 to 1917 UT at the Arecibo Observatory. At this frequency the antenna beamwidth is 3.3, and the system sensitivity is 8 K per Jy at zenith ($1 \text{ Jy} = 10^{-23} \text{ ergs s}^{-1} \text{ cm}^{-2} \text{ Hz}^{-1}$). Both the left-hand circularly polarized (LCP) signals and the right-hand circularly polarized (RCP) signals were recorded using separate receivers. Linear polarization was not obtained. The ellipticity was 0.95, and the uncertainty in circular polarization due to cross talk between the two receivers was 5%. A bandwidth of 4 MHz was employed, with an integration time of 5 ms. The flux density scale was established by calibration observations of PKS 0453+22 (3.25 Jy at 1415 MHz) and PKS 0333+12 (1.8 Jy at 1415 MHz) immediately before and after the observations of AD Leonis.

As illustrated in Figure 1, a circularly polarized (LCP) burst with a maximum flux density of $S_{\text{max}} = 30$ mJy, a total duration of $\tau = 50$ s, and a degree of circular polarization of 50%–100% was observed around 1819 UT. Another, weaker burst with $S_{\text{max}} = 10$ mJy, $\tau = 25$ s, and 100% LCP was observed about 20 s after the decay of the more intense burst. Because no similar variations in signal level were observed during this observation or during 20 hours of other observations of AD Leonis, we assume that the variations lasting 50 s and 20 s represent bursts rather than a slowly varying background that would be expected to continue during the rest of the observations. The burst flux densities reported here are therefore absolute values with respect to negligible quiescent radiation from the star. (No other bursts were detected at 1415 MHz during 2 hours centered at transit at the Arecibo Observatory on 1984 November 7–10 and 1985 July 13, 14, 16, 19, 20, and 21.)

A sequence of five quasi-periodic pulsations, or oscillations, with a mean periodicity of $\tau_p = 3.2 \pm 0.3$ s and a total duration of $\tau_D = 25$ s were superposed upon the more intense 50 s burst (see Fig. 1). The strongest pulse had $S_{\text{max}} = 70$ mJy when the data were averaged by running means over 312 ms. The pulses had circular polarizations of 50%–100%. (Quasi-periodic, highly left-hand circularly polarized (100%) burst emission at 1400 MHz with fluctuations at time scales of ~ 2 s, 10 s, and 25 s were previously reported for AD Leonis (Lang *et al.* 1983), but no single periodicity dominated the data.)

When the strongest pulse, marked A in Figure 1, was observed with 5 ms integration time, it was found to be composed of a train of five quasi-periodic spikes with a mean periodicity of $\tau_p = 32 \pm 5$ ms and total duration of $\tau_D = 150$ ms (Fig. 2). These spikes had $S_{\text{max}} = 300$ mJy and circular polarizations of $\sim 33\%$ with respect to the longer lasting 50 s burst. The pulses immediately before and after pulse A (see Fig. 1) were resolved in time with durations of ~ 1 s, and they exhibited no detectable structure on shorter time scales.

Here we also note that higher flux densities are obtained with shorter integration times. The long integration of ~ 10 s at the VLA and other large radio telescopes would smooth out the individual spikes, leading to a serious underestimate of the flux density and perhaps reducing the quasi-periodic spikes to undetectable levels.

As illustrated in Figure 3, the time, Δt , between spikes was not completely regular, but instead showed a tendency to increase with $\Delta t = 25, 30, 40$, and 32 ms for sequential spikes: a sixth spike occurred at $\Delta t = 80$ ms. The individual quasi-periodic spikes had rise times $\tau_R \leq 5$ ms, and isolated, nonperiodic spikes like 2A (Fig. 2) and B (Fig. 1) had similar rise times. Spike B was $100\% \pm 5\%$ left-hand, circularly polarized, with a rise time of $\tau_R \leq 5$ ms (see Fig. 4).

An upper limit to the linear size of the emitting region is $L \leq 1.5 \times 10^8$ cm, the distance that light travels in 5 ms. This size is only 0.005 of the estimated radius of AD Leonis ($R = 3.0 \times 10^{10}$ cm; Pettersen 1980). Provided that the spike emitter is symmetric, it has an area which is less than 2.5×10^{-5} of the surface area of the star's visible disk.

We can use the maximum flux density, $S_{\text{max}} = 300$ mJy, to infer a lower limit to the brightness temperature $T_b \geq 10^{16}$ K using the Rayleigh-Jeans expression (Lang 1980) and assuming a symmetric source of linear size $L \leq 1.5 \times 10^8$ cm, a distance $D = 4.85$ pc $= 1.55 \times 10^{19}$ cm, and a frequency of 1415 MHz $= 1.415 \times 10^9$ Hz.

III. DISCUSSION

What accounts for the millisecond spikes emitted by AD Leonis at 1415 MHz? The high circular polarization of up to 100% indicates an intimate connection with strong stellar magnetic fields, whereas the high brightness temperatures of $T_b \geq 10^{16}$ K suggest a coherent emission mechanism. Similar short-lived (≤ 20 ms), highly circularly polarized (100%), bright ($T_b \geq 10^{12}$ K) spikes have been observed at decimetric wavelengths during solar bursts (Droge 1977; Slottje 1978, 1980). These spikes have been explained in terms of electron-cyclotron (or gyrosynchrotron) masers at the gyrofrequency and perhaps its low harmonics. (Maser is the acronym for microwave amplification by stimulated emission of radiation.) We know that solar bursts at 1415 MHz occur near the apex of coronal loops (Willson 1983; Lang and Willson 1983, 1984; Kundu and Lang 1985), and we may therefore argue by analogy that the spikes from AD Leonis are due to the maser

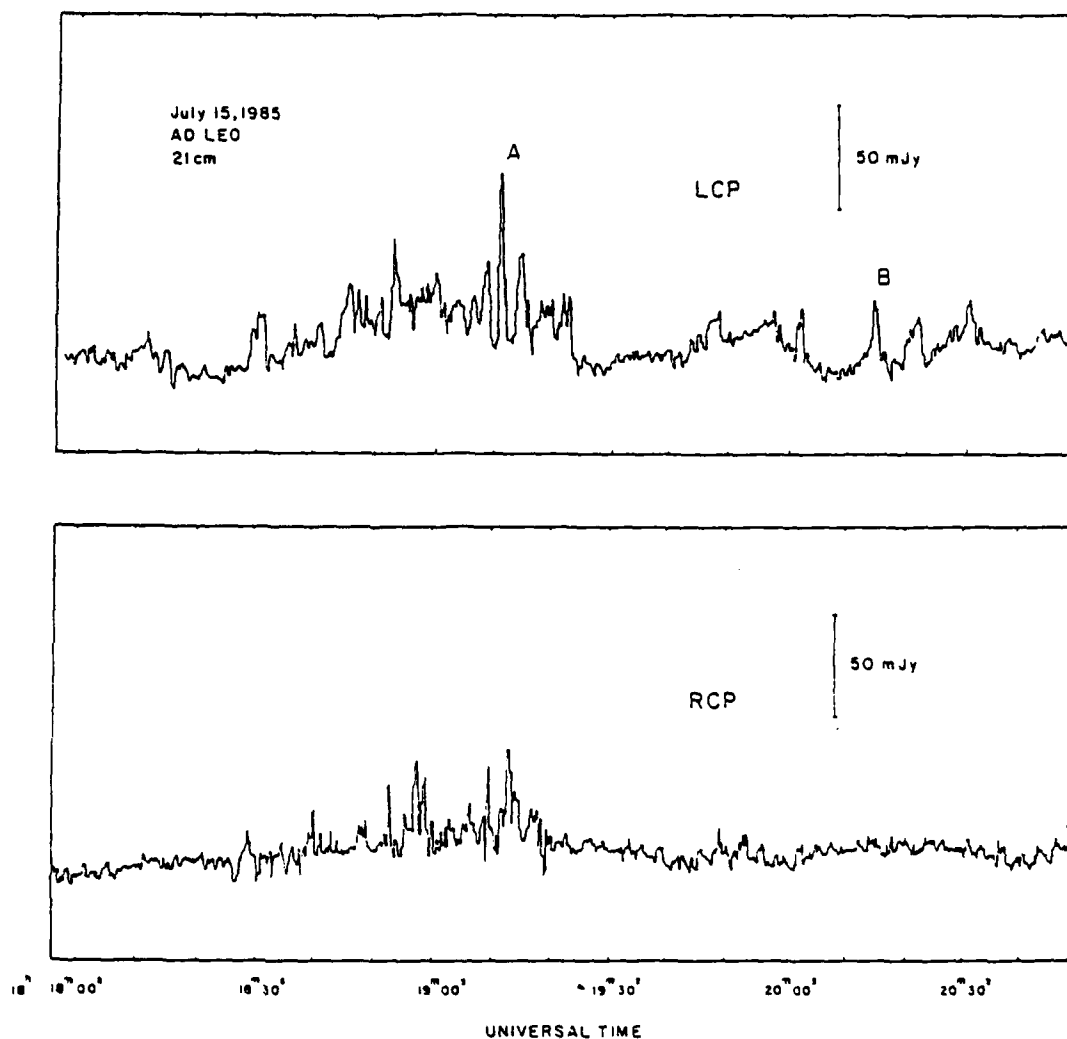


FIG. 1.—Total power detected at a frequency of 1415 MHz (21.2 cm) while tracking the dwarf M star AD Leonis. Both the left-hand circularly polarized (LCP, top) and the right-hand circularly polarized (RCP, bottom) signals are shown. Here the data have been smoothed by running means to give an effective integration time of 312 ms. The LCP plot exhibits two circularly polarized bursts lasting ~ 50 s and 25 s. A quasi-periodic sequence of five pulses is superposed upon the longer burst near the strongest pulse A. These pulses had a mean periodicity of $\tau_p = 3.2 \pm 0.3$ s and a total duration of $\tau_D = 25$ s. The features marked A and B are shown with a 5 ms integration time in Figs. 2–4.

action of electrons trapped in stellar loops. If this is the case, we would not expect a strong correlation between radio bursts and optical flares of dwarf M stars. In fact, there is no strong correlation between bursts observed in these two spectral regions (Spangler and Moffet 1976).

The theory of electron-cyclotron maser emission from coronal loops was first investigated by Twiss (1958) and Twiss and Roberts (1958), and Wu and Lee (1979) delineated the conditions at which the coherent emission will escape from magnetic loops. The theory has been subsequently developed in greater detail and applied to coronal loops by Holman, Eichler, and Kundu (1980), Melrose and Dulk (1982), Sharma, Vlahos, and Papadopoulos (1982), Holman (1983), Melrose, Hewitt, and Dulk (1984), Sharma and Vlahos (1984), and Dulk (1985). The coherent radiation of solar bursts emitted from coronal loops can be generated at the first or second harmonic of the gyrofrequency $\nu_H = 2.8 \times 10^6 H_l$ Hz, where H_l is the longitudinal magnetic field strength.

A relatively strong magnetic field and low-density plasma are required for the electron-cyclotron maser to work. That is, the gyrofrequency ν_H must be greater than or equal to the plasma frequency $\nu_p = 8.9 \times 10^3 N_e^{1/2}$ Hz, where N_e is the electron density in cm^{-3} . For $\nu_H > 3\nu_p$, radiation at the first harmonic of the gyrofrequency grows the fastest and extracts most of the free energy. However, the radiation must pass through overlying atmospheric layers where the radiation frequency is equal to 2 or 3 times the gyrofrequency. The radiation will therefore suffer severe gyroresonance absorption and will most likely never reach the observer.

The problem of gyroresonant absorption may be overcome if the escaping radiation is generated by a maser at the second harmonic where the radiation frequency $\nu = 2\nu_H$ (Melrose and Dulk 1982; Vlahos, Sharma, and Papadopoulos 1983; Melrose, Hewitt and Dulk 1984). The much faster growth of the first harmonic must then be suppressed and this is possible for $\nu_H \approx \nu_p$. It is unlikely that significant amplification will

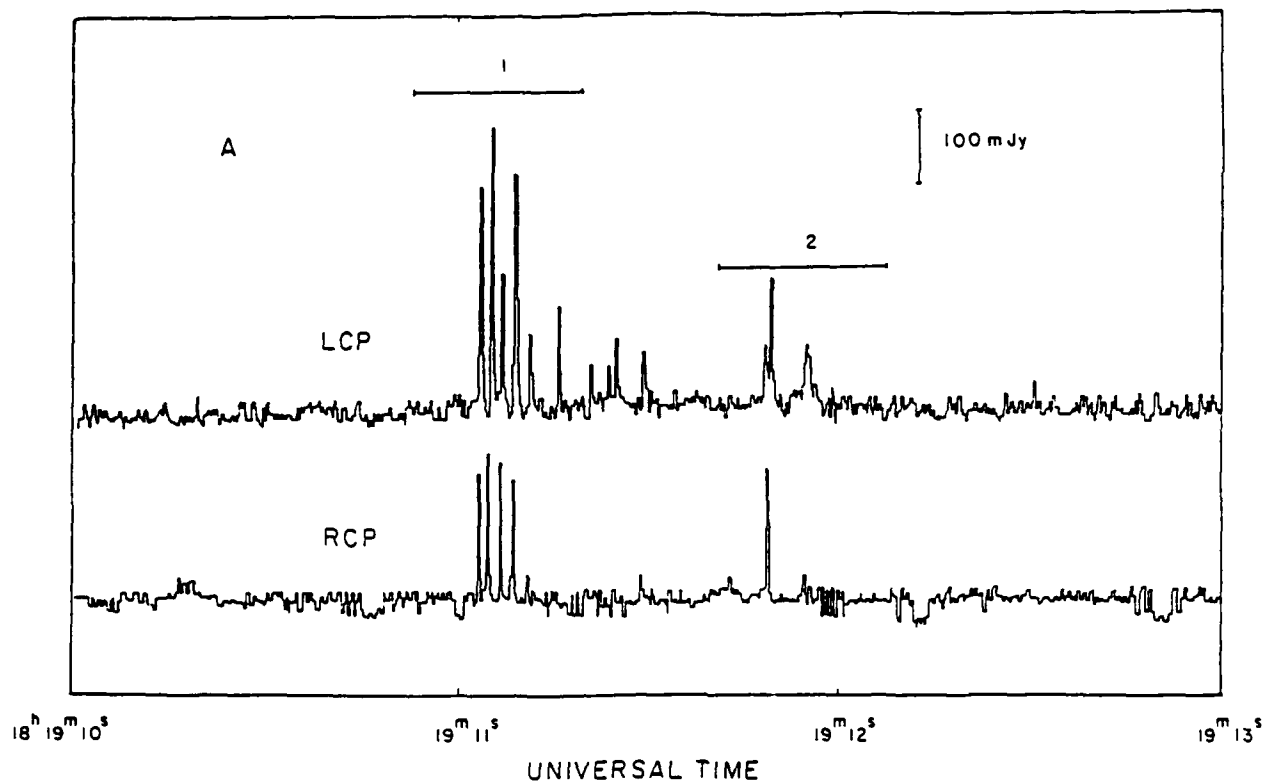


FIG. 2.—The strongest pulse marked A in Fig. 1 is displayed with a 5 ms integration time. Here the background level of the longer burst has been subtracted from the data, and the flux density scale is with respect to this background. Pulse A is composed of a train of five quasi-periodic spikes with a mean periodicity of $\tau_p = 32 \pm 5$ ms and a total duration of $\tau_D = 150$ ms. The emission contained within the horizontal bar marked 1 is shown on an expanded scale in Fig. 3.

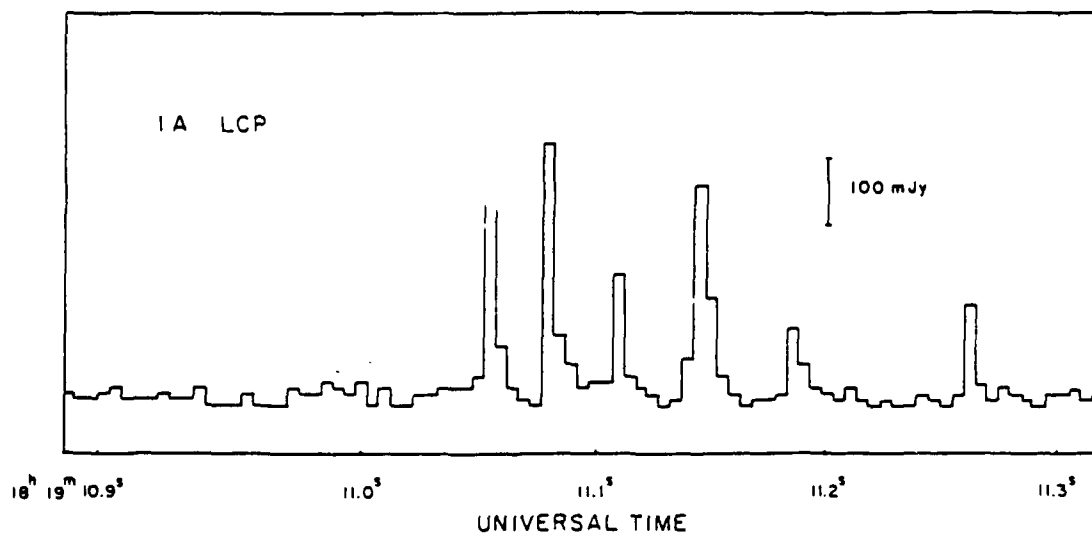


FIG. 3.—Quasi-periodic spikes from pulse A are exhibited on an expanded scale with 5 ms integration time. Each of these spikes had a rise time of $\tau_R \leq 5$ ms, leading to an upper limit to the linear size $L \leq 1.5 \times 10^8$ cm for the spike emitter.

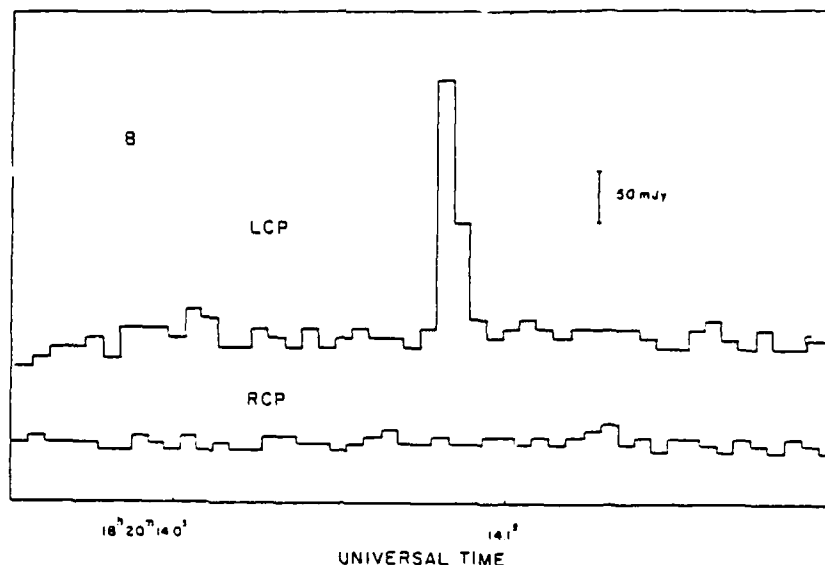


FIG. 4.—The burst feature marked B in Fig. 1 with 5 ms integration time. It is a single spike that is 100% left-hand circularly polarized. The spike has a rapid rise time of $\tau_r \leq 5$ ms, providing an upper limit to the linear size $L \leq 1.5 \times 10^9$ cm for the spike emitter.

occur at harmonics greater than two because faster growth at the first and second harmonics would extract all the free energy (Dulk 1985).

These conditions provide constraints on the electron density, N_e , and the longitudinal magnetic field strength, H_l . For $\nu = 1.4 \times 10^9$ Hz $= 2\nu_H$, we obtain $H_l = 250$ G, and for $\nu_p \approx \nu_H = 7.0 \times 10^8$ Hz, an electron density of $N_e \approx 6 \times 10^9$ cm $^{-3}$ is inferred.

Although electron-cyclotron maser emission at the second harmonic of the gyrofrequency may explain the observed spikes from AD Leonis, it is not necessarily the only explanation. For example, under conditions that apply to the low solar corona, second harmonic maser emission may never reach appreciable levels (Sharma and Vlahos 1984).

The high brightness temperature, high circular polarization, and rapid variations of the millisecond spikes might be explained by coherent plasma radiation. For $\nu_H \ll \nu_p$, plasma radiation is favored over electron-cyclotron emission.

Radiation at the first harmonic of the plasma frequency can be seriously attenuated by collisional damping (electron-ion collisions) in the overlying layers of an extensive stellar corona. For the Sun, the first harmonic is strongly absorbed for frequencies higher than 100–500 MHz, whereas the second harmonic is observed up to 2–5 GHz. If solar conditions prevail on AD Leonis, we might be seeing spikes at the second harmonic of the plasma frequency. Nevertheless, we might imagine a stellar corona with less extent and absorption, thereby permitting radiation at the first harmonic of the plasma frequency to escape.

For a radiation frequency $\nu = 1.4 \times 10^9$ Hz equal to ν_p or $2\nu_p$, we infer an electron density $N_e = 2 \times 10^{10}$ cm $^{-3}$ and $N_e = 6 \times 10^9$ cm $^{-3}$, respectively. The condition that $\nu_H \ll \nu_p$ then leads to the constraint $H_l \ll 500$ G for the first harmonic and $H_l \ll 250$ G for the second harmonic.

But what accounts for the quasi-periodic spikes and pulsations? Some process must modulate the coherent burst emitter in a quasi-periodic manner. Here we can draw upon the rich literature on modulations and oscillations of solar bursts.

Quasi-periodic solar pulsations with a mean periodicity of

$\tau_p \approx 1$ s have been observed at decametric (Achon 1974), meter (Tapping 1978), and decimetric (Gorwols 1972) wavelengths during type IV bursts. Quasi-periodic fluctuations with periodicities of 0.1–8 s have even been detected during solar bursts at X-ray wavelengths (Dennis, Frost, and Orwig 1981; Orwig, Frost, and Dennis 1981; Kane *et al.* 1983; and Kiplinger *et al.* 1983), and there is some evidence for hard X-ray variations with rise times of $\tau_r \leq 20$ ms.

Extensive observations of quasi-periodic solar oscillations have been carried out at meter wavelengths for nearly two decades. Trains of pulses with a range of periodicities of $\tau_p = 50$ ms to 5 s and durations of $\tau_D = 1$ –50 s have been observed. Tapping (1978) showed that the duration times, τ_D , decrease systematically with decreasing pulsation period τ_p . Moreover, Pick and Trotter (1978) showed that enhanced pulses recurring with $\tau_p = 1.7$ s contain trains of spikes of mean periodicity $\tau_s = 0.37$ s. The pulses and spikes that we have observed from AD Leonis exhibit analogous behavior, with τ_D decreasing with decreasing τ_p , and rapid spikes occurring within a pulse of slower periodicity. Moreover, Gary, Linsky, and Dulk (1982) observed quasi-periodic oscillations with $\tau_p = 56 \pm 5$ s during a circularly polarized 6 cm burst from L726–8A, the dwarf M companion of UV Ceti.

One currently popular explanation for the quasi-periodic solar bursts is magnetoacoustic oscillations in a coronal loop. According to this theory, small amplitude radial oscillations are excited in a magnetic flux tube with periods on the order of the tube radius, a , divided by the Alfvén velocity, V_A (Rosenberg 1970, 1972). Meerson, Sasorov, and Stepanov (1978) noticed that the fast magnetohydrodynamic waves in Rosenberg's theory are radiatively damped to such an extent that they cannot account for the long-lasting solar oscillations. They proposed that energetic protons trapped within closed magnetic structures provide the energy to feed the waves and continually excite them. Roberts, Edwin, and Benz (1983, 1984) have alternatively argued that density enhancements in coronal loops support and trap the fast waves that are naturally excited by an impulsive source such as a stellar burst.

Regardless of the exact mechanism of excitation, the

maximum periodicity of these coronal oscillations is given by $\tau_p = 2.6a/v_A$. For sizes $a \approx 10^8$ cm and Alfvén velocities $v_A \approx 3 \times 10^8$ cm s⁻¹, maximum periodicities of ~ 1 s are obtained.

For impulsively generated oscillations, the onset time and duration of the quasi-periodic phase can be related to the size, a , and the height, h , of the emitter (Roberts, Edwin, and Benz 1983, 1984). Moreover, the duration time, τ_D , is related to the pulsation period, τ_p . At fixed h and v_A , the duration time τ_D will decrease with decreasing τ_p .

Our observations of quasi-periodic spikes and pulsations indicate that τ_D decreases with decreasing τ_p , as predicted by the theory of coronal oscillations. In addition, plausible physical parameters can be obtained from the observed periodicities. For a magnetic field strength of 250 G, as inferred from coherent emission at the second harmonic of the gyrofrequency, we obtain an Alfvén velocity of $v_A = (H^2/4\pi\rho)^{1/2} = 2 \times 10^9$ cm s⁻¹ for a plausible density of $N = 10^9$ cm⁻³ (ρ is the mass density). Pulsation periodicities of $\tau_p = 3.2$ s and 32 ms then require sizes $a_1 = 2 \times 10^9$ cm and $a_2 = 2 \times 10^7$ cm, respectively.

Coronal loops on the Sun have sizes on the order of 2×10^9 cm, and the smaller size of 2×10^7 cm for the faster spikes is well below that inferred from the light travel time argument. We might view the smaller size as an inhomogeneity in a larger stellar loop. Duration times of 0.15 and 25 s are consistent with a constant height of $h = 2 \times 10^9$ cm and a time

of ~ 1 s between the generation of the disturbance and the onset of the quasi-periodic phase.

Gary, Linsky, and Dulk (1982) reasoned that the 56 s oscillations observed in the 6 cm burst from L727-8A might be caused by a periodic modulation of the source by an external agent or by a periodic modulation of the energy release mechanism. We agree with their conclusion that flux tube oscillations might modulate coherent maser action. However, this is not the only plausible mechanism for producing apparent periodicities. Energetic particles might be trapped within closed magnetic structures, bouncing between magnetic mirrors at times $\tau \approx L/c$, where L is the size of the magnetic trap and c is the velocity of light. Perhaps mirroring energetic particles interfere with and modulate the coherent maser action.

Radio astronomical studies of the Sun and other active stars at Tufts University are supported under grant AFOSR-83-0019 with the Air Force Office of Scientific Research. Our VLA observations of the Sun are supported by contract N00014-86-K-0068 with the Office of Naval Research (ONR). Investigations of dwarf M flare stars and RS CVn stars at Tufts University are also supported by NASA grant NAG 5-477. The Arecibo Observatory is part of the National Astronomy and Ionosphere Center, which is operated by Cornell University under contract with the NSF.

REFERENCES

- Achon, A. 1974, *Solar Phys.*, 37, 477.
 Davis, R. J., Lovell, B., Palmer, H. P., and Spencer, R. E. 1978, *Nature*, 273, 644.
 Dennis, B. R., Frost, K. J., and Orwig, L. E. 1980, *Ap. J. (Letters)*, 244, L167.
 Droge, F. 1977, *Astr. Ap.*, 57, 235.
 Dulk, G. A. 1985, *Ann. Rev. Astr. Ap.*, 23, 169.
 Fisher, P. L., and Gibson, D. M. 1982, *Smithsonian Ap. Ob. Spec. Rept.*, No. 392, 109.
 Gary, D. E. 1985, in *Radio Stars*, ed. R. M. Hjellming and D. M. Gibson (Dordrecht: Reidel), p. 385.
 Gary, D. E., Linsky, J. L., and Dulk, G. A. 1982, *Ap. J. (Letters)*, 263, L79.
 Gotwols, B. L. 1972, *Solar Phys.*, 25, 232.
 Holman, G. D. 1983, in *Advances in Space Research* Vol. 2, No. 11 (COSPAR: Oxford: Pergamon) p. 181.
 Holman, G. D., Eichler, D., and Kundu, M. R. 1980, in *IAU Symposium 86, Radio Physics of the Sun*, ed. M. R. Kundu and T. E. Gergely (Dordrecht: Reidel), p. 457.
 Kane, S. R., Kai, D., Kosugi, T., Enome, S., Landecker, P. B., and McKenzie, D. L. 1983, *Ap. J.*, 271, 376.
 Kiplinger, A. L., Dennis, B. R., Emslie, A. G., Frost, K. J., and Orwig, L. E. 1983, *Ap. J. (Letters)*, 265, L99.
 Kundu, M. R., and Lang, K. R. 1985, *Science*, 228, 9.
 Lang, K. R. 1980, *Astrophysical Formulae* (2d ed.; New York: Springer Verlag), p. 23.
 Lang, K. R., Bookbinder, J., Golub, L., and Davis, M. M. 1983, *Ap. J. (Letters)*, 272, L15.
 Lang, K. R., and Willson, R. F. 1983, *Advances in Space Research*, Vol. 2, No. 11 (COSPAR: Oxford: Pergamon), p. 91.
 ———, 1984, *Advances in Space Research*, Vol. 4, No. 7 (COSPAR: Oxford: Pergamon), p. 105.
 ———, 1986, *Ap. J. (Letters)*, 302, L17.
 Linsky, J. L., and Gary, D. E. 1983, *Ap. J.*, 274, 776.
 Lovell, B. 1969, *Nature*, 222, 1126.
 Meerson, B. I., Sasorov, P. V., and Stepanov, A. V. 1978, *Solar Phys.*, 58, 165.
 Melrose, D. B., and Dulk, G. A. 1982, *Ap. J.*, 259, 844.
 Melrose, D. B., Hewitt, R. C., and Dulk, G. A. 1984, *J. Geophys. Res.*, 87, 5140.
 Orwig, L. E., Frost, K. J., and Dennis, B. R. 1981, *Ap. J. (Letters)*, 244, L163.
 Pallavicini, R., Willson, R. F., and Lang, K. R. 1985, *Astr. Ap.*, 149, 95.
 Pettersen, B. R. 1980, *Astr. Ap.*, 82, 53.
 Pick, M., and Trotter, G. 1978, *Solar Phys.*, 60, 353.
 Roberts, B., Edwin, P. M., and Benz, A. O. 1983, *Nature*, 305, 688.
 ———, 1984, *Ap. J.*, 279, 857.
 Rosenberg, H. 1970, *Astr. Ap.*, 9, 159.
 ———, 1972, *Solar Phys.*, 25, 188.
 Sharma, R. R., and Vlahos, L. 1984, *Ap. J.*, 280, 405.
 Sharma, R. R., Vlahos, L., and Papadopoulos, K. 1982, *Astr. Ap.*, 112, 337.
 Slottje, C. 1978, *Solar Phys.*, 59, 145.
 ———, 1980, in *IAU Symposium 86, Radio Physics of the Sun*, ed. M. R. Kundu and T. E. Gergely (Dordrecht: Reidel), p. 193.
 Spangler, S. R., and Moffett, T. J. 1976, *Ap. J.*, 203, 497.
 Spangler, S. R., Rankin, J. M., and Shawhan, S. D. 1974, *Ap. J. (Letters)*, 194, L43.
 Spangler, S. R., Shawhan, S. D., and Rankin, J. M. 1974, *Ap. J. (Letters)*, 190, L129.
 Tapping, K. F. 1978, *Solar Phys.*, 59, 145.
 Topka, K., and Marsh, K. A. 1982, *Ap. J.*, 254, 641.
 Twiss, R. Q., 1958, *Australian J. Phys.*, 11, 564.
 Twiss, R. Q., and Roberts, J. A. 1958, *Australian J. Phys.*, 11, 424.
 Willson, R. F. 1983, *Solar Phys.*, 83, 285.
 Wu, C. S., and Lee, L. C. 1979, *Ap. J.*, 230, 621.

KENNETH R. LANG and ROBERT F. WILLSON: Department of Physics and Astronomy, Robinson Hall, Tufts University, Medford, MA 02155

27. COMPACT, VARIABLE SOURCES ON THE SUN AT 2 CENTIMETER WAVELENGTH

ROBERT F. WILLSON and KENNETH R. LANG

Department of Physics and Astronomy, Tufts University, Medford, MA 02155, U.S.A.

(Received 14 May, in revised form 2 August, 1987)

Abstract. Very Large Array (VLA) observations of compact transient sources on the Sun at 2 cm wavelength are presented. These sources have angular sizes of $\theta \approx 5''$ – $25''$, brightness temperatures of $T_B \approx 1$ – 3×10^5 K, and lifetimes ranging between a few minutes to several hours. The emission originates in regions of diffuse plage and quiet Sun, where the photospheric magnetic fields are relatively weak ($H \leq 100$ G). In some cases the 2 cm radiation may be explained as the thermal bremsstrahlung of a dense ($N_e \leq 10^{10} \text{ cm}^{-3}$) plasma in the transition region. For other sources, the relatively high circular polarization ($p_c \approx 40$ – 50%) suggests a nonthermal emission mechanism, such as the gyrosynchrotron radiation of mildly relativistic electron with a power-law spectrum.

1. Introduction

VLA observations of solar active regions have shown that the quiescent emission at 2 cm wavelength often originates in compact ($\theta < 5''$) highly circularly polarized ($p_c = 80$ – 90%) sources in regions of strong magnetic fields near sunspots (Lang *et al.*, 1983; Shevgaonkar and Kundu, 1984). The observed brightness temperatures of $T_B = 10^5$ – 10^6 K suggest that this emission originates in the transition region or low solar corona. More recent observations have revealed a different class of 2 cm sources which are also compact and often highly circularly polarized but which originate in regions of apparently weak photospheric field (Akhmedov *et al.*, 1986; Willson and Lang, 1986). The nature of these sources is enigmatic because magnetic fields of $H \approx 1500$ – 2000 G are required if the observed brightness temperatures and degrees of circular polarization are to be attributed to thermal gyroresonance emission or to propagation effects (thermal bremsstrahlung). Alternatively, the 2 cm emission could be attributed to nonthermal radiation such as the gyrosynchrotron radiation of subrelativistic electrons in low magnetic fields.

These compact sources are also observed to vary on time-scales of a few tens of seconds to several hours. In one case Willson and Lang (1986) observed the apparent emergence and disappearance of a compact ($\theta < 10''$) dipolar loop which evolved on a time-scale of about 60 s. These variations could be due to fluctuations in the magnetic field strength or to a variable nonthermal electron density, possibly brought about by changes in the acceleration mechanism. The time-scales of the variations are similar to those observed at ultraviolet wavelengths from small sources in the transition region and to optical wavelength fluctuations of so-called ephemeral regions (Porter *et al.*, 1984; Martin *et al.*, 1985).

In this paper we discuss new VLA observations of the Sun at 2 cm wavelength. In

Section 2 we present these observations and show that compact, transient sources are detected in both regions of weak plage without sunspots as well as in regions of the quiet Sun. There also does not appear to be any clear association between these transient sources and the photospheric $H\alpha$ emission. In Section 3 we discuss these observations in light of both thermal and nonthermal radiation processes. We show that the unpolarized 2 cm emission could be attributed to the thermal bremsstrahlung of dense, compact sources in the transition region. The moderate circular polarization ($\rho_c = 40\text{--}50\%$) of other sources, however, suggests either a nonthermal emission mechanism such as gyrosynchrotron radiation or else unexpectedly high magnetic fields in the transition region or corona. Here we also comment on the possibility of detecting transient sources at other radio wavelengths.

2. Observations

The VLA was used (*D* configuration) to observe a region of diffuse plage on 1986 January 17. The position of this region was S 10 W 62 at 13:00 UT on this day. Observations (*B* configuration) were also made toward another plage region as well as toward two regions of quiet Sun on 1986 August 24. The plage was located at S 10 W 08 at 13:00 UT, and the two quiet-Sun regions were located at N 30 W 00 and S 30 W 00. On 1986 January 17, the region was observed during an eight hour period between 15:00 and 23:00 UT. The entire VLA was used to observe the Sun at 2.1 and 6.1 cm

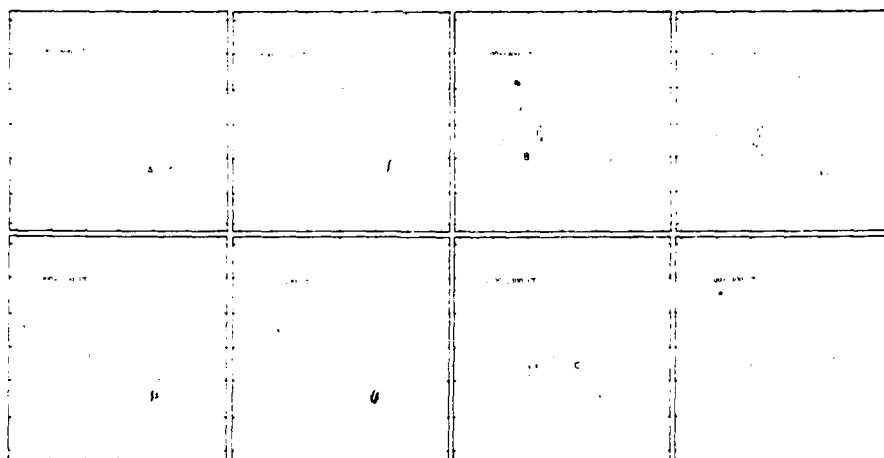


Fig. 1. VLA synthesis maps of the total intensity of the radiation from compact sources at 2.1 and 6.1 cm (lower right-hand box) during an eight hour period on 1986 January 17. Each map begins and ends at the time indicated. Here each box refers to the same area on the surface of the Sun, and the fiducial marks are separated by $60''$. The contours mark levels of equal brightness temperature. At 2.1 cm, the outermost contour is drawn at 5.2×10^4 K with a contour interval of 1.8×10^4 K. The inner contour and contour interval of the 6 cm map are equal to 1.0×10^5 K.

for 20 m and 10 m, respectively, followed by successive 2 min observations on a nearby calibration source. On 1986 August 24, the plage and the northern and southern hemisphere quiet-Sun regions were observed at 2.1 cm for successive periods of 4.5, 2.5, and 2.5 hr, respectively, beginning at 15 : 00 UT. On both days the bandwidth was 12.5 MHz. At 2.1 cm the half-power beamwidth of the antennas is $\sim 3.5'$. At this wavelength the synthesized beamwidths in the *B* and *D* configurations are $\sim 0.4'' \times 0.5''$ and $4.2'' \times 4.6''$, respectively.

The right and left circularly polarized signals were sampled every 10 s and were calibrated using the standard VLA solar calibration procedures. These data were then used to produce CLEANED synthesis maps of the total intensity, *I*, and circular polarization, *V*, over an area of $\sim 5' \times 5'$ on the Sun on time-scales as short as 30 s.

In Figure 1 we show a series of 1–2 hour maps of total intensity for the plage region observed on 1986 January 17. Here each box refers to the same region on the Sun. This figure shows several compact 2 cm sources with angular sizes of $\theta_s < 25''$ and maximum brightness temperatures of $T_s \approx 2 \times 10^5$ K. These sources lie within more extended 6 cm emission whose peak brightness temperature is $T_B \approx 10^6$ K. Comparisons with a Kitt Peak magnetogram (taken at 16 : 05 UT) and SOON and Big Bear Solar Observatory H α pictures show that these sources were located in regions of diffuse plage with weak photospheric magnetic fields ($H \leq 100$ G) and no sunspots. The 2 cm sources were also unpolarized ($\rho_c = V/I \leq 15\%$) suggesting optically thick emission from regions where $T_s = T_B \approx 1\text{--}2 \times 10^5$ K.

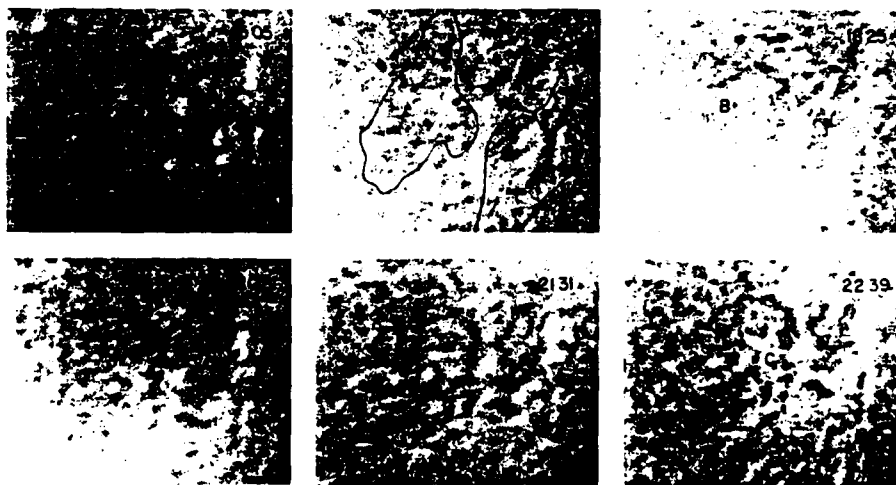


Fig. 2. A series of SOON H α images taken at the UT time indicated in the upper right-hand corner. The outermost contours of the 6 cm emission shown in Figure 1 are drawn on the image at 16 : 45 UT. The locations of the variable 2 cm sources *A*, *B*, and *C*, also shown in Figure 1, are indicated in the frames at 15 : 05, 18 : 25, and 22 : 39 UT, respectively.

It is clear from Figure 1 that these compact sources varied substantially in intensity on time-scales of hours. Source *B*, for example, appeared to emerge between $\sim 17:00$ and $19:00$ UT, and then faded and reappeared a few hours later. Likewise, source *C* emerged between $22:00$ and $23:00$ UT. A series of maps on hourly time-scales was also made for the 6 cm data, but they failed to reveal any significant changes in structure or intensity at this wavelength. Examination of $H\alpha$ images obtained by the SOON observatories also failed to reveal any obvious changes in the structure or brightness of the plage emission.

Figure 1 also shows that the most intense and long lasting source *A* appeared to move laterally towards the southeast during these observations. The angular displacement between the centroids of source *A* between $15:00$ and $23:00$ UT is $\sim 50''$, and corresponds to a transverse velocity of $\sim 1.3 \text{ km s}^{-1}$. Since the VLA was made to continuously track the same point on the Sun with an accuracy of $\sim 1''$, this shift in position cannot be attributed to systematic pointing errors.

In Figure 2 we show SOON $H\alpha$ images taken throughout the day. The universal time that the image was taken is given in the upper right-hand corner of each frame. Here

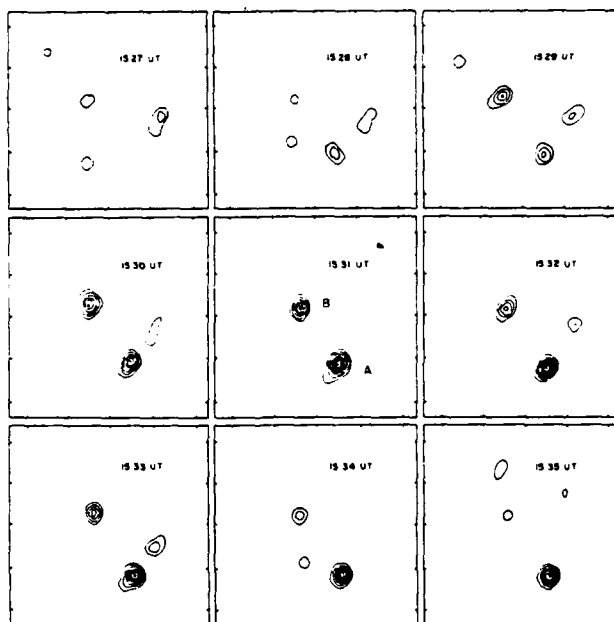


Fig. 3. VLA snapshot maps of the total intensity of compact variable sources at 2.1 cm wavelength. Each map is for 1 min of data beginning at the time indicated. These sources were located within a region of weak plage. The two sources *A* and *B* appear to have emerged together at $\sim 15:41$ UT. Source *A* lasted for ~ 12 min until $\sim 15:41$ UT, while source *B* lasted only until $\sim 15:34$ UT. Here the contours mark levels of equal brightness temperature with an outermost contour and contour interval of 3.5×10^4 K. The fiducial marks on the axes are separated by $10''$.

we have also superimposed the outer contours of the 6 cm emission on the image at 16:45 UT together with the locations of the 2 cm sources *A*, *B*, and *C*, shown in Figure 1. Source *A*, as well as the most intense 6 cm emission, might be associated with two patches of $H\alpha$ emission in the western half of the frame, but there is no such association for the variable sources *B* and *C*. Furthermore, although the $H\alpha$ data are not of the highest quality, it appears that there were no major changes in the intensity or structure of this diffuse $H\alpha$ emission during the day, unlike at 2 cm.

In Figure 3 we show a series of 60 snapshot maps of two compact variable sources detected within the diffuse plage region observed on 1986 August 24. The peak brightness temperatures and circular polarizations of the two sources, *A* and *B*, are

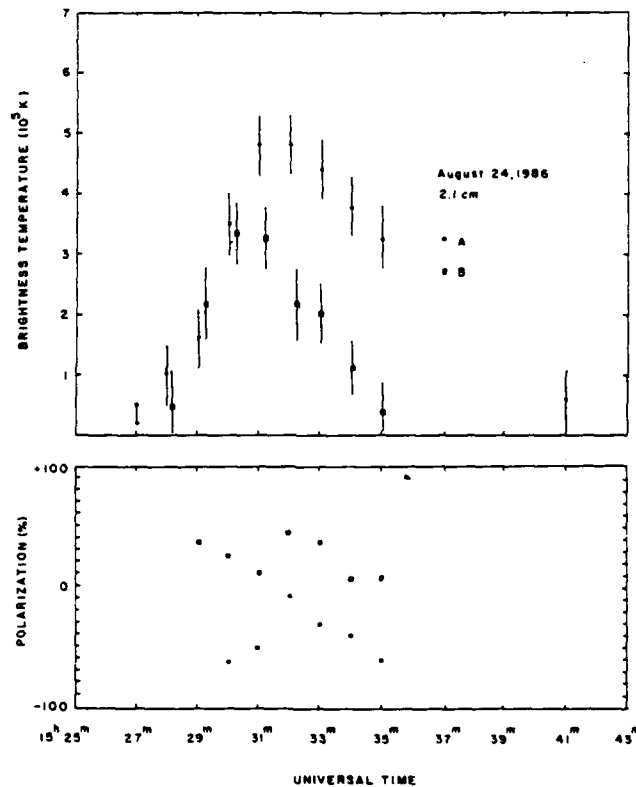


Fig. 4. Plots of the total intensity, $I = (RCP + LCP)/2$ (top) and circular polarization, $p_c = (RCP - LCP)/(RCP + LCP)$ (bottom), for the compact sources *A* and *B* shown in Figure 2.

plotted as a function of time in Figure 4. These data indicate that a bipolar region of about $10''$ in size emerged at $\sim 15:29$ UT and reached a maximum brightness a few minutes later. The weaker right circularly polarized source *B*, however, decreased in intensity more rapidly than the left circularly polarized source *A*, which lasted until

$\sim 15:41$ UT. Here the gap in the data between $15:35$ and $15:40$ UT corresponds to a calibration period. It is interesting to note the abrupt increase in circular polarization of source *B* to $\rho_c = 40\text{--}50\%$ between $15:32$ and $15:33$ UT, followed by an abrupt decrease at $15:34$ UT. Subsequent maps made on 1 min time intervals showed no evidence for the reappearance of sources at this position or for the emergence of any other sources ($T_B \leq 10^5$ K) during the following 4 hours that this region was observed.

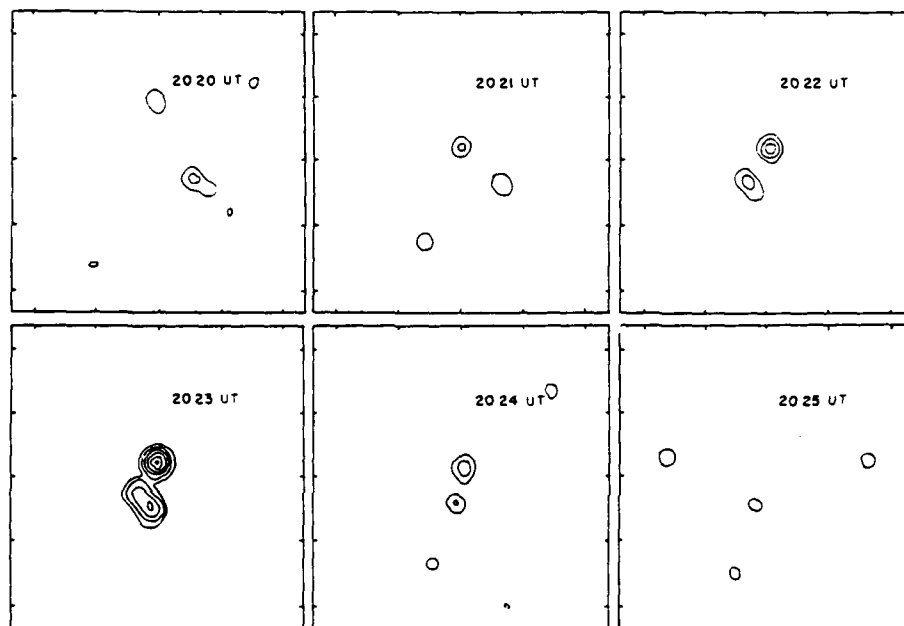


Fig. 5. VLA snapshot maps of the total intensity of a compact source at 2.1 cm wavelength. Each map is for 1 min of data, beginning at the time indicated. Here the fiducial marks are separated by $10''$. The contours mark levels of equal brightness-temperatures with an outermost contour and contour interval equal to 3.5×10^4 K.

In Figure 5 we show a series of snapshot maps depicting the emergence and decay of another 2 cm source located within a region of quiet Sun near the center of the disk (N30 W00). Again, the maps show the evolution of two compact sources on a time-scale of a few minutes. These sources, however, were, unlike those discussed previously, unpolarized ($\rho_c \leq 15\%$). Thus we cannot say whether these two sources represent the optically thick emission from the feet of a compact loop, or the unresolved emission from two separate loops.

Observations toward the quiet-Sun region in the southern hemisphere (S30 W00) yielded no detectable emission ($T_B \leq 10^5$ K) during the 2.5 hours that this region was observed. Thus, only two cases of transient 2 cm emission were observed over an area of $\sim 5' \times 5''$ during the 9.5 hr period of observation.

3. Discussion

Our results have confirmed the presence of often highly circularly polarized 2 cm emission in regions of apparently weak photospheric magnetic fields. These sources are resolved with angular sizes of between 2" and 25" and undergo variations in intensity on time-scales of a few minutes to several hours. The inferred brightness temperatures of $T_B = 1-3 \times 10^5$ K are characteristic of the transition region. These sources are found both in plage regions without sunspots as well as in areas of quiet Sun. The fact that they are nearly always present within our relatively small field of view suggests they may be quite common on the Sun. The more rapidly varying 2 cm sources have temperatures, sizes, and lifetimes that are comparable to sources of rapid brightenings observed in the transition region at ultraviolet wavelengths (Vernazza *et al.*, 1975; Bruner and Lites, 1979; Athay *et al.*, 1980; Lites, 1981; Porter *et al.*, 1984). These brightenings occur frequently throughout active regions with lifetimes of 20 to 60 s, and appear to come from regions with angular sizes of $\leq 3''$. High-resolution EUV observations of small bipolar magnetic features, or ephemeral regions, indicate similar source characteristics (Roussel-Dupre *et al.*, 1984). Porter *et al.* (1984) suggest that the rapid brightenings may represent regions of small-scale heating in which magnetic loops emerge and reconnect with the existing magnetic field structure.

The high degree of circular polarization of the 2 cm sources is somewhat enigmatic. High circular polarization can be accounted for by propagation effects (thermal bremsstrahlung) or gyroresonant absorption in the presence of magnetic fields of $B \approx 2000$ G. Both explanations have been invoked to describe the compact 2 cm sources above sunspots (Lang *et al.*, 1983; Shevgaonkar and Kundu, 1984). However, the compact sources described here did not lie near sunspots and in fact lay above regions of apparently weak photosphere magnetic field ($B \leq 100$ G). Although gyroresonant absorption might account for the circular polarization, the weak magnetic field requires a very high harmonic ($n > 50$). The optical depth due to gyroresonant absorption is then negligibly small and cannot account for the observed brightness temperature of $T_B \approx 10^5$. Thermal bremsstrahlung, however, might explain the unpolarized sources (Figures 1 and 4) if the emission measure within the source is sufficiently high.

Recently, for example, Habbal *et al.* (1986) used the VLA to observe 20 cm emission from a number of so-called coronal bright points. These sources are variable on time-scales of a few minutes and have brightness temperatures between 1 and 5×10^5 K. These observations suggest that the radiation is dominated by emission in the transition region.

Some of these sources were also moderately circularly polarized with $\rho_c \leq 40\%$, yet there was no indication of exceptionally strong bipolar features underlying the radio emission. Habbal *et al.* (1986) interpreted these fluctuations in terms of density and temperature fluctuations in the transition region combined with plasma motions along changing magnetic fields. The 20 cm polarization was interpreted as a propagation effect in a thermal plasma with magnetic fields of between 50 and 200 G.

They showed the observed brightness temperature of a thermal plasma in the extraordinary and ordinary modes, T_{B_e} and T_{B_o} , could be expressed in terms of the coronal temperature, T_{cor} , the gas pressure, P_0 , and the conductive flux, F_c , in the transition region as

$$T_{B_{x,0}} = \frac{a_{x,0} T_{cor}}{a_{x,0} + 1},$$

where

$$a_{x,0} = \frac{1.95 \times 10^{-7} P_0^2}{v^2 (1 \mp v_H/v)^2 F_c}$$

and

$$P_0 = N_e T_e,$$

$$F_c = 1.1 \times 10^{-6} T_e^{5/2} \frac{dT_e}{dl}.$$

Here, v is the observing frequency, v_H is the gyrofrequency corresponding to a magnetic field H , N_e is the electron density, and T_e is the electron temperature.

The observed degree of circular polarization, ρ_c , is

$$\rho_c = \frac{T_{B_e} - T_{B_o}}{T_{B_e} + T_{B_o}}.$$

With $T_{cor} = 1.5 \times 10^6$ K, they showed that the observed brightness temperatures at 20 cm could be explained for $P_0^2/F_c \approx 2 \times 10^{24}$, consistent with quiet-Sun values (Withbroe and Noyes, 1977). For the same values, however, the predicted brightness temperatures at 2 cm wavelength are about a factor of 100 smaller and, therefore, cannot explain the present observations.

Under what conditions might we expect to observe the thermal bremsstrahlung from compact transient sources? Roussel-Dupré *et al.* (1984), for example, derive electron temperatures of $T_e = 1.6 \times 10^4 - 3 \times 10^5$ K and electron densities of $N_e = 10^{11} - 10^{12} \text{ cm}^{-3}$ from EUV observations of an ephemeral region. These regions are similar to the 2 cm sources in that they sometimes appear to move as they grow and evolve, typically with velocities of $\approx 0.5 \text{ km s}^{-1}$ (e.g., Martin *et al.*, 1985). For a pressure of $P_0 = 3 \text{ dyne cm}^{-2}$, a magnetic field strength of $H \leq 100$ G, and a conductive flux of $F_c = 2 \times 10^6 \text{ erg cm}^{-2} \text{ s}^{-1}$, typical of a quiet-Sun transition region, we would expect a brightness temperature of $T_{B_e} \approx T_{B_o} \approx 3 \times 10^5$ K at 2 cm wavelength. Therefore, if the transient microwave sources are related to ephemeral regions, or other regions of enhanced pressure, then their brightness temperatures could be attributed to a thermal plasma. However, we cannot explain the high degree of circular polarization ($\rho_c = 40\text{--}50\%$) unless there are unexpectedly high magnetic fields ($H \approx 2000$ G) in the regions where the 2 cm emission originates.

An alternative explanation, discussed by Willson and Lang (1986) is that the compact 2 cm sources arise from the nonthermal gyrosynchrotron-radiation of mildly relativistic electrons in relatively weak magnetic fields. This idea has also been suggested as the explanation for the high brightness temperatures ($T_B \geq 2 \times 10^6$ K) of 6 cm sources that are found close to neither enhanced X-ray emission nor sunspots (Webb *et al.*, 1983; Chiuderi Drago and Melozzi, 1984).

A fundamental difficulty with this model is the uncertain nature of the mechanism that accelerates electrons to near-relativistic energies. One possibility is that there are small-scale magnetic loops in the transition region or corona where electrons can be accelerated and confined in a magnetic bottle (e.g., Takakura and Kai, 1966; Brown and Hoyng, 1975). This so-called magnetic trap model has, for example, been successful in explaining the characteristics of hard X-ray and microwave bursts. It has been observed that the flux within small ($\theta \leq 3''$) knots in the photosphere can change on relatively rapid time-scales (Komle, 1979; Wilson and Simon, 1983; Topka and Tarbell, 1983; Simon and Wilson, 1985), and it is the evolution of these fields that might lead to the acceleration of electrons. These evolving fields might also give rise to isolated magnetic elements, or plasmoids (Cargill and Pneumann, 1984) which in turn might explain explosive events representing high-velocity mass ejections that have been observed at ultraviolet wavelengths (Karpen *et al.*, 1982).

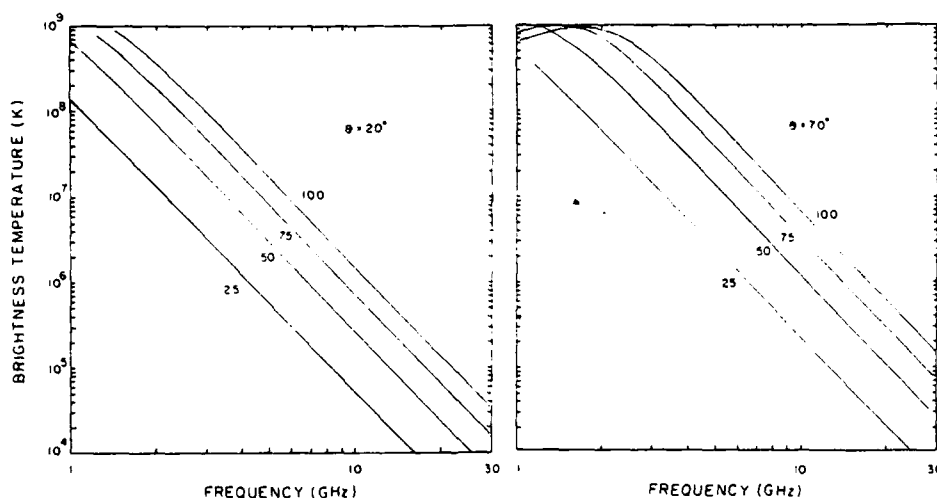


Fig. 6. Plots of the brightness temperature for nonthermal (power-law) radiation source. These spectra were generated assuming a power-law index of $\delta = 3.0$, a nonthermal electron density of $N = 5 \times 10^7 \text{ cm}^{-3}$, a path length $L = 5 \times 10^7 \text{ cm}$, viewing angles θ of 20° (left) and 70° (right) and magnetic field strengths of $H = 25, 50, 75$, and 100 G .

In Figure 6 we show theoretical spectra of nonthermal (power-law) radiation from electrons in magnetic fields of $H = 25\text{--}100 \text{ G}$. These spectra were computed using the relationships given by Dulk and Marsh (1982) and Dulk (1984) for a power-law index

of $\delta = 3.0$, a nonthermal electron density of $N = 5 \times 10^7 \text{ cm}^{-3}$, a path length of $L = 5 \times 10^7 \text{ cm}$, viewing angles of $\theta = 20^\circ$ and 70° , and magnetic field strengths ranging between 25 and 100 G. These spectra indicate that brightness temperatures of $T_B > 10^5 \text{ K}$ can be produced at 2 cm wavelength in relatively low magnetic fields of $H > 75 \text{ G}$. With these values of δ , N , and L , the circular polarization may be as high as $\rho_c = 40\text{--}50\%$ for viewing angles of $\theta \approx 20^\circ$, and magnetic fields of $H > 75 \text{ G}$. The variable polarization of the compact source shown in Figures 3 and 4 may, therefore, reflect changes in some combination of the electron energy, density, or magnetic field strength as the source evolved.

Figure 6 also shows that the brightness temperature increases towards the longer wavelength, reaching $T_B \approx 10^9 \text{ K}$ at $\lambda = 20 \text{ cm}$. In this case, nonthermal emission from compact resources would also be detectable at the longer wavelengths (6 and 20 cm), available at the VLA. However, if the nonthermal emission is generated in the transition region, then the surrounding thermal plasma might significantly attenuate this emission at the longer wavelengths. This is because for a given electron density, temperature, and path length, the opacity of the thermal plasma increases as the square of the wavelength.

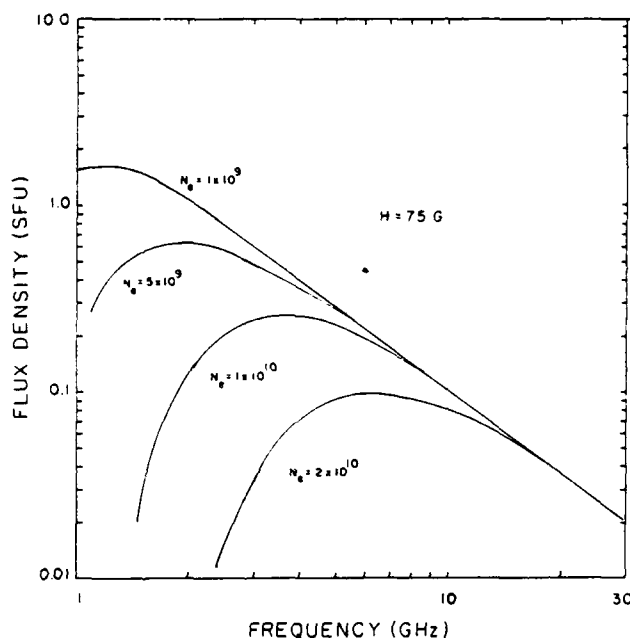


Fig. 7. Flux-density spectra of a nonthermal radiation source in the presence of a thermal plasma. These spectra were generated assuming a source size of $\theta = 5''$, a power law index of $\delta = 3.0$, a nonthermal electron density of $N = 5 \times 10^7 \text{ cm}^{-3}$, a path length of $L = 5 \times 10^7 \text{ cm}$, a magnetic field strength of $H = 75 \text{ G}$, a viewing angle of $\theta = 20^\circ$, and thermal electron densities ranging from $N_e = 1 \times 10^9 \text{ cm}^{-3}$ to $2 \times 10^{10} \text{ cm}^{-3}$. These plots indicate that the nonthermal emission may be significantly attenuated at the lower frequencies for $N_e > 5 \times 10^9 \text{ cm}^{-3}$.

In Figure 7 we show plots of the flux density of a nonthermal source embedded within such an absorbing plasma. Here, we assumed a constant source size of $\theta = 5''$, typical of the transient sources discussed in Section 2. These plots were generated by solving the equation of transfer for the brightness temperature using the density and temperature structure of the quiet-Sun transition region and corona as given by Vernazza *et al.* (1981). For a quiet-Sun transition region pressure of $N_e T_e = 10^{15} \text{ cm}^{-3} \text{ K}$, our calculations indicate that the nonthermal radiation would not be significantly attenuated. However, for higher densities of $N_e > 10^{10} \text{ cm}^{-3}$ and $T_e = 2 \times 10^5 \text{ K}$, the optical depth due to thermal absorption could be large enough to screen the nonthermal emission and effectively prevent the transient sources from being detected at the longer wavelengths. For example, the minimum 20 cm detectable flux of a source $5''$ in size during a 60 s integration (10:1 signal-to-noise ratio) at the VLA in the A or B configuration (synthesized beamwidths $\theta = 1.2''$ and $4.4''$, respectively) is $\sim 0.015 \text{ SFU}$ and 0.0015 SFU , respectively. This would therefore suggest that nonthermal transient sources originating in regions where $N_e \geq 2 \times 10^{10} \text{ cm}^{-3}$ would not be detectable at this wavelength with the VLA. Finally, as pointed out by Chiuderi Drago and Melozzi (1984), collisions with thermal electrons will decrease the energy of the nonthermal particles, thereby limiting the time that they radiate. For electron velocities of $v \geq 0.5c$ and thermal electron densities of $N_e \geq 10^{10} \text{ cm}^{-3}$, the so-called energy exchange time is less than 6 min, much shorter than the radiative lifetime of about 5 hours in a magnetic field of $H \leq 100 \text{ G}$. Simultaneous observations at several wavelengths of the brightness temperature and lifetimes of transient sources could, therefore, place useful constraints on their emission mechanism and place of origin.

Acknowledgements

The VLA is a facility of the National Radio Astronomy Observatory, which is operated by associated Universities, Inc., under contract with the National Science Foundation. Radio Astronomical studies of the Sun at Tufts University are supported under grant AFOSR-83-0019 with the Air Force Office of Scientific Research and contract N0014-86-K-0068 with the office of Naval Research (ONR). Comparisons of VLA and Solar Maximum Mission (SMM) data are supported by our NASA-SMM Guest Investigator grant NAG5-501.

References

- Akhmedov, Sh. B. *et al.*: 1986, *Astrophys. J.* **310**, 760.
- Athay, R. G., White, O. R., Lites, B. W., and Bruner, E. C.: 1980, *Solar Phys.* **66**, 357.
- Brown, J. C. and Hoyng, P.: 1975, *Astrophys. J.* **200**, 734.
- Bruner, E. C. and Lites, B. W.: 1979, *Astrophys. J.* **228**, 322.
- Cargill, P. J. and Pneuman, G. W.: 1984, *Astrophys. J.* **276**, 369.
- Chiuderi Drago, F. and Melozzi, M.: 1984, *Astron. Astrophys.* **131**, 103.
- Dulk, G. A.: 1985, *Ann. Rev. Astron. Astrophys.* **23**, 169.
- Dulk, G. A. and Marsh, K. A.: 1982, *Astrophys. J.* **259**, 350.
- Habbal, S. H., Ronan, R. S., Withbroe, G. L., Shevgaonkar, R. K., and Kundu, M. R.: 1986, *Astrophys. J.* **306**, 740.

- Karpen, J. T., Oran, E. S., Mariska, J. T., Boris, J. P., and Brueckner, G. E.: 1982, *Astrophys. J.* **261**, 375.
- Komle, N.: 1979, *Solar Phys.* **64**, 213.
- Lang, R. R., Willson, R. F., and Gaizauskas, V.: 1983, *Astrophys. J.* **267**, 455.
- Lites, B. W.: 1981, *Solar Phys.* **71**, 329.
- Martin, S. F., Livi, S. H. B., Wang J., and Shi, Z.: 1985, *NASA Conf. Publ.*, NASA CP-2374, p. 403.
- Porter, J. G., Toomre, J., and Gebbie, K. B.: 1984, *Astrophys. J.* **283**, 879.
- Roussel-Dupré, R., Wrathall, J., Nicolas, K. R., Bartoe, J. D. F., and Brueckner, G. E.: 1984, *Astrophys. J.* **278**, 428.
- Shevgaonkar, R. K. and Kundu, M. R.: 1984, *Astrophys. J.* **283**, 413.
- Simon, G. W. and Wilson, P. R.: 1985, *Astrophys. J.* **295**, 241.
- Takakura, T. and Kai, K.: 1966, *Publ. Astron. Soc. Japan* **18**, 57.
- Topka, K. and Tarbell, T.: 1983, in S. Keil (ed.), *Small-Scale Dynamical Processes in Quiet Stellar Atmospheres*, Proc. Nat. Soc. Obs. Conf., Sunspot, N.M.: NSO, pp. 278–286.
- Vernazza, J. E., Avrett, E. H., and Loeser, R.: 1981, *Astrophys. J. Suppl.* **45**, 635.
- Vernazza, J. E., Foubert, P. V., Huber, M. C. E., Noyes, R. W., and Reeves, E. M.: 1975, *Astrophys. J.* **199**, L123.
- Webb, D. F., Davis, J. M., Kundu, M. R., and Velusamy, T.: 1983, *Solar Phys.* **85**, 267.
- Willson, R. F. and Lang, K. R.: 1986, *Astrophys. J.* **308**, 443.
- Wilson, P. R. and Simon, G. W.: 1983, *Astrophys. J.* **273**, 805.
- Withbroe, G. L. and Noyes, R. G.: 1977, *Ann. Rev. Astron. Astrophys.* **15**, 363.

28. MULTIPLE WAVELENGTH MICROWAVE OBSERVATIONS OF THE RS CANUM VENATICORUM STARS UX ARIETIS, HR 1099, HR 5110, AND II PEGASI

ROBERT F. WILLSON AND KENNETH R. LANG

Department of Physics and Astronomy, Tufts University

Received 1985 November 18; accepted 1986 June 26

ABSTRACT

The VLA was used to observe the RS CVn stars, UX Arietis, HR 1099, HR 5110, and II Pegasi with a time resolution of 6.6 s at two pairs of wavelengths near 4835 MHz and 1415 MHz. Variable emission was detected from UX Arietis at 4835 MHz on time scales ranging from 30 s to more than 1 hr, but there were no detectable variations at 1415 MHz. From the rise time of the shortest variation of ~ 30 s, we use the light-travel time argument to obtain an upper limit to the source size of $L \leq 9 \times 10^{11}$ cm, or about 4 times smaller than the halo size determined from VLBI techniques. More plausible Alfvén velocities of 2×10^8 cm s $^{-1} \leq V_A \leq 7 \times 10^9$ cm s $^{-1}$ imply source sizes of 6×10^9 cm $\leq L \leq 2 \times 10^{11}$ cm for the 30 s variations. These sizes are smaller than the binary separation and most-likely smaller than the size of an individual star. Here we also derive a magnetic field of $H \leq 15$ G for the varying source and show that the relatively rapid time scales of the variations cannot be due to synchrotron radiation losses. Instead we suggest that the variations may be due to absorption by a thermal plasma located between the stars.

Subject headings: stars: binaries — stars: individual — stars: radio radiation — radio sources: variable

I. INTRODUCTION

Observations of RS CVn stars at centimeter wavelengths have shown that some of these objects exhibit strong and variable emission on time scales of minutes to several days. Among the more active and well studied RS CVn stars are UX Arietis (G5 V + K1 IV) and HR 1099 (G5 IV + K1 IV). Gibson, Hjellming, and Owen (1975) showed that the flux from UX Arietis at 2095 MHz and 8085 MHz decreased by about a factor of ~ 2.5 over a 24 hr period. Feldman *et al.* (1978) subsequently discovered variations on a time scale of a few hours from HR 1099 at 10.5 GHz. Shorter variations were reported from HR 1099 by Brown and Crane (1978); the 2695 MHz flux underwent rapid, and possibly periodic, fluctuations on a time scale of about 4 minutes.

The microwave radiation from UX Arietis and HR 1099 is often highly circularly polarized, especially, but not exclusively, during periods of little variation (Brown and Crane 1978; Mutel and Weisberg 1978; Mutel *et al.* 1985; Pallavicini, Willson, and Lang 1985). During a variation, the radio spectrum is usually inverted, with a spectral index, $\alpha \approx 1$. These properties suggest that the emission mechanism is gyrosynchrotron radiation from mildly relativistic electrons radiating in magnetic fields of a few tens of gauss (Owen, Jones, and Gibson 1976).

Recent VLBI observations have provided information about the sizes of a number of RS CVn Stars. Mutel *et al.* (1985) and Lestrade *et al.* (1985) have shown that UX Arietis contains an unresolved core (size $L \leq 3 \times 10^{11}$ cm) embedded in extended halo of about 3.2×10^{12} cm in size and that HR 1099 contains a single unresolved component whose size is $L \leq 1.1 \times 10^{12}$ cm. The separations between the binary components of UX Arietis and HR 1099 are, $\sim 1.5 \times 10^{12}$ cm, and 8.4×10^{11} cm, respectively. Observations of HR 5110 at 8.4 Lestrade *et al.* (1984) indicate a source size of 1.1×10^{12} cm, comparable to the overall size of the binary system. The VLBI size estimates, together with the observed flux densities indicate peak brightness temperatures of $T_B \geq 4 \times 10^8$ K for HR 5110 and $T_B \geq$

10^{10} K for UX Ari and HR 1099. A temperature of 10^{10} K is not inconsistent with the idea that the radio emission is due to gyrosynchrotron emission, but significantly higher brightness temperatures might indicate a coherent emission mechanism such as an electron-cyclotron maser (Melrose and Dulk 1982).

More stringent limits to the size and brightness temperature can be obtained by measuring the rise time of the variable emission using the light-travel time argument to place an upper limit to the size. This approach has, for example, recently been used to derive brightness temperatures of $T_B \geq 10^{16}$ K from intense millisecond spikes emitted by the dwarf M star AD Leonis (Lang and Willson 1986).

In this paper we present 6.6 s VLA observations of UX Arietis at HR 1099, HR 5110, and II Peg at two pairs of frequencies near 1415 MHz and 4835 MHz. The RS CVn stars HR 5110 and II Peg were studied because both are known to vary at radio wavelengths (Feldman 1979; Viner 1979; Spangler, Owen, and Hulse 1977). In § II we present the data and show that UX Arietis exhibited variations on time scales ranging between ~ 30 s to more than 1 hr. In § III we discuss these observations and derive an upper limit of $L \leq 1.98 \times 10^{11}$ cm for the source size. Here we also derive a magnetic field of $H \leq 15$ G for the varying source and show that the time scale of the variations cannot be due to synchrotron radiation losses. Instead we suggest that the variations may be due to absorption by a thermal plasma located between the stars.

II. OBSERVATIONS

The RS CVn stars UX Arietis HR 1099, HR 5110, and II Peg were observed with the VLA (B configuration) on 1985 June 10. One subarray containing 13 antennas was used to observe at frequencies of 1415 MHz and 1465 MHz and another subarray containing 14 antennas was used to observe at frequencies of 4835 MHz and 4885 MHz. In all cases the bandwidth was 50 MHz. The fringe visibilities were sampled at a rate of 6.67 s, and the data were calibrated from observations

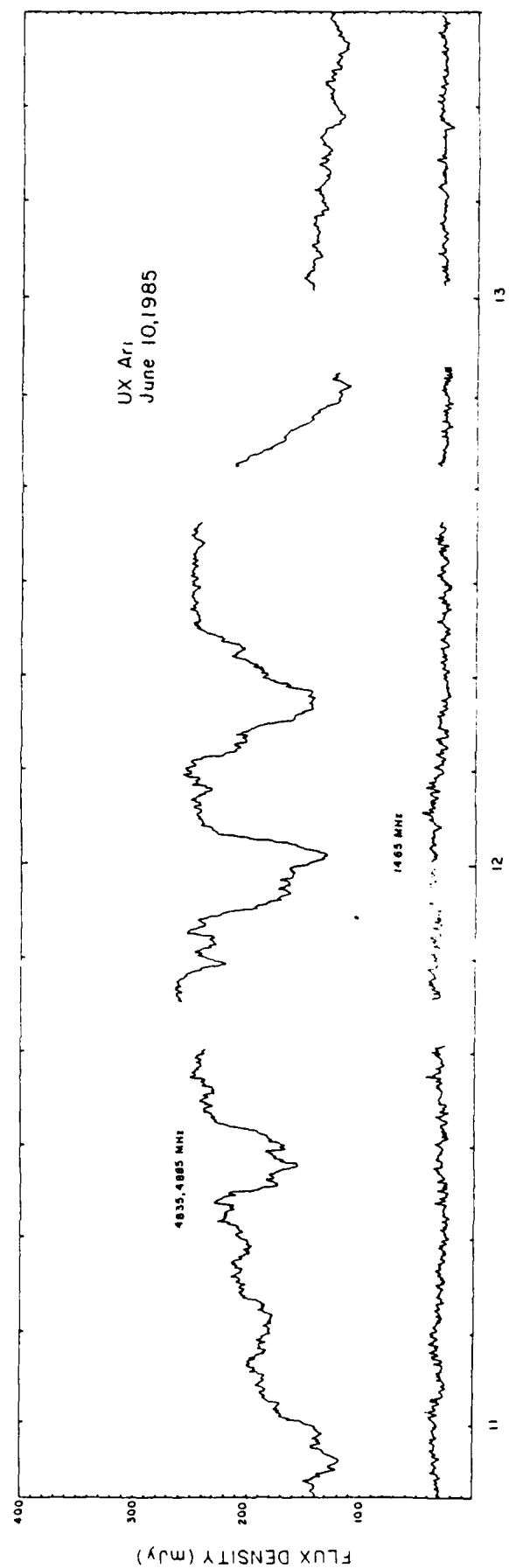


FIG. 1.—A plot of the total intensity, I , observed at 1465 MHz, 4835 MHz, and 4885 MHz from the RS CVn star UX Ariens on 1985 June 10. The visibility data were phase-shifted to the source center and then vector-averaged, baseline by baseline, over a 6.67 s interval to produce these time profiles.

of 3C 236 (14.51 Jy at 1465 MHz and 7.4 Jy at 4835 MHz) and 0333+321 (3.14 Jy at 1465 MHz and 2.64 Jy at 4835 MHz). The raw data were first examined, baseline by baseline, for the presence of interference or any obviously bad data.

The edited data were then calibrated and used to make synthesis maps of the sources which were then cleaned and fitted with two-dimensional Gaussian functions in order to determine their locations to within about one-tenth of the beamwidth (1.9×2.0 at 4885 MHz, 3.7×5.0 at 1465 MHz). The 6.6 s data were then phase-shifted to bring the sources exactly into the center of the map. Finally, these data were vector-averaged, baseline by baseline, and used to construct plots of total intensity, I , and circular polarization, p_c , as a function of time for the 2 hr observation interval. For a 6.6 s integration time the theoretical 3σ rms noise level is ~ 7 mJy at 1415 MHz and 1465 MHz and ~ 6 mJy at 4835 MHz and 4885 MHz.

Our observations indicate that HR 1099, HR 5110, and II Peg exhibited no significant fluctuations in intensity on any time scales ranging from 6.6 s to more than 1 hr, but that UX Ari varied significantly throughout the 2.5 hr period of observation. In Table 1, we give the total intensity and circular polarization at 6 and 20 cm wavelength for each of the four sources. For HR 1099, HR 5110, and II Peg, the 3σ errors were determined from the rms noise levels on the synthesis maps.

In Figure 1 we show the plots of total intensity for UX Arietis at 4835 MHz, 4885 MHz, and 1465 MHz. These plots indicate that UX Arietis was much more intense and time variable at 4835 MHz and 4885 MHz. There was no detectable circular polarization at any frequency, to a limit of 5%. The major variations in flux occur on time scales of ~ 10 –20 minutes, but faster variations are also apparent in the data. The peak flux occurs at ~ 1145 UT with an amplitude of ~ 270 mJy. In contrast, the flux at 1415 MHz and 1465 MHz has a nearly constant value of ~ 30 mJy. In Figure 2 we show a section of data with variations as short as 30 s. Here, the data at 4835 MHz and 4885 MHz have been averaged together in order to improve the signal-to-noise ratio. The burst denoted by an arrow has an amplitude of ~ 30 mJy and a rise time of ~ 30 s. In order to check that these fluctuations are real and not caused by instrumental effects, we constructed a series of 2 minute snapshot maps at both 4835 MHz and 4885 MHz at various times during these observations. Small phase errors, for example, might mimic rapid time variations if the effective phase center varies by a small fraction of the synthesized beam over time scales of a few minutes. Examination of these maps, however, confirmed that the fluxes derived from them were nearly identical at 4835 MHz and 4885 MHz and that they agreed with the values determined by vector-averaging the data.

III. DISCUSSION

Our observations of UX Arietis indicate that the 6 cm flux varied on time scales ranging from ~ 30 s to more than 1 hr. From the shortest variations of ~ 30 s, we can place an upper limit of $L \leq 9 \times 10^{11}$ cm for the size of the emitting region under the assumption that the source cannot move faster than the velocity of light. This size is 4 times smaller than that of the halo component obtained from 6 cm VLBI observations (Mutel, Doiron, and Phillips 1984; Mutel *et al.* 1985), but comparable to the size of the core component ($l \leq 3 \times 10^{11}$ cm) found by Mutel *et al.* (1985). With an amplitude of ~ 30 mJy and a size of $L \leq 9 \times 10^{11}$ cm, we derive a brightness temperature of $T_B \geq 10^9$ K.

Velocities considerably below the velocity of light are most likely. For example, plausible magnetic field strengths of $H = 10$ –100 G and electron densities of $N_e = 10^7$ – 10^8 cm $^{-3}$ (Gibson, Hicks, and Owen 1974; Mutel, Doiron, and Phillips 1984), result in an Alfvén velocity of 2×10^8 cm s $^{-1} \leq V_A \leq 7 \times 10^9$ cm s $^{-1}$. This implies a source size of $L = 6 \times 10^9$ cm to 2×10^{11} cm and a brightness temperature of $T_B \geq 10^{11}$ K to $T_B \geq 10^{13}$ K for the rapid 30 s variations. These sizes are small compared to the separation between the two stars ($L = 1.4 \times 10^{12}$ cm) and to the sizes of the stars themselves ($L = 1.4 \times 10^{11}$ cm and 4.2×10^{11} cm).

Dulk and Marsh (1982) have shown that brightness temperatures of up to $\sim 10^{10}$ K may be explained in terms of gyrosynchrotron emission from nonthermal particles radiating in magnetic fields of a few tens of gauss, but that significantly higher brightness temperatures may require a coherent emission mechanism such as an electron cyclotron maser. In principle, the possibility of a brightness temperature as high as 10^{13} K would favor a coherent emission mechanism. However, since electron-cyclotron maser emission is expected to be highly circularly polarized (Melrose and Dulk 1982), the unpolarized variable emission discussed here would seem to exclude this particular coherent emission mechanism.

Synchrotron self-absorption with a spectral index of $\alpha = 2.5$ has been invoked to explain the inverted spectra often observed during radio bursts from RS CVn stars (Owen, Jones, and Gibson 1976; Spangler 1977; Hjellming and Gibson 1980). The turnover frequency due to synchrotron self-absorption is $\nu_{sa} = 8.1 \times 10^{-4} (S_m/\Omega)^{2/5} H^{1/5}$ (Slysh 1963), where ν_{sa} is given in MHz, Ω is the source solid angle, and H is the magnetic field strength in G. If it is assumed that the absence of burst emission at 21 cm is due to synchrotron self-absorption, then the source size may be estimated. Adopting $\nu \approx 5000$ MHz, $S_m = 270$ mJy, and $H = 100$ G, we derive a source size of $L \approx 10^{12}$ cm, which exceeds the upper limits established from plausible

TABLE 1
JOURNAL OF OBSERVATIONS

	Date (1985)	UT Time	Wavelength (cm)	Flux (mJy)	Polarization (%)
HR 5110	Jun 9	2308–0411	6	17.2 ± 0.2	$+11.7$
			20	20.1 ± 0.25	≤ 5
II Pegasi	Jun 10	0903–0951	6	9.2 ± 0.4	$+10$
UX Arietis	Jun 10	1052–1330	6	$120\text{--}270$	≤ 5
			20	30	≤ 5
HR 1099	Jun 10	2103–2253	6	11.8 ± 0.3	< 5
			20	16.8 ± 0.4	-27

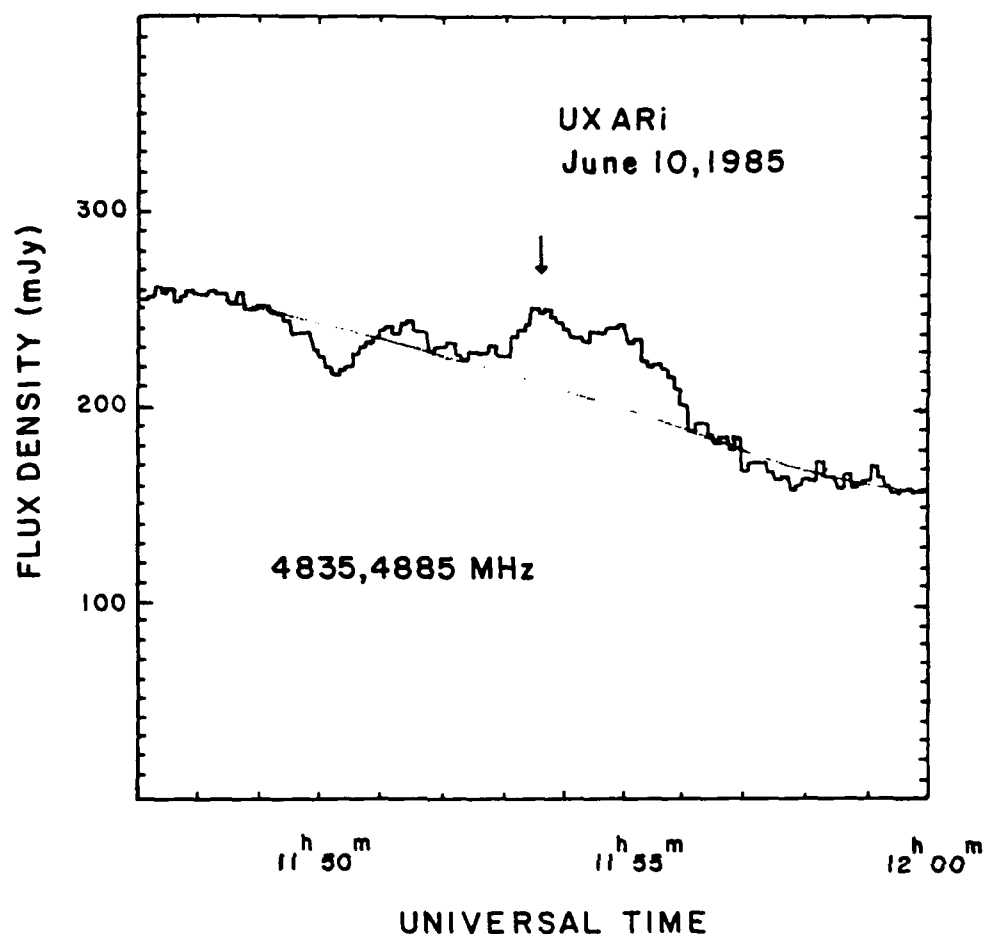


FIG. 2.—A plot of the total intensity, I , observed at 4835 MHz and 4885 MHz from UX Arietis. Here the data at these two frequencies have been averaged together. The time resolution of this plot is 6.67 s; the arrow shows a burst with a rise time of ~ 30 s.

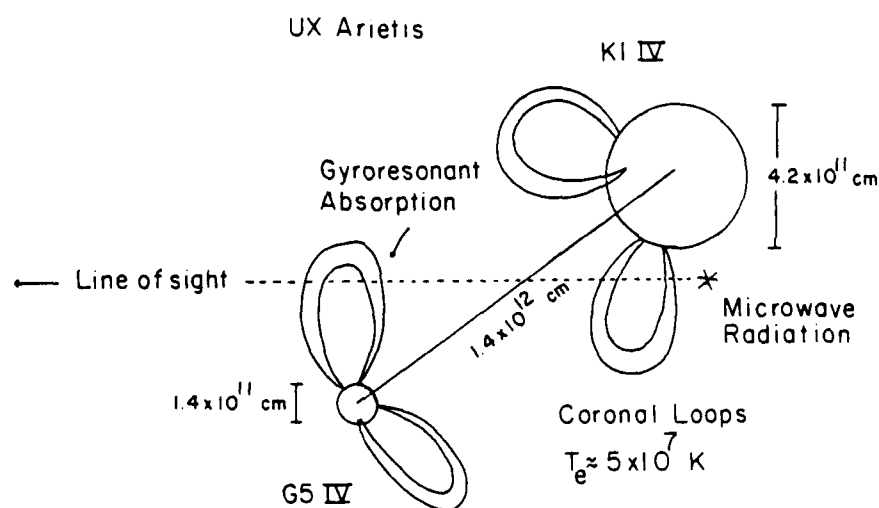


FIG. 3.—A schematic view of UX Arietis showing the orientation of the two components during the time of our observation. Six cm burst emission occurring on the more active K1 star may have passed through a coronal loop located between the two stars, giving rise to thermal absorption. The orbital inclination, $i \approx 55^\circ$, is inferred from the data of Carlos and Popper (1971).

Alfvén velocities for the 30 s variations. However, smaller magnetic fields of $H \approx 10$ G imply a smaller size of $L \approx 3 \times 10^{11}$ cm under synchrotron self-absorption hypothesis.

Fields as small as 10 G are in fact suggested by the lack of polarization of the 6 cm burst emission. Dulk and Marsh (1982) have shown that the degree of circular polarization, ρ_c , of optically thin gyrosynchrotron radiation from mildly relativistic electrons having a power law distribution in energy is

$$\rho_c = 1.26 \times 10^{0.035\delta} \times 10^{-0.071 \cos \theta} \left(\frac{\nu_H}{\nu} \right)^{[-0.782 + 0.545 \cos \theta]}$$

Here, $\nu_H = 2.8 \times 10^6 H$ is the gyrofrequency, δ is the electron energy index, and θ is the angle between the magnetic field and the line of sight. For $\delta = 3-4$, we require $H \leq 15$ G and $\theta \geq 70^\circ$ in order to yield a circular polarization of less than about 5%, the approximate upper limit obtained from the VLA observations.

Fields as low as 15 G may, however, present a problem regarding the relatively rapid timescales of the 6 cm variations. According to Mullan (1985), an outburst observed from an RS CVn star has a time scale that is controlled by the evolutionary time scale of a coronal loop that expands outward from the stellar surface. Eventually the outburst will "turn off" when the loop de-couples from the stellar interior. When this happens it is expected that the burst lifetime will be determined by the synchrotron radiative loss lifetime (Chiuderi and Chiuderi-Drago 1967)

$$t_{1/2} \approx \frac{1.8 \times 10^8}{H^2} \text{ s.}$$

For $H = 15$ G, we find $t_{1/2} = 222$ hr, which is inconsistent with the much shorter time scales of variability reported here.

One possibility is that the major dips in intensity during the peak of the gradual burst are due to absorption by thermal plasma located between the stars. Observations of the Sun at centimeter wavelengths sometimes show "negative" bursts in which the flux decreases abruptly before or during gradual rise and fall bursts (Covington and Dodson 1952; Tanaka and Kakinuma 1960; Covington 1969). These events are sometimes associated with H α prominences or filament activity that obscure the underlying microwave sources for brief periods of time (Sawyer 1977a, b).

A model that might explain the relatively abrupt variations of less than 10–20 minutes is one in which the variable emission is absorbed by a thermal plasma lying between the two stars. There is ample evidence for thermal plasma within the UX Arietis system. X-ray observations indicated the presence of two emission components with electron temperatures $T_e \approx 8 \times 10^6$ and $\sim 5 \times 10^7$ K (Swank *et al.* 1981). The lower temperature emission is believed to arise in coronal loops whose lengths are a small fraction of the radius of the more active star. The higher temperature plasma may reside in coronal loops which are comparable in size to the binary system. Simon, Linsky, and Schiffer (1980) have also found evidence for loops which interconnect two stars and which serve as conduits for mass exchange. These loops may provide the mechanism by which particles are accelerated, giving rise to radio bursts (Uchida and Sakurai 1983; Mullan 1985).

The orbital phase of UX Arietis during the time of our

observations was $\phi = 0.457-0.472$, as computed from the ephemeris of Carlos and Popper (1971), where zero phase corresponds to the cooler, more active K0 IV star in front. This means that the more active star was situated on the far side of its orbit, as shown schematically in Figure 3, so that burst emission which was generated near that star had a greater probability of passing through material lying between the two stars than at any other time.

Observations indicate that both gyroresonant and thermal bremsstrahlung processes contribute to the centimeter wavelength opacity on the Sun (Lang, Willson, and Rayrole 1982; Dulk and Gary 1983; Lang, Willson and Gaizauskas 1983; McConnell and Kundu 1984). Under the assumption that gyroresonance absorption is the dominant mechanism at 6 cm wavelength, field strengths of 445–595 G are required if the absorption occurs at the third or fourth harmonic of the gyrofrequency. In the present case, however, unless the absorption occurs close to the secondary G5 star, fields as high as these imply surface fields which are much larger than those deduced from starspot analyses of RS CVn and late-type stars (Bonsack and Simon 1983; Marcy 1983). Thus it seems unlikely that gyroresonance absorption plays a role in modulating the burst emission from the active star in UX Arietis.

The optical depth due to thermal bremsstrahlung however does not depend on the magnetic field, and is given by

$$\tau_{TB} = \frac{9.78 \times 10^{-3} N_e^2}{\nu^2 T_e^{3/2}} \ln \frac{(4.7 \times 10^{10} T_e)}{\nu} L,$$

where N_e is the electron density, T_e is the electron temperature, and L is the path length through the absorbing medium. For a temperature of $T_e = 10^7$ K, an electron density of $N_e = 1.5 \times 10^9 \text{ cm}^{-3}$ and a path length $L = 10^{12}$ cm (the approximate size of the binary system) we have $\tau_{TB} \approx 0.5$ at $\nu = 4.8 \times 10^9$ Hz. If the unattenuated flux of the slowly varying emission is taken to be 220 mJy at 1130 UT, for example, then the flux after absorption by the thermal plasma is ~ 140 mJy, in good agreement with the observed value. The relatively rapid dips in total intensity at 1130 UT, 1200 UT and 1215 UT might then reflect changing physical conditions within coronal loops lying between the stars. Absorption by thermal plasma between the active loops might also explain the total absence of variations at 20 cm. Since the thermal optical depth varies nearby as λ^2 , where λ is the wavelength, the opacity from this surrounding plasma might be negligible at 6 cm, but not at 20 cm. If the optical depth is high enough, the underlying source of variable emission (as well as the effect of the changing loops) would not be detected. In this case, the quiescent 20 cm emission would likely originate in a larger halo surrounding the stars. High time resolution observations over a range of frequencies at different phases of the 6.43 day binary orbit would provide a useful test of this model.

Radio astronomical studies of the Sun and other active stars at Tufts University are supported under grant AFOSR-83-0019 with the Air Force Office of Scientific Research and contract N00014-86-K-0068 with the Office of Naval Research (CONR). Investigations of dwarf M flare stars and RS CVn Stars are also supported by NASA grant NAG 5-477. The Very Large Array is operated by Associated Universities, Inc., under contract with the National Science Foundation.

REFERENCES

- Bonsack, W. K., and Simon, T. 1983, in *IAU Symposium 102, Solar and Stellar Magnetic Fields: Origin and Coronal Effects*, ed. J. O. Stenflo (Dordrecht: Reidel), p. 35.
- Brown, R. L., and Crane, P. C. 1978, *A.J.*, **83**, 1504.
- Carlos, R. C., and Popper, D. M. 1971, *Pub. A.S.P.*, **83**, 504.
- Chiuderi, C., and Chiuderi-Drago, F. 1986, *Nuovo Cimento*, **48**, 186.

- Covington, A. E. 1969, *J.R.A.S. Canada*, **63**, 125.
 Covington, A. E., and Dodson, H. 1953, *J.R.A.S. Canada*, **47**, 207.
 Dulk, G. A., and Gary, D. E. 1983, *A.J.*, **124**, 103.
 Dulk, G. A., and Marsh, K. A. 1982, *Ap. J.*, **259**, 350.
 Feldman, P. A. 1979, *IAU Circ.*, 3366.
 Feldman, P. A., Taylor, A. R., Gregory, P. C., Seaquist, E. R., Balonek, T. J., and Cohen, N. L. 1978, *A.J.*, **83**, 1471.
 Gibson, D. M., Hjellming, R. M., and Owen, F. N. 1975, *Ap. J. (Letters)*, **200**, L99.
 Gibson, D. M., Hicks, P. D., and Owen, F. N. 1978, *A.J.*, **83**, 1495.
 Hjellming, R. M., and Gibson, D. M. 1980, in *IAU Symposium 86, Radiophysics of the Sun*, ed. M. R. Kundu and T. E. Gehrels (Dordrecht: Reidel), p. 209.
 Lang, K. R., and Willson, R. F. 1986, *Ap. J.*, **305**, 363.
 Lang, K. R., Willson, R. F., and Gaizauskas, V. 1983, *Ap. J.*, **267**, 455.
 Lang, K. R., Willson, R. F., and Rayrole, J. 1982, *Ap. J.*, **258**, 384.
 Lestrade, J. F., Mutel, R. L., Preston, R. A., and Phillips, R. B. 1985, in *Radio Stars*, ed. R. M. Hjellming and D. M. Gibson (Dordrecht: Reidel), p. 275.
 Lestrade, J. F., Mutel, R. L., Preston, R. A., Scheid, J. A., and Phillips, R. B. 1984, *Ap. J.*, **279**, 184.
 Marcy, G. W. 1983, in *IAU Symposium 102, Solar and Stellar Magnetic Fields: Origin and Coronal Effects*, ed. J. O. Stieffo (Dordrecht: Reidel), p. 3.
 McConnell, D., and Kundu, M. R. 1984, *Ap. J.*, **279**, 421.
 Melrose, D. B., and Dulk, G. A. 1982, *Ap. J.*, **259**, 844.
 Muilan, D. 1985, in *Radio Stars*, ed. R. M. Hjellming and D. M. Gibson (Dordrecht: Reidel), p. 173.
 Mutel, R. L., Doiron, D. J., and Phillips, R. B. 1984, *Ap. J.*, **278**, 220.
 Mutel, R. L., Lestrade, J. F., Preston, R. A., and Phillips, R. B. 1985, *Ap. J.*, **289**, 262.
 Mutel, R. L., and Weisberg, J. M. 1978, *A.J.*, **83**, 1499.
 Owen, F. N., Jones, T. W., and Gibson, D. M. 1976, *Ap. J.*, **210**, 127.
 Pallavicini, R., Willson, R. F., and Lang, K. R. 1985, *Astr. Ap.*, **149**, 95.
 Sawyer, C. 1977a, *Solar Phys.*, **51**, 195.
 ———. 1977b, *Solar Phys.*, **51**, 203.
 Simon, T., Linsky, J. L., and Schiffer, F. H. 1980, *Ap. J.*, **239**, 911.
 Slysh, V. I. 1963, *Nature*, **199**, 682.
 Spangler, S. R. 1977, *A.J.*, **82**, 169.
 Spangler, S. R., Owen, F. N., and Hulse, R. A. 1977, *A.J.*, **82**, 989.
 Swank, J. H., White, N. E., Holt, S. S., and Becker, R. H. 1981, *Ap. J.*, **246**, 208.
 Tanaka, H., and Kakinuma, T. 1960, *Proc. Res. Inst. Atmospheric, Nagoya University*, **7**, 72.
 Uchida, Y., and Sakurai, T. 1983, in *IAU Colloquium 71, Activity in Red Dwarf Stars*, ed. P. B. Byrne and M. Rodonó (Dordrecht: Reidel), p. 629.
 Viner, M. R. 1979, *IAU Circ.*, 3368.

KENNETH R. LANG and ROBERT F. WILLSON: Department of Physics and Astronomy, Robinson Hall, Tufts University, Medford, MA 02155

29. VLA OBSERVATIONS OF A SOLAR NOISE STORM

KENNETH R. LANG AND ROBERT F. WILLSON

Department of Physics and Astronomy, Tufts University

Received 1986 October 6; accepted 1987 January 21

ABSTRACT

We present the first Very Large Array (VLA) observations of the Sun at 92 cm wavelength (328 MHz). A solar noise storm, which lasted at least 3 hr, was detected at this wavelength; it consisted of burstlike spikes superposed on a slowly varying background, and both storm components were $95\% \pm 5\%$ right-hand circularly polarized. A long-duration soft X-ray event preceded the radio radiation by 30 minutes, suggesting a disturbance moving outward at a velocity of $v = 78 \text{ km s}^{-1}$. The 92 cm noise storm was resolved with an angular resolution of $9''$ for time intervals as short as 13 s. During the onset and early phases, the storm consisted of four compact sources, each with an angular diameter of $40''$, oriented within an elongated source with angular dimensions of $40'' \times 200''$. During the subsequent hour the most intense emission was located in two $40''$ sources separated by $100''$. Snapshot maps revealed a persistent elongated source at successive peaks, with a scatter in the source position. A systematic position shift of $\Delta\theta, \geq 15''$ can be produced by Earth's ionosphere, but these effects can be removed by frequent observations of a nearby calibrator source. Our observations confirm previously reported trends for a decrease in source size at higher frequencies, but they suggest a hitherto unresolved complexity in source structure. The new VLA results are also consistent with previous observations of noise storm polarization and height. The VLA can potentially resolve both the burst and continuum components of noise storms, while also detecting the effects of anisotropic scattering in the corona. The high angular resolution and large collecting area of the VLA may either lead to the detection of the second harmonic of the storm plasma frequency or establish important limits to it.

Subject headings: interferometry — polarization — Sun: corona — Sun: radio radiation

I. INTRODUCTION

Noise storms are the most common phenomenon observed on the Sun at decimetric and metric wavelengths (see Elgaroy [1977] and Kai, Melrose, and Suzuki [1985] for reviews). Here we will present a brief synopsis of their properties, thereby providing a perspective for our subsequent observations and discussion.

The noise storms consist of a slowly varying, wide-band continuum radiation with superposed short-lived, narrow-band bursts. The background continuum, which is usually observed between 50 and 350 MHz, normally continues for a few hours and sometimes lasts for days. The noise storms are clearly associated with solar active regions, but there is no clear-cut association with solar flares.

Literally thousands of storm bursts are emitted, each with a bandwidth between 2 and 10 MHz and a duration of 0.1 to 2 s. These bursts have been designated type I bursts in order to distinguish them from other types of solar bursts. They are superposed upon a continuum that is not thought to be composed of numerous bursts.

Both the background continuum and the bursts are strongly circularly polarized (up to 100%), usually with the same sense and degree of polarization. This polarization is attributed to coronal magnetic fields that connect with underlying sunspots. The sense of circular polarization usually corresponds to the ordinary mode of wave propagation in the magnetic field of the nearest leading spot; right-handed circular polarization therefore corresponds to negative magnetic polarity with the magnetic field lines pointed in toward the Sun.

It is thought that noise storms are some kind of plasma radiation emitted at the plasma frequency, and this is consistent with circular polarization in the ordinary mode. The emission originates in the lower solar corona at altitudes of

between 0.1 and $0.5 R_{\odot}$ (solar radii) above the photosphere. Radiation at lower frequencies originates at higher altitudes where the electron density and plasma frequency are smaller than those at lower altitudes. The inferred electron density at a given altitude is greater than that of the quiet corona at this altitude, suggesting an origin in closed magnetic loops (coronal loops) that contain a high-density plasma.

II. OBSERVATIONS

a) Time Profile

The VLA was used to observe the solar active region AR 4732 in the A-configuration between 1300 UT and 2400 UT on 1986 May 29. The position of AR 4732 was $0^{\circ}\text{N } 40^{\circ}\text{W}$ on this day. The array was divided into two subarrays with 12 antennas operating at 92 cm wavelength (328 MHz) with a 3.12 MHz bandwidth, and 15 antennas operating at 21 cm wavelength (1420 MHz) with a 12.5 MHz bandwidth. The beamwidth of the individual antennas at 21 cm was $31.5''$ and included the active region AR 4731 located at $6^{\circ}\text{S } 50^{\circ}\text{W}$ at 1300 UT on May 29. The individual antennas had beamwidths of $138''$ at 92 cm, which includes the entire visible disk of the Sun, but AR 4731 and AR 4732 were the only active regions on the visible solar surface during our observations.

All four Stokes parameters were sampled every 6.67 s, and the data were calibrated by observing 3C 84 every 30 minutes. The flux density of 3C 84 was assumed to be 32.0 Jy and 8.0 Jy at 21 cm and 92 cm, respectively.

As illustrated in Figure 1, a noise storm was detected at 92 cm between about 1930 UT and 2400 UT. No noise storm was detected at 21 cm, but this is not surprising as plasma radiation at this wavelength would be absorbed in the overlying solar atmosphere. The 92 cm noise storm consisted of numerous burstlike spikes superposed on slowly varying emission.

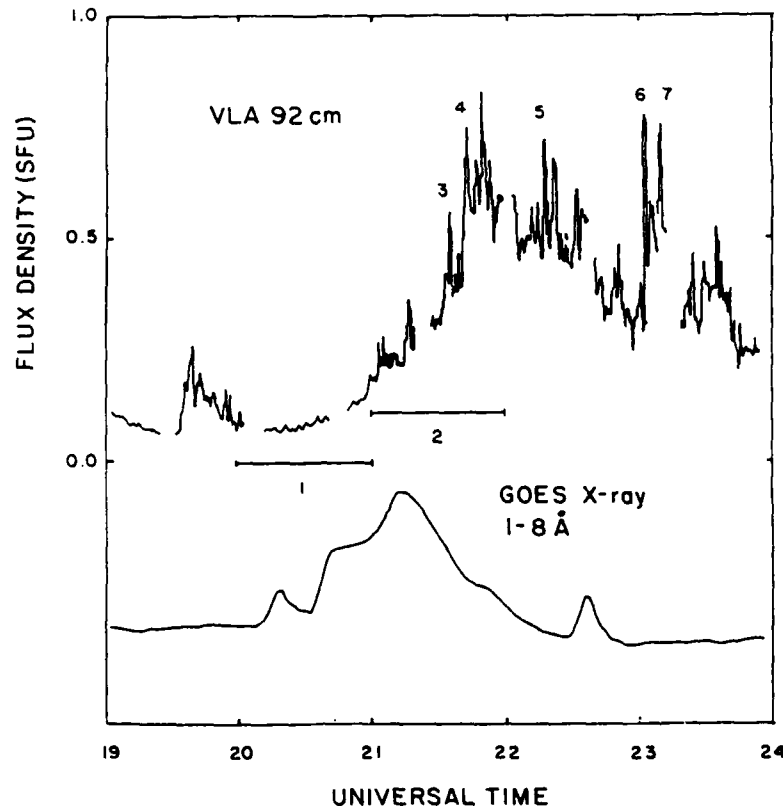


FIG. 1.—The time profile of a solar noise storm observed with one interferometer pair of the Very Large Array (VLA) at 92 cm wavelength (*top*) is compared with the soft X-ray emission detected by the GOES satellite (*bottom*). The separation of the two antennas was 0.8 km, providing an angular resolution of $240''$ at 92 cm during source transit. Here the data have been smoothed over 33.3 s. Spikelike bursts are superposed upon a slowly varying background; both of these components were $95\% \pm 5\%$ right-hand circularly polarized. VLA maps covering the intervals denoted by 1 and 2 are shown in Fig. 2, and VLA snapshot maps of the spikes denoted by 3, 4, 5, 6, and 7 are presented in Fig. 3. The X-ray emission precedes the 92 cm radiation by about 30 minutes. If we assume that the noise storm is excited by a disturbance that originates during the soft X-ray event at a distance of $0.2 R_{\odot}$, then that disturbance must travel outward at a velocity of $v \sim 78 \text{ km s}^{-1}$.

The burstlike spikes are analogous to type I bursts, but the observed data have relatively long integration times that probably integrate the emission of several type I bursts or chains of bursts. The slowly varying emission resembles the background continuum of a typical noise storm. Both the burstlike spikes and the slowly varying background emission were $95\% \pm 5\%$ right-hand circularly polarized.

A long-duration soft X-ray event (also shown in Fig. 1) may provide a clue to the triggering mechanism for the 92 cm noise storm that followed it by about 30 minutes. The noise storm may have been triggered by a disturbance moving outward from the source of the X-ray radiation. If the sources of radiation in the two spectral regions are separated by a distance of $0.2 R_{\odot}$, then the disturbance moves at a velocity of $v = 78 \text{ km s}^{-1}$.

b) Observations with High Angular Resolution

The VLA can provide angular resolutions that are more than an order of magnitude better than those of previous observations of solar noise storms. It is capable of $5''$ angular resolution at 92 cm wavelength (328 MHz). By way of comparison, the Culgoora and Nançay radioheliographs had respective beamwidths of ~ 2.0 and ~ 1.3 at 160 MHz.

As illustrated in Figure 2, the onset and first maximum of the 92 cm noise storm consisted of four compact sources, each about $40''$ in angular diameter, that were arranged within an

elongated $40'' \times 200''$ source. During the subsequent hour, the 92 cm emission was concentrated within the same elongated source, but it was most intense in two $40''$ sources separated by $100''$. For comparison, the tapered beamwidth of $9'' \times 9''$ is shown as a small black dot.

The VLA also has the capability of making snapshot maps at time intervals as short as 3 s. As an example, Figure 3 shows VLA snapshot maps of successive peaks in the emission of the 92 cm noise storm shown in Figure 1 (peaks 3, 4, 5, 6, and 7). These peaks originate in an elongated source that has a persistent, unchanging shape with half-power angular dimensions of about $40'' \times 120''$. The scatter in the locations of the most intensive emission is real, but there were no apparent trends in the location change.

Refraction in Earth's ionosphere will produce a systematic shift in source position. This shift is smallest at source transit and largest near the horizon. It is also relatively large at sunrise and at times of increased solar activity.

When theoretical formulae given by Komesaroff (1960) are combined with measurements of the ionosphere's electron density, Stewart and McLean (1982) obtain a noontime ionospheric shift of $\Delta\theta_i = 60''$ at 160 MHz. Because refraction scales as the inverse square of the observing frequency, we would expect $\Delta\theta_i = 15''$ at 92 cm (328 MHz). This is consistent with the observations of Erickson (1984) at 80 MHz and with those of Spoelstra (1983) at 600 MHz. The systematic position

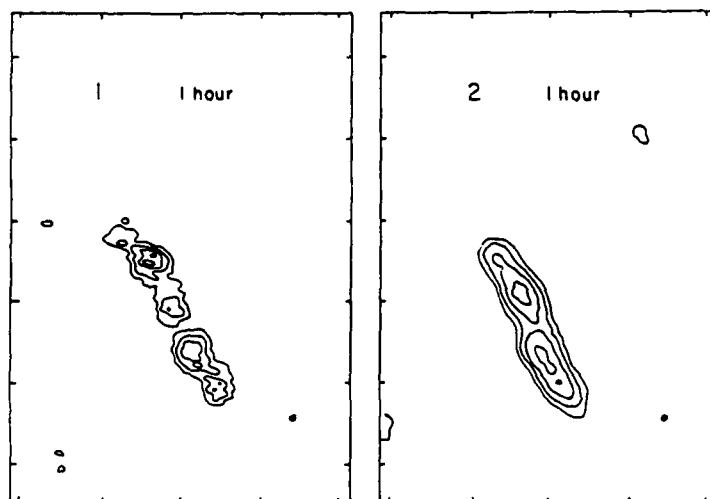


FIG. 2.—Very Large Array (VLA) synthesis maps for a 1 hr interval that includes the beginning of a solar noise storm (left) and for the subsequent 1 hr interval (right). These two intervals are respectively denoted by 1 and 2 in Fig. 1. Both the onset and early excitation of the 92 cm noise storm consist of four sources with angular diameters of $40''$ and a total angular extent of $200''$. Emission in the two central $40''$ sources became more intense later in the noise storm (see Fig. 3). The fiducial marks on the axes are separated by $100''$, and the contours mark levels of equal brightness temperature T_b , with an outermost contour of $T_b = 1.0 \times 10^6$ K and a contour interval of 7.2×10^5 K. The synthesized beamwidth is denoted by the black spot.

shift, $\Delta\theta$, can be automatically removed from future VLA data by frequent observations of a nearby calibrator source, but a smaller, random shift should remain because of the fluctuating component of the ionosphere's electron density.

III. DISCUSSION

a) Comparisons with Previous Results

Observations of noise storms with the Culgoora radioheliograph at two frequencies (80 and 160 MHz) and with the Clark Lake facility at several frequencies between 20 and 65 MHz suggest that the higher frequency radiation originates in more compact sources (Gergely and Kundu 1975; Stewart 1976; McLean 1981). This downward trend in source size with increasing frequency was also suggested by a small sample of storm sources observed with the Culgoora instrument at 80, 160, and 327 MHz (Sheridan *et al.* 1983). Characteristic half-power angular sizes of $\theta \sim 6'$, $3'$, and $1.5'$ were respectively obtained at 80, 160, and 327 MHz.

However, storm sources are also often unresolved with even the largest radio telescopes, and the telescope beamwidths exhibit a disturbingly similar downward trend with increasing frequency. There have been no systematic high-resolution investigations of the size and shape of solar noise storms because of the poor resolving power of the existing radio telescopes.

Although the new VLA observations are not inconsistent with previous observations of a decrease in source size at higher frequencies, they do suggest that complex source structure will be revealed at high resolution. Such complexity may well rule out a simple model in which noise storms originate within a conical column (diverging magnetic fields) whose size increases with height (McLean 1973, 1981).

The new VLA results are also consistent with previous polarization observations. The sense of circular polarization should correspond with that of the ordinary mode expected from plasma radiation in a strong magnetic field (Dulk and Nelson 1973; Stewart 1985). Right-handed circular polariz-

ation is therefore associated with negative magnetic polarity in which the magnetic field is directed away from the observer and into the Sun. Left-handed circular polarization is similarly associated with positive magnetic polarity in which the magnetic field is directed toward the observer.

Because our observed storm was $95\% \pm 5\%$ right-hand circularly polarized, it should originate in coronal magnetic fields that are connected with the dark, negative-polarity magnetogram features shown in Figure 4. Because the noise storm projects radially downward to the more central active region (AR 4732), the storm source is most likely associated with magnetic fields that connect to the dark, dominant leading spot of AR 4732. As a matter of fact, noise storms are usually related to the dominant, leading sunspot of the associated active region.

Thus the storm source is most likely plasma radiation on magnetic fields connected to the dark, leading spot of AR 4372. As illustrated in Figure 4, the angular size and distance of the noise storm are nevertheless larger than the angular separation of the leading and trailing spots of AR 4372. If the storm originates in closed magnetic loops, they may not be solely connected to the bipolar AR 4372. Large-scale magnetic fields may instead connect the leading spots of the two active regions AR 4371 and AR 4372. A similar model has been proposed by Kai and Sheridan (1974) for other noise storms. However, our observations cannot by themselves rule out the possibility of open magnetic field lines that extend out into the interplanetary medium.

The height of a noise storm can be found if we assume that it lies radially above the associated sunspot. Under this assumption, the average observed heights, h , at 160 MHz and 80 MHz were $h = 0.4 R_\odot$ and $h = 0.8 R_\odot$ above the photosphere (Stewart 1976). Noise storms at the higher frequencies of 327 MHz and 408 MHz have estimated heights of $h = 0.2 R_\odot$ and $h = 0.1 R_\odot$, respectively (Sheridan *et al.* 1983; Clavelier 1967).

Thus the average height of the noise storm source decreases with increasing frequency. Our observations also support this conclusion. The angular displacement of the noise storm from

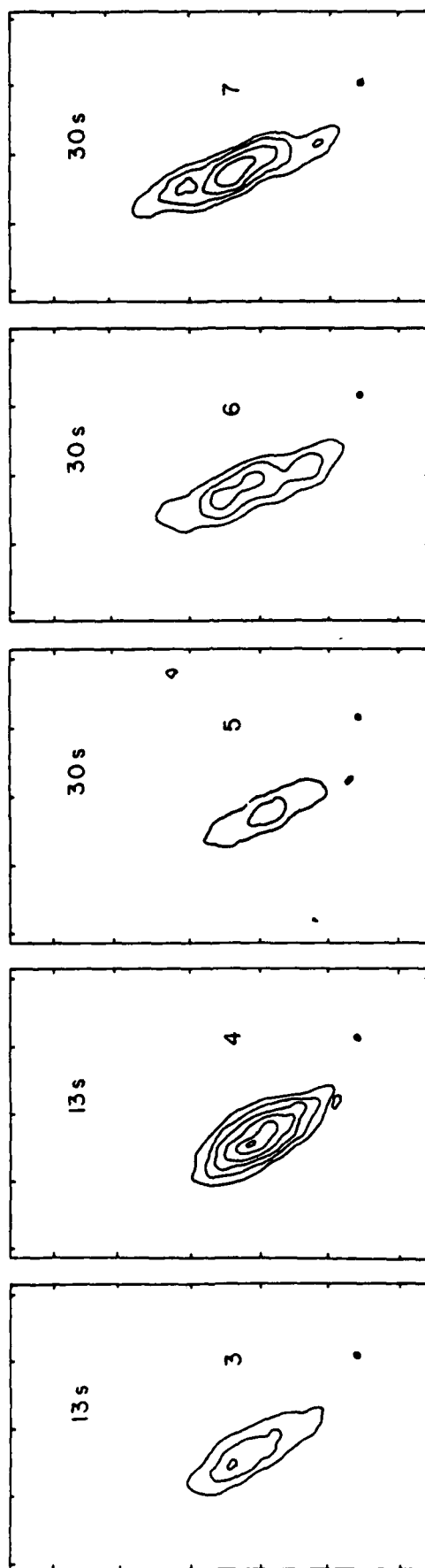


FIG. 3.—Very Large Array snapshot maps of successive peaks in a solar noise storm at 92 cm wavelength. These peaks are denoted by 3, 4, 5, 6, and 7 in Fig. 1. The snapshot maps, each lasting 13 s or 30 s, show no substantial change in the shape or size of the storm source over a period of 2 hr. Here the synthesized beamwidth is denoted by the black dot, and the fiducial marks on the axes are separated by $100''$. The contours mark levels of equal brightness temperature, T_b , with an outermost contour of $T_b = 3.8 \times 10^6$ K, a contour interval of 2.5×10^6 K, and a peak brightness temperature of $T_p = 1.6 \times 10^7$ K.



FIG. 4—A Very Large Array (VLA) synthesis map of a solar noise storm at 92 cm wavelength is superposed on a Kitt Peak National Observatory (KPNO) magnetogram taken on the same day. The VLA map covered the 1 hr time interval between 2300 and 2400 UT; its synthesized beamwidth is denoted by the black spot. The contours mark levels of equal brightness temperature, T_b , with an outermost contour of $T_b = 1.0 \times 10^6$ K and a contour interval of 7.2×10^5 K. Dark areas on the magnetogram correspond to negative magnetic polarity with the magnetic field lines pointing in toward the Sun, whereas light magnetogram areas correspond to outward regions of positive magnetic polarity. Two dipolar regions are shown on the magnetogram—AR 4731 near the limb and AR 4732. The 92 cm source is attributed to plasma radiation in the ordinary mode of wave propagation along magnetic field lines connected to the dark negative spot of AR 4732. The angular displacement between this spot and the 92 cm source corresponds to radial altitude of about $0.2 R_\odot$ above the photosphere. The magnetogram was kindly provided by Jack Harvey of the National Solar Observatory.

its associated spot is $\Delta\theta = 2.3$ (when corrected for ionospheric refraction), and this displacement corresponds to a radial height of $h = 1.0 \pm 0.2 \times 10^{10}$ cm $= 0.15 \pm 0.03 R_{\odot}$.

At our observing frequency of $\nu = 328$ MHz, we infer an electron density of $N_e = 1.4 \times 10^9$ cm $^{-3}$ for the height $h = 1.0 \times 10^{10}$ cm from the condition that $\nu = \nu_p$, where the plasma frequency $\nu_p = 8.9 \times 10^3 N_e^{1/2}$ Hz. The plasma radiation will dominate over thermal cyclotron radiation when $\nu = \nu_p \gg \nu_H$, where the gyrofrequency $\nu_H = 2.8 \times 10^6 H$ Hz and H is the magnetic field strength in gauss. Thus, we have $H \leq 100$ G in the storm source at a height of $h = 1.0 \times 10^{10}$ cm above the photosphere. The condition for suppression of the extraordinary mode of wave propagation, with the resultant escape of the ordinary mode, similarly requires $H \leq 100$ G at this height.

b) Future VLA Potential

The VLA can potentially resolve noise storm sources with an angular resolution of $5''$ at 92 cm wavelength. Snapshot synthesis maps can be made with this resolution for intervals as short as 3 s, which is comparable to the duration of chains of type I bursts. The observing bandwidth, $\Delta\nu$, can be comparable to that of type I bursts ($\Delta\nu \sim 6$ MHz), and an improvement in VLA integration time to 0.1 s would permit observations of individual type I bursts.

As illustrated in § II, the VLA has already been used to resolve noise storm sources with an angular diameter of $40''$. This diameter corresponds to a linear size, L , of $L = 3 \times 10^9$ cm at the Sun's distance. Waves moving at the velocity of light would cross this dimension in a time, $\tau = 0.1$ s. Because nothing can move faster than the velocity of light, the duration, τ , of a source with this dimension must be $\tau \geq 0.1$ s. The observed limit to the duration of individual type I bursts is also $\tau \geq 0.1$ s (Elgaroy 1977). The VLA resolution of $5''$ therefore seems to be fully capable of resolving the type I burst emitters.

The VLA can probably distinguish between the two principal components of noise storms, thereby resolving the sources of type I bursts and the background continuum for the first time. Future VLA observations will therefore probably determine if the two sources have comparable or different sizes, and if one of them resides within the other.

The VLA can also potentially detect the effects of scattering on field-aligned density inhomogeneities. This anisotropic scattering was first proposed to reconcile the narrow bandwidths and apparently large sizes of some type I bursts at 169 MHz (Bougeret and Steinberg 1977). As illustrated in § II, the 92 cm (328 MHz) VLA observations have resolved elongated sources that were predicted by the scattering theory.

Both the fundamental and the second harmonic of the plasma frequency might be detected if an intense noise storm is observed with both the VLA and a smaller patrol-type solar radio telescope. The fundamental plasma radiation is all that has been previously observed, primarily because of the low brightness temperature of the harmonic. The large collecting area and high angular resolution of the VLA will vastly improve detection thresholds. For instance, observations at twice the frequency of strong type I bursts indicate that the flux of the associated second harmonic emission is less than 0.001 of the fundamental (Jaeggi and Benz 1982). Future VLA observations should improve this limit by more than an order of magnitude, or else detect the second harmonic, thereby providing important constraints to theoretical explanations of noise storms (see Benz and Wentzel 1981).

We thank the staff of the Very Large Array and, in particular, Durga Bagri and Ray Gonzalez, for help with the observations. Radio astronomical studies of the Sun at Tufts University are supported under grant AFOSR-83-0019 with the Air Force Office of Scientific Research and contract N00014-86-K-0068 with the Office of Naval Research (ONR). Our simultaneous VLA and *Solar Maximum Mission* (SMM) observations of the Sun are supported by NASA grant NAG 5-501. Collaborative long-wavelength solar observations by Tufts University and the Observatoire de Paris are supported by National Science Foundation (NSF) grant INT-8602285 and Centre National de la Recherche Scientifique grant 920038. The Very Large Array is operated by Associated Universities, Inc., under contract with the National Science Foundation.

REFERENCES

- Benz, A. O., and Wentzel, D. G. 1981, *Astr. Ap.*, **94**, 100.
 Bougeret, J. L., and Steinberg, J. L. 1977, *Astr. Ap.*, **61**, 777.
 Clavelier, B. 1967, *Ann. d'Ap.*, **30**, 895.
 Duik, G. A., and Nelson, G. J. 1973, *Proc. Astr. Soc. Australia*, **2**, 211.
 Elgaroy, O. 1977, *Solar Noise Storms* (New York: Pergamon Press).
 Erickson, W. C. 1984, *J. Ap. Astr.*, **5**, 55.
 Gergely, T. E., and Kundu, M. R. 1975, *Solar Phys.*, **41**, 163.
 Jaeggi, M., and Benz, A. O. 1982, *Astr. Ap.*, **107**, 88.
 Kai, K., Melrose, D. B., and Suzuki, S., 1985, in *Solar Radiophysics*, ed. D. J. McLean and N. R. Labrum (New York: Cambridge University Press), p. 415.
 Kai, K., and Sheridan, K. V. 1974, *Solar Phys.*, **35**, 181.
 Komesaroff, M. M. 1960, *Australian J. Phys.*, **13**, 153.
 McLean, D. J. 1973, *Proc. Astr. Soc. Australia*, **2**, 222.
 ———. 1981, *Proc. Astr. Soc. Australia*, **4**, 132.
 Sheridan, K. V., Labrum, N. R., Payten, W. J., Nelson, G. J., and Hill, E. R. 1983, *Solar Phys.*, **83**, 167.
 Spoelstra, T. A. T. 1983, *Astr. Ap.*, **120**, 313.
 Stewart, R. T. 1976, *Solar Phys.*, **50**, 437.
 ———. 1985, *Solar Phys.*, **96**, 381.
 Stewart, R. T., and McLean, D. J. 1982, *Proc. Astr. Soc. Australia*, **4**, 386.

KENNETH R. LANG and ROBERT F. WILLSON: Department of Physics and Astronomy, Robinson Hall, Tufts University, Medford, MA 02155

30. SIMULTANEOUS SMM FLAT CRYSTAL SPECTROMETER AND VERY LARGE ARRAY OBSERVATIONS OF SOLAR ACTIVE REGIONS

KENNETH R. LANG AND ROBERT F. WILLSON
Department of Physics and Astronomy, Tufts University

AND

KERMIT L. SMITH AND KEITH T. STRONG

Lockheed Palo Alto Research Laboratory

Received 1987 January 27; accepted 1987 May 4

ABSTRACT

We compare high-resolution images of the quiescent emission from two solar active regions at 20 cm (VLA) and soft X-ray (SMM FCS) wavelengths. There are regions where the X-ray coronal loops have been completely imaged at 20 cm wavelength. In other regions, the X-ray radiation was detected without detectable 20 cm radiation, and vice versa. The X-ray data were used to infer average electron temperatures, T_e , of about 3×10^6 K and average electron densities of about $2.5 \times 10^9 \text{ cm}^{-3}$ for the X-ray emitting plasma in the two active regions. The thermal bremsstrahlung of the X-ray emitting plasma is optically thin at 20 cm wavelength. The 20 cm brightness temperatures, T_B , were always less than T_e , which is consistent with optically thin bremsstrahlung. However, the thermal gyroresonance radiation from the X-ray emitting plasma ought to be optically thick at 20 cm wavelength. The low T_B can then be explained if a higher, cooler plasma covers the hotter X-ray emitting plasma. Thermal gyroresonance radiation must account for the intense 20 cm radiation near and above sunspots where no X-ray radiation is detected. The potential of 20 cm (VLA) and soft X-ray (SMM FCS) comparisons is discussed.

Subject headings: radiation mechanisms — Sun: corona — Sun: radio radiation — Sun: X-rays

1. INTRODUCTION

High-resolution observations with X-ray telescopes orbiting above the atmosphere have transformed our understanding of the solar corona. The corona is now viewed as a highly inhomogeneous distribution of closed magnetic loops that are anchored in the Sun, and open magnetic fields that extend out into interplanetary space (see Vaiana and Rosner [1978] for a review). The hot, dense plasma that is trapped within coronal loops gives rise to intense X-ray radiation, and observations of X-ray spectral lines can be used to infer the electron temperature, electron density, and emission measure of this plasma.

The development of aperture synthesis telescopes like the Very Large Array (VLA) has permitted ground-based microwave observations of the solar corona with angular resolutions that are comparable to those of X-ray telescopes. The high-resolution microwave observations can uniquely specify the strength and structure of the coronal magnetic field. VLA synthesis maps of the total intensity, I , describe the two-dimensional distribution of source brightness, whereas synthesis maps of circular polarization, or Stokes parameter V , can provide information about the coronal magnetic field (see Kundu and Lang [1985] for a review).

The microwave brightness temperature, T_B , of the quiescent, or nonflaring, corona is nearly equal to the coronal electron temperature, T_e , with $T_B \approx T_e \approx 10^6$ K. This suggests that the quiescent microwave emission is thermal. However, there are two possible thermal radiation mechanisms. They are thermal bremsstrahlung, or free-free emission, and thermal gyroresonance radiation, or cyclotron emission. In contrast, the quiescent X-ray emission of the solar corona is mainly due to thermal bremsstrahlung.

To identify the dominant thermal radiation mechanism at microwave wavelengths, one needs to know the electron temperature, the electron density and the magnetic field strength, as well as the thickness of the radiating layer, the scale length of the magnetic field, and the angle between the line of sight and the magnetic field. Thermal gyroresonance will generally dominate radiation at centimeter wavelengths when the electron density is relatively low and the magnetic field is strong.

Early evidence for thermal gyroresonance radiation at coronal levels above sunspots was provided by comparison of the soft X-ray and centimeter-wavelength radiation of active regions (Kundu, Schmahl, and Gerassimenko 1980; Pallavicini, Sakurai, and Vaiana 1981). Bright microwave radiation was found in the strong magnetic fields above sunspots, but the X-ray observations indicated a relatively low electron density in these regions. This meant that the high microwave brightness temperatures above sunspots could not be due to thermal bremsstrahlung, but it could be explained by thermal gyroresonant radiation at the second or third harmonic of the gyrofrequency.

These early low-resolution comparisons were fully confirmed when high-resolution synthesis maps at 6 cm wavelength were compared with simultaneous soft X-ray images obtained with the X-ray polychromator (XRP) aboard the *Solar Maximum Mission* (SMM) satellite (Chiuderi-Drago *et al.* 1982; Schmahl *et al.* 1982; Shibasaki *et al.* 1983; Strong, Alissandrakis, and Kundu 1984). Soft X-ray spectral lines were used to determine the electron temperature and electron density of the X-ray emitting plasma that coincided with the sunspot-associated 6 cm sources. These parameters were then used to compute the bremsstrahlung brightness temperature at 6 cm. Because the computed value was much less than the

observed brightness temperature, additional 6 cm opacity due to gyroresonance absorption above sunspots was required.

Thermal gyroresonance radiation at 6 cm in coronal regions above sunspots was additionally confirmed by the detection of circularly polarized ring-shaped or horseshoe-shaped structures (Alissandrakis and Kundu 1982; Lang and Willson 1982). The highly polarized (up to 100%) structures were predicted by the theory of cyclotron radiation in the curved magnetic fields above sunspots (Gel'freikh and Lubyshev 1979). Depressions in the 6 cm brightness temperature above sunspot umbrae have been attributed to cool material in these regions (Strong, Alissandrakis, and Kundu 1984).

What about the microwave counterpart of the intense X-ray sources? The brightest 6 cm sources are not usually associated with the brightest X-ray sources, and the detailed correspondence between the radiation at the two wavelengths is poor (Schmahl *et al.* 1982; Webb *et al.* 1983). However, this result is not particularly surprising. It would be expected if the dominant radiation mechanisms are different in the two wavelength domains. Thermal bremsstrahlung is often too optically thin to be detected at 6 cm wavelength where gyroresonant radiation dominates. Different structures are observed at the two wavelengths because 6 cm gyroresonance absorption occurs in the strong magnetic fields above sunspots, while the X-ray emission originates in coronal loops that stretch between sunspots of opposite magnetic polarity.

The hot temperatures, slow evolution, and long lifetime of X-ray coronal loops make them ideal candidates for aperture synthesis techniques. Of course, low-lying loops have occasionally been detected at 6 cm (Strong, Alissandrakis and Kundu 1984; Webb *et al.* 1987), but radiation at this wavelength originates at relatively low heights and is usually dominated by gyroresonance absorption. Higher levels are observed at 20 cm wavelength where the thermal bremsstrahlung of coronal loops can become optically thick. In fact, when VLA observations were extended to the longer 20 cm wavelength, quiescent looplike coronal features were discovered (Lang, Willson, and Rayrole 1982).

The coronal loops seen at 20 cm strongly resemble their X-ray counterparts (Lang and Willson 1983, 1984). They have million-degree temperatures and stretch across regions of opposite magnetic polarity in the underlying photosphere. The size and shape of the loops observed at 20 cm are also similar to those of arcades of X-ray coronal loops, with linear extents $L \approx 10^9$ – 10^{10} cm. In addition, the electron temperature and electron density inferred from X-ray observations of other loops are consistent with the idea that the microwave loops are due to thermal radiation from the X-ray emitting plasma. All of these similarities suggest that the microwave counterpart of X-ray coronal loops can be observed in VLA synthesis maps at 20 cm.

Numerous authors have now identified elongated, looplike features at 20 cm with coronal loops, but the exact radiation mechanism for the 20 cm emission remains controversial. Many authors have attributed this radiation to the optically thick thermal bremsstrahlung of a hot, dense plasma trapped within coronal magnetic loops that connect with underlying sunspots (Lang, Willson, and Rayrole 1982; Dulk and Gary 1983; Lang, Willson, and Gaizauskas 1983; Lang and Willson 1983, 1984; Gary and Hurford 1987; Holman 1986). Others reason that optically thick thermal gyroresonance radiation may dominate the 20 cm emission of coronal loops (McConnell and Kundu 1983; Shevgaonkar and Kundu 1984;

Lang *et al.* 1987). Both radiation mechanisms could play a role, with gyroresonance radiation becoming important at relatively high brightness temperatures or relatively low electron densities.

One can distinguish between the two thermal radiation mechanisms for the 20 cm emission from the coronal loops if the VLA synthesis maps are compared with simultaneous X-ray images. This has been done only twice. Chiuderi-Drago *et al.* (1982) used X-ray spectral lines from the SMM FCS to infer the electron temperature and emission measure of the X-ray emitting plasma, concluding that one 20 cm source is the optically thin bremsstrahlung of this plasma. The angular extent of the X-ray source was comparable to that of the 20 cm one, but the observations at both wavelengths were of relatively poor angular resolution. Another sunspot-associated 20 cm source had to be attributed to gyroresonance radiation, for there was no detectable X-ray radiation from this region. Webb *et al.* (1987) used X-ray data taken during a recent rocket flight to conclude that one of several 20 cm features was due to optically thick thermal bremsstrahlung associated with X-ray coronal loops. They noticed that the 20 cm radiation was concentrated at the tops of the X-ray loops and attributed this apparent concentration to absorption in a cool external plasma. However, such a concentration was not apparent in the data of Chiuderi-Drago *et al.* (1982).

In this paper, we present comparisons of high-resolution 20 cm maps from the VLA with simultaneous X-ray images from the SMM FCS. These comparisons are given in § II. In one instance, all of the X-ray emitting plasma was detected at 20 cm, and additional 20 cm emission was observed near sunspots where no X-ray radiation was detected. However, the 20 cm radiation was concentrated at the apex of the more extensive X-ray coronal loops of another active region. In § III, we discuss the absorption and radiation mechanisms for coronal loops at 20 cm. We next use X-ray measurements of electron temperature and electron density to place constraints on these mechanisms. The observed 20 cm features are then explained. Our results are summarized in § IV, where we also discuss the potential of future 20 cm (VLA) and soft X-ray (SMM FCS) comparisons.

II. OBSERVATIONS

We have used the VLA and the SMM FCS to observe solar active regions AR 4508 and AR 4532 on 1984 June 4 and 1984 July 8, respectively. The VLA was in the C-configuration on June 4 and in the hybrid C–D-configuration on July 8. In both instances, the signal wavelength was 20.7 cm (1446 MHz) and the bandwidths were 12.5 MHz. Active region AR 4508 was observed with the VLA between 1500 UT and 2300 UT on June 4; its position on the solar surface was 06° N and 57° E at 1300 UT on this day. Active region AR 4532 was observed between 1800 UT and 2300 UT on July 8; its position on the solar surface was 07° S and 18° E on this day. The flat crystal spectrometer (FCS) observed six prominent soft X-ray lines: Ov III at 18.9 Å, Ne IX at 13.4 Å, Mg XI at 9.2 Å, Si XIII at 6.7 Å, S XV at 5.0 Å, and Fe XXV at 1.9 Å. The FCS observed AR 4508 and AR 4532 throughout the time the VLA was observing these regions.

The half-power beamwidth of the individual VLA antennas was about 30' at 20 cm wavelength, and the synthesized maps constructed from up to 325 interferometer pairs had beamwidths of 12'6 × 15'5 in the C-configuration and 12'6 × 36'0

in the C-D-configuration. The June 4 data were calibrated by 5 minute observations of the calibrator source PKS 0528 + 134 every 35 minutes, while the July 8 data were similarly calibrated with the source PKS 0742 + 103. The flux densities of PKS 0528 + 134 and PKS 0742 + 103 were 1.5 Jy and 3.3 Jy at 1446 MHz, respectively. The calibrated data for the entire observing period were used together with the standard CLEAN procedure to make synthesis maps of both the total intensity, I , and the circular polarization, or Stokes parameter, V . No solar bursts or flares were observed, and the synthesis maps therefore refer to the quiescent, or nonflaring, radio emission. That is, plots of the visibility data exhibited no variations that could be attributed to solar activity. There was no detectable circular polarization ($V/I \leq 15\%$) for both active regions.

The 14" collimated field of view of the FCS was rastered over a $7' \times 7'$ field of view on June 4 and over a $4' \times 4'$ field of view on July 8; in each case the pixel spacing was $10'' \times 10''$. X-ray images were obtained for each of the six spectral lines during the orbital day at a cadence of 410 s. All of the available data for each spectral line were then summed and averaged during each orbit to improve the statistical uncertainty on the count rate from each pixel. Significant emission was only detected from the three softest channels—O VIII, Ne IX, and Mg XI. The peak formation temperatures for these lines are 3×10^6 K, 4×10^6 K, and 7×10^6 K, respectively. The failure to detect emission in the harder, more energetic, channels indicates that the active regions were unperturbed by flaring activity during the periods of observation. The SMM bent crystal spectrometer (BCS) confirmed the absence of flares as no significant brightenings were observed in its Ca XIX channel during these observations.

The XRP also produced a white-light image that showed the sunspots, making it possible to align the X-ray images with the sunspots to an accuracy of $10''$. The VLA maps of the total intensity, I , at 20 cm were aligned with H α photographs of the same sunspots with a similar $10''$ accuracy. This enabled us to compare the soft X-ray and 20 cm data with the same field of view and angular scale. The 20 cm radiation of AR 4508 is concentrated in the central regions of a more extensive system of X-ray loops (Fig. 1). In this instance, the 20 cm radiation was aligned along the magnetic neutral line (Fig. 2). There is a sharp drop in the intensity of the radio emission along the edges of the magnetic neutral line where there ought to be a sharp gradient in the magnetic field strength.

However, all of the X-ray emitting plasma of AR 4532 was detected at 20 cm, and additional 20 cm emission was observed near and above sunspots where no X-ray radiation was detected. Intense X-ray radiation and intense 20 cm radiation were detected from coronal loops or arcades of loops that are connected with underlying sunspots (Fig. 3). These loops were about $60''$ across or about 5×10^9 cm in linear extent. Both X-ray and 20 cm radiation were also emitted from regions of bright plage. In addition, Lang *et al.* (1987) presented simultaneous FCS-VLA data in which an entire system of X-ray loops was completely imaged at 20 cm.

Thus, the same coronal loops are often detected at both 20 cm and X-ray wavelengths, with extra information at 20 cm near and above sunspots. Of course, the 20 cm coronal loops can also be limited to a smaller volume than their X-ray counterparts, but our FCS-VLA comparisons and other VLA observations suggest that this is not usually the case. We will now turn our attention to the absorption and radiation mechanisms that account for the 20 cm coronal loops.

III. DISCUSSION

Because the microwave brightness temperature, T_b , of the quiescent coronal loops is nearly equal to the electron temperature, T_e , the quiescent radiation from 20 cm loops is most likely thermal. The two possible thermal radiation mechanisms at 20 cm wavelength are thermal bremsstrahlung, or free-free emission, and thermal gyroresonance radiation, or cyclotron emission. In order to identify the dominant thermal radiation mechanism at 20 cm wavelength, we will evaluate the electron temperature, T_e , and the electron density, N_e , using the X-ray radiation that is attributed to thermal bremsstrahlung alone.

As previously mentioned, the active regions were so quiescent that they were only detectable in the three softest X-ray channels (O VIII, Ne IX, and Mg XI). Because the O VIII to Ne IX line intensity ratio is insensitive to temperature variations over the range typical of solar active regions, the ratios of the other two lines (O VIII to Mg XI and Ne IX to Mg XI) were used as temperature diagnostics. The temperatures inferred from the two ratios were averaged to obtain our estimate for the electron temperature.

An emission measure was inferred from the temperatures and the observed X-ray fluxes. The electron density was then calculated using a volume of 3×10^{27} cm³, which equals the product of the FCS pixel area and a typical soft X-ray scale height of 3×10^9 cm.

The mean electron temperatures, T_e , and electron densities, N_e , for AR 4508 were determined for the areas marked A, B, and C in Figure 4. These parameters are given in Table 1 together with the maximum observed brightness temperature, T_b , at 20 cm wavelength and the optical depth $\tau = T_b/T_e$. The mean T_e and N_e for AR 4532 were similarly inferred for the areas marked A, B, C, D, E, and F in Figure 5; they are given in Table 2 together with the relevant T_b and τ .

The mean values for different areas were then combined to give average values of $T_e = 3.0 \pm 0.2 \times 10^6$ K and $N_e = 2.7 \pm 0.3 \times 10^9$ cm⁻³ for AR 4508 and $T_e = 3.0 \pm 0.1 \times 10^6$ K and $N_e = 2.4 \pm 0.4 \times 10^9$ cm⁻³ for AR 4532. Here the uncertainties correspond to the standard deviation of the line ratios. These values of T_e and N_e are typical values for quiescent coronal loops in active regions.

TABLE 1
PHYSICAL PARAMETERS FOR AR 4508

Region	T_e (10^6 K)	N_e (10^9 cm ⁻³)	T_b (10^6 K)	τ	W (10^9 cm)
A	3.3	2.7	0.8	0.27	3
B	2.9	3.0	1.7	0.88	6
C	3.0	2.8	1.0	0.41	3
Average	3.1	2.8	1.2	0.52	4

TABLE 2
PHYSICAL PARAMETERS FOR AR 4532

Region	T_e (10^6 K)	N_e (10^9 cm ⁻³)	T_b (10^6 K)	τ	W (10^9 cm)
A	2.9	2.4	1.3	0.60	6
B	2.8	2.1	0.8	0.34	4
C	3.1	2.1	0.8	0.30	4
D	3.3	3.0	1.4	0.55	4
E	2.7	2.1	1.4	0.73	8
F	2.7	2.1	0.7	0.30	4
Average	2.9	2.3	1.1	0.47	5

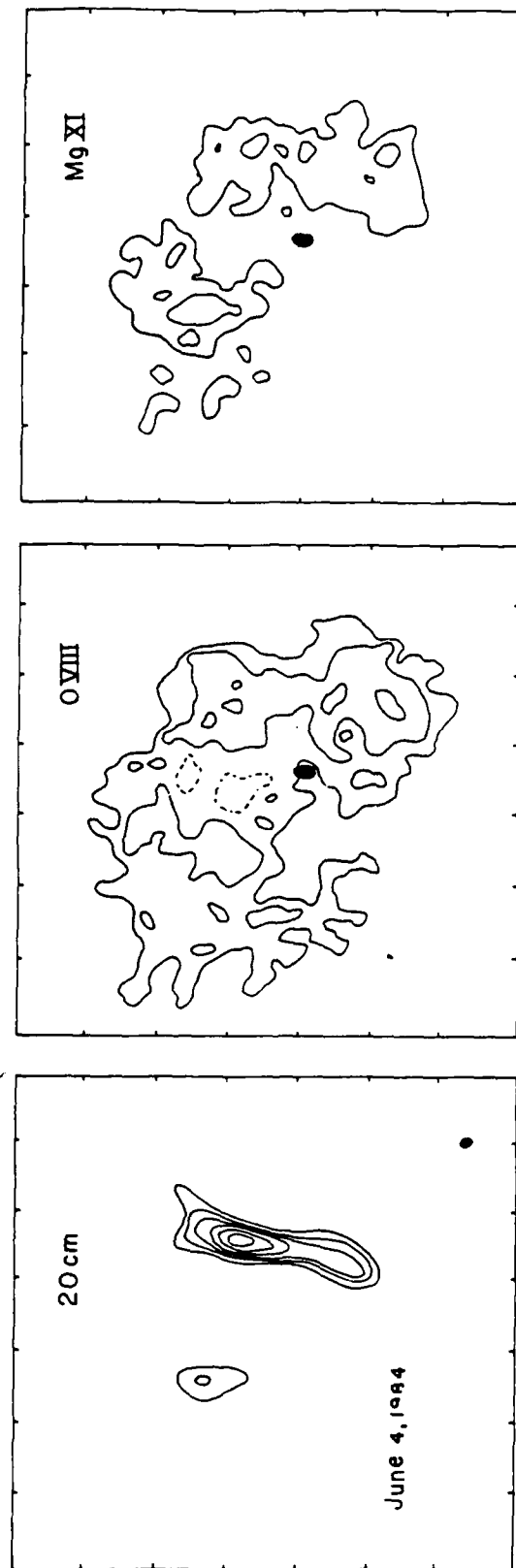


FIG. 1.—A comparison of a 20 cm VLA synthesis map of AR 4508 with SMM FCS images in the O VIII (18.9 Å) and Mg XI (9.2 Å) lines on 1984 June 4. The field of view of all three images is the same, and the angular scale can be inferred from the 60" spacing between fiducial marks on the axes. The contours of the 20 cm map mark levels of equal brightness temperature corresponding to 0.4, 0.5, 0.6, ..., 1.0 times the maximum brightness temperature of 1.7×10^6 K. The contours of the O VIII image correspond to 4, 8, and 15 counts s^{-1} above the background level of 10 counts s^{-1} with a maximum signal of 20 counts s^{-1} . The contours of the Mg XI image are the same as those of O VIII with a background level of 5 counts s^{-1} and with a maximum signal of 15 counts s^{-1} . The small dark spot on the 20 cm map denotes the VLA beam, and the large dark spot on the O VIII and Mg XI images denotes the white light sunspot.



FIG. 2.—The 20 cm contours of equal brightness temperature (solid black lines) are superposed on a Kitt Peak National Observatory (KPNO) magnetogram of AR 4508 on 1984 June 4. The radio emission is concentrated along the magnetic neutral line that separates regions of negative (black) and positive (white) magnetic polarity. Sharp magnetic field gradients may exist along the neutral line. The KPNO magnetogram was kindly provided by Jack Harvey of the National Solar Observatory.

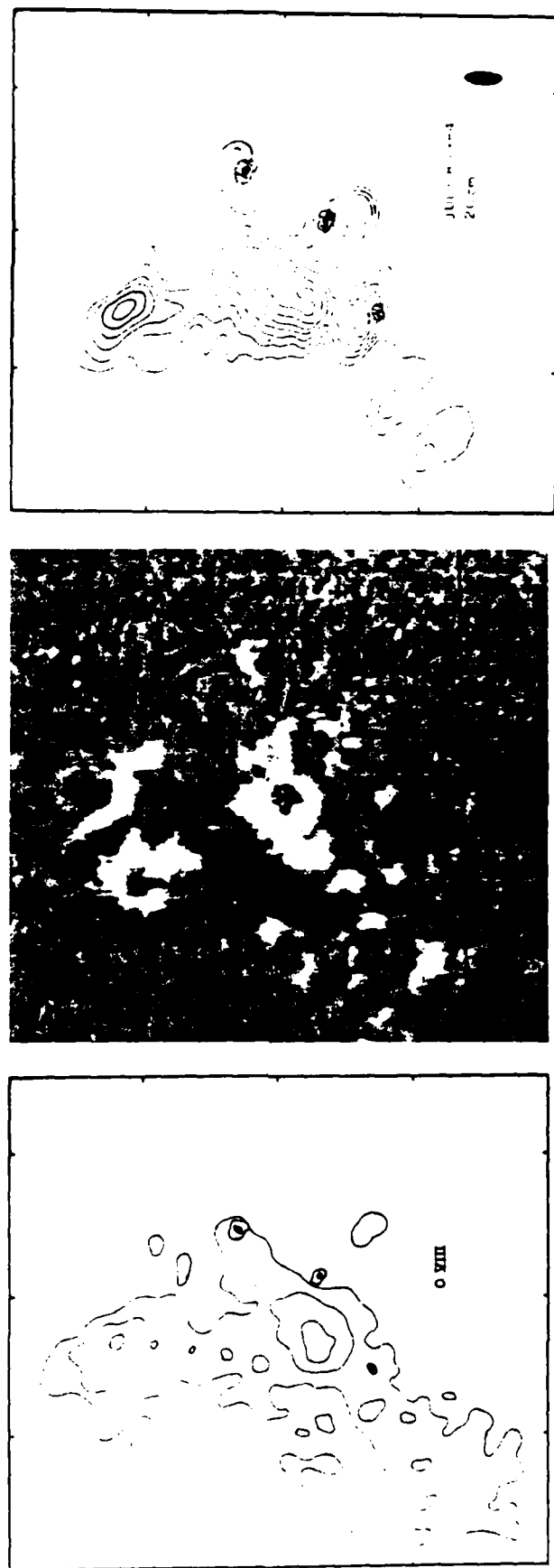


FIG. 3.—A comparison of soft X-ray (SMM FCS: *left*), H α (SOON: *middle*), and 20 cm (VLA: *right*) images of AR 4532 on 1984 July 8. The field of view of all three images is the same, and the angular scale can be inferred from the 120" spacing between the fiducial marks on the axes. The contours of the 20 cm map mark levels of equal brightness temperature corresponding to 0.4, 0.5, 0.6, ..., 1.0 times the maximum brightness temperature of 1.4×10^6 K. The soft X-ray data were taken in the O VIII line (18.9 Å) with contours corresponding to 4, 8, and 15 counts s^{-1} above a background level of 10 counts s^{-1} with a maximum signal of 20 counts s^{-1} . Here the sunspots are denoted by small black dots with a circle around them. The large black dot on the 20 cm map denotes the VLA beam.

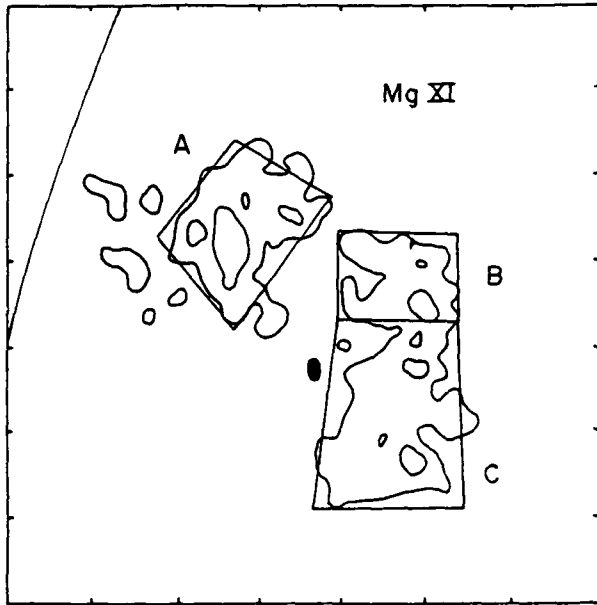


FIG. 4.—A soft X-ray map of AR 4508 taken in the Mg XI line (9.2 Å) with contours corresponding to 4, 8, and 15 counts s^{-1} . The ratios of the O VIII and Mg XI line intensities were used to determine the mean electron temperatures in the regions marked A, B, and C. These temperatures, the mean electron density, 20 cm brightness temperature, optical depth, and loop width are given in Table 1. The image represents the averaged sum of two maps taken at 17:03 UT and 18:37 UT on 1984 June 4. The solar limb is shown by the line in the upper left corner, and the black dot denotes the white light sunspot.

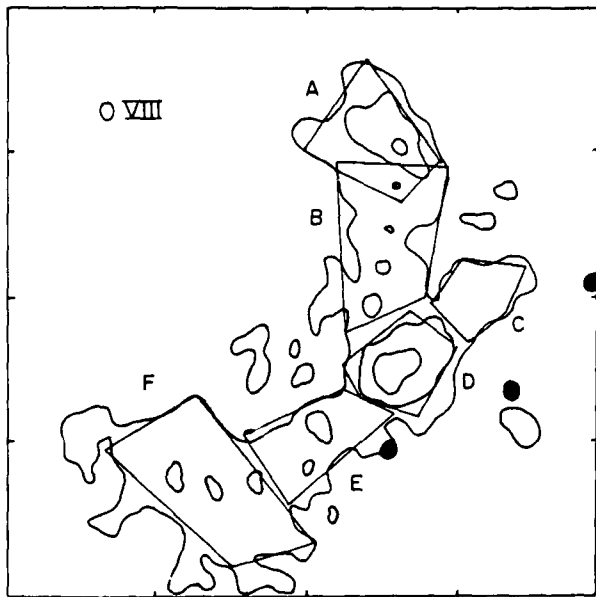


FIG. 5.—A soft X-ray map of AR 4532 taken in the O VIII line (18.9 Å) with contours corresponding to 4, 8, and 15 counts s^{-1} . The ratios of the O VIII and Mg XI line intensities were used to determine the mean electron temperature in the regions marked A, B, C, D, E, and F. These temperatures, the mean electron density, 20 cm brightness temperature, optical depth, and loop width are given in Table 2. The image represents the averaged sum of four maps taken at 18:06 UT, 19:40 UT, 21:15 UT, and 22:49 UT on 1984 July 8. There is no detectable X-ray emission associated with the white light sunspots (black dots), but these regions are associated with intense radiation at 20 cm wavelength (also see Fig. 3).

Within the uncertainties, the observed loops were isothermal. They also all had optical depths $\tau < 1$ (optically thin). We will therefore evaluate the loop width or thickness, W , that would give rise to optically thin thermal bremsstrahlung at our observing frequency of $\nu = 1446$ MHz (20.75 cm). According to Lang (1980):

$$W \leq \frac{102 \tau_{ff} \nu^2 T_e^{3/2}}{N_e^2 \ln(4.7 \times 10^{10} T_e / \nu)}, \quad (1)$$

or

$$W \leq \frac{2.13 \times 10^{20} \tau_{ff} T_e^{3/2}}{N_e^2 \ln(32.5 T_e)} \text{ cm},$$

where τ_{ff} is the optical depth for bremsstrahlung. The N_e and T_e obtained from the X-ray observations were substituted into equation (1) to provide the widths, W , given in Tables 1 and 2. The average values of W for the two active regions were $W \leq 4 \times 10^9$ cm and $W \leq 5 \times 10^9$ cm, which are certainly plausible.

In fact, the free-free optical depth, τ_{ff} , at 20 cm wavelength can be directly inferred from the X-ray measurements of electron temperature and emission measure, $N_e^2 W$. They imply $\tau_{ff} \approx 0.3$, suggesting that at least part of the 20 cm radiation is optically thin bremsstrahlung.

However, we will next evaluate the optical depth τ_{gr} for gyroresonance absorption by using the equation (Zheleznyakov 1970)

$$\tau_{gr} = 0.052 \frac{n^{2n}}{2^{n+1} n!} \frac{N_e}{\nu} (1.7 \times 10^{-10} T_e)^{n-1} L_H \times (1 \pm \cos \alpha)^2 \sin^{2n-2} \alpha, \quad (2)$$

where the magnetic scale length L_H has typical values of $L_H \sim 1 \times 10^9$ cm the angle between the line of sight and the direction of the magnetic field lines is α , and our observing frequency $\nu = 1446$ MHz and the harmonic n is related to ν through the relation

$$\nu = 2.8 \times 10^6 n H \text{ Hz}, \quad (3)$$

where the magnetic field strength is H .

When our average X-ray values of $N_e \sim 2.5 \times 10^9 \text{ cm}^{-3}$ and $T_e \sim 3 \times 10^6$ K are substituted into equation (2), we obtain optically thick conditions $\tau_{gr} \geq 1.0$ with low circular polarization at either the third or fourth harmonic ($n = 3$ or 4) and nearly transverse magnetic field lines ($\alpha = 60^\circ$ to 70°). Plausible magnetic field strengths of $H = 172$ G and 129 G are inferred for $n = 3$ and 4, respectively.

Thus we expect thermal gyroresonance radiation to be optically thick for plausible loop widths and magnetic scale lengths. This is consistent with the lack of any detectable circular polarization at 20 cm. The observed brightness temperature, T_b , at 20 cm wavelength should therefore be equal to the electron temperature with $T_b = T_e$, but the values of T_b are about 5 times smaller than T_e . To resolve this paradox, we call attention to an idea first proposed by Holman (1986).

To explain the restriction of one 20 cm loop to the apex of an X-ray loop, Holman argued that cooler material with $T_e \sim 10^5$ K exists either as a sheath around the loops or as part of an external medium. The 20 cm radiation emitted by the X-ray loops will be partly absorbed in the cooler, higher plasma, thereby reducing its brightness temperature. The cooler, higher material would, however, be invisible in X-rays because of its low temperature and relatively small emission measure.

If the cool plasma is part of an external medium that is more extensive than the X-ray loops, we would expect the observed 20 cm loops to be cospatial with the X-ray ones, but with a lowered brightness temperature. This is in fact observed for AR 4532. When the cool plasma is part of a sheath around the X-ray loops, the line of sight through the low-temperature plasma will be greatest at the loop edges and footpoints, and the observed 20 cm emission will be concentrated at the apexes of the X-ray coronal loops. This is observed for AR 4508.

What about the bright 20 cm radiation near and above sunspots? There is no detectable X-ray radiation in these regions, and this can be attributed to a low electron density, N_e . Because the optical depth for free-free absorption scales with N_e^2 while that for gyroresonance absorption scales with N_e , the low electron density favors gyroresonance absorption. The high magnetic field strength above sunspots also favors this process. We therefore attribute the 20 cm radiation near and above sunspots to thermal gyroresonance radiation.

IV. SUMMARY

The quiescent, or nonflaring, X-ray radiation of solar active regions is attributed to thermal bremsstrahlung, but the quiescent microwave radiation may be due to either thermal bremsstrahlung or thermal gyroresonant radiation. In the Introduction, we reviewed evidence for thermal gyroresonance radiation at 6 cm in coronal regions above sunspots. This evidence includes comparisons of 6 cm VLA maps with simultaneous soft X-ray data, as well as the detection of highly circularly polarized horseshoe-shaped structures above sunspots at 6 cm.

Although the thermal bremsstrahlung of coronal loops is usually optically thin at 6 cm, it might become optically thick at the longer 20 cm wavelength where looplike coronal structures are observed. These 20 cm coronal loops stretch between regions of opposite magnetic polarity in the underlying photosphere, and the temperatures, sizes, and shapes of the 20 cm coronal loops resemble those of soft X-ray coronal loops.

In this paper we have compared high-resolution 20 cm maps (VLA) with simultaneous high-resolution X-ray images (SMM FCS) of two active regions. The X-ray coronal loops in AR 4532 were completely imaged at 20 cm, while the 20 cm emission of AR 4508 was concentrated along the magnetic neutral line within more extended X-ray loops. The X-ray data were used to infer an average $T_e = 3.0 \pm 0.2 \times 10^6$ K and an average $N_e = 2.7 \pm 0.3 \times 10^9$ cm $^{-3}$ for AR 4532 and the average $T_e = 3.0 \pm 0.1 \times 10^6$ K and $N_e = 2.4 \pm 0.4 \times 10^9$ cm $^{-3}$ for AR 4508.

The microwave brightness temperatures, T_b , at 20 cm were always less than the average electron temperature, with optical depths $\tau = T_e/T_b$ of $0.2 \leq \tau \leq 0.5$. The X-ray values of T_e and

N_e indicate that thermal bremsstrahlung ought to be optically thin at 20 cm for plausible loop widths, but the thermal gyroresonance radiation can be optically thick at 20 cm for plausible magnetic field strengths and scale heights. Optically thick radiation is also consistent with the lack of detectable circular polarization at 20 cm. Thermal gyroresonance radiation must account for the intense 20 cm radiation near and above sunspots where no X-ray radiation is detected.

The unexpectedly low values of T_b can be explained if the X-ray emitting coronal loops lie beneath a higher, cooler plasma. The hot, dense plasma in the X-ray coronal loops would emit optically thick radiation at 20 cm wavelength, but the brightness temperature of this radiation would be reduced during subsequent propagation through the cooler, absorbing plasma. The observations of AR 4532 can be explained if the cooler plasma extends across and beyond the X-ray loops, while the AR 4508 results might be explained by the presence of a cool sheath around the X-ray loops. The cooler material would not be detected at X-ray wavelengths because of its low temperature and relatively small emission measure. The results given in this paper indicate that the structure and dominant radiation mechanisms in the low corona are much more complex and inhomogeneous than was previously thought. Systems of coronal loops within a single active region apparently have different temperatures and different radiation mechanisms that can be detected only by observations at both X-ray and 20 cm wavelength. Future comparisons of high-resolution images at these two wavelengths will lead to detailed information about the plasma and magnetic structure of the low solar corona. Physical parameters such as electron temperature, electron density, and magnetic field strength can be specified, and the detailed variation of these parameters within the coronal atmosphere can be determined. Such information will provide important constraints on theories and models of coronal loops as well as general theories for the structure and heating of solar active regions.

Radio astronomical studies of the Sun at Tufts University are supported under grant AFOSR-83-0019 with the Air Force Office of Scientific Research and contract N00014-86-K0068 with the Office of Naval Research (ONR). Simultaneous VLA and SMM FCS observations of the Sun are supported by NASA grant NAG 5-501. K.L.S. and K.T.S. are supported by NASA contract NAS 5-23758 and the Lockheed Independent Research Program. The XRP was built by a consortium of three groups: Lockheed Palo Alto Research Laboratory, Mullard Space Science Laboratory, and the Rutherford and Appleton Laboratories. The VLA is operated by Associated Universities, Inc., under contract with the National Science Foundation.

REFERENCES

- Alissandrakis, C. E., and Kundu, M. R. 1982, *Ap. J. (Letters)*, **253**, L49.
 Chiuderi-Drago, F., Bandiera, R., Falciani, R., Antonucci, E., Lang, K. R., Willson, R. F., Shibasaki, K., and Slotje, C. 1982, *Solar Phys.*, **80**, 71.
 Duik, G. A., and Gary, D. E. 1983, *Astr. Ap.*, **124**, 103.
 Gary, D. E., and Hu \ddot{o} rd, G. J. 1987, *Ap. J.*, **317**, 522.
 Gef \ddot{u} riekh, G. B., and Lubyshev, B. I. 1979, *Soviet Astr.*, **23**, 316.
 Holman, G. D. 1986, "High-Spatial-Resolution Microwave and Related Observations as Diagnostics of Coronal Loops," to be published in *Coronal And Prominence Plasmas*.
 Kundu, M. R., and Lang, K. R. 1985, *Science*, **228**, 9.
 Kundu, M. R., Schmahl, E. J., and Gerassimenko, M. 1980, *Astr. Ap.*, **82**, 265.
 Lang, K. R. 1980, *Astrophysical Formulae* (2d ed.; New York: Springer Verlag).
 Lang, K. R., and Willson, R. F. 1982, *Ap. J. (Letters)*, **255**, L111.
 ———, 1983, *Adv. Space Res.*, **2**, No. 11, 91.
 ———, 1984, *Adv. Space Res.*, **4**, No. 7, 105.
 Lang, K. R., Willson, R. F., and Gaizauskas, V. 1983, *Ap. J.*, **267**, 455.
 Lang, K. R., Willson, R. F., and Rayrole, J. 1982, *Ap. J.*, **258**, 384.
 Lang, K. R., Willson, R. F., Smith, K. L., and Strong, K. T. 1987, "Solar Active Region Physical Parameters Inferred From A Thermal Cyclotron Line and Soft X-ray Spectral Lines," submitted to *Ap. J.*
 McConnell, D., and Kundu, M. R. 1983, *Ap. J.*, **269**, 698.
 Pallavicini, R., Sakurai, T., and Vaiana, G. S. 1981, *Astr. Ap.*, **98**, 316.
 Schmahl, E. J., Kundu, M. R., Strong, K. T., Bentley, R. D., Smith, J. B., and Krall, K. R., 1982, *Solar Phys.*, **80**, 233.

- Shevgaonkar, R. K., and Kundu, M. R. 1984, *Ap. J.*, **283**, 413.
Shibasaki, K., Chiuderi-Drago, F., Melozzi, M., Slottje, C., and Antonucci, E. 1983, *Solar Phys.*, **89**, 307.
Strong, K. T., Alissandrakis, C. E., and Kundu, M. R. 1984, *Ap. J.*, **277**, 865.
Vaiana, G. S., and Rosner, R. 1978, *Ann. Rev. Astr. Ap.*, **16**, 393.
Webb, D. F., Davis, J. M., Kundu, M. R., and Velusamy, T. 1983, *Solar Phys.*, **85**, 267.
Webb, D. F., Holman, G. D., Davis, J. M., Kundu, M. R., and Shevgaonkar, R. K. 1987, *Ap. J.*, **315**, 716.
Willson, R. F. 1985, *Ap. J.*, **298**, 911.
Zheleznyakov, V. V. 1970, *Radio Emission of the Sun and Planets* New York: Pergamon, p. 454.

KENNETH R. LANG and ROBERT F. WILLSON: Department of Physics and Astronomy, Robinson Hall, Tufts University, Medford, MA 02155

KERMIT L. SMITH and KEITH T. STRONG: Code 602.6, Bldg. 7-XRP, Goddard Space Flight Center, Greenbelt, MD 20771

31. SOLAR ACTIVE REGION PHYSICAL PARAMETERS INFERRED FROM A THERMAL CYCLOTRON LINE AND SOFT X-RAY SPECTRAL LINES

KENNETH R. LANG AND ROBERT F. WILLSON
Department of Physics and Astronomy, Tufts University

AND

KERMIT L. SMITH AND KEITH T. STRONG
Lockheed Palo Alto Research Laboratory

Received 1987 January 27; accepted 1987 May 4

ABSTRACT

We present simultaneous high-resolution observations of coronal loops at 20 cm wavelength with the VLA and at soft X-ray wavelengths with the SMM FCS. The images at 20 cm and soft X-ray wavelengths have nearly identical sizes and ellipsoidal shapes, with a linear extent of about 5×10^9 cm. This emission stretches between and across regions of opposite magnetic polarity in the underlying photosphere. Complete X-ray coronal loops can therefore be imaged at 20 cm, and the VLA maps describe the radio wavelength counterpart of X-ray coronal loops. X-ray spectral lines were used to obtain values of electron temperature $T_e = 2.6 \pm 0.1 \times 10^6$ K and electron density $N_e = 3.1 \pm 0.3 \times 10^9$ cm $^{-3}$ averaged over the emitting area. These parameters are used with plausible estimates for the loop thickness, magnetic scale height, and magnetic field strength to show that the plasma is optically thin to thermal bremsstrahlung, but that it might be optically thick to thermal gyroresonance radiation at 20 cm. The absence of detectable circular polarization is consistent with an optically thick plasma. The observed brightness temperature was roughly equal to the electron temperature of the coronal plasma. The VLA maps at 10 closely spaced frequencies between 1440 and 1720 MHz describe the same coronal loops or arcades of loops. A plot of the maximum brightness temperature of these loops as a function of observing frequency exhibits a linelike feature with a central frequency of 1650 MHz and a half-width of 80 MHz. This spectral feature is attributed to a thermal cyclotron line and indicates that the optical depth of thermal gyroresonance radiation must be greater than that of thermal bremsstrahlung at these frequencies. The X-ray values for T_e and N_e are combined with plausible values of magnetic scale height and optical depth for gyroresonance absorption to show that the harmonic of the gyrofrequency is 4. The central frequency and narrow width of the thermal cyclotron line are combined with this harmonic to show that the magnetic field strength of the coronal loops is 147 ± 5 G.

Subject headings: radiation mechanisms — Sun: corona — Sun: magnetic fields — Sun: radio radiation — Sun: X-rays

1. INTRODUCTION

Very Large Array (VLA) observations of solar active regions at 20 cm wavelength delineate looplike features that are probably the radio wavelength counterpart of the coronal loops seen at X-ray wavelengths. The 20 cm coronal loops stretch across regions of opposite magnetic polarity and have sizes, shapes, and temperatures that are similar to those of X-ray coronal loops (Lang, Willson, and Rayrole 1982; Lang, Willson, and Gaizauskas 1983; Lang and Willson 1983, 1984). Because the radio brightness temperatures are nearly equal to the electron temperatures of coronal loops, the radio radiation is most likely due to a thermal radiation mechanism.

The two possible thermal processes are thermal bremsstrahlung, or free-free emission, and thermal gyroresonance radiation, or cyclotron emission. The electron temperatures and electron densities inferred from X-ray observations of coronal loops can be consistent with either optically thin or optically thick thermal bremsstrahlung at 20 cm wavelength, but these parameters can also be combined with plausible estimates of the coronal magnetic field strength to show that thermal gyroresonance radiation can also become optically thick at this wavelength (McConnell and Kundu 1983; Shevgaonkar and Kundu 1984).

When thermal gyroresonance dominates, one might detect

individual cyclotron lines as narrow-band enhancements in the radio spectra of coronal loops. Theoreticians have predicted that such thermal cyclotron lines might be observed if the radiation is emitted from relatively thin layers in the corona where the magnetic field is nearly constant (Syrovatskii and Kuznetsov 1980; Zheleznyakov and Zlotnik 1980; Kuznetsov and Syrovatskii 1981). The spectrum of a linelike feature was subsequently observed at wavelengths near 20 cm when the apex of a coronal loop was resolved (Willson 1985). Observations of these lines provide an unusually accurate method of specifying the coronal magnetic field strength. The central frequency of the line must be a harmonic of the gyrofrequency, and the narrow linewidth provides tight constraints on that frequency and the relevant magnetic field strength.

Although there have been rapid recent developments in the observations of 20 cm coronal loops, there have been relatively few comparisons of simultaneous 20 cm and soft X-ray observations. Such comparisons can help specify the dominant 20 cm radiation mechanism, while also establishing the physical parameters of the coronal plasma. X-ray spectral lines can, for example, be used to calculate the electron temperature and electron density while the radio observations can uniquely specify the strength and structure of the magnetic field.

In this paper, we provide an example in which the coronal

radiation at 20 cm and X-ray wavelengths coincide. The observations are presented in § II, where we also present radio spectra that are attributed to a thermal cyclotron line. In § III, we provide values for the electron density, electron temperature, and magnetic field strength in these coronal loops and attribute the 20 cm radiation to thermal gyroresonance emission. The X-ray values of electron density and electron temperature are combined with the 20 cm brightness temperature and the cyclotron line to calculate the harmonic of the gyrofrequency. Our results are summarized in § IV.

II. OBSERVATIONS

We have used the VLA and the SMM FCS to observe the solar active region AR 4663 on 1985 June 7. The VLA was used in the B-configuration at 10 different wavelengths between 21.8 cm (1440 MHz) and 17.4 cm (1720 MHz) with bandwidths of 12.5 MHz between 1500 UT and 2400 UT on June 7, and the FCS observed five prominent soft X-ray lines (O VIII, Mg XI, Si XIII, S XV, and Fe XXV) between 1500 UT and 1940 UT on June 7. The position of AR 4663 on the solar surface was 01° N and 65° E at 1300 UT on June 7.

The half-power beamwidth of the individual VLA antennas ranged between $26'$ and $31'$, and the synthesized maps constructed from up to 325 interferometer pairs had beamwidths between $3''.0 \times 3''.5$ and $3''.6 \times 4''.2$. The active region was observed with the VLA at successive pairs of wavelengths for 5 minutes each, so that all 10 wavelengths could be observed in 25 minutes. This sequence of observations was followed by successive 2 minute observations of the calibrator source PKS 0552+398 whose flux density was 1.7 Jy at 1465 MHz. The calibrated data for the 9 hr interval were used with the standard CLEAN procedure to make synthesis maps of both the total intensity, I , and circular polarization or Stokes parameter V . No solar bursts or flares were observed during this interval, and the synthesis maps therefore refer to the quiescent, or nonflaring, radio emission. That is, plots of the visibility data exhibited no variations that could be attributed to solar activity. There was no detectable circular polarization ($V/I \leq 15\%$).

The $14''$ collimated field of view of the FCS was rastered over a $4'' \times 4''$ area with a pixel spacing of $10'' \times 10''$. X-ray images were obtained simultaneously in the five soft X-ray emission lines every 990 s throughout the orbital day which lasts about 60 minutes. All of the available data for each spectral line during each orbit were then summed and averaged to improve the statistical uncertainty on the count rate from each pixel. Significant emission was detected in the two softest channels—O VIII and Mg XI. The peak formation temperatures for these lines are 3×10^6 K and 7×10^6 K, respectively. The failure to detect emission in the harder, more energetic channels indicates that the active region was unperturbed by any flaring throughout the period of observation. The SMM bent crystal spectrometer (BCS) confirmed the absence of flares as no significant brightenings were observed in its Ca XIX channel during these observations.

The FCS also produced a white-light image that showed the sunspots, making it possible to align the X-ray images with the sunspots to an accuracy of $10''$. The VLA maps of the total intensity, I , at 20 cm wavelength were aligned with H α photographs of the same sunspots with a similar $10''$ accuracy. This enabled us to compare the soft X-ray and 20 cm data for the same field of view and angular scale.

The 20.3 cm (1480 MHz) radiation and the soft X-ray (O VIII) emission originated in the same area (Fig. 1). Observations at

TABLE 1
SPECTRAL DATA FOR AR 4336

Frequency (MHz)	$T_{b,max}$ (10^6 K)
1440	1.7
1480	1.9
1515	2.0
1558	2.3
1585	2.2
1620	2.8
1658	3.8
1690	2.4
1705	2.0
1725	1.8

both wavelengths apparently describe the same coronal loops or arcades of loops. They are about $60''$ across, which corresponds to a linear extent, L , of about 5×10^9 cm. Both the radio and the X-ray emission are displaced toward the limb. If this displacement is attributed to a projection effect, then at a longitude of $\sim 65^\circ$ we infer a radial height of $h \approx 3 \times 10^9$ cm for both the radio and X-ray sources above the photosphere. Both sources stretch between and across regions of opposite magnetic polarity seen in magnetograms of the underlying photosphere (Fig. 2).

The radio-wavelength coronal loops exhibited the same ellipsoidal shape and extent at 10 closely spaced frequencies ranging from between 1440 MHz (20.8 cm) and 1725 MHz (17.4 cm) (Fig. 3). The maximum brightness temperatures are given in Table 1. The highest brightness temperature of $T_{b,max} = 3.8 \times 10^6$ K requires a hot spatially distinct region that was not detected with the soft X-rays. The failure to detect the associated X-ray emission places a 1σ limit of 3×10^{-3} to the volume emission measure of the hot plasma.

The maximum brightness temperatures are plotted as a function of observing frequency in Figure 4. This spectrum contains a linelike feature with a central frequency, $\nu = 1650$ MHz and a full width to half-maximum, $\Delta\nu$, of 80 MHz. As discussed in more detail in § III, we attribute this feature to a thermal cyclotron line and use it to obtain an estimate of the coronal magnetic field strength.

III. DISCUSSION

To identify the dominant thermal radiation mechanism at 20 cm, one needs to know the electron temperature, electron density, and the magnetic field strength. The X-ray data were therefore used to infer the mean electron temperature, T_e , and the mean electron density N_e , for the regions marked A, B, and C in Figure 5. As previously mentioned, the active region was quiescent and was only detectable in the two softest X-ray channels (O VIII and Mg XI). The ratios of the two lines (O VIII to Mg XI) were used as temperature diagnostics.

An emission measure was inferred from the temperature and the observed X-ray fluxes. The electron density was then calculated using a volume of 3×10^{27} cm 3 , which equals the product of the FCS pixel area and a typical soft X-ray scale height of 3×10^9 cm.

The mean temperatures and densities are given in Table 2. We obtain average values of $T_e = 2.6 \pm 0.1 \times 10^6$ K and $N_e = 3.1 \pm 0.3 \times 10^9$ cm $^{-3}$ when averaged over all the coronal loops or arcades of loops. Here, the uncertainties correspond to the maximum possible deviation that reproduces the flux in all the detected X-ray lines to within 1 standard deviation of

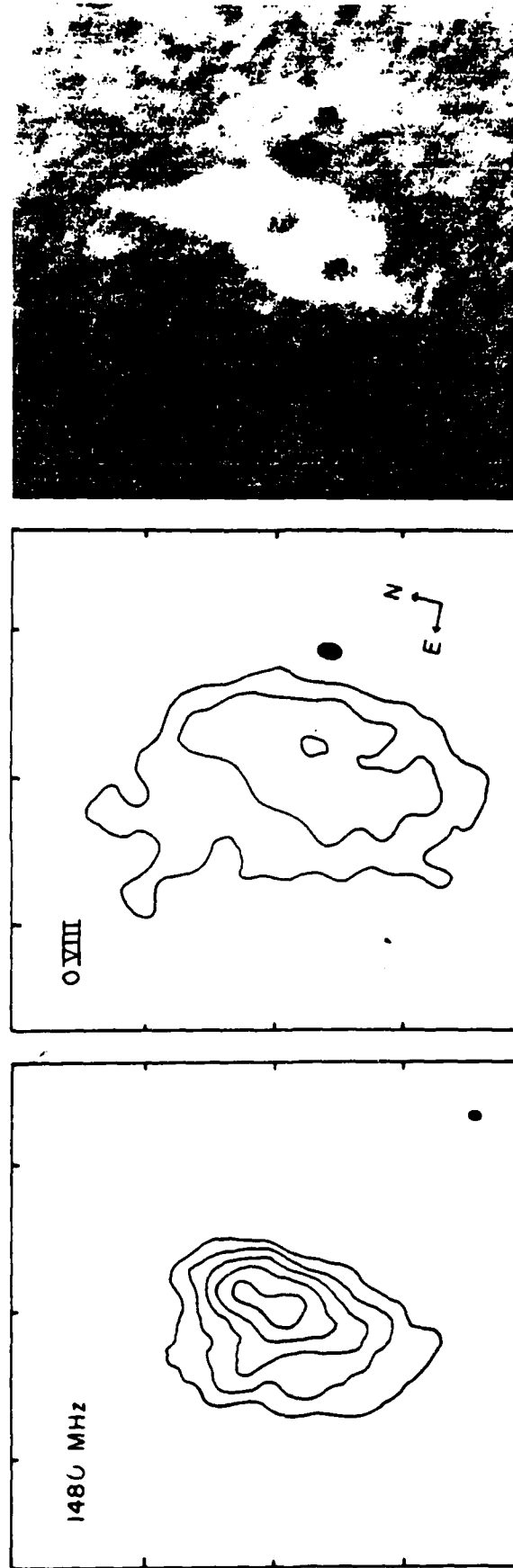


FIG. 1.—A comparison of 20 cm (VLA: left), soft X-ray (SMM: center) and H α (SOON: right) images of AR 4663 on 1985 June 7. The field of view of all three images is identical, and the identical angular scale can be inferred from the 60" spacing between fiducial marks on the axes. The contours of the 20 cm map mark levels of equal brightness temperature corresponding to 0.2, 0.4, ... 1.0 times the maximum brightness temperature of 1.8×10^6 K. The soft X-ray data were taken in the O VIII line (18.9 Å) with contours corresponding to 3, 7, 14, and 24 counts s^{-1} above a background level of 10 counts s^{-1} with a maximum signal of 18 counts s^{-1} .

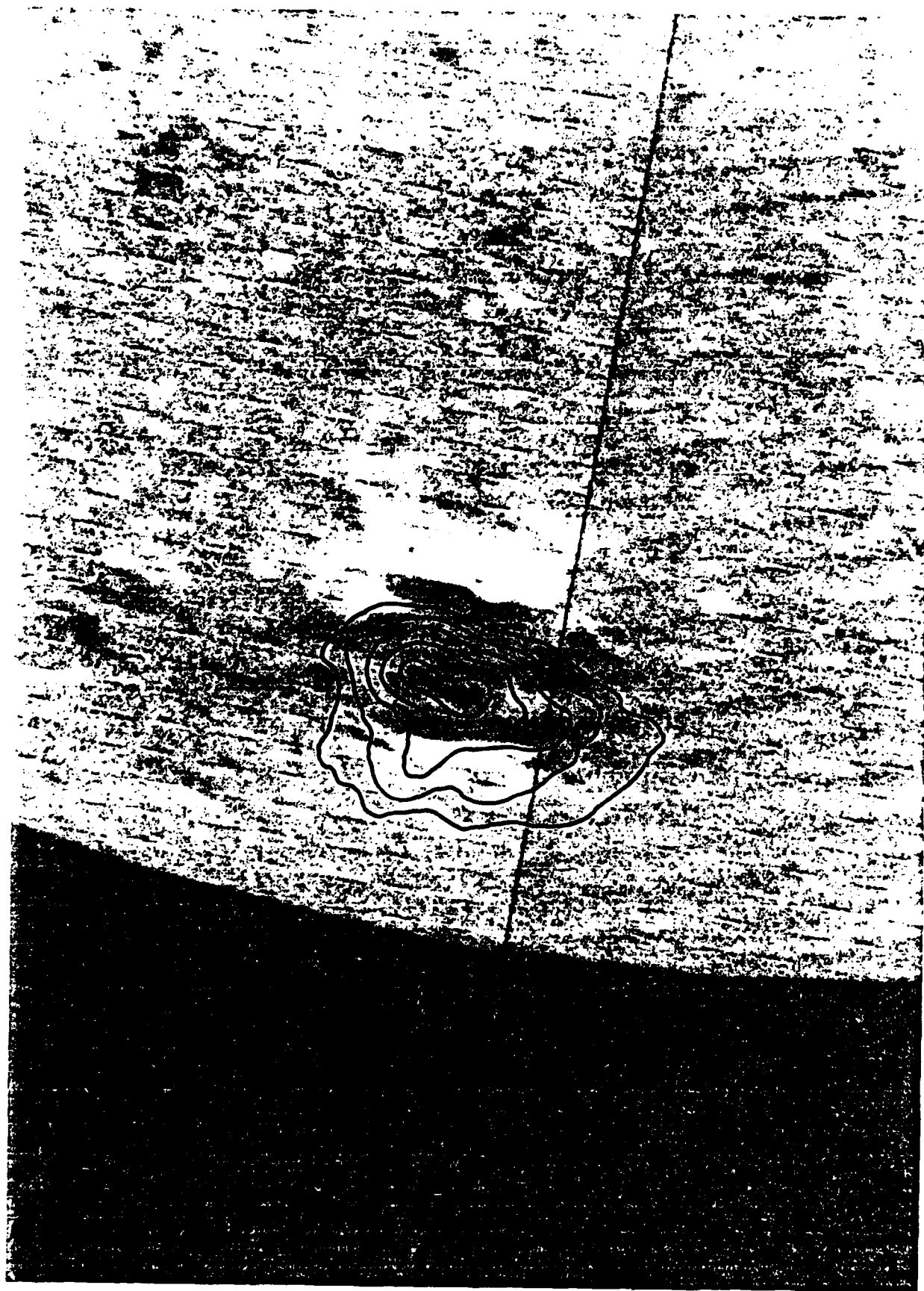


FIG. 2.—The 30 cm contours of equal brightness temperature (solid black lines) are superposed on a Kitt Peak National Observatory (KPNO) magnetogram of AR 4663 on 1985 June 7. The black magnetogram features indicate regions of negative magnetic polarity with magnetic fields pointed in toward the Sun, while the white magnetogram areas are regions of positive magnetic polarity with magnetic field lines pointed out toward the observer. The KPNO magnetogram is courtesy of Jack Hurvey of the National Solar Observatory.

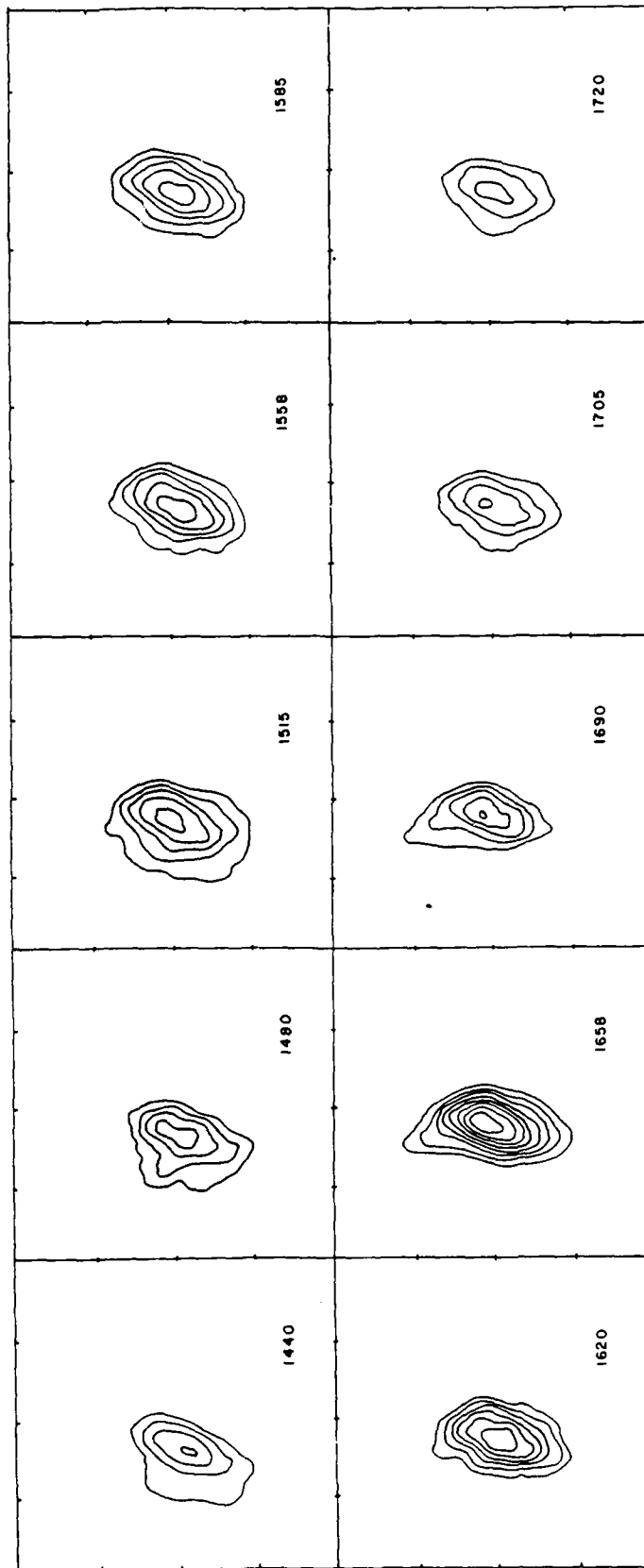


FIG. 3.—VLA synthesis maps of the total intensity, I , of AR 4663 at 10 closely spaced frequencies during a 9 hr period on 1985 June 7. The synthesized beamwidth was about $3'' \times 4''$, and the spacing between fiducial marks on the axes is $60''$. The map contours mark levels of equal brightness temperature, with an outermost contour of 7.6×10^5 K and a contour interval of 3.8×10^5 K. The maximum brightness temperatures are given in Table 1 and plotted in Fig. 4.

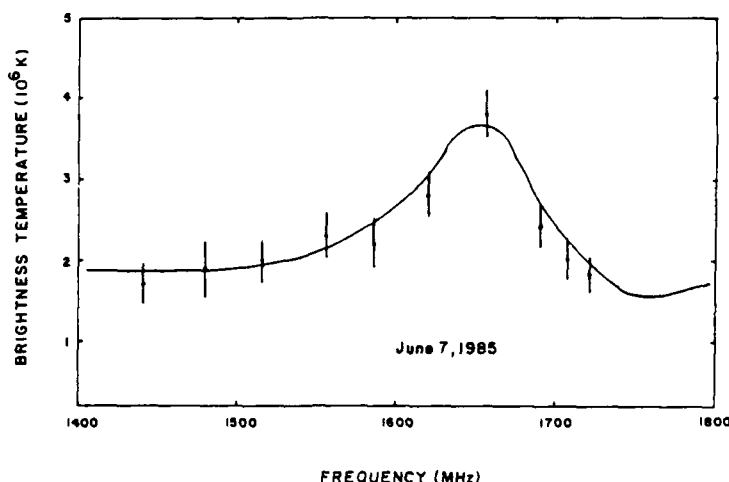


FIG. 4.—The maximum brightness temperature of the coronal loops of AR 4663 at 10 closely spaced frequencies on 1985 June 7. The maximum temperatures were inferred from the 9 hr synthesis maps shown in Fig. 3, and the error bars correspond to the peak-to-peak fluctuations in the background temperature of the synthesis maps.

the observed values. The inferred values of electron temperature and electron density are typical of those of quiescent coronal active region loops. Within the uncertainties, the observed loops were isothermal and isobaric, but there was a statistically uncertain tendency for a hotter temperature at the loop apex.

We may use the parameters derived from X-ray observations to estimate the optical depth and brightness temperature of the X-ray emitting plasma at radio wavelengths. Assuming an isothermal source of electron temperature, T_e , and optical depth,

τ , the observed radio brightness temperature, T_B , will be given by

$$T_B = \tau T_e \quad \text{for } \tau \ll 1 \text{ (optically thin)}$$

and

$$T_B = [1 - \exp(-\tau)] T_e \quad \text{for } \tau \geq 1 \text{ (optically thick).} \quad (1)$$

The free-free optical depth, τ_{ff} , for an isothermal loop with electron temperature, T_e , and width or thickness, W , is (Lang 1980)

$$\tau_{ff} = 9.8 \times 10^{-3} \frac{N_e^2 W}{v^2 T_e^{3/2}} \ln \left(4.7 \times 10^{10} \frac{T_e}{v} \right), \quad (2)$$

where v is the observing frequency in Hz and N_e is the electron density in cm^{-3} . Using $v = 1.65 \times 10^9$ Hz, corresponding to the center of our linelike feature, together with the X-ray values of $T_e = 2.6 \times 10^6$ K and $N_e = 3.1 \times 10^9 \text{ cm}^{-3}$ and a typical loop thickness of $W \leq 3 \times 10^9$ cm in equation (2), we obtain $\tau_{ff} \leq 0.4$. Free-free emission might therefore be important for some of the radiation with brightness temperatures $T_B < T_e$, but not for the hotter, spatially distinct regions with $T_B \approx 3.8 \times 10^6$ K.

We must therefore examine the alternative possibility of thermal gyroresonance radiation. The optical depth, τ_{gr} , due to gyroresonance absorption is given by (Zheleznyakov 1970)

$$\tau_{gr} = 2\pi^2 \frac{n^{2n}}{2^{n+1}n!} \frac{v_p^2}{cv} \left(\frac{kT_e}{mc^2} \right)^{n-1} L_H (1 \pm \cos \alpha)^2 \sin^{2n-2\alpha}, \quad (3)$$

where $n = 1, 2, 3, \dots$ is the harmonic number, the plasma

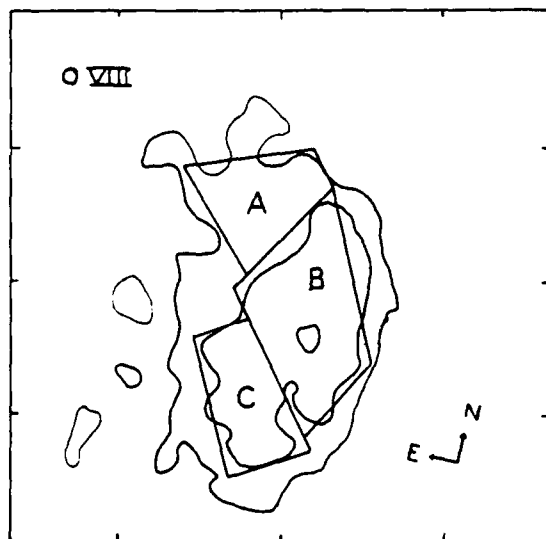


FIG. 5.—A soft X-ray map of AR 4663 taken in the O VII line (18.9 Å) with contours corresponding to 3, 7, and 14 counts s^{-1} . The image represents the averaged sum of two maps taken at 15:11 UT and 19:55 UT on 1985 June 7. Each map took 590 s to accumulate. The ratio of the O VII and Mg XI line intensities were used to determine the mean electron temperature in the regions marked A, B, and C. These temperatures are given together with estimates for the mean electron density in Table 2.

TABLE 2
PHYSICAL PARAMETERS FOR AR 4336

Region	T_e (10^6 K)	N_e (10^9 cm^{-3})
A	2.8	2.1
B	2.7	3.2
C	2.2	3.6
Average	2.6	3.1

frequency $\nu_p = 8.9 \times 10^3 N_e^{1/2}$ Hz, the velocity of light $c = 2.9979 \times 10^{10}$ cm s⁻¹, Boltzmann's constant $k = 1.38 \times 10^{-16}$ ergs K⁻¹, the electron mass $m = 9.1 \times 10^{-28}$ g, the scale height of the magnetic field is L_H , and α is the angle between the line of sight and the direction of the magnetic field lines. Collecting terms, we obtain

$$\tau_{gr} = 0.052 \frac{n^{2n}}{2^{n+1}n!} \frac{N_e}{\nu} \times (1.7 \times 10^{-10} T_e)^{n-1} L_H (1 \pm \cos \alpha)^2 \sin^{2n-2\alpha}. \quad (4)$$

The harmonic n is related to the observing frequency ν and the magnetic field strength H through the relation

$$\nu = 2.8 \times 10^6 nH \text{ Hz}. \quad (5)$$

For gyroresonance absorption to dominate free-free absorption at our reference frequency $\nu = 1.65 \times 10^9$ Hz, the layers must be optically thick with $\tau_{gr} > \tau_{ff} \approx 0.4$.

Optically thick gyroresonance emission with low circular polarization can be obtained using the X-ray values of $N_e = 3.1 \times 10^9$ cm⁻³ and $T_e = 2.6 \times 10^6$ K in equation (4) with $n = 3$ or 4 and $\alpha = 60^\circ$ or 70° , respectively. We can then use equation (5) with $n = 3$ or 4 and $\nu = 1.65 \times 10^9$ Hz to obtain a magnetic field strength of $H = 196$ or 147 G, respectively. This is consistent with model calculations of the spectrum of another thermal cyclotron line (Willson 1985), but in the case presented here, we do not have to make ad hoc assumptions about N_e and T_e . Observations of these lines may provide an unusually accurate method of specifying the coronal magnetic field strength.

If the magnetic field strength is highly variable, the width of the cyclotron line will depend on this variation; but if the field is relatively constant, the width depends on Doppler broadening and the central frequency of the cyclotron line gives an accurate measurement of the field strength—provided the harmonic can be isolated. For instance, the observed line half-width is only 80 MHz, indicating that H is known with a precision of better than 5 G or $H = 147 \pm 5$ G if we assume $n = 4$.

However, these are general arguments based upon homogeneous, isothermal models. When Table 1 and Figure 4 are examined in greater detail, we notice that inhomogeneities are required. For example, the 20 cm brightness temperature, T_b , is usually lower than the electron temperature, T_e , suggesting that the radio emission from the hot, optically thick loops is partially absorbed in a cooler external plasma. In addition, the T_b at 1650 MHz is greater than T_e , suggesting a thin, hot gyroresonance layer similar to that proposed by Willson (1985). The detailed radio spectrum is probably due to a mixture of hot and cool loops whose average properties are inferred from X-ray observations.

Here we should point out that individual cyclotron lines are observed near the apex of coronal loops where the magnetic

field is relatively constant and a steep temperature gradient may exist. Neutral currents might also play a role, leading to intense radio emission from a relatively thin layer near the loop apex. The cyclotron lines from loop legs will, however, exhibit a great deal of spatial structure if the loops are thin enough (Holman and Kundu 1985). Observations of thin loops at an oblique angle with wavelengths of about 6 cm should lead to the spatial resolution of cyclotron-emitting layers along the loop legs, while observations of the loop apex at $\lambda \approx 20$ cm can resolve cyclotron lines in this region. Both techniques can provide a powerful diagnostic of the magnetic and thermal properties of coronal loops.

IV. SUMMARY

Simultaneous high-resolution observations of AR 4663 with the VLA and the SMM FCS indicate that the radiation at 20 cm and soft X-ray wavelengths originates from the same region, and that 20 cm VLA maps can image X-ray coronal loops. The X-ray spectral lines were used to infer an average electron temperature of about $2.9 \pm 0.1 \times 10^6$ K and an average electron density of $3.1 \pm 0.3 \times 10^9$ cm⁻³. These parameters were used to show that the layers emitting 20 cm radiation can be optically thick to either thermal bremsstrahlung or thermal gyroresonance radiation, depending upon unknown but plausible values of loop thickness, magnetic scale height, and magnetic field strength.

The absence of circular polarization suggests that these coronal loops are optically thick at wavelengths near 20 cm and the detection of a linelike feature in the radio spectrum indicates that gyroresonance absorption exceeds free-free absorption. This feature is attributed to a thermal cyclotron line. The X-ray values for T_e and N_e were combined with plausible values for gyroresonant optical depth and the magnetic scale height to show that the 20 cm radiation is probably at the fourth harmonic of the gyrofrequency. The central frequency and relatively narrow width of the thermal cyclotron line were combined with this harmonic to infer a magnetic field strength of 147 ± 5 G at the apexes of these coronal loops.

Radio astronomical studies of the Sun at Tufts University are supported under grant AFOSR-83-0019 with the Air Force Office of Scientific Research and contract N00014-86-K-0068 with the Office of Naval Research (ONR). Simultaneous VLA and SMM observations of the Sun are supported by NASA grant NAG 5-501. K.L.S. and K.T.S. are supported by NASA contract NAS 5-23758 and the Lockheed Independent Research Program. The FCS and BCS were built by a consortium of three groups: Lockheed Palo Alto Research Laboratory, Mullard Space Science Laboratory, and the Rutherford Appleton Laboratories. The VLA is operated by Associated Universities, Inc., under contract with the National Science Foundation.

REFERENCES

- Holman, G. O., and Kundu, M. R. 1985, *Ap. J.*, **292**, 291.
 Kuznetsov, V. S., and Syrovatskii, S. I. 1981, *Solar Phys.*, **69**, 391.
 Lang, K. R. 1980, *Astrophysical Formulae* (2d ed.; New York: Springer Verlag), p. 47.
 Lang, K. R., and Willson, R. F. 1983, *Adv. Space Res.*, **2**, No. 11, 91.
 ———, 1984, *Adv. Space Res.*, **4**, No. 7, 105.
 Lang, K. R., Willson, R. F., and Gaizauskas, V. 1983, *Ap. J.*, **267**, 455.
 Lang, K. R., Willson, R. F., and Rayrole, J. 1982, *Ap. J.*, **258**, 384.

McConnell, D., and Kundu, M. R. 1983, *Ap. J.*, **269**, 698.

Shevgaonkar, R. K., and Kundu, M. R. 1984, *Ap. J.*, **283**, 413.

Syrovatskii, S. I., and Kuznetsov, V. D. 1980, in *IAU Symposium 86, Radio Physics of the Sun*, ed. M. R. Kundu and T. E. Gergely (Dordrecht: Reidel), p. 109.

Willson, R. F. 1985, *Ap. J.*, **298**, 911.

Zheleznyakov, V. V. 1970, *Radio Emission of the Sun and Planets* (New York: Pergamon), p. 454.

Zheleznyakov, V. V., and Zlotnik, E. Ya. 1980, in *IAU Symposium 86, Radio Physics of the Sun*, ed. M. R. Kundu and T. Gergely (Dordrecht: Reidel), p. 87.

KENNETH R. LANG and ROBERT F. WILLSON: Department of Physics and Astronomy, Robinson Hall, Tufts University, Medford, MA 02155

KERMIT L. SMITH and KEITH T. STRONG: Code 602.6, Bldg. 7-XRP, Goddard Space Flight Center, Greenbelt, MD 20771

32. ULTRAVIOLET AND RADIO FLARES FROM UX ARIETIS AND HR 1099

KENNETH R. LANG AND ROBERT F. WILLSON
 Department of Physics and Astronomy, Tufts University
 Received 1987 June 29; accepted 1987 November 5

ABSTRACT

We present simultaneous observations of the RS CVn systems UX Ari and HR 1099 with the *International Ultraviolet Explorer* (IUE) satellite and the Very Large Array (VLA). Flaring activity is observed at ultraviolet wavelengths with the IUE when none is detected at radio wavelengths with the VLA. We have also observed radio flares with no detectable ultraviolet activity. Thus, flares in the two spectral regions are either uncorrelated or weakly correlated. The flaring emission probably originates in different regions at the two wavelengths. Radio flares from RS CVn stars may originate in sources that are larger than, or comparable to, a star in size. This is in sharp contrast to compact, coherent radio flares from dwarf M stars. The ultraviolet flares from RS CVn stars probably originate in sources that are smaller than a component star.

Subject headings: stars: binaries — stars: flare — stars: individual (UX Ari, HR 1099) — stars: radio radiation — ultraviolet: spectra

I. INTRODUCTION

The RS CVn systems like UX Ari and HR 1099 are binary stars whose components are late-type dwarfs or subgiants with spectral type G or K. Variations in their light curves and observations of Ca II H and K lines have been associated, respectively, with photospheric starspots and chromospheric plages that are probably on the K star (see Gondoin 1986 for HR 1099). Extended transition regions are suggested by observations of intense ultraviolet emission lines (see Simon and Linsky 1980 for UX Ari and HR 1099), and the fact that essentially all RS CVn systems have been identified with soft X-ray sources suggests the presence of high-temperature coronal plasmas (Walter *et al.* 1980).

However, the relationship between the starspots, chromospheric activity, and the hypothetical coronal loops is not clear, particularly at times of stellar flares. Observations of asymmetries in the wings of ultraviolet emission lines have been interpreted in terms of mass upflow in unspotted regions (see Baliunas and Dupree 1982 for λ And), and similar asymmetries during an ultraviolet flare from UX Ari have been interpreted in terms of mass flow along magnetic flux tubes that connect the K star to the G star (see Simon, Linsky, and Schiffer 1980). Speculations about mass flow between or around (as in mass loss) the component stars might, at first sight, be related to radio flares from RS CVn stars, for they have been interpreted in terms of nonthermal gyrosynchrotron radiation from a volume that is several times larger than a star's volume (see Feldman *et al.* 1978 for HR 1099). However, previous coordinated ultraviolet and radio observations suggest that the ultraviolet emission is confined to a smaller volume on one star and that there may not be a causal relation between activity in the two spectral regions (see Weiler *et al.* 1978 for UX Ari and HR 1099).

In this paper we present simultaneous observations of UX Ari and HR 1099 at ultraviolet and radio wavelengths. Flaring activity is observed at ultraviolet wavelengths when none is detected at radio wavelengths, and vice versa. The observations are given in § II where we show that flares in the two spectral regions are either uncorrelated or only weakly correlated. In § III we discuss these observations and use them with

other data to argue that the flaring emission originates in different regions at the two wavelengths. Radio flares from RS CVn systems most likely originate in sources that are larger than, or comparable to, a star in size; but this is in sharp contrast to the radio radiation from dwarf M stars that emit coherent radiation from compact sources. Ultraviolet flares from RS CVn systems probably originate in sources that are smaller than a component star.

II. OBSERVATIONS

The RS CVn systems UX Ari (HD 21242) and HR 1099 (HD 22468, V711 Tau) were observed simultaneously with the *International Ultraviolet Explorer* (IUE) satellite and the Very Large Array (VLA) on 1987 January 6 and 7. UX Ari was observed with the VLA from 0251 to 0757 UT on January 6 and with the IUE during the 8 hr US 2 shift on the same day (roughly 0000–0800 UT). HR 1099 was observed with the VLA from 2219 UT on January 6 to 0805 UT on January 7 and with the IUE during the 8 hr US 2 shift on January 7.

The VLA (C configuration) was divided into two subarrays of 13 antennas each in order to simultaneously observe at four frequencies. One subarray was used to observe at frequencies of 1465 MHz and 1515 MHz and the other one was used at 4835 MHz and 4885 MHz. The fringe visibilities were sampled at a rate of 6.67 s, and the data were calibrated from observations of PKS 0333+321 for 5 minutes every 40 minutes. The flux density scale was established from observations of 3C 286 (7.5 Jy at 4835 MHz and 14.7 Jy at 1465 MHz).

The VLA data were first examined, baseline by baseline for any interference or obviously bad data. The edited data were then calibrated and used to make synthesis maps of the source which were then cleaned and fitted with two-dimensional Gaussian functions in order to determine their locations to within about one-tenth of the beamwidth ($3''.7 \times 4''.3$ at 6 cm and $12''.7 \times 14''.4$ at 20.4 cm). The 6.6 s data were then phase-shifted to bring the sources exactly into the center of the map. Finally, these data were vector-averaged, baseline by baseline, and used to construct plots of total intensity, I , and circular polarization, p_c , as a function of time. Because the fluxes at the two closely spaced IF's at 6 cm and 20 cm showed no evidence

of narrow-band structure, they were averaged together to improve the signal-to-noise ratio. For a 6.6 s integration time the 3σ rms noise level on the averaged maps is ~ 10 mJy at 20.4 cm and ~ 7 mJy at 6 cm.

The *IUE* observations were made by alternately using the short-wavelength (1150–1975 Å) SWP camera and the long-wavelength (1910–3300 Å) LWP camera. The SWP observations were made at low dispersion (spectral resolution ~ 6 Å), while the LWP observations were made at high dispersion (spectral resolution ~ 0.2 Å). In both cases the stars were observed through the large $10'' \times 20''$ aperture. Observations with the SWP camera consisted of two or three multiple exposures placed side-by-side in the large aperture and perpendicular to the spectral dispersion. Each SWP exposure was about 10 minutes long, while the LWP observations consisted of a single 15 minute exposure. During these observations the background radiation level was moderately low and fairly constant with flux counts, DN, of 18–25 for the SWP camera and 32–45 for the LWP camera.

The spectra were extracted from the photometrically corrected images, and the absolute flux calibration of Bohlin and Holm (1980) was applied to the SWP data. Because the absolute calibration of the high-resolution LWP spectra is still controversial, we decided to analyze relative spectral values only. We also examined the spectra for cosmic-ray events or "hits," but none were found.

In Figures 1–4 we show the *IUE* spectra for both stars. Here, third order polynomial baselines have been removed from the data. The SWP spectra contain a number of chromospheric and transition region ($T_e = 10^4$ – 2×10^5 K) lines, of which the most prominent are C IV, O I, and C II. The LWP spectra show the relative intensities of the Mg II *k* line at a wavelength of ~ 2796 Å. Each spectral feature was fitted, using a least-squares procedure, with a Gaussian profile in order to determine the peak intensity, ΔI_L , the full width at half-maximum, $\Delta \lambda_L$, and the central wavelength, λ_L , of the line. The integrated line intensity was then taken to be equal to $1.06 \Delta I_L \Delta \lambda_L$, appropriate for a Gaussian function. When no variations were detected, the spectrum from each 10 minute SWP exposure was averaged to give an integrated line intensity over an interval of 30 minutes.

The combined VLA and *IUE* data are shown in Figures 5 and 6. An intense ultraviolet flare was observed from UX Ari at about 0530 UT on January 6 (Fig. 5), but there was no detectable radio burst at either 6 cm or 20 cm. Here, we have plotted the variations in the integrated line intensity of the C IV line at 1549 Å, but similar variations were observed from some of the other prominent SWP lines (Fig. 1). Our analysis of the LWP spectra (Fig. 2) also indicates that the relative intensity of the Mg II *k* line increased more or less monotonically by about a factor of 1.6 ± 0.1 during the 5 hr period of observation.

In Table 1 we give the intensities of the SWP lines during the quiescent period preceding the flare (spectrum A at 0005 UT) and at the flare peak (spectrum D3 at 0522 UT). We note that the intensities of these lines are in reasonably good agreement with those given by Simon and Linsky (1980), also during a period of quiescence.

As illustrated in Figure 6, a circularly polarized radio flare was observed from HR 1099 at 1465 MHz at about 0500 UT on January 7, but there was no detectable flare at either 4885 MHz or at ultraviolet wavelengths. Both of the latter two wavelengths refer to lower levels in the stellar atmosphere than the longer 20.4 cm (1465 MHz) wavelength where the flare

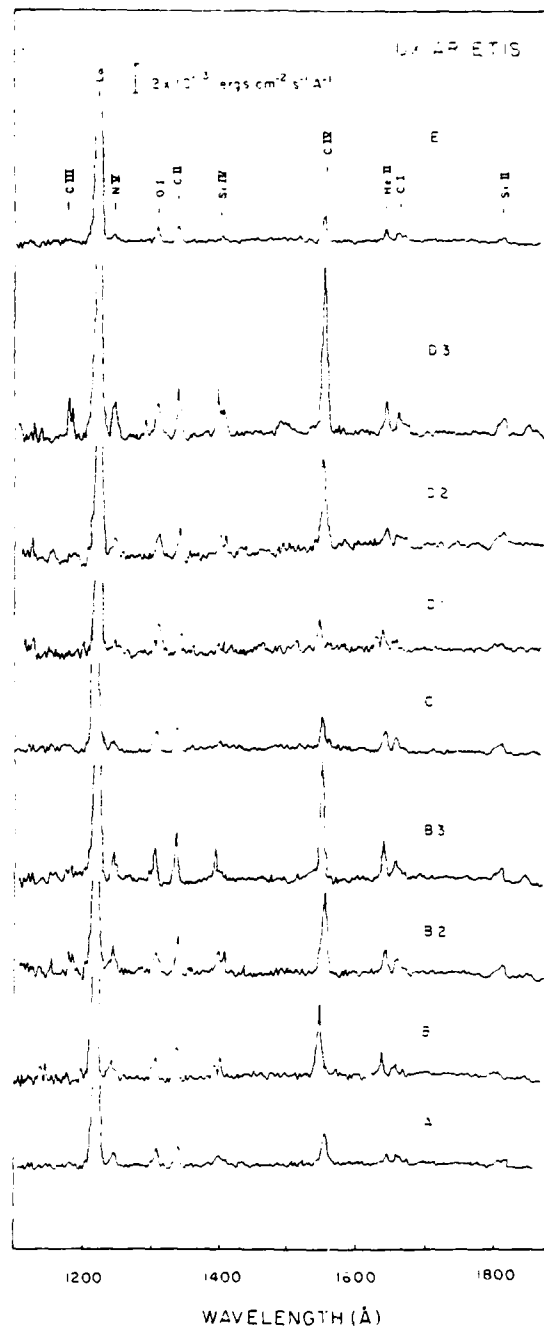


FIG. 1.—Short-wavelength (SWP), low-dispersion spectra of UX Ari on 1987 January 6. The time covered by each exposure can be inferred from Fig. 5, which shows the integrated intensity of the C IV line (1549 Å) throughout the day.

occurred. There is a possibility that the slow 5 hr increase in the integrated intensity of the C IV line (Fig. 3) was related to subsequent triggering of the radio flare observed at higher levels in the stellar atmosphere, but the flare itself was not detected at the lower levels. There were also no detectable variations in the intensity of the Mg II *k* line, to an uncertainty of $\sim 10\%$ (Fig. 4).

Thus, our simultaneous VLA-*IUE* observations of UX Ari

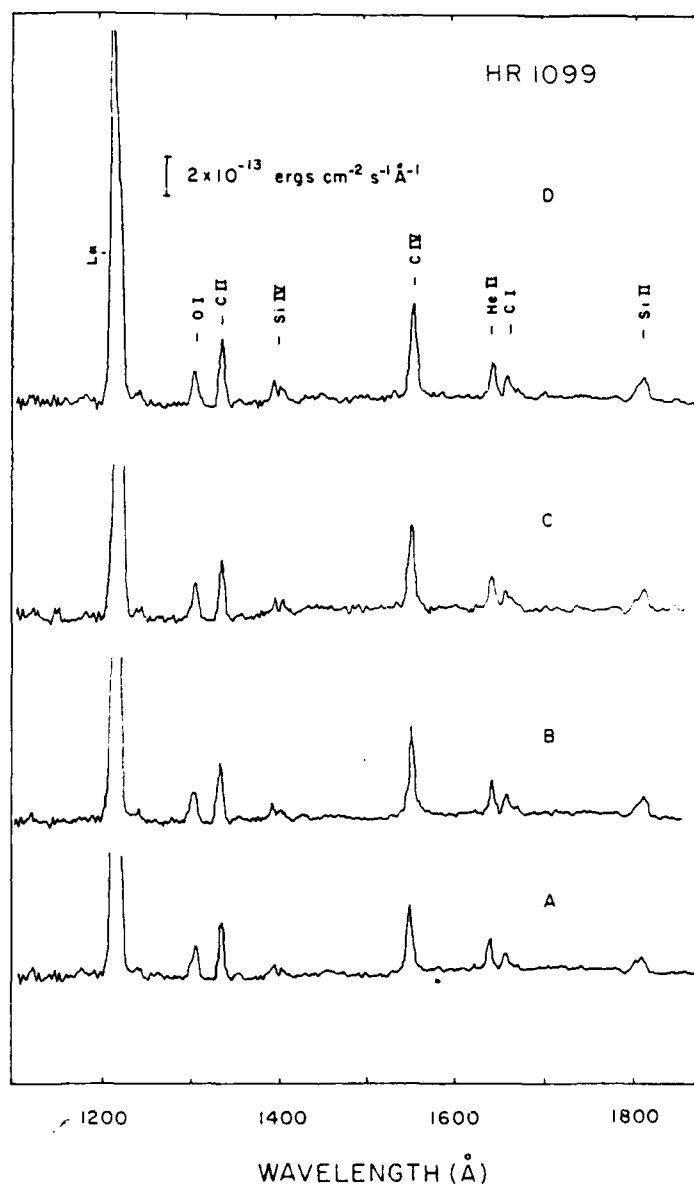


FIG. 2.—Long-wavelength (LWP), high-dispersion spectra of UX Ari on 1987 January 5 and 6, showing the relative intensities of the Mg II *k* line. Here, time increases toward the top of the figure.

TABLE 1
INTEGRATED LINE FLUXES FOR QUIESCENT AND FLARE SPECTRA OF UX ARIETIS

LINE	λ (Å)	FLUX	
		Quiescent ($\times 10^{-13}$ ergs cm^{-2} s^{-1})	Flare ($\times 10^{-13}$ ergs cm^{-2} s^{-1})
C III	1175	<2	13
N V	1240	<2	16
O I	1304	10	23
C II	1335	10	25
C IV	1549	18	85
He II	1640	5	14
C I	1657	4	16
Si II	1808, 1817	5	9

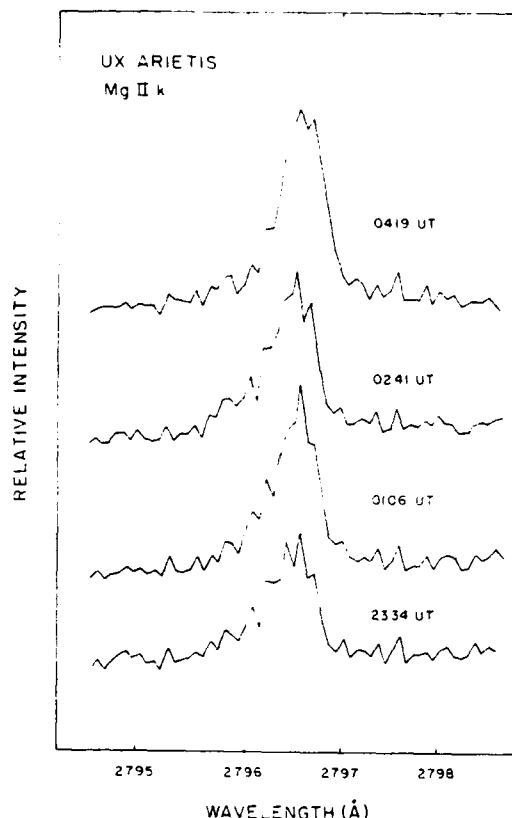


FIG. 3.—Short-wavelength (SWP), low-dispersion spectra of HR 1099 on 1987 January 7. The time covered by each exposure can be inferred from Fig. 6, which shows the integrated intensity of the C IV line (1549 Å) throughout the day.

and HR 1099 indicate that intense ultraviolet flares are emitted from RS CVn systems when no radio flares are detected and that a radio flare is observed when no counterpart is detected at ultraviolet wavelengths. Previous observations of the RS CVn system λ And also indicated ultraviolet variations that were not detected at radio wavelengths with the VLA (Willson and Lang 1986), and previous radio variations from UX Ari at 4885 MHz were not detected at either 1465 MHz with the VLA or at ultraviolet wavelengths with the IUE (Willson and Lang 1987). As discussed in greater detail in the next section, the flaring emission at different wavelengths probably originates in different regions, with shorter wavelengths referring to smaller regions that are deeper within the atmosphere of the active K star.

III. DISCUSSION

Weakly polarized ($p_c \leq 20\%$) radio radiation was always observed during our observations of HR 1099 with flux densities $S \approx 50$ mJy. A circularly polarized ($p_c \approx 55\%$) radio flare with $S \approx 120$ mJy was superposed upon the weaker, more slowly varying, radiation. If the radius, R , of the radio source is comparable to the separation of the component stars ($R \approx 10^{12}$ cm), then the brightness temperatures, T_b , corresponding to these two values of flux density are $T_b = 2.3 \times 10^9$ K and $T_b = 5.6 \times 10^9$ K (using the Rayleigh-Jeans law with a distance of 33 pc). Similar brightness temperatures are inferred for the radio radiation from UX Ari if the source is

comparable in size to the separation of the component stars (Willson and Lang 1987).

Thus, plausible brightness temperatures are inferred if the radio radiation originates in sources that are larger than the stellar size and comparable to the binary star separation. The radio flares can then be explained by nonthermal gyrosynchrotron radiation. The low-frequency cutoff of the spectrum of one burst from HR 1099 has been explained by synchrotron self-absorption in a source of this size with plausible magnetic field strengths, H , of $H = 10$ – 100 G (Feldman *et al.* 1978). Such a large radio source size is consistent with VLBI observations of UX Ari and HR 1099 at 4.98 GHz. UX Ari has a radio halo with a linear size, L , of $L \approx 3 \times 10^{12}$ cm and a core of size $L \leq 3 \times 10^{11}$ cm (Mutel *et al.* 1985), and the upper limit to the radio size of HR 1099 is $L \leq 1 \times 10^{12}$ cm (Mutel *et al.* 1984). Detailed considerations of the self-absorption of gyrosynchrotron radiation indicate that the source size will increase at lower frequencies (Klein and Chiuderi-Drago 1987), so even larger sources are expected at our observing frequencies near 1.4 GHz.

If the radio sources were smaller than a star in size, with radii $R \leq 10^{11}$ cm, then the brightness temperatures would be $T_b \geq 10^{12}$ K at our observing frequency of 1465 MHz (for a distance of 33 pc and an assumed flux of 120 mJy). Such a high brightness temperature suggests a coherent radiation mechanism. Compact, coherent radio sources have, in fact, been inferred from the rapid, millisecond variations in radio bursts from the dwarf M star AD Leo (Lang and Willson 1986a). The

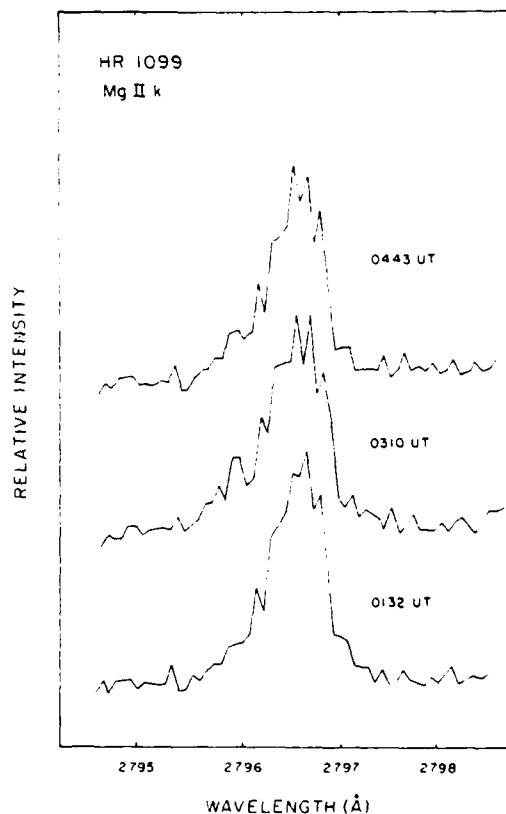


FIG. 4.—Long-wavelength (LWP), high-dispersion spectra of HR 1099 on 1987 January 7, showing the relative intensities of the Mg II k line.

narrow-band structure expected for coherent radiation has also been observed in the radio radiation from other dwarf M stars, including YZ Cmi (Lang and Willson 1986b, 1987) and UV Ceti (Bastian and Bookbinder 1987). If the RS CVn stars radiate similar narrow-band coherent emission, we might have detected a difference in the radiation observed at 1465 MHz and 1515 MHz. The variations and the signal level observed at these two frequencies were, within the observational uncertainties, identical during our observations of HR 1099. Moreover, the observed variations in the radio radiation had time scales $\tau \geq 30$ s, suggesting $L \geq 10^{12}$ cm, if the source expands at the speed of light. Thus, the available data suggest that the RS CVn stars do not emit coherent radio radiation from compact sources that are much smaller than a star in size, and in this respect they differ from the dwarf M stars.

Radio bursts from RS CVn stars may originate in large-scale coronal loops that are anchored in the active K star but exceed it in size. Such loops have been suggested by extrapolations from transition region pressures using a hydrostatic scaling law (Simon and Linsky 1980). They would be large enough to permit gyrosynchrotron radiation with plausible brightness temperatures and synchrotron self-absorption at low radio frequencies. The hot plasma trapped within these loops could also be of sufficiently low electron density, N_e , to permit the

radio radiation to escape. Radiation at frequencies, ν , less than the plasma frequency $\nu_p = 8.9 \times 10^3 N_e^{1/2}$ would be absorbed. In order to detect the radiation observed from HR 1099 at 1465 MHz, the electron density must be $N_e \leq 10^{10} \text{ cm}^{-3}$.

Much higher electron densities are required to account for the ultraviolet emission lines observed during ultraviolet flares from RS CVn stars. This suggests that these flares originate close to the stellar transition region in sources that are most likely smaller than a component star in size. The fact that the ultraviolet flares were not correlated with radio flares, and vice versa, is consistent with different sources for the radiation emitted in these two spectral regions, and the radiation at the shorter ultraviolet wavelengths most likely originates in smaller sources that lie deeper in the atmosphere of the K star. This suggests that mass flow between stars is not responsible for the ultraviolet flares of RS CVn stars and that there must be some other explanation for the line asymmetries that led to speculations about such mass flows (Simon, Linsky, and Schiffer 1980).

We thank the referee for suggesting improvements to our paper. Radio astronomical studies of the Sun and other active stars at Tufts University are supported under grant AFOSR-

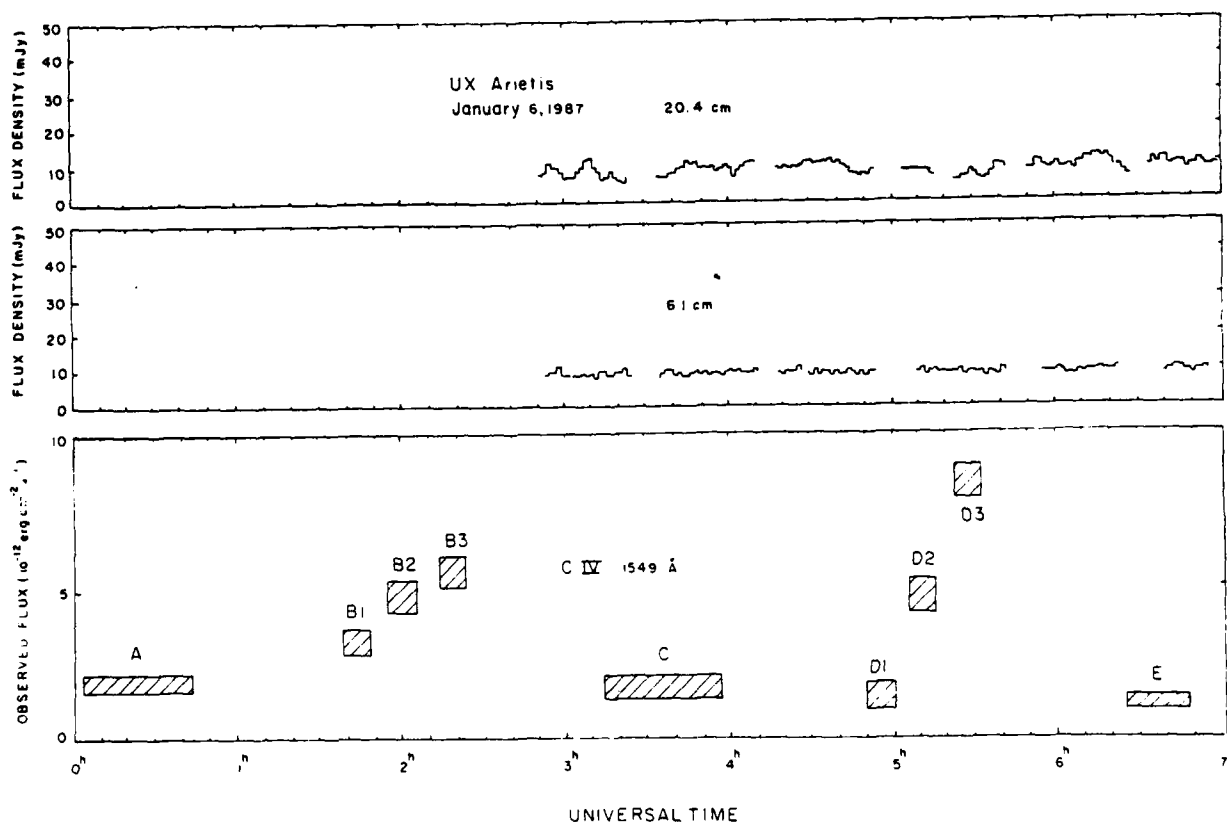


FIG. 5.—VLA and IUE observations of UX Ari on 1986 January 6. Plots of the total intensity, I , observed with the VLA at 1465 MHz and 1515 MHz (top) and 4835 MHz 4885 MHz (middle) are compared with a plot of the integrated intensity of the C IV line (1549 Å) observed with the IUE (bottom). Here the VLA data have been averaged over a time interval of 60 s. The vertical extent of each box corresponds to the 3σ uncertainty in line intensity, determined by our fitting procedure, while the horizontal extent of each box denotes the time interval for each spectrum. The labels refer to the SWP spectra shown in Fig. 1. In this case, the VLA observations did not begin until almost 3 hr after those with the IUE, but they did show that there was no detectable radio emission during the ultraviolet flare occurring at about 0530 UT.

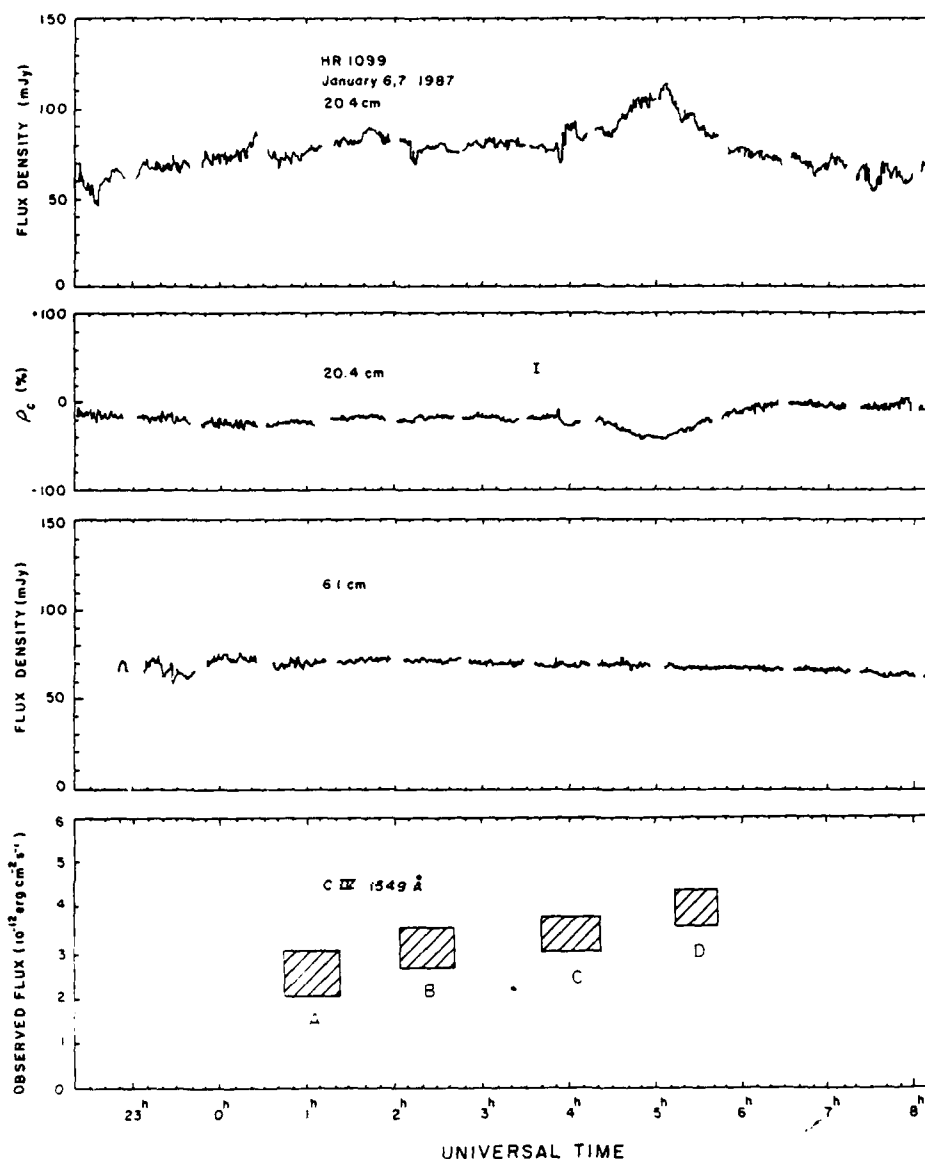


FIG. 6.—VLA and IUE observations of HR 1099 on 1987 January 6 and 7. Plots of total intensity, I , and degree of circular polarization, ρ_c , observed with the VLA at 1465 MHz and 1515 MHz (top) are compared with a plot of the total intensity observed with the VLA at 4835 MHz and 4885 MHz (middle) and a plot of the integrated line intensity of the C IV line (1549 Å) observed with the IUE (bottom). Here, the VLA data have been averaged over a time interval of 33.3 s, and the vertical bar on the polarization plot is the 3σ uncertainty of $\sim 10\%$ in ρ_c . The vertical extent of each box corresponds to the 3σ uncertainty in line intensity, determined by our fitting procedure, while the horizontal extent denotes the time interval for each spectrum. The labels refer to the SWP spectra shown in Fig. 3. Although there is a slow increase in the flux of the C IV line between 0100 and 0500 UT, the circularly polarized burst observed at 20 cm around 0500 UT was not detected at either 6 cm or at ultraviolet wavelengths.

83-0019 with the Air Force Office of Scientific Research. Simultaneous observations of active stars with the *International Ultraviolet Explorer* (IUE) satellite and the Very Large Array

(VLA) are also supported by NASA grant NAG 5-477. The VLA is operated by Associated Universities, Inc., under contract with the National Science Foundation.

REFERENCES

- Baliunas, S. L., and Dupree, A. K. 1982, *Ap. J.*, **252**, 668.
 Baliunas, S. L., Guinan, E. F., and Dupree, A. K. 1984, *Ap. J.*, **282**, 733.
 Bastian, T., and Bookbinder, J. 1987, *Nature*, **326**, 678.
 Bohlin, R. C., and Holm, A. J. 1980, *IUE NASA Newsletter*, No. 10, p. 37.
 Feldman, P. A., et al. 1978, *A.J.*, **83**, 1471.
 Gondoin, P. 1986, *Astr. Ap.*, **160**, 73.
 Klein, K. L., and Chiuderi-Drago, F. 1987, *Astr. Ap.*, **175**, 179.
 Lang, K. R., and Willson, R. F. 1986a, *Ap. J.*, **305**, 363.
 Lang, K. R., and Willson, R. F. 1986b, *Ap. J. (Letters)*, **302**, L17.
 ———, 1987, *Ap. J.*, in press.
 Mutel, R. L., Doiron, D. J., Lestrade, J. F., and Phillips, R. B. 1984, *Ap. J.*, **278**, 220.
 Mutel, R. L., Lestrade, J. F., Preston, R. A., and Phillips, R. B. 1985, *Ap. J.*, **289**, 262.
 Simon, T., and Linsky, J. L. 1980, *Ap. J.*, **241**, 759.
 Simon, T., Linsky, J. L., and Schiffer, F. H. 1980, *Ap. J.*, **239**, 911.

Walter, F. M., Cash, W., Charles, P. A., and Bowyer, C. S. 1980, *Ap. J.*, **236**, 212.
Weiler, E. J., et al. 1978, *Ap. J.*, **225**, 919.

Willson, R. F., and Lang, K. R. 1986, in *New Insights in Astrophysics* (ESA SP-263), p. 57.
———. 1987, *Ap. J.*, **312**, 278.

KENNETH R. LANG and ROBERT F. WILLSON: Department of Physics and Astronomy, Robinson Hall, Tufts University, Medford, MA 02155

33. VLA observations of dwarf M flare stars and magnetic stars

R.F. Willson, K.R. Lang, and P. Foster*

Department of Physics and Astronomy, Tufts University, Medford, MA 02155, USA

Received September 14, accepted December 17, 1987

Summary. The VLA has been used to search for 6 cm emission from 16 nearby dwarf M stars, leading to the detection of only one of them – Gliese 735. The dwarf M flare stars AD Leonis and YZ Canis Minoris were also monitored at 6 cm and 20 cm wavelength in order to study variability. Successive oppositely circularly polarized bursts were detected from AD Leo at 6 cm, suggesting the presence of magnetic fields of both magnetic polarities. An impulsive 20 cm burst from YZ CMi preceded slowly-varying 6 cm emission. The VLA was also used, unsuccessfully, to search for 6 cm emission from 13 magnetic Ap stars, all of which exhibit kilogauss magnetic fields. Although the Ap magnetic stars have strong dipolar magnetic fields, the failure to detect gyroresonant radiation suggests that these stars do not have hot, dense coronae. The quiescent microwave emission from GL 735 is probably due to nonthermal radiation, since unusually high ($H \geq 5 \cdot 10^4$ G) surface magnetic fields are inferred under the assumption that the 6 cm radiation is the gyroresonant radiation of thermal electrons.

Key words: late-type stars – stars: magnetic field – radio radiation of stars

1. Introduction

Nearby main sequence stars of nearly all spectral types exhibit quiescent X-ray emission whose absolute luminosity may be two orders of magnitude greater than that of the Sun (Johnson, 1981; Vaiana et al., 1981; Pallavicini et al., 1981). Since spatially resolved X-ray observations have shown that magnetic fields are responsible for the structure of the solar corona, the detection of X-ray emission from other stars suggests that they may also have large-scale coronal loops and intense magnetic fields. If this is the case, quiescent microwave emission might also be emitted by electrons trapped in these loops or by energetic electrons trapped in magnetic fields above starspots.

Recent centimeter wavelength investigations of one class of X-ray stars – the dwarf M flare stars have begun to provide a wealth of new information about a number of physical processes that occur on these stars. Quiescent, or non-flaring radiation,

has been detected from the binary stars UV Ceti, EQ Pegasi, YY Geminorum and Wolf 630 and from the single stars YZ Canis Minoris and AU Microscopium (Gary and Linsky, 1981; Topka and Marsh, 1982; Linsky and Gary, 1983; Cox and Gibson, 1984; Pallavicini et al., 1985). The quiescent emission from YZ CMi is slowly variable over timescales of hours and it exhibits narrow-band characteristics expected from coherent radiation processes (Lang and Willson, 1986a; Lang and Willson, 1987). White et al. (1986) have detected narrow-band microwave emission from AD Leo and UV Cet. Bastian and Bookbinder (1987) have also recently observed highly circularly polarized, narrow-band bursts from UV Cet. Stellar bursts have been observed from both components of UV Cet (Fisher and Gibson, 1982), and highly circularly polarized bursts have been observed from AD Leo and YZ CMi (Lang et al., 1983; Lang and Willson, 1986a,b).

The exact radiation mechanism of the quiescent emission from dwarf M flare stars is not well understood. One possibility is gyroresonant radiation from thermal electrons spiralling in magnetic loops that are several times larger than the star (Linsky and Gary, 1983). An alternative explanation is gyrosynchrotron radiation from non-thermal electron accelerated more or less continuously in coronal magnetic fields above starspots (Pallavicini et al., 1985). The intense ($T_e \geq 10^{10}$ K) rapid (rise times less than 5 ms) highly circularly polarized ($\rho_c \approx 100\%$) 20 cm bursts observed from flare stars such as AD Leo on the other hand, suggest a coherent emission mechanism for stellar bursts (Lang and Willson, 1986b).

There is another class of stars whose intense magnetic fields have already been directly observed – the peculiar A and B stars. These stars have magnetic fields of a few hundred to several thousand gauss which are distributed over the entire surface of the star (e.g. Borra et al., 1982). The observed field strengths vary in a roughly sinusoidal fashion with periods of between 1 and 10 days. Most of these stars also vary in brightness and have spectral lines that vary in strength. In all cases the periods of these variations are the same as those of the magnetic fields. The magnetic variations can be explained by a dipolar magnetic field that is frozen into the star, so that as the star rotates, the observer detects different aspects of the magnetic geometry.

X-ray observations of magnetic stars are sparse, but observation of the stars ω Her, ω Oph, β Scl and χ^2 CVn indicate moderately high luminosities of $L_X \approx 5 \cdot 10^{29}$ ergs s^{-1} (Vaiana et al., 1981; Cash and Snow, 1982). These X-ray observations also indicate electron temperatures of $T_e \leq 10^7$ K and electron densities of $N_e \approx 10^{19}$ cm $^{-3}$ at radii comparable to the radius of the star. One might therefore expect that thermal electrons with these

Send offprint requests to: R.F. Willson

* Present address: Department of Astronomy, University of Virginia, Charlottesville, VA, USA

temperatures and densities would give rise to gyroresonance emission in the strong magnetic fields of the stars. Detailed calculations by Zheleznyakov and Tikhomorov (1984) suggest that microwave emission may in fact be detectable from a number of close magnetic stars. Positive detection of microwave emission from magnetic stars would confirm the presence of hot, dense corona around these stars, while systematic monitoring of the radio intensity would provide information about the magnetic field orientation.

In this paper we present VLA observations of dwarf M flare stars and magnetic stars. In Sect. 3 we describe the results of a 6 cm survey of nearby dwarf M flare stars, reporting the first detection of microwave radiation from GL 735. Here we also describe observations of stellar bursts from AD Leo and YZ CMi at 6 cm and 20 cm wavelength. This section concludes with a discussion of an unsuccessful search for 6 cm emission from 13 magnetic stars. In Sect. 3 we interpret the 6 cm flux from GL 735 in light of thermal (gyroresonance) and nonthermal (gyrosynchrotron) emission processes. Here we also compute the expected intensity of gyroresonant emission from the undetected magnetic stars assuming the dipolar model of Zheleznyakov and Tikhomorov (1985).

2. Observations

2.1. Observations of dwarf M stars

On 1986 June 22, we used the Very Large Array (VLA) to search for microwave emission from sixteen nearby ($d \leq 25$ pc) dwarf M stars at 6 cm wavelength. In Table 1 we list these stars, together with their Gliese catalog numbers, spectral classifications, distances, and when available, their X-ray luminosities as given by Johnson (1983). The entire VLA (A/B hybrid configuration) was used to observe each star for one hour at 4835 MHz and 4885 MHz with a bandwidth of 50 MHz. These data were phase-calibrated from observations of nearby standard sources every 30 minutes and the flux density scale was established from observations of 3C 286 (5.41 Jy at 4835 MHz). These data were then

used to produce cleaned synthesis maps of a $4' \times 4'$ field of view centred on the position of each star. The results of our observations are given in the last column of Table 1, where the upper limits refer to the 3σ noise levels on the cleaned maps. Only one of the stars, Gliese 735, was detected. In Sect. 3 we will discuss the radiation mechanisms that may account for the microwave emission from this star.

On 1986 June 23, we used the VLA to observe the dwarf M flare stars YZ CMi and AD Leo for about three hours each. In order to obtain spectral information about bursts and other variations, the array was divided into two subarrays so that one subarray, containing 13 antennas, had signal frequencies of 4835 MHz and 4885 MHz, and the other subarray, containing 14 antennas, had signal frequencies of 1415 MHz and 1465 MHz. The right and left hand circularly polarized signals were recorded every 10 s and calibrated as on the previous day. The raw visibility data were first inspected for malfunctioning antennae, interference or correlator errors, then edited, calibrated, and used to construct synthesis maps of each source. The cleaned components of nearby continuum sources were then subtracted from the visibility data, according to the procedure described by Gary (1985). The 10 s data were then phase-shifted to bring the microwave sources of AD Leo and YZ CMi exactly into the center of the map. These data were then vector averaged, baseline by baseline with running means as long as 2 minutes and used to construct plots of the total intensity, I , and circular polarization, ρ_c , at each frequency. In order to check on the integrity of this procedure, we also made cleaned snapshot maps on the same time-scales which were used to determine the source intensity. Both the vector averaging and straightforward mapping procedures gave essentially the same results.

AD Leo (GL 388) is an active dwarf M flare star known to exhibit frequent and intense bursts at optical and radio wavelengths. Rapid, highly circularly polarized spikes have, for example, been observed at 20-cm wavelength by Lang et al. (1983) and Lang and Willson (1986b). The rise times of these spikes have been as short as the integration time of 5 ms, yielding lower limits to the source size of $L \leq 1.5 \cdot 10^8$ cm, and brightness tem-

Table 1. Results of a search for 6 cm emission from dwarf M flare stars

Star name	Gliese number	Spectral class	Distance (pc)	L_x $10^{26} \text{ erg s}^{-1}$	Flux density (mJy)
GX And	15 A,B	dM1e, dM6e	3.5	14	<0.15
	29.1 A,B	dM0e	23.2	—	<0.15
σ^2 Eri	166 A,B		4.9	—	<0.17
	182	dM1e	14.7	—	<0.20
V 371 Ori	207.1	dM5e	15.2	—	<0.15
	229	dM1e	5.7	6	<0.12
Ross 614	234 A,B	dM7e	4.0	8	<0.18
Wolf 359	406	dM8e	2.3	10	<0.17
	424	dM1	8.4	—	<0.15
Ross 128	447	dM5	3.3	4.2	<0.19
	494	dM2e	12.2	—	<0.14
	517	K5	18.9	—	<0.15
	725 A,B	dM4, dM5	3.5	—	<0.18
VB10	735	dM2e	10.8	835	0.45 ± 0.15
	752 A,B	dM3.5e, dM5e	5.8	10	<0.17
	873	dM4.5e	5.2	—	<0.18

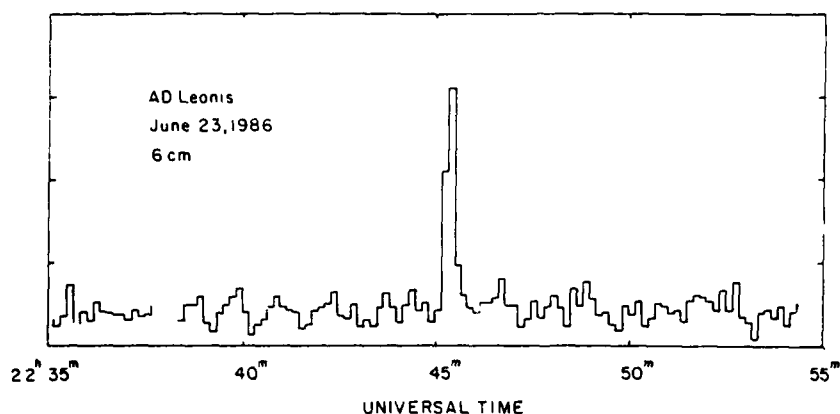


Fig. 1. A plot of the total intensity observed with the VLA at 4835 MHz (6.1 cm) from AD Leo. The burst shown here has a rise time of ≤ 10 s and is 100% right circularly polarized

peratures of $T_B \geq 10^{16}$ K. The high brightness temperatures require a coherent burst mechanism and the high circular polarization suggest a connection with stellar magnetic fields.

Our VLA observations of AD Leo resulted in the detection of two bursts at 6 cm wavelength (Figs. 1 and 2). The first occurred at ~ 2245 UT on 1986 June 23 and consisted of a 100% right circularly polarized event whose rise time was shorter than the 10 s integration time. This burst was followed about 2 hours later by a more complicated 100% left circularly polarized burst. In neither case was there any detectable quiescent or burst emission at 20 cm.

The reversal in polarity of these two successive bursts is of some interest. Microwave bursts from AD Leo were observed with up to 100% left hand circular polarization on 1983 February 1; 1984 November 8, and 1985 July 15 (Lang et al., 1983; Willson and Lang, 1986; Lang and Willson, 1986b). More recently, burst emission with up to 100% right hand circular polarization has been observed on 1985 December 15 and 1986 May 23 (White et al. 1986; this paper).

The constancy of the sense of circular polarization over long periods of time might indicate that the burst emission originates in magnetic fields of only one polarity, possibly due to a domi-

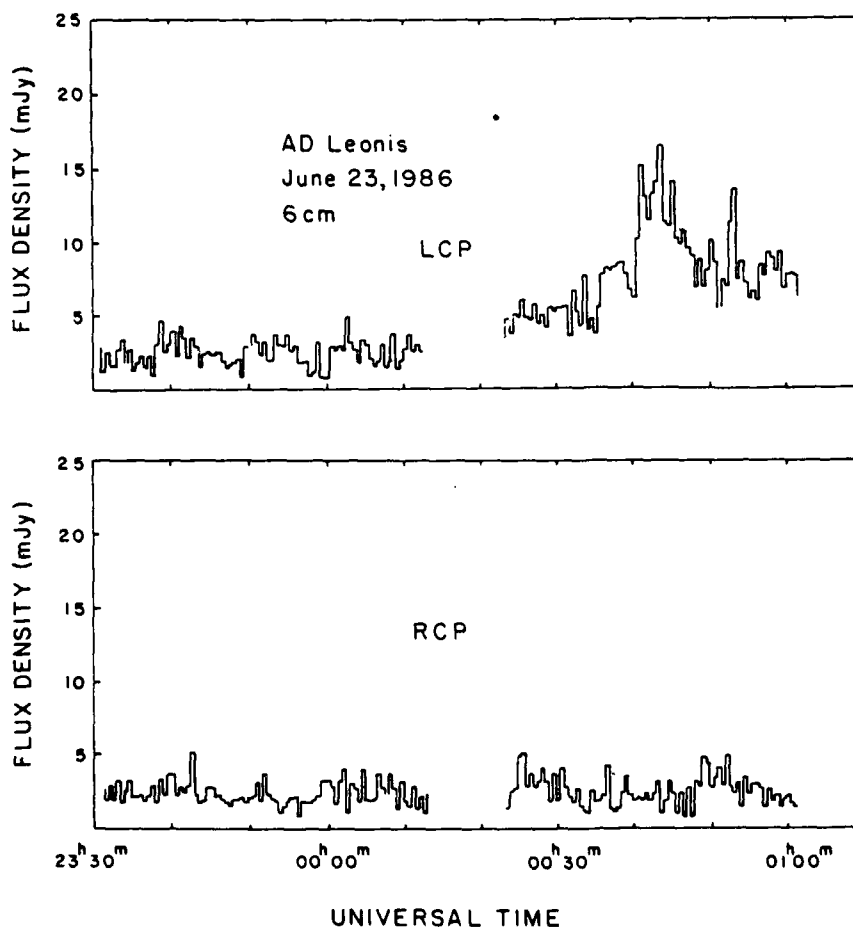


Fig. 2. A plot of the left hand circularly polarized (LCP) and right hand circularly polarized (RCP) signals observed at 4835 MHz (6.1 cm) from AD Leo. Here a complex 100% left circularly polarized burst lasting ~ 20 m was detected. The data in this plot have been vector averaged to yield an effective integration time of 30 s

nant starspot, and that a change in circular polarization may reveal long-term activity cycles. However, if both bursts were emitted in the extraordinary mode, then our observations of both left and right hand circular polarization for successive bursts indicate that magnetic fields of both polarities exist on AD Leo. We note that Bastian and Bookbinder (1987) have also recently observed oppositely circularly polarized bursts from UV Cet within a period of a few hours.

YZ CMi (GL 285) is another active flare star that has been well studied at optical and radio wavelengths. Coordinated optical, radio, and X-ray observations have resulted in the detection of a large number of flares, but few of these appear to have been detected simultaneously in all three wavelength ranges (Karpen et al., 1977; Kahler et al., 1982).

VLA observations of YZ CMi at 6 cm wavelength indicate that the source is variable on timescales of ten minutes to an hour (Pallavicini et al., 1985). Recent observations near 20 cm indicate that the radiation exhibits narrow-band structure that rules out broad-band continuum processes such as gyroresonant

emission or synchrotron radiation and suggests a coherent emission process such as coherent plasma radiation or an electron-cyclotron maser (Lang and Willson, 1986a).

Our VLA observations on 1986 June 23 indicate both slowly varying emission at 6 cm and moderately rapid (~ 20 minutes) emission at 20 cm (Fig. 3). The interesting aspect of the activity shown in Fig. 3 is that the 20 cm burst occurred at the onset of the increase in left circularly polarized flux at 6 cm. The 20-cm burst was unpolarized ($p_c \leq 15\%$) and there was no evidence of narrow-band structure. That is, the time profiles of the 1415 MHz and 1465 MHz emission were identical to within the noise level. The 6-cm emission is seen to be $\sim 50\%$ left circularly polarized from the beginning of our observations until ~ 2000 UT, at which time the left circularly polarized flux increased while the right circularly polarized flux remained nearly constant. Since longer wavelength radiation generally refers to higher levels in solar or stellar coronae, these observations suggest a disturbance which travelled downward in the stellar corona triggering the 6-cm variation.

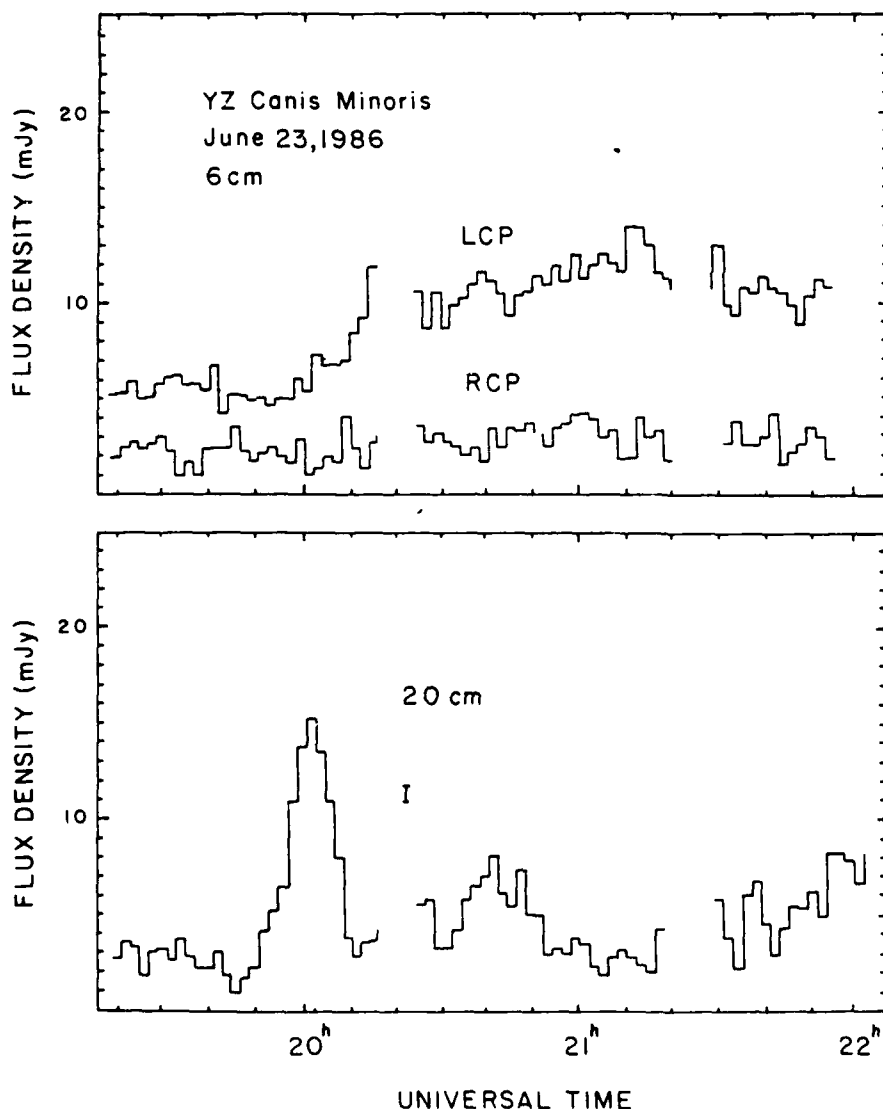


Fig. 3. Plots of the emission from YZ CMi at 4835 MHz (6.1 cm) (top) and 1465 MHz (20.47 cm) (bottom). Here the data have been vector averaged to yield an effective resolution of 2 m. Notice that left hand circularly polarized 6-cm emission began to increase immediately following the 20 cm burst

Table 2. Results of a search for 6 cm emission from magnetic stars

Star name	m_p	Rotation period (days)	B_p (Gauss)	Spectral type	Distance (pc)	Flux density (mJy)
α And	2.1	0.96	1500	B9 P	41.6	≤ 0.23
i Cas	4.5	1.74	3000	A5 P	47.6	≤ 0.35
53 Cam	6.0	8.03	51000	A2 P	70.0	≤ 0.21
30 UMa	5.0	11.58	3600	A0 P	25.0	≤ 0.20
γ Vir	3.0	—	1300	F0 P	9.9	≤ 0.20
ϵ UMa	1.8	50.09	3000	A0 P	20.0	≤ 0.25
α^2 CVn	2.9	5.47	10500	A0 P	43.5	≤ 0.20
i Lib	4.5	—	900	A0 P	43.5	≤ 0.20
β CrB	3.7	18.49	18000	F0 P	32.3	≤ 0.18
χ Ser	5.3	1.60	5400	A0 P	33.3	≤ 0.23
ω Her	4.6	1.53	6000	B9 P	30.3	≤ 0.23
γ Cyg	2.2	—	5200	F8 IB	—	≤ 0.20
γ Equ	4.7	—	10500	F0 P	47.6	≤ 0.20

2.2. Observation of magnetic stars

On 1986 February 10 and 11, the VLA (A/D hybrid configuration) was used to search for 6-cm emission from 13 magnetic stars. These stars are listed in Table 2, together with relevant physical parameters given by Didelon (1983) and Catalano and Benson (1984). These objects were chosen for study on the basis of their high magnetic fields ($H \approx 900$ –51,000 G) and relatively close distances ($D \leq 50$ pc). Each star was observed for about 1 hour using the entire VLA at 4835 MHz and 4885 MHz with a bandwidth of 50 MHz. The data were calibrated from observations of nearby calibrators and the overall flux density scale was established from observations of 3C 286. The data were then used to make synthesis maps of the region surrounding each star as described in the previous section. Our results indicate that none of the magnetic stars was detected above a 3σ noise level ~ 0.2 mJy. These results may be compared with those of a previous VLA survey of magnetic stars by Drake et al. (1985), who failed to detect 2 cm emission from the stars ω Her, ϵ UMa, α^2 CVn and 53 Cam at about the 3σ level of ~ 0.45 mJy.

3. Discussion

Our observations of dwarf M flare stars and magnetic stars allow us to place constraints on the physical conditions within the outer atmospheres of these stars. It is interesting to note that the only dwarf M star detected in our survey, GL 735, also has the highest X-ray luminosity ($L_X = 8.3 \cdot 10^{28} \text{ erg s}^{-1}$) of the 16 stars observed (Johnson, 1983). This is consistent with the results of previous studies of late-type stars which show that stars with detectable microwave emission (Linsky and Gary, 1983) are also intense X-ray emitters. In order to determine if the 6 cm flux from GL 735 represents quiescent or burst emission, we made a series of snapshot maps throughout the 60 minute period of observation. These maps gave no indication of source variability on any timescale between 10 s and 1 hour. We therefore conclude that the 6 cm emission is due either to a long lasting burst ($\tau > 1$ hour), or to quiescent emission from the stellar corona.

Our observations can also place some constraints on the radiation mechanism that gives rise to this emission. It has been

suggested that gyroresonance radiation of thermal electrons in stellar coronae may account for the slowly varying quiescent emission from dwarf M stars (Gary and Linsky, 1981; Topka and Marsh, 1982). The gyroresonant layers in a stellar corona will lie outside the star and will be generated at a maximum harmonic, n , for which the corona remains optically thick. Using the Rayleigh-Jeans law together with the observed flux density of 0.45 mJy at 6 cm wavelength, a coronal temperature of $T_e = 3 \cdot 10^6$ K, as suggested by the detected X-ray emission, a stellar radius of $R_* = 0.35 R_\odot$, and a distance of $d = 10.9$ pc, we find that the microwave source must have a radius of 6 – $11 R_\odot$. If the 6 cm source is to remain optically thick at the third or fourth harmonic of the gyrofrequency, then magnetic fields of $H \sim 430$ to 500 G must be present at 6 – 11 stellar radii. If a potential magnetic field configuration is assumed to be valid, then the inferred surface magnetic fields must be on the order of $H \geq 5 \cdot 10^4$ G. Such fields are at least an order of magnitude greater than those in sunspots as well as those that have been observed in the dwarf M flare star AD Leo (Saar, et al., 1986). The observed 6 cm radiation is therefore most-likely not due to thermal gyroresonance radiation.

An alternative explanation for the 6 cm radiation is nonthermal gyrosynchrotron emission from mildly relativistic electrons (Linsky and Gary, 1983; Pallavicini, et al., 1985). An attractive feature of non-thermal emission is that relatively high brightness temperatures can be produced with low magnetic fields. Using the relationship for gyrosynchrotron emission given by Dulk (1985), we find, for example, that a brightness temperature of $T_b \sim 3 \cdot 10^6$ K can be achieved for a power law index of $\delta = 3$, a nonthermal electron density of $N \sim 10^7 \text{ cm}^{-3}$, a scale length of $L \sim 10^8$ cm and a magnetic field strength of $H \sim 40$ G. In this case, surface magnetic fields about an order of magnitude smaller than those inferred under the assumption of thermal radiation would be expected.

What about our failure to detect 6 cm emission from the magnetic stars? If the high magnetic fields of these stars are in dipolar configurations with no stresses or reconnection, there may not be enough free energy for particle acceleration and nonthermal radiation. However, as shown by Zheleznyakov and Tikhomirov (1984), a rotating magnetic star with a hot ($T_e \approx 10^7$ K), dense

($\int N_e^2 dV \approx 10^{54} \text{ cm}^{-3}$) corona may emit thermal gyroresonant, or cyclotron, radiation at levels that are detectable with the VLA.

Observations of the Ap stars ω Her and α^2 CVn indicate that they are intense X-ray emitters ($L_X = 5-10 \cdot 10^{38} \text{ erg s}^{-1}$) whereas all of the stars in our survey have high magnetic fields of $H \geq 900$ Gauss. We have therefore used the model discussed by Zheleznyakov and Tikhomorov (1983) to compute the microwave spectrum of each of the stars observed. In order to compute the optical depth, brightness temperature and flux at any harmonic, it is necessary to know the magnetic field strength at the pole of the star, B_0 . The magnetic field at any distance r , from the center of the star can then be calculated using the dipolar field approximation

$$B = B_0(1 + 3 \cos^2 \theta)^{1/2} / 2(r/R_*)^3 \quad (1)$$

where θ is the angle between the dipolar axis and the radius vector r , and R_* is the stellar radius. Values of B_0 , taken from the literature, are given in Table 2. In some cases, B_0 has been obtained directly from fits to a rotating dipolar model, while in other cases, we have assumed that $B_0 = 3.0B_e$ where B_e is the maximum or minimum effective longitudinal magnetic field observed on each star (Didelon, 1983).

We also assumed a stellar radius of $R_* = 3R_\odot$, a coronal temperature of $T_e = 5 \cdot 10^6$ K and an electron density distribution $N_e(r)$ that varies with distance r as

$$N_e(r) = N_{e,0} \left(\frac{r}{R_*} \right)^{-6} \quad (2)$$

where $N_{e,0}$ is the density at the surface of the star. The r^{-6} variation of the electron density is characteristic of the quiescent solar corona (Allen, 1973), although there is no certainty that it applies for magnetic stars. In our calculations we also assumed that $N_{e,0} = 10^9 \text{ cm}^{-3}$, consistent with the densities inferred from observations of the coronae of the Sun and other active stars. The optical depth and brightness temperature at harmonics up to $n = 7$ was then computed along the line of sight through the stellar corona using the formulae for gyroresonance absorption given by Zlotnik (1968). The microwave flux was then computed numerically by integrating over the gyroresonant surfaces surrounding the star. These calculations were made both for the case in which the magnetic axis of the star is oriented parallel to the line of sight and in which it is perpendicular. For most stars, however, there is little difference in the shape or peak intensity for these two different cases.

Our results indicate that at 6 cm wavelength, the corona remains optically thick up to the fourth harmonic of the gyrofrequency ($H = 595$ Gauss). For a star with a polar magnetic field of $B_0 = 3000$ Gauss, this corresponds to a projected size of $r \approx 1.4R_*$. In Table 3 we give the computed flux densities at 6 cm and 2 cm wavelength for each of the stars, assuming a coronal base electron density of $N_{e,0} = 10^9 \text{ cm}^{-3}$, an electron temperature of $T_e = 5 \cdot 10^6$ K, and parallel alignment of the magnetic dipolar axis and the line of sight. Our results indicate that except for γ Vir, ϵ UMa and β CrB, the computed fluxes are consistent with the 6 cm upper limits given in Table 2 and with the 2 cm upper limits given by Drake et al. (1985). These authors for example find 3σ upper limits of ~ 0.45 mJy for ϵ UMa and β CrB, whereas our predicted 2 cm fluxes are 1.5 mJy and 1.3 mJy, respectively.

These discrepancies, however, could be reconciled by adjusting the electron density or temperature or both, since the optical

Table 3. Predicted gyroresonance flux density at 6 cm and 2 cm wavelength

Star	6 cm (mJy)	2 cm (mJy)
α And	0.04	$1 \cdot 10^{-4}$
i Cas	0.07	0.25
53 Cam	0-0.05	0.23
30 UMa	0.20	0.96
γ Vir	0.74	$\leq 10^{-6}$
ϵ UMa	0.32	1.5
α^2 CVn	0.10	0.52
i Lib	0.03	$\leq 10^{-4}$
β CrB	0.23	1.3
χ Ser	0.13	0.70
ω Her	0.20	0.80
γ Cyg	-	-
γ Equ	0.09	0.44

depth of gyroresonant emission depends on these parameters. In Fig. 4, for example, we show cyclotron spectra of γ Vir for different values of the electron density, $N_{e,0}$. This figure shows that the observed 3σ upper limit of 0.20 mJy is consistent with $N_{e,0} \leq 5 \cdot 10^8 \text{ cm}^{-3}$, or about two or three orders of magnitude smaller than the densities observed in coronal loops on the Sun, and those inferred from X-ray observations of late-type stars (Swank et al., 1981; Swank and Johnson, 1982). For ϵ UMa and β CrB we find that $N_e \leq 5 \cdot 10^7 \text{ cm}^{-3}$ yields fluxes consistent with the observations, again implying relatively low coronal densities for these stars.

Finally, Drake et al. (1987) recently reported the detection of the helium-weak magnetic stars IQ Aur (A0p, $S_1 = 0.48 \pm 0.09$ mJy, $D = 165$ pc) and GL Lac (B8p, $S_1 = 0.95 \pm 0.06$ pc, $D = 850$ pc). The longitudinal magnetic field data given by Didelon (1983) and by Borra and Landstreet (1978) suggests that these stars have polar magnetic fields of $B_p \approx 1800$ G (IQ Aur) and $B_p = 56,000-115,000$ G (GL Lac). Based on these values our model predicts 6 cm fluxes that are about two orders of magnitude smaller than those observed. Drake et al. (1987), also observed variable microwave emission ($\lambda = 2, 6$ and 20 cm) from the helium-strong magnetic stars δ Ori C, σ Ori E, and HR 1890 (spectral classes B1, B2). They found that this emission could not be attributed to a stellar wind, as in the case for other early type stars, but was consistent with gyrosynchrotron emission from mildly relativistic electrons trapped in closed magnetic fields. The fact that thermal cyclotron radiation cannot explain the emission from IQ Aur and GL Lac may therefore indicate a nonthermal mechanism for these stars.

Acknowledgements. Microwave studies of the Sun and other active stars at Tufts University are supported under grant AFOSR-83-0019 with the Air Force Office of Scientific Research. Our VLA observations of the Sun are supported by contract N0014-86-K-0068 with the Office of Naval Research (ONR). Investigations of dwarf M flare stars and RSCVn stars are also supported by NASA grant NAG 5-477. The National Radio Astronomy Observatory is operated by Associated Universities, Inc., under contract with the National Science Foundation.

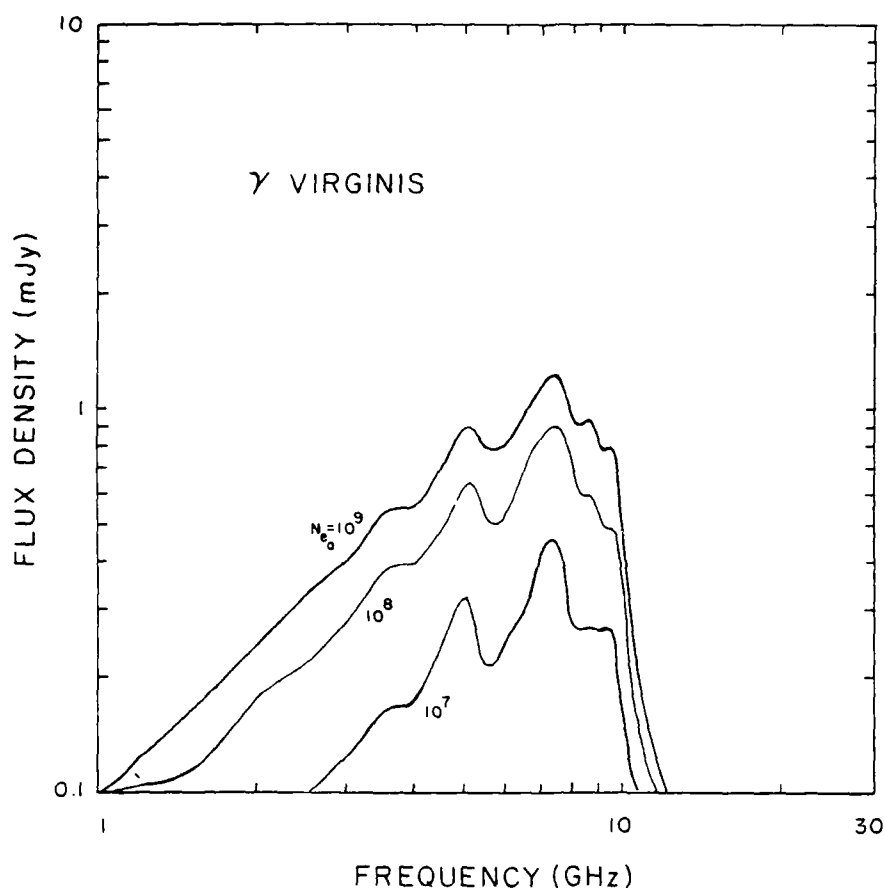


Fig. 4. Cyclotron radiation spectra for the magnetic star γ Vir. These spectra were computed assuming a polar magnetic field strength of $B_0 = 3600$ Gauss, a coronal electron temperature of $T_e = 5 \cdot 10^6$ K, parallel alignment of the magnetic dipole axis with respect to the line of sight and different values of the coronal base electron density, $N_{e,0}$, as indicated

References

- Allen, C.W.: 1973, *Astrophysical Quantities*, 3rd ed., Athlone Univ. Press, London
- Bastian, T.S., Bookbinder, J.A.: 1987, *Nature* **326**, 678
- Borra, E.F., Landstreet, J.D.: 1978, *Astrophys. J.* **222**, 226
- Borra, E.F., Landstreet, J.D., Mestel, L.: 1982 *Ann. Rev. Astron. Astrophys.* **20**, 191
- Cash, W., Snow, T.P.: 1982, *Astrophys. J. Letters* **263**, L59
- Catalano, F.A., Benson, P.: 1984, *Astron. Astrophys. Suppl. Ser.* **55**, 371
- Cox, J.J., Gibson, D.M.: 1984, in *Radio Stars*, eds. R.M. Hjellming, D.M. Gibson, Reidel, Dordrecht, p. 233
- Didelon, P.: 1983, *Astron. Astrophys. Suppl. Ser.* **53**, 119
- Drake, S.A., Simon, T., and Linsky, J.L.: 1985, in *Radio Stars*, eds. R.M. Hjellming, D.M. Gibson, Reidel, Dordrecht, p. 247
- Drake, S.A., Abbott, D.C., Bastian, T.S., Bieging, J.H., Churchwell, E., Dulk, G., Linsky, J.L.: 1987, *Astrophys. J.* **322**, 902
- Dulk, G.A.: 1985, *Ann. Rev. Astron. Astrophys.* **23**, 169
- Fisher, P.L., and Gibson, D.M.: 1982, in *Second Cambridge Workshop on Cool Stars, Stellar Systems and the Sun*, eds. M.S. Giampapa, L. Golub, Smithsonian Observatory Special Report No. 392, p. 109
- Gary, D.E., Linsky, J.L.: 1981, *Astrophys. J.* **250**, 284
- Gary, D.E.: 1985, in *Radio Stars*, eds. R.M. Hjellming, D.M. Gibson, Reidel, Dordrecht, p. 385
- Johnson, H.M.: 1981, *Astrophys. J.* **243**, 234
- Johnson, H.M.: 1983, *Astrophys. J.* **273**, 702
- Kahler, S. et al.: 1982, *Astrophys. J.* **252**, 239
- Karpen, J.T. et al.: 1977, *Astrophys. J.* **216**, 479
- Lang, K.R., Bookbinder, J., Golub, L., Davis, M.M.: 1983, *Astrophys. J. Letters* **272**, L15
- Lang, K.R., Willson, R.F.: 1986a, *Astrophys. J. Letters* **302**, L17
- Lang, K.R., Willson, R.F.: 1986b, *Astrophys. J.* **305**, 363
- Lang, K.R., Willson, R.F.: 1987, *Astrophys. J.*
- Linsky, J.L., Gary, D.E.: 1983, *Astrophys. J.* **274**, 776
- Pallavicini, R., Golub, L., Rosner, R., Vaina, G.S., Ayres, T., Linsky, J.L.: 1981, *Astrophys. J.* **248**, 279
- Pallavicini, R., Willson, R.F., Lang K.R.: 1985, *Astron. Astrophys.* **149**, 95
- Saar, S.H., Linsky, J.L.: 1985, *Astrophys. J. Letters* **299**, L47
- Saar, S.H., Linsky, J.L., and Beckers, J.M.: 1986, *Astrophys. J.* **302**, 777
- Swank, J.H., White, N.E., Holt, S.S., Becker, R.H.: 1981, *Astrophys. J.* **246**, 208
- Swank, J.H., Johnson, H.M.: 1982, *Astrophys. J. Letters* **259**, L67
- Topka, K., Marsh, K.A.: 1982, *Astrophys. J.* **254**, 641
- Vaiana, G.S. et al.: 1981, *Astrophys. J.* **244**, 163
- White, S., Kundu, M.R., Jackson, J.: 1986, *Astrophys. J.* **311**, 814
- Willson, R.F., Lang, K.R.: 1986, *Simultaneous IUE and VLA Observations of Flare Stars, New Insights in Astrophysics: Eight Years of Observations with IUE*
- Zheleznyakov, V.U., Tikhomorov, Yu. V.: 1984, *Astrophys. Space Sci.* **102**, 189

34. High-resolution VLA maps of the quiescent corona at 90 cm wavelength

K. R. Lang^{2,*}, R. F. Willson¹, and G. Trottet²¹ Department of Physics and Astronomy, Tufts University, Medford, MA 02155, USA² Observatoire de Paris, Section d'Astrophysique de Meudon UA 324, F-92195 Meudon Principal Cedex, France

Received June 15, 1987; accepted February 25, 1988

Summary. We present the first Very Large Array (VLA) synthesis maps of the quiescent corona at 90 cm wavelength and compare them with optical solar features. When the quiet Sun is observed at 90 cm with moderate angular resolution of 100" to 200", structures are observed with angular extents, θ , of $\theta = 3'$ to $10'$ and brightness temperatures, T_B , of $T_B = 0.5$ to $5.7 \cdot 10^5$ K. Some of these structures are relatively stable over a two-day interval, with positions shifted westward by the amount expected from solar rotation; while others disappear or evolve during this interval. These intense, quiescent 90 cm sources are not associated with active regions; in contrast, simultaneous 20 cm observations reveal coronal loops that are associated with active regions. When the quiet Sun is observed with the VLA at 90 cm wavelength at high angular resolution of 15" to 30", compact components are detected with $\theta = 50''$ to $200''$ and $T_B = 2.1$ to $4.0 \cdot 10^5$ K. There is no systematic association of any of the 90 cm sources with any optical counterpart, including active regions, filaments, sunspots and the magnetic neutral line in the underlying photosphere. There is no intense 90 cm radiation in the polar regions where $T_B \leq 0.5 \cdot 10^5$ K, and this apparent depression is at least partly due to coronal holes. We confirm previous meter-wavelength results that indicate that noise storms are the only sources, other than flares, associated with active regions.

Key words: Sun: atmosphere – Sun: corona – Sun: coronal holes – Sun: coronal loops – Sun: magnetic field – Sun: noise storms – Sun: radio radiation

1. Introduction

The radio emission of the quiescent, or non-flaring, corona is dominated by different structures at different wavelengths. The most intense quiescent radiation at 20 cm wavelength is due to a hot, dense plasma trapped within relatively compact coronal loops associated with individual active regions (Kundu and Lang, 1985; Lang et al., 1987a, b). In contrast, the most intense emission of the quiescent corona at meter wavelengths (80 and 160 MHz) is not associated with active regions or with bright regions in the centimeter maps (Sheridan and McLean, 1985). This emission

might be associated with relatively large coronal loops or with extended magnetic structures such as coronal streamers.

This paper presents the first VLA images of the quiescent corona at 90 cm wavelength. It therefore refers to a spectral region located between the shorter 20 cm region and the longer meter wavelength one. Our 90 cm observations are presented in Sect. 2, where they are also compared with optical features. Our conclusions are summarized in Sect. 3.

2. Observations

The half-power beamwidth of the VLA's 25-meter telescopes is 32' at 20 cm wavelength, and this is just equal to the angular extent of the Sun at mean Earth distance. So, the entire solar disk can be imaged at either 20 cm or 90 cm, but with a varying degree of completeness that depends on the array configuration. That is, the 27 individual telescopes can be moved in and out along the Y-shaped arms of the array, creating a radio zoom lens that provides higher angular resolution at the expense of more incomplete information on larger angular structures. For example, the synthesized half-power beamwidth, θ , at 20 cm is $\theta \approx 1'', 4'', 13''$ and $44''$ for the A, B, C and D configurations, respectively, while the corresponding values at 90 cm are $\theta \approx 5'', 18'', 60''$ and $200''$.

The VLA was used to observe the Sun in the C-D hybrid configuration between 2013 UT on 20 February 1987 and 0015 UT on 21 February 1987 and between 1905 UT on 22 February 1987 and 0020 UT on 23 February 1987. The array was divided into two subarrays with 15 antennas operating at 90 cm wavelength (333 MHz) with 3.125 MHz bandwidth and 12 antennas operating at 20.7 cm wavelength (1446 MHz) with 12.5 MHz bandwidth. The beamwidth of the individual antennae was 138' at 90 cm and 32' at 20.7 cm.

All four Stokes parameters were sampled every 6.67 s, and the data were calibrated by observing 3C 48 for five minutes every 70 min. The flux density of 3C 48 was assumed to be 47.0 Jy and 14.6 Jy at 90 cm and 20.7 cm respectively.

In order to construct reliable 90 cm synthesis maps, we had to delete data from the shortest baselines at the end of the day. These data, which corresponded to fringe spacings of 36' and 48', were omitted because the large correlated flux exceeded the dynamic range of the correlators. There were no such problems at the beginning of our observations because the projected baselines were longer with correspondingly smaller fringe spacings and correlated fluxes. Shadowing of the antennae at the end of the day

Send offprint requests to: K. R. Lang

* Currently on sabbatical leave at the Observatoire de Paris, Meudon

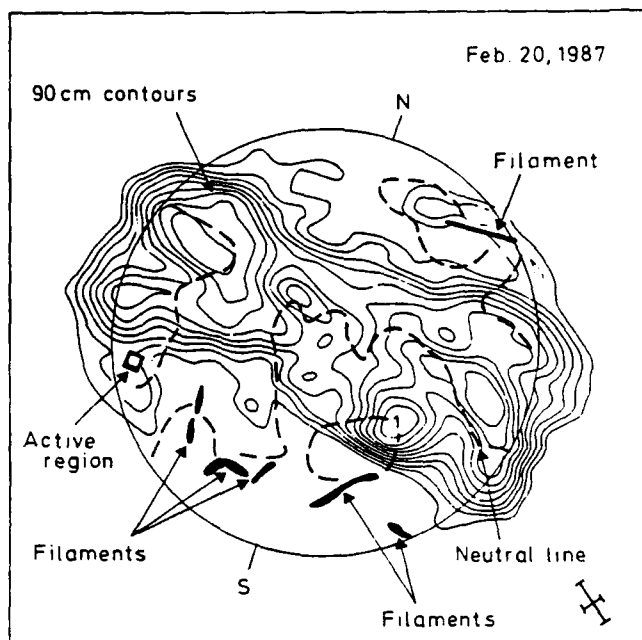


Fig. 1. Four-hour VLA synthesis map of the Sun at 90 cm wavelength on 20 February 1987 is compared with optical solar features including active regions (squares), filaments (solid lines) and the magnetic neutral line (dashed line). The most intense 90 cm emission is not systematically associated with any optical counterpart. There is no intense 90 cm radiation in the polar regions, and this is at least partly due to polar coronal holes. The array was in the C-D hybrid configuration with a synthesized beamwidth denoted by the crosses. The contours mark levels of equal brightness temperature, T_B , with an outermost contour of $T_B = 5.5 \times 10^4$ K, a contour interval of 5.5×10^4 K, and a peak brightness temperature of $T_B = 5.7 \times 10^5$ K. All of the sources are positive and all of the optical data have been extracted from Solar Geophysical Data (1987).

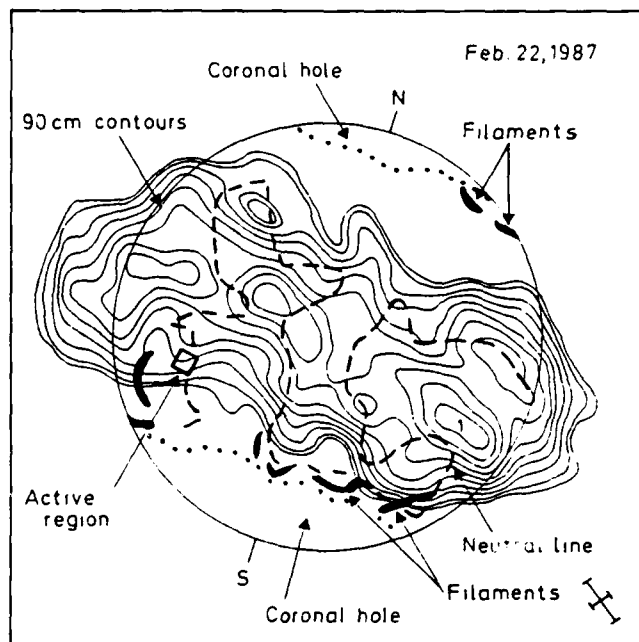


Fig. 2. Four-hour VLA synthesis map of the Sun at 90 cm wavelength on 22 February 1987 is compared with optical solar features including active regions (squares), coronal hole boundaries (dotted lines), filaments (solid lines) and the magnetic neutral line (dashed line). The most intense 90 cm emission is not systematically associated with any optical counterpart. There is no intense 90 cm radiation in the polar regions, and this is at least partly due to polar coronal holes. The array was in the C-D hybrid configuration with a synthesized beamwidth denoted by the crosses. The contours mark levels of equal brightness temperatures, T_B , with an outermost contour of $T_B = 5.5 \times 10^4$ K, a contour interval of 5.5×10^4 K, and a peak brightness temperature of $T_B = 5.5 \times 10^5$ K. All of the sources are positive, all of the optical data have been extracted from Solar Geophysical Data (1987) and the coronal hole boundaries have been inferred from the He 10830 map supplied by Jack Harvey.

can also produce erroneous fringe amplitude changes and incorrect images.

The calibrated and edited data were used together with the standard CLEAN procedure to produce the synthesis maps shown in Figs. 1 and 2. Each map refers to 4 h of observation with a synthesized beamwidth of $113'' \times 237''$. All of the sources shown in each cleaned map were also present in the dirty map, so the cleaning procedure did not introduce any artifacts. The level of negative residuals was 15 to 20% of the dirty map maximum.

The most intense 20 cm emission on both days was associated with an active region with strong photospheric magnetic fields. We attribute this emission to the coronal loops that have been previously detected in the low corona at 20 cm and soft X-ray wavelengths. The association of intense 20 cm emission with coronal loops in active regions has now been documented by numerous VLA observations (see Lang et al., 1987a, b and references within it), so we do not give our 20 cm maps here.

In contrast to the 20 cm coronal loops, the most intense 90 cm radiation of the quiescent, or non-flaring, corona (see Figs. 1 and 2) is not related to active regions. The 90 cm sources are concentrated near the equatorial regions and provide a distinctly inhomogeneous component to the quiescent corona. The 90 cm structures have brightness temperatures, T_B , of $T_B = 0.5$ to 5.7×10^5 K, which are slightly less than those of the 20 cm coronal

loops, but that are comparable to the brightness temperature $T_B \approx 6 \times 10^5$ K of the entire quiet Sun (Sheridan and McLean, 1985).

In several cases, the 90 cm sources shown in Figs. 1 and 2 remain, within the uncertainty of measurements, at the longitudes expected from solar rotation (see source 1), but some of the latitudes also apparently change and some sources have disappeared, changed shape or emerged during the two-day interval. These results suggest that the large-scale structures detected at 90 cm wavelength are both inhomogeneous and variable on time scales of a few days.

Assuming an angular radius $\theta \approx 4'$ and a brightness temperature of $T_B \approx 5 \times 10^5$ K, we can use the Rayleigh-Jeans law to show that the flux density, S , in a typical intense 90 cm source is $S \approx 1$ s.f.u., where 1 s.f.u. = 10^4 Jy (see Lang, 1980). But there are at least five such sources, so their combined flux density is 5 s.f.u., or roughly half the 10 s.f.u. flux density of the quiet Sun at this wavelength (Sheridan and McLean, 1985). Thus, as much as half the total flux density of the quiescent corona at 90 cm wavelength may be emitted from undetected structures. This essentially follows from the fact that the intense 90 cm sources have a brightness temperature comparable to the entire quiet Sun at this wavelength, so if they occupy roughly half the surface area of the Sun they account for roughly half the total flux density.

A comparison of the 90 cm sources with optical features (Figs. 1, 2) indicates that the intense, quiescent 90 cm emission is not systematically associated with any optical counterpart, at least for our observations. Although the north-west filament on 20 February 1987 is apparently associated with an extended 90 cm source, the other filaments on this day and on 22 February are not associated with detectable 90 cm emission. All of the 90 cm sources on these days are concentrated within equatorial regions away from active regions and sunspots. There is a noticeable depression, or lack of intense 90 cm emission, at the poles, and this is at least partly due to polar coronal holes.

Some of the extended 90 cm sources lie on or near the neutral line, but other sources do not. Moreover, some minima in brightness temperature also lie on or near that line, and the 90 cm emission certainly does not trace out all of the neutral line. So, relations with that line may be due to chance, and there is no systematic association with it.

When the VLA zeroes in for a closer look, the 90 cm structures are resolved into compact components. For example, the VLA was used to observe the Sun in the B configuration between 1545 UT and 2230 UT on 23 August 1986. An array of 13 antennas operating at 90 cm wavelength with a bandwidth of 3.125 MHz was used to produce the synthesis map shown in Fig. 3. In this case, the data were calibrated by observing 3C 286 (90 cm flux 29.0 Jy) for 5 min every 40 min, and the synthesized beamwidth was $16'' \times 29''$.

Components with angular dimensions, θ , of $\theta \approx 50''$ to $200''$ and brightness temperatures, T_B , of $T_B = 2.1$ to 4.0×10^5 K were detected. As indicated in Fig. 3, these sources are not directly related to the active regions that would have been detected if we had simultaneous VLA observations at 20 cm wavelength.

The only possible optical counterpart of the intense compact 90 cm sources is the inversion line (magnetic neutral line) of the photospheric magnetic field, but these sources do not trace out the full magnetic neutral line. If the quiescent 90 cm sources are related to the magnetic neutral line, some additional factor is causing them to be concentrated over only small parts of it. This factor is apparently unrelated to H α filaments: an examination of Meudon data (DASOP) indicated no detectable H α filament or plage at the latitudes of the enhanced 90 cm emission, either on the day of observation or on three rotations before or after that day.

There is, however, one source of 90 cm radiation that is associated with active regions: it is the ubiquitous noise storms. This nonthermal radiation is the most common type of activity observed on the Sun at decimetric and metric wavelengths. The noise storms might be confused with quiescent radiation because of their long durations (hours to days); but they are actually sources of continued activity, apparently located in large magnetic arches that connect active regions with their surroundings (Mercier et al., 1984). Metric wavelength observations of noise storms provided some of the first evidence for stable magnetic connections between solar active regions and more distant areas on the Sun (Lantos-Jarry, 1970; Daigne et al., 1971).

When the VLA is used to resolve a noise storm at 90 cm wavelength, it is indeed found near the apex of large-scale magnetic loops that apparently connect two active regions (Lang and Willson, 1987). Intense radiation at 183 cm wavelength is also associated with this loop system (see Fig. 4). This radiation could be due to low-level noise storm activity, for such noise storm continua are an important source of slowly varying radiation at 183 cm wavelength (Alissandrakis et al., 1985; Lantos et al., 1987). Other extended quiescent coronal features at 183 cm, such as the one observed on the center of the map shown in Fig. 4, resemble those

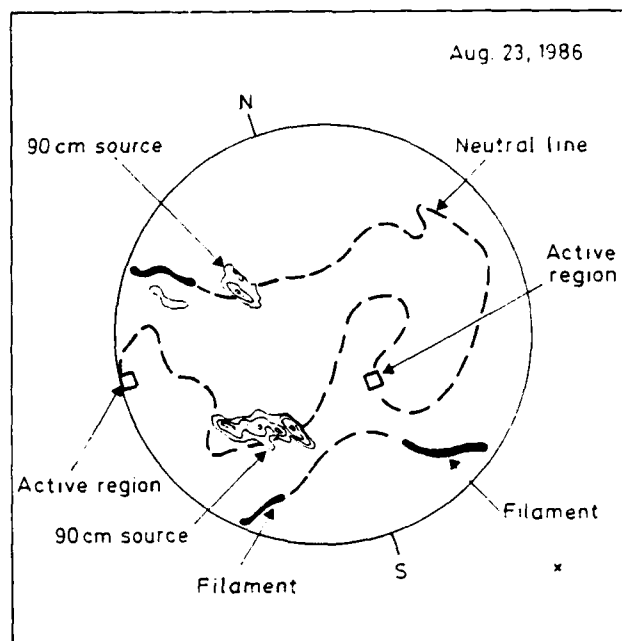


Fig. 3. A VLA synthesis map at 90 cm wavelength during a 6^h45 min. period on 23 August 1986 is compared with optical solar features including active regions (squares), filaments (solid lines) and the probable magnetic neutral line (dashed line). At least three compact 90 cm sources have been detected with angular dimensions of $50'' \times 200''$. Here the 90 cm contours mark levels of equal brightness temperature, T_B , with an outermost contour of $T_B = 2.1 \times 10^5$ K, a contour interval of 4.1×10^4 K and a peak brightness temperature of $T_B = 4.0 \times 10^5$ K. The VLA was in the B configuration with a $16'' \times 29''$ synthesized beamwidth denoted by the small solid cross in the lower right corner. All of the optical data have been extracted from Solar Geophysical Data (1986).

found at 90 cm with the VLA, with no apparent correlation with any optical counterpart and comparable brightness temperatures.

Our results are in accord with previous observations which showed that intense quiescent emission at meter wavelengths (80 and 169 MHz) is not associated with active regions (Axisa et al., 1971; Sheridan and McLean, 1985). A statistical study of numerous one-dimensional Nançay scans at 169 MHz indicated, however, that the longitudes of many quiescent sources are associated with filament corridors as seen on H α synoptic maps and not on daily maps (Axisa et al., 1971). In contrast, fewer two-dimensional maps at the same frequency show a poor apparent association with filaments and a possible association with the magnetic neutral line in the underlying photosphere (Alissandrakis et al., 1985; Lantos et al., 1987). Our observations do not confirm either result, indicating no systematic association with any optical counterpart; but we can not rule out such associations, particularly during different parts of the solar cycle.

Correlations of radio sources with optical counterparts are confused by nonradial divergence, refraction effects and solar tilt. There are additional uncertainties due to random correlations with the long magnetic neutral line; its placement on the solar surface differs by several degrees depending on the technique used. A deeper understanding of the quiescent coronal sources is likely to come from multiple-wavelength observations in the radio part of the electromagnetic spectrum.

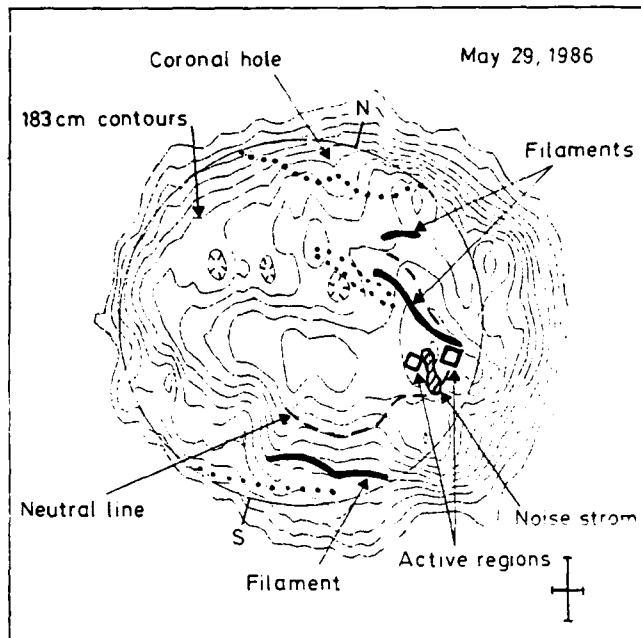


Fig. 4. A Nançay Radioheliograph synthesis map at 183 cm wavelength during an 8 h period is compared with a 90 cm noise storm (VLA-hatched area) and various optical solar features including active regions (squares), coronal hole boundaries (dotted lines), filaments (solid lines) and the magnetic neutral line (dashed line). The 90 cm noise storm emission apparently comes from large-scale magnetic loops that connect active regions, and the apex of these loops is probably associated with a maximum in the intensity of the 183 cm radiation. Here the 183 cm contours mark levels of equal brightness temperature, T_B , with an outermost contour of $T_B = 2.0 \cdot 10^5$ K, a contour interval of $5.0 \cdot 10^4$ K and a peak brightness temperature of $7.5 \cdot 10^5$ K. A detailed understanding of these sources will require greater angular resolution and spectral information. The 1.2×4.5 synthesized beamwidth is denoted by crosses in the lower right corner, and all of the optical data have been extracted from Solar Geophysical Data (1986).

3. Conclusions

The quiescent corona at 90 cm wavelength is very inhomogeneous and variable, with the most intense emission concentrated within structures near the equatorial regions. This emission may be the thermal bremsstrahlung of a coronal plasma that might be confined in large-scale magnetic structures. The 90 cm sources are not systematically associated with any optical counterpart including active regions, filaments, sunspots and the magnetic neutral

line, at least for the observations presented here. There is no intense 90 cm radiation in the polar regions, and this is at least partly due to coronal holes. More compact 90 cm sources in the quiescent corona also show no systematic correlation with optical counterparts. Associations with the magnetic neutral line are uncertain, and future multiple-wavelength radio observations might provide new insights to the paradoxical quiescent coronal structures.

Acknowledgements. Radio astronomical studies of the Sun at Tufts University are supported under grant AFOSR-83-0019 with the Air Force Office of Scientific Research and contract N00014-86-K-0068 with the Office of Naval Research. Collaborative long-wavelength solar observations by Tufts University and the Observatoire de Paris are supported by National Science Foundation grant INT-8602285 and Centre National de la Recherche Scientifique grant 920038. The Very Large Array is operated by Associated Universities Inc., under contract with the National Science Foundation. We thank C.E. Alissandrakis, K.-L. Klein, P. Lantos, C. Mercier and M. Pick for useful discussions.

References

- Alissandrakis, C.E., Lantos, P., Nicolaidis, E.: 1985, *Solar Phys.* **97**, 267
- Axisa, F., Avignon, Y., Martres, M.J., Pick, M., Simon, P.: 1971, *Solar Phys.* **19**, 110
- Daigne, G., Lantos-Jarry, M.F., Pick, M.: 1971, in *Solar Magnetic Fields*, ed. Howard, p. 609
- Kundu, M.R., Lang, K.R.: 1985, *Science* **228**, 9
- Lang, K.R.: 1980, in *Astrophysical Formulae*, 2nd ed., New York, Springer-Verlag, p. 23
- Lang, K.R., Willson, R.F.: 1987, *Astrophys. J.* **319**, 514
- Lang, K.R., Willson, R.F., Smith, K.L., Strong, K.T.: 1987a, b, *Astrophys. J.* **322**, 1035, 1044
- Lantos, P., Alissandrakis, C.E., Gergely, T., Kundu, M.R.: 1987, *Solar Phys.* **112**, 325
- Lantos-Jarry, M.F.: 1970, *Solar Phys.* **15**, 40
- Mercier, C., Elgaroy, O., Tlamicha, A., Zlobek, P.: 1984, *Solar Phys.* **92**, 375
- Saito, K.: 1970, *Ann. Tokyo Astron. Obs. Ser.* **2**, **12**, 53
- Sheridan, K.V., Labrum, N.R., Payten, W.J., Nelson, G.J., Hill, E.R.: 1983, *Solar Phys.* **83**, 167
- Sheridan, K.V., McLean, D.J.: 1985, in *The Quiet Sun at Metre Wavelengths*, *Solar Radiophysics*, eds. D.J. McLean, N.R. Labrum, New York, Cambridge University Press, p. 443
- Solar Geophysical Data: 1986, 1987, Part 1, No 503, p. 53, No 506, p. 47, No 512, p. 50, 52

35. NARROW-BAND, SLOWLY VARYING DECIMETRIC RADIATION FROM THE DWARF M FLARE STAR YZ CANIS MINORIS. II.

KENNETH R. LANG AND ROBERT F. WILLSON

Department of Physics and Astronomy, Tufts University

Received 1987 May 29; accepted 1987 August 21

ABSTRACT

The Very Large Array has been used in the spectral-line mode to obtain the frequency spectra of the radiation from the dwarf M star YZ Canis Minoris at frequencies, ν , near 1465 MHz. The slowly varying (minutes) radiation was, within the observational uncertainties, 100% left-hand circularly polarized. The radiation during several 10 minute intervals exhibited evidence for narrow-band structure with a bandwidth $\Delta\nu \approx 30$ MHz and a fractional bandwidth of $\Delta\nu/\nu \approx 0.02$. Broad-band radiation with $\Delta\nu \geq 50$ MHz and $\Delta\nu/\nu \geq 0.03$ was observed during other 10 minute intervals. The highly polarized, slowly varying, narrow-band emission is attributed to coherent radiation from an electron-cyclotron maser in a magnetic field of strength $H \approx 260$ G. If this radiation is from coronal loops similar to those observed on the Sun, then a source size of $L_s \approx 2 \times 10^7$ cm and brightness temperature $T_b \approx 0.5 \times 10^{17}$ K are inferred for the narrow-band source. The observed broad-band radiation may be due to the superposition of many rapid, narrow-band bursts with different central frequencies. The fact that the observed narrow-band radiation persists for 10 minutes indicates that there was no substantial change in the source height, size, magnetic field strength, or electron density during this time. The "quiescent" microwave radiation of some dwarf M stars might be due to the superposition of nearly continuous, low-level coherent bursts; this activity might play a role in the heating of stellar coronae.

Subject headings: radiation mechanisms — stars: flare — stars: individual (YZ CMi) — stars radio radiation

I. INTRODUCTION

Radio and microwave bursts from dwarf M stars have been attributed to coherent radiation mechanisms. High brightness temperatures of $T_b \geq 10^{12}$ – 10^{15} K were, for example, inferred from the flux densities of rare, powerful bursts under the assumption that the radio emitter was smaller than the stellar disk; coherent processes are required to explain these high brightness temperatures (see Lang and Willson 1986a for a review). Observations with high time resolution indicated that the 20 cm bursts from one dwarf M star, AD Leonis, had rise times of milliseconds, relatively small sizes $L \leq 10^8$ cm, and high brightness temperatures $T_b \geq 10^{16}$ K (Lang *et al.* 1983; Lang and Willson 1986a). These bursts were up to 100% circularly polarized, suggesting an intimate connection with the star's magnetic fields.

Lang and Willson (1986b) first provided evidence for the narrow-band frequency structure expected from a coherent radiation process. They showed that the variation in the radiation from the dwarf M star YZ Canis Minoris had a bandwidth $\Delta\nu \leq 100$ MHz. This was because there was no correlation between the variations detected at 1415 and 1515 MHz.

This two-frequency experiment was repeated with similar results for the dwarf M stars AD Leonis and L726-8A (White, Kundu, and Jackson 1986). A 2 hr variation in the radiation from AD Leonis was observed at 1415 MHz but did not appear at 1515 MHz. The flux and evolution of a flare from L726-8A differed at the two frequencies.

Intensity was plotted as a function of both time and frequency (dynamic spectra) for radiation from the dwarf M star UV Ceti (L726-8B) near 1415 MHz (Bastian and Bookbinder 1987). One left circularly polarized burst showed no variation as a function of frequency across the 41 MHz band, but

another right circularly polarized burst exhibited complex frequency structure with narrow-band components whose fractional bandwidths were as small as the frequency resolution (bandwidth $\Delta\nu \leq 3$ MHz and $\Delta\nu/\nu \leq 0.002$). Jackson, Kundu, and White (1987) similarly produced dynamic spectra for UV Ceti by observing four frequencies simultaneously. Although the bandwidths were not measured, the dynamic spectrum of one 10 minute burst suggested complex frequency-time structure with both positive and negative frequency drifts. The features that showed a positive drift were interpreted in terms of disturbances traveling downward in the star's corona where they excite radiation at higher frequencies or shorter wavelengths.

In this paper we report measurements of the frequency spectra of YZ Canis Minoris using 15 continuous 3.125 MHz bands. In § II we present observations of frequency structure with narrow bandwidths $\Delta\nu \approx 30$ MHz that persist over 10 minutes of time without evidence for a drift. The fractional bandwidth $\Delta\nu/\nu \approx 0.02$. Here we also show that radiation over other 10 minute intervals appears to be broad band with $\Delta\nu \geq 50$ MHz, but these spectra could represent the time average of many rapid, narrow-band events. In § III we interpret the narrow-band, 30 MHz structure in terms of electron-cyclotron maser emission. Here we also draw attention to certain solar bursts that may require a similar coherent radiation mechanism. We conclude by mentioning the implications of continued coherent burst activity for the heating of stellar coronae.

II. OBSERVATIONS

The dwarf M star YZ Canis Minoris (GL 285, dM4.5e) was observed with the Very Large Array (VLA) between 08:10 and 12:22 UT on 1987 January 6 in the C-configuration. The VLA

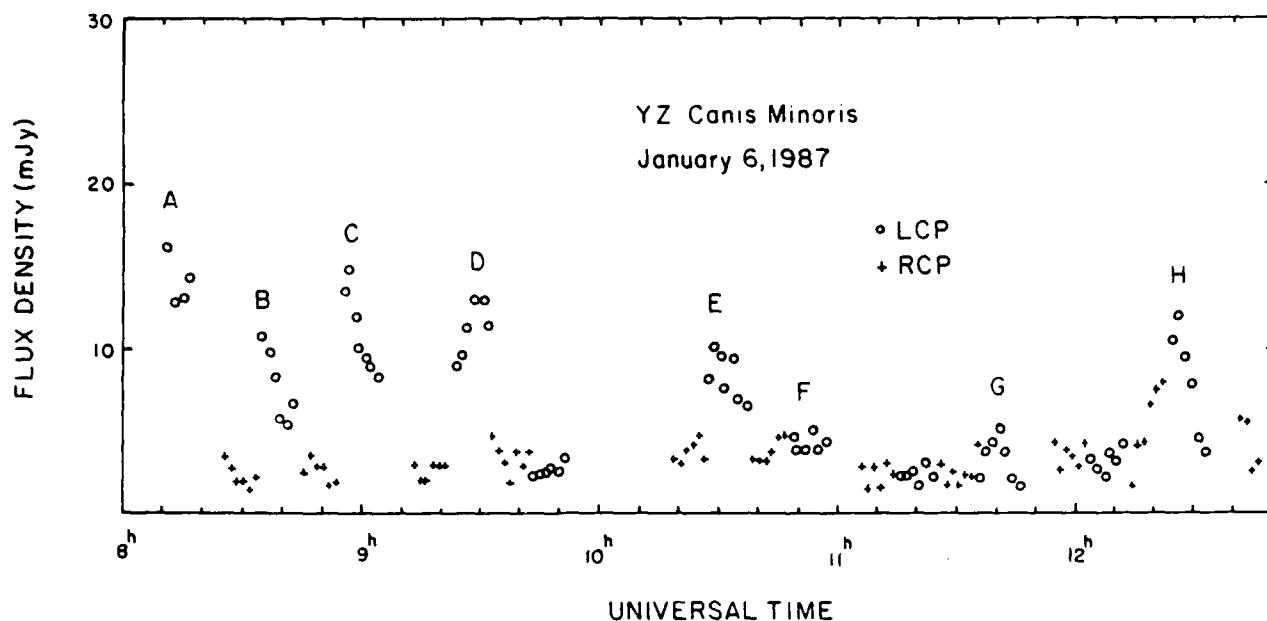


FIG. 1.—The total intensity of the radiation received from the dwarf M flare star YZ Canis Minoris is plotted as a function of time. The left circularly polarized (LCP) and right circularly polarized (RCP) signals were alternately recorded for 10 minute intervals within a 50 MHz bandwidth centered at 1464.9 MHz. Here the visibility data of all baselines from the 15 independent channels has been averaged over a 1.5 minute time interval with a 3σ noise level of 2.9 mJy. Frequency spectra of the slowly varying LCP radiation marked by the letters A, B, C, ..., H are shown in Figs. 2 and 3.

was used in the 16-channel spectral line mode centered at 1464.9 MHz. At this frequency, the half-power beamwidth of the antennas is $\sim 31'$ and the synthesized beamwidth is $\sim 13'' \times 22''$. The 50 MHz bandwidth was divided into 15 continuous channels of 3.125 MHz width; the 16th channel was used to record the integral flux over the inner 37.5 MHz of the bandwidth. The full array of 26 antennas was used to sample the signal intensity every 10 s, and the left circularly polarized (LCP) and right circularly polarized (RCP) signals were observed for alternate 10 minute intervals. A bandpass calibration for each of the 16 channels was applied to the visibilities during the observations. The phase data were calibrated by observing PKS 0735+178 for a 3 minute interval every 40 minutes, and the flux density calibration was made from observations of 3C 286 whose flux density is 14.7 Jy at 1465 MHz ($1 \text{ Jy} = 10^{-23} \text{ ergs cm}^{-2} \text{ s}^{-1} \text{ Hz}^{-1}$).

The raw visibilities were first examined, baseline-by-baseline and channel-by-channel for interference or other corrupted data, and then edited. The calibrated visibility data for the 16 channels were then averaged, baseline-by-baseline, with running means over 1.5 minutes and then vector-averaged. A synthesis map was then made for each 1.5 minute time interval using the standard CLEAN procedure.

The source flux densities were determined from these maps and plotted as a function of time in Figure 1. Here the flux density scale is in mJy, 10^{-3} Jy , and the 3σ noise level is 2.9 mJy. The observed radiation was 100% left-hand circularly polarized, within an observational uncertainty of about 10%. The highly polarized radiation also exhibited variations on time scales of minutes; these variations are relatively slow when compared with those of more impulsive stellar bursts (milliseconds to seconds).

The 10 s visibility data observed within each 3.125 MHz

channel was then averaged, baseline-by-baseline, with running means over 10 minutes and then vector-averaged. A synthesis map was then made for each of the 15 channels using the standard CLEAN procedure. The flux densities determined from these maps are plotted as a function of observing frequency in Figures 2 and 3. Several of these 10 minute spectra provide evidence for narrow-band radiation with a bandwidth $\Delta\nu \approx 30 \text{ MHz}$ near a central frequency $\nu = 1465 \text{ MHz}$, or $\Delta\nu/\nu \approx 0.02$. Other spectra have broad bandwidths $\Delta\nu \geq 50 \text{ MHz}$, or $\Delta\nu/\nu \geq 0.03$.

III. DISCUSSION

The highly polarized emission may be attributed to coherent radiation from an electron-cyclotron maser. The maser will radiate at harmonics, n , of the gyrofrequency $\nu_H = 2.8 \times 10^6 H \text{ Hz}$, where H is the magnetic field strength. Although the first harmonic may be absorbed in overlying atmospheric layers, the second harmonic can escape with up to 100% circular polarization (Melrose and Dulk 1982). For $n = 2$ and our observing frequency of $\nu = n\nu_H = 1.465 \times 10^9 \text{ Hz}$, the required magnetic field strength is $H \approx 260 \text{ G}$.

The electron-cyclotron maser emission is confined to a thin cone at large angles $\theta_0 = 70^\circ$ to 85° with respect to the magnetic field. A narrow relative bandwidth of $\Delta\nu/\nu \approx \cos^2 \theta_0 \approx 0.01$ to 0.10 is expected.

The observed bandwidth will depend on the gradient of the magnetic field and the size of the source. A sharper field gradient will produce a wider range of gyrofrequencies and a broader bandwidth, while a smaller source size will limit the magnetic field variation and produce a narrower bandwidth.

If the emission is confined to magnetic loops like those on the Sun, then the magnetic scale height $L_H \approx 10^9 \text{ cm}$. Such a scale height is plausible for coronal loops on YZ Canis Minoris

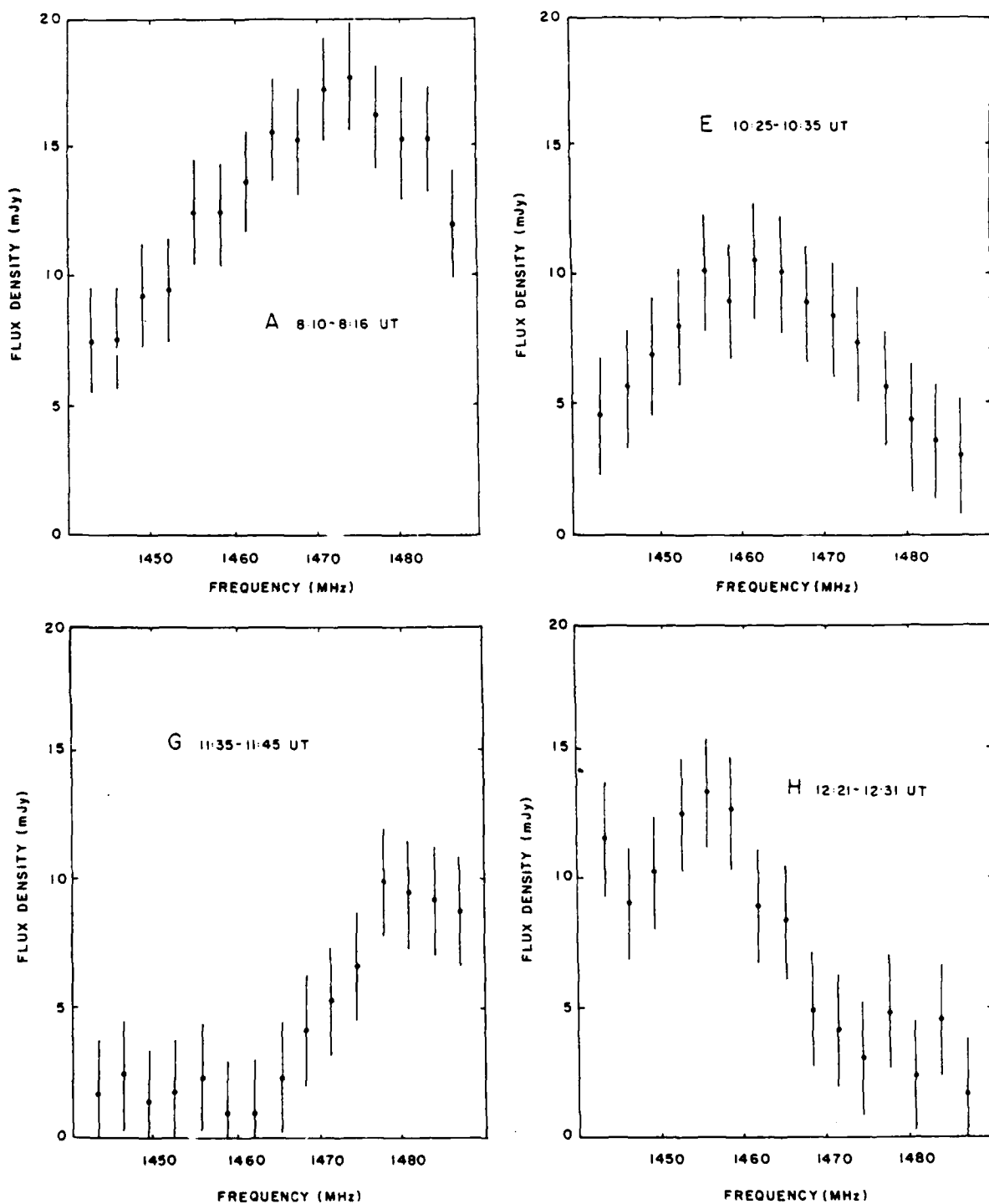


FIG. 2.—Frequency spectra of the left circularly polarized radiation from YZ Canis Minoris for the intervals marked A, E, G, and H in Fig. 1. Here we have plotted the total intensity received in 15 contiguous channels, each 3.125 MHz wide, during the time interval denoted on each plot. The observed value is plotted as a small circle with two vertical bars, each denoting the 3σ noise level for the relevant time interval and bandwidth. These spectra have been grouped together because they all show evidence for narrow-band radiation with a bandwidth $\Delta\nu \approx 30$ MHz near a central frequency $\nu = 1465$ MHz, or $\Delta\nu/\nu \approx 0.02$.

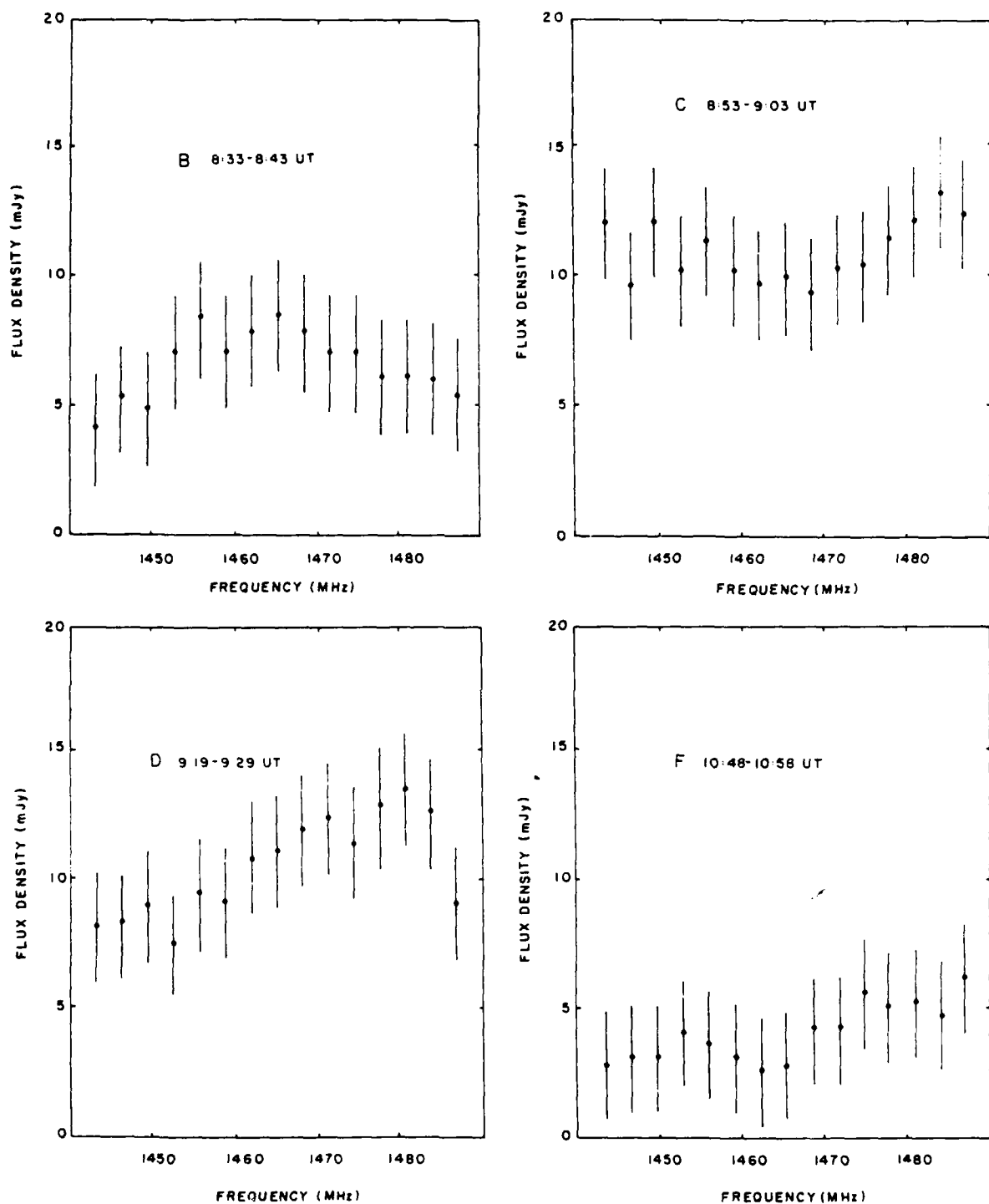


FIG. 3.—Frequency spectra of the left circularly polarized radiation from YZ Canis Minoris for the intervals marked B, C, D, and F in Fig. 1. Here we have plotted the total intensity received in 15 contiguous channels, each 3.125 MHz wide, during the time interval denoted on each plot. The observed value is plotted as a small circle with two vertical bars, each denoting the 3σ noise level for the relevant time interval and bandwidth. These spectra have been grouped together because they all show evidence for broad-band radiation with a bandwidth $\Delta\nu \geq 50$ MHz near a central frequency $\nu = 1465$ MHz, or $\Delta\nu/\nu \geq 0.03$.

whose radius $R \approx 2.6 \times 10^{10}$ cm (Pettersen 1980). The size, L_s , of the masing source with a 30 MHz bandwidth is then given by

$$L_s = L_H \frac{\Delta\nu}{\nu} \approx 2 \times 10^7 \text{ cm}, \quad (1)$$

and its brightness temperature, T_B , is

$$T_B \approx 10^{13} \frac{SD^2}{\nu^2 L_s^2} \approx 0.5 \times 10^{17} \text{ K}, \quad (2)$$

where the flux density $S = 0.015$ Jy, the star's distance $D = 1.8 \times 10^{19}$ cm, our observing frequency $\nu = 1.465 \times 10^9$ Hz, and $L_s = 2 \times 10^7$ cm. Melrose and Dulk (1982) have shown that an electron-cyclotron maser can produce similar brightness temperatures of $T_B = 10^{16}$ to 10^{17} K.

Of course, the broad-band radiation from YZ Canis Minoris can also be attributed to coherent radiation from an electron-cyclotron maser. The 10 minute spectra may have averaged over several narrow-band bursts of short duration and different central frequencies, thereby producing broad-band spectra. In fact, microwave spikes emitted during solar burst have short durations of $\tau_D \leq 10$ ms, high brightness temperatures of $T_B \geq 10^{12}$ K, and relative bandwidths of $\Delta\nu/\nu \approx 0.015$ (Benz 1985), and these spike bursts have been attributed to electron-cyclotron maser emission (Holman, Eichler, and Kundu 1980). Decimetric bursts from the dwarf M star AD Leonis are also composed of millisecond spikes with rise times of $\tau_R \leq 5$ ms and durations of $\tau_D \leq 10$ ms (Lang and Willson 1986a). Such spikes would not be resolved with the 10 s integration time at the VLA.

In fact, the interesting aspect of the narrow-band radiation from YZ Canis Minoris is that it persists for 10 minutes with a well-defined bandwidth and central frequency. If this radiation is composed of bursts with shorter duration, they have to be coming from a region in which there is no substantial change of physical parameters such as height, size, magnetic field strength, and electron density. A substantial change in height, size, or magnetic field strength would produce a drift in the central frequency which is not observed. If there is any drift it has to be slower than 0.05 MHz s^{-1} . A substantial increase in the electron density above $N_e \approx 6 \times 10^9 \text{ cm}^{-3}$ would make the

plasma frequency ν_p exceed the gyrofrequency, and plasma radiation would dominate the emission.

As discussed by Lang and Willson (1986a, b) and by Bastian and Bookbinder (1987), an alternative coherent process might be plasma radiation. Solar type II, III, and IV bursts as well as weaker narrow-band decimetric bursts or blips with $\Delta\nu/\nu \leq 0.1$ have been attributed to plasma radiation (Furst, Benz, and Hirth 1982; Benz, Bernold, and Dennis 1983). As pointed out by Bastian and Bookbinder (1987) one difficulty with this interpretation is that plasma radiation tends to rapidly drift toward lower frequencies as the disturbance travels outward into the lower density corona. The drift rate, $\Delta\nu/\Delta t \approx 0.5 U_b \nu/H_g$, where U_b is the velocity of the disturbance and H_g is the scale height. For $H_g \approx 10^{10}$ cm, $\nu = 1465$ MHz, and $\Delta\nu/\Delta t < 0.5 \text{ MHz s}^{-1}$, we require that $U_b < 7 \text{ km s}^{-1}$, or about 30–200 times slower than the speeds observed in moving type IV bursts (Robinson 1978). For higher speeds, the frequency drift rate is correspondingly higher and would give rise to an apparently broad-band spectrum.

Finally, we also note that YZ Canis Minoris appears to undergo nearly continuous coherent burst activity for periods as long as 4 hr (see Fig. 1). The "quiescent" microwave emission of some dwarf M stars might therefore be due to the superposition of many low-level coherent bursts. Similar continued low-level variability has been reported for the X-ray emission from dwarf M stars (Butler *et al.* 1986; Ambruster, Sciortino, and Golub 1987). The continued variability might well be related to emerging magnetic flux that plays a role in heating the stellar coronae. It is interesting to note that Melrose and Dulk (1982) have shown that cyclotron maser emission at the second harmonic may heat the overlying coronal plasma to $T_e \approx 3 \times 10^7$ K, thereby giving rise to X-ray bursts.

Radio astronomical studies of the Sun and other nearby active stars at Tufts University are supported under grant AFOSR-83-0019 with the Air Force Office of Scientific Research. Related solar observations are supported by contract N00014-86-K-0068 with the Office of Naval Research (ONR). The Very Large Array is operated by Associated Universities, Inc., under contract with the National Science Foundation.

REFERENCES

- Ambruster, C. W., Sciortino, S., and Golub, L. 1987, *Ap. J. Suppl.*, **65**, 273.
 Bastian, T. S., and Bookbinder, J. A. 1987, *Nature*, **326**, 678.
 Benz, A. O. 1985, *Solar Phys.*, **96**, 357.
 Benz, A. O., Bernold, T. E. X., and Dennis, B. R. 1983, *Ap. J.*, **271**, 355.
 Butler, C. J., Rodono, M., Foing, B. H., and Haisch, B. M., 1986, *Nature*, **321**, 679.
 Furst, E., Benz, A. O., and Hirth, W. 1982, *Astr. Ap.*, **107**, 178.
 Holman, G. D., Eichler, D., and Kundu, M. R., 1980, in *IAU Symposium 86, Radio Physics of the Sun*, ed. M. Kundu and T. Gergely (Dordrecht: Reidel), p. 457.
 Jackson, P. D., Kundu, M. R., and White, S. M., 1987, *Ap. J. (Letters)*, **316**, L85.
 Lang, K. R., Bookbinder, J., Golub, L., and Davis, M. M. 1983, *Ap. J. (Letters)*, **272**, L15.
 Lang, K. R., and Willson, R. F. 1986a, *Ap. J.*, **305**, 363.
 ———, 1986b, *Ap. J. (Letters)*, **302**, L17.
 Melrose, D. B., and Dulk, G. A. 1982, *Ap. J.*, **259**, 844.
 Pettersen, B. R. 1980, *Astr. Ap.*, **82**, 53.
 Robinson, R. D. 1978, *Solar Phys.*, **60**, 383.
 White, S. M., Kundu, M. R., and Jackson, P. D. 1986, *Ap. J.*, **311**, 814.

KENNETH R. LANG and ROBERT F. WILLSON: Department of Physics and Astronomy, Robinson Hall, Tufts University, Medford, MA 02155

36. MICROWAVE OBSERVATIONS OF SOLAR AND STELLAR CORONAE

ROBERT F. WILLSON
Department of Physics and Astronomy
Tufts University
Medford, Ma 02155

ABSTRACT

We summarize recent high resolution microwave observations of the coronae of the Sun and other nearby active stars. VLA observations near 20 cm wavelength have been combined with simultaneous soft X-ray (SMM-XRP) observations to obtain the electron density and temperature in coronal loops and to specify the radiation mechanism within the emitting plasma. Observations near 90 cm wavelength outline large-scale coronal structures that may connect areas of weak magnetic fields. VLA observations of a solar noise storm at 90 cm have resolved the burst-emitting region into a number of compact components. These observations confirm previously reported trends for a decrease in burst size at shorter wavelengths, and they also suggest a hitherto unresolved complexity in source structure. The results of a search for 6 cm microwave emission from stars with short rotation periods and high magnetic fields or intense X-ray emission indicate that these properties alone do not guarantee the stars will be radio emitters. VLA and Arecibo observations of the dwarf M flare stars VZ Canis Minoris and AD Leonis reveal both slowly-varying and impulsive narrow-band emission, suggesting a nonthermal radiation mechanism such as plasma emission or electron-cyclotron maser emission.

1. INTRODUCTION

Recent high resolution microwave observations of the Sun have provided new insights to the structure of the solar corona and transition region. These include such things as the three-dimensional structure and magnetic field strengths of coronal loops, the preburst heating and magnetic triggering of loops, and the evolution of solar microwave bursts (see Kundu and Lang 1985 and Dulk 1985, for recent reviews). These results have come about through the unprecedented spatial resolution of radio synthesis instruments such as the Very Large Array (VLA) which can produce microwave images on angular scales of few seconds of arc and on timescales as short as a few seconds. The high sensitivity of the VLA, and the Arecibo Observatory also makes it possible to detect quiescent and burst emission from nearby stars. These observations can be used to specify the magnetic field strength in stellar coronae, to resolve the components of binary star systems, and to place stringent limits on the size of burst-emitting regions.

**SOLAR AND STELLAR CORONAL
STRUCTURE AND DYNAMICS**
A Festschrift in Honor of Dr. John W. Evans

PROCEEDINGS OF THE NINTH SACRAMENTO
PEAK SUMMER SYMPOSIUM, SUNSPOT, NM
17 – 21 AUGUST 1987

Sponsored by:
The National Solar Observatory
The NASA Solar Maximum Mission
The U. S. Air Force

Edited by:

Richard C. Altrock
Air Force Geophysics Laboratory
Sunspot, New Mexico

JULY 1988
NATIONAL SOLAR OBSERVATORY/SACRAMENTO PEAK
SUNSPOT, NEW MEXICO 88349

In this paper we discuss some recent VLA and Arecibo observations of the Sun and other active stars. We begin by discussing simultaneous VLA-SMM observations of coronal loops for which the microwave and soft X-ray data were combined to specify the radiation mechanisms of the emitting plasma. We then discuss observations of quiescent and burst emission from the Sun at 90 cm. Finally, we present the results of a recent VLA survey of active stars and discuss observations of narrow-band burst emission that provides evidence for non-thermal, coherent emission processes in stellar coronae.

3. MICROWAVE OBSERVATIONS OF THE SOLAR CORONA

3.1 Simultaneous Microwave and Soft X-ray Observations of Coronal Loops.

VLA observations of active regions at 20 cm wavelength outline coronal loops that appear to stretch between areas of opposite magnetic polarity in the photosphere (Lang, Willson and Rayrole 1982; Lang, Willson and Gaizauskas 1983). These loops have lengths ($L=10^9 - 10^{10}$ cm), temperatures ($T = 1 - 3 \times 10^6$ K) and shapes that are similar to those inferred from X-ray observations of the Sun. Although the soft X-ray emission is attributed to the thermal bremsstrahlung of a hot dense plasma, there are two possible thermal emission mechanisms at centimeter wavelengths. These are the thermal bremsstrahlung of electrons accelerated in the electric fields of ions, and the gyroresonant emission of electrons accelerated in coronal magnetic fields. Although both mechanisms are sensitive to the electron temperature and electron density, only gyroresonant emission provides a direct estimate of the magnetic field strength.

In order to determine which of these two competing mechanisms is the dominant one, it is necessary to know the temperature, density, magnetic field strength, and scale height of the coronal loop. X-ray observations provide estimates of T_e and N_e , so that comparisons of simultaneous X-ray and microwave observations might be used to specify the dominant microwave emission mechanism, and also establish the physical properties of the coronal plasma.

In Figure 1 we compare a 20 cm VLA synthesis map of an active region with a Solar Maximum Mission Flat Crystal Spectrometer (FCS) image in the O VIII line and with an H α image (Lang et al. 1987a). This figure shows that all of the X-ray emitting plasma was detected at 20 cm, with additional 20 cm emission above and near sunspots where no X-ray radiation was detected. Both X-ray and 20 cm emission was detected from coronal loops or arcades of loops that have sizes of $\sim 5 \times 10^9$ cm. The emission measure and electron temperature were inferred from ratios of different line intensities, and the electron density was calculated using a volume of 3×10^{27} cm³, which equals the product of the FCS projected area and a typical scale height of 3×10^9 cm. Our analysis indicates that the electron temperature and density were fairly uniform throughout the region, with $T_e = 2.7 - 3.1 \times 10^6$ K indicate that thermal bremsstrahlung ought to be optically thin for plausible loop widths, and that thermal gyroresonance radiation can be optically thick for plausible magnetic fields strength of $H > 130$ gauss.



Figure 1. A comparison of soft x-ray (SMM-FCS-left), H α (SOON-middle) and 20 cm (VLA-right) images of AR 4532 on 1984 July 9. The angular scale can be inferred from the 120" spacing between the fiducial marks on the axes. The contours of the 20 cm map mark levels of equal brightness temperature corresponding to 0.4, 0.5 ... 1.0 times the maximum brightness temperature of 1.4×10^6 K. The soft X-ray data were taken in the O VIII line (18.9 Å) with contours corresponding to 4, 8 and 15 counts s $^{-1}$.

Conclusive evidence for the importance of thermal gyroresonance emission comes from observations of sharp line-like enhancements in the microwave brightness temperature spectra of some active regions (Willson 1985; Lang et al 1987b). It has been predicted that thermal cyclotron lines might be observed if the radiation is emitted from hot, thin regions, or current sheets where the magnetic field is relatively constant (Syrovatskii 1977; Zheleznyakov and Zlotnik 1980; Kuznetsov and Syrovatskii 1981). Figure 2 shows a comparison between a 20 cm loop and SMM and H α images for another active region, while Figure 3 shows the brightness temperature spectrum at 10 different frequencies, as measured at the top of the loop. The peak brightness-temperature at $\nu = 1650$ MHz is higher than the electron temperature inferred from the X-ray data ($T_e = 2.6 \times 10^6$ K) while the brightness temperature at neighboring frequencies is lower. If the spectral feature is attributed to a thermal cyclotron line, then it indicates that the optical depth of thermal gyroresonance radiation must be greater than that of thermal bremsstrahlung at these frequencies, and that the coronal loop is inhomogeneous, with higher temperatures in some parts of the loop. The central frequency and narrow width of the line-like feature suggest that the magnetic field strength in this hotter layer is $B = 196 \pm 5$ or 147 ± 5 gauss, if the cyclotron radiation is generated at the third or fourth harmonic of the gyrofrequency, respectively.

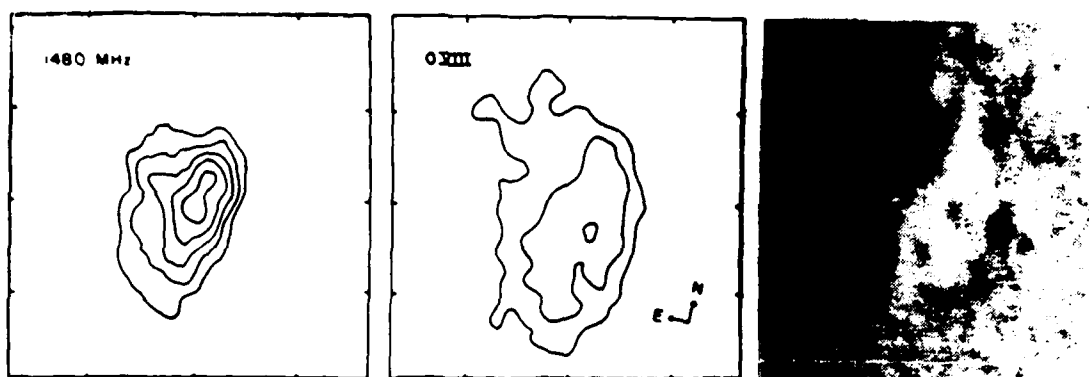


Figure 2. A comparison of 20 cm (VLA-left), soft X-ray (SMM-FOS-center) and $H\alpha$ (SOON-right) images of AR 4663 on 1985 June 7. The field of view of all three images is identical, and the angular scale can be inferred from the 60" spacing between fiducial marks on the axes. The contours of the 20 cm map mark levels of equal brightness temperature corresponding to 0.2, 0.4, ... 1.0 times the maximum brightness temperature of 1.8×10^6 K. The soft X-ray data were taken in the OVIII line (18.9 Å) with contours corresponding to 3, 7, 14 and 24 counts s^{-1} above a background level of 10 counts s^{-1} with a maximum signal of 18 counts s^{-1} .

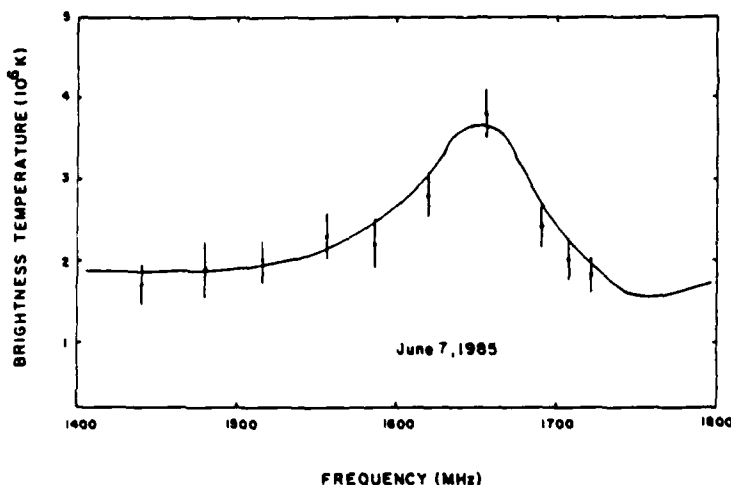


Figure 3. The maximum brightness temperatures of the coronal loop of AR 4663 at 10 closely spaced frequencies.

3.2 Large-Scale Coronal Loops at 90 cm Wavelength.

Recent developments at the VLA have made it possible to observe the Sun at 90 cm wavelength. When the VLA is in the most extended configuration the angular resolution is about 5 seconds of arc or about a factor of 20 better than that available on other instruments at this wavelength. In Figure 4 we show full-disk synthesis maps of the Sun at 20 cm and 90 cm on February 20, 1987. During these observations, the

VLA was in the C-D hybrid configuration which provided synthesized beamwidths of $\sim 26'' \times 54''$ at 20 cm and $\sim 113'' \times 237''$ at 90 cm (crosses).

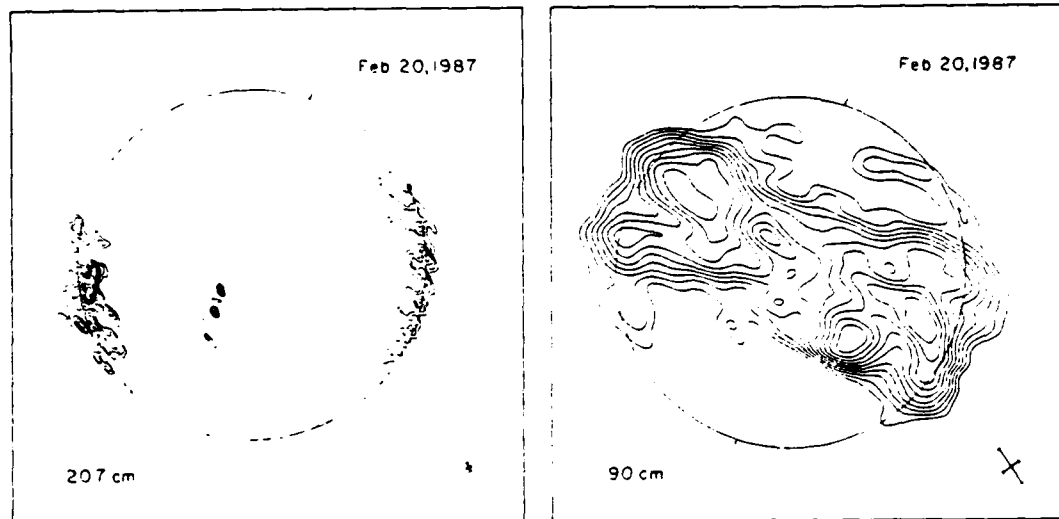


Figure 4. Four-hour VLA synthesis maps of the Sun at 20.7 cm (left) and 90 cm (right) wavelength on 20 February 1987. The contours mark levels of equal brightness temperature, T_B . The 20.7 cm map has an outermost contour of $T_B = 1.3 \times 10^5$ K a contour interval of 6.5×10^4 K and peak brightness temperature of $T_B = 6.5 \times 10^5$ K. The 90 cm map has an outermost contour of $T_B = 5.5 \times 10^4$ K a contour interval of 5.5×10^4 K, and a peak brightness temperature of $T_B = 5.7 \times 10^5$ K. The circles denote the edge of the optically-visible solar disk, and the Sun's north-south axis is denoted by the two short lines that intersect each circle.

A comparison with a Kitt Peak magnetogram shows that the 20 cm emission was associated with bipolar active regions (sizes $2'-3'$) with strong magnetic fields similar to the situation described in the previous section. The emission at 90 cm however indicates six or seven elongated structures with angular extents ranging between $3'$ and $10'$. These sources have no obvious association with strong magnetic fields or other optical features. Since observations at longer wavelengths generally refer to greater heights in the solar atmosphere, these results suggest that the coronal region where the 90 cm emission originates is highly structured, but that it is concentrated in more extended loops that connect areas of less intense magnetic fields. In this sense, high resolution full-disk 90 cm maps may act as "coronagraphs" that outline the structure of global magnetic fields, just as Kitt peak magnetograms delineate more intense, smaller scale photospheric fields. A comparison of the 90 cm map with one made two days later reveals that some of the sources have evolved or even disappeared during the day between observations. These observations indicate that the middle corona is dynamic, with evolutionary timescales of a few days or less.

3.3 Observations of a Solar Noise Storm.

We have also used the VLA at 90 cm to study a solar noise storm (Lang and Willson 1987). Noise storms are, in fact, the most common type of solar activity at decimetric and metric wavelengths (see e.g. Elgaroy 1977 and Kai, Melrose and Suzuki 1985). They consist of thousands of narrow-band, impulsive spikes or bursts superimposed on a wide-band continuum. The continuum is usually observed between ~ 50 and 350 MHz and normally lasts for a few hours to several days.

In Figure 5 we show a plot of the noise storm intensity together with a plot of the 1-8 Å GOES X-ray flux. The noise storm consisted of many burst-like spikes superimposed on a slowly-varying component. The most intense 90 cm emission followed a soft X-ray burst by about 30 minutes, and may have been triggered by an outward moving disturbance from the source of the X-ray event. The radio spikes are similar to Type I bursts but the relatively long VLA integration time of 6.7 seconds may have averaged the emission of several Type I bursts or chains of bursts. Both the spikes and the slowly varying emission were $95 \pm 5\%$ right hand circularly polarized.

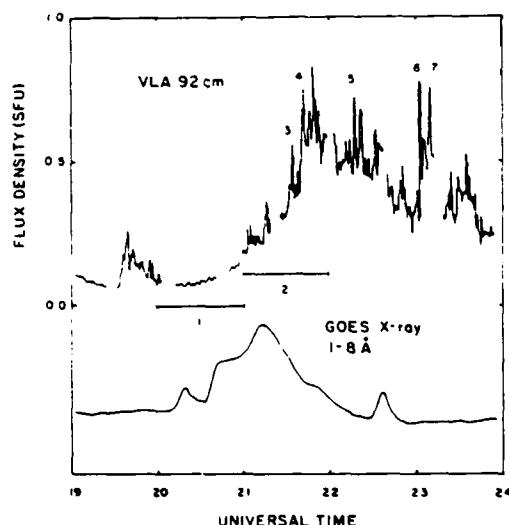


Figure 5. The time profile of a solar noise storm observed with one interferometer pair of the VLA at 92 cm wavelength (top) is compared with the soft X-ray emission detected by the GOES satellite (bottom). The data have been smoothed over 33.2 s. Spike-like bursts are superimposed upon a slowly-varying background; both of these components were $95 \pm 5\%$ right-hand circularly polarized.

A series of VLA snapshot maps made at successive peaks (Figure 6) depict the evolution of the noise storm. The peaks originate in an elongated region that has a nearly constant shape with a half-power size of $\sim 40'' \times 120''$. Figure 7 shows that these sources were located between widely separated active regions (separation $\sim 6'$) seen in the underlying photosphere.

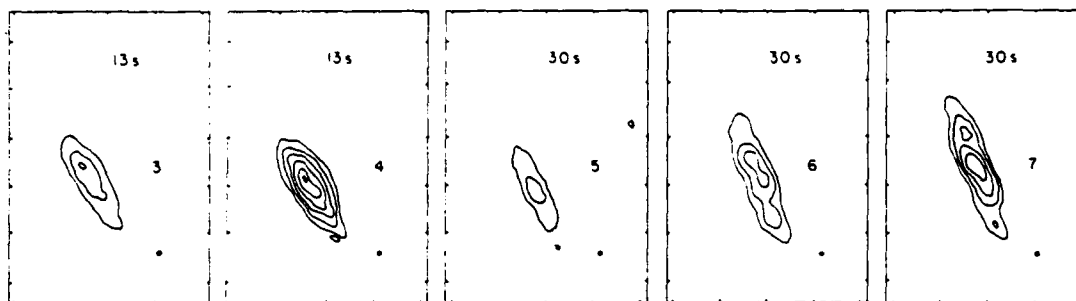


Figure 6. VLA snapshot maps of successive peaks in a solar noise storm at 92 cm wavelength. These peaks are denoted by 3, 4, 5, 6 and 7 in Figure 5. The contours mark levels of equal brightness temperature, T_B , with an outermost contour of $T_B = 3.3 \times 10^6$ K, a contour interval of 2.5×10^6 K, and a peak brightness temperature of $T_B = 1.0 \times 10^7$ K.

Previous observations of solar noise storms suggest that sense of circular polarization should correspond to the ordinary mode of wave propagation expected from plasma radiation in a strong magnetic field (Dulk and Nelson 1973; Stewart 1985). The high right handed circularly polarized source might therefore originate in coronal magnetic fields that are associated with the leading negative polarity sunspot shown in Figure 7. If this is the case, and if the source projects radially upward from this spot, then from the limbward projection of the source we infer a height of $h = 0.15 \pm 0.03 R_\odot$ for the noise storm. Under the assumption that the radiation is emitted at the fundamental of the plasma frequency ν_p , we infer an electron density of $N_e = 1.4 \times 10^9 \text{ cm}^{-3}$, and a magnetic field strength of $H \ll 100$ gauss, if $\nu_H \ll \nu_p$, where $\nu_H = 2.8 \times 10^6 \text{ Hz}$ is the gyrofrequency.



Figure 7. A Very Large Array (VLA) synthesis map of solar noise storm at 92 cm wavelength is superimposed on a Kitt Peak National Observatory (KPNO) magnetogram taken on the same day. The VLA map covered the one hour time interval between 2300 and 2400 UT. Its synthesized beamwidth is denoted by the black spot. The contours mark levels of equal brightness temperature, T_B , with an outermost contour of $T_B = 1.0 \times 10^6$ K and a contour interval of 7.2×10^5 K. The magnetogram was kindly provided by Jack Harvey of the National Solar Observatory.

4. MICROWAVE OBSERVATIONS OF THE CORONAE OF ACTIVE LATE-TYPE STARS

4.1 A VLA Survey of Active Cool Stars at 6 cm Wavelength

Observations using the High Energy Astronomical Observatory (HEAO-1) and Einstein (HEAO-B) satellites indicate that most active cool stars of spectral type F-M are intense X-ray emitters (see Rosner, Golub and Vaina 1985) for a recent review). If the solar analogy applies, then there stars must also have hot ($T_e = 10^6 - 10^8$ K) coronae with large-scale loops and intense photospheric magnetic fields. The coronal X-ray luminosity appears to increase with the square of the stellar rotation rate (Pallavicini et al 1981) and this correlation is probably related to the internal dynamo mechanism that generates the stellar magnetic field. Chromospheric activity also increases with the rotational velocity, but it additionally depends on spectral type, or equivalently, with the depth of the convection zone (Noyes et. al 1984).

If these stars have large-scale magnetic loops, then quiescent microwave emission might also be detected from thermal or non-thermal electrons trapped in these loops. Quiescent emission has in fact been detected from at least one class of late-type stars, the dwarf M flare stars using the VLA (Gary and Linsky 1981; Topka and Marsh 1982; Linsky and Gary 1983; Pallavicini, Willson and Lang 1985; Willson, Lang and Foster 1987).

The radiation mechanism that gives rise to this emission is somewhat controversial. The emission from the star EQ Peg has been interpreted as thermal gyroresonance radiation by electrons spiralling in regions of high magnetic field (Gary and Linsky 1981; Topka and Marsh 1982). This interpretation is suggested by the analogy with the Sun, in which intense, highly circularly polarized centimeter wavelength emission is usually observed from magnetic field regions overlying sunspots. However, for coronal temperatures of $T_e = 10^6 - 10^7$ K, this explanation requires magnetic field strengths of several hundreds gauss in loops that are many times larger than the star, and photospheric magnetic field strengths that may be at least an order of magnitude higher than observed on late-type stars. An alternative explanation is gyrosynchrotron-radiation from non-thermal electrons accelerated more or less continuously in weaker magnetic fields above starspots (Pallavicini, Willson and Lang 1985; Willson, Lang and Foster 1987).

Since it would be interesting to correlate intrinsic properties of the stars with microwave emission, we have recently begun a 6 cm VLA survey of nearby active stars of spectral type F, G, and K (Table 1). All of these stars exhibit chromospheric activity and many of them rotate faster than the Sun. Some of them also have strong photospheric magnetic fields, and some exhibit chromospheric variability, indicative of stellar activity cycles. The results of our initial observations are summarized in Table 1, where we give the rotation period, distance, and when available the photospheric magnetic field strength and X-ray luminosity, and either the flux or 3 σ upper limits. Of the 18 stars observed, two were detected, namely BY Draconis and BD + 26° 730. Both are members of the BY Draconis class of stars,

and both show evidence of long-term photometric variations, suggestive of activity cycles (Phillips and Hartmann 1978). BY Draconis was $\sim 8\%$ left hand circularly polarized, while ED + 260730 was less than 5% circularly polarized. BD 260730 also systematically increased in intensity by about a factor of two during our observation period of 60 minutes, but there was no evidence for narrow-band emission as has been observed from some active stars (see section 4.2). Our preliminary results indicate that in general, rapid rotation and/or high surface magnetic fields are not sufficient to yield detectable radio emission, suggesting that these fields do not extend far out into the corona, or that the coronal loops do not have a high enough density of thermal or nonthermal particles. (see Willson and Lang (1987) for a detailed discussion of these results).

Table 1. Results of a 6 cm VLA Survey of Active Cool Stars

STAR NAME	No. CL.	θ (days) ^a	D (pc)	M (solar)	L_X (10^{26} erg s ⁻¹)	S (mJy)
9 Oct	12	7.7	20.4			< 0.16
HD 4638	12	39	6.9			< 0.17
HD 16160	13	45	7.2			< 0.16
ε Per	12	11.3	3.3	2850 ^a	200 ^b	< 0.15
HD 21998	17	2.6	27			< 0.15
ED + 260730	45	-	-			2.5 - 7.5
GL 202	19	2.6	15.6			< 0.15
HD 45099	13	7.1	12.0			< 0.19
GL 311	11.5	3.7	15.6			< 0.15
HD 82845	08	19.1	9.2			< 0.16
GL 417	12	5.3	23.8			< 0.15
β Com	00	12.4	8.3		2000	< 0.15
HD 152391	09	11.1	16.9			< 0.17
36 Oph	11, 15	22.9	5.4	2080 ^a		< 0.15
HD 156026	15	18.0	5.4			< 0.16
HD 190007	12	29.3	14.1			< 0.14
RT Dra	16	-	15.6		3200 ^d	3.8
61 Cyg	15, 17	38.48	3.4	3240 ^a	~30 ^b	< 0.19

Refs. a) March (1984)
 b) Johnson (1981)
 c) Valina et al (1981)
 d) Golub (1983)
 e) Reeves et al (1984)

4.2 Observations of Narrow Band Microwave Bursts from Stars.

The high sensitivity of instruments such as the VLA and Arecibo has made it possible to study burst emission from active stars. These bursts are often highly circularly polarized, suggesting an intimate connection with stellar magnetic fields. Brightness temperatures of $T_b > 10^{10}$ K are often inferred from observations of millisecond spikes observed from the dwarf M flare star AD Leonis (Lang et al 1983; Lang and Willson 1986b). These characteristics are suggestive of a coherent radiation mechanism.

Conclusive evidence of a coherent mechanism came when observers began to study the dynamic spectra of stellar microwave bursts and found that some showed evidence of narrow-band characteristics. Lang and Willson (1986a) found that variations in the 20 cm flux from YZ Canis Minoris had a fractional bandwidth of $\Delta\nu/\nu_0 < 0.03$. Similar results were obtained for the stars AD Leonis and L726-8A by White, Kundu and Jackson (1986). Dynamical spectra in both time and frequency for one burst emitted by the flare star TV Ceti showed no variations as a function of frequency across a band of 41 MHz, while another circularly polarized exhibited complex frequency structure with narrow-band components of $\Delta\nu < 3.0$ MHz. (Bastian and Bookbinder (1987)).

In Figure 8 we show our most recent Arecibo observations of burst emission from AD Leonis. These observations were made at wavelengths near 20 cm using a 64 channel autocorrelator and a bandwidth of 40 MHz (For a description of our observing technique, see Willson and Lang (1987)). Here, the time resolution of the data is 1.25 seconds. This burst was ~ 100% right circularly polarized and consisted of a number of individual components each with a lifetime of few seconds. The intensity of the burst decreases rapidly with increasing frequency, with spectral indices, α , ($S_\nu \propto \nu^\alpha$) ranging from -55 to -70. Such high spectral indices cannot be accounted for by an incoherent emission process such as gyrosynchrotron radiation which predicts more broad-band emission.

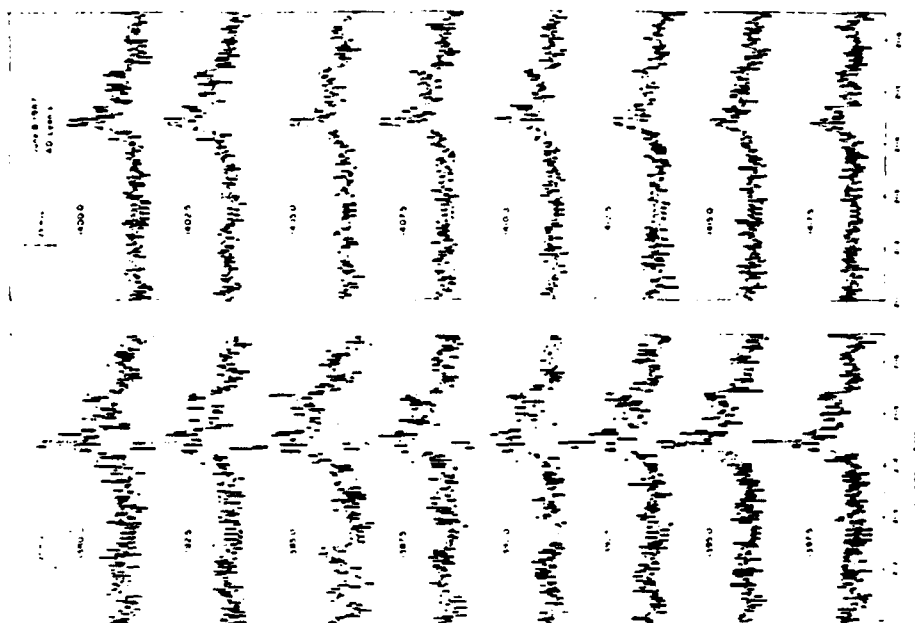


Figure 8. The right circularly polarized intensity of a 20 cm burst observed from AD Leonis over a 40 MHz bandwidth. Each channel is ~ 2.5 MHz wide and is centered at the given frequency, in MHz.

Finally, in Figure 9 and 10 we show recent VLA dynamical spectral observations of YZ Canis Minoris (Lang and Willson 1988). In Figure 9 we plot the left and right circularly polarized signals which represent the averages of 15 contiguous frequency channels covering a bandwidth of ~ 50 MHz. Here the data have been averaged over a time interval of 1.5 minutes. This figure shows that the emission is nearly 100% left circularly polarized and variable on timescales of tens of minutes. In Figure 10 we show spectra for different intervals denoted on each plot. These spectra indicate that, in some cases, the emission has a relatively-narrow bandwidth ($\Delta\nu < 50$ MHz) whose central frequency shifts with time. The total intensity at other times appears to be broad-band with $\Delta\nu > 50$ MHz, but these spectra could represent the average of many narrow-band emission. The interesting aspect of the narrow-band emission is that it persists for relatively long time intervals of ten minutes with a well defined bandwidth and central frequency. Coherent emission processes such as an electron-cyclotron maser emission or plasma

plasma radiation can produce narrow band radiation at the first or second harmonic of the gyrofrequency or plasma frequency, but if the magnetic field or electron-density change significantly within the source during the periods of observation, then the average emission profile will be smeared, resulting in wide-band spectrum. The fact that the narrow-band emission persisted for ten minutes therefore is surprising and suggests that these parameters remained remarkably constant in the stellar corona.

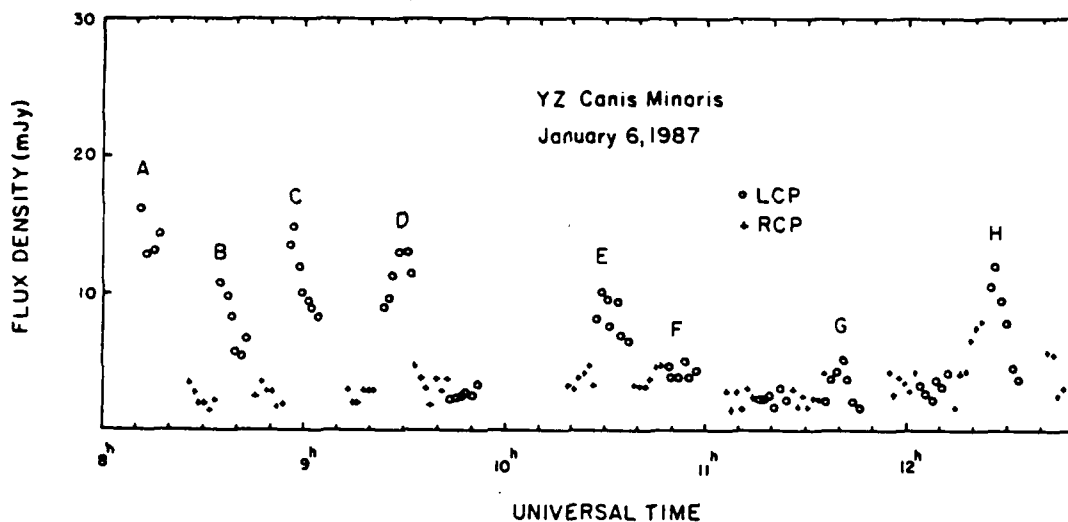


Figure 9. The right and left circularly polarized intensity of the radiation observed from YZ Canis Minoris, plotted as a function of time. The oppositely polarized signals were alternately recorded for 10 minutes intervals within a 50 MHz bandwidth centered on 1464.0 MHz. Here the data have been averaged over a time interval of 1.5 minutes. Frequency spectra of the slowly varying LCP radiation marked by the letters A, E, G and H are shown in Figure 10.

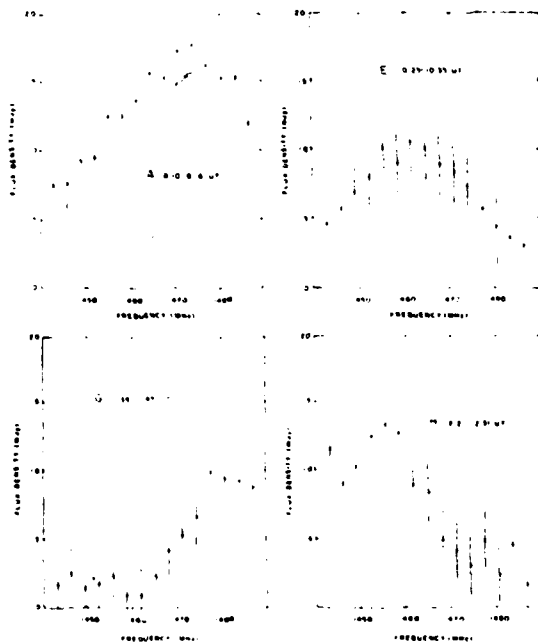


Figure 10. Frequency spectra of the left circularly polarized emission from YZ Canis Minoris for the intervals marked A, E, G and H in Figure 9. Each of the 15 frequency channels is 3.125 MHz wide. The error bars denote the 3σ noise level for the relevant time interval and bandwidth. These spectra all show evidence for narrow band radiation with $\Delta\nu < 30$ MHz. At other times, the radiation appears to have a width greater than the 50 MHz bandwidth.

Acknowledgements

All of these observations were made in collaboration with Kenneth R. Lang at Tufts University. Radio Astronomical studies of the Sun and other active stars at Tufts University are supported under grant AFOSR-93-0019 with the Air Force Office of Scientific Research and by contract N00014-96-K-0068 with the office of Naval Research (ONR). Investigations of dwarf flare stars at Tufts are also supported by NASA grant NAG 5-477. The Very Large Array is operated by Associated Universities, Inc., under contract with the National Science Foundation. The Arecibo Observatory is part of the National Astronomy and Ionosphere Center which is operated by Cornell University under contract with the National Science Foundation.

References

- Bastian, T.S., and Bookbinder, J.A., 1987, *Nature*, 326, 678.
 Dulk, G.A. 1985, *Ann. Rev. Astron. Ap.*, 23, 169.
 Dulk, G.A., and Nelson, G.J. 1973, *Proc. Astr. Soc. Austr.* 2, 211.
 Elgarov, O. 1977, *Solar Noise Storms*. (New York; Pergamon Press).
 Activity in Red Dwarf Stars ed. M. Rodono
 Gary, D.E., and Linsky, J.L., 1981, *Ap. J.* 250, 284.
 Golub, L., 1983 in *IAU Colloquium 71*, and P.R. Bryne (Dordrecht: Reidel).
 Johnson, H.M., 1981, *Ap.J.*, 243, 234.
 Kuznetsov, V.S., and Syrovatskii, S.I. 1981, *Solar Phys.*, 69, 391.
 Kai, K., Melrose, D.B., and Suzuki, S. 1985, "Storms", in *Solar Radiophysics*, eds. D.J. McClean and N.R. Labrum (New York: Cambridge University Press) pp. 415-441.
 Kundu, M.R., and Lang, K.R., 1985, *Science*, 228, 9.
 Lang, K.R., and Willson, R.F., 1986a *Ap. J. (Letters)*, 302, L17.
 Lang, K.R., and Willson, R.F., 1986b, *Ap.J.*, 305, 363.
 Lang, K.R., and Willson, R.F. 1987, *Ap.J.* 319, 514.
 Lang, K.R., and Willson, R.F. 1988, *Ap.J.* (in press).
 Lang, K.R., Willson, R.F., and Rayrole, J. 1982, *Ap.J.* 258, 384.
 Lang, K.R., Willson, R.F., and Gaizauskas, V. 1983, *Ap.J.*, 267, 455.
 Lang, K.R., Bookbinder, J., Golub, L. and Davis, M.M. 1983, *Ap. J. (Letters)*, 272, L15.
 Lang, K.R., Willson, R.F., Smith, K., and Strong, K.T. 1987a, *Ap.J.*, (in press).
 Lang, K.R., Willson, R.F., Smith, K., and Strong, K.T. 1987b, *Ap.J.*, (in press).
 Marcy, G.W., 1984, *Ap.J.*, 276, 286.
 Noyes, R.W., Hartmann, L., Baliunas, S., Duncan, D., and Vaughan, A.H. 1984, *Ap. J.*, 279, 763.
 Pallavicini, R.P., Golub, L., Rosner, R., Vaina, G.S., Avres, T., and Linsky, J.L. 1981, *Ap.J.* 248, 279.
 Pallavicini, R., Willson, R.F., and Lang, K.R., 1985, *Astron. Ap.*, 149, 95.
 Phillips, M.J., and Hartmann, L. 1978, *Ap.J.*, 224, 82.
 Rosner, R., Golub, L., and Vaina, G.S., 1985, *Ann. Rev. Astron. Ap.*, 23, 413.
 Stewart, R.T. 1985, *Solar Phys.* 96, 381.
 Syrovatskii, V.D. 1977, *Astr. Zh (letters)*, 3, 133.
 Topka, K., and Marsh, K.A., 1982, *Ap.J.*, 254, 641.
 Vaina, G.S., et al., 1981, *Ap.J.*, 244, 163.
 White, S., Kundu, M.R., and Jackson, J. 1986, *Ap.J.*, 311, 814.
 Willson, R.F. 1985, *Ap.J.*, 298, 911.
 Willson, R.F., and Lang, K.R. 1987. (in preparation).
 Willson, R.F., Lang, K.R., and Foster, P. 1987, *Astron. Ap.* (submitted).
 Zheleznyakov, V.V., and Zlotnik, E. Ya., 1980, in *IAU Symposium 86, Radio Physics of the Sun*, eds. M.R. Kundu and T. Gergely (Dordrecht: Reidel) p. 87.

37. SIMULTANEOUS VLA-SATELLITE
OBSERVATIONS OF THE SUN*

Kenneth R. Lang**
D.A.S.O.P.
Observatoire de Paris - Meudon
92195 MEUDON PRINCIPAL CEDEX
FRANCE

*Presented at the XXVII COSPAR (Committee on Space Research) meeting in Helsinki, Finland during Workshop XV - Scientific Planning for the Next Solar Maximum and Beyond on 26 July 1988.

**On sabbatical leave from the Department of Physics and Astronomy, Robinson Hall, Tufts University, MEDFORD, MA 02155, U.S.A.

ABSTRACT

The Very Large Array (VLA) and satellite-borne telescopes can be used in the 1990s to provide unique observations of the quiescent and active corona with comparable resolution in time and space. Recently available 90-cm VLA data specify closed and open magnetic structures in the low solar corona, providing unique information about the initiating source of coronal mass ejections observed by satellite coronagraphs. The physical properties of quiescent coronal loops can be inferred from combined soft X-ray (electron density and temperature) and 20-cm VLA (magnetic field strength and structure) data. Systems of coronal loops within a single active region have different temperatures and different radiation mechanisms that can only be detected by observations in both spectral domains. The combined VLA-satellite observations will also specify magnetic interaction and particle acceleration before and during flares, including magnetic triggering in the corona (VLA) and preflare heating (VLA-satellite).

INTRODUCTION

The Very Large Array (VLA) can provide unique information about large-scale magnetic structures, coronal holes, and coronal loops. Newly-developed receiving systems at 92-cm wavelength permit observations of quiescent and active emission from filaments and coronal holes, while 20-cm observations provide similar information for coronal loops within active regions.

FILAMENTS AND CORONAL HOLES

The first VLA synthesis maps of the quiescent corona at 92-cm wavelength (327 MHz) revealed intense, elongated structures that were not systematically associated with any optical counterpart, including active regions, filaments, sunspots and magnetic neutral lines /1/. Filaments are sometimes associated with enhanced 92-cm emission, however, and there is a reduction in brightness over polar coronal holes at this wavelength /1/, /2/.

The ubiquitous noise storms are the only source of intense 92-cm radiation associated with solar active regions. These storms are apparently located in large-scale magnetic loops that connect with more distant areas on the Sun /3/. Individual noise storm bursts and the background continuum can be resolved in both space and time by using simultaneous observations with the VLA and the Nancay Radioheliograph /4/. Such information will provide important constraints to our future understanding of noise storms and related activity on the Sun.

Recent VLA synthesis maps indicate that intense, quiescent 92-cm radiation is definitely associated with the large-scale magnetic structures detected as dark filaments in H α photographs (see Fig. 1, 2). Such an association was first suggested by a statistical study of numerous one-dimensional scans of moderate angular resolution at meter wavelengths (169 MHz) /5/, but subsequent two-dimensional maps at this wavelength suggested that extended quiescent filaments have no radio counterpart /6/, /7/. The results shown in Figures 1 and 2 indicate that this is not

always the case at 92-cm.

Future VLA observations of large-scale magnetic structures can be used to test models for the origin of coronal mass ejections. These outward-moving magnetic bubbles are currently thought to be initiated by global magnetic changes; associated chromospheric activity, detected as erupting prominences or H α flares, is thought to be the result, rather than the cause, of these changes /8/. Such models have been derived from observations with satellite-borne coronagraphs whose occulting disks block the visible photosphere and the low corona. VLA observations at 92-cm wavelength can enhance and extend future coronagraph investigations by observing the formation of coronal mass ejections in the low solar corona at both the limb and across the entire solar disk.

Reductions or depressions in the 92-cm radiation are apparently associated with coronal holes in both the polar and equatorial regions (see /1/ and Fig. 1). Future VLA observations can therefore provide new insights to the formation and evolution of coronal holes and the high-speed solar wind that probably originates in them. Comparisons with satellite observations may resolve current uncertainties about the density and temperature of these coronal holes /9/.

Although intense, quiescent 92-cm sources are not associated with active regions, the quiescent emission at 20-cm wavelength is dominated by radiation from coronal loops that are often anchored within single active regions. These magnetic loops are smaller than the large-scale magnetic structures detected at the longer wavelength; but the 20-cm loops dominate the coronal structure of active regions and store the magnetic energy that is released during powerful eruptions from them /10/, /11/.

When the 20-cm VLA results are combined with satellite observations of spectral lines at soft X-ray wavelengths, the physical properties and dominant radiation mechanisms can be specified /12/. There are coronal structures that are detected at 20-cm but remain invisible at X-ray wavelengths and vice versa (see Fig. 3). Future VLA data will also uniquely specify the strength and structure of the coronal magnetic fields.

Observations of the 20-cm loops during the coming solar maximum will help establish magnetic changes that probably trigger solar eruptions /13/, /14/. The magnetic interaction of coronal loops apparently involves reconnection processes that release stored magnetic energy and accelerate particles near their tops (see Fig. 4). Simultaneous satellite observations at soft and hard X-ray wavelengths will help unravel the detailed triggering and acceleration mechanism.

ACKNOWLEDGEMENTS

Radio astronomical studies of the Sun at Tufts University are supported under grant AFOSR-83-0019 with the Air Force Office of Scientific Research and contract N00014-86-K-0068 with the Office of Naval Research. Collaborative long-wavelength solar observations by Tufts University and the Observatoire de Paris are supported by National Science Foundation grant INT-8602235 and Centre National de la Recherche

Scientifique grant 920038. Simultaneous SMM and VLA observations of the Sun are supported by NASA grant NAG 5-501. The Very Large Array is operated by Associated Universities Inc., under contract with the National Science Foundation.

REFERENCES

1. K. R. Lang, R. F. Willson, and G. Trottet, High-resolution VLA maps of the quiescent corona at 90-cm wavelength, Astron. Astrophys. in press (1988).
2. R. K. Shevgaonkar, M. R. Kundu, and P. D. Jackson, Variability of Metric Emission from the Sun, Astrophys. J., submitted (1988).
3. K.R. Lang, and R. F. Willson, Astrophys. J. 319, 514-519 (1987). Also see M. F. Lantos-Jarry, Solar Phys., 15, 40 (1970).
4. A. Kerdraon, G. Trottet, K. R. Lang, and R. F. Willson, High-resolution VLA-Nancay observations of the Sun, this issue.
5. F. Axisa, Y. Avignon, M. J. Martres, M. Pick, and P. Simon, Solar Phys. 19, 110-127 (1971).
6. C. E. Alissandrakis, P. Lantos, and E. Nicolaidis, Solar Phys., 97, 267-282 (1985).
7. P. Lantos, C. E. Alissandrakis, T. Gergely, and M. R. Kundu, Solar Phys., 112, 325-340 (1987).
8. A. J. Hundhausen, The origin and propagation of coronal mass ejections, Solar Wind Six, in press (1988).
9. G. A. Dulk, K. V. Sheridan, S. F. Smerd, and G. L. Withbroe, Solar Phys. 52, 349-367 (1977).
10. K. R. Lang, and R. F. Willson, Adv. Space Res., 2, No. 11, 91-## (1983).
11. K. R. Lang, and R. F. Willson, Adv. Space Res. 4, No. 7, 105-## (1984).
12. K. R. Lang, R. F. Willson, K. L. Smith, and K. T. Strong, Astrophys. J., 322, 1035-1043, 1044-1051 (1987).
13. M. R. Kundu, and K. R. Lang, Science, 228, 9-15 (1985).
14. K. R. Lang, and R. F. Willson, Adv. Space Res. 6, No. 6, ###-## (1986).

FIGURE LEGENDS

Fig. 1. Three-hour VLA synthesis map at 92-cm wavelength (327.0 MHz) on 15 May, 1988 between 13 h and 16 h U.T. The regions of enhanced 92-cm emission are well correlated with dark filaments shown in a H α photograph taken on the same day (see Figure 2). The elongated filaments have similar shapes at 92-cm and H α wavelengths. Active regions (squares) are not associated with enhanced 92-cm radiation; but they dominate the intense radiation at 20-cm wavelength and are observed as bright H α features. Regions of depressed 92-cm emission are at least partly due to equatorial coronal holes. The contours mark levels of equal brightness temperature, T_b , with an outermost contour of $T_b = 7.8 \times 10^4$ K, a contour interval of 7.8×10^4 K, and a peak brightness temperature of $T_b = 7.8 \times 10^5$ K. The synthesized beamwidth is denoted by the small black spot in the lower left-hand corner; it has angular dimensions of 80" x 55" at a position angle of -20° .

Fig. 2. AnH α spectroheliogram taken at 6 h and 36 m U.T. on 15 May 1988 at the Observatoire de Paris, Meudon. Five dark filaments are well correlated with regions of enhanced emission at 92-cm wavelength (see Figure 1); the elongated shape of the longer filaments is also detected in the radio data. Areas of bright H α emission (plage-active regions) are not associated with enhanced 92-cm emission; but they dominate the radiation at 20-cm wavelength.

Fig. 3. A comparison of soft X-ray (Solar Maximum Mission Satellite) and 20 cm (Very Large Array) images of AR 4532 on 1984 July 8. The field of view of all two images is the same, and the angular scale can be inferred from the 120" spacing between the fiducial marks on the axes. The contours of the 20 cm map mark levels of equal brightness temperature corresponding to 0.4, 0.5, 0.6...1.0 times the maximum brightness temperature of 1.4×10^6 K. The soft X-ray data were taken in the O VIII line (18.9 Å) with contours corresponding to 4, 8, and 15 counts s $^{-1}$ above a background level of 10 counts s $^{-1}$ with a maximum signal of 20 counts s $^{-1}$. Here the sunspots are denoted by small black dots with a circle around them.

Fig. 4. A VLA snapshot map during a 10-second interval at 20 cm wavelength catches a powerful eruption at the site of particle acceleration. The energetic particles originate at the apex of coronal loops; some of them travel to the Earth where they interfere with radio communication and high-flying aircraft. The VLA contours are superposed on an H α photograph of flare emission at lower levels in the solar atmosphere.

VLA 3 hour synthesis map
visible solar disk at 327 MHz

MAY 15, 1988

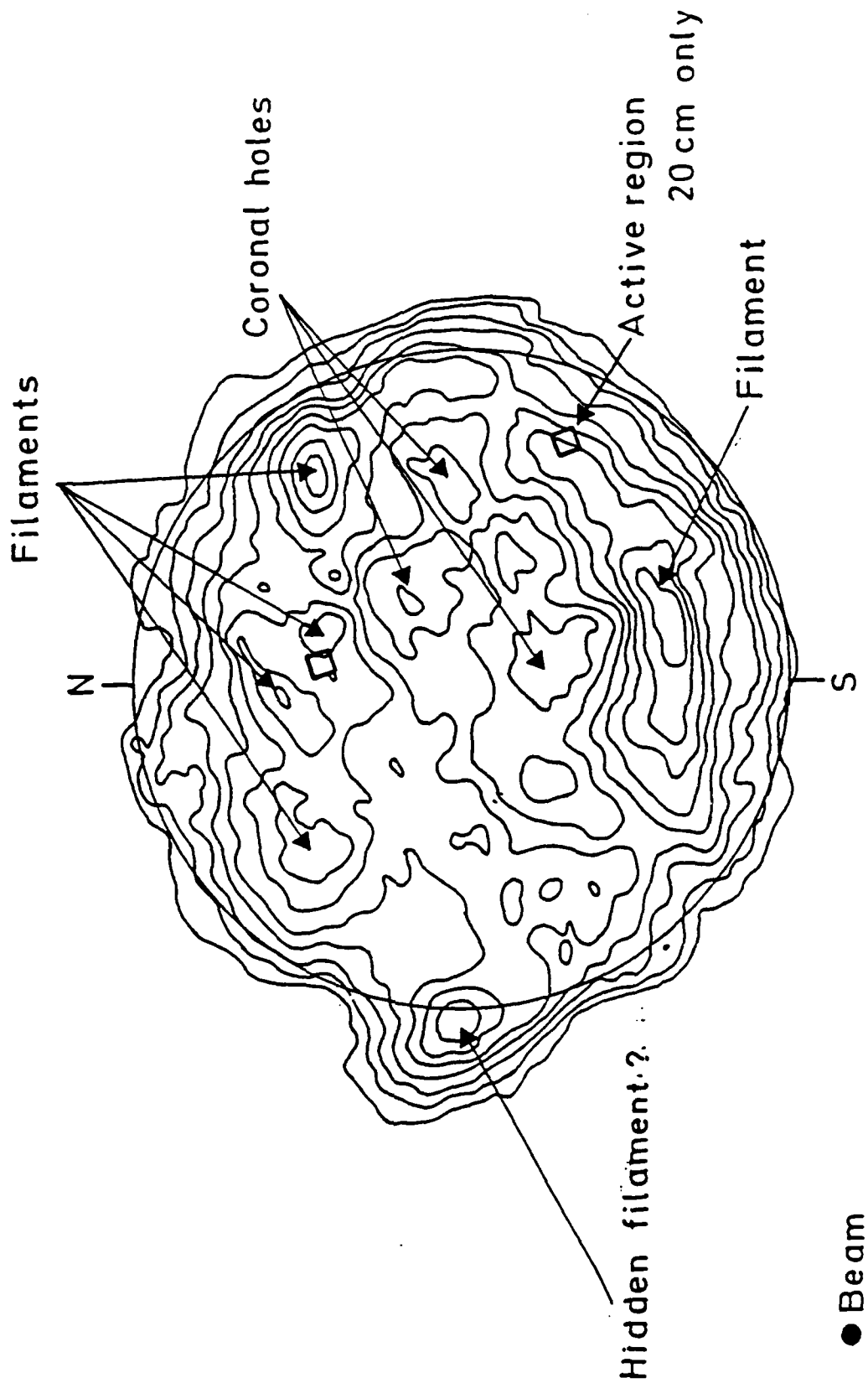


Fig. 1.

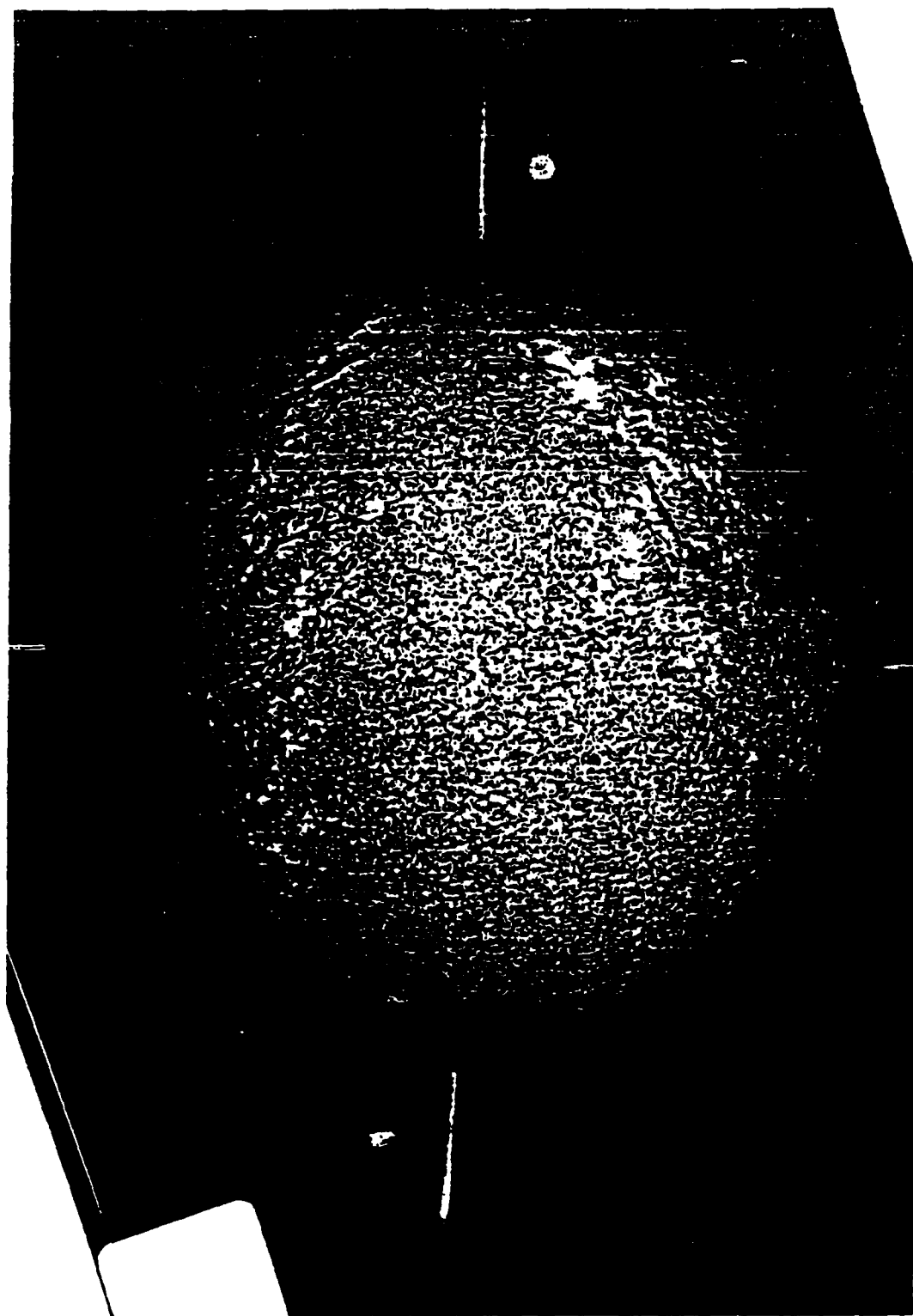
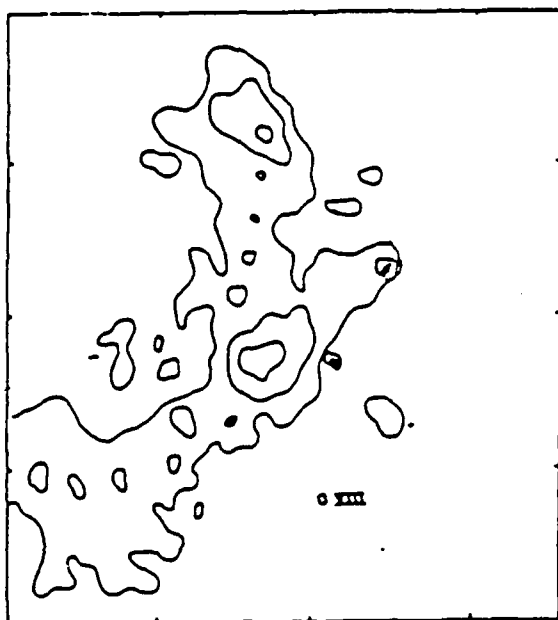
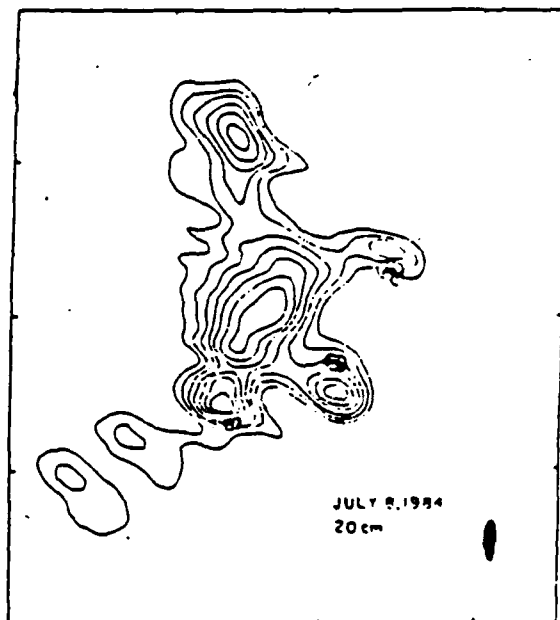


Fig. 2.



X - Rays
SMM SATELLITE



RADIO RADIATION
VERY LARGE ARRAY

Fig. 3.

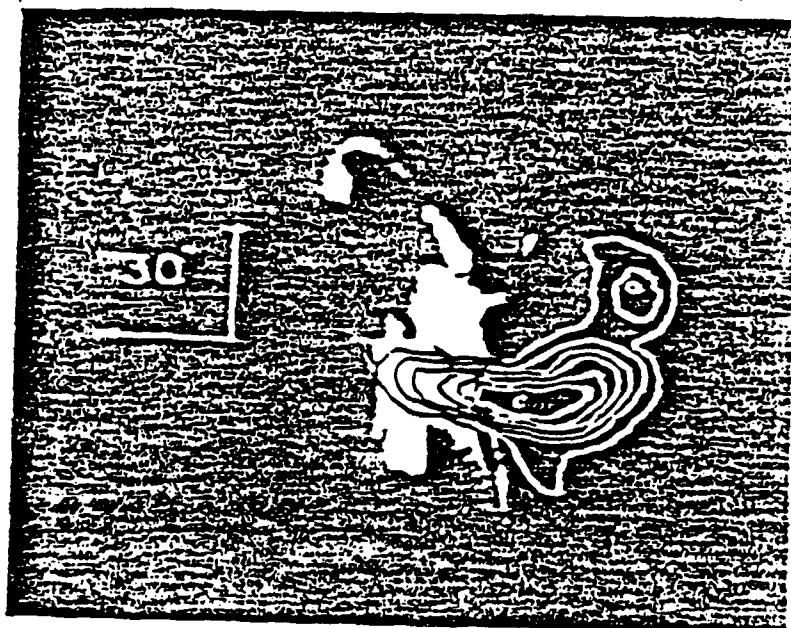


Fig. 4.

38. HIGH RESOLUTION VLA - NANCAY OBSERVATIONS OF THE SUN *

Alain Kerdraon and Gérard Trottet
D.A.S.O.P.
Observatoire de Paris - Meudon; CNRS-UA 324
92195 MEUDON PRINCIPAL CEDEX
FRANCE

Kenneth R. Lang ** and Robert F. Willson
Department of Physics and Astronomy
Robinson Hall
Tufts University
MEDFORD, MA 02155
U.S.A.

* Presented at the XXVII COSPAR (Committee on Space Research) meeting in Helsinki, Finland, during Workshop XV - Scientific Planning for the Next Solar Maximum and Beyond on 26 July 1988.

** On sabbatical leave from Tufts University at the Observatoire de Paris - Meudon.

A B S T R A C T

The Very Large Array (VLA) and the Nançay Radioheliograph (NR) can be used in the 1990s to provide unique observations of the quiescent and active corona. The combined data can specify the evolution and magnetic structure at a variety of heights in the quiescent corona, from compact to extended structures such as loops, streamers and coronal holes. The scientific potential of simultaneous VLA - NR research is illustrated by observations of solar noise storms with hitherto unavailable resolution in space (VLA), time (NR). Unique information will also be provided for other types of solar bursts, leading to an improved understanding of solar activity during the coming maximum.

NOISE STORMS

Noise storms are the most common type of solar activity observed at metric wavelengths. They consist of a slowly-varying, wide-band continuum radiation with superposed short-lived, narrow-band bursts. These bursts have been designated Type I bursts to distinguish them from other types of solar bursts. The background continuum, which is usually observed between 50 and 350 MHz, normally continues for a few hours, while individual bursts have bandwidths between 2 and 10 MHz and durations of 0.1 to 2 seconds /1/.

Both the background continuum and the bursts are usually strongly circularly polarized (up to 100 %), but unpolarized bursts are occasionally observed. The sense of circular polarization is constant throughout the storm; it is attributed to the ordinary mode of plasma radiation in a strong magnetic field /3/.

Noise storms have been extensively studied with the Culgoora and Nançay radioheliographs, whose respective beamwidths are $\theta \sim 2.0$ and 1.3 at 160 MHz. The resolved storm sources have sizes that tend to increase with height, and radiation at lower frequencies originates at higher altitudes

(see Fig. 1 and /4/). These sources appear to be located in large-scale magnetic loops extending high into the corona from one or more active region /5/, /6/; suggesting plasma radiation within the legs of magnetic loops whose field lines diverge with height /7/, /8/. At a given frequency, successive Type I bursts may come from either a fixed or different locations /9/, /10/, and can have a variety of sizes /11/.

Storm sources were nevertheless often unresolved with the Culgoora and Nançay instruments, for they were often operating at the limits of their capability. The Very Large Array (VLA) now provides a substantial improvement in angular resolution, θ with $\theta \approx 5''$ at 92 cm wavelength (327 MHz) in the A configuration. It has been used to fully resolve one noise storm that had an elongated shape (40" x 200"), and contained four compact components, each 40" across, during the onset and early stages /12/. Such complexity may rule out the simple conical model, or at least involve its extension to include magnetic flux tubes or scattering on field-aligned density inhomogeneities.

Because the VLA has limited integration times of $\tau \geq 3.3$ sec., simultaneous observations with the Nançay Radioheliograph ($\tau \geq 0.02$ sec.). are required to isolate individual bursts and to discriminate between the bursts and background continuum. We have therefore begun such observations during the period of common solar visibility (13 h to 16 h U.T.). This collaborative program will continue throughout the coming maximum in solar activity, thereby enhancing the scientific return of both ground-based and balloon or satellite-borne instruments.

Simultaneous observations of a solar noise storm were carried out on 27 June 1987 with the VLA in the A configuration and operating at a signal frequency of 333.0 MHz with a bandwidth of 3.125 MHz; the Nançay Radioheliograph (NR) operated at 327.0 MHz with a 700 kHz bandwidth. The integrated signal from all the VLA interferometer pairs was plotted as a function of time and compared with a similar NR record to determine bursts that were detected by both telescopes.

The VLA was then used to make successive 10-second snapshot maps for intervals of several minutes centered at the common burst time. Two examples are shown in Fig. 2. The unpolarized and polarized bursts both have elongated shapes, but they originate in different sources that are separated by 60". The unpolarized burst (degree of circular polarization $g_c \approx 10\%$) consists of a single elongated source with angular dimensions of 30" x 80", whereas the polarized one ($g_c \approx 70\%$) contained two components separated by $\approx 20''$ and embedded within an elongated 40" x 60" structure. Although previous observers have established similar overall source sizes, the VLA has determined the elongated shape, source complexity and separate burst positions for the first time.

The NR has been used to determine the time profiles shown in Fig. 3. The unpolarized burst has a rapid rise and exponential decay; its most intense component is resolved in time with a duration of ≈ 2 sec. The time of the VLA snapshot map for one of them is designated by the horizontal bar. Successive 10-second snapshot maps throughout the two-minute interval indicate that the entire chain of bursts came from the same elongated source located at the same position. Subsequent highly-polarized chains of Type I bursts may originate in other sources, however, and the unpolarized burst definitely does.

PHYSICS OF SOLAR BURSTS

These previously-unpublished noise storm results illustrate the scientific potential of simultaneous VLA-NR observations of solar activity. They will be extended during the coming maximum to include other types of solar bursts, thereby providing constraints to theoretical models. The dynamical evolution of the source size is, for example, required as an input to models of the gradual and impulsive phases of solar flares. VLA-NR observations with high resolution in time, space and frequency are also required to provide fresh insights to the physics of burst phenomena such as pulsations /13/.

ACKNOWLEDGEMENTS

ACKNOWLEDGEMENTS

Radio astronomical studies of the Sun at Tufts University are supported under grant AFOSR-83-0019 with the Air Force Office of Scientific Research and contract N00014-86-K-0068 with the Office of Naval Research. Collaborative long-wavelength solar observations by Tufts University and the Observatoire de Paris are supported by National Science Foundation grant INT-8602285 and Centre National de la Recherche Scientifique grant 920038. Simultaneous SMM and VLA observations of the Sun are supported by NASA grant NAG 5-501. The Very Large Array is operated by Associated Universities Inc., under contract with the National Science Foundation. The Nançay Radioheliograph is supported by INSU. (Institut National des Sciences de l'Univers) by CNRS (Centre National de la Recherche Scientifique) and by Paris Observatory.

REFERENCES

1. O. Elgaroy, Solar Noise Storms, (New York : Pergamon Press, 1977).
2. C. Mercier, O. Elgaroy, A. Tlâmicha, and P. Zlobec, Solar Phys., 92 375-381 (1984).
3. K. Kai, P.B. Melrose, and S. Suzuki, Storms, in Solar Radiophysics, ed. D.J. McLean and N.R. Labrum (New York : Cambridge University Press, 1985), pp. 415-442.
4. J.V. Sheridan, N.R. Labrum, W.J. Payten, G.J. Nelson, and E.R. Hill, Solar Phys., 83 167-177 (1983).
5. M.F. Lantos-Jarry, Solar Phys., 15, 40-47 (1970).
6. P. Lantos, A. Kerdraon, G.G. Rapley, and R.D. Bentley, Astron. Astrophys., 101, 33-38 (1981).
7. D.J. McLean, Proc. Astron. Soc. Austr., 4, 132-138 (1981).
8. K.V. Sheridan, Storm-Source structure from two-dimensional radio-heliograph observations at meter wavelengths, in Solar Radio Storms, ed. A.O. Benz and P. Zlobec (Osservatorio Astronomico : Trieste, 1982), pp. 12-25.
9. A. Kerdraon, and C. Mercier, New observational results on noise storms, in Solar Radio Storms, ed. A.O. Benz and P. Zlobec (Osservatorio Astronomico : Trieste, 1982), pp. 27-37.
10. R.A. Duncan, Solar Phys., 97, 137-182 (1985).
11. A. Kerdraon, Astron. Astrophys., 71, 266-268 (1979).
12. K.R. Lang, and R.F. Willson, Astrophys. J., 319, 514-519 (1987).
13. G. Trottet, A. Kerdraon, A.O. Benz, and R. Treumann, Astron. Astrophys., 93, 129-132 (1981).

FIGURE LEGENDS

Fig. 1. Multiple-frequency observations of a solar noise storm with the Nançay Radioheliograph on 3 February 1986 at 150 and 164 MHz (small solid circle), 327 MHz (dashed circle) and 408 MHz (dark spot). The square denotes the position of the associated active region in the underlying photosphere. The noise storm is displaced away from a radial projection above the active region. Lower frequencies are emitted in higher regions, and the source size tends to increase with height.

Fig. 2. Very Large Array (VLA) synthesis maps for ten second intervals during a polarized burst ($\sim 50\%$ - right) and an unpolarized burst (left) on 27 June 1987. The two intervals began at 14h 30m 36.0s and 14h 46m 16s U.T., respectively. The fiducial marks on the axes are separated by $60''$, and the contours mark levels of equal brightness temperature, T_B , with an outermost contour and contour interval of 4.4×10^7 K. The peak brightness temperatures for the two intervals are 6.2×10^8 K and 3.1×10^8 K, respectively. The synthesized beam is denoted by the black spot in the lower left-hand corner; it has an angular extent of $\theta \approx 6''$. The time profiles for the two bursts are given in Figure 3.

Fig. 3. Intensity plotted as a function of time for an unpolarized burst (top) and a polarized burst ($\sim 50\%$ - bottom) with 0.5 second time resolution over two minutes on 27 June 1987. These time profiles were taken with the Nançay Radioheliograph at the same observing frequency as the VLA (~ 327 MHz) and included the times of the 10 second VLA maps shown in Figure 2.

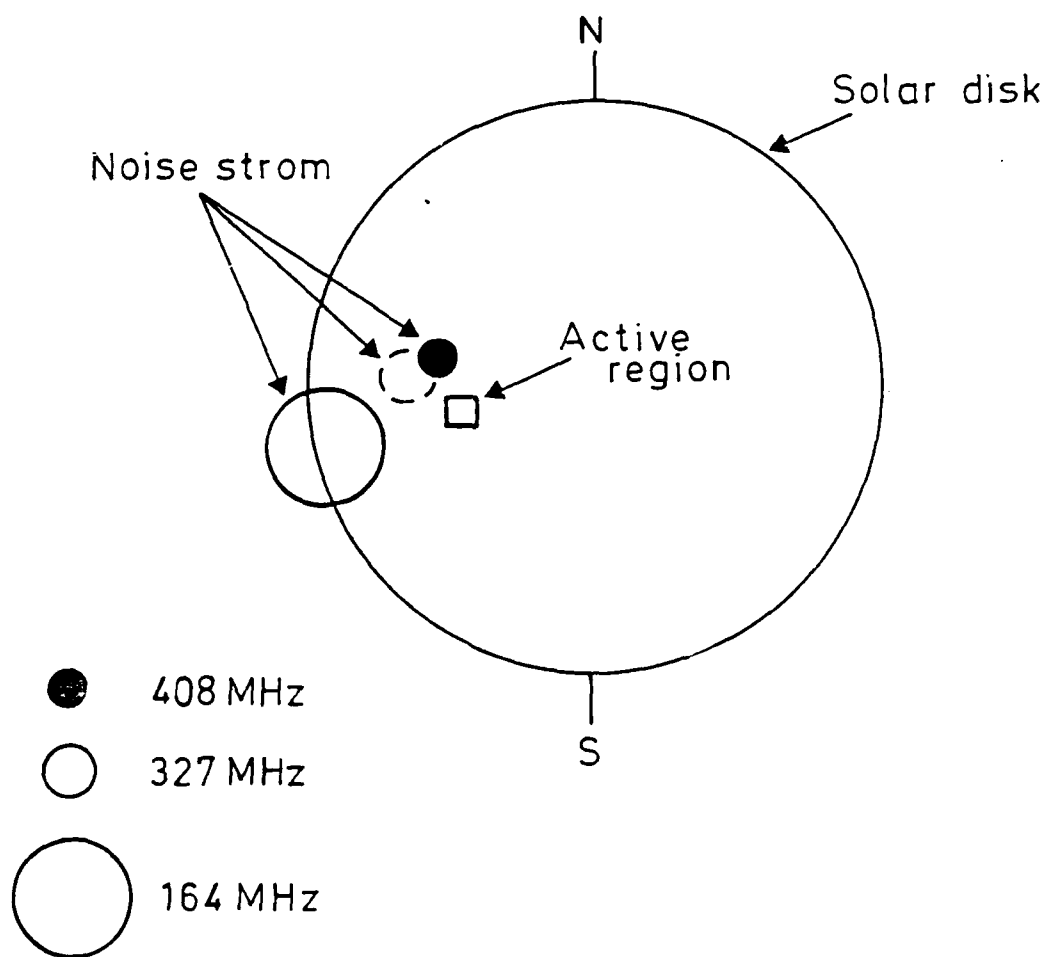


Figure 1

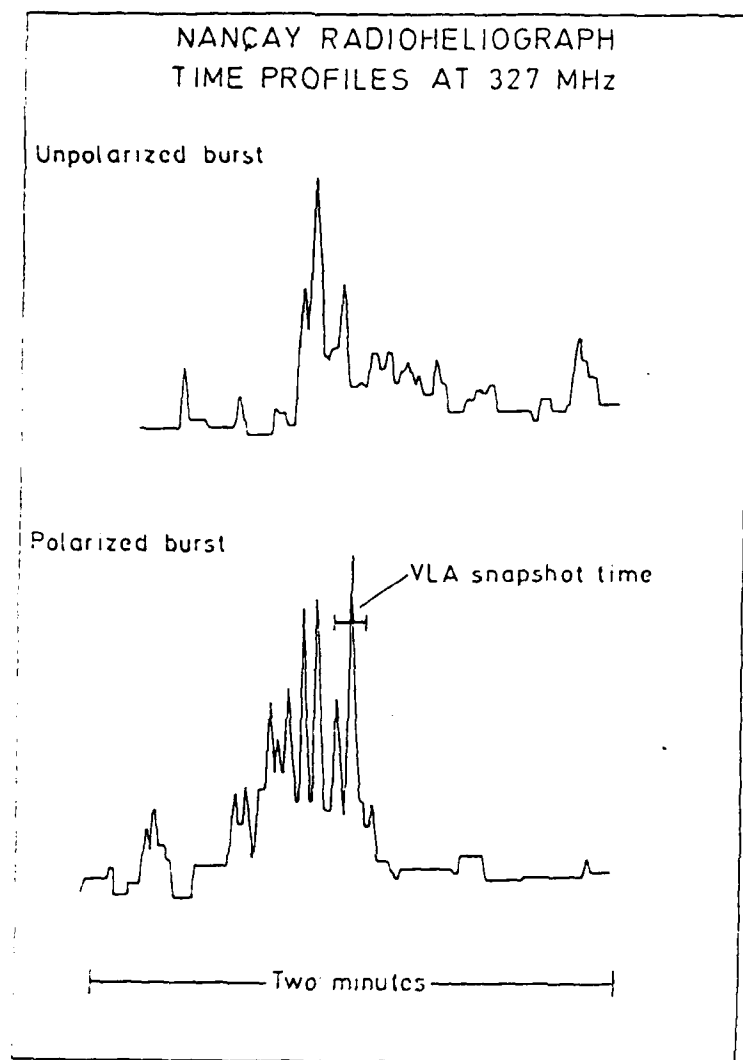


Figure 3

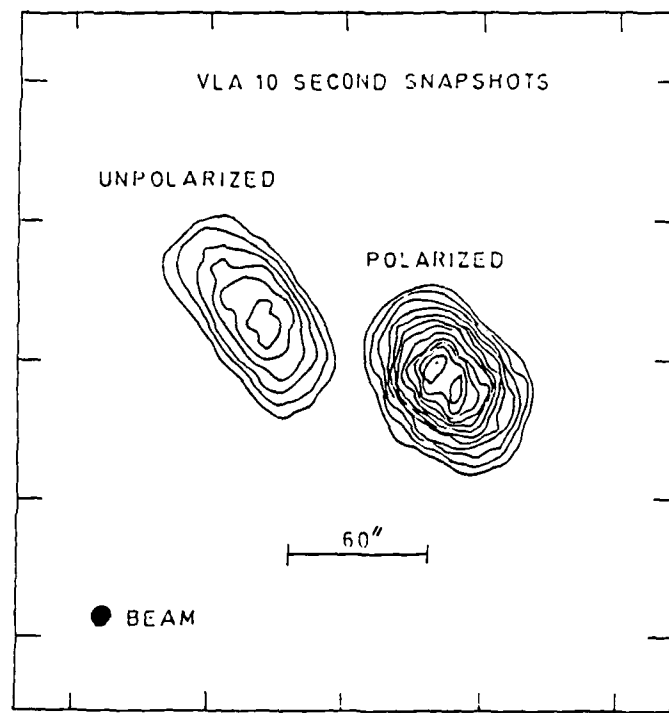


Figure 2